# Source rock development and oil-source correlation in eastern China basins

By

Huiyuan (Ian) Xu

A thesis submitted to Macquarie University
for the degree of Doctor of Philosophy
Department of Earth and Planetary Sciences

January 2019

MACQUARIE
University
SYDNEY·AUSTRALIA

This thesis is being submitted to Macquarie University in accordance with the Cotutelle agreement dated on 24 June 2015. To the best of my knowledge and belief, the thesis contains no material previously published or written by another person except where due reference is made in the thesis itself.

Huiyuan Xu

# Acknowledgements

First of all, I would like to give many thanks to my principal supervisor **Simon C. George**. I wouldn't have made it without his generous help and support. He gave me the opportunity to work in the Organic Geochemistry group and to pursue my PhD degree at Macquarie University. In the past three years, I have learned a lot from his very patient mentoring in the office and laboratory. I have obtained much knowledge from the discussions with him. I shall not forget his professional attitude as a scientist, his encouragement as a mentor, and his kindness as a friend.

I would like to thank my home university supervisor **Dujie Hou**. He gave me the chance to begin an academic life when I was still an undergraduate student. He shared his professional knowledge and experience with me. Also he encouraged me a lot with his passion for geosciences. He generously provided me with his best assistance.

I would like to give my thanks to my associate supervisor **Stefan C. Löhr**. He shared me with his expertise in sedimentology and palaeontology. He helped me a lot with the

experimental designs. Also, many useful suggestions were provided by him.

I would like to give my sincere thanks to my beloved, my wife, **Li (Ada) Wan**. She is not only my family but also my closest friend. We shared every beautiful moment of life. As PhD students, we talked and debated about geosciences. She respected and protected every one of my thoughts from cooking to science. She totally understood my stress and also my ambition. My life would be much less colourful without her company.

**Se Gong** at CSIRO is thanked for her help on conducting experiments. My fellow colleagues at Macquarie University are sincerely thanked: **Tim Leefmann**, **Carl Peters**, **Konstantinos Kotzakoulakis**, **Sarah Houlahan**, **Hongwei Ping**, **Kaikai Li**, **Oluwatoosin Agbaje**, **Sophia Aharonovich**, **Soumaya Abbassi**, **Yueyue Bai**, **Bronwyn Campbell, Lian Jiang**, **Xiong Cheng**, **Habibur Rahman**, **Bonnie Teece**, **Abah Linda Anghuno**, **Hindol Ghatak** and **Brave Manda.** I was happy to work together with them. They are very nice and would love to give me a hand when I came across problems. I have learned how to enjoy work from them. They are OJ in my PhD period.

Also many thanks to my fellow colleagues at China University of Geosciences (Beijing): **Fan Zhang**, **Zhibin Jia**, **Ziming Zhang**, **Yuhan Jiang**, **Wenjing Ding**, **Jiang Wu**, **Qinqin Su**, **Yixiong Huang**, **Dashuang He**, **Yingya Liu**, **Huaqing**, **Xu**, **Rong Mao**, **Zhe Zhao**, **Xiu Chen**, **Mei Hong**, **Zhe Chang**, **Piao Wu**. They helped me with scientific questions and CUGB communications.

I will never forget a bunch of lovely friends called ‘EPS 188 Squad’ in Macquarie

University. They are all good chefs. The weekly feast really gave me lots of security when I was homesick. Boys and girls from the football team are thanked for winning games together. That ‘tuned’ my brain to the best condition.

Finally I give my deepest appreciation to my father **Zongsheng Xu**, my mother **Xianai Jin**, and my elder sister **Naina Xu**. They have always been supporting me and praying for me. I have got confidence and strength from their spiritual support.

Thanks to China University of Geosciences (Beijing) and Macquarie University for a co-tutelle PhD scholarship. Macquarie University is thanked for the MQ-CSC Top-up scholarship. China Scholarship Council is thanked for providing funding and stipend. Macquarie University Marine Research Centre is thanked for analytical support funds.

# Abstract

In the Dongying Depression, Bohai Bay Basin of eastern China, lacustrine source rocks in the Eocene Shahejie Formation are analogous to those in the Nenjiang Formation in the Songliao Basin and the Green River Formation in Colorado, USA. The rich organic carbon in these types of source rocks (TOC > 10%) has been extensively discussed. However, uncertainty remains as to (1) the depositional environments and the organic matter inputs for adjacent laminae on the millimetre scale, (2) what triggers the change from one laminae to another, and (3) apart from the important algal contribution, what role aerobic and anaerobic bacteria played in the preservation of organic matter. It is necessary to know how subtly different depositional environments (e.g. bottom water anoxia, photic zone euxinia, etc.) and organic source inputs (e.g. bacteria, algae, land plants, etc.) interacted to produce the observed hydrocarbon heterogeneity.

Thirty eight low thermal maturity (Ro = 0.3–0.65%), organic-rich and well laminated bulk shales were subjected to organic geochemical analysis so as to understand the organic matter inputs, the depositional environment, and marine transgressions in the Dongying Depression. The paucity of terrigenous land plant biomarkers, the relationship of aqueous

organisms to biomarkers that would suggest terrigenous input, and abundant algal and bacterial biomarkers together support an organic matter input that was primarily controlled by palaeowater conditions. The detection of 24-*n*-propylcholestanes suggests an additional sporadic marine organic matter input into the Dongying palaeolake. Some shale sample were sliced at the millimetre scale so as to assess hydrocarbon heterogeneity, and thus unveil the precise mechanisms of organic matter accumulation and preservation at the microscale. Significantly, photic zone euxinia was documented on the millimetre scale, hence it was critical for phototrophs to oxidise $H_2S$ that was released from bacterial sulphate reduction. The obligate anaerobes significantly degraded and altered the organic matter that was initially provided by phytoplankton in the surface water layers. Micro-changes in palaeowater conditions are shown by varying aryl isoprenoid ratios, relative amounts of isorenieratane, and other markers including the relative abundance of dibenzothiophene, dibenzofuran, methyldibenzothiophene, methyltrimethyltridecylchromans, etc. The sliced samples have been interpreted as embodiments of different levels of euxinic water conditions. These findings reinforce (1) the main aqueous organisms that contributed to hydrocarbons, (2) the association between the open sea and the Dongying palaeolake, (3) the importance of bacterial sulphate reduction in carbon and sulphur cycling, and (4) the anaerobic respiration control on preservation of organic carbon. The controls on hydrocarbon variability at the millimetre scale will enhance our understanding and utilisation of organic geochemistry. This thesis demonstrates a comprehensive investigation into organic matter enrichment, the dynamic mechanisms for preserving organic matter, and the applicability of various biomarkers in a lacustrine setting.

A combined analysis of biomarkers and compound-specific isotopes was used to discriminate the relative hydrocarbon contribution of mudstones and associated coals to petroleum in the Xihu Depression, East China Sea Basin. Abundant diterpanes (e.g., isopimarane, phyllocladane) are present in all the samples. For samples dominated by terrigenous organic matter, long chain *n*-alkanes with a large proportion of gymnosperm input are approximately 2-3‰ enriched in $^{13}C$ relative to those with more angiosperm input, regardless of lithology. This provides a way of differentiating specific source contributions of coals and associated mudstones to petroleum.

# Contents

# List of Figures

matter contributions are shown by the abundant 24-*n*-propylcholestanes (peaks A, B, C and D). (b). Partial mass chromatograms (*m/z* 184) of the tetramethylnaphthalenes (TeMN) and dibenzothiophene (DBT) show the differences between slice C and slice I. Peak assignments: q = 24-ethyl-13β(H),17α(H)-diacholestane (20S); r = 24-ethyl-13β(H),17α(H)-diacholestane (20R); u = 24-ethyl-5α(H),14α(H),17α(H)-cholestane (20S); v = 24-ethyl-5α(H),14β(H),17β(H)-cholestane (20R); x = 24-ethyl-5α(H),14α(H),17α(H)-cholestane (20R); y = 24-*n*-propyl-13β(H),17α(H)-diacholestane (20S); z = 24-*n*-propyl-13β(H),17α(H)-diacholestane (20R); K = 4α-methyl-24-ethylcholestane 20S; P = 4α,23S,24S-trimethylcholestane (20R); Q = 4α,23S,24R-trimethylcholestane (20R); R = 4α-methyl-24-ethylcholestane (20R); S = 4α,23R,24R-trimethylcholestane (20R); T = 4α,23R,24S-trimethylcholestane (20R); 1367 TeMN means 1,3,6,7-tetramethylnaphthalene, etc.

Fig. 4.7 Representative *m/z* 133 mass chromatograms for slice A in detail (a) and all the slices (b), showing the characteristic aryl isoprenoids in the aromatic hydrocarbon fractions. The detailed chromatogram (a) shows the monoaryl isoprenoids (Axx), the diaryl isoprenoids (Dxx) and the triaryl isoprenoids (Txx) with 2,3,6/2,3,4-trimethyl substitution pattern, and the $C_{40}$ biomarker isorenieratane (iR) and other structurally unidentified derivative $C_{33}$ and $C_{40}$ compounds which are typical biomarkers for green sulphur bacteria. The chemical structure of isorenieratane with 1-alkyl-2,3,6-trimethyl substitution is shown, and the insets are the mass spectra of isorenieratane and two of the corresponding derivatives. These hydrocarbons were identified by comparison of retention times and typical mass spectra with reference samples.

# List of Tables

# Chapter 1

# 1. Introduction

## 1.1. Source rock quality, and relationship to sequence stratigraphy

Source rocks are defined as the fine-grained sedimentary rocks that have generated and expelled hydrocarbons to form a commercial accumulation of petroleum in a natural process. (Hunt, 1996). Organic matter abundance determines if a source rock is qualified to generate commercial hydrocarbon deposits. The organic matter types of the source rock determines the hydrocarbon generation potential. Thermal maturity determines the characteristics of the generated hydrocarbons. Of the components of the petroleum system, most attention should be paid to the effectiveness of the source rock, as this is the most crucial component. A relic effective source rock is a rock that has generated and expelled a large amount of hydrocarbons, and has contributed to oil and gas reservoirs. It has three main features: (1) abundant organic matter; (2) at the thermally mature stage; (3) and high expulsion effectiveness. A potential source rock is a relatively less mature rock that has not effectively generated or expelled hydrocarbons, but has great potential to generate significant amounts of

hydrocarbons under appropriate conditions.

### 1.1.1. Productivity, depositional environment and sedimentation rate

In the 1980s, Tissot and Welte (1984) researched the relationship between the kerogen in source rocks and the petroleum. In the 1990s, Hunt (1996) researched kerogen and the burial that source rocks experience, and showed that hydrocarbon generation is initiated when at a maturity indicative of Ro = 0.5-0.6%. The hydrocarbon generation peak occurs when Ro = 0.9%. The relationship between kerogen types and hydrocarbon generation potential was also investigated. Since the 1980s, petroleum scientists have studied the influencing factors on the formation of source rocks, such as palaeoenvironment, palaeoclimate, productivity, redox conditions, sedimentation rate, etc. Oehler (1984) suggested that the depositional environment controls organic matter enrichment. Jones (1987) pointed out that the main controlling factors on the organic facies are: the redox conditions during deposition, the distance to the provenance, palaeoenvironment, and palaeoclimate. Organic facies is a similar concept as depositional facies, and is determined by the organic matter content, organic matter source and the depositional environment. Organic facies can be divided into four main types, A, B, C and D, and three sub-types, AB, BC, and CD. This category can be applied to describe the amounts and types of organic matter as well as their relationships with the generation rate and petroleum properties. Katz et al. (1993) studied three sets of source rocks in North America, South America and Southeast Asia, and pointed out that the depositional environment (water depth, climate, etc.) determines the development and distribution of source rocks, as well as

the organic matter fractions and hydrocarbon generation potential in the thermally mature stage. Mello et al. (1993) studied four sets of source rocks in five Brazilian basins formed in different depositional environments (including marine and lacustrine environments), and showed that the depositional environment influences the organic geochemistry of specific source rocks. Mark et al. (1998) studied two sets of source rocks with different abundance of organic matter in the Arabian basin and suggested that productivity was the primary control on organic richness. Schulte et al. (2000) suggested that the appropriately matched sedimentation rate results in high total organic carbon (TOC). Vető et al. (2000) suggested that 36–89% of organic matter is preserved during sedimentation, and the proportion is mainly controlled by the sedimentation rate and the settling rate of the organic matter. Tyson (2001) also established an association between marine organic matter and sedimentation rate. The exploration risks of source rocks are commonly addressed by geochemical or stratigraphic models based on factors that lead to the formation of organic-rich sediments. Three independent models have been proposed: (1) an elevated primary productivity model; (2) an enhanced organic preservation model; and (3) a burial rate model (Tyson, 2001, 2005; Gallego-Torres et al., 2007). No model based on a single factor provides a fully predictive source-rock model, thus a more robust source rock model needs to account for the interplay of these factors (Katz, 2005). Although a few organic accumulations are dominated by one or another of these factors, most organic-rich sediments and rocks record a variety of optimized interactions of all variables. Organic matter enrichment can be expressed as an overall simple relation that is quite complex in detail because of the interdependencies of the variables:

Organic-matter enrichment = Production – (Destruction + Dilution) (Bohacs et al., 2005). Although organic matter-rich intervals can be hundreds of meters thick, vertical variability in TOC is high (<1-3 meters) and is controlled by stratigraphic and biotic factors (Passey et al., 2010). The co-evolution of environments and organisms controlled by tectonic subsidence and climate accounted for the deposition and distribution of high quality lacustrine source rocks with distinctly different geochemical characteristics (Hao et al., 2011).

### 1.1.2. The control of the system tract

Sequence stratigraphy was developed and widely applied into research on source rocks after the 1990s (Creaney and Passey, 1993; van Buchem et al., 1996; Passey et al., 2010). Research related to sequence stratigraphy has focussed on (1) the relationship between the geochemical properties of source rocks and the corresponding depositional environment, (2) the relationship between eustatic sea level changes and the preservation of organic matter, and (3) the organic matter fractions and hydrocarbon generation potential of source rocks from different system tracts.

Bohacs and Isaksen (1991) suggested that the low-stand system tract (LST) leads to oxidising conditions in the source rocks, and the early transgression system tract (TST) and the high-stand system tract (HST) are typified by suboxic-anoxic environments. Pasley et al. (1993) studied the upper Cretaceous Mancos Shale in the San Juan Basin in the USA, and showed that in continental margins the shale in the TST contains more organic matter. Terrigenous organic matter content in rocks deposited during the maximum flooding surface is

the lowest, and the total organic matter content in the LST and HST is the lowest. The analysis of organic matter fractions shows that terrigenous organic matter is more abundant in the regressive system tract (RST) than that in the TST. Rich land plant detritus was maintained well in the LSTs, whereas land plant detritus in the TST was highly amorphous and thus degraded (Pasley et al., 1993). This implies that the type and preservation of organic matter is related to the supply rate of terrigenous detritus and the redox conditions in the bottom waters. Therefore, organic matter content and type are predictable with the assistance of sequence stratigraphy. The source rocks with the highest hydrocarbon generation potential can be developed in TSTs, rather than only in condensed sections. During regressions the terrigenous organic matter content increases from the bottom to the top as sea level falls, while the TOC decreases due to increasing dilution of sedimentation. On the contrary, the terrigenous organic matter content decreases during transgressions, while the amount of marine organic matter and the TOC increase.

Meyers (1993) studied early Cretaceous strata in the northwest of Australia using Ocean Drilling Program data. He suggested that TOC decreases during basin subsidence. The palaeoenvironment was terrigenously dominated, and the terrigenous supply decreased with the migration landward of the deltas. Lambert (1993) studied the Devonian Chattanooga shale in Oklahoma and Kansas, USA and suggested that the shales were deposited in a complete sequence during transgression. The TOC is highest in the early HST, and is dominated by type I and II marine organic matter. The shales are widely distributed and have great thickness, and are characterised by palaeoenvironments with deep water and anoxia. The lower (early TST)

shale mainly contains type III organic matter, whereas the upper shale (late HST) contains large amounts of terrigenous organic matter, suggest that sea level was falling and the delta prograding seaward during deposition.

Wignall and Maynard (1993) suggested a transgressive deposition model for black shales, formed during maximum flooding and basal transgressive shales. Black shales usually form in condensed sections near maximum flooding surface, in TSTs. Steffen and Gorin (1993) studied carbonates from three Upper Tithonian-Berriasian field sections in southeastern France using organic petrology and palynology, and established a method to interpret sequence stratigraphy by organic facies. The relationship between organic facies and system tracts, as well as the relationship between the eustatic sea level changes and the distribution of particulate organic matter, were discussed. Creaney and Passey (1993) studied the TOC of marine source rocks in different system tracts. It was suggested that maximum TOC is generally related with maximum flooding surfaces. Above this surface, progradation in the HST leads to a large amount of terrigenous detritus. Thus, marine sediments are diluted and TOC is reduced. Below this surface the water depth increases, and the sedimentation rate decreases in the TST, which favours the accumulation of organic matter. Thus TOC increases upwards and seaward. This observation led to the HTB (high TOC at base) model that was established (Creaney and Passey, 1993).

Chandra et al. (1993) studied sea level changes and tectonic events in the Cretaceous sedimentary sequence from the Cauvery Basin in eastern India by micropaleontology. This study focussed on the controls of formation of organic-rich shales (sea level, anoxia, TOC). It

demonstrated that in the early TST source rocks have a high organic matter content and high hydrogen index. In the later TST the source rocks have lower organic matter content. Mancini et al. (1993) studied the hydrocarbon generation potential of the Upper Jurassic Smackover Formation carbonate mudstones in a condensed section deposits of southwest Alabama, USA. Only two sets of good source rocks were identified. This indicates that even if the condensed section is the most favourable section in the stratigraphy for source rocks, the local palaeoenvironment and preservation condition are also important controls. Robison et al. (1996) used a comprehensive method combining organic geochemistry, organic petrology and sequence stratigraphy to study the differences in the organic facies and lithofacies in the Triassic Shublik Formation source rocks in Alaska, USA. This study showed that the TST is more oil related.

Mann and Stein (1997) studied the distribution and hydrocarbon generation potential of organic facies in a sequence stratigraphic frame. The analyses of organic geochemical data and organic matter fractions show that there are four types of organic facies in the Cretaceous black shale in the upper Magdalena Valley, Quebrada, Columbia. The organic facies are distributed in different system tracts and show diversity in their organic geochemistry. Fleck et al. (2002) studied the organic geochemistry of the Cretaceous Marcoule Formation siliciclastic marine deposits in southeastern France. The strata section includes a marine flooding facies of a single transgressive–regressive cycle. Biomarkers show that these formations contain both marine and terrigenous organic matter inputs. The characteristics of molecular fossils were influenced by the organic matter source (marine or terrigenous), preservation (clay protection

and early diagenesis), redox conditions, and bioturbation. Frimmel et al. (2004) analysed the Toarcian Posidonia black shale in a cement quarry in Dotternhausen in the southeastern Germany using high resolution sequence stratigraphy and multi-proxy geochemical stratigraphy. This study showed that eustatic sea level changes affect the original organic matter fraction, and reducing conditions controlled the preservation of organic matter. The variation of productivity and the ratio of terrigenous/marine organic matter occur during early deposition of black shale (Fig. 1.1). Bacterial organic matter was developed in the LST and the lower TST, whereas marine planktonic organic matter was developed in the upper TST, HST and the maximum flooding surface (Frimmel et al., 2004).

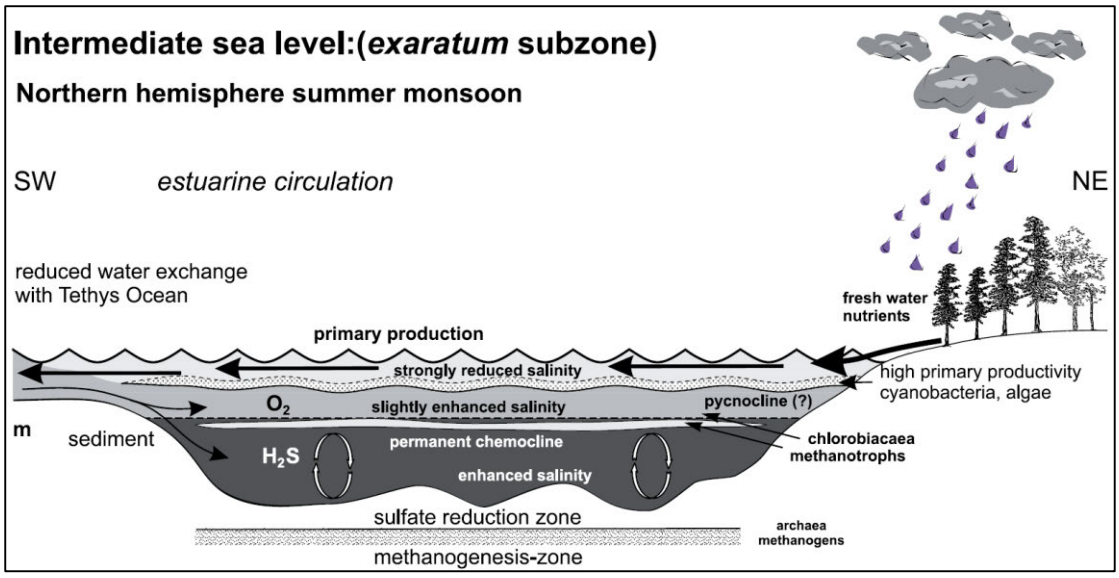


Fig. 1.1 Intermediate sea level due to restriction of water exchange with the Tethys Ocean promotes excellent preservation of organic matter produced during the summer monsoon (Frimmel et al., 2004).

In summary, the controls on the formation and quality of source rocks include depositional environment, sea level change, lithology, and organic matter source. Excellent marine source rocks in the early HST and the late TST have the best quality, followed by

effective marine source rocks in the early TST. However, in terrigenous lacustrine basins, lake level changes are more complicated in comparison to the marine environment, due to the smaller water catchment of lakes, the varying palaeoclimate, water stability, multiple organic matter sources, and uncertain condensed sections, etc.

## 1.2. Dongying Depression, Bohai Bay Basin

### 1.2.1 Geology

The Jiyang Sub-basin is a typically petroliferous depression in eastern China. After oil and gas exploration over four decades, it has 33 oil fields, and it has proven reserves of $23.4 \times 10^8$ t oil. Now exploration is in the mature stage and mainly focuses on subtle reservoirs, such as lithological traps, and shale oil. The Jiyang Sub-basin is an inland basin formed in the Mesozoic-Cenozoic under the influence of the Tanlu Fault. The depocenters include the Huimin Depression and the Dongying Depression (Fig. 1.2). The Paleogene Shahejie deposition period was dominated by rifting, which changed to deposition in a semi-graben towards the north-east in the $4^{th}$ member of Shahejie period of deposition. A large amount of sags and faults towards the north-east were formed, including four depositional depressions, namely the Dongying, Zhanhua, Huimin, and Chezhen depressions.

The Dongying Depression is in the southeast of the Jiyang Sub-basin. It is bounded by the Qingtuozi salient in the east, the Luxi and Guangrao uplifts in the south, the Qingcheng salient in the west, and the Chenjiazhuang-Binxian salient in the north (see Chapter 2.2). It is 90 km in length in the E-W direction, 65 km in width in the N-S direction, and has an area of

~5850 km$^2$. It is a complex of rifts and depressions formed during the late Cretaceous–Paleogene, and is surrounded by uplifts. The Dongying Depression is elongated along the NE-SW direction. Faults on the northern boundaries have a strike direction of NNE-SSW, and control the depositional evolution of the whole depression. From the northeast to the southwest the Dongying Depression can be divided into several tectonic zones, including the Minfeng sag, the Lijin sag, the Niuzhuang-Liuhu sags and the Boxing sag (see Chapter 2.2).

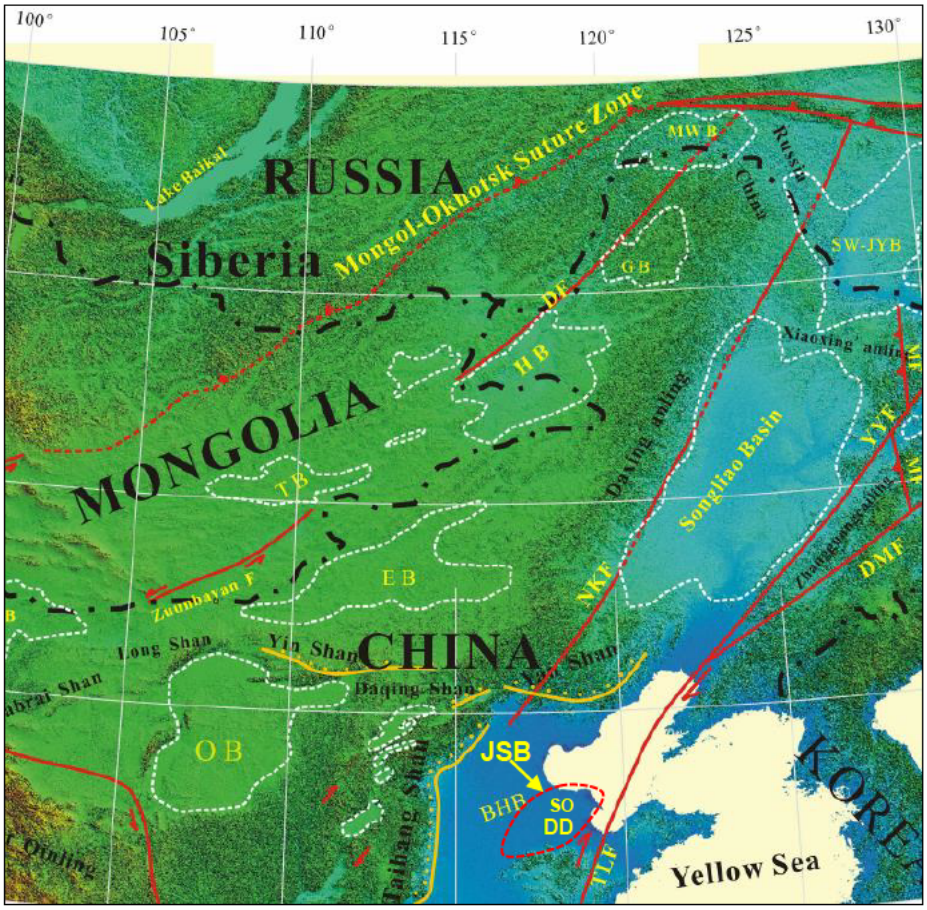


Fig. 1.2 Location and tectonic map of the Bohai Bay Basin. OB = Ordos Basin; EB = Erlian Basin; BHB = Bohai Bay Basin; SO = Shengli oilfield; DD = Dongying Depression; JSB = Jiyang Sub-basin; TLF = Tanlu Fault. Modified after Hu et al. (2015).

In profile the Dongying Depression is composed of three tectonic sets (Fig. 1.3). The basal tectonic set was formed in the early Mesozoic. The middle tectonic set is rifted-

depression controlled, and consists of the upper Jurassic–lower Cretaceous and the overlying Paleogene, with an angular unconformity between them. The upper tectonic set consists of Neogene sediments, which have undergone only minor deformation. The latter is widely distributed and thins towards the basin edge. In the Paleogene the subsidence rate was higher, faults rapidly developed and the basin moved into the rifting stage. During this stage, there were multiple instances of transgressions and regressions. Lacustrine sediments were very well developed, and formed >1000 m of dark Paleogene shales. Lacustrine source rocks were deposited in saline to fresh water environments. Consequently, this stage is critical for hydrocarbon generation and petroleum prospectivity of the Dongying Depression.

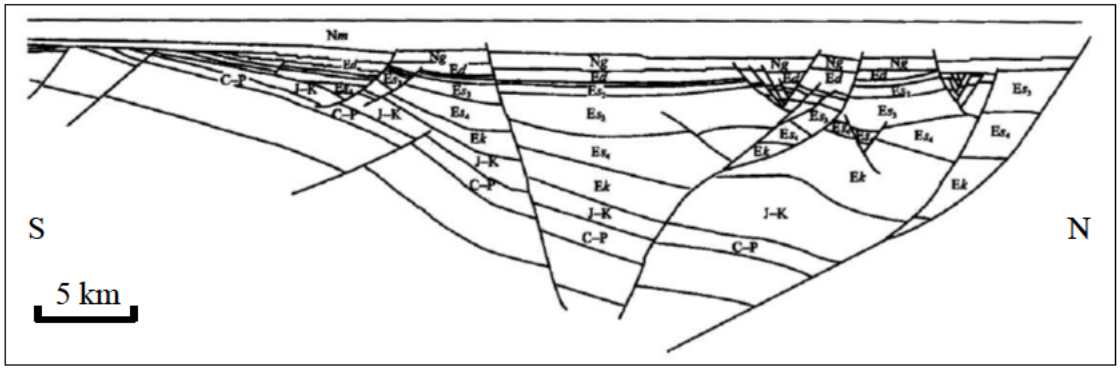


Fig. 1.3 S-N trending cross section showing the structural framework of the Dongying Depression. C-P = Carboniferous-Permian, J-K = Jurassic-Cretaceous, Ek = Eogene Kongdian Formation, $Es_4$ = Eogene 4th member of Shahejie Formation, $Es_3$ = Eogene 3rd member of Shahejie Formation, $Es_2$ = Eogene 2nd member of Shahejie Formation, Ed = Eogene Dongying Formation, Ng = Neogene Guantao Formation. Modified after Zhang et al. (2009).

### 1.2.2 Lacustrine source rocks

Kelts (1988) summarised the origins and depositional environments of lacustrine source rocks. Also the production, deposition and preservation of organic matter in lacustrine system

was discussed by Kelts (1988). Talbot (1988) studied six modern tropical lakes in Africa and discussed the origin of lacustrine source rocks. Particularly this paper emphasised the controls of climate and lake level on the accumulation of organic matter. Bohacs et al. (2000) compared a large number of modern and ancient lacustrine sediments. These authors suggested that the balance between the sediment supply rate and the increasing rate of accommodation controls the initiation, distribution and architecture of lacustrine systems. Lacustrine lakes are classified into three types: over-filled lakes, balanced-filled lakes, and under-filled lakes (Carroll and Bohacs, 1999, 2001). Balanced-filled and over-filled lakes are often associated with relatively closed hydrology, while under-filled lakes are dominated by open hydrology. The TOC is low to medium in over-filled lakes, and the kerogen type can vary from I–III, with distinct lateral variations of organic facies. In balanced-filled lakes, the TOC is medium to high, and the kerogen is typically type I (type I to III at flooding surfaces). The organic facies is uniform and continuous laterally in balanced-filled lakes. In under-filled lakes, the TOC is rather low but the kerogen type is typically type I.

### 1.2.3 Dongying Depression source rocks

Source rocks in the Dongying Depression have differences not only due to variations in the depositional environment, lithology and lake level at the time of deposition, leading to variations in organic matter content, organic matter type, and biomarkers. The source rocks in the Shahejie Formation have relatively high organic matter content (2–9%) and are dominated by type I kerogen. Source rocks in part of this formation have relatively low organic

abundance (< 2%) and contain types II and III kerogen. (Zhang et al., 2009). The significant variation of aliphatic and aromatic hydrocarbon markers in the Shahejie Formation is a function of burial depth, which explains the uncertainty associated with the maturity assessment and genetic modelling for so-called 'immature oils' (Li et al., 2003). The biogenic assemblage has the characteristics of high differentiation and high abundance, and includes dinoflagellates (*Defladrea*, *Senegalinium*, *Subtilisphaera luxadinium*, *Bohaidina granulata* subsp *minor* and *Palacostomocysts* species), green algae (*Reticuloffenesira bohaiensis*), blue algae (*Pediastrum*), and *Botryococcus* genera. The palaeo-lake depths ranged from shallow lake to semi-deep lake in the 4$^{th}$ member of the Shahejie Formation, and then to a deep lake in the 3$^{rd}$ member of the Shahejie Formation. The salinity of the lake water has a large variation from hypersaline water, saline water, brackish water, and fresh water. Another important feature of the Dongying source rocks is that they are highly heterogeneous at both the macro-scale (e.g. system tracts, sedimentary facies and rhythmicity) and micro-scale (e.g. laminae characteristics, minerals) (Li et al., 2003). Marine organic matter input to the Dongying Depression has not been previously ascertained (Hou et al., 1997). The possibility of a marine influx on the organic matter would be important, because a marine transgressive event may have significantly improved the lake productivity and increased the salinity of the palaeolake, hence improving preservation (Hou et al., 1997; Wang et al., 2008; Yuan et al., 2008). A marine transgression would also have influenced the system tracts.

In general, lacustrine basins are smaller and receive multiple sources of sediment supply compared with marine basins in the open sea. Therefore the vertical distribution of lacustrine

and marine source rocks in the sequence stratigraphic framework are different (Bohacs et al., 2000). For the Dongying lacustrine basin, the condensed sections are distributed in the lower HST or upper TST (Feng et al., 2013). The best source rocks in the Jiyang Sub-basin were discovered in large amounts in the Dongying Depression, Bohai Bay Bain. These account for the most important oil field in China, the Shengli oil field (Fig. 1.2). The Dongying Depression is a large paralic basin formed from the Paleogene to the Neogene. Because rifted-basins such as the Dongying Depression are formed by multiple tectonic events, they are extremely complicated. Moreover, the Dongying Depression shows multiple cycles of sedimentary evolution (Zhang et al., 2009). Consequently, there are many difficulties in petroleum exploration. Petroleum geologists need to solve the following problems: How much remaining oil and gas potential is there? How are the oil and gas fields distributed? Where are the next exploration targets? These questions are significant for the future of petroleum exploration in the Dongying Depression, which is the most important depression in the Jiyang Sub-basin. Also, addressing these questions will assist in research on the generation and accumulation of petroleum in lacustrine basins more generally.

This study focuses specifically on the Dongying Depression in eastern China. This study will help to evaluate the resource potential of the Dongying Depression, and will determine the target area of shale oil exploration in the future. Additionally, the research will provide new insights and research case studies for the other lacustrine rifted-basins.

## 1.3. Xihu Depression, East China Sea Basin

The East China Sea Basin is located on the eastern Chinese margin with an effective

exploration area of $24 \times 10^4$ km$^2$. It has been filled with sediments since the Jurassic, which have a maximum thickness of 15,000 m. It has an estimated petroleum resource of $6 \times 10^9$ tons of oil (Hou et al., 2015). The Xihu Depression is in the central Zhedong Depression of the East China Sea Basin (Fig. 1.4), with an area of $4.6 \times 10^4$ km$^2$. The Xihu Depression is separated into five tectonic belts which are designated, from west to east, the West Slope Belt, the West Sub-depression, the Central Inversion Tectonic Belt, the East Sub-depression, and the East Fault Belt (Fig. 1.5).

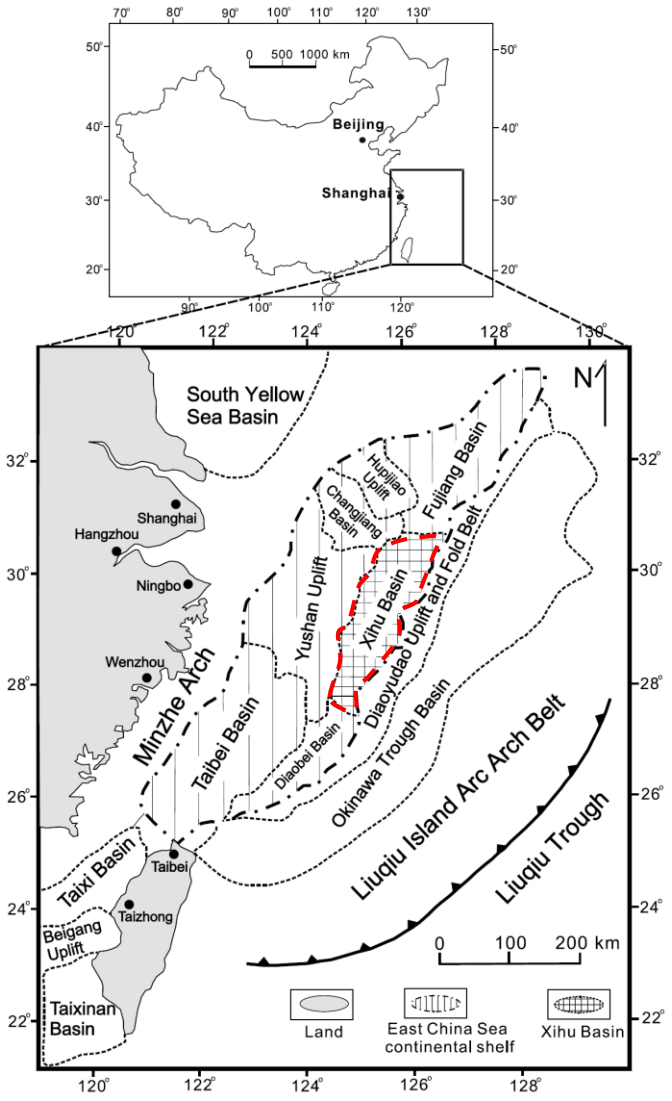


Fig. 1.4 A schematic diagram showing the East China Sea continental shelf with its major tectonic units and the location of the Xihu Depression (red dashed line). From Ye et al. (2007)

Petroleum exploration since the 1970s shows that the Xihu Depression has the most petroleum potential in the East China Sea Basin (Li and Li, 2003; Ye et al., 2007). In 1980, the first well (LJ-1) was drilled in the Jiaxing structural belt. In 1982, the PH-1 well was drilled in the Pinghu structural belt and found commercial petroleum. Up to present, eight oil fields have been discovered, including the Pinghu, Chunxiao, and Tianwaitian oilfields (see Chapter 6.1). The natural gas resources of the Xihu Depression are $1.7\times10^{12}$ m$^3$ in the target area. However, large petroleum traps have only been discovered in the Oligocene Huagang Formation and the Eocene Pinghu Formation. The proven reserves of natural gas are less than $500\times10^{8}$ m$^3$.

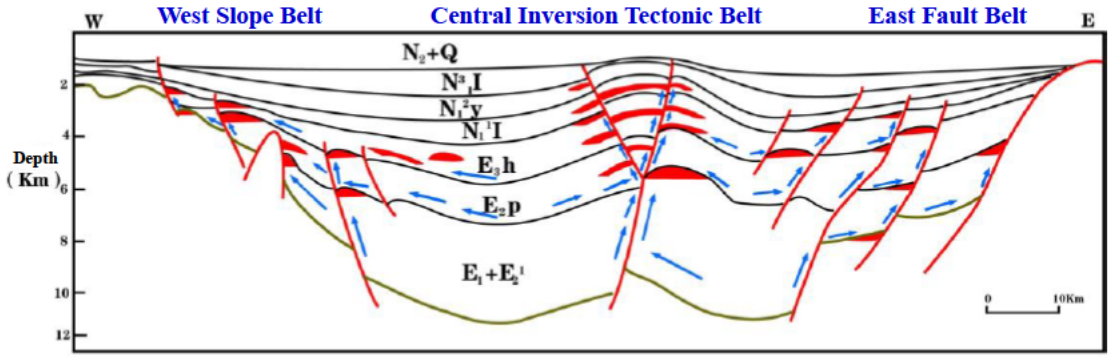


Fig. 1.5 W-E trending cross section showing the structural framework of the Xihu Depression. $E_2p$ = Eogene Pinghu Formation, $E_3h$ = Eogene Huagang Formation, $N_1^1I$ = Neogene Longjing Formation, $N_1^2y$ = Neogene Yuquan Formation, $N_1^3I$ = Neogene Liulang Formation, $N_2$+Q = upper Neogene+Quaternary. From Hou et al. (2015).

The depositional environment and organic matter sources are complex in the Xihu Depression. The source rocks mainly contain kerogen types III (Fig. 1.6). The question of the source of the discovered oil and gas, and the accumulation and migration system, have not yet been fully understood (Ye et al., 2007). The Xihu Depression may contain oil and gas from

deeper source rocks, rather than just the Pinghu and Huagang formations. Additionally, another key question waiting to be addressed is the relative contribution of mudstones and the associated coals to the discovered oil and gas.

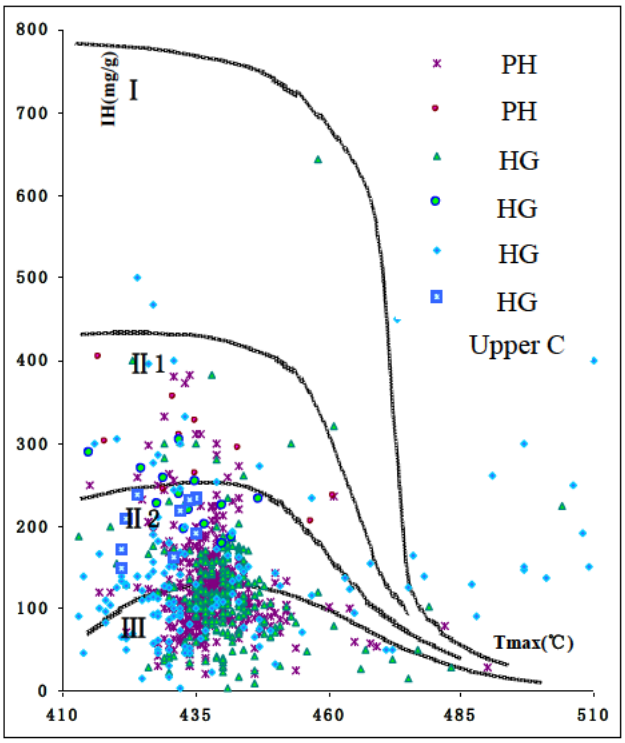


Fig. 1.6 Organic matter types in mudstones (M) and coals (C) in the Xihu Depression. PH = Pinghu Formation, HG = Huagang Formation. From Hou et al. (2015).

## 1.4. Thesis aims

The aims of this thesis are to use mainly organic geochemical methodologies to assess the depositional environments and organic matter inputs of the organic-rich source rocks (shales and mudstones) in the Dongying Depression, Bohai Bay Basin. The thesis also aims to discriminate the relative contributions of mudstones and coals to the oil and gas in the Xihu Depression, East China Sea Basin.

## References

Bohacs, K.M., Isaksen, G.H., 1991. Source quality variations tied to sequence development: Integration of physical and chemical aspects, Lower to Middle Triassic, western Barents Sea. AAPG Bulletin 75, 544-544.

Bohacs, K.M., Carroll, A.R., Neal, J.E., Mankiewicz, P.J., 2000. Lake-basin type, source potential, and hydrocarbon character: an integrated sequence stratigraphic geochemical framework. Lake basins through space and time: AAPG Studies in Geology 46, 3-34.

Bohacs, K.M., Grabowski Jr, G.J., Carroll, A.R., Mankiewicz, P.J., Miskell-Gerhardt, K.J., Schwalbach, J.R., Wegner, M.B., Simo, J.T., 2005. Production, destruction, and dilution—the many paths to source-rock development. SEPM Special Publication 82, 61-101.

Carroll, A.R., Bohacs, K.M., 1999. Stratigraphic classification of ancient lakes: Balancing tectonic and climatic controls. Geology 27, 99-102.

Carroll, A.R., Bohacs, K.M., 2001. Lake-type controls on petroleum source rock potential in nonmarine basins. AAPG Bulletin 85, 1033-1053.

Chandra, K., Raju, D.S.N., Mishra, P.K., 1993. Sea level changes, anoxic conditions, organic matter enrichment, and petroleum source rock potential of the Cretaceous sequences of the Cauvery Basin, India: Chapter 9, SG 37: Source Rocks in a Sequence Stratigraphic Framework, pp. 131-146.

Creaney, S., Passey, Q.R., 1993. Recurring patterns of total organic carbon and source rock quality within a sequence stratigraphic framework. AAPG Bulletin 77, 386-401.

Feng, Y., Li, S., Lu, Y., 2013. Sequence stratigraphy and architectural variability in Late Eocene lacustrine strata of the Dongying Depression, Bohai Bay Basin, Eastern China. Sedimentary Geology 295, 1-26.

Fleck, S., Michels, R., Ferry, S., Malartre, F., Elion, P., Landais, P., 2002. Organic geochemistry in a sequence stratigraphic framework. The siliciclastic shelf environment of Cretaceous series, SE France. Organic Geochemistry 33, 1533-1557.

Frimmel, A., Oschmann, W., Schwark, L., 2004. Chemostratigraphy of the Posidonia black shale, SW Germany: I. Influence of sea-level variation on organic facies evolution. Chemical Geology 206, 199-230.

Gallego-Torres, D., Martínez-Ruiz, F., Paytan, A., Jiménez-Espejo, F.J., Ortega-Huertas, M., 2007. Pliocene–Holocene evolution of depositional conditions in the eastern Mediterranean: Role of anoxia vs. productivity at time of sapropel deposition. Palaeogeography Palaeoclimatology Palaeoecology 246, 424-439.

Hao, F., Zhou, X., Zhu, Y., Yang, Y., 2011. Lacustrine source rock deposition in response to co-evolution of environments and organisms controlled by tectonic subsidence and climate, Bohai Bay Basin, China. Organic Geochemistry 42, 323–339.

Hou, D., Wang, T., Zhang, Y., 1997. Dinosteranes in the Tertiary terrestrial deposits, Eastern China: The marker of marine transgression facies. Geological Review 43, 524-528.

Hou, D., Xu, H., Wu, J., Diao, H., Cao, B., Chen, X., 2015. 125 National Science and Technology Major Project. Shanghai Branch of China National Offshore Oil Corporation, Shanghai.

Hu, J.F., Peng, P.A., Liu, M.Y., Xi, D.P., Song, J.Z., Wan, X.Q., Wang, C.S., 2015. Seawater incursion events in a Cretaceous paleo-lake revealed by specific marine biological markers. Scientific Reports 5, 9508.

Hunt, J., 1996. Petroleum geochemistry and geology. W.H. Freeman, New York.

Jones, R.W., 1987. Organic facies, Organic Geochemistry in Oil Exploration, pp. 15-30.

Katz, B.J., Breaux, T., Colling, E., Darnell, L., Elrod, L., Jorjorian, T., Royle, R., Robison, V., Szymczyk, H., Trostle, J., 1993. Implications of stratigraphic variability of source rocks. Source rocks in a sequence stratigraphic framework. American Association of Petroleum Geologists Studies in Geology 37, 5-16.

Katz, B.J., 2005. Controlling factors on source rock development—a review of productivity, preservation, and sedimentation rate.

Kelts, K., 1988. Environments of deposition of lacustrine petroleum source rocks: an introduction. Geological Society, London, Special Publications 40, 3-26.

Lambert, M.W., 1993. Internal stratigraphy and organic facies of the Devonian-Mississippian Chattanooga (Woodford) shale in Oklahoma and Kansas: Chapter 11, SG 37: Source Rocks in a Sequence Stratigraphic Framework, pp. 163-176.

Li, S., Li, C., 2003. Analysis on the petroleum resource distribution and exploration potential of the Xihu depression, the East China Sea. Petroleum Geology and Experiment 25, 728-733.

Li, S., Pang, X., Li, M., Jin, Z., 2003. Geochemistry of petroleum systems in the Niuzhuang South Slope of Bohai Bay Basin—part 1: source rock characterization. Organic

Geochemistry 34, 389–412.

Mancini, E.A., Tew, B.H., Mink, R.M., 1993. Petroleum source rock potential of Mesozoic condensed section deposits of southwest Alabama. Geological Survey of Alabama.

Mann, U., Stein, R., 1997. Organic facies variations, source rock potential, and sea level changes in Cretaceous black shales of the Quebrada Qcal, Upper Magdalena Valley, Colombia. AAPG Bulletin 81, 556-576.

Mello, M.R., Koutsoukos, E.A.M., Neto, E.V.S., Jr, A.C.S.T., 1993. Geochemical and micropaleontological characterization of lacustrine and marine hypersaline environments from Brazilian sedimentary basins, SG 37: Source Rocks in a Sequence Stratigraphic Framework, pp. 17-34.

Meyers, P.A., 1993. Types and maturity of organic matter accumulated during Early Cretaceous subsidence of the Ex-mouth Plateau, Northwest Australia margin. AAPG studies in Geology 37, 119-130.

Oehler, J.H., 1984. Carbonate source rocks in the Jurassic Smackover trend of Mississippi, Alabama, and Florida, SG 18: Petroleum Geochemistry and Source Rock Potential of Carbonate Rocks, pp. 63-69.

Pasley, M.A., Riley, G.W., Nummedal, D., 1993. Sequence stratigraphic significance of organic matter variations: Example from the upper Cretaceous mancos shale of the San Juan Basin, New Mexico: Chapter 14, SG 37: Source Rocks in a Sequence Stratigraphic Framework, pp. 221-241.

Passey, Q.R., Bohacs, K., Esch, W.L., Klimentidis, R., Sinha, S., 2010. From oil-prone source

rock to gas-producing shale reservoir-geologic and petrophysical characterization of unconventional shale gas reservoirs, International oil and gas conference and exhibition in China. Society of Petroleum Engineers, Beijing, China.

Robison, V.D., Liro, L.M., Robison, C.R., Dawson, W.C., Russo, J.W., 1996. Integrated geochemistry, organic petrology, and sequence stratigraphy of the Triassic Shublik Formation, Tenneco Phoenix# 1 well, North Slope, Alaska, USA. Organic Geochemistry 24, 257-272.

Schulte, S., Mangelsdorf, K., Rullkötter, J., 2000. Organic matter preservation on the Pakistan continental margin as revealed by biomarker geochemistry. Organic Geochemistry 31, 1005-1022.

Steffen, D., Gorin, G., 1993. Palynofacies of the Upper Tithonian-Berriasian deep-sea carbonates in the Vocontian Trough (SE France). Bulletin des Centres de Recherches Exploration-Production Elf-Aquitaine 17, 235-247.

Talbot, M.R., 1988. The origins of lacustrine oil source rocks: evidence from the lakes of tropical Africa. Geological Society, London, Special Publications 40, 29-43.

Tissot, B.P., Welte, D.H., 1984. From kerogen to petroleum, in: Tissot, B.P., Welte, D.H. (Eds.), Petroleum formation and occurrence, 2nd Edition. Springer, Berlin Heidelberg, pp. 160–198.

Tyson, R.V., 2001. Sedimentation rate, dilution, preservation and total organic carbon: some results of a modelling study. Organic Geochemistry 32, 333-339.

Tyson, R.V., 2005. The "productivity versus preservation" controversy: cause, flaws, and

resolution, in: Harris, N.B. (Ed.), The Deposition of Organic-carbon-rich Sediments: Models, Mechanisms, and Consequences. SEPM Special Publication, pp. 17-33.

van Buchem, F.S.P., Razin, P., Homewood, P.W., Philip, J.M., Eberli, G.P., Platel, J.-P., Roger, J., Eschard, R., Desaubliaux, G.M.J., Boisseau, T., 1996. High resolution sequence stratigraphy of the Natih Formation (Cenomanian/Turonian) in northern Oman: distribution of source rocks and reservoir facies. GeoArabia 1, 65-91.

Vető, I., Hetényi, M., Hámor-Vidó, M., Hufnagel, H., Haas, J., 2000. Anaerobic degradation of organic matter controlled by productivity variation in a restricted Late Triassic basin. Organic Geochemistry 31, 439-452.

Wang, G., Wang, T.G., Simoneit, B.R.T., Chen, Z., Zhang, L., Xu, J., 2008. The distribution of molecular fossils derived from dinoflagellates in Paleogene lacustrine sediments (Bohai Bay Basin, China). Organic Geochemistry 39, 1512–1521.

Wignall, P.B., Maynard, J.R., 1993. The sequence stratigraphy of transgressive black shales. Source Rocks in a Sequence stratigraphic framework 37, 35-47.

Ye, J., Qing, H., Bend, S.L., Gu, H., 2007. Petroleum systems in the offshore Xihu Basin on the continental shelf of the East China Sea. AAPG Bulletin 91, 1167-1188.

Yuan, B., Chen, S., Yuan, W., Zhu, J., 2008. Characteristics of strontium and sulfur isotopes in Shahejie Formation of Jiyang Depression. Journal of Jilin University (Earth Science Edition) 38, 613–617. (in Chinese).

Zhang, L., Liu, Q., Zhu, R., Li, Z., Lu, X., 2009. Source rocks in Mesozoic-Cenozoic continental rift basins, East China: A case from Dongying Depression, Bohai Bay

Basin. Organic Geochemistry 40, 229–242.

Chapter 2

# 2. The occurrence of isorenieratane, 2α-methylhopanes, crocetane, 24-*n*-propylcholestanes and 24-norcholestanes in Paleogene lacustrine source rocks from the Dongying Depression, Bohai Bay Basin: Implications for bacterial sulphate reduction, photic zone euxinia and seawater incursions

Huiyuan Xu[a, b, *], Simon C. George[b, *], Dujie Hou[a, *]

[a] School of Energy Resources, China University of Geosciences (Beijing), Haidian District, Beijing 100083, China

[b] Department of Earth and Planetary Sciences and MQMarine Research Centre, Macquarie University, Sydney, NSW 2109, Australia

**Chapter 2** is a comprehensive demonstration of aliphatic hydrocarbons and biomarkers in the source rocks in the Dongying Depression, one of the main lacustrine source rock formations in China. This chapter helps readers better understand the organic matter input, lipids preservation and water chemistry of the Dongying Depression.

**Statement of Author's Contribution:** This chapter is an original research paper that has been published in the journal *Organic Geochemistry* (2019). 85% of the work was done by the first author Huiyuan Xu, including developing the project plan and timeframe, sampling, conducting laboratory experiments, processing and analysing the data, and writing the manuscript. Simon C. George helped with sampling, designing the laboratory experiments, directing the research, and improving the manuscript, which accounts for 10%. Dujie Hou helped with developing the project plan and timeframe, sampling, and improving the manuscript, which accounts for 5%.

# Abstract

Lacustrine organic-rich source rocks (shales and mudstones) were examined to assess the palaeo depositional environment and organic input sources of the third and fourth members of the Eocene Shahejie Formation, Bohai Bay Basin, China. Major organic contributions to the Shahejie Formation from dinoflagellates, diatoms, *Botryococcus* and marine pelagophyte/chrysophyte algae were determined by *n*-alkane distributions, gammacerane index and diagnostic steranes. The scarcity of higher plant biomarkers in the sediments analysed suggests that terrigenous organic inputs were limited. The pervasive presence of β-carotane, aryl isoprenoids, paleorenieratane, renieratane, isorenieratane, 2α-methylhopanes and crocetane indicate significant organic contributions from bacterial communities including cyanobacteria, purple sulphur bacteria (*Chromatiaceae*), green sulphur bacteria (*Chlorobiaceae*) and sulphate-reducing bacteria. The extent of $H_2S$ content, bacterial sulphate reduction, and photic zone euxinia (PZE) were evaluated by determining the aryl isoprenoids ratio (AIR), the presence of isorenieratene derivatives, and the fate of sulphur in palaeo-water. There was a decrease of PZE extent and duration from the northeast to the southwest of the palaeo-lake, and there was a decrease of water body salinity and bottom water anoxia from the fourth to the third member of the Shahejie Formation. Abrupt environmental perturbations in the third member of the Shahejie Formation are indicated not only by significant changes in parameters such as the pristane/phytane (0.34–1.53) and β-carotane/*n*-$C_{20}$ alkane ratios (0.0–26.9), the gammacerane index (0.04–2.5), the isorenieratane/$C_{18}$ aryl isoprenoid (0.0–71), and the AIR (0.7–9.0), but also by the time lag in the expansion of cyanobacterial lineages after the expansion of purple/green sulphur bacteria, as well as seawater incursions. The occurrence of intact $C_{30}$ 4-desmethylsteranes (24-*n*-propylcholestanes) in the Shahejie Formation is first reported here, after crosstalk checking, and provides unambiguous biological evidence for at least two marine transgression events reaching the Eocene lake. The organic enrichment of the

petroleum source rocks in the Shahejie Formation is a consequence of combined indigenous lacustrine algal production, the constrained and favourable preservation conditions, and significant bacterial contributions and marine organic matter inputs to the lake.

*Keywords:* Lacustrine; organic-rich; 24-*n*-propylcholestane; marine transgression; methylhopanes; isorenieratane; photic zone euxinia; Dongying Depression; Bohai Bay Basin.

## 2.1. Introduction

The evolution of depositional environments and the primary mechanism of accumulation of organic matter in the Dongying Depression, Bohai Bay Basin, eastern China, has been widely discussed. The formation of excellent petroleum source rocks usually depends on a high productivity of algal blooms and restricted preservation conditions, with a low clastic sedimentation rate to avoid dilution also important (Gallois, 1976; Fleet et al., 1988; Parnell, 1988; Katz, 1990, 1995). For instance, the lacustrine organic-rich shales in the Dongying Depression were deposited under anoxic environments from a saline and stratified water column (Li et al., 2003; Xiong et al., 2007; Zhang et al., 2009; Hao et al., 2011; Liu and Wang, 2013; Wang et al., 2015; He et al., 2017). Nevertheless, the possibility that marine transgressional events may be associated with the formation of massive hydrocarbon-rich shales and mudstones in the Dongying Depression has been proposed (Peng et al., 1989; Tang, 1993; Yang, 2000; Yuan et al., 2005, 2006; Yuan, 2006; Yuan et al., 2008a; Yuan et al., 2008b). The Eocene Dongying Depression was deposited during a period of global marine transgressions with high sea level (Haq et al., 1987). The seawater incursions may have increased the water salinity and nutrient level of the lake, leading to high primary productivity and eutrophication. Various lines of evidence support marine-related deposition in the Dongying Depression, including fossils (*Deflandrea* dinoflagellates, *Petalocrinus* crinoids, foraminifera), minerals and rocks (algal reef limestones, collophane, and glauconite) (Hou, 1978; Qian et al., 1980; Hao and Li, 1984; He et al., 2003; Ge, 2004), the evaporation and crystallisation order of various saline minerals (Yuan et al., 2006), molecular fossils (a series of $C_{30}$ and $C_{31}$ steranes, e.g. dinosteranes) and inorganic geochemical parameters (B/Ga, Sr/Ba, Br $\times 10^{-3}$/Cl, Th/U, and the $\delta^{13}C$ and $\delta^{18}O$ in carbonates; Li and Xiao, 1988; Ren et al., 2000; Yuan et al., 2005; He et al., 2017). Nonetheless, no unambiguous marine sedimentary

rocks occurred in northern China during the Cretaceous and Cenozoic, and these marine indicators are not widespread across the whole of the Dongying Depression.

Inland brackish lakes can contain dinoflagellates and glauconite, etc., so these indicators are no longer thought to be specific to marine settings (Wang, 1983; Mao and Yu, 1990). Liu et al. (2002) suggested the presence of marine-terrestrial fossils by analyses of O, C and Sr isotopes. It appears that some of the marine facies features in the Dongying Depression are merely related to water salinity. Another hypothesis is that marine climate events such as the East Asian monsoon (Wang et al., 2013a), winter storms and summer hurricanes are most likely to occur within 25 °–45 °latitude (Marsaglia and Klein, 1983; Duke, 1985, 1987). Thus, the paralic Dongying Depression, which had a palaeo-latitude of 39 °north in the Eocene (Boucot et al., 2009), could possibly be affected by these marine-related events in the northwest Pacific Ocean region. Furthermore, the heterogeneity (i.e. stability and consistency) of depositional environments both temporally and spatially across the whole of the Dongying Depression have rarely been discussed. It is uncertain to what extent water column stratification, bottom water anoxia, photic zone euxinia, and bacterial activity occurred, and the association between multiple sources of organic matter and the water body conditions is also unknown. The exact trigger(s) leading to the formation of organic-rich shales/mudstones in the Dongying Depression remains unclear.

Source rocks of the lower part of the third and upper part of the fourth members of the Shahejie Formation have relatively high organic matter content and are dominated by type I kerogen (Zhang et al., 2009). Algal blooms are the primary control on the formation of lacustrine petroleum source rocks (Liu and Wang, 2013). Thermal evolution studies show that the upper part of the fourth member is in the early stage of the hydrocarbon generation process, and can generate immature oils, while the lower and middle parts of the third member have a relatively late and simple hydrocarbon generation process, and mainly generate mature

oils (Zhang et al., 2009). No strict groupings of the source rocks was determined as samples show intermediate hydrocarbon characteristics (Li et al., 2003). So-called 'immature oils' are usually defined on the basis of the presence of biomarkers with "biological" configurations (Li et al., 2003).

The well-preserved low maturity lacustrine shales and mudstones in the Dongying Depression, Bohai Bay Basin are well suited for comprehensively testing organic geochemical parameters that respond to a changing depositional environment. The occurrence of exclusively marine biomarkers will track the earliest marine algae contributions to organic-rich source rocks in the Dongying Depression. The present work complements previous study of organic matter inputs and unravels the relationship between depositional environment and enrichment of organic matter by analysing Shahejie Formation samples throughout the depression from the third to the fourth member, and from the northeast to the southwest of the Dongying Depression.

## 2.2. Geological setting

The rise of upper mantle behind the Western Pacific subduction margin caused the rifting of continental crust during the Late Mesozoic-Cenozoic (Fu and Sheng, 1989). The Bohai Bay Basin is an intracontinental extensional rift basin that formed since the Late Jurassic, and is located in the east of the North China Craton, adjacent to the Bohai Sea, and is bounded by the Tanlu Fault in the east. The Bohai Bay Basin experienced high geothermal heat flow and has a high geothermal gradient (4.3 ℃/100 m; Zhang et al., 2008). There are six sub-basins within the Bohai Bay Basin. The Jiyang Sub-basin is the most petroliferous one, and formed in the rifting and subsiding phase. It is situated in the south of the Bohai Bay Basin, and covers most of the Yellow River Delta, with an area of 25,000 $km^2$, with a width of 120 km and length of 200 km, and is northeast-southwest trending. The Dongying Depression

developed in the southern part of the Jiyang Sub-basin, and covers an area of 5,500 km$^2$ (Fig. 2.1).

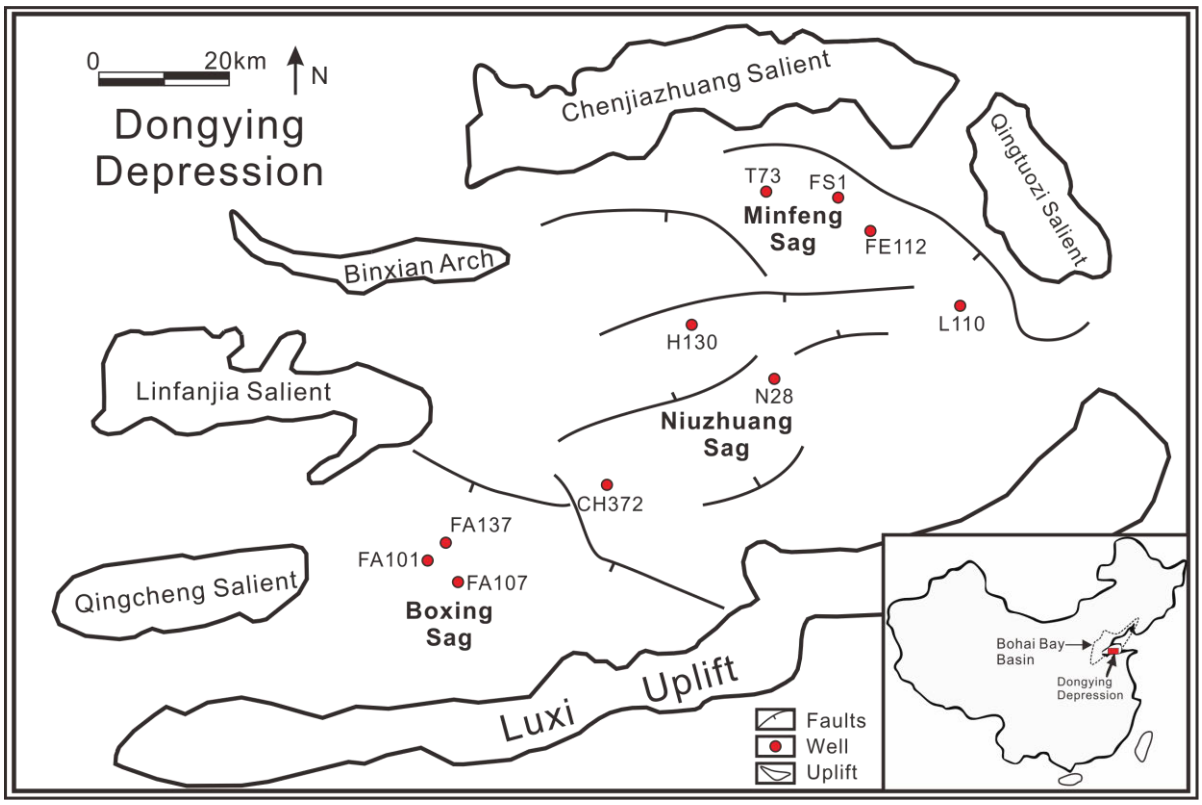


Fig. 2.1 Location map of the Dongying Depression, Bohai Bay Basin, showing the position of the subdivided sags, the wells and the structural elements.

The Dongying Depression is the second largest oil field in China, and contains five major Paleogene and Neogene formations. The Pliocene Minghuazhen Formation and the Miocene Guantao Formation are composed of alluvial and fluvial sediments, whereas the Oligocene Dongying Formation and the Eocene Shahejie and Kongdian formations are composed of lacustrine sediments. The widely distributed Eocene Shahejie Formation (designated Es in Fig. 2.2) is further subdivided into four members: the Sha1 (Es1), Sha2 (Es2), Sha3 (Es3) and Sha4 (Es4) members. Much evidence suggests that the Es1, the lower part of Sha3 (Es3L) and the upper part of Sha4 (Es4U) are the main oil-bearing intervals (Li et al., 2003; Zhang et al., 2009). The Es4 member was deposited in a shallow, semi-enclosed brackish-saline lacustrine setting during the early stage of rift development, and the Es3 member was deposited in a

deeper and wider lake with fresh-brackish water salinity during the peak period of paralic lake development and regional subsidence (Bao and Li, 2001; Wang et al., 2013b). The sandy Es2 member has proven to be the main reservoir unit. The Es1 member was deposited in a brackish water depositional environment. Although the Paleogene and Neogene sediments in the Jiyang Sub-basin have been affected by extensive extrusive and intrusive igneous activity, the Shahejie Formation contains high-quality hydrocarbon source rocks of lacustrine laminated calcareous mudstones and shales (Zhu et al., 2007) and was rarely influenced by any igneous activity. The laminated features of the fine grained rocks in the Shahejie Formation in the Dongying Depression probably indicate seasonal water stratification that may have arisen from seasonal palaeoclimate conditions (Zhang, 2008). The small scale micro-bioturbation in the Es3 member suggests hypoxic conditions for the bottom water (Chen et al., 2016).

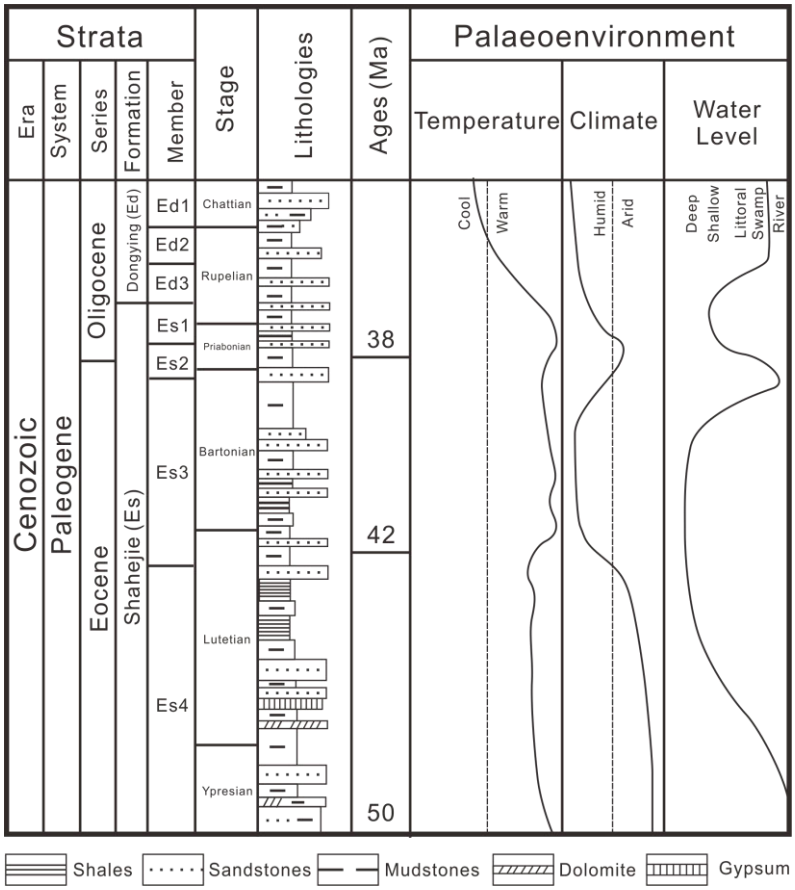


Fig. 2.2 Stratigraphic chart showing Eocene to Oligocene strata of the Dongying Depression, Bohai Bay Basin.

## 2.3. Samples and analytical methods

### 2.3.1. Samples

For the present study, a suite of thirty eight source rock samples was obtained from the middle part of the Sha3 member (Es3M), the lower part of the Sha3 member (Es3L) and the upper part of the Sha4 member (Es4U) from cores from ten different wells in the Dongying Depression, Bohai Bay Basin (Fig. 2.1). Twenty one samples are from three wells (FE112, FS1 and T73) in the north-eastern Minfeng Sag, nine samples are from three wells (H130, N28 and L110) in the eastern Niuzhuang Sag, and eight samples are from four wells (FA107, FA101, FA137 and CH372) in the south-western Boxing Sag.

### 2.3.2. Solvent extraction and fractionation

All source rock samples were crushed into powder in a rotary mill. The homogenised powdered samples were extracted using an azeotropic solvent mixture of dichloromethane/methanol (9:1 v/v) in an accelerated solvent extractor (Dionex ASE300). The extracts were fractionated using two stage silica gel column liquid chromatography. Total hydrocarbons (THC) were collected from the EOM by eluting with *n*-hexane/dichloromethane (4:1 v/v). Aliphatic hydrocarbons were collected from the THC by eluting with *n*-hexane, and aromatic hydrocarbons were then collected by eluting with *n*-hexane/dichloromethane (4:1 v/v). UV light monitoring was used to ensure there were no mixed elution of aliphatic and aromatic hydrocarbons. In this chapter, and elsewhere in the thesis, the solvents used were mainly as follows: dichloromethane, B&J Brand, ~50ppm cyclohexane preservative (HPLC, GC, pesticide residue, spectro.); methanol, AH230-4 Methanol ACS (HPLC certified); *n*-hexane, 99%, LC1083-G4L, Chem-Supply.

### 2.3.3. Gas chromatography–mass spectrometry (GC–MS)

Gas chromatography–mass spectrometry (GC–MS) analyses of the aliphatic and aromatic hydrocarbon fractions were performed on an Agilent GC (6890N) coupled to an Agilent Mass Selective Detector (5975B) equipped with a J&W DB-5MS fused silica column (length 60 m, inner diameter 0.25 mm, film thickness 0.25 μm). The programmable temperature vaporizing (PTV) inlet was held at 35 ℃ for 3 min., then was programmed to 310 ℃ (0.4 min. isothermal) at a rate of 700 ℃/min. Samples (1 μL) were injected in splitless mode. The temperature of the GC oven was initially held at 35 ℃ for 4 min., then programmed to 310 ℃ at 4 ℃ /min, held for 40 min. Helium (99.999%) was used as the carrier gas, with a constant flow rate of 1.5 mL/min. The ion source of the mass spectrometer was operated in EI mode at 70 eV. The MS data were acquired in full scan modes. The relative abundance of compounds was determined from peak areas (using selected mass chromatograms for the integration of the compounds). External standards, including North Sea Oil 1 (NSO-1), were also analysed for comparison of retention times.

### 2.3.4. Gas chromatography–metastable reaction monitoring–mass spectrometry (GC–MRM–MS)

GC–MRM–MS analysis of the aliphatic hydrocarbon fraction was also performed on a Thermo Trace Ultra GC interfaced with a high resolution Thermo DFS GC–MS system. Gas chromatography was carried out on a J&W DB-5MS fused silica column (60 x 0.25 mm i.d., 0.25 μm film thickness). Aliphatic hydrocarbons (1 μL) were injected using a splitless technique with an injector temperature of 260 ℃ and constant flow of 1.5 mL/min. The mass spectrometer was tuned to 1000 resolution (electron energy 70 eV; source temperature 280 ℃). The GC oven was programmed for an initial temperature of 40 ℃ held for 2 min., followed by heating at 20 ℃ $min^{-1}$ to 200 ℃ and then a second heating ramp at 2 ℃ $min^{-1}$ to

310 ℃. The aliphatic fractions were analysed using a metastable reaction monitoring (MRM) programme with the following *m/z* transitions to examine the $C_{25-30}$ steranes: 344→217, 358→217, 372→217, 386→217, 400→217, 414→217, 414→231. An external standard (AGSO_NADD) was analysed for comparison of retention times.

### 2.3.5. Total organic carbon and nitrogen

500 mg of well ground samples were immersed in 10% HCl and were heated in a water bath at 50 ℃ for 36 hours to remove the carbonates and dolomites (inorganic carbon). After HCl treatment, the samples were rinsed and centrifuged 3 times with deionised water to remove the acid, and then were dried in an oven for 24 hours at 55 ℃. Dried samples were mixed well, and then 5–10 mg were analysed using a Euro Vector EA3000 CHNS-O Elemental Analyser. The reaction gas products ($CO_2$ and $NO_x$) were carried by helium flow to a copper reactor where excess $O_2$ was consumed to produce CuO, and NOx products were converted to $N_2$. The products were carried through a packed GC column that provided separation of the combustion gases which were detected by a thermal conductivity detector. Soil#6 (C = 3.429%; N = 0.228%) and acetanilide were used as standards every eight samples.

## 2.4. Results

Bulk geochemical measurements, total organic carbon (TOC), total nitrogen content (TN), and the extractable organic matter yield (EOM) are reported for individual samples in Table 2.1. The Es3M member source rocks consist of massive grey mudstones and black shales, with TOC contents of 4.7-14.9% (average 8.1%), TN contents of 0.46–0.66% (average 0.55%), and EOM contents of 5.9–19.9 mg/g (average 12.5 mg/g). The Es3L member samples are composed of black and grey mudstones, laminated mudstones and black shales, with TOC of 1.12–10.0%, (average 4.6%), TN of 0.48–0.83% (average 0.62%) and EOM of 2.4–29.2

mg/g (average 9.5 mg/g). The Es4U member samples are comprised mainly of calcareous laminated dark mudstones and black shales, with TOC of 0.26–13.5% (average 5.5%), TN of 0.19–0.79% (average 0.45%) and EOM of 0.6–15.0 mg/g (average 7.6 mg/g).The C/N ratio ranges from 8.3–22.5 (average 14.2), 1.4–14.4 (average 7.5) and 5.4–23.0 (average 12.9) for the Es3M, Es3L and Es4U member samples, respectively (Table 2.1).

The TOC content correlates well with the C/N ratio and EOM content, and the general organic richness has been ascribed to microbial activity by heterotrophic bacteria, cyanobacteria and chemoautotrophic bacteria, as well as purple and green sulphur bacteria with strong denitrification (van Mooy et al., 2002), and anoxic conditions for preservation of organic matter (Meyers et al., 2009). Other sample details, and aliphatic and aromatic hydrocarbon parameters are provided in Table 2.1. Selectedsterane parameters from the GC–MRM–MS analyses for the selected samples are provided in Table 2.2. Peak assignments are listed in Table 2.3.

## 2.5. Discussion

The molecular composition of the bitumen extracted from the cores reflects the biotic input, depositional conditions, and level of thermal alteration. Variations are observed in the distribution of n-alkanes, isoprenoids, saturated biomarkers and aromatic hydrocarbons that can be used to infer these conditions.

The relative proportions of different molecular weight *n*-alkanes generally represents the extent and magnitude of organic inputs derived from different biological origins, e.g. bacteria, algae, macrophytes and terrestrial higher plants. For instance, larger proportions of low molecular weight (LMW), medium molecular weight (MMW) and high molecular weight (HMW) *n*-alkanes generally indicate origins from bacteria/algae, aquatic macrophytes and terrigenous higher plants, respectively (Eglinton and Hamilton, 1967; Cranwell, 1977; Philp,

1985; Tegelaar et al., 1989; Ficken et al., 2000). HMW *n*-alkanes with a marked odd-over-even carbon number predominance are also a good indication of terrigenous higher plants. However, other sources of HMW waxy *n*-alkanes have also been proposed, including specific algae (e.g. lacustrine *Botryococcus braunii* biosynthesise precursors of exclusively odd carbon numbered $C_{25–31}$ *n*-alkanes) and aquatic microorganisms (Derenne et al., 1988; Metzger et al., 1991; Huang et al., 2003; Feng et al., 2007; Riboulleau et al., 2007; Bechtel et al., 2012). Probable origins of MMW and HMW *n*-alkanes from macrophytes and bacteria, respectively, have also been noted (Volkman et al., 1998; Zhang et al., 2004). Additionally, inferred terrigenous organic matter inputs of *n*-alkanes could be disproportionate, due to land plants containing more *n*-alkanes than other sources (Derenne et al., 1988).

Biomarkers are recalcitrant molecular fossils from particular organisms that exist in geological strata. Steranes are widely applied biomarkers that provide genetic information on sources of eukaryotic organisms (Volkman, 2005), while hopanes are evidence for the presence of prokaryotic microbes (Ourisson et al., 1987). The 24-*n*-propylcholestanes are diagnostic biomarkers for marine pelagophyte/chrysophyte algae of the order *Sarcinochrysidales* (Moldowan et al., 1990). The 24-iso-propylcholestanes originate from demosponges (McCaffrey et al., 1994; Love et al., 2009). Triaromatic dinosteranes, dinosteranes (4,23,24-trimethylcholestane) and $C_{30}$ 4α-methyl-24-ethyl-cholestane are considered to be exclusively derived from dinoflagellates, although similar dinosterols have been reported in diatoms (Volkman, 2005, 2006; Volkman et al., 2008). Significant abundances of 2α-methylhopanes most likely indicate primary producers of aerobic/anaerobic-photosynthetic cyanobacteria, (Summons et al., 1999), although additional prokaryotic sources are known (Rashby et al., 2007; Welander et al., 2010). The aryl isoprenoids and isorenieratene and its derivatives are biomarkers for phototrophic purple sulphur bacteria (*Chromatiaceae*) and green sulphur bacteria (*Chlorobiaceae*) (Grice et al.,

1996), and indicate photic zone euxinia and high hydrogen sulphide contents. The age-specific 24-norcholestanes mainly originate from diatoms, with a potential additional source from dinoflagellates (Holba et al., 1998a; Rampen et al., 2007; Wang et al., 2008). However, only 0.2% of total 24-norcholesterols in the dinoflagellate *Gymnodinium simplex* have been identified, and an increase of 24-norcholestanes during the Cenozoic is likely related to diatom expansion (Rampen et al., 2007). The biogeographical distribution of 24-norcholestane concentrations at low palaeolatitudes are likely from dinoflagellates (Rampen et al., 2007). The *Chrysophyceae* and certain highly resistant taxa were recognised by siliceous fossils in the form of diatoms (Livingston, 1984), but no diatom fossils have been identified, although dinoflagellate/coccolith laminae and cyanophytes/chlorophytes were identified by scanning electron microscopy and back scattered electron images analyses in the Dongying Depression (Li et al., 2003; Liu and Wang, 2013). These inconsistencies encourage further work exploring the existence of diatoms using organic geochemical approaches is required (Belt et al., 2017), i.e., highly branched isoprenoids, which are important biomarkers for some diatoms (Löhr et al., 2018). Recently, positive isotope excursions of pyritic sulphur and the hydrogen of individual *n*-alkanes were used to evaluate seawater incursions in the Songliao Basin, which brought in external organic inputs (Huang et al., 2013; Cao et al., 2016b). Alternatively, a high relative abundance of 24-*n*-propylcholestanes or 24-*iso*-propylcholestanes is a good indication for whether a palaeo-lake was connected with the open ocean (Moldowan et al., 1990; Peters et al., 2005; Hu et al., 2015).

### 2.5.1. Algal-derived high molecular weight *n*-alkanes

The possibility of a lacustrine setting with potential marine organic matter inputs will complicate interpretation of the *n*-alkane distributions from the *m/z* 57 mass chromatograms, so these data have to be supported with other analyses. Organic geochemical data are listed in

Table 2.1. The *n*-alkanes in the aliphatic fractions have variable molecular weight distributions, even of sub-members (Fig. 2.3). In accordance with the characteristics and distributions of the *n*-alkanes and acyclic isoprenoids, and their consistency with regular steranes, the samples were tentatively divided into four groups as follows (Fig. 2.3). Group 1 samples have variation in the relative proportions of LMW, MMW and HMW *n*-alkanes that generally corresponds with the variation in the carbon number distribution of the steranes. In addition, the *n*-alkanes have varying odd-over-even carbon number predominance. Group 2 samples have unimodal or slightly bimodal distributions of *n*-alkanes, with comparable amounts of LMW and HMW *n*-alkanes, or sometimes are dominated by MMW *n*-alkanes. In addition, regular steranes are either dominated by $C_{27}$ or $C_{29}$ isomers. Group 3 samples have bimodal *n*-alkane distributions that are overwhelmingly dominated by HMW *n*-alkanes relative to LMW *n*-alkanes, with maxima at $C_{17}$ and $C_{27}$ or $C_{28}$. Moreover, these samples either have an odd-over-even or even-over-odd carbon number predominance, with dominant $C_{27}$ steranes. The group 4 samples are characterised by abundant LMW *n*-alkanes and prominent acyclic isoprenoids ($C_{11}$–$C_{20}$). The regular steranes are dominated by the 5α(H),14β(H),17β(H) epimers, and their relative abundance is in the order $C_{29}>C_{27}\geq C_{28}$. In contrast, groups 1–3 have sterane distributions dominated by 5α(H),14α(H),17α(H) 20R epimers.

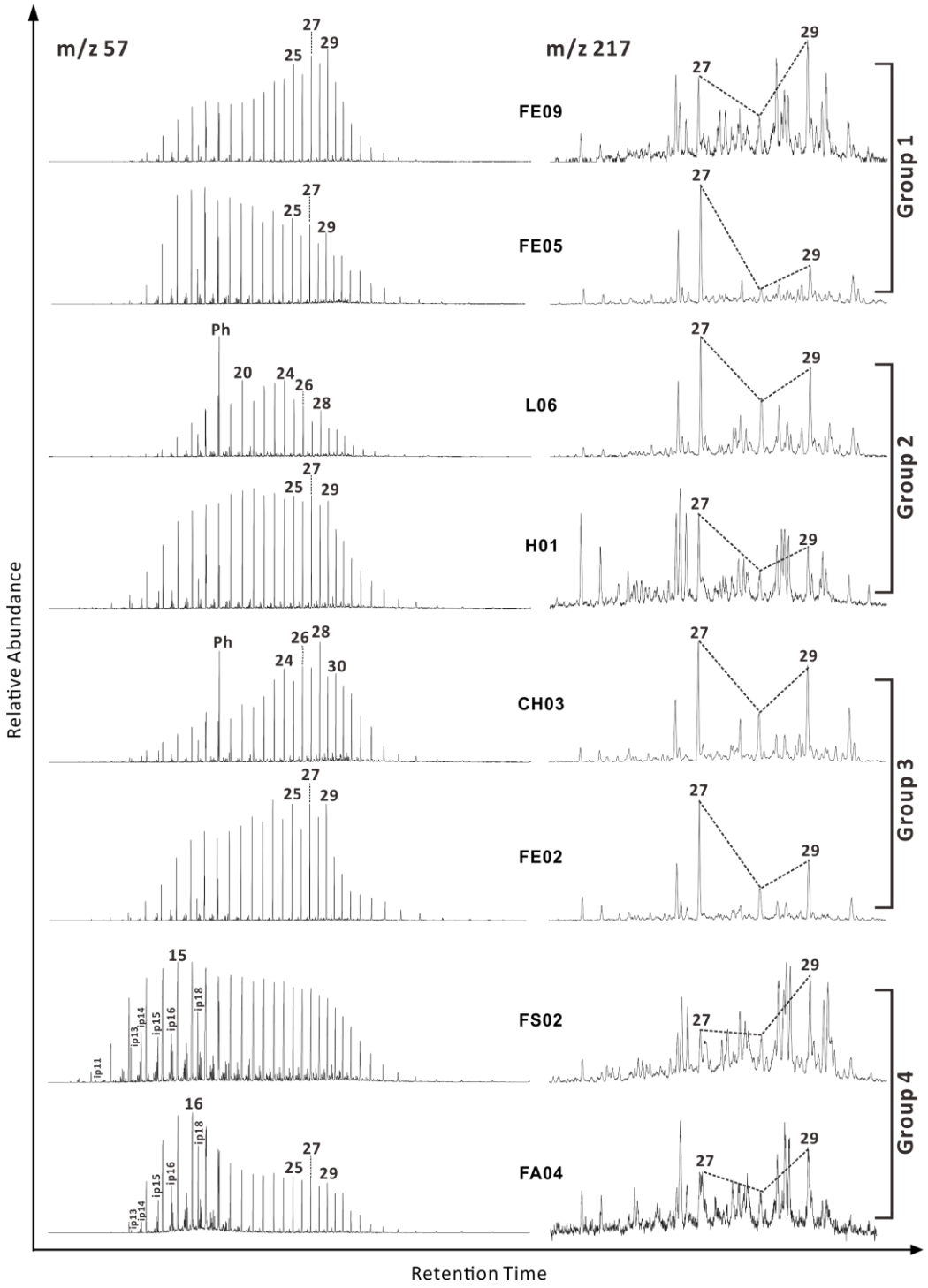


Fig. 2.3 Representative *m/z* 57 and partial *m/z* 217 mass chromatograms, showing the distribution of *n*-alkanes and regular steranes in typical rock samples from four different groups defined in Section 2.5.1. The sample codes are given in the centre of the figure. Numbers on peaks are *n*-alkane and sterane (ααα R isomer) carbon numbers, Ph = phytane, ipxx = Cxx acyclic isoprenoids.

The Minfeng Sag samples mainly have group 1 *n*-alkane distributions, with two samples in group 2 (FE15 and FE16, from the basal Es3L and Es4U members in the FE112 well), two

samples in group 3 (FE01 and FE02, from the upper Es3M member in the FE112 well), and one sample in group 4 (FS02, from the basal Es4U member in the FS1 well) (Fig. 2.4). The carbon preference index ($CPI_{22–32}$; 0.99–1.33) generally decreases with increasing burial depth (Table 2.1). The samples from the Es3M member are characterised by a high abundance of LMW and MMW *n*-alkanes with relatively higher CPI values, whereas samples from the deeper Es3L and Es4U member are characterised by HMW and MMW *n*-alkanes (Fig. 2.4) with CPI values close to 1.0 (Table 2.1). The Es3M samples have a predominance of $C_{27}$ regular steranes, which indicates that the organic matter originated mainly from algae, bacteria or aquatic micro-organism, whereas the Es3L and Es4U samples have a predominance of $C_{29}$ regular steranes, interpreted as suggesting derivation from aquatic macrophytes and terrigenous land plants. Interestingly, the group 3 Es3M samples FE01 and FE02 have an high abundance of MMW and HMW *n*-alkanes with a prominent odd-over-even carbon number predominance, probably suggesting fresh water algae organic inputs or an increased contribution of organic matter from macrophytes (Ficken et al., 2000), which is still in agreement with the higher relative abundances of $C_{27}$ steranes. The Es3L member sample FE15 and the Es4U member sample FE16 (both group 2) have high relative amounts of LMW *n*-alkanes, but are more enriched in $C_{29}$ regular steranes. The possible effect of thermal maturation or depositional environment cannot account for these phenomena, as samples with almost identical depth (e.g. FE14; group 1; Table 2.1) have completely different *n*-alkane distributions. Thus, the unusual group 2 distributions probably reflect different OM inputs. It is worth noting that 24-*n*-propylcholestane, a biomarker of marine organisms, was detected in these samples, especially in FE16 (see Chapter 2.4.4). The FS02 sample (group 4) is dominated by LMW *n*-alkanes with much greater abundance of regular acyclic isoprenoids (Fig. 2.3), which is inconsistent with the high relative abundance (53%) of $C_{29}$ steranes, which more typically reflects greater terrigenous land plant OM contributions.

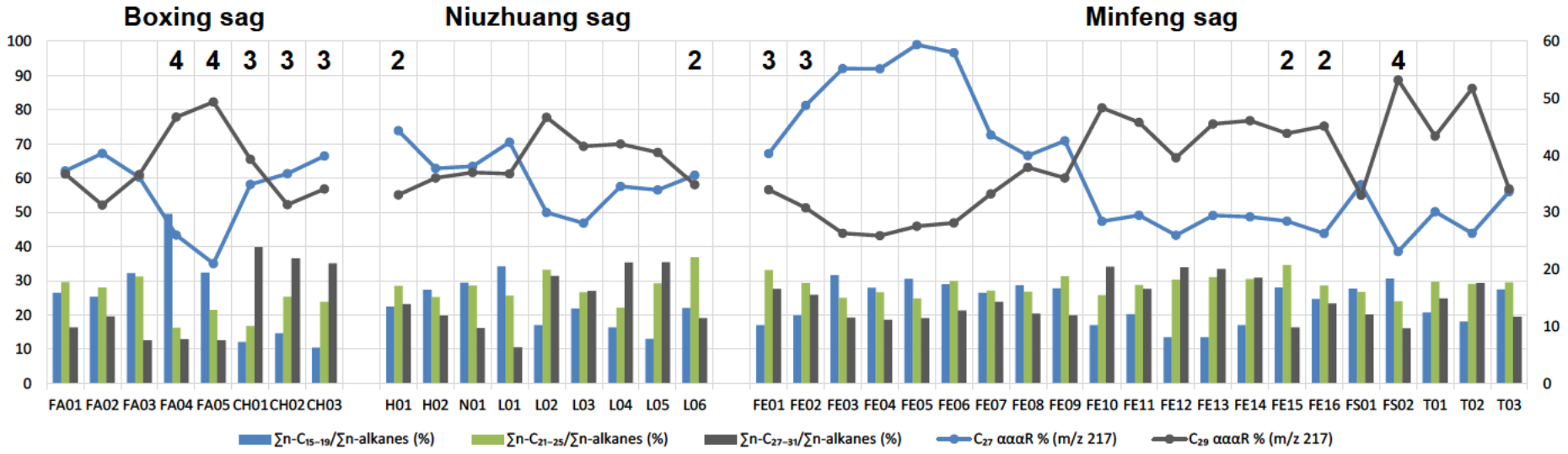


Fig. 2.4 Composite *n*-alkane column charts (left axis is applied) and regular sterane line charts (right axis is applied), showing the relative changes of these compounds reflecting the organic matter input from the north-eastern Minfeng Sag, the Niuzhuang Sag, and the south-western Boxing Sag. Numbers refer to the group numbers defined in Section 2.5.1, unnumbered samples are from Group 1.

The Niuzhuang sag samples mainly have group 1 *n*-alkane distributions, with two samples in group 2 (H01 from the Es3L member of the H130 well, and L06 from the Es4U member of the L110 well). The Es4U samples from the L110 well have $CPI_{22–32}$ values of 0.89–1.09, whereas the Es3L samples from the H130 and N28 wells have $CPI_{22–32}$ values of 1.11–1.14 (Table 2.1). There is a greater proportion of $C_{29}$ steranes in the Es4U member than in the Es3L member. The Es3L sample H01 (group 2) has a unimodal *n*-alkane distribution with an odd-over-even carbon number predominance for the HMW *n*-alkanes ($\Sigma nC_{15–19}$: 22.4%; $\Sigma nC_{21–25}$: 28.5% $\Sigma nC_{27–31}$: 23.2%; $CPI_{26–32}$: 1.16) and significant $C_{27}$ steranes (44%) (Fig. 2.3), indicating a non-marine algal input for the organic matter, probably due to a contribution from *Botryococcus* A race that exclusively biosynthesise odd-carbon-numbered *n*-alka-dienes/trienes in the $C_{25}$–$C_{31}$ carbon number range (Metzger et al., 1991). However, the other group 2 sample (L06; Es4U member) has a unimodal *n*-alkane distribution with a clear even-over-odd carbon number predominance ($CPI_{26–32}$: 0.85) and a carbon number distribution of the regular steranes in the order $C_{27}$>$C_{29}$>$C_{28}$ (Fig. 2.3). Furthermore, this sample has the lowest pristane/phytane (Pr/Ph) ratio of the dataset (0.34), the highest $C_{29}$ sterane/$C_{29}$ αβ hopane ratio (10.8), the highest gammacerane index (2.5), and the highest $C_{35}$/($C_{35}$+$C_{34}$) homohopane ratio (0.64), and it also has a high β-carotane/$C_{20}$ *n*-alkane ratio (11.4; Table 2.1). These biomarker distributions of L06 attest to an algal/bacterial origin for organic matter preserved in a black shale under stable reducing hypersaline bottom water conditions. Another Es4U member sample (L01, group 1) is dominated by mainly LMW *n*-alkanes exhibiting a bimodal pattern maximised at $C_{16}$ and $C_{23}$, which is consistent with its regular sterane distributions in the order $C_{27}$>$C_{29}$>$C_{28}$. In sharp contrast to sample L06, L01 has a higher Pr/Ph ratio (1.53), a lower sterane/hopane ratio (0.61) and a lower gammacerane index (0.19), and a lower β-carotane content (Table 2.1). The rest of the Es4U member

samples from the L110 well (L02, L03, L04 and L05) have *n*-alkane maxima at $C_{28}$, and variable even-over-odd or odd-over-even carbon number predominances.

Group 1 (FA01, FA02 and FA03 samples), group 3 (CH01, CH02 and CH03 samples) and group 4 (FA04 and FA05 samples) *n*-alkane distributions are recognised in the Boxing Sag samples, with $CPI_{22\text{-}32}$ varying from 0.81-1.13. Bimodal distributions for the Es3 member FA01, FA02 and FA03 samples indicate mixed sources of aqueous and terrigenous organic inputs. The Es4U member CH01, CH02 and CH03 samples are characterised by slightly bimodal *n*-alkane distributions maximising at $C_{17}$ and $C_{28}$ with significant even-over-odd carbon number predominance ($\Sigma nC_{15\text{–}19}$: 10.5–14.7%; $\Sigma nC_{21\text{–}25}$: 16.8–25.3% $\Sigma nC_{27\text{–}31}$: 35.1–39.8%; $CPI_{22\text{–}32}$: 0.81–0.99), and a higher relative abundance of the $C_{27}$ regular steranes ($C_{27}$:$C_{29}$ = 37.2%:34.9% on average). These parameters, and the Pr/Ph ratios (0.34–0.8), gammacerane indices (0.41–0.53), the $C_{35}/(C_{35}+C_{34})$ homohopane ratios (0.57–0.66) and the presence of β-carotane, suggests the origins of organic matter in the CH01, CH02 and CH03 samples to be from lacustrine algae under reducing bottom water conditions. The likely cause of the high amounts of HMW *n*-alkanes is hydrolysis of the wax forming *n*-fatty acids and alcohols, the reduction of phytanic acid or phytol being stronger than the effect of oxidative decarboxylation under reducing conditions (Dembicki et al., 1976).

The other Boxing Sag Es4U member samples (FA04 and FA05; group 4) are similar to sample FE02 in the Minfeng Sag, and have slightly bimodal *n*-alkane distributions maximising at $C_{15}$ or $C_{16}$ and $C_{23}$ (Fig. 2.3). The samples are dominated by LMW *n*-alkanes ($\Sigma nC_{15\text{–}19}$: 32.4–49.5%; $\Sigma nC_{21\text{–}25}$: 16.3–21.5% $\Sigma nC_{27\text{–}31}$: 12.6–12.9%), have little odd- or even-carbon number predominance ($CPI_{22\text{–}32}$: 1.00–1.08), abundant $C_{10+}$ regular isoprenoids, and have higher abundances of $C_{29}$ steranes ($C_{27}$:$C_{29}$ = 23.5%:48.2% on average). One possible explanation for these features is that the HMW *n*-alkanes were cracked to lighter products during maturation and microbial reworking (Kissin, 1987; Mango, 2000). Most regular

acyclic isoprenoids containing twenty or fewer carbon atoms, including pristane and phytane, originate primarily from the phytol side chain of chlorophyll a during diagenesis (Rontani and Volkman, 2003). The relative abundance of $C_{10+}$ regular isoprenoid hydrocarbons probably suggests a proportion of higher plant and bacterial wax contribution for the Es4U member in the Boxing Sag.

The relative proportions of $\Sigma nC_{15-19}$, $\Sigma nC_{21-25}$ and $\Sigma nC_{27-31}$ to total *n*-alkanes for thirty eight samples from the whole Dongying Depression are 17.0–31.6% (average 26.6%), 24.8–33.1% (average 28.4%) and 16.3–27.6% (average 21.2%) for the Es3M member, 13.4–32.2% (average 22.7%), 25.2–34.6% (average 29.1%) and 12.6–34.1% (average 24.0%) for the Es3L member, and 10.5–49.5% (average 23.0%), 24.8–33.1% (average 25.9%) and 16.3–36.9% (average 25.6%) for the Es4U member (Table 2.1). On the whole, a decrease in the relative proportions of *n*-$C_{15-19}$ alkanes and *n*-$C_{21-25}$ alkanes, and an increase in the relative proportions of *n*-$C_{27-31}$ alkanes is observed from the top Es3M member, through the Es3L member to the bottom Es4U member. The average terrigenous/aquatic ratios [TAR = (*n*-$C_{27}$ + *n*-$C_{29}$ + *n*-$C_{31}$)/(*n*-$C_{15}$ + *n*-$C_{17}$ + *n*-$C_{19}$)] are 0.92 for the Es3M member, 1.28 for the Es3L member and 1.4 for the Es4U member, thus increasing with age (Silliman et al., 1996; Peters et al., 2005). There is a decrease in the relative abundance of $C_{27}$ steranes and an increase in the relative abundance of $C_{29}$ steranes from the Es3M member to the Es3l and Es4U members (Supplementary Fig. 2.1). Average $CPI_{22-32}$ values are 1.20, 1.07 and 0.99 for the Es3M, Es3L and Es4U member, respectively, corresponding to increasing maturity with burial depth.

Although thermal maturation and alternative microbial origins can affect the Pr/Ph ratio (Goossens et al., 1984; Tissot and Welte, 1984; Volkman and Maxwell, 1986; ten Haven et al., 1987), in this study the main control on this ratio appears to be the redox conditions (Didyk et al., 1978). The Pr/Ph ratios are 0.89–1.43 (average 1.10) for the Es3M member, 0.38–1.52 (average 0.79) for the Es3L member, and 0.34–1.53 (average 0.69), for the Es4U

member. These data indicate an anoxic to suboxic bottom water environments for the three members, and an overall slight increase of oxygen content during deposition of the Shahejie Formation (Didyk et al., 1978).

Based on these results, it is postulated that there was a significant contribution of terrigenous land plants and/or specific algae (e.g. *Botryococcus braunii*) to organic matter deposited in the Es4U member, and slightly increased oxygenation of the water column and increased input of allochthonous aqueous micro-organisms in the Es3M member due to freshwater run-off or seawater incursions. This is also suggested by that the relative proportions of $C_{27}$ steranes and *n*-$C_{15–19}$ alkanes, which correspond well to the Pr/Ph ratio (Table 2.1), thus imply an association between water column redox conditions and variation in contributions from aqueous micro-organisms. As the $CPI_{22–32}$ does not exceed 2.0, even in the lowest maturity samples (i.e. samples from the L110 well), the greater proportions of HMW *n*-alkanes may not be related to terrigenous higher plants inputs. This is also supported by minor presence of higher plant biomarkers such as oleanane (see below). The various and complex patterns of *n*-alkanes represent the diverse algae inputs thriving in specific palaeoenvironments in the Shahejie Formation, Dongying Depression. Li et al. (2003) also recognised abundant well-preserved algae structures (e.g. phyla of dinoflagellates, green algae and blue algae) and amorphous sapropelic material in the Shahejie Formation.

### 2.5.2. Algal-derived $C_{29}$ regular steranes

Regular steranes have been proposed for characterisation of the relative proportions of eukaryotic organic matter inputs that originated from algae, microorganisms or land plants (Huang and Meinschein, 1979; Grantham and Wakefield, 1988; Peters et al., 2005). Generally, the $C_{27}$ steranes are derived from phytoplankton/algae, while the $C_{29}$ steranes are associated with terrigenous land plants (Volkman et al., 1998; Volkman, 2005). Alternative

micro-algal sources (e.g. brown/green algae contain 24-ethylcholesterols) for $C_{29}$ steranes have also been demonstrated (Volkman et al., 1998). The carbon number distribution of the regular steranes in the aliphatic fractions are illustrated in Supplementary Fig. 2.1. The Es4U and Es3L member samples contain $C_{29}$ steranes ≥ $C_{27}$ steranes, whereas the Es3M member samples contain larger proportions of $C_{27}$ steranes relative to $C_{29}$ steranes. This could be consistent with a greater contribution of organic matter from terrigenous land plants/plankton for the Es4U and Es3L members, and a greater algal/planktonic contribution for the Es3M member. Whilst, the Es3L and Es4U member samples (FE10–FE16) from the FE112 well have a predominance of $C_{29}$ steranes, the lack significant amounts of higher plants biomarkers such as oleanane. The $C_{23}$ tricyclic terpane, a biomarker for algal input, is most abundant relative to other tricyclic and tetracyclic terpanes in the Es3L and Es4U member samples from the FE112 well, which is inconsistent with the greater proportions of HMW and MMW *n*-alkanes in these samples (Fig. 2.4). This suggests the HMW *n*-alkanes and $C_{29}$ regular steranes have alternative sources.

The ratio of regular steranes versus hopanes can reflect the relative input of eukaryotic (mainly algae and higher plants) organisms versus prokaryotic organisms (bacteria in general) to the source rocks (Grantham and Wakefield, 1988; Peters et al., 2005). Gammacerane is a reduction product of tetrahymanol in bacterivorous ciliates living at the boundary of an enhanced salinity water layer with an upper layer of less saline water (chemocline). Elevated concentrations of gammacerane indicate enhanced water salinity, water column stratification accompanied with anoxic conditions, and possible photic zone anoxia (ten Haven et al., 1987; Sinninghe Damsté et al., 1995), conditions that are favourable for the algae contributing to steroidal biomarkers. Note gammacerane appears highly specific for water-column stratification, such states may not necessarily be caused by salinity.

There is a very good correlation ($R^2$ = 0.92) between the gammacerane index and the $C_{29}$ steranes/$C_{29}$ αβ hopane ratio (St/H) (Figs 2.5a and 2.6), which suggests a close association between organism inputs, redox conditions, and palaeoenvironments in the water column. Therefore, the predominance of $C_{29}$ steranes over $C_{27}$ and $C_{28}$ steranes as an indicator of higher plant input into the source rock is questionable, and may be invalid. Algal sources for high molecular weight *n*-alkanes and $C_{29}$ steranes (Volkman et al., 1998) need to be considered in this study. Additionally, almost all samples from the Es4U member have St/H >1.0 (as high as 12.6), which suggests major contributions from plankton/algae in a marine facies with a high bio-productivity. The Es3M and Es3L member samples generally have St/H ≤ 1.0, indicating dominant bacterially/microbially reworked organic matter in a lacustrine facies (Mackenzie, 1984; Tissot and Welte, 1984; Moldowan et al., 1985). The lack of consistency between the four groups defined by *n*-alkane molecular weight distributions and the carbon number distribution of the steranes are likewise supportive of contributions of plankton/algae to the HMW *n*-alkanes and $C_{29}$ steranes. Moreover, TOC generally correlates with the relative abundance of $C_{27}$ steranes (Table 2.1).

Liu and Wang (2013) suggested that the occurrence of organic-rich source rocks in the Jiyang Sub-basin was controlled by algal blooms, which thus account for the accumulation of organic matter in lacustrine petroleum source rocks. The sterane and *n*-alkane distributions, and the minor amounts of higher plant biomarkers, support the hypothesis that phytoplankton/algae were the dominant sources of the organic matter in the shales and mudstones investigated. Additionally, for the studied source rocks, the relative abundance of $C_{28}$ regular steranes is as high as 34%, and the $C_{28}/C_{29}$ regular sterane ratio is as high as 1.02, which is consistent with phytoplankton/algae flourishing during deposition of the Paleogene Shahejie Formation, Dongying Depression (Grantham and Wakefield, 1988).

The $C_{27}$ βα diasterane/$C_{27}$ ααα sterane ratio ranges from 0.09–0.34 (average 0.18), 0.14–0.93 (average 0.36) and 0.03–0.94 (average 0.28) for the Es3M, Es3L and Es4U member samples, respectively. There is no obvious correlation of the diasterane/sterane ratio with other parameters for depositional environments, but there is a good correlation with Ts/(Ts+Tm) ($R^2$ = 0.79) and $C_{29}$ αββ/(αββ+ααα) ($R^2$ = 0.79) (Supplementary Fig. 2.2). Thus, the variation of diasteranes/sterane ratio for this study are most likely related to thermal maturity in this study, and are not related to any changes in organic matter inputs or depositional environments.

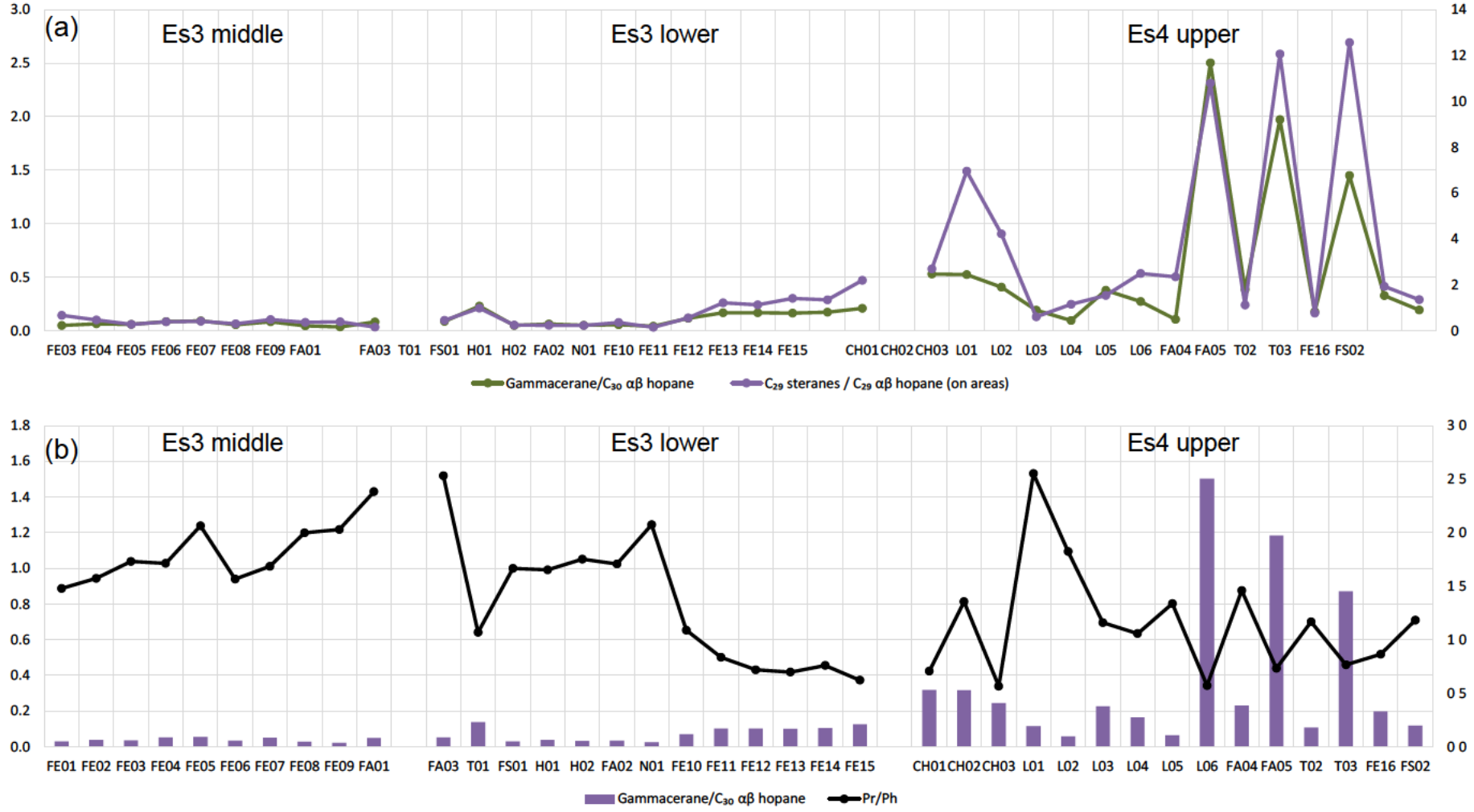


Fig. 2.5 Composite line charts of (a) gammacerane/$C_{30}$ αβ hopane ratio (left axis is applied) and $C_{29}$ sterane/$C_{29}$ αβ hopane ratio (right axis is applied), showing a good corresponding change of these two ratios from the top Es3M member, through the Es3L member to the Es4U member of the Shahejie Formation. Composite line charts of (b) gammacerane/$C_{30}$ αβ hopane ratio column chart (right axis is applied) and Pr/Ph ratio (left axis is applied), showing the relative changes of these ratios reflecting the depositional environment.

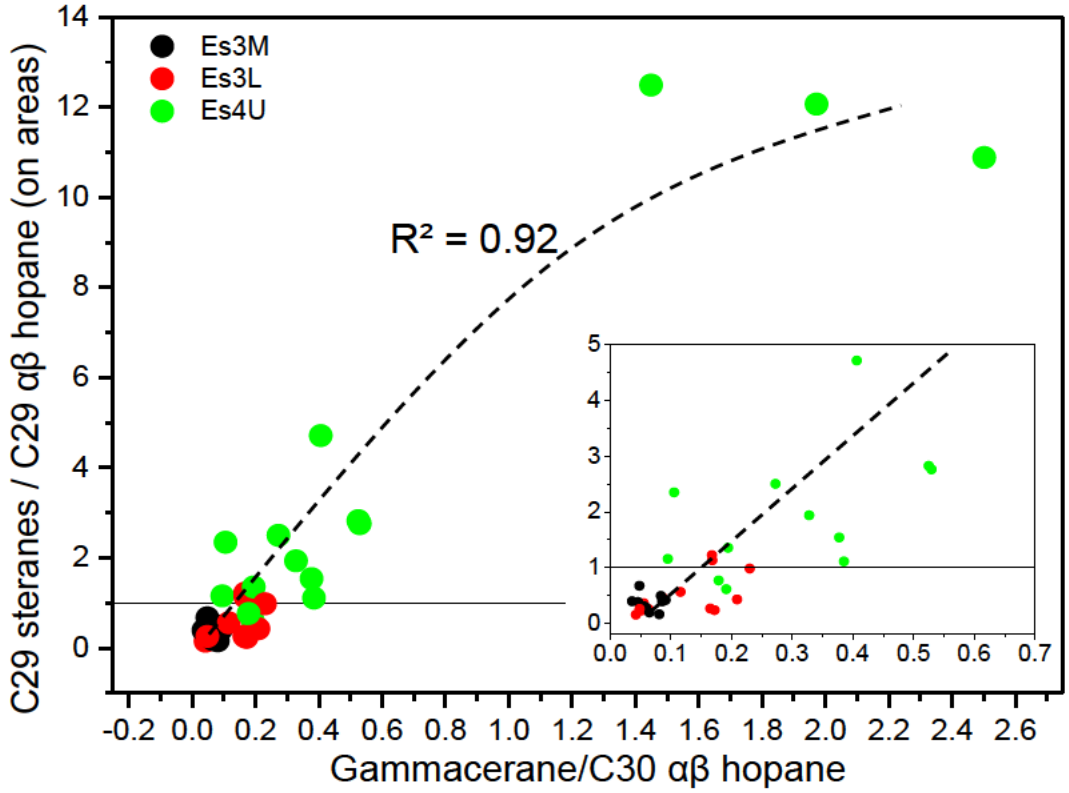


Fig. 2.6 Cross-plot of gammacerane/$C_{30}$ αβ hopane versus $C_{29}$ steranes/$C_{29}$ αβ hopane (based on peak areas), showing a good correlation ($R^2$ = 0.92) between these two parameters. The inset is the magnified portion of these plots near the origin.

The $C_{27}$ βα diasterane/$C_{27}$ ααα sterane ratio ranges from 0.09–0.34 (average 0.18), 0.14–0.93 (average 0.36) and 0.03–0.94 (average 0.28) for the Es3M, Es3L and Es4U member samples, respectively. There is no obvious correlation of the diasterane/sterane ratio with other parameters for depositional environments, but there is a good correlation with Ts/(Ts+Tm) ($R^2$ = 0.79) and $C_{29}$ αββ/(αββ+ααα) ($R^2$ = 0.79) (Supplementary Fig. 2.2). Thus, the variation of diasteranes/sterane ratio for this study are most likely related to thermal maturity in this study, and are not related to any changes in organic matter inputs or depositional environments.

### 2.5.3. Limited terrigenous organic input

The angiosperm high plant biomarker oleanane was detected in relatively low abundance, with the oleanane/$C_{30}$ αβ hopane ratio (O/H) ranging from 0.02–0.35 (0.08 on

average) (Supplementary Fig. 2.3). This is interpreted as generally indicating restricted angiosperm plant contributions to the organic matter during deposition of the Shahejie Formation. Nonetheless, amongst the thirty eight samples there are four samples from the FA137 and T73 wells (the FA03–05 and T03 samples) that have higher O/H ratios (0.23–0.35, 0.28 on average; Table 2.1, Supplementary Fig. 2.3), indicating considerable angiosperm contributions to the organic matter of these four samples. This may be attributed to the localities of these four samples near the edge of the Dongying Depression, thus enabling them to have received more terrigenous input. Tricyclic terpanes are less abundant than the pentacyclic terpanes (Supplementary Fig. 2.3). Most samples are characterised by more abundant $C_{23}$ and $C_{24}$ members of the tricyclic terpanes series, which is a distribution typical of marine algae. The exceptions are the FA137 (FA04–05 samples), L110 (L02 sample) and FS1 (FS02 sample) wells, which have relatively more abundant $C_{20}$ and $C_{21}$ tricyclic terpanes (Table 2.1; Supplementary Fig. 2.3). Diterpanes, which are characteristic markers of a terrigenous conifer plant-derived contribution (Otto and Wilde, 2001), are absent from the *m/z* 123 chromatograms, and the higher plant index (HPI = [iHMN + cadalene + retene]/1,3,6,7-tetramethylnaphthalene) is low for the Dongying Depression samples (Table 2.1). Thus, terrigenous organic matter input is very limited in the Dongying Depression.

### 2.5.4. Significant bacterial inputs

The bacteria-derived hopanes (Ourisson et al., 1979; Sinninghe Damsté and Schouten, 1997) are present in varying relative abundance compared with the regular steranes, as measured by the St/H ratio (Table 2.1). The Es3M and Es3L member samples contain more hopanes compared to steranes than the Es4U member samples (Fig. 2.6), showing that there was relative more bacterial activity in the Es3M and Es3L members in the Shahejie Formation. An increase in the St/H ratio was observed from the top Es3M member, through

the Es3L member to the basal Es4U member. Specific bacteria are potentially associated with specific organic matter inputs or water column environments. This was supported by the detection of various diagnostic biomarkers, including phytane, gammacerane, β-carotane, isorenieratane, 2α-methylhopane, and crocetane.

## 2.5.5. Water column environments

### *2.5.5.1. Salinity and redox conditions*

In the Dongying Depression, the hopanes mainly consist of Ts, Tm, 17α(H),21β(H)-hopanes, 17β(H),21α(H)-hopanes (moretanes) and homohopanes. The $C_{30}$ αβ hopane is the most abundant compound in most of the samples (Supplementary Fig. 2.3). Exceptions are three of the Es4U member samples (FA05 in the FA137 well, Supplementary Fig. 2.3; L06 in the L110 well, and T03 in the T73 well), which are overwhelmingly dominated by gammacerane, with gammacerane indices (G/H = gammacerane/$C_{30}$ αβ hopanes) of 2.0, 2.5 and 1.5, respectively (Fig. 2.5a). In the Es4U member, the gammacerane index has episodically high values (G/H: 0.09–2.5, average = 0.65), and drops abruptly in the Es3L member (0.04–0.23, average = 0.12) and the Es3M member (0.04–0.09, average = 0.07). This decline is interpreted as reflecting a decrease in water salinity from the basal Es4U member, through the Es3L member to the top Es3M member. The elevated gammacerane concentrations suggest an extensively stratified water column and probable photic zone euxinia (PZE) in the Es4U member. It is noteworthy that the gammacerane index is negatively correlated with the Pr/Ph ratio (Table 2.1 and Fig. 2.5b; $R^2$ = 0.51 by power exponent), suggesting that gammacerane is influenced by increased oxygen content (Bohacs, 2012). This accounts for the episodically lower concentration of gammacerane with relatively higher Pr/Ph in the Es4U member (sawtooth-like pattern in Fig. 2.5b).

A high relative abundance of $C_{35}$ homohopanes is usually associated with either saline lacustrine deposition (Peters et al., 2005; Wang et al., 2010) or marine carbonates/evaporates (Connan et al., 1986; Clark and Philp, 1989). Oxygen-deficient redox conditions are favourable for the formation of $C_{35}$ homohopanes (Peters and Moldowan, 1991). The Es4U member samples have higher $C_{35}/(C_{35}+C_{34})$ homohopanes ratios than the Es3L and Es3M member samples, consistent with higher water salinity in the Es4U member. Moreover, the $C_{35}/(C_{35}+C_{34})$ homohopanes ratio decreases with increasing burial depth (Table 2.1), probably due to the instability of $C_{35}$ homohopanes at higher levels of thermal stress (Peters and Moldowan, 1991).

β-Carotane has a carotenoid skeleton and is present in considerable quantities in the aliphatic fractions of almost all rock extracts investigated (Supplementary Fig. 2.4), indicating anoxic saline lacustrine depositional environments, or a highly restricted marine depositional setting (Fu et al., 1990; Irwin and Meyer, 1990). Similarly high concentrations of β-carotane occur in the Green River oil shales (Murphy et al., 1967), the Junggar Basin Permian oil shales (Carroll et al., 1992), and the Jianghan Basin oil shales (Brassell et al., 1988). β-Carotane is more abundant in the Es4U member samples than that in the Es3M and Es3L member samples (Table 2.1; Fig. 2.7b), probably suggesting more reducing bottom water conditions for the preservation of β-carotane in the Es4U member, which is consistent with the Pr/Ph ratio and the gammacerane index.

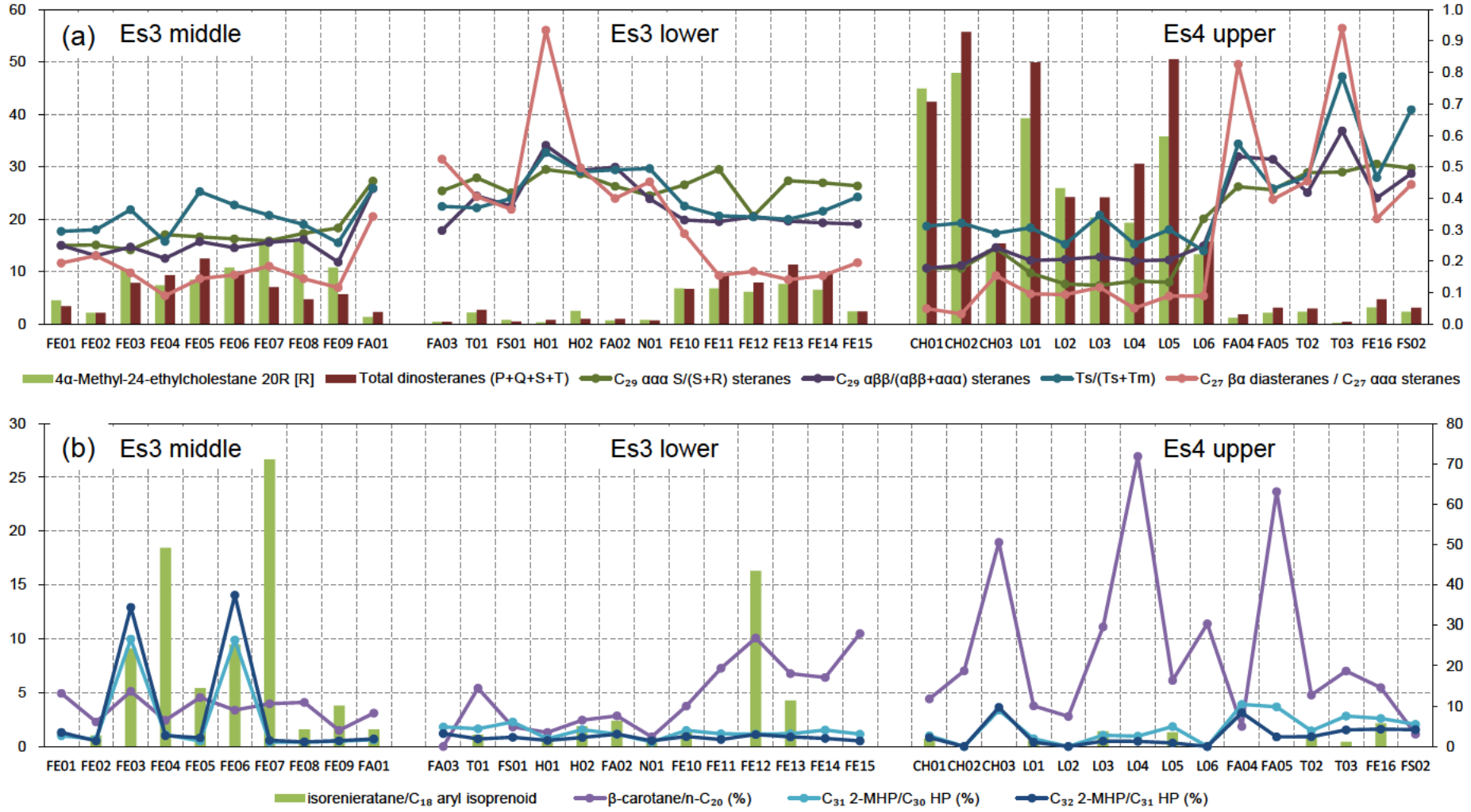


Fig. 2.7 Composite diagram of the relative abundance of biomarker parameters with depth through the Shahejie Formation, showing changes from the top Es3M member, through the Es3L member to the Es4U member. (a) Column charts of the relative abundance of the 4α-methyl-24-ethylcholestane 20R [R] and total dinosteranes (P+Q+S+T) (left y axis are normalised amounts to 13β(H),17α(H)-diacholestane 20S); and line charts of $C_{29}$ ααα S/(S+R) steranes, $C_{29}$ αββ/(αββ+ααα)

steranes, Ts/(Ts+Tm) and $C_{27}$ βα diasteranes/$C_{27}$ ααα steranes ratio (right y axis is for the ratios). There is an inverse correlation between changes in the column and line charts. (b) Composite isorenieratane/$C_{18}$ aryl isoprenoid ratio column chart, and line charts of the β-carotane/*n*-$C_{20}$ (%) ratio, 2-MHP index ($C_{31}$ 2-MHP/$C_{30}$ HP, based on areas in the *m/z* 205 and 191 mass chromatograms, %) and $C_{32}$ 2α-methylhopanes/$C_{31}$ αβ hopane ($C_{32}$ 2-MHP/$C_{31}$ HP) ratio (based on areas in the *m/z* 205 and 191 mass chromatograms, %). The left y axis applies to the $C_{32}$ 2-MHP/$C_{31}$ HP and β-carotane/*n*-$C_{20}$ (%) ratios, the right y axis applies to the 2-MHP index and the isorenieratane/$C_{18}$ aryl isoprenoid ratio. Note that the two maxima of the $C_{32}$ 2-MHP/$C_{31}$ HP ratio temporally lag the two maxima of the isorenieratane/$C_{18}$ aryl isoprenoid ratio in the Es3M member, which may indicate the relationship between the microorganism community expansion between cyanobacteria and green/purple sulphur bacteria in the ecosystem.

*2.5.5.2. Photic zone euxinia*

In aromatic fractions, the most prominent carotenoid skeleton compounds are monoaryl, diaryl and triaryl isoprenoids (with a 2,3,6/2,3,4/3,4,5-trimethyl substitution pattern) and isorenieratene derivatives. These tail-to-tail-structure aromatic hydrocarbons include abundant monoaryl isoprenoids from $C_{11}$ to $C_{22}$ with a maxima at $C_{13}$ or $C_{19}$, diaryl isoprenoids from $C_{21}$ to $C_{26}$, $C_{32}$ triaryl isoprenoid, paleorenieratane, isorenieratane, renieratane, and three unknown compounds with a prominent *m/z* 133 molecular ion (Fig. 2.8). The monoaryl and diaryl isoprenoids were detected in all samples from the Dongying Depression, but the intact paleorenieratane, isorenieratane, renieratane were identified in variable amounts (Fig. 2.8). The aryl isoprenoids have two known sources consisting of isorenieratene or β-isorenieratene in green sulphur bacteria, and β-isorenieratene from the ubiquitous carotenoid pigment β-carotene (Koopmans et al., 1996). Only the occurrence of $^{13}$C-rich or isorenieratane-sourced aryl isoprenoids in geological sediments indicates photic zone euxinia (PZE) (Grice et al., 1996).

Under these environmental conditions, the isorenieratane is exclusively biosynthesised by anaerobic, photosynthetic green sulphur bacteria living in a quiescent and organic-rich water column where the electron donor hydrogen sulphide is abundant, hence being critical for the photosynthesis of the green sulphur bacteria (Summons, 1993; Koopmans et al., 1996; Grice et al., 1998). Renieratane is derived from purple sulphur bacteria (Brocks and Schaeffer, 2008), whilst no okenone was detected. In the Dongying Depression, isorenieratane, renieratane and aryl isoprenoids are present in considerable quantities, with just a few exceptions (e.g. samples FA04–05 from the FA137 wells which only contain β-carotanes, but no isorenieratane or derivatives), which provides unambiguous evidence for PZE conditions

and green sulphur bacteria/purple sulphur bacteria organic inputs during deposition of the Shahejie Formation.

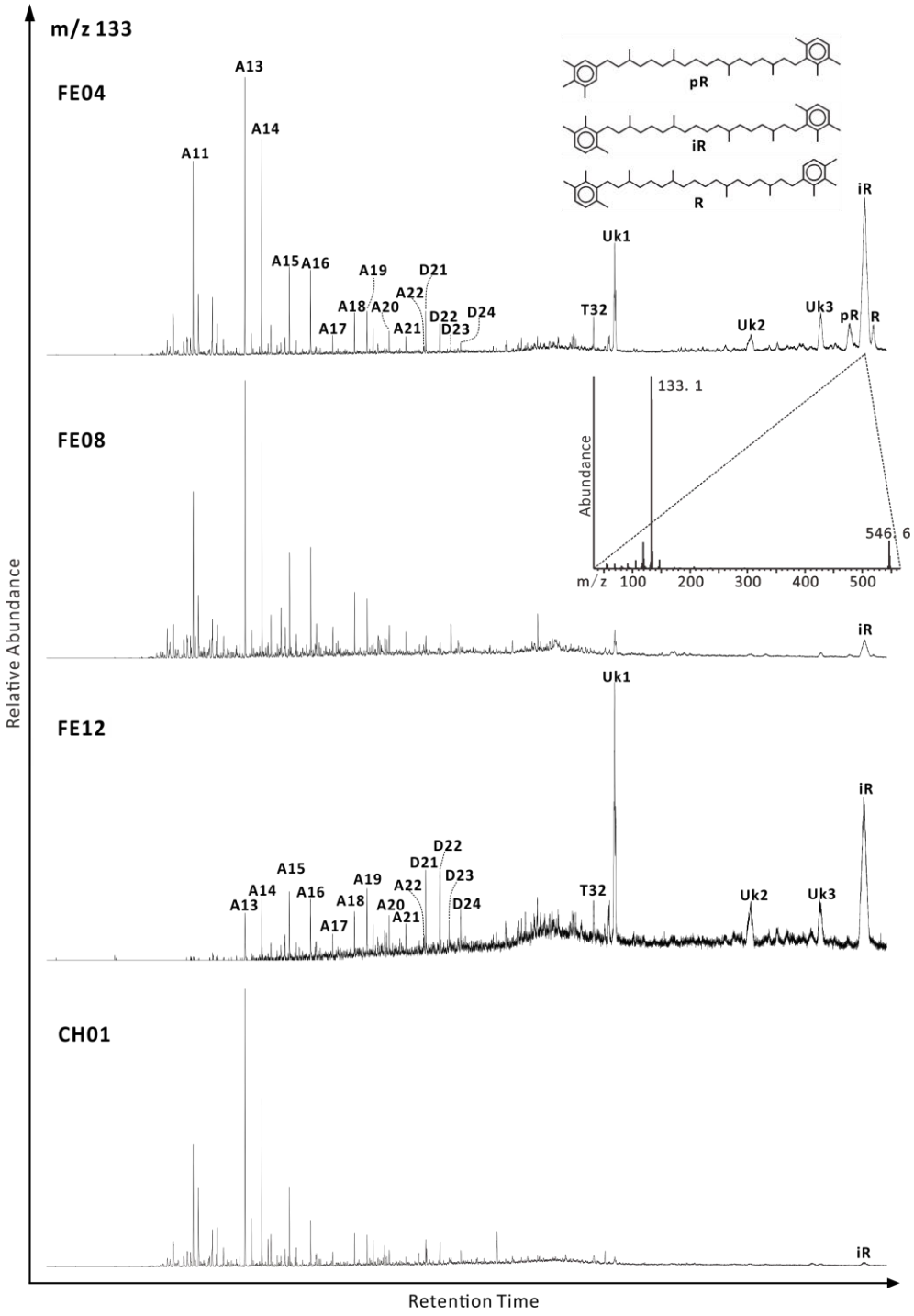


Fig. 2.8 Representative *m/z* 133 mass chromatograms characteristic of the aryl isoprenoids in the aromatic hydrocarbon fraction extracted from representative source rocks (FE04 and FE08 are from the Es3M member, FE12 is from the Es3L member, and CH01 is from the Es4U member) in the Shahejie Formation, Donying Depression, Bohai Bay Basin. The chromatograms show the monoaryl isoprenoids (Axx), the diaryl isoprenoids (Dxx) and the triaryl isoprenoids (Txx) with 2,3,6/2,3,4/3,4,5-trimethyl substitution pattern, and the $C_{40}$ biomarkers paleorenieratane (pR), isorenieratane (iR) and renieratane (R) which are typical biomarkers for green sulphur bacteria (*Chlorobiaceae*). Ukx = unknown compounds. The chemical

structures of paleorenieratane, isorenieratane and renieratane with 1-alkyl-2,3,6-trimethyl substitution are shown, and the inset is the mass spectra of isorenieratane. These hydrocarbons were identified by comparison of the retention times and typical mass spectra with reference samples.

The duration and seasonal fluctuation of PZE can be evaluated by the relative abundance of derivatives of the green sulphur bacteria lipids. The intensive aerobic degradation of aryl isoprenoids leads to more low molecular aryl isoprenoids. Accordingly, Schwark and Frimmel (2004) proposed the aryl isoprenoid ratio (AIR) for comparing the low molecular weight to the medium molecular weight aryl isoprenoids (defined as $\sum C_{13-17}/\sum C_{18-22}$ monoaryl isoprenoids) to assess the variability and persistence of PZE. A low value of the AIR suggests persistent PZE, whereas a high AIR value (>3.0) suggests short-term episodic PZE conditions. The Pr/Ph ratios are generally low in the Dongying Depression, especially for Es4U member samples (Table 2.1), which is consistent with the presence of aryl isoprenoids and isorenieratene derivatives.

In order to obtain reliable ratios, the 9 samples without isorenieratane were not used when calculating the AIR, as aryl isoprenoids derived from β-carotane cannot be ruled out without isotopic data. Most of the evaluated samples have more abundant low molecular weight aryl isoprenoids than medium molecular weight aryl isoprenoids (Fig. 2.8), except for a few samples from the FE112 well (Table 2.1). The mostly lower AIR and Pr/Ph values for the samples from the FE112 and T73 wells in the Minfeng sag in the northeast of the Dongying Depression suggest relatively more persistent PZE conditions (Fig. 2.9). The higher AIR and Pr/Ph values indicate short-termed episodic PZE conditions for the samples in the southwest of the depression. Thus there is a decrease in persistency of the PZE from the northeast Minfeng sag to the southwest Boxing sag (Fig. 2.9). Note that the AIRs are never below the value of 0.5 that Schwark and Frimmel (2004) suggested as indicative of persistent PZE, so overall, the PZE conditions in the Dongying Depression were episodic. The detailed causes of extension of anoxic conditions from the bottom water to the upper photic zone are

still unknown. Melendez et al. (2013) suggested that a phytoplankton bloom along with limited water circulation promoted anoxic conditions in a Devonian reef facies, eventually leading to the development of PZE in a stratified palaeo-water column. A similar mechanism is possible for the present case because of the algal blooms (Liu and Wang, 2013). However, in lacustrine settings saturated $H_2S$ in the photic zone is necessary for anoxygenic photosynthesis by green sulphur bacteria. One hypothesis is that episodic seawater flooding carried abundant sulphate into the palaeo-lake, and that sulphate reducing bacteria supplied $H_2S$ to green sulphur bacteria by reducing aqueous sulphate ($SO_4^{2-}$) to sulphides (Cai et al., 2005).

Crocetane (2,6,11,15-tetramethylhexadecane) and 2,6,10,15,19-pentamethylicosane (PMI) are tail-to-tail-linked isoprenoid hydrocarbons, which together are diagnostic for methanogenic archaea, methanotrophic archaea and sulphate-reducing bacteria (Elvert et al., 1999; Pancost et al., 2000; Barber et al., 2001). In the Dongying Depression samples, only crocetane was probably detected (Supplementary Fig. 2.5b), and there is no detectable PMI, so an archaeal source is not indicated. Maslen et al. (2009) suggested that green sulphur bacteria-derived carotenoids are precursors for crocetane by analysing the structures and carbon isotopes, which thus makes crocetane a potential marker for PZE.

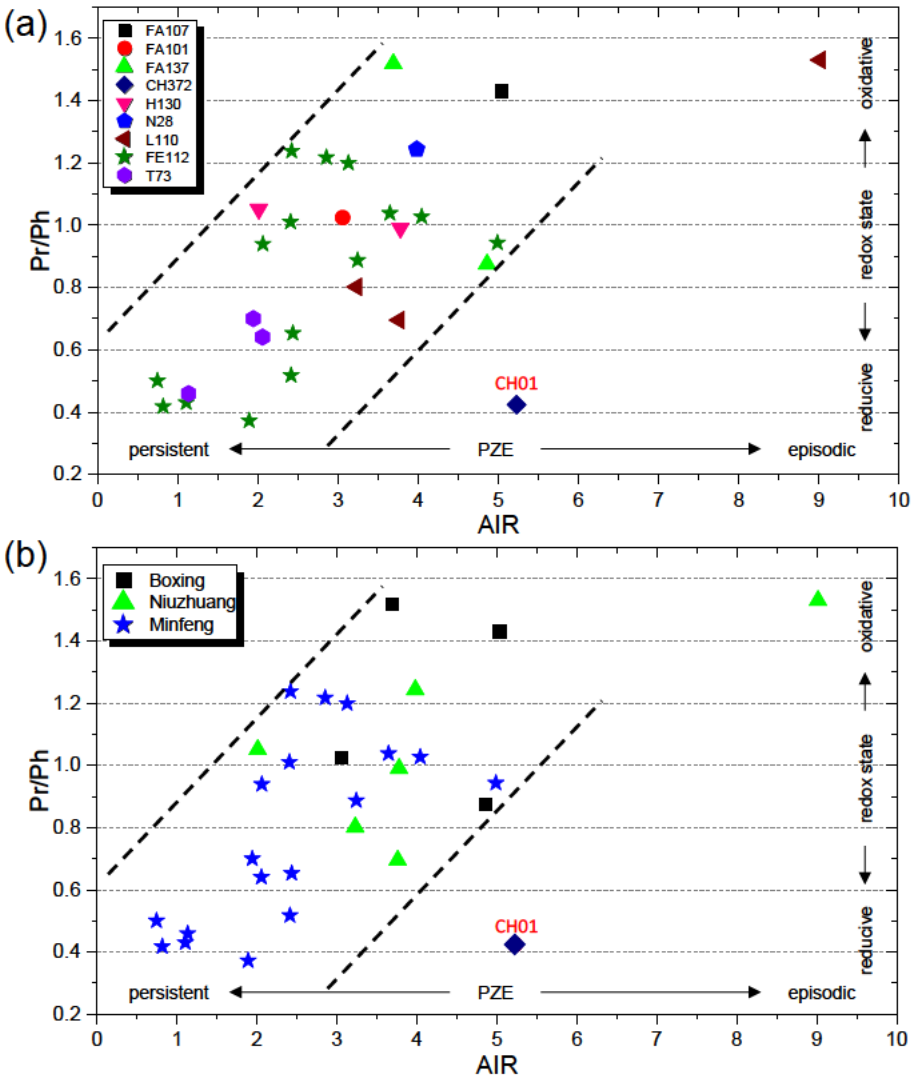


Fig. 2.9 Cross-plot of the molecular redox indicators pristane/phytane (Pr/Ph) ratio against aryl isoprenoid ratio (AIR), which are colour and shape indexed by (a) the wells, and (b) the subdivided sags in the Dongying Depression from the NE to the SW. Low AIR and Pr/Ph ratios indicate permanent PZE, whereas high ratios indicate episodic PZE conditions (Schwark and Frimmel, 2004). The AIR increases with the decreasing preservation of the aryl isoprenoids. The AIR compares low molecular weight to medium molecular weight aryl isoprenoids, and is defined as $\sum C_{13-17}/\sum C_{18-22}$ monoaryl isoprenoids.

*2.5.5.3. 2α-Methylhopane and crocetane*

The occurrence of 2α-methylhopane derived from 2α-methyl-bacteriohopanepolyols precursors is characteristic of cyanobacteria (Summons et al., 1999). The relative cyanobacteria component of the bacterial population were expressed by the $C_{31}$ 2α-methylhopane/$C_{30}$ αβ hopane ratio (the 2-MHP index) and the $C_{32}$ 2α-methylhopane/$C_{31}$ αβ hopane ratio (32MHP%) (both based on integrated areas in the *m/z* 205 and 191 mass chromatograms; Supplementary Fig. 2.5a). The 2-MHP index mostly ranges from 0.41% to

3.9% (average 1.4%) in the three studied sections, with the exception that in the Es3M member, there are two samples with 2-MHP indices of 10.0% and 9.9% (34.5% and 37.5% for 32MHP%) (Table 2.1; Fig. 2.7b). This probably reflects a variation in the cyanobacteria community, likely in response to the environment or a nutrient change in the water column (Xie et al., 2005). However, there is no significant correlation of the 2-MHP index with TOC, Pr/Ph, the gammacerane index, the β-carotane/ *n*-$C_{20}$ (%) ratio, or the isorenieratane/$C_{18}$ aryl isoprenoid ratio. In addition, due to the constant low St/H ratio (indication of the relative input of the eukaryotes compared to bacteria) during deposition of the Es3M member (Fig. 2.6), the change in 2α-methylhopane content can only reflect the cyanobacterial rather than total bacterial community structure.

The 2-methylhopanoids were originally thought to be biomarkers for cyanobacterial oxygenic photosynthesis (Summons et al., 1999). However, Rashby et al. (2007) noted an anoxygenic photoautotroph (*Rhodopseudomonas palustris*) that is capable of generating 2α-methylhopanes, and others have been detected since (Welander et al., 2010; Welander et al., 2012). The 2α-methylhopanes studied herein are more likely related to anaerobic photoautotrophs (e.g. cyanobacteria) due to the oxygen-deficient water column.

The reason for the sudden expansion of cyanobacteria within bacteria in general in the Es3M member, and its relationship with green sulphur bacteria and sulphate reducing bacteria are unknown. In the Es3M member samples, it is noteworthy that the two dramatic maxima of 2α-methylhopane abundance temporally lag the two maxima of the isorenieratane/$C_{18}$ aryl isoprenoid ratio (Fig. 2.7), which likely reflects the response of the anoxygenic photoautotrophs and green/purple sulphur bacteria community in the ecosystem to an environmental perturbation, marine-related events (such as the East Asian monsoon or summer hurricanes), or even catastrophic events (Grice et al., 2005; Xie et al., 2005; 2007). A

similar offset in the timing of biomarker distribution changes at the P/Tr boundary was also noticed by Xie et al. (2005).

### 2.5.6. Dinoflagellate, pelagophyte/chrysophyte and diatom biomarkers

Steranes derived from cell membranes can survive in the organic matter in sediments from a variety of geological process, and can record valuable information on organic matter sources, the depositional environment, or thermal maturity. A series of 24-norcholestanes ($C_{26}$), 4-methylsteranes ($C_{21}$–$C_{22}$ and $C_{28}$–$C_{30}$), dinosteranes ($C_{30}$ with trace amounts of $C_{31}$), triaromatic dinosteranes, and 24-*n*-propylcholestanes ($C_{30}$) were identified in the Shahejie Formation (Figs 2.10 and 2.11). Monoaromatic steranes, triaromatic steranes and pregnane are also present.

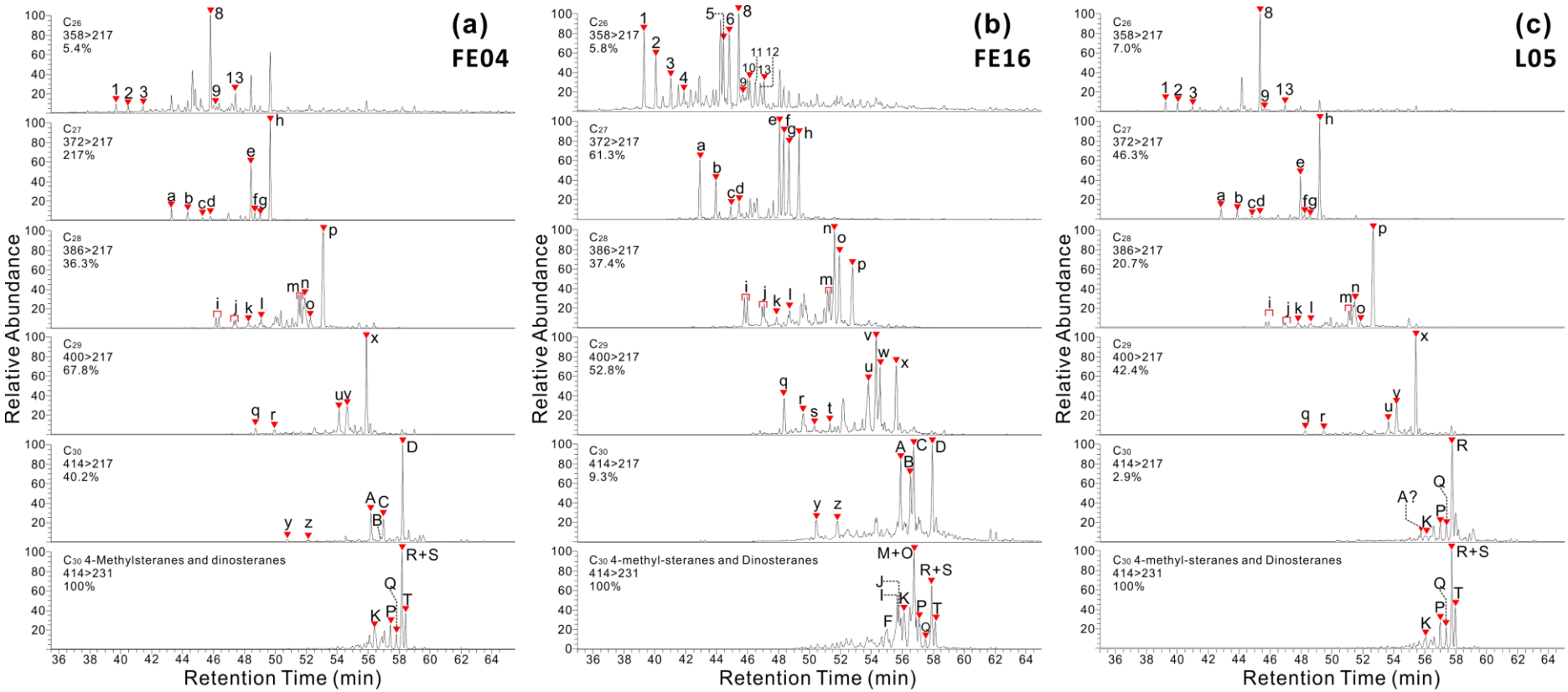


Fig. 2.10 Partial MRM GC–MS mass chromatograms showing the distribution of $C_{26}$–$C_{30}$ steranes, diasteranes and methylsteranes in the source rock samples from the Shahejie Formation, Dongying Depression. The sterane parameters are provided in Table 2.2. Peak assignments are given in Table 2.3. Representative samples are: (a) the Es3M member (sample FE04); (b) the Es4U member (sample FE16); and (c) the Es4U member (sample L05). The xx% indicates the relative signal intensity for each MRM channel, compared to *m/z* 414→231 (100%). Marine organic matter contributions are shown by the abundant 24-*n*-propylcholestanes (peaks A, B, C and D). Because of the very low relative signal intensity of the *m/z* 414→217 mass transition to the *m/z* 414→231 mass transition for the Es4U member L05 sample, 24-*n*-propylcholestanes herein are most likely absent.

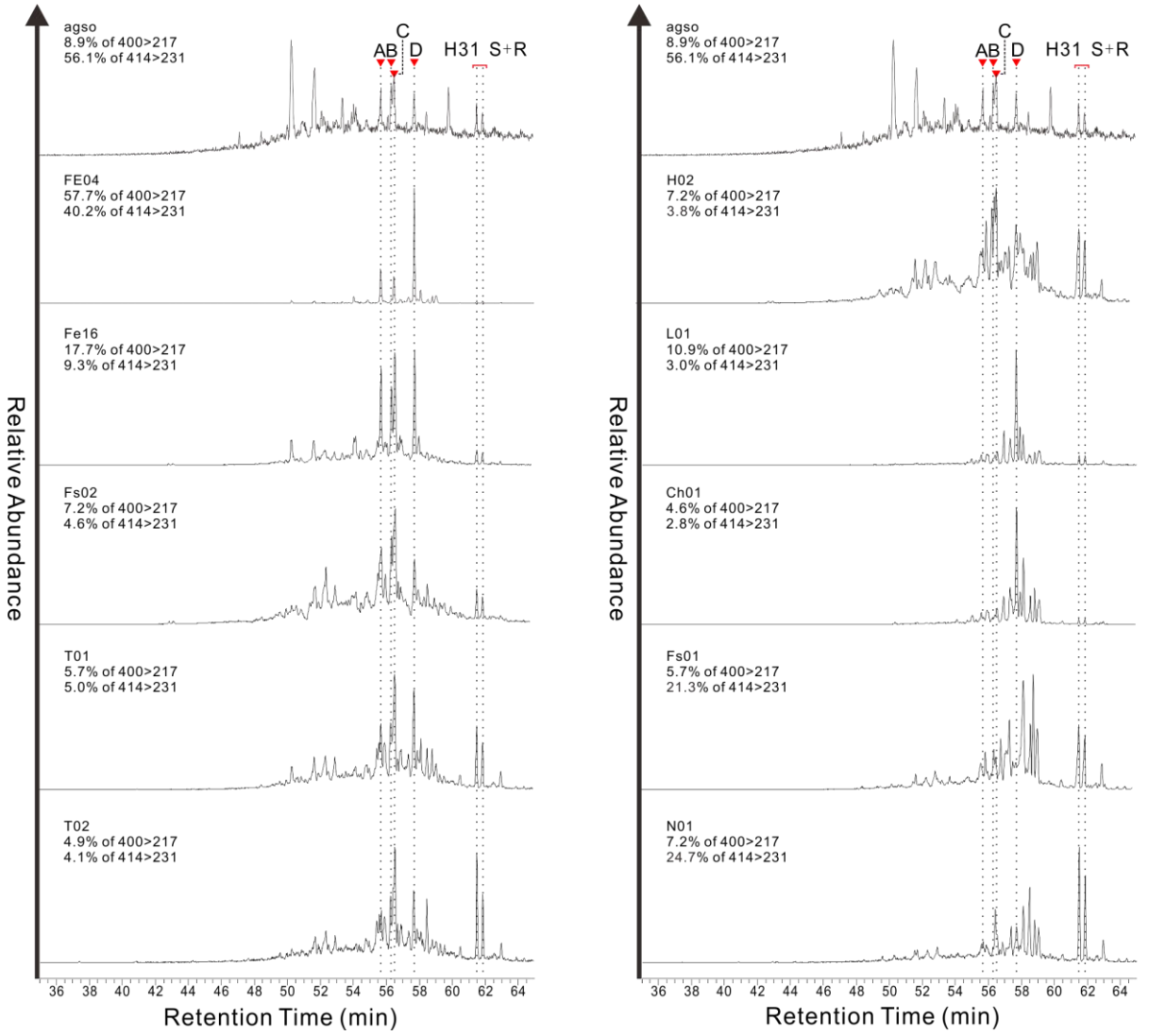


Fig. 2.11 Partial MRM GC–MS mass chromatograms (*m/z* 414→217 transition) for representative samples, showing the detection of $C_{30}$ steranes (24-*n*-propylcholestanes) in high amounts (AGSO standard; FE04 and FE16 samples), in a minority (FS02, T01, T02 and H02 samples), in very low abundance (L01 and CH01 samples), and absent (FS01 and N01 samples). The signal intensity of the *m/z* 414→217 mass transition ($C_{30}$ steranes) chromatogram relative to the signal intensity of the *m/z* 400→217 mass transition ($C_{29}$ steranes) and the *m/z* 414→231 mass transition (4-methylsteranes and dinosteranes) chromatograms are indicated as xx%. The response of MRM cross-talk from the $C_{31}$ αβ hopanes (S + R) is noticeable in the $C_{30}$ sterane channel. The elution times of four 24-*n*-propylcholestane isomers and two $C_{31}$ αβ hopanes are labelled. The $C_{30}$ sterane trace of the AGSO_NADD oil standard is provided for comparison. Peak assignments are given in Table 2.3, H31 = $C_{31}$ homohopanes.

### *2.5.6.1. Dinoflagellate biomarkers*

The 4α-methyl-24-ethylcholestanes (4-methylsteranes), 4,23,24-trimethylcholestanes (only four 4α dinosteranes were detected and no 4β epimers were above detection limits) and triaromatic dinosteranes were identified in all the samples in the Dongying Depression. These

biomarkers are derived from 4-methyl-24-ethylsterol and dinosterol precursors produced by certain algal dinoflagellates in marine or lacustrine environments (Withers, 1983; Robinson et al., 1984; Volkman et al., 1990; Summons et al., 1992; Moldowan et al., 1996; Moldowan and Talyzina, 1998). In addition, some bacteria, microalgae and diatoms have been related to the dinosterol (Bird et al., 1971; Volkman et al., 1990; 1993). Dinosteranes are not only present in high concentrations in marine and saline water, but also in freshwater environments, as shown by the different genera of dinoflagellates in water columns of different palaeosalinities (Wang et al., 2008). The triaromatic dinosteranes are age-related biomarkers derived from the dinosterols that are products of dinoflagellates (Moldowan and Talyzina, 1998). Dinoflagellates play an important role in hydrocarbon generation (Al-Ameri, 2011; Liu and Wang, 2013). The characteristics of the oil-prone organic matter in the Shahejie Formation are similar to the oil shales in the Eocene-Oligocene Elko Formation from the north-eastern Nevada (Palmer, 1984), including the low Pr/Ph ratio, more $C_{27}$ and $C_{28}$ regular steranes than $C_{29}$ regular steranes, the presence of gammacerane, and abundant $C_{28}$, $C_{29}$, and $C_{30}$ 4-methylsteranes.

4-Methylsteranes and dinosteranes were detected in high concentrations in some of the samples from the Dongying Depression, which provides evidence for a source contribution and likely the flourishing of dinoflagellates (or diatoms) in the palaeowater column during deposition of the Shahejie Formation. However in some samples from the FA101, FA107, FA137, H130, N28, FS1 and T73 wells, 4α-methyl-24-ethylcholestanes and dinosteranes were only detected in relatively minor amounts. The relative abundance of 4-methylsteranes and dinosteranes has no obvious correlation with the gammacerane index, the Pr/Ph ratio or the $C_{35}/(C_{34}+C_{35})$ homohopanes ratio, which are related to palaeowater conditions, but has a good relationship to maturity parameters such as $C_{29}$ ααα S/(S+R) steranes, $C_{29}$ αββ/(αββ+ααα) steranes, $C_{31}$ αβ S/(S+R) hopanes and Ts/(Ts+Tm) (Fig. 2.7a).

Due to the co-elution of $C_{30}$ 4α-methyl-24-ethylcholestane 20R (peak R) and the 4α,23R,24R-trimethylcholestane 20R (peak S), and the co-elution of 4α-methyl-24-ethylcholestane 14β,17β(H) 20S (peak M) and the 3β-methyl-24-ethylcholestane (20R), we defined the dinosterane index (DSI) as P+Q+T/(P+Q+T+F+I+J) (peak letters referred to in Table 2.3). The average DSI values are 0.79, 0.45 and 0.67 for the Es3M, Es3L and Es4U member samples, respectively (Table 2.2). The 4-methylsterane index (4MSI) were defined as 4-methylsteranes/$C_{29}$ regular steranes. The average 4MSI values are 0.62, 0.48 and 0.61 for the Es3M, Es3L and Es4U member samples, respectively. The DSI and 4MSI slightly decrease with increasing burial depth, showing an influence of thermal maturity (Supplementary Fig. 2.6a and 6b). The DSI is well correlated ($R^2$ = 0.93) with the $C_{29}$ ααα 20S/(20S+20R) sterane ratio (Supplementary Fig. 2.6e). This is consistent with Wang et al. (2008), who noted that both dinosteranes and triaromatic dinosteranes are affected by thermal maturation. Thus, the variation in the relative abundance of dinosteranes within the Shahejie Formation (Fig. 2.7a) can be attributed to either the extent of algal contributions, or the effect of thermal maturation. Given dinosteranes and triaromatic dinosteranes are almost exclusively sourced from dinoflagellates (Moldowan et al., 1996; Moldowan and Talyzina, 1998), the high concentrations of dinosteranes and triaromatic dinosteroids corroborate an essential contribution from algae flourishing in the water column (Liu and Wang, 2013).

*2.5.6.2. Pelagophyte/chrysophyte biomarkers*

Due to cross-talk and co-elution of the $C_{30}$ 24-*n*-propylcholestanes ($C_{30}$ 4-desmethylcholestanes) with the $C_{30}$ 4α-methyl-24-ethylcholestanes on the *m/z* 414→217 mass transition, the identification of the 24-*n*-propylcholestanes has to be carefully verified to avoid using biased information. Rohrssen et al. (2015) noted that 24-*n*-propylcholestanes are not always present above detection limits in marine rocks over certain extended intervals of the

Lower Palaeozoic era. Considering that the 4α-methyl-24-ethylcholestanes have minor *m/z* 217 fragments, yielding peaks in the *m/z* 414→217 mass transition, and that the retention times of the ααα 20R and αββ 20R stereoisomers of the 4α-methyl-24-ethylcholestanes are nearly identical to those of the same stereoisomers of the 24-*n*-propylcholestanes, the presence of small amounts of 24-*n*-propylcholestanes can be difficult to verify (Peters et al., 2005). In the case of the GC–MS used in this study, the signal intensities of the *m/z* 414→217 mass transition peaks of the 4α-methyl-24-ethylcholestanes are less than the 10% of the *m/z* 414→231 mass transition intensities that Peters et al. (2005) suggested. The relative signal intensity of 4α-methyl-24-ethylcholestanes in the *m/z* 414→231 mass transition is 3–34 times higher than that in the *m/z* 414→217 mass transition.

After careful comparison with the external standard (AGSO_NADD), the four prominent peaks that elute in the *m/z* 414→217 mass transition were assigned to be the following 24-*n*-propylcholestanes: $C_{30}$ ααα 20S (A), αββ 20R (B), αββ 20S (C) and ααα 20R (D) (Fig. 2.10). The relative signal intensity of these stereoisomers in the *m/z* 414→217 mass transition is ~10% of the signal intensity on the *m/z* 414→231 mass transition. This value in the FE04 sample is ~40% (Fig. 2.10a), showing that 24-*n*-propylcholestanes are certainly present in this sample. However, for sample L05 the pattern of peaks on the *m/z* 414→217 mass transition is almost completely identical with the pattern of peaks on the *m/z* 414→231 mass transition, and the signal intensity is only 2.9% of those on the *m/z* 414→231 mass transition (Fig. 2.10c). Thus, these peaks are most likely due to the *m/z* 217 fragments of the 4α-methyl-24-ethylcholestanes, or in other words, such small amounts of 24-*n*-propylcholestanes are undetectable and unreliable. If the $C_{30}$ steranes are too minor relative to the $C_{30}$ methylsteranes, the identification of the 24-*n*-propylcholestanes is questionable even with correct retention times, and in this study such samples were not further taken into consideration.

The presence of $C_{30}$ 24-*n*-propylcholestanes is commonly thought to be an indicator of a marine depositional environment (Moldowan, 1984; Moldowan et al., 1990). These biomarkers originate from 24-*n*-propylcholesterols that are biosynthesised exclusively by pelagophyte/chrysophyte algae of the order *Sarcinochrysidales* that are commonly ingested by marine invertebrates (Raederstorff and Rohmer, 1984; Moldowan et al., 1990; McCaffrey et al., 1994; Volkman, 2003; Grosjean et al., 2009). In the studied samples these biomarkers indicate marine organic matter input to the Shahejie Formation in the Dongying Depression (Fig. 2.10). The presence of $C_{30}$ 24-*n*-propylcholestanes in some of the samples indicates an episodic marine organic matter input to the Shahejie Formation in the Minfeng sag of the Dongying Depression, but not in the other sags (Table 2.2). In a similar way Cao et al. (2016a) and Hu et al. (2015) reported episodic marine incursions in the Songliao Basin palaeo-lake by demonstrating the sporadic presence of 24-*n*-propylcholestanes and 24-*iso*-propylcholestanes.

The relative concentration and magnitude of the 24-*n*-propylcholestanes is expressed as the ratios of $C_{30}/C_{29}$ ααα R steranes (%) and $C_{30}/(C_{27}–C_{30})$ ααα R steranes (%) (Table 2.2). In the sixteen aliphatic fractions examined, the 24-*n*-propylcholestanes are present in considerable quantity in the Es4U member samples only from the FE112, FS1 and T73 wells (e.g. samples FE16 and FS02, Fig. 2.11), and in the Es3 member samples from the FE112 and T73 wells (e.g. samples FE04, T01, Fig. 2.11). For samples such as the Es4U member T02 and the Es3L member H02 (Fig. 2.11), the first epimer (24-*n*-propyl-5α(H),14α(H),17a(H)-cholestane (20S); peak A) is as low in abundance as the cross-talk peaks I and J (3β – methylsteranes) from the *m/z* 414→231 mass transition, thus the identification and integration of $C_{30}$ 24-*n*-propylcholestanes is not reliable. Other samples such as the Es4U member L01 and CH01 (Fig. 2.11) barely have four epimers of the $C_{30}$ 24-*n*-propylcholestanes, and the dominant peak D is most likely the cross-talk peak R+S from the *m/z* 414→231 mass

transition, due to the <3.0% signal relative intensity to the *m/z* 414→231 mass transition, and the almost identical patterns of peaks in *m/z* 414→231 and *m/z* 414→217 (Fig. 2.11). Some samples such as the Es4U member FS01 and the Es3L member N01 are overwhelmed by the cross-talk from hopanes (Fig. 2.11), so provide no evidence that $C_{30}$ 24-*n*-propylcholestanes occurred during deposition, Their absence is also supported by the trace amounts of dinosteranes in the *m/z* 98 mass chromatograms for these kind of samples.

This stepwise abundance of $C_{30}$ 24-*n*-propylcholestanes may reflect the temporal and lateral extent of marine organic matter inputs and seawater incursions in the Dongying Depression. Temporally, the distribution of 24-*n*-propylcholestane indicates that seawater incursions occurred episodically during deposition of the Es4U and Es3M members of the Shahejie Formation. Laterally, the samples that contain 24-*n*-propylcholestanes are almost all from localities to the northeast of the Dongying Depression in the Minfeng sag. The Es4U member probably received a marine input of pelagophyte/chrysophyte when seawater entered the Dongying Depression. Interestingly, the lack of significant 24-*n*-propylcholestanes in all the Es3M, Es3L and Es4U member samples in the south-western part of the Dongying Depression can be interpreted as indicating that the seawater incursions came from the NE direction (Scotese, 2001; Meng et al., 2017).

Between the time of deposition of the Es4U and Es3M members there were probably periods of cessation of seawater incursions, which may be due to tectonic events or alternatively eustatic sea level changes. The FE04 sample has the highest $C_{30}/(C_{27}\text{-}C_{30})$ ααα R sterane ratio (10.1%), the highest $C_{30}/C_{29}$ ααα R sterane ratio (48.6%), the highest relative abundance of $C_{27}$ ααα R regular steranes (55% of the total $C_{27}\text{-}C_{29}$ ααα R regular steranes) and the highest TOC (14.9%; compared to the average TOC of 5.0%). These data suggest the marine organic matter input could be associated with the organic-rich source rocks. However, it seems that the magnitude of the marine organic matter contribution cannot always exceed

the indigenous/non-marine bio-productivity, as shown by the relatively low TOC (4.3–6.2%) for the FE16, FS02 and T02 samples, which contain $C_{30}$ 24-*n*-propylcholestanes.

Yuan et al. (2008a) reported $^{87}Sr/^{86}Sr$ ratios (0.7076-0.7099) and pyrite sulphur isotope data ( $\delta^{34}S$ = 15-24‰) for sediments in the Es4U member in the Shahejie Formation, which also indicate that marine transgression events happened in the Dongying Depression. In comparison, 24-*n*-propylcholestanes are absent from the lacustrine sediments of the Biyang Basin, which is a Paleogene faulted saline lake basin located in the southern part of Henan Province in central China, although abundant $C_{30}$ dinosteranes are present (Chen and Summons, 2001).

*2.5.6.3. Diatom biomarkers*

Diatoms are likely to be a major source for 24-norcholestanes in oils and rocks (Moldowan et al., 1991). Rampen et al. (2007) noticed 6–10% 24-norsterols of total sterols in diatoms and only 0.2% of total sterols in dinoflagellates, suggesting that both can be sources of 24-norcholestanes. The high concentration of 24-norcholestanes in Cretaceous and younger strata has been related to the expansion of dinoflagellates and diatoms (Holba et al., 1998b; Volkman, 2003; Rampen et al., 2007). Wang et al. (2008) noted a good relationship between the 24-norcholestane ratio (NCR = 24-norcholestanes/(24-norcholestanes + 27-norcholestanes) and the triaromatic dinosteroid hydrocarbon index (TDHI) = triaromatic dinosteroids/(triaromatic dinosteroids + triaromatic 3-methyl-24-ethylcholestanes), indicating a close association of the occurrence of 24-norcholestanes and triaromatic dinosteranes.

The presence of dinoflagellate laminae in the Dongying Depression indicating algal blooms (i.e. dinoflagellate) was noted by Liu and Wang (2013). The studied samples from the Dongying Depression contain thirteen $C_{26}$ norcholestane homologues, which consists of four 24-norcholestane isomers, four 27-norcholestane isomers, four 24/27-nordiacholestane

isomers and one 21-norcholestane (Fig. 2.10b). The NCR and 24-nordiacholestane ratio (NDR) calculated as 24-nordiacholestane/(24-nordiacholestane+24-nordiacholestane) were used to characterise the relative concentrations of 24-norcholestanes (Wang et al., 2008). The NCR of the Dongying Depression samples ranges from 0.54 to 0.90 (average = 0.74), which is a typical range for Paleogene sediments (Holba et al., 1998a), and could be a consequence of organic matter contributions from dinoflagellates and/or diatoms.

The NCR decreases with burial depth (Supplementary Fig. 2.6d), and correlates well with the $C_{29}$ ααα S/(S+R) sterane ratio (Supplementary Fig. 2.6f), which implies a thermal maturity control. This phenomenon is somewhat similar with the 4MSI, DSI and TDHI, which also show the effects of thermal maturation (Supplementary Fig. 2.6). Thus, solely depending on the dinoflagellate-derived biomarkers, it is ambiguous to differentiate the non-marine organic matter from the marine influenced lacustrine setting.

In addition to a major contribution of dinoflagellates to the organic matter in the Paleogene Dongying Depression, the low proportion of 24-norsterols in dinoflagellates, the dinosterol and other 4-methyl sterols in a marine diatom (Volkman et al., 1993) and the possible marine transgression have increased the likelihood of the existence of diatoms. However, no definitive diatom frustules or siliceous diatom skeletons have been separated from the strata of the Shahejie Formation (Wang et al., 2008), although diatom fossils could be degraded during thermal stress. Moreover, the mechanisms of predation and uptake of the dinoflagellates are very diverse, and fully autotrophic species are very rare (Schnepf and Elbrächter, 1992). Certain mixed-nutrition-strategies enable dinoflagellates to feed heterotrophically on bacteria, cyanobacteria, small dinoflagellates, ciliates and diatoms (Norris, 1969; Elbrächter, 1979). No evidence of diatom-specific biomarkers such as highly branched isoprenoids (HBIs) (Brown et al., 2014; Belt et al., 2017) were detected in the Dongying Depression samples. When Fe levels are low, organic matter tends to be preserved

through sulphurisation under anoxic conditions by $H_2S$ produced by bacterial sulphate reduction (BSR) at early stages of diagenesis (Sinninghe Damsté and de Leeuw, 1990). It is possible that HBIs are sulphurised, so in future work it is recommended that Raney nickel desulphurisation of the polar fractions is carried out to test for polar-bound diatom biomarkers.

### 2.5.7. The palaeoenvironment, sulphur cycle and seawater incursions

Algal blooms offer a very high rate of primary productivity, and were likely responsible for the formation of organic-rich shales and mudstones in the Dongying Depression (Liu and Wang, 2013). Simultaneously along with a strongly stratified water column, the algal blooms furthered bottom water anoxia which episodically extended into upper water column PZE. PZE is favourable for intensive bacterial activity by sulphate-reducing bacteria, green sulphur bacteria, purple sulphur bacteria, and cyanobacteria. Terrigenous inputs were minor, and the predominant algal contributions to the organic matter were controlled by water salinity and redox conditions. Bacteria contributed to the organic matter, notably in the Es3 member of the Shahejie Formation. The restricted circulatory environment in the water column is shown by several biomarkers, including the low Pr/Ph ratio, the abundant β-carotane and isorenieratane, and the elevated gammacerane and $C_{35}$ homohopane abundances. From the basal Es4U member to the top Es3M member there was a decrease in duration and extent of restriction. Bottom water anoxia and episodic PZE can lead to exceptional skeletal/vertebrate fossils (including soft tissue) preservation (Long and Trinajstic, 2010; Melendez et al., 2013), and also plays a pivotal role in preventing organic matter in the Shahejie Formation being aerobically degraded.

Very low organic sulphur content is demonstrated by the very low dibenzothiophene/phenanthrene (DBT/P) ratios (average = 0.13, 0.06 and 0.16 for the Es3M,

Es3L and Es4U members, respectively). Additionally, elemental sulphur content of the EOM was also low, as shown by barely any reaction with fresh copper. However, almost all the samples contain abundant aryl isoprenoids and isorenieratene derivatives, with the isorenieratane/$C_{18}$ aryl isoprenoid ratio as high as 71 (Table 2.1). This is evidence for the thriving of green sulphur bacteria and purple sulphur bacteria that oxidised $H_2S$ to elemental sulphur. This oxidation process is required for anoxygenic photosynthesis by the green sulphur bacteria and purple sulphur bacteria. Sulphate-reducing bacteria can then reduce elemental sulphur back to $H_2S$, which the green sulphur bacteria can use as an electron donor (Madigan et al., 2009). Consequently, the mostly likely source for the free $H_2S$ extending into the photic zone was BSR.

The sources of sulphate in the palaeo-lake water must be seriously considered, as marine settings contain much higher concentrations of dissolved sulphate than lakes (Berner and Raiswell, 1984). Canfield (2001) proposed four possible external inputs of sulphate into lake waters: dissolved gypsum ($\delta^{34}S$ of 10 to 30‰) or pyrite ($\delta^{34}S$ of –40 to 5‰) in ancient sediments, atmospheric precipitation ($\delta^{34}S$ of 3 to 15‰), emission from volcanoes or hydrothermal systems ($\delta^{34}S$ of –10 to 15‰), and marine sulphate from seawater incursions. The BSR process of transforming aqueous sulphate ($SO_4^{2-}$) into sulphide (e.g. $H_2S$) in anoxic marine and lacustrine environments can result in sulphur isotopic fractionation (depletion in $^{34}S$) of up to 70‰ (Meyer and Kump, 2008), after which the $^{34}S$ depleted and reduced sulphur may be incorporated into organic matter or pyrite (Sinninghe Damsté et al., 1989).

Alternatively, if there was PZE, green sulphur bacteria and purple sulphur bacteria could firstly recycle this released $H_2S$ to the isotopically lighter sulphate (Zerkle et al., 2009), then sulphate-reducing bacteria could reduce them back to even lighter $H_2S$. Ultimately, after PZE more $^{34}S$ depleted pyrite-bound sulphur or organic sulphur relative to its parent sulphate source is expected (Cai et al., 2005; 2009). The high concentrations of isorenieratene

derivatives suggest that elevated concentrations of $H_2S$ existed in the water column, which would have been an excess for the formation of pyrite if there was available dissolved iron.

Yuan et al. (2008a) reported a highly positive $\delta^{34}S$ values of 26.0 to 31.0‰ (average = 29.6‰) for the gypsum in the Es4U member, and relatively lighter pyrite in the Es4U member ($\delta^{34}S$ of 2.6‰, 12.0‰, 17.5‰ and 18.0‰). Additionally, there are a suite of gypsum and halite interbeds in the Es4 member in the northeast Dongying Depression where the FE112, FS1 and T73 wells are situated (Li et al., 2003). Therefore, one possible origin of sulphate for BSR is dissolved gypsum or pyrite from the Es4 member. Nonetheless, marine sources of sulphate cannot be ruled out, not only because of the sulphur isotopes, but also because of the presence of 24-*n*-propylcholestanes in both the Es4U and Es3M members (Figs 2.10 and 2.11).

The Es3M member is thought to have been deposited under a relatively fresh water column (Zhang et al., 2009; Hao et al., 2011), but the FE04 sample has the highest $C_{30}/(C_{27}–C_{30})$ ααα R sterane ratio (10.1%), the highest $C_{30}/C_{29}$ ααα R sterane ratio (48.6%), the highest TOC (14.9%), the highest C/N ratio (22.5), the almost highest relative abundance of the $C_{27}$ regular sterane (55%), the highest isorenieratane/$C_{18}$ aryl isoprenoid ratio, and the second highest EOM content (19.9 mg/g). The differences in the sulphur isotopes between gypsum and pyrite and the consistency with the $\delta^{34}S$ of 15 to 24‰ in the Paleogene Ocean (Holser and Kaplan, 1966), the PZE conditions (as shown by the abundant isorenieratane derivatives) and the presence of 24-*n*-propylcholestanes lead to the hypothesis that with intense bacterial activity the green sulphur bacteria recycled the $H_2S$ from the BSR. This led to a significant isotopic fractionation relative to the parent sulphate, and marine sulphates and marine organisms contributing to the productivity in the coastal Dongying palaeo-lake (Fig. 2.12). Furthermore, $PO_4^{3-}$ can be liberated from ferrophosphorus, promoting the eutrophication of palaeo-water (Mort et al., 2007).

The seawater incursions were probably controlled by the eustatic sea level changes. The global sea level was high during deposition of the Eocene Shahejie Formation (Haq et al., 1987, 1988; Miller et al., 2005; 2008), although sea level fell from the Eocene to the Oligocene. From the Es4 member to the Es3 member there was a transgression in the Dongying palaeo-lake (Wang et al., 2010), which is also consistent with global sea level changes during the Lutetian and Bartonian (Fig. 2.2). Accompanied the sea level increases, the East Asian monsoon (Wang et al., 2013a), winter storms, and summer hurricanes (Emanuel, 1987; Houghton et al., 1996) could have induced heavy precipitation, bringing significant amounts of sulphate ($\delta^{34}S$ of 3 to 15‰ from sea water), algae and nutrients to the Dongying palaeo-lake. In addition to a climate control on the development of the palaeo-lake in the Dongying Depression, the biomarker-proven episodic marine influence provides another way for addressing questions such as the causes for the salinization and the stratification (thermal or salinity) of the palaeo-water body, although the detailed mechanisms are not understood fully. Due to the many other influencing factors, further investigations into the exact timing, extent, duration and outcome of the seawater incursions into the Dongying palaeo-lake are needed.

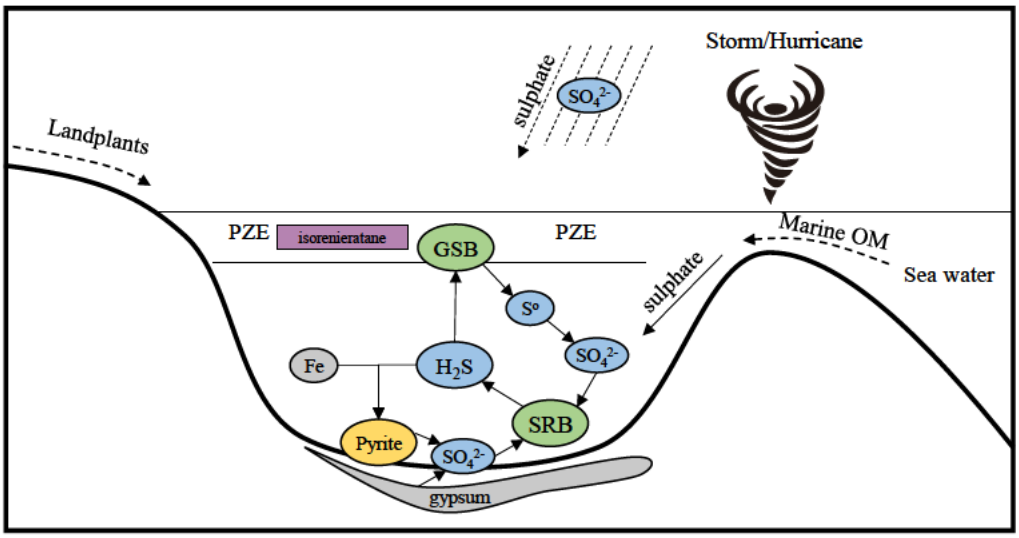


Fig. 2.12 A schematic illustration of the sulphate cycle and the organic inputs in the Dongying Depression, Bohai Bay Basin. OM = organic matter, GSB = green sulphur bacteria, SRB = sulphate-reducing bacteria, PZE = photic zone euxinia.

## 2.5. Conclusions

We used multiple organic-geochemical approaches to track environmental change and organic matter inputs associated with the key members of the Shahejie Formation, Dongying Depression, Bohai Bay Basin.

The interpretation of *n*-alkanes and regular steranes in complex and paralic lacustrine settings is challenging, especially when these compounds are not present in very characteristic patterns. The abundant HMW *n*-alkanes and the $C_{29}$ regular steranes were likely derived from specific algae. Terrigenous land plant contributions to the organic matter in the Shahejie Formation were limited. The identification of 24-*n*-propylcholestanes should consider cross-talk of 4-methylsteranes and dinosteranes into the *m/z* 414→217 mass transition, particularly in samples with low concentrations of 24-*n*-propylcholestanes. No diatom biomarkers in the aliphatic fractions were detected, but the polar fractions should be released by Raney nickel reduction and tested and analysed for sulphurised polar-bound diatom biomarkers.

The pervasive presence of β-carotane, aryl isoprenoids and isorenieratene derivatives was inferred to indicate a stratified water column and episodic PZE condition during deposition of the Shahejie Formation. There was a decreasing PZE persistence from the NE to the SW in the palaeo-lake. This was probably due to enhanced water salinity, and it played a pivotal role in the preservation of organic matter. Algal blooms may have given rise to the oxygen-deficient conditions. In addition to abundant phytoplankton contributions, there was intensive bacterial activity, including from purple sulphur bacteria (*Chromatiaceae*), green sulphur bacteria (*Chlorobiaceae*), cyanobacteria, and sulphate reducing bacteria, that contributed to the organic matter in the depositional environment. Two periods of episodic seawater incursions into the Dongying palaeo-lake occurred during deposition of the Es3M and the Es4U members, as shown by the unambiguous occurrence of 24-*n*-propylcholestanes,

signifying marine pelagophyte/chrysophyte organic matter inputs into the Shahejie Formation. In the Dongying Depression, the high generative potential of the organic-rich source rocks is not only a consequence of high algal productivity and the anoxic preservation conditions, but also of significant bacterial organic matter input during deposition of the Shahejie Formation.

## Acknowledgements

This research was supported by the National Natural Science Foundation of China (Grant No. 41472108). The authors acknowledge the experimental assistance of Carl A. Peters, Sophia Aharonovich, Konstantinos Kotzakoulakis, Huaqing Xu, and Xiong Cheng. We thank CSIRO for assistance with the MRM GC–MS analyses. HX thanks the China University of Geosciences (Beijing) and Macquarie University for a co-tutelle PhD scholarship, and Macquarie University for analytical support funds.

# References

Al-Ameri, T.K., 2011. Khasib and Tannuma oil sources, East Baghdad oil field, Iraq. Marine and Petroleum Geology 28, 880–894.

Bao, J., Li, M., 2001. Unprecedented occurrence of novel $C_{26}$-$C_{28}$ 21-norcholestanes and related triaromatic series in evaporitic lacustrine sediments. Organic Geochemistry 32, 1031–1036.

Barber, C.J., Grice, K., Bastow, T.P., Alexander, R., Kagi, R.I., 2001. The identification of crocetane in Australian crude oils. Organic Geochemistry 32, 943–947.

Bechtel, A., Jia, J., Strobl, S.A.I., Sachsenhofer, R.F., Liu, Z., Gratzer, R., Püttmann, W., 2012. Palaeoenvironmental conditions during deposition of the Upper Cretaceous oil shale sequences in the Songliao Basin (NE China): Implications from geochemical analysis. Organic Geochemistry 46, 76–95.

Belt, S.T., Brown, T.A., Smik, L., Tatarek, A., Wiktor, J., Stowasser, G., Assmy, P., Allen, C.S., Husum, K., 2017. Identification of $C_{25}$ highly branched isoprenoid (HBI) alkenes in diatoms of the genus Rhizosolenia in polar and sub-polar marine phytoplankton. Organic Geochemistry 110, 65–72.

Berner, R.A., Raiswell, R., 1984. C/S method for distinguishing freshwater from marine sedimentary rocks. Geology 12, 365–368.

Bird, C.W., Lynch, J.M., Pirt, F.J., Reid, W.W., Brooks, C.J.W., Middleditch, B.S., 1971. Steroids and squalene in Methylococcus capsulatus grown on methane. Nature 230, 473–474.

Bohacs, K., 2012. Relation of hydrocarbon reservoir potential to lake-basin type: an integrated approach to unraveling complex genetic relations among fluvial, lake-plain, lake margin, and lake center strata, in: Baganz, O.W., Bartov, Y., Bohacs, K., Nummedal,

D. (Eds.), Lacustrine Sandstone Reservoirs and Hydrocarbon Systems, American Association of Petroleum Geologists Memoir 95, pp. 13–56.

Boucot, A.J., Chen, X., Scotese, C.R., Fan, J., 2009. Reconstruction of Global Paleoclimate in Phanerozoic (in Chinese). Science Press, Beijing.

Brassell, S.C., Eglinton, G., Sheng, G., Fu, J., 1988. Biological markers in lacustrine Chinese oil shales, in: Fleet, A.J., Kelts, K., Talbot, M.R. (Eds.), Lacustrine petroleum source rocks. Geological Society, Special Publications, London, pp. 299–308.

Brocks, J.J., Schaeffer, P., 2008. Okenane, a biomarker for purple sulfur bacteria (*Chromatiaceae*), and other new carotenoid derivatives from the 1640 Ma Barney Creek Formation. Geochimica et Cosmochimica Acta 72, 1396–1414.

Brown, T.A., Belt, S.T., Cabedo-Sanz, P., 2014. Identification of a novel di-unsaturated C25 highly branched isoprenoid in the marine tube-dwelling diatom Berkeleya rutilans. Environmental Chemistry Letters 12, 455–460.

Cai, C., Worden, R.H., Wolff, G.A., Bottrell, S., Wang, D., Li, X., 2005. Origin of sulfur rich oils and $H_2S$ in Tertiary lacustrine sections of the Jinxian Sag, Bohai Bay Basin, China. Applied Geochemistry 20, 1427–1444.

Cai, C., Zhang, C., Cai, L., Wu, G., Jiang, L., Xu, Z., Li, K., Ma, A., Chen, L., 2009. Origins of Palaeozoic oils in the Tarim Basin: Evidence from sulfur isotopes and biomarkers. Chemical Geology 268, 197–210.

Canfield, D.E., 2001. Biogeochemistry of sulfur isotopes. Reviews in Mineralogy and Geochemistry 43, 607–636.

Cao, H., Hu, J., Peng, P.a., Xi, D., Tang, Y., Lei, Y., Shilling, A., 2016a. Paleoenvironmental reconstruction of the Late Santonian Songliao paleo-lake. Palaeogeography, Palaeoclimatology, Palaeoecology 457, 290–303.

Cao, H., Kaufman, A.J., Shan, X., Cui, H., Zhang, G., 2016b. Sulfur isotope constraints on marine transgression in the lacustrine Upper Cretaceous Songliao Basin, northeastern China. Palaeogeography, Palaeoclimatology, Palaeoecology 451, 152–163.

Carroll, A.R., Brassell, S.C., Graham, S.A., 1992. Upper Permian lacustrine oil shales, Southern Junggar Basin, Northwest China. AAPG Bulletin 76, 1874–1902.

Chen, J.H., Summons, R.E., 2001. Complex patterns of steroidal biomarkers in Tertiary lacustrine sediments of the Biyang Basin, China. Organic Geochemistry 32, 115–126.

Chen, Z., Huang, W., Liu, Q., Zhang, L., Zhang, S., 2016. Geochemical characteristics of the Paleogene shales in the Dongying depression, eastern China. Marine and Petroleum Geology 73, 249–270.

Clark, J.P., Philp, R.P., 1989. Geochemical characterization of evaporite and carbonate depositional environments and correlation of associated crude oils in the Black Creek Basin, Alberta. Bulletin of Canadian Petroleum Geology 37, 401–416.

Connan, J., Bouroullec, J., Dessort, D., Albrecht, P., 1986. The microbial input in carbonate-anhydrite facies of a sabkha palaeoenvironment from Guatemala: A molecular approach. Organic Geochemistry 10, 29–50.

Cranwell, P.A., 1977. Organic geochemistry of Cam Loch (Sutherland) sediments. Chemical Geology 20, 205–221.

Dembicki, H., Meinschein, W.G., Hattin, D.E., 1976. Possible ecological and environmental significance of the predominance of even-carbon number $C_{20}$-$C_{30}$ *n*-alkanes. Geochimica et Cosmochimica Acta 40, 203–208.

Derenne, S., Largeau, C., Casadevall, E., Connan, J., 1988. Comparison of torbanites of various origins and evolutionary stages. Bacterial contribution to their formation. Causes of the lack of botryococcane in bitumens. Organic Geochemistry 12, 43–59.

Didyk, B.M., Simoneit, B.R.T., Brassell, S.C., Eglinton, G., 1978. Organic geochemical indicators of palaeoenvnonmental conditions of sedimentation. Nature 272, 216–222.

Duke, W.L., 1985. Hummocky cross‐stratification, tropical hurricanes, and intense winter storms. Sedimentology 32, 167–194.

Duke, W.L., 1987. Hummocky cross‐stratification, tropical hurricanes, and intense winter storms. Sedimentology 34, 344–344.

Eglinton, G., Hamilton, R.J., 1967. Leaf epicuticular waxes. Science 156, 1322–1335.

Elbrächter, M., 1979. On the taxonomy of unarmored dinophytes (Dinophyta) from the Northwest African upwelling region. Meteor'Forschungs 3, 1–22.

Elvert, M., Suess, E., Whiticar, M.J., 1999. Anaerobic methane oxidation associated with marine gas hydrates: superlight C-isotopes from saturated and unsaturated C20 and C25 irregular isoprenoids. Naturwissenschaften 86, 295–300.

Emanuel, K.A., 1987. The dependence of hurricane intensity on climate. Nature 326, 483–485.

Feng, Z., Fang, W., Zhang, J., Li, Z., Huang, C., Wang, X., Zhao, Q., Huo, Q., 2007. Distribution and significance of $C_{40+}$ alkanes in the extracts of Cretaceous source rocks from the Songliao Basin. Science in China Series D: Earth Sciences 50, 1510-1520.

Ficken, K.J., Li, B., Swain, D.L., Eglinton, G., 2000. An *n*-alkane proxy for the sedimentary input of submerged/floating freshwater aquatic macrophytes. Organic Geochemistry 31, 745–749.

Fleet, A.J., Kelts, K., Talbot, M., 1988. Lacustrine petroleum source rocks. Blackwell Scientific Publications, Boston.

Fu, J., Sheng, G., 1989. Biological marker composition of typical source rocks and related crude oils of terrestrial origin in the People's Republic of China: a review. Applied Geochemistry 4, 13–22.

Fu, J., Sheng, G., Xu, J., Eglinton, G., Gowar, A.P., Jia, R., Fan, S., Peng, P., 1990. Application of biological markers in the assessment of paleoenvironments of Chinese non-marine sediments. Organic Geochemistry 16, 769-779.

Gallois, R.W., 1976. Coccolith blooms in the Kimmeridge Clay and origin of North Sea Oil. Nature 259, 473–475.

Ge, R., 2004. Occurrence and geological significance of glauconite in Cenozoic Group of Jiyang Depression. Acta Sedimentologica Sinica 22, 276–280. (in Chinese).

George, S.C., Volk, H., Ahmed, M., Pickel, W., Allan, T., 2007. Biomarker evidence for two sources for solid bitumens in the Subu wells: Implications for the petroleum prospectivity of the East Papuan Basin. Organic Geochemistry 38, 609–642.

Goossens, H., de Leeuw, J.W., Schenck, P.A., Brassell, S.C., 1984. Tocopherols as likely precursors of pristane in ancient sediments and crude oils. Nature 312, 440–442.

Grantham, P.J., Wakefield, L.L., 1988. Variations in the sterane carbon number distributions of marine source rock derived crude oils through geological time. Organic Geochemistry 12, 61–73.

Grice, K., Schaeffer, P., Schwark, L., Maxwell, J.R., 1996. Molecular indicators of palaeoenvironmental conditions in an immature Permian shale (Kupferschiefer, Lower Rhine Basin, north-west Germany) from free and S-bound lipids. Organic Geochemistry 25, 131–147.

Grice, K., Schouten, S., Peters, K.E., Sinninghe Damsté, J.S., 1998. Molecular isotopic characterisation of hydrocarbon biomarkers in Palaeocene-Eocene evaporitic, lacustrine source rocks from the Jianghan Basin, China. Organic Geochemistry 29, 1745–1764.

Grice, K., Cao, C., Love, G.D., Bottcher, M.E., Twitchett, R.J., Grosjean, E., Summons, R.E., Turgeon, S.C., Dunning, W., Jin, Y., 2005. Photic zone euxinia during the Permian-Triassic superanoxic event. Science 307, 707-709.

Grosjean, E., Love, G.D., Stalvies, C., Fike, D.A., Summons, R.E., 2009. Origin of petroleum in the Neoproterozoic-Cambrian South Oman salt basin. Organic Geochemistry 40, 87–110.

Hao, F., Zhou, X., Zhu, Y., Yang, Y., 2011. Lacustrine source rock deposition in response to co-evolution of environments and organisms controlled by tectonic subsidence and climate, Bohai Bay Basin, China. Organic Geochemistry 42, 323–339.

Hao, Y., Li, H., 1984. The occurrence and significance of the Early Tertiary calcareous nannofossil in the coast of the Bohai Sea. Chinese Science Bulletin 29, 741–741. (in Chinese).

Haq, B.U., Hardenbol, J., Vail, P.R., 1987. Chronology of fluctuating sea levels since the Triassic. Science 235, 1156–1167.

Haq, B.U., Hardenbol, J., Vail, P.R., 1988. Mesozoic and Cenozoic chronostratigraphy and cycles of sea-level change. Special Publications of SEPM 42, 71–108.

He, J., Ding, W., Jiang, Z., Jiu, K., Li, A., Sun, Y., 2017. Mineralogical and chemical distribution of the Es3L oil shale in the Jiyang Depression, Bohai Bay Basin (East China): Implications for paleoenvironmental reconstruction and organic matter accumulation. Marine and Petroleum Geology 81, 196–219.

He, W., Jin, K., Hao, D., 2003. Characteristics and their significance of mudstone source and reservoir rock in the 3rd member of Shahejie Formation in the GUO-7 well, Jiyang Depression. Oil & Gas Geology 24, 375–379.

Holba, A.G., Dzou, L.I.P., Masterson, W.D., Hughes, W.B., Huizinga, B.J., Singletary, M.S., Moldowan, J.M., Mello, M.R., Tegelaar, E., 1998a. Application of 24-norcholestanes for constraining source age of petroleum. Organic Geochemistry 29, 1269–1283.

Holba, A.G., Tegelaar, E.W., Huizinga, B.J., Moldowan, J.M., Singletary, M.S., McCaffrey, M.A., Dzou, L.I.P., 1998b. 24-norcholestanes as age-sensitive molecular fossils. Geology 26, 783–786.

Holser, W.T., Kaplan, I.R., 1966. Isotope geochemistry of sedimentary sulfates. Chemical Geology 1, 93–135.

Hou, Y., 1978. The ostracods in the Early Tertiary Bohai Bay Basin. Science Press, Beijing. (in Chinese).

Houghton, J.T., Meiro Filho, L.G., Callander, B.A., Harris, N., Kattenburg, A., Maskell, K., 1996. The science of climate change: contribution of WG I to the second assessment report of the intergovernmental panel on climate change. Cambridge University Press, Cambridge.

Hu, J.F., Peng, P.A., Liu, M.Y., Xi, D.P., Song, J.Z., Wan, X.Q., Wang, C.S., 2015. Seawater incursion events in a Cretaceous paleo-lake revealed by specific marine biological markers. Scientific Reports 5, 9508.

Huang, H., Zheng, Y., Zhang, Z., Li, J., 2003. Lacustrine biomass: An significant precursor of high wax oil. Chinese Science Bulletin 48, 1987–1994.

Huang, W., Meinschein, W.G., 1979. Sterols as ecological indicators. Geochimica et Cosmochimica Acta 43, 739-745.

Huang, Y., Yang, G., Gu, J., Wang, P., Huang, Q., Feng, Z., Feng, L., 2013. Marine incursion events in the Late Cretaceous Songliao Basin: Constraints from sulfur geochemistry records. Palaeogeography, Palaeoclimatology, Palaeoecology 385, 152–161.

Irwin, H., Meyer, T., 1990. Lacustrine organic facies. A biomarker study using multivariate statistical analysis. Organic Geochemistry 16, 197–210.

Katz, B.J., 1990. Controls on distribution of lacustrine source rocks through time and space, in: Katz, B.J. (Ed.), Lacustrine basin exploration: Case studies and modern analogs. AAPG Memoir 50, pp. 61–76.

Katz, B.J., 1995. Factors controlling the development of lacustrine petroleum source rocks - An update, in: Alain-Yves, H. (Ed.), Paleogeography, Paleoclimate, And Source Rocks. Studies in Geology 40, pp. 61–79.

Kissin, Y.V., 1987. Catagenesis and composition of petroleum: origin of n-alkanes and isoalkanes in petroleum crudes. Geochimica et Cosmochimica Acta 51, 2445–2457.

Koopmans, M.P., Schouten, S., Kohnen, M.E.L., Sinninghe Damsté, J.S., 1996. Restricted utility of aryl isoprenoids as indicators for photic zone anoxia. Geochimica et Cosmochimica Acta 60, 4873–4876.

Löhr, S., Kennedy, M., George, C.S., Williamson, R., Xu, H., 2018. Sediment microfabric records mass sedimentation of colonial cyanobacteria, rapid onset of seafloor anoxia and extensive metazoan reworking in Pliocene sapropels. The Depositional Record, in press.

Li, C., Xiao, J., 1988. The application of trace element to the study on paleosalinities in Shahejie Formation of Dongying Basin, Shengli oil field. Acta Sedimentologica Sinica 6, 100–107.

Li, S., Pang, X., Li, M., Jin, Z., 2003. Geochemistry of petroleum systems in the Niuzhuang South Slope of Bohai Bay Basin—part 1: source rock characterization. Organic Geochemistry 34, 389–412.

Liu, C., Zhao, Q., Wang, P.-x., 2002. Water chemistry of the Paleogene Dongying Lake: evidence from fossil assemblages and shell isotopes. Acta Geoscientia Sinica 23, 237–242.

Liu, C., Wang, P., 2013. The role of algal blooms in the formation of lacustrine petroleum source rocks - Evidence from Jiyang depression, Bohai Gulf Rift Basin, eastern China. Palaeogeography Palaeoclimatology Palaeoecology 388, 15–22.

Livingston, D., 1984. The preservation of algal remains in recent lake sediment, in: Haworth, E.Y., Lund, J.W.G. (Eds.), Lake sediment and environmental history. University of Minnesota Press, Minneapolis, pp. 191–202.

Long, J.A., Trinajstic, K., 2010. The Late Devonian Gogo Formation lägerstatte of Western Australia: exceptional early vertebrate preservation and diversity. Annual Review of Earth and Planetary Sciences 38, 255–279.

Love, G.D., Grosjean, E., Stalvies, C., Fike, D.A., Grotzinger, J.P., Bradley, A.S., Kelly, A.E., Bhatia, M., Meredith, W., Snape, C.E., 2009. Fossil steroids record the appearance of Demospongiae during the Cryogenian period. Nature 457, 718–721.

Mackenzie, A.S., 1984. Applications of biological markers in petroleum geochemistry, in: Brooks, J., Welte, D.H. (Eds.), Advances in petroleum geochemistry. Academic Press, London, pp. 115–214.

Madigan, M.T., Martinko, J.M., Dunlap, P.V., Clark, D.P., 2009. Brock biology of microorganisms. Pearson Benjamin Cummings, San Francisco.

Mango, F.D., 2000. The origin of light hydrocarbons. Geochimica et Cosmochimica Acta 64, 1265–1277.

Mao, S., Yu, J., 1990. Origin and evolution of terrestrial dinoflagellates and their significance in source potential for petroleum. Earth Science: Journal of China University of Geosciences 15, 283–291.

Marsaglia, K.M., Klein, G.D., 1983. The paleogeography of Paleozoic and Mesozoic storm depositional systems. The Journal of Geology 91, 117–142.

Maslen, E., Grice, K., Gale, J.D., Hallmann, C., Horsfield, B., 2009. Crocetane: A potential marker of photic zone euxinia in thermally mature sediments and crude oils of Devonian age. Organic Geochemistry 40, 1–11.

McCaffrey, M.A., Moldowan, J.M., Lipton, P.A., Summons, R.E., Peters, K.E., Jeganathan, A., Watt, D.S., 1994. Paleoenvironmental implications of novel $C_{30}$ steranes in Precambrian to Cenozoic age petroleum and bitumen. Geochimica et Cosmochimica Acta 58, 529–532.

Melendez, I., Grice, K., Trinajstic, K., Ladjavardi, M., Greenwood, P., Thompson, K., 2013. Biomarkers reveal the role of photic zone euxinia in exceptional fossil preservation: An organic geochemical perspective. Geology 41, 123–126.

Meng, Q., Bruch, A.A., Sun, G., Liu, Z.-j., Hu, F., Sun, P.-c., 2017. Quantitative reconstruction of Middle and Late Eocene paleoclimate based on palynological records from the Huadian Basin, northeastern China: Evidence for monsoonal influence on oil shale formation. Palaeogeography, Palaeoclimatology, Palaeoecology.

Metzger, P., Largeau, C., Casadevall, E., 1991. Lipids and macromolecular lipids of the hydrocarbon-rich microalga *Botryococcus braunii*. Chemical structure and biosynthesis. Geochemical and biotechnological importance, in: Herz, W., Kirby, G.W., Steglich, W., Tamm, C. (Eds.), Progress in the Chemistry of Organic Natural Products. Springer, Verlag, pp. 1–70.

Meyer, K.M., Kump, L.R., 2008. Oceanic euxinia in Earth history: causes and consequences. Annual Review of Earth and Planetary Sciences 36, 251–288.

Meyers, P.A., Yum, J.G., Wise, S.W., 2009. Origins and maturity of organic matter in mid-Cretaceous black shales from ODP Site 1138 on the Kerguelen Plateau. Marine and Petroleum Geology 26, 909–915.

Miller, K.G., Kominz, M.A., Browning, J.V., Wright, J.D., Mountain, G.S., Katz, M.E., Sugarman, P.J., Cramer, B.S., Christie-Blick, N., Pekar, S.F., 2005. The Phanerozoic record of global sea-level change. Science 310, 1293–1298.

Miller, K.G., Browning, J.V., Aubry, M.P., Wade, B.S., Katz, M.E., Kulpecz, A.A., Wright, J.D., 2008. Eocene-Oligocene global climate and sea-level changes: St. Stephens Quarry, Alabama. Geological Society of America Bulletin 120, 34–53.

Moldowan, J.M., 1984. $C_{30}$ steranes, novel markers for marine petroleums and sedimentary rocks. Geochimica et Cosmochimica Acta 48, 2767–2768.

Moldowan, J.M., Seifert, W.K., Gallegos, E.J., 1985. Relationship between petroleum composition and depositional environment of petroleum source rocks. AAPG Bulletin 69, 1255–1268.

Moldowan, J.M., Fago, F.J., Lee, C.Y., Jacobson, S.R., Watt, D.S., Slougui, N.E., Jeganathan, A., Young, D.C., 1990. Sedimentary 24-*n*-propylcholestanes, molecular fossils diagnostic of marine-algae. Science 247, 309–312.

Moldowan, J.M., Lee, C.Y., Watt, D.S., Jeganathan, A., Slougui, N.-E., Gallegos, E.J., 1991. Analysis and occurrence of $C_{26}$ steranes in petroleum and source rocks. Geochimica et Cosmochimica Acta 55, 1065–1081.

Moldowan, J.M., Dahl, J., Jacobson, S.R., Huizinga, B.J., Fago, F.J., Shetty, R., Watt, D.S., Peters, K.E., 1996. Chemostratigraphic reconstruction of biofacies: molecular evidence linking cyst-forming dinoflagellates with pre-Triassic ancestors. Geology 24, 159–162.

Moldowan, J.M., Talyzina, N.M., 1998. Biogeochemical evidence for dinoflagellate ancestors in the Early Cambrian. Science 281, 1168–1170.

Mort, H.P., Adatte, T., Föllmi, K.B., Keller, G., Steinmann, P., Matera, V., Berner, Z., Stüben, D., 2007. Phosphorus and the roles of productivity and nutrient recycling during oceanic anoxic event 2. Geology 35, 483–486.

Murphy, S.M.T.J., McCormick, A., Eglinton, G., 1967. Perhydro-β-carotene in the Green River shale. Science 157, 1040–1042.

Norris, D.R., 1969. Possible phagotrophic feeding in Ceratium lunula Schimper. Limnology and Oceanography 14, 448–449.

Otto, A., Wilde, V., 2001. Sesqui-, di-, and triterpenoids as chemosystematic markers in extant conifers-a review. The Botanical Review 67, 141–238.

Ourisson, G., Albrecht, P., Rohmer, M., 1979. The hopanoids: palaeochemistry and biochemistry of a group of natural products. Pure and Applied Chemistry 51, 709–729.

Ourisson, G., Rohmer, M., Poralla, K., 1987. Prokaryotic hopanoids and other polyterpenoid sterol surrogates. Annual Reviews in Microbiology 41, 301–333.

Palmer, S.E., 1984. Hydrocarbon source potential of organic facies of lacustrine Elko Formation (Eocene-Oligocene), northeastern Nevada. AAPG Bulletin 68, 945–945.

Pancost, R.D., Sinninghe Damsté, J.S., Lint, S.D., Maarel, M.J.E.C.v.d., Gottschal, J.C., 2000. Biomarker Evidence for Widespread Anaerobic Methane Oxidation in Mediterranean Sediments by a Consortium of Methanogenic Archaea and Bacteria. Applied and Environmental Microbiology 66, 1126–1132.

Parnell, J., 1988. Lacustrine petroleum source rocks in the Dinantian Oil Shale Group, Scotland: a review, in: Fleet, A.J., Kelts, K., Talbot, M.R. (Eds.), Lacustrine petroleum source rocks. Geological Society, Special Publications, London, pp. 235–246.

Peng, S., Xu, H., Wen, Z., 1989. A Prelimnary discussion about transgressions and hydrocarbons of Shahejie Formation in the Bohai Bay Basin. Marine Geology & Quaternary Geology 9, 17–28.

Peters, K.E., Moldowan, J.M., 1991. Effects of source, thermal maturity, and biodegradation on the distribution and isomerization of homohopanes in petroleum. Organic Geochemistry 17, 47–61.

Peters, K.E., Walters, C.C., Moldowan, J.M., 2005. The Biomarker Guide. Cambridge University Press, Cambridge

Philp, R.P., 1985. Petroleum formation and occurrence. Eos, Transactions American Geophysical Union 66, 643–644.

Qian, K., Wang, S., Liu, S., Shi, H., 1980. Discovery of the Lower Tertiary reef limestone in the northern part of East China and its significance in petroleum geology. Chinese Science Bulletin 25, 1025–1029.

Raederstorff, D., Rohmer, M., 1984. Sterols of the unicellular algae Nematochrysopsis roscoffensis and Chrysotila lamellosa: isolation of (24E)-24-n-propylidenecholesterol and 24-n-propylcholesterol. Phytochemistry 23, 2835–2838.

Rampen, S.W., Schouten, S., Abbas, B., Panoto, F.E., Muyzer, G., Campbell, C.N., Fehling, J., Sinninghe Damsté, J.S., 2007. On the origin of 24-norcholestanes and their use as age-diagnostic biomarkers. Geology 35, 419–422.

Rashby, S.E., Sessions, A.L., Summons, R.E., Newman, D.K., 2007. Biosynthesis of 2-methylbacteriohopanepolyols by an anoxygenic phototroph. Proceedings of the National Academy of Sciences 104, 15099–15104.

Ren, L., Lin, G., Zhao, Z., Wang, X., 2000. Early Tertiary marine transgression in Dongpu Depression. Acta Palaeontologica Sinica 39, 557–570.

Riboulleau, A., Schnyder, J., Riquier, L., Lefebvre, V., Baudin, F., Deconinck, J.-F., 2007. Environmental change during the Early Cretaceous in the Purbeck-type Durlston Bay section (Dorset, Southern England): A biomarker approach. Organic Geochemistry 38, 1804–1823.

Robinson, N., Eglinton, G., Brassell, S.C., Cranwell, P.A., 1984. Dinoflagellate origin for sedimentary 4α-methylsteroids and 5α (H)-stanols. Nature 308, 439–442.

Rohrssen, M., Gill, B.C., Love, G.D., 2015. Scarcity of the $C_{30}$ sterane biomarker, 24-*n*-propylcholestane, in lower Paleozoic marine paleoenvironments. Organic Geochemistry 80, 1–7.

Rontani, J.-F., Volkman, J.K., 2003. Phytol degradation products as biogeochemical tracers in aquatic environments. Organic Geochemistry 34, 1–35.

Schnepf, E., Elbrächter, M., 1992. Nutritional strategies in dinoflagellates: a review with emphasis on cell biological aspects. European Journal of Protistology 28, 3–24.

Schwark, L., Frimmel, A., 2004. Chemostratigraphy of the Posidonia black shale, SW-Germany: II. Assessment of extent and persistence of photic-zone anoxia using aryl isoprenoid distributions. Chemical Geology 206, 231–248.

Scotese, C.R., 2001. The plate tectonic reconstructions. PALEOMAP Project. http://www.scotese.com/newpage9.htm

Silliman, J.E., Meyers, P.A., Bourbonniere, R.A., 1996. Record of postglacial organic matter delivery and burial in sediments of Lake Ontario. Organic Geochemistry 24, 463–472.

Sinninghe Damsté, J.S., Rijpstra, W.I.C., Kock-van Dalen, A.C., De Leeuw, J.W., Schenck, P.A., 1989. Quenching of labile functionalised lipids by inorganic sulphur species: evidence for the formation of sedimentary organic sulphur compounds at the early stages of diagenesis. Geochimica et Cosmochimica Acta 53, 1343–1355.

Sinninghe Damsté, J.S., de Leeuw, J.W., 1990. Analysis, structure and geochemical significance of organically-bound sulphur in the geosphere: State of the art and future research. Organic Geochemistry 16, 1077–1101.

Sinninghe Damsté, J.S., Kenig, F., Koopmans, M.P., Köster, J., Schouten, S., Hayes, J., de Leeuw, J.W., 1995. Evidence for gammacerane as an indicator of water column stratification. Geochimica et Cosmochimica Acta 59, 1895–1900.

Sinninghe Damsté, J.S., Schouten, S., 1997. Is there evidence for a substantial contribution of prokaryotic biomass to organic carbon in Phanerozoic carbonaceous sediments? Organic Geochemistry 26, 517–530.

Summons, R.E., Thomas, J., Maxwell, J.R., Boreham, C.J., 1992. Secular and environmental constraints on the occurrence of dinosterane in sediments. Geochimica et Cosmochimica Acta 56, 2437–2444.

Summons, R.E., 1993. Biogeochemical cycles, Organic Geochemistry. Springer, pp. 3–21.

Summons, R.E., Jahnke, L.L., Hope, J.M., Logan, G.A., 1999. 2-Methylhopanoids as biomarkers for cyanobacterial oxygenic photosynthesis. Nature 400, 554–557.

Tang, X., 1993. Calcareous Nannofossil paleoecology and depositional environment of Shahejie Formation in Bohaiwan basin. Marine Geology & Quaternary Geology 13, 41–45.

Tegelaar, E.W., Matthezing, R.M., Jansen, J.B.H., Horsfield, B., De Leeuw, J.W., 1989. Possible origin of *n*-alkanes in high-wax crude oils. Nature 342, 529–531.

ten Haven, H.L., De Leeuw, J.W., Rullkötter, J., Sinninghe Damsté, J.S., 1987. Restricted utility of the pristane/phytane ratio as a palaeoenvironmental indicator. Nature 330, 641–643.

Tissot, B.P., Welte, D.H., 1984. From kerogen to petroleum, in: Tissot, B.P., Welte, D.H. (Eds.), Petroleum formation and occurrence, 2nd Edition. Springer, Berlin Heidelberg, pp. 160–198.

van Mooy, B.A.S., Keil, R.G., Devol, A.H., 2002. Impact of suboxia on sinking particulate organic carbon: Enhanced carbon flux and preferential degradation of amino acids via denitrification. Geochimica et Cosmochimica Acta 66, 457–465.

Volkman, J.K., Maxwell, J.R., 1986. Acyclic isoprenoids as biological markers. Methods in Geochemistry and Geophysics 24, 1–42.

Volkman, J.K., Kearney, P., Jeffrey, S.W., 1990. A new source of 4-methyl sterols and 5α (H)-stanols in sediments: prymnesiophyte microalgae of the genus Pavlova. Organic Geochemistry 15, 489–497.

Volkman, J.K., Barrett, S.M., Dunstan, G.A., Jeffrey, S.W., 1993. Geochemical significance of the occurrence of dinosterol and other 4-methyl sterols in a marine diatom. Organic Geochemistry 20, 7–15.

Volkman, J.K., Barrett, S.M., Blackburn, S.I., Mansour, M.P., Sikes, E.L., Gelin, F., 1998. Microalgal biomarkers: A review of recent research developments. Organic Geochemistry 29, 1163–1179.

Volkman, J.K., 2003. Sterols in microorganisms. Applied Microbiology and Biotechnology 60, 495-506.

Volkman, J.K., 2005. Sterols and other triterpenoids: source specificity and evolution of biosynthetic pathways. Organic Geochemistry 36, 139–159.

Volkman, J.K., 2006. Lipid markers for marine organic matter, in: Volkman, J.K. (Ed.), Marine organic matter: Biomarkers, isotopes and DNA. Springer, pp. 27–70.

Volkman, J.K., Revill, A.T., Holdsworth, D.G., Fredericks, D., 2008. Organic matter sources in an enclosed coastal inlet assessed using lipid biomarkers and stable isotopes. Organic Geochemistry 39, 689–710.

Wang, D., Lu, S., Han, S., Sun, X., Quan, C., 2013a. Eocene prevalence of monsoon-like climate over Eastern China reflected by hydrological dynamics. Journal of Asian Earth Sciences 62, 776–787.

Wang, G., Wang, T.G., Simoneit, B.R.T., Chen, Z., Zhang, L., Xu, J., 2008. The distribution of molecular fossils derived from dinoflagellates in Paleogene lacustrine sediments (Bohai Bay Basin, China). Organic Geochemistry 39, 1512–1521.

Wang, G., Li, S., Wang, T., Zhang, L., 2010. Applications of molecular fossils in lacustrine stratigraphy. Chinese Journal of Geochemistry 29, 15–20.

Wang, G., Wang, T.G., Simoneit, B.R.T., Zhang, L., 2013b. Investigation of hydrocarbon biodegradation from a downhole profile in Bohai Bay Basin: Implications for the origin of 25-norhopanes. Organic Geochemistry 55, 72–84.

Wang, G., Chang, X., Wang, T.G., Simoneit, B.R.T., 2015. Pregnanes as molecular indicators for depositional environments of sediments and petroleum source rocks. Organic Geochemistry 78, 110–120.

Wang, Y.H., 1983. Discovery and primary study of glauconite in modern lacustrine sediments from Fuxian Lake. Chinese Science Bulletin 28, 1388–1392.

Welander, P.V., Coleman, M.L., Sessions, A.L., Summons, R.E., Newman, D.K., 2010. Identification of a methylase required for 2-methylhopanoid production and implications for the interpretation of sedimentary hopanes. Proceedings of the National Academy of Sciences of the United States of America 107, 8537–8342.

Welander, P.V., Doughty, D.M., Wu, C.H., Mehay, S., Summons, R.E., Newman, D.K., 2012. Identification and characterization of *Rhodopseudomonas palustris* TIE-1 hopanoid biosynthesis mutants. Geobiology 10, 163–177.

Withers, N., 1983. Dinoflagellate sterols, in: Scheuer, P.J. (Ed.), Marine Natural Products: Chemical and Biological Perspectives. Academic Press, New York, pp. 87–130.

Xie, S., Pancost, R.D., Yin, H., Wang, H., Evershed, R.P., 2005. Two episodes of microbial change coupled with Permo/Triassic faunal mass extinction. Nature 434, 494–497.

Xie, S., Pancost, R.D., Huang, J., Wignall, P.B., Yu, J.Z., Tang, X., Chen, L., Huang, X., Lai, X., 2007. Changes in the global carbon cycle occurred as two episodes during the Permian-Triassic crisis. Geology 35, 1083–1086.

Xiong, Y., Wang, Y., Wang, Y., Xu, S., 2007. Compound-specific C- and H-isotope compositions of enclosed organic matter in carbonate rocks: Implications for source identification of sedimentary organic matter and paleoenvironmental reconstruction. Applied Geochemistry 22, 2553–2565.

Yang, J., 2000. Storm deposits in the upper Sha-3 member of Eogene system in western central uplift belt of Huimin Depression. Journal of China University of Petroleum (Natural Science Edition) 24, 26–29.

Yuan, B., Chen, S., Yuan, W., Zhu, J., 2008a. Characteristics of strontium and sulfur isotopes in Shahejie Formation of Jiyang Depression. Journal of Jilin University (Earth Science Edition) 38, 613–617. (in Chinese).

Yuan, J., 2006. The sedimentary characteristics and models of Paleogene tempestites in Huimin Sag, Shandong Province. Acta Sedimentologica Sinica 24, 43–49.

Yuan, W., Chen, S., Zeng, C., 2005. Research development and prospects on Paleogene sea transgression in Bohai Bay Basin. Acta Sedimentologica Sinica 23, 604–612. (in Chinese).

Yuan, W., Chen, S., Zeng, C., 2006. Study on marine transgression of Paleogene Shahejie Formation in Jiyang Depression. Acta Petrolei Sinica 27, 40–49. (in Chinese).

Yuan, W., Chen, S., Zeng, C., 2008b. Characteristic of dinosterane and $C_{31}$ sterane in Paleocene saline Formation of Jiyang Depression. Acta Sedimentologica Sinica 26, 683–687. (in Chinese).

Zerkle, A.L., Farquhar, J., Johnston, D.T., Cox, R.P., Canfield, D.E., 2009. Fractionation of multiple sulfur isotopes during phototrophic oxidation of sulfide and elemental sulfur by a green sulfur bacterium. Geochimica et Cosmochimica Acta 73, 291–306.

Zhang, L., 2008. The progress on the study of lacustrine source rocks. Petroleum Geology & Experiment 30, 591–595.

Zhang, L., Liu, Q., Zhu, R., Li, Z., Lu, X., 2009. Source rocks in Mesozoic-Cenozoic continental rift basins, East China: A case from Dongying Depression, Bohai Bay Basin. Organic Geochemistry 40, 229–242.

Zhang, T., Zhang, M., Bai, B., Wang, X., Li, L., 2008. Origin and accumulation of carbon dioxide in the Huanghua depression, Bohai Bay Basin, China. AAPG Bulletin 92, 341–358.

Zhang, Z., Zhao, M., Yang, X., Wang, S., Jiang, X., Oldfield, F., Eglinton, G., 2004. A hydrocarbon biomarker record for the last 40 kyr of plant input to Lake Heqing, southwestern China. Organic Geochemistry 35, 595–613.

Zhu, D., Jin, Z., Hu, W., Song, Y., Gao, X., 2007. Effect of igneous activity on hydrocarbon source rocks in Jiyang Sub-basin, Eastern China. Journal of Petroleum Science and Engineering 59, 309–320.

# Tables

Table 2.1 Organic geochemical parameters of the investigated Paleogene lacustrine core samples from the Dongying Depression, Bohai Bay Basin.

| Sample Name | Sag | Well | Formation | Depth (m) | C% | N% | C/N | EOM (mg/g) | Pr/Ph | Pr/*n*-$C_{17}$ | Ph/*n*-$C_{18}$ | $CPI_{22-32}$ |
|---|---|---|---|---|---|---|---|---|---|---|---|---|
| FA01 | Boxing | FA107 | Es3M | 3171.00 | 5.0 | 0.5 | 9.5 | 5.9 | 1.43 | 0.55 | 0.43 | 1.03 |
| FA02 | Boxing | FA101 | Es3L | 3282.44 | 5.5 | 0.5 | 10.9 | 5.9 | 1.02 | 0.50 | 0.49 | 1.00 |
| FA03 | Boxing | FA137 | Es3L | 2847.60 | 1.1 | 0.8 | 1.4 | 2.4 | 1.52 | 0.81 | 0.58 | 1.05 |
| FA04 | Boxing | FA137 | Es4U | 3166.40 | 0.3 | 0.2 | 1.4 | 0.6 | 0.88 | 0.54 | 1.03 | 1.08 |
| FA05 | Boxing | FA137 | Es4U | 3259.52 | 4.4 | 0.2 | 22.1 | 3.8 | 0.44 | 1.07 | 2.77 | 1.01 |
| CH01 | Boxing | CH372 | Es4U | 2571.50 | 6.1 | 0.4 | 14.9 | 6.3 | 0.42 | 0.99 | 2.44 | 0.87 |
| CH02 | Boxing | CH372 | Es4U | 2573.50 | nd | nd | nd | nd | 0.80 | 1.86 | 2.19 | 1.00 |
| CH03 | Boxing | CH372 | Es4U | 2583.00 | 7.4 | 0.3 | 23.0 | 15.0 | 0.34 | 1.63 | 4.33 | 0.83 |
| H01 | Niuzhuang | H130 | Es3L | 3222.00 | 3.6 | 0.5 | 7.1 | 7.6 | 0.99 | 0.53 | 0.52 | 1.12 |
| H02 | Niuzhuang | H130 | Es3L | 3235.25 | 5.9 | 0.7 | 8.8 | 11.3 | 1.05 | 0.48 | 0.56 | 1.11 |
| N01 | Niuzhuang | N28 | Es3L | 3282.43 | 1.9 | 0.5 | 4.0 | 4.0 | 1.24 | 0.67 | 0.63 | 1.14 |
| L01 | Niuzhuang | L110 | Es4U | 2747.70 | 13.5 | 0.6 | 22.5 | 5.7 | 1.53 | 2.31 | 2.13 | 1.09 |
| L02 | Niuzhuang | L110 | Es4U | 2752.10 | nd | nd | nd | nd | 1.06 | 1.66 | 1.66 | 0.97 |
| L03 | Niuzhuang | L110 | Es4U | 2767.50 | 4.0 | 0.3 | 12.0 | 5.5 | 0.70 | 1.24 | 2.37 | 1.02 |
| L04 | Niuzhuang | L110 | Es4U | 2770.40 | nd | nd | nd | nd | 0.63 | 1.88 | 3.57 | 1.06 |
| L05 | Niuzhuang | L110 | Es4U | 2779.80 | 6.2 | 0.4 | 14.6 | 7.8 | 0.80 | 1.19 | 1.47 | 0.95 |
| L06 | Niuzhuang | L110 | Es4U | 2897.80 | nd | nd | nd | nd | 0.34 | 1.35 | 3.11 | 0.89 |
| FE01 | Minfeng | FE112 | Es3M | 3116.80 | 4.7 | 0.5 | 9.9 | nd | 0.89 | 0.51 | 0.59 | 1.33 |
| FE02 | Minfeng | FE112 | Es3M | 3120.00 | nd | nd | nd | nd | 0.95 | 0.71 | 0.78 | 1.23 |
| FE03 | Minfeng | FE112 | Es3M | 3122.00 | 14.3 | 0.7 | 21.7 | 17.2 | 1.04 | 1.23 | 1.39 | 1.18 |
| FE04 | Minfeng | FE112 | Es3M | 3122.00 | 14.9 | 0.7 | 22.4 | 19.9 | 1.03 | 0.78 | 0.87 | 1.20 |
| FE05 | Minfeng | FE112 | Es3M | 3123.40 | nd | nd | nd | nd | 1.28 | 1.09 | 0.99 | 1.19 |
| FE06 | Minfeng | FE112 | Es3M | 3124.90 | 5.7 | 0.5 | 10.9 | nd | 0.95 | 1.30 | 1.41 | 1.17 |
| FE07 | Minfeng | FE112 | Es3M | 3134.10 | 4.7 | 0.6 | 8.3 | nd | 1.05 | 0.90 | 1.01 | 1.26 |
| FE08 | Minfeng | FE112 | Es3M | 3135.80 | 5.2 | 0.5 | 11.3 | 7.0 | 1.20 | 0.68 | 0.74 | 1.24 |
| FE09 | Minfeng | FE112 | Es3M | 3137.90 | 10.2 | 0.5 | 19.8 | nd | 1.21 | 0.59 | 0.60 | 1.17 |
| FE10 | Minfeng | FE112 | Es3L | 3337.70 | nd | nd | nd | 5.8 | 0.65 | 0.88 | 1.35 | 1.15 |
| FE11 | Minfeng | FE112 | Es3L | 3340.20 | nd | nd | nd | nd | 0.50 | 0.99 | 2.14 | 1.05 |
| FE12 | Minfeng | FE112 | Es3L | 3340.50 | 7.3 | 0.7 | 10.0 | 29.2 | 0.43 | 1.08 | 2.14 | 1.05 |
| FE13 | Minfeng | FE112 | Es3L | 3341.00 | nd | nd | nd | 12.2 | 0.42 | 1.08 | 2.23 | 1.06 |
| FE14 | Minfeng | FE112 | Es3L | 3341.40 | 10.0 | 0.7 | 14.4 | nd | 0.47 | 1.05 | 2.17 | 1.06 |
| FE15 | Minfeng | FE112 | Es3L | 3341.50 | nd | nd | nd | nd | 0.38 | 1.05 | 2.97 | 1.01 |
| FE16 | Minfeng | FE112 | Es4U | 3430.68 | 6.2 | 0.7 | 9.0 | 11.4 | 0.52 | 0.69 | 1.35 | 1.02 |
| FS01 | Minfeng | FS1 | Es3L | 3217.93 | 2.5 | 0.6 | 3.9 | 4.2 | 1.00 | 0.48 | 0.61 | 1.09 |
| FS02 | Minfeng | FS1 | Es4U | 3690.40 | 4.3 | 0.8 | 5.4 | 3.6 | 0.71 | 0.24 | 0.42 | 1.04 |
| T01 | Minfeng | T73 | Es3L | 3158.00 | 3.7 | 0.5 | 6.8 | 12.1 | 0.64 | 0.90 | 1.44 | 1.06 |
| T02 | Minfeng | T73 | Es4U | 3269.38 | 5.3 | 0.5 | 10.2 | 14.6 | 0.70 | 0.93 | 1.39 | 1.05 |
| T03 | Minfeng | T73 | Es4U | 3341.66 | 3.0 | 0.5 | 6.6 | 9.5 | 0.46 | 0.84 | 1.58 | 0.99 |

Table 2.1 (*continued*)

| $CPI_{26-32}$ | $\beta/C_{20}$ (%) | TAR | $\Sigma n$-$C_{15-19}$ (%) | $\Sigma n$-$C_{21-25}$ (%) | $\Sigma n$-$C_{27-31}$ (%) | $C_{27}$ αα α 20R % | $C_{28}$ αα α 20R % | $C_{29}$ αα α 20R % | $C_{29}$ 20S | $C_{29}$ αββ | D/S | Ts/ (Ts+Tm) |
|---|---|---|---|---|---|---|---|---|---|---|---|---|
| 1.03 | 3.1 | 0.63 | 26 | 30 | 16 | 37 | 26 | 37 | 0.45 | 0.43 | 0.34 | 0.43 |
| 1.01 | 2.8 | 0.78 | 25 | 28 | 20 | 40 | 28 | 31 | 0.44 | 0.50 | 0.40 | 0.49 |
| 1.04 | 0.0 | 0.41 | 32 | 31 | 13 | 36 | 27 | 37 | 0.42 | 0.30 | 0.52 | 0.37 |
| 1.13 | 1.9 | 0.28 | 49 | 16 | 13 | 26 | 27 | 47 | 0.44 | 0.53 | 0.83 | 0.57 |
| 1.01 | 23.7 | 0.39 | 32 | 21 | 13 | 21 | 30 | 49 | 0.43 | 0.52 | 0.40 | 0.43 |
| 0.85 | 4.4 | 2.85 | 12 | 17 | 40 | 35 | 26 | 39 | 0.18 | 0.18 | 0.05 | 0.31 |
| 0.99 | 7.0 | 2.43 | 15 | 25 | 37 | 37 | 32 | 31 | 0.18 | 0.19 | 0.03 | 0.32 |
| 0.81 | 18.9 | 3.04 | 10 | 24 | 35 | 40 | 26 | 34 | 0.24 | 0.24 | 0.15 | 0.29 |
| 1.15 | 1.3 | 1.08 | 22 | 29 | 23 | 44 | 23 | 33 | 0.49 | 0.57 | 0.93 | 0.55 |
| 1.11 | 2.5 | 0.75 | 27 | 25 | 20 | 38 | 26 | 36 | 0.48 | 0.49 | 0.50 | 0.48 |
| 1.15 | 0.9 | 0.58 | 29 | 29 | 16 | 38 | 25 | 37 | 0.41 | 0.40 | 0.45 | 0.49 |
| 1.11 | 3.8 | 0.32 | 34 | 26 | 11 | 42 | 21 | 37 | 0.16 | 0.20 | 0.10 | 0.31 |
| 0.90 | 2.8 | 1.69 | 17 | 33 | 31 | 30 | 23 | 47 | 0.13 | 0.21 | 0.09 | 0.25 |
| 0.99 | 11.1 | 1.18 | 22 | 27 | 27 | 28 | 30 | 42 | 0.12 | 0.21 | 0.12 | 0.35 |
| 1.03 | 26.9 | 2.05 | 16 | 22 | 35 | 35 | 23 | 42 | 0.14 | 0.20 | 0.05 | 0.25 |
| 0.91 | 6.1 | 2.39 | 13 | 29 | 35 | 34 | 26 | 41 | 0.13 | 0.20 | 0.09 | 0.30 |
| 0.86 | 11.4 | 0.86 | 22 | 37 | 19 | 37 | 29 | 35 | 0.33 | 0.25 | 0.09 | 0.23 |
| 1.31 | 4.9 | 1.83 | 17 | 33 | 28 | 40 | 26 | 34 | 0.25 | 0.25 | 0.19 | 0.29 |
| 1.26 | 2.3 | 1.40 | 20 | 29 | 26 | 49 | 20 | 31 | 0.25 | 0.22 | 0.22 | 0.30 |
| 1.22 | 5.1 | 0.65 | 32 | 25 | 19 | 55 | 18 | 26 | 0.24 | 0.25 | 0.16 | 0.36 |
| 1.23 | 2.4 | 0.70 | 28 | 27 | 19 | 55 | 19 | 26 | 0.28 | 0.21 | 0.09 | 0.26 |
| 1.23 | 4.6 | 0.67 | 31 | 25 | 19 | 59 | 13 | 28 | 0.28 | 0.26 | 0.14 | 0.42 |
| 1.22 | 3.4 | 0.82 | 29 | 30 | 21 | 58 | 14 | 28 | 0.27 | 0.24 | 0.16 | 0.38 |
| 1.32 | 4.0 | 0.99 | 26 | 27 | 24 | 44 | 23 | 33 | 0.26 | 0.26 | 0.18 | 0.35 |
| 1.27 | 4.1 | 0.78 | 29 | 27 | 20 | 40 | 22 | 38 | 0.29 | 0.27 | 0.14 | 0.32 |
| 1.17 | 1.5 | 0.76 | 28 | 31 | 20 | 43 | 21 | 36 | 0.31 | 0.20 | 0.12 | 0.26 |
| 1.19 | 3.7 | 2.16 | 17 | 26 | 34 | 28 | 23 | 48 | 0.44 | 0.33 | 0.29 | 0.38 |
| 1.05 | 7.3 | 1.37 | 20 | 29 | 28 | 30 | 25 | 46 | 0.49 | 0.33 | 0.15 | 0.34 |
| 1.06 | 10.1 | 2.57 | 13 | 30 | 34 | 26 | 34 | 40 | 0.34 | 0.34 | 0.17 | 0.34 |
| 1.09 | 6.8 | 2.54 | 13 | 31 | 33 | 29 | 25 | 46 | 0.46 | 0.33 | 0.14 | 0.33 |
| 1.08 | 6.4 | 1.86 | 17 | 31 | 31 | 29 | 25 | 46 | 0.45 | 0.32 | 0.15 | 0.36 |
| 0.98 | 10.5 | 0.60 | 28 | 35 | 16 | 28 | 28 | 44 | 0.44 | 0.32 | 0.20 | 0.40 |
| 1.03 | 5.5 | 0.98 | 25 | 29 | 23 | 26 | 29 | 45 | 0.51 | 0.40 | 0.33 | 0.47 |
| 1.10 | 1.8 | 0.74 | 28 | 27 | 20 | 35 | 32 | 33 | 0.42 | 0.37 | 0.36 | 0.40 |
| 1.06 | 1.2 | 0.53 | 31 | 24 | 16 | 23 | 24 | 53 | 0.50 | 0.48 | 0.44 | 0.68 |
| 1.06 | 5.4 | 1.22 | 21 | 30 | 25 | 30 | 27 | 43 | 0.46 | 0.41 | 0.41 | 0.37 |
| 1.08 | 4.8 | 1.64 | 18 | 29 | 29 | 26 | 22 | 52 | 0.48 | 0.42 | 0.45 | 0.47 |
| 0.99 | 7.0 | 0.76 | 27 | 30 | 19 | 34 | 32 | 34 | 0.48 | 0.61 | 0.94 | 0.79 |

Table 2.1 (*continued*)

| 35/ (35+34) | O/H | G/H | (19+20) /23 | 23/21 | St/H | 28/29 | 2-MHP index | 32MHP % | HPI | Dino | DBT/P | AIR | Iso/$C_{18}$ |
|---|---|---|---|---|---|---|---|---|---|---|---|---|---|
| 0.38 | 0.03 | 0.08 | 0.71 | 1.14 | 0.15 | 0.71 | 0.6 | 1.9 | 0.54 | 233 | 0.07 | 5.0 | 4.2 |
| 0.42 | 0.04 | 0.06 | 0.85 | 1.16 | 0.36 | 0.91 | 1.2 | 3.1 | 0.33 | 100 | 0.07 | 3.1 | 6.4 |
| 0.48 | 0.23 | 0.09 | 1.34 | 0.92 | 0.45 | 0.74 | 1.8 | 3.2 | 0.70 | 42 | 0.04 | 3.7 | nd |
| 0.43 | 0.26 | 0.39 | 3.26 | 0.51 | 1.12 | 0.58 | 3.9 | 8.4 | 0.92 | 185 | 0.02 | 4.9 | nd |
| 0.50 | 0.29 | 1.97 | 0.58 | 1.30 | 12.1 | 0.60 | 3.7 | 2.4 | 0.18 | 313 | 0.005 | nd | nd |
| 0.57 | 0.10 | 0.53 | 0.55 | 1.92 | 2.70 | 0.66 | 1.0 | 2.2 | 3.10 | 4240 | 0.45 | 5.2 | 1.9 |
| 0.66 | 0.15 | 0.53 | 0.14 | 2.86 | 6.96 | 1.02 | nd | nd | 4.10 | 5568 | 0.39 | nd | nd |
| 0.59 | 0.06 | 0.41 | 0.42 | 1.88 | 4.22 | 0.76 | 3.4 | 9.7 | 2.88 | 1536 | 0.27 | nd | nd |
| 0.36 | 0.03 | 0.06 | 0.70 | 1.29 | 0.24 | 0.68 | 0.7 | 1.5 | 0.28 | 76 | 0.09 | 3.8 | 2.0 |
| 0.37 | 0.02 | 0.05 | 0.67 | 1.38 | 0.23 | 0.73 | 1.6 | 2.3 | 0.32 | 103 | 0.11 | 2.0 | 5.0 |
| 0.41 | 0.02 | 0.04 | 0.76 | 1.46 | 0.15 | 0.67 | 0.4 | 1.4 | 0.44 | 70 | 0.05 | 4.0 | 1.5 |
| 0.49 | 0.07 | 0.19 | 0.97 | 1.13 | 0.61 | 0.57 | 0.7 | 1.1 | 2.62 | 4993 | 0.29 | 9.0 | 1.7 |
| 0.46 | 0.07 | 0.09 | 1.05 | 0.67 | 1.15 | 0.50 | 1.5 | 2.9 | 2.69 | 2421 | 0.10 | nd | nd |
| 0.50 | 0.09 | 0.38 | 0.54 | 1.51 | 1.54 | 0.73 | 1.0 | 1.3 | 5.26 | 2417 | 0.23 | 3.8 | 3.8 |
| 0.53 | 0.07 | 0.27 | 0.34 | 1.85 | 2.50 | 0.56 | 1.0 | 1.3 | 3.68 | 3057 | 0.14 | nd | nd |
| 0.45 | 0.09 | 0.11 | 0.52 | 1.14 | 2.35 | 0.63 | 1.8 | 0.9 | 0.63 | 5053 | 0.31 | 3.2 | 3.5 |
| 0.64 | 0.08 | 2.50 | 0.22 | 2.19 | 10.8 | 0.82 | nd | nd | 1.82 | 1574 | 0.12 | nd | nd |
| 0.39 | 0.04 | 0.05 | 0.16 | 1.66 | 0.67 | 0.76 | 1.0 | 3.5 | 1.03 | 341 | 0.11 | 3.2 | nd |
| 0.35 | 0.03 | 0.06 | 0.73 | 1.40 | 0.47 | 0.66 | 0.7 | 1.4 | 1.06 | 212 | 0.07 | 5.0 | 2.8 |
| 0.35 | 0.03 | 0.06 | 0.50 | 1.47 | 0.28 | 0.70 | 10.0 | 34.5 | 1.13 | 787 | 0.15 | 3.6 | 24.3 |
| 0.38 | 0.03 | 0.09 | 0.63 | 1.40 | 0.39 | 0.73 | 1.1 | 2.7 | 0.93 | 931 | 0.15 | 4.0 | 49.2 |
| 0.34 | 0.03 | 0.09 | 0.47 | 1.48 | 0.41 | 0.47 | 0.5 | 2.2 | 1.54 | 1252 | 0.07 | 2.4 | 14.4 |
| 0.33 | 0.03 | 0.06 | 0.32 | 1.69 | 0.30 | 0.49 | 9.9 | 37.5 | 1.66 | 964 | 0.11 | 2.1 | 25.3 |
| 0.38 | 0.02 | 0.08 | 0.30 | 1.81 | 0.49 | 0.70 | 0.4 | 1.5 | 1.21 | 704 | 0.15 | 2.4 | 71.1 |
| 0.38 | 0.04 | 0.05 | 0.71 | 1.48 | 0.37 | 0.58 | 0.4 | 1.1 | 1.07 | 474 | 0.17 | 3.1 | 4.2 |
| 0.45 | 0.03 | 0.04 | 0.56 | 1.37 | 0.39 | 0.59 | 0.5 | 1.4 | 1.30 | 565 | 0.28 | 2.9 | 10.2 |
| 0.31 | 0.06 | 0.12 | 0.52 | 1.21 | 0.56 | 0.48 | 1.5 | 2.5 | 0.65 | 667 | 0.04 | 2.4 | 3.7 |
| 0.38 | 0.04 | 0.17 | 0.56 | 1.26 | 1.22 | 0.54 | 1.2 | 1.7 | 0.86 | 978 | 0.04 | 0.7 | 0.0 |
| 0.41 | 0.05 | 0.17 | 0.47 | 1.40 | 1.13 | 0.87 | 1.2 | 3.0 | 0.77 | 791 | 0.06 | 1.1 | 43.5 |
| 0.37 | 0.04 | 0.16 | 0.49 | 1.28 | 1.41 | 0.55 | 1.2 | 2.4 | 0.75 | 1136 | 0.06 | 0.8 | 11.4 |
| 0.37 | 0.03 | 0.17 | 0.69 | 1.23 | 1.35 | 0.54 | 1.5 | 2.0 | 0.78 | 973 | 0.04 | nd | nd |
| 0.37 | 0.05 | 0.21 | 0.50 | 1.16 | 2.20 | 0.63 | 1.2 | 1.4 | 0.72 | 243 | 0.04 | 1.9 | nd |
| 0.36 | 0.04 | 0.33 | 0.64 | 1.20 | 1.93 | 0.63 | 2.6 | 4.3 | 0.55 | 472 | 0.02 | 2.4 | 5.8 |
| 0.36 | 0.05 | 0.05 | 1.06 | 1.27 | 0.24 | 0.97 | 2.3 | 2.3 | 1.02 | 50 | 0.02 | nd | nd |
| 0.38 | 0.07 | 0.19 | 1.69 | 0.89 | 1.35 | 0.44 | 2.1 | 4.2 | 0.29 | 314 | 0.01 | nd | nd |
| 0.39 | 0.06 | 0.23 | 0.82 | 1.24 | 0.98 | 0.61 | 1.7 | 1.9 | 0.99 | 269 | 0.06 | 2.1 | 2.9 |
| 0.36 | 0.05 | 0.18 | 0.78 | 1.15 | 0.77 | 0.42 | 1.5 | 2.4 | 1.14 | 296 | 0.02 | 1.9 | 2.4 |
| 0.52 | 0.35 | 1.45 | 1.03 | 1.19 | 12.6 | 0.95 | 2.8 | 4.1 | 0.48 | 42 | 0.05 | 1.1 | 1.2 |

EOM = extractable organic matter; $CPI_{22–32}$ = $2*(C_{23}+C_{25}+C_{27}+C_{29}+C_{31})/(C_{22}+2*C_{24}+2*C_{26}+2*C_{28}+2*C_{30}+C_{32})$ *n*-alkanes; $CPI_{26–32}$ = $2*(C_{27}+C_{29}+C_{31})/(C_{26}+2*C_{28}+2*C_{30}+C_{32})$ *n*-alkanes; $\beta/C_{20}$ (%) = β-carotane/*n*-$C_{20}$ (%); TAR = terrigenous/aquatic ratio, $(C_{27} + C_{29} + C_{31})/(C_{15} + C_{17} + C_{19})$ *n*-alkanes; $\sum n\text{-}C_{15\text{-}19}$ (%) = $\sum n\text{-}C_{15\text{-}19}/\sum n$-alkanes (%); $\sum n\text{-}C_{21\text{-}25}$ (%) = $\sum n\text{-}C_{21\text{-}25}/\sum n$-alkanes (%); $\sum n\text{-}C_{27\text{-}31}$ (%) = $\sum n\text{-}C_{27\text{-}31}/\sum n$-alkanes (%); $C_{29}$ 20S = $C_{29}$ ααα 20S/(20S + 20R) steranes; $C_{29}$ αββ = $C_{29}$ αββ/(αββ + ααα) steranes; D/S = $C_{27}$ βα diasteranes/$C_{27}$ ααα steranes; 35/(35 + 34) = $C_{35}$ αβ hopanes/($C_{35}$ αβ hopanes + $C_{34}$ αβ hopanes); O/H = Oleanane/$C_{30}$ ab hopane; G/H = Gammacerane/$C_{30}$ αβ hopane; (19 + 20)/23 = ($C_{19}$ tricyclic terpane + $C_{20}$ tricyclic terpane)/$C_{23}$ tricyclic terpane; 23/21 = $C_{23}$ tricyclic terpane/$C_{21}$ tricyclic terpane; St/H = $C_{29}$ (ααα + αββ) steranes/$C_{29}$ αβ hopanes (based on areas in m/z 191 and m/z 217); 28/29 = $C_{28}$/$C_{29}$ ααα 20R steranes; 2-MHP index = $C_{31}$ 2α-methylhopane/$C_{30}$ αβ hopanes (based on areas of m/z 205 and 191); 32MHP% = $C_{32}$ 2α-methylhopane/$C_{31}$ αβ hopanes (based on areas in m/z 205 and 191). HPI = ([iHMN + Cadalene + Retene]/1,3,6,7-tetramethylnaphthalene); Dino = Relative abundance of total dinosteranes (P + Q + S + T), normalised to 13β(H),17α(H)-diacholestane 20S, peaks defined in Table 3; DBT/P =

dibenzothiophene/phenanthrene; AIR = $C_{13-17}/C_{18-22}$ monoaryl isoprenoids; Iso/$C_{18}$ = isorenieratane/$C_{18}$ aryl isoprenoid; nd = not determined.

Table 2.2 Selected lipid biomarker parameters from the MRM GC–MS analysis of the investigated Paleogene lacustrine core samples from the Dongying Depression, Bohai Bay Basin.

| Sample Name | Sags | Wells | Formation | Depth | NCR | DSI | 4MSI | TDHI | $C_{29}$ 20S | $C_{30}$% | $C_{30/29}$% |
|---|---|---|---|---|---|---|---|---|---|---|---|
| CH01 | Boxing | CH372 | Es4U | 2571.5 | 0.82 | 0.86 | 0.58 | 0.91 | 0.19 | nd | nd |
| CH03 | Boxing | CH372 | Es4U | 2583.0 | 0.81 | 0.81 | 0.69 | 0.96 | 0.22 | nd | nd |
| H02 | Niuzhuang | H130 | Es3L | 3235.3 | 0.66 | 0.41 | 0.66 | 0.85 | 0.59 | nd | nd |
| N01 | Niuzhuang | N28 | Es3L | 3282.4 | 0.59 | 0.46 | 0.30 | 0.85 | 0.51 | nd | nd |
| L01 | Niuzhuang | L110 | Es4U | 2747.7 | 0.85 | 0.89 | 0.75 | 0.93 | 0.19 | nd | nd |
| L03 | Niuzhuang | L110 | Es4U | 2767.5 | 0.88 | 0.86 | 0.53 | 0.91 | 0.15 | nd | nd |
| L05 | Niuzhuang | L110 | Es4U | 2779.8 | 0.90 | 0.88 | 0.66 | 0.96 | 0.15 | nd | nd |
| FE04 | Minfeng | FE112 | Es3M | 3122.0 | 0.77 | 0.76 | 0.59 | 0.94 | 0.24 | 10.1 | 48.6 |
| FE08 | Minfeng | FE112 | Es3M | 3135.8 | 0.69 | 0.82 | 0.64 | 0.84 | 0.31 | nd | nd |
| FE10 | Minfeng | FE112 | Es3L | 3337.7 | 0.71 | 0.54 | 0.63 | 0.91 | 0.48 | 3.0 | 6.9 |
| FE12 | Minfeng | FE112 | Es3L | 3340.5 | 0.74 | 0.48 | 0.52 | 0.88 | 0.47 | 1.7 | 3.9 |
| FE16 | Minfeng | FE112 | Es4U | 3430.7 | 0.68 | 0.38 | 0.61 | 0.87 | 0.53 | 6.4 | 17.7 |
| FS01 | Minfeng | FS1 | Es3L | 3217.9 | 0.54 | 0.39 | 0.25 | 0.63 | 0.46 | nd | nd |
| FS02 | Minfeng | FS1 | Es4U | 3690.4 | 0.71 | 0.31 | 0.56 | 0.82 | 0.59 | 3.5 | 7.8 |
| T01 | Minfeng | T73 | Es3L | 3158.0 | 0.66 | 0.44 | 0.51 | 0.90 | 0.52 | 2.2 | 5.8 |
| T02 | Minfeng | T73 | Es4U | 3269.4 | 0.76 | 0.37 | 0.52 | 0.90 | 0.55 | 1.9 | 4.2 |

NCR = 24-norcholestane ratio (24-norcholestanes/(24-norcholestanes + 27-norcholestanes)); DSI = dinosterane index (P + Q + T/(P + Q + T + F + I + J), for peak abbreviations see Table 3; 4MSI = 4-methylsterane index (4-methylsteranes/$C_{29}$ regular steranes); TDHI = triaromatic dinosteroid hydrocarbon index (triaromatic dinosteroids/[triaromatic dinosteroids + triaromatic 3-methyl-24-ethylcholestanes]); $C_{29}$ 20S = $C_{29}$ ααα 20S/(20S + 20R) steranes; $C_{30}$% = $C_{30}$/($C_{27}$ + $C_{28}$ + $C_{29}$+$C_{30}$) ααα 20R steranes (%); $C_{30/29}$%=$C_{30}$/$C_{29}$ ααα 20R steranes (%); nd = not determined.

Table 2.3 Peak assignments for steranes, diasteranes, methylsteranes and dinosteranes in the MRM chromatograms in Figs 2.10 and 2.11. Modified after George et al. (2007).

| Peak | Sterane, diasterane and methylsterane peak assignments |
|---|---|
| 1 | 13β(H),17α(H)-24-nordiacholestane (20S) |
| 2 | 13β(H),17α(H)-24-nordiacholestane (20R) |
| 3 | 13β(H),17α(H)-27-nordiacholestane (20S) |
| 4 | 13β(H),17α(H)-27-nordiacholestane (20R) |
| 5 | 5α(H),14α(H),17α(H)-24-norcholestane (20S) |
| 6 | 5α(H),14β(H),17β(H)-24-norcholestane (20R) |
| 7 | 5α(H),14β(H),17β(H)-24-norcholestane (20S) |
| 8 | 5α(H),14α(H),17α(H)-24-norcholestane (20R) |
| 9 | 5α(H),14α(H),17α(H)-21-norcholestane + 5α(H),14β(H),17β(H)-21-norcholestane |
| 10 | 5α(H),14α(H),17α(H)-27-norcholestane (20S) |
| 11 | 5α(H),14β(H),17β(H)-27-norcholestane (20R) |
| 12 | 5α(H),14β(H),17β(H)-27-norcholestane (20S) |
| 13 | 5α(H),14α(H),17α(H)-27-norcholestane (20R) |
| a | 13β(H),17α(H)-diacholestane (20S) |
| b | 13β(H),17α(H)-diacholestane (20R) |
| c | 13α(H),17β(H)-diacholestane (20S) |
| d | 13α(H),17β(H)-diacholestane (20R) |
| e | 5α(H),14α(H),17a(H)-cholestane (20S) |
| f | 5α(H),14β(H),17β(H)-cholestane (20R) |
| g | 5α(H),14β(H),17β(H)-cholestane (20S) |
| h | 5α(H),14α(H),17α(H)-cholestane (20R) |
| i | 24-methyl-13β(H),17α(H)-diacholestane (20S)* |
| j | 24-methyl-13β(H),17α(H)-diacholestane (20R)* |
| k | 24-methyl-13α(H),17β(H)-diacholestane (20S) |
| l | 24-methyl-13α(H),17β(H)-diacholestane (20R)* |
| m | 24-methyl-5α(H),14α(H),17α(H)-cholestane (20S)* |
| n | 24-methyl-5α(H),14β(H),17β(H)-cholestane (20R) |
| o | 24-methyl-5α(H),14β(H),17β(H)-cholestane (20S) |
| p | 24-methyl-5α(H),14α(H),17α(H)-cholestane (20R) |
| q | 24-ethyl-13β(H),17α(H)-diacholestane (20S) |
| r | 24-ethyl-13β(H),17α(H)-diacholestane (20R) |
| s | 24-ethyl-13α(H),17β(H)-diacholestane (20S) |
| t | 24-ethyl-13α(H),17β(H)-diacholestane (20R) |
| u | 24-ethyl-5α(H),14α(H),17a(H)-cholestane (20S) |
| v | 24-ethyl-5α(H),14β(H),17β(H)-cholestane (20R) |
| w | 24-ethyl-5α(H),14β(H),17β(H)-cholestane (20S) |
| x | 24-ethyl-5α(H),14α(H),17a(H)-cholestane (20R) |
| y | 24-n-propyl-13β(H),17a(H)-diacholestane (20S) |
| z | 24-n-propyl-13β(H),17a(H)-diacholestane (20R) |
| A | 24-n-propyl-5α(H),14α(H),17a(H)-cholestane (20S) |
| B | 24-n-propyl-5α(H),14β(H),17β(H)-cholestane (20R) |
| C | 24-n-propyl-5α(H),14β(H),17β(H)-cholestane (20S) |
| D | 24-n-propyl-5α(H),14α(H),17α(H)-cholestane (20R) |
| F | 3β-methyl-24-ethylcholestane (20S) |
| I | 3β-methyl-24-ethylcholestane (14β,17β(H), 20R) |
| J | 3β-methyl-24-ethylcholestane (14β,17β(H), 20S) |
| L | 4α-methyl-24-ethylcholestane (14β,17β(H), 20R) |
| M | 4α-methyl-24-ethylcholestane (14β,17β(H), 20S) |
| N | 2α-methyl-24-ethylcholestane (20R) |
| O | 3β-methyl-24-ethylcholestane (20R) |
| R | 4α-methyl-24-ethylcholestane (20R) |
| P | 4α,23S,24S-trimethylcholestane (20R) (dinosterane) |
| Q | 4α,23S,24R-trimethylcholestane (20R) (dinosterane) |
| S | 4α,23R,24R-trimethylcholestane (20R) (dinosterane) |
| T | 4α,23R,24S-trimethylcholestane (20R) (dinosterane) |

*Isomeric peaks (24S and 24R).

## Supplementary figures and tables

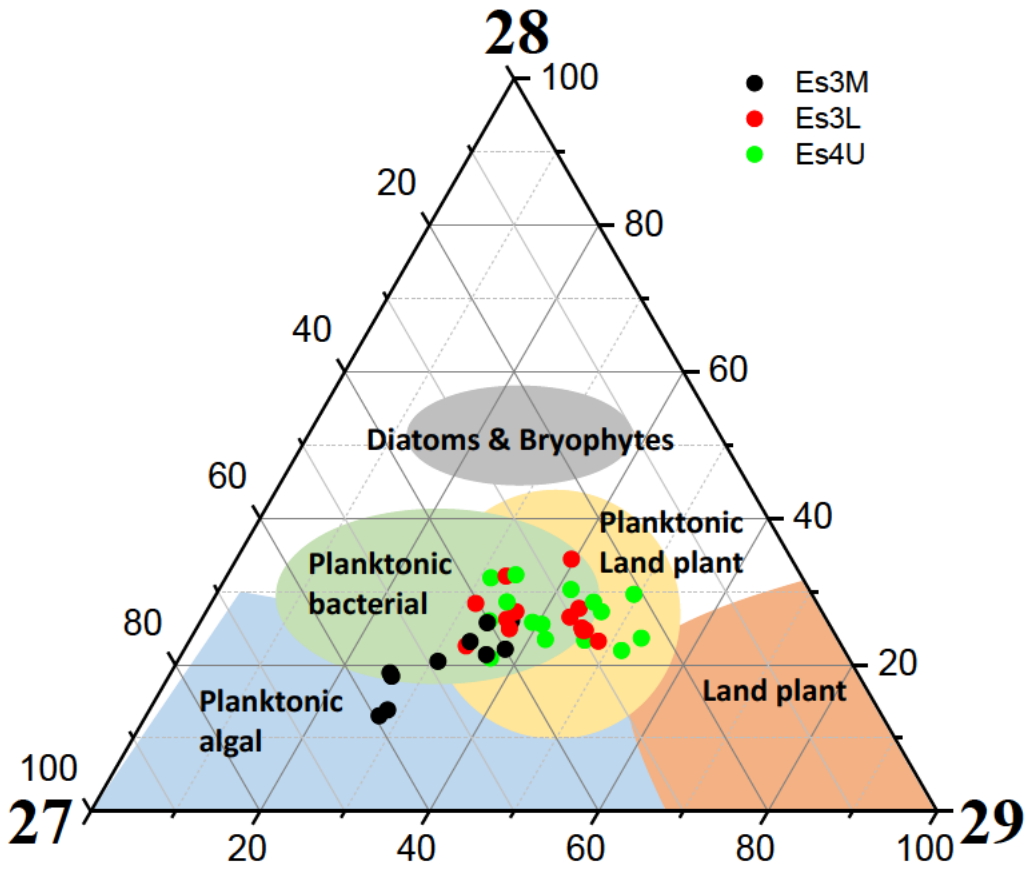


Supplementary Fig. 2.1 Ternary diagram showing the relative abundance of $C_{27}$, $C_{28}$ and $C_{29}$ ααα 20R steranes in the aliphatic fractions of source rock extracts from the Es3M, Es3L and Es4U members of the Shahejie Formation. 27 = $C_{27}$ ααα 20R % (*m/z* 217), 28 = $C_{28}$ ααα 20R % (*m/z* 217), 29 = $C_{29}$ ααα 20R % (*m/z* 217).

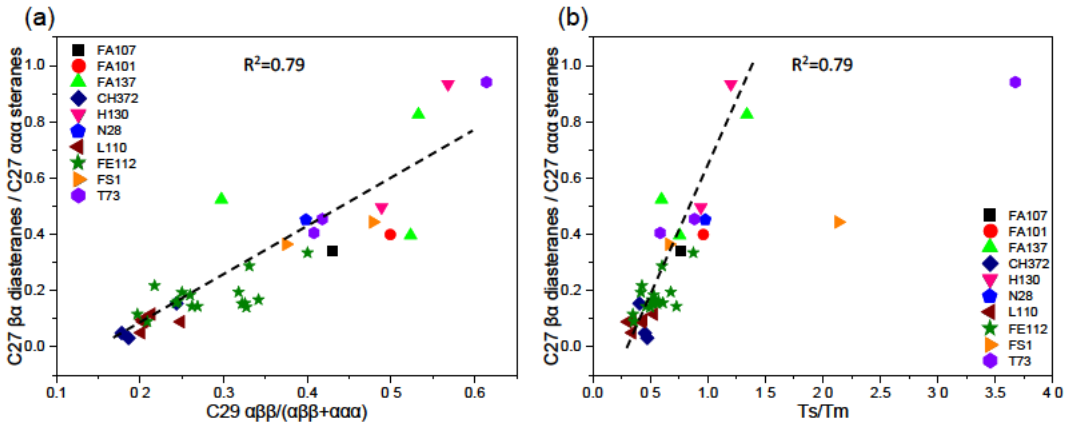


Supplementary Fig. 2.2 Cross-plot of the $C_{27}$ βα diasterane/$C_{27}$ ααα sterane ratio versus maturity parameters (a) $C_{29}$ αββ/(αββ+ααα) steranes, and (b) Ts/Tm, showing good correlation ($R^2$ = 0.79) between the rearrangement of $C_{27}$ steranes and thermal maturation.

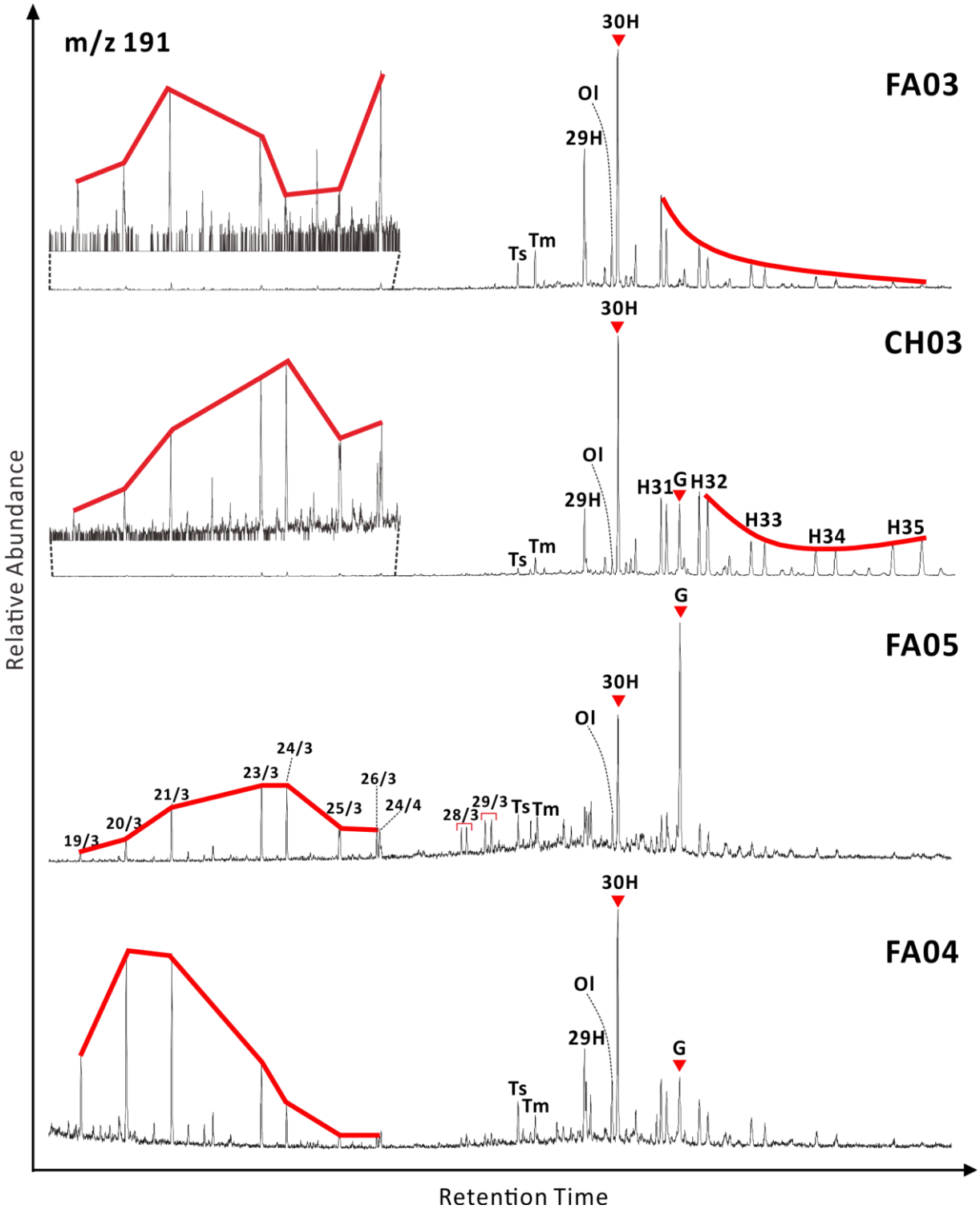


Supplementary Fig. 2.3 Partial *m/z* 191 mass chromatograms, showing the distribution of terpanes in four representative rock samples. The sample codes are given in the right of the figure. Two insets are the expanded parts of the FA03 and CH03 samples. Peak assignments: 19/3 to 29/3 = $C_{19}$-$C_{29}$ tricyclic terpanes, 24/4 = $C_{24}$ tetracyclic terpane, Ts = 18α(H),22,29,30-trisnorneohopane, Tm = 17α(H),22,29,30-trisnorhopane, Ol = oleanane, 30H = $C_{30}$ αβ hopane, 29H = $C_{29}$ αβ hopane, G = gammacerane, H31 to H35 = $C_{31}$–$C_{35}$ αβ homohopanes (S+R).

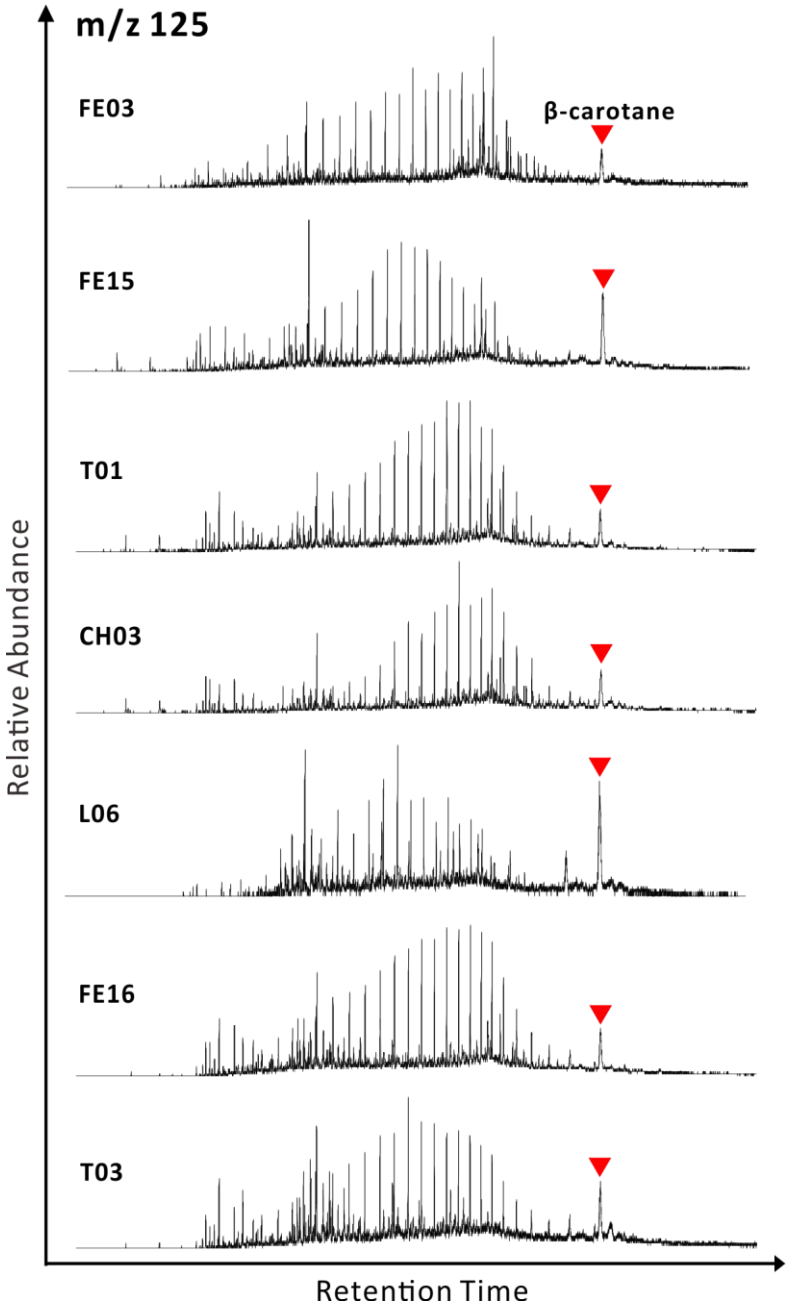


Supplementary Fig. 2.4 Representative *m/z* 125 mass chromatograms, showing the widespread occurrence of β-carotane in aliphatic fractions of the Es3M member sample (e.g. FE03), the Es3L member samples (e.g. FE15 and T01) and the Es4U member samples (e.g. CH03, L06, FE16 and T03).

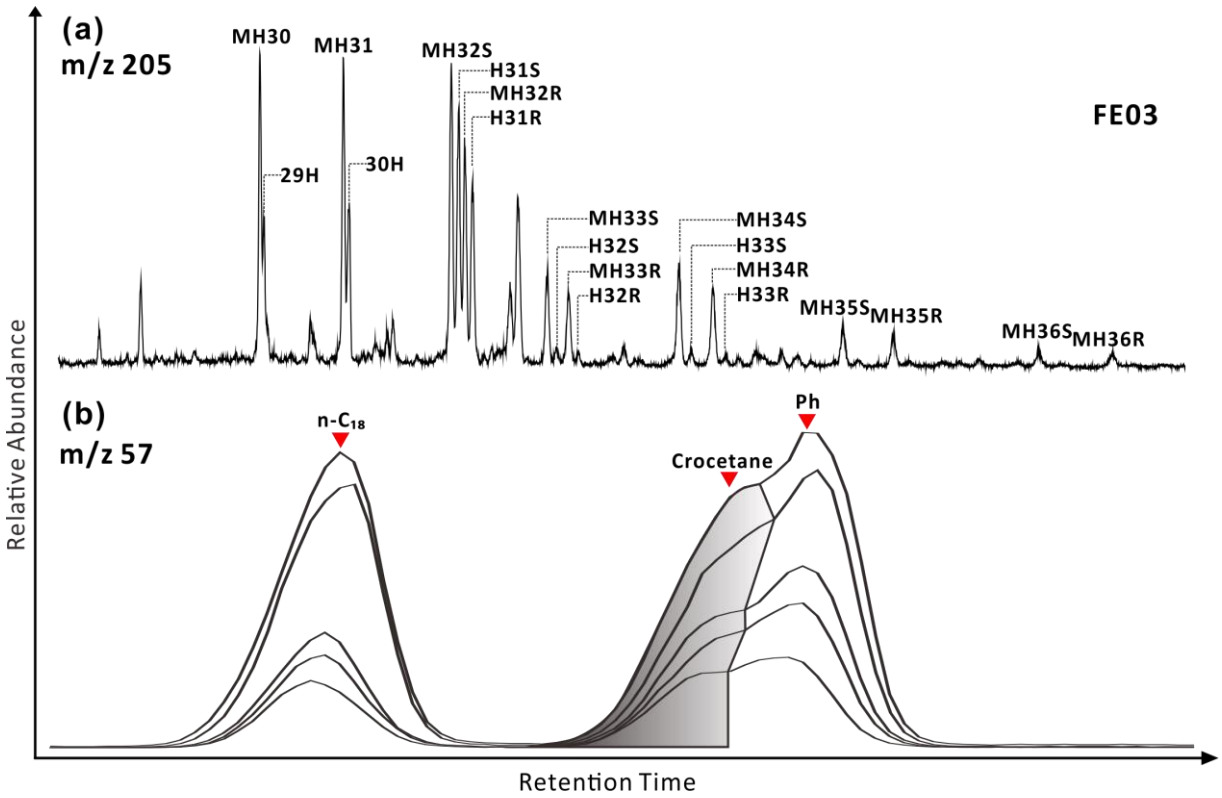


Supplementary Fig. 2.5 Partial (a) *m/z* 205 and (b) *m/z* 57 mass chromatograms, showing the distribution of methylhopanes in the aliphatic fraction of the FE03 sample, and the partial separation of crocetane (shaded part) from phytane (Ph). MHxx = $C_{xx}$ 2α-methylhopanes, 30H = $C_{30}$ αβ hopane, 29H = $C_{29}$ αβ hopane, Hxx = $C_{xx}$ αβ homohopanes (S+R)

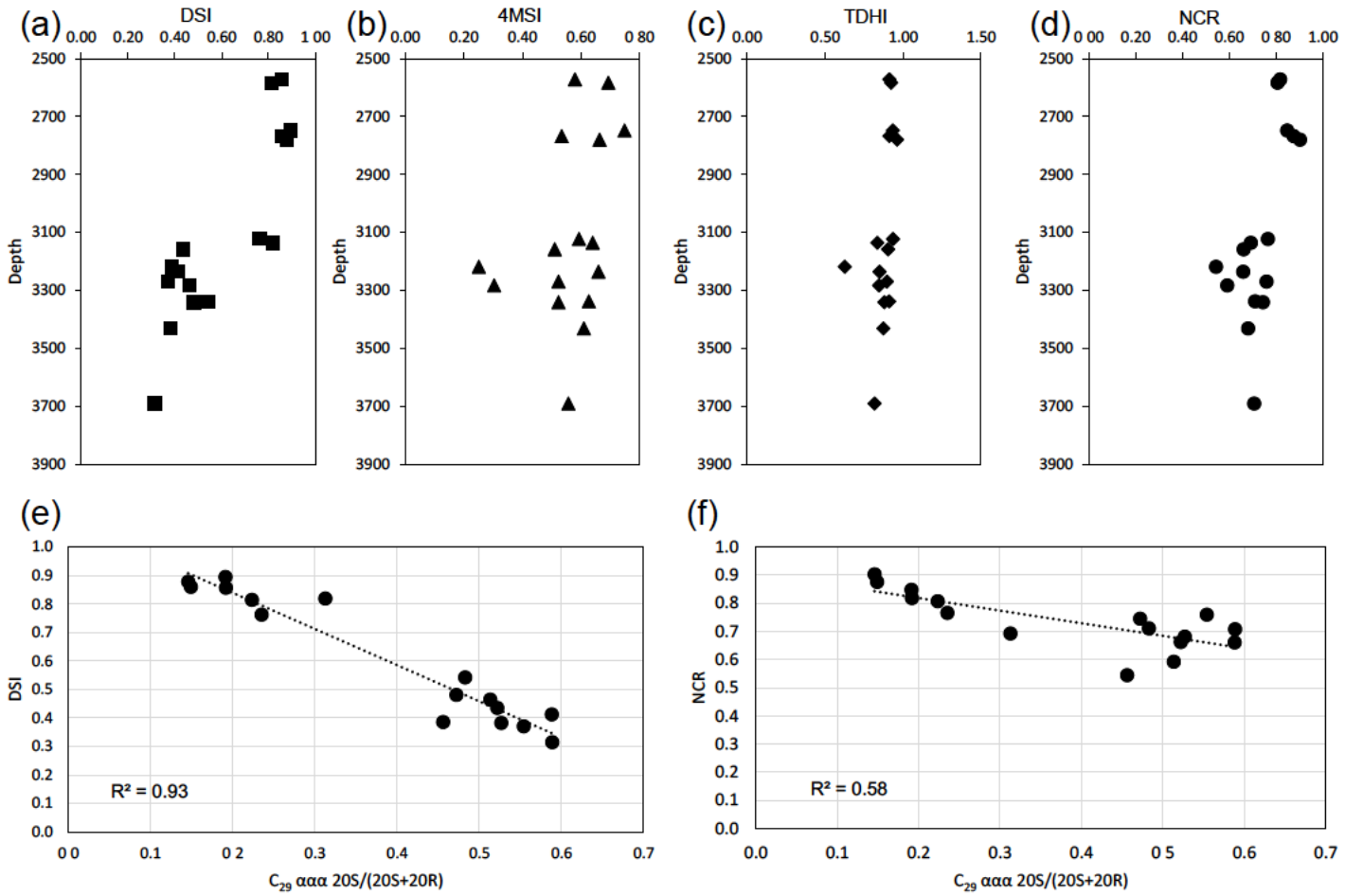


Supplementary Fig. 2.6 Cross-plot of burial depth versus (a) dinosterane index (DSI), (b) 4-methylsterane index (4MSI), (c) triaromatic dinosterane hydrocarbon index (TDHI), and (d) 24-norcholestane ratio (NCR), and cross-plots of $C_{29}$ ααα S/(S+R) steranes versus (e) DSI and (f) NCR. For ratio definitions see Table 2.2.

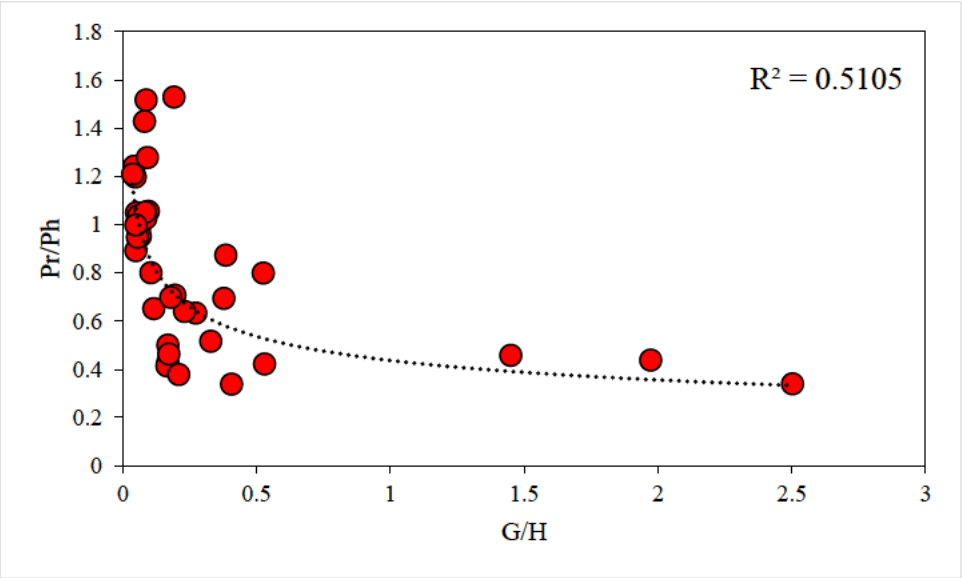


Supplementary Fig. 2.7 Cross-plot of Pr/Ph versus Gammacerane/$C_{30}$ αβ hopane (G/H). Pr/Ph = pristane/phytane.

Supplementary Table 2.1 Diagnostic biomarkers in the Dongying Depression and their biological and environmental interpretation.

| Group of organisms | | Biomarker or biomarker pattern | Environmental interpretation and age constraints | Other known potential sources |
|---|---|---|---|---|
| **Eukarya** | Eukaryotes in general | Cholestane and aromatic analogs | Possible minor contribution from myxococcales (myxobacteria) | |
| | Pelagophyte algae ("brown tides" and Sarcinochrysidales) | 24-*n*-Propylcholestane | Commonly found only in marine environments | |
| | Dinoflagellates | 4-Methylsterane | | Minor component in other eukaryotes |
| | | Dinosterane | Mostly Mesozoic and Cenozoic (minor concentrations in Paleozoic, possibly of "protodinoflagellate" origin) | Rare in diatoms |
| | Diatoms | 24-Norcholestane ($C_{26}$) | Cretaceous to Cenozoic | |
| | Ciliates | Gammacerane | The main source is possibly bacterivorous ciliates inhabiting the chemocline of stratified waters | Gammacerane precursors were also observed in a fungus, a fern, and the ubiquitous a-proteobacterium Rhodopseudomonas |
| | Terrestrial plants in general | *n*-Alkanes > $C_{25}$ with oddover-even carbon number preference, derived from higher plant waxes | Proximity to terrestrial organic matter sources; post-Silurian age | Non-marine algae |
| | | Retene | Possible occurrence in algae and microorganisms | |
| | Angiosperms | Oleanane, precursors are betulins, taraxerenes, and others triterpenoids | Predominantly Upper Cretaceous to Cenozoic | Precursors also occur in lichens and ferns in minor concentrations |
| **Bacteria** | Bacteria in general | $C_{30}$-hopanes | | Some cryptogams, ferns, mosses, lichens, filamentous fungi, and protists |
| | | Hopanes with extended side chain (homohopanes ($C_{31}$) – pentakishomohopane ($C_{35}$)) | | |
| | Cyanobacteria | 2-Methylhopanes | | Pseudomonadales, rhizobiales |
| | Green sulfur bacteria (Chlorobiaceae) | Isorenieratane(brown pigmented species) | Photic zone euxinia | Some sponges, Actinomycetales |
| | | 2,3,6-Trimethyl aryl isoprenoids | Photic zone euxinia | Aromatization and degradation of bcarotene |
| | | Palaerenieratane and 3,4,5- trimethyl aryl isoprenoids | Photic zone euxinia; restricted to the Paleozoic? | |
| | Purple sulfur bacteria (Chromatiaceae) | Renieratane | Photic zone euxinia | Sponges or sponge symbionts |
| | | 2,3,4-Trimethyl aryl isoprenoids | Photic zone euxinia | Cyanobacterial synechoxanthin? |
| | Phototrophs in general | Pristane, phytane | From chlorophylls of cyanobacteria and phototrophic eukaryotes, BChl a and b of phototrophic bacteria | Tocopherols and other acyclic isoprenoids, archaeal membrane lipids |
| **Archaea** | Anaerobic methane oxidizers (ANME) | Crocetane | Typical habitats are subsea gas sources, gas hydrates, and mud volcanoes | Degradation product of diaromatic carotenoids |

Chapter 3

# 3. Algal-derived polycyclic aromatic hydrocarbons in Paleogene lacustrine sediments from the Dongying Depression, Bohai Bay Basin, China

Huiyuan Xu[a, b, c, *], Simon C. George[b, *], Dujie Hou[a, *]

[a] School of Energy Resources, China University of Geosciences (Beijing), Haidian District, Beijing 10083, China

[b] Department of Earth and Planetary Sciences and MQMarine Research Centre, Macquarie University, Sydney, NSW 2109, Australia

[c] State Key Laboratory of Shale Oil and Gas Enrichment Mechanisms and Effective Development, Beijing 100083, China

**Chapter 3** is a comprehensive description and interpretation of aromatic hydrocarbons in the source rocks in the Dongying Depression. This chapter casts doubt on previous interpretations, and suggests an algal derivation for several aromatic hydrocarbons, consistent with the organic matter inputs shown by the aliphatic biomarkers.

**Statement of Author's Contribution:** This chapter is an original research paper that has been published in the journal *Marine and Petroleum Geology* (2019). 85% of

the work was done by the first author Huiyuan Xu, including developing the project plan and timeframe, sampling, conducting laboratory experiments, processing and analysing the data, and writing the manuscript. Simon C. George helped with sampling, designing the laboratory experiments, directing the research, and improving the manuscript, which accounts for 10%. Dujie Hou helped with developing the project plan and timeframe, sampling, and improving the manuscript, which accounts for 5%.

## Abstract

The sources and origins of polycyclic aromatic hydrocarbons (PAHs) in thirty eight Paleogene organic-rich shales and mudstones from the Shahejie Formation in the Dongying Depression, Bohai Bay Basin have been assessed. Phenanthrene, retene, cadalene, fluoranthene, pyrene, benz[a]anthracene, triphenylene, chrysene, benzofluoranthenes, benzo[e]pyrene, benzo[a]pyrene, indeno[1,2,3-cd]pyrene, benzo[ghi]perylene and coronene were identified in the sediments. The symmetrical 4-ring triphenylene was unequivocally identified by comparison with mass spectra and a synthetic standard. Key PAH ratios including fluoranthene/(fluoranthene + pyrene), benz[a]anthracene/(benz[a]anthracene + chrysene), indeno[1,2,3-cd]pyrene/(indeno[1,2,3-cd]pyrene + benzo[ghi]perylene) and benzofluoranthene/(benzofluoranthene + benzo[e]pyrene) indicate a mainly diagenetic/catagenetic origin for the PAHs. The relative low abundance of the 6-ring indeno[1,2,3-cd]pyrene and benzo[ghi]perylene and the 7-ring coronene suggest the absence of larger, high temperature wildfires, either due to inadequate seasonality of the humid-arid climate, or limited terrigenous organic matter input. Phenanthrene and alkylphenanthrenes are likely derived from phytoplankton, based on the correlation of the relative abundance of $C_{27}$ regular steranes and 1-methylphenanthrene and 9-methylphenanthrene. The methylphenanthrenes, triphenylene, alkyltriphenylenes and benzo[e]pyrene may share a common source as their occurrences are closely correlated. Four groups of samples were differentiated on the basis of the relative abundance and distribution patterns of benz[a]anthracene, triphenylene and chrysene, showing that these compounds are useful PAH markers in petroleum geochemistry. Thermal maturation effects are the major control on the relative abundance and distribution of the non-combustion derived PAHs (e.g. biphenyl, fluorene, fluoranthene, pyrene, benz[a]anthracene, triphenylene) in lacustrine sediments. Benz[a]anthracene decreases in relative abundance while triphenylene increases in relative

abundance with burial depth. Correlation of the newly defined triphenylene-chrysene ratio (TCR; triphenylene/(triphenylene + chrysene) with burial depth and biomarker maturity parameters was observed, suggesting that it may be a useful maturity indicator for lacustrine oils and sediments in the Dongying Depression.

*Keywords***:** PAH; aromatic hydrocarbon; lacustrine; shale; Dongying Depression; Bohai Bay Basin

## 3.1. Introduction

The aromatic hydrocarbons preserved in sediments result from transformations of biological precursors, either through microbial processes or the subsequent effects of temperature, pressure and the catalytic action of the mineral matrix during diagenesis (Albrecht and Ourisson, 1971). Aromatic hydrocarbons can provide information on both the origin of the deposited organic matter and on the geochemical transformations during thermal maturity. Polycyclic aromatic hydrocarbons (PAHs) identified in the geosphere are mainly derived from three origins: combustion-derived (sometimes known as pyrolytic PAHs), higher-plant-derived and diagenetic-derived.

Pre-depositional combustion-derived PAHs have been attributed to being the products of palaeo-wildfires, representing the incomplete combustion of biomass/solid fuel or plants (Laflamme and Hites, 1978; 1979; Wakeham et al., 1980b; Prahl and Carpenter, 1983; Kawamura et al., 1987; Venkatesan and Dahl, 1989; Killops and Massoud, 1992; Jiang et al., 1998; Hasegawa, 2001; Yunker and Macdonald, 2003; Luo et al., 2006; Grice et al., 2007; Yunker et al., 2011). Combustion-derived PAH are typically unsubstituted with three or more rings, and include phenanthrene, anthracene, fluoranthene), pyrene, benzo[a]anthracene, benzo[b]anthracene, triphenylene, chrysene, benzo[e]pyrene, benzo[a]pyrene, benzo[b,j,k]fluoranthene, benzo[ghi]perylene, indeno[1,2,3-cd]pyrene and coronene. A list of names and abbreviations of aromatic hydrocarbons discussed in this paper is provided in Table 3.1, with structures in the Appendix. The combustion-derived PAH can be used to reconstruct palaeoenvironments and palaeoclimates. They can also be produced through abnormal thermal stress on organic matter, as shown for example by the occurrence of combustion-derived PAHs in hydrothermal petroleum in the Guaymas Basin, Escanaba Trough and Middle Valley (Simoneit and Lonsdale, 1982; Kawka and Simoneit, 1990;

Simoneit and Fetzer, 1996). Volcanic activity and igneous intrusion also provide the geological conditions that generate these type of PAHs. For example, abundant unsubstituted PAHs are present in Chinese Lower Palaeozoic carbonate rocks where volcanic tuffs exist (Jiang et al., 1995). The abnormal heating rate accelerates aromatisation and yields predominantly unsubstituted PAHs, whereas normal thermal heating induced by geological burial produces considerably greater amounts of alkyl-substituted components (Murchison and Raymond, 1989; Jiang et al., 1998; Huang et al., 2015). Unsubstituted PAHs also occur in deep space and in meteorites (e.g., Messenger et al., 1998), and can be formed in the laboratory by synthesis from benzene (Mimura, 1995). The derivation of a microbial metabolism for PAHs has also been noticed by Grice et al. (2007), who showed that combustion-derived benzo[e]pyrene can originate from algal sources.

PAHs derived from natural biological precursors such as higher plants are termed higher-plant PAHs. These include cadalene, retene and simonellite, which can be formed during sedimentary diagenesis (Simoneit, 1977; Wakeham et al., 1980a) and from the decomposition of kerogen during catagenesis (Lu and Kaplan, 1992). Higher-plant PAHs have been used to characterise the specific type of organic matter inputs in terrigenous environments (Thomas, 1969; Laflamme and Hites, 1978; Wakeham et al., 1980a; Tan and Heit, 1981; Ramdahl, 1983; Simoneit et al., 1986; Alexander et al., 1988, 1992b; 1993; 1996; van Aarssen et al., 1996; Jiang et al., 1998; Zhou et al., 2000). For example, retene and simonellite have different plant precursors from those of cadalene. Diterpenoids, such as abietane-related compounds that are commonly thought to be derived from coniferous resins, have been proposed as the precursors for retene and simonellite, which can form due to thermal degradation during diagenesis (Alexander et al., 1992a; Tan et al., 1996). Cadalene is derived from compounds with cadalene molecular skeleton in higher plants (van Aarssen et

al., 1996). Nevertheless, a possible microbial or combustion source for retene should not be ignored (Jiang et al., 1995; Bechtel et al., 2007).

Perylene and benzo[ghi]perylene are diagenetic PAHs which will yield a different sedimentary distribution from those of the combustion-derived PAHs and higher-plant PAHs. Land-based organisms are likely to be a source for perylene precursors due to (1) good correlation between perylene and terrigenous material in sediments (Aizenshtat, 1973), (2) sufficient amounts of perylenequinones (perylene precursors) detected in soils from the surroundings of Lake Harun where perylene increases progressively with burial depth of sediments (Ishiwatari et al., 1980), (3) the widespread occurrence of perylene in peats and bituminous coal (Venkatesan, 1988) and (4) the co-occurrence of gymnosperm-derived retene and perylene in Baffin Bay sediments (Rullkötter et al., 1994). Several authors have suggested a link between fungi and perylene (Grice et al., 2009; Marynowski et al., 2013). The relative abundance of perylene increases rapidly with burial depth, which suggests that perylene is not only derived from the natural sources, but also can be formed after deposition (Marynowski et al., 2013; Varnosfaderany et al., 2014; Kumar et al., 2017). There is also evidence in support of biomass combustion sources for perylene (Oros and Simoneit, 2001; Oros et al., 2006; Fan et al., 2011; Yunker et al., 2011; 2012). An anoxic marine environment is favourable for Diels-Alder reactions which are conducive for the formation of benzo[ghi]perylene from perylene, allowing for the assessment of water salinity (Jiang, 1998). In addition, other aromatic hydrocarbons including biphenyl, terphenyl, phenylnaphthalenes, phenylphenanthrene, phenylanthracene, and binaphthyl, and heterocyclic aromatic compounds such as dibenzothiophene, phenyldibenzothiophene and phenyldibenzofuran, have also been detected in sedimentary organic matter (Kruge, 2000; Marynowski et al., 2002; 2007; 2008; Rospondek et al., 2009; Li et al., 2012b; 2013b; 2013a; 2016). Diagenesis or catagenesis of organic matter seems to be a major control on their occurrence.

Higher plant-derived PAHs can be representative biomarkers for assemblages and variations of specific types of plants inhabiting different paleoenvironments. Similarly, combustion-derived PAHs, as a consequence of exposure of organic matter to high temperatures (Blumer and Youngblood, 1975), ancient wildfires and abnormal geothermal activity (Murchison and Raymond, 1989), can reveal the paleoclimate conditions in terms of humidity, aridity, and seasonality (Scott and Jones, 1994). This can be achieved by assessing the frequency, temperature and materials of combustions, or possible geological events associated with a temperature anomaly. As fungi are the most likely source of perylene, its presence predicts a humid climate for decaying wood during early diagenetic processes (Moore, 1969; Stubblefield et al., 1985; Jiang et al., 2000; Grice et al., 2009; Suzuki et al., 2010). Reducing depositional conditions are necessary, but which are insufficient for the diagenetic formation of perylene during or after deposition (Hites et al., 1980; Tan and Heit, 1981; Louda and Baker, 1984). Jiang (1998) noted that sediments of Toarcian age (late Early Jurassic) deposited under a relatively persistent humid climate exhibit abundant higher-plant PAHs and scarce combustion-derived PAHs, and sediments in the Aalenian (top Lower Jurassic) deposited under a humid and seasonal climate contain relative high concentrations of both combustion and higher-plant PAH markers.

The effect of thermal maturity on PAHs and their methylated homologues has been documented (Garrigues et al., 1988; Kruge, 2000; Li et al., 2012a; Li et al., 2012b; Li et al., 2013a; Li et al., 2013b; Fang et al., 2015; Li et al., 2016). Their distribution patterns, relative and absolute concentrations have been widely used to indicate thermal maturity. For example, ratios of alkylated PAHs with isomers having a high degree of β-substitution to those with a high degree of α-substitution are sensitive to changes of thermal maturity (Alexander et al., 1985), because β-substituted isomers are more thermally stable.

More generally, the aromatic hydrocarbon source and maturity parameters generally associated with terrigenous organic matter, (e.g., conifer resins, angiosperms woods) have been widely applied over several decades (Volk et al., 2004). However, due to source and environmental influences, these parameters are not widely suitable for samples from lacustrine settings (Li et al., 2003). These maturity parameters need to be recalibrated for specific basins and formations.

The features of source rocks from different types of hydrologically-closed lake basins are controlled by climate. The water level in a lake is commonly the result of the interaction of climate-influenced water supply and tectonically-controlled accommodation space, thus resulting in high frequency wet-dry alternations recorded in lacustrine sediments (Carroll and Bohacs, 1999). The Eocene Shahejie Formation in the Dongying Depression was deposited in a balanced and over-filled lake, with strong climate-driven rhythmicity (Zhang et al., 2009). The resistivity logs show a rhythmic pattern that is consistent with seasonal lamination in the source rocks (Zhang et al., 2009) and alternating palaeoclimate conditions, as also indicated by a series of transgressive-regressive parasequences as evidence for periodic stratification and hypersalinity (Liu et al., 2004). The abundant algal organic matter inputs to the Dongying Depression include dinoflagellates of the *Defladrea*, *Senegalinium*, *Palacostomocysts* species, and green algae (*Bohaiensis*, *Pediastrum* and *Botryococcus* genera) (Li et al., 2003). It is reasonable to speculate these algae may have contributed to the formation of the PAHs. However, igneous activity from the time of the Himalayan Orogeny has been well documented in Paleogene sediments in the Jiyang Sub-basin, Bohai Bay Basin, in which extrusive basalts and other volcanic rocks and intrusive diabases and dolerites were extensively developed (Jin et al., 2004; Zhu et al., 2007; Zhang et al., 2008; Wang et al., 2012; Luo et al., 2017). The high heat flow released from the magma could have influenced the

occurrence and distribution of the pyrolytic PAHs. Hence caution should be taken in interpretation of the PAHs in the Dongying Depression.

The transitional-paralic Dongying palaeo-lake contains indigenous algal organic matter, allochthonous terrigenous organic matter, and probably occasional marine organic matter input (Hou et al., 1997). Thus it is an ideal place for studying multi-sourced PAHs. On the basis of the occurrence and distribution of various types of PAHs in the Dongying Depression sedimentary sequences, correlated with traditional aliphatic biomarkers, this paper aims:

(1) to predict the source, origin and significance of the PAHs, and to assess and compare the Dongying PAHs with those normally attributed to the combustion of biomass/ solid fuel;

(2) to reveal the palaeoenvironment (e.g. redox conditions and water salinity) and palaeoclimate (e.g. vegetation types, wildfires, humidity, aridity and seasonality) relationship of the PAHs;

(3) Explore the potential of aromatic hydrocarbon maturity indicators based on unsubstituted PAHs for oils and sediments from the Dongying lacustrine setting.

## 3.2. Geological setting of the Dongying Depression

The rise of upper mantle behind the Western Pacific subduction margin caused the rifting of continental crust in eastern China during the Late Mesozoic-Cenozoic (Fu and Sheng, 1989). The Bohai Bay Basin is an intracontinental extensional rift basin that formed in the Late Jurassic, and is located in the east of the North China Craton adjacent to the Bohai Sea (Fig. 3.1a). It is bounded by the Tanlu Fault in the east. The basin has experienced high geothermal heat flow, with a geothermal gradient of 4.3 ℃/100m (Zhang et al., 2008). Of the six sub-basins in the Bohai Bay Basin, the Jiyang Sub-basin is the most petroliferous one. It was formed in the rifting and subsiding phase, and is situated in the south of the Bohai Bay

Basin (Fig. 3.1a). The Jiyang Sub-basin covers most of the Yellow River delta, a northeast-southwest trending area of 25,000 $km^2$, with a width of 120 km and a length of 200 km. The Dongying Depression developed in the southern part of the Jiyang Sub-basin and covers an area of 5,500 $km^2$ (Fig. 3.1a). The Dongying Depression is the second largest oil field in China. It contains 5 major Cenozoic formations, including the Pliocene Minghuazhen Formation and the Miocene Guantao Formation, which are composed of alluvial and fluvial sediments, the lacustrine Oligocene Dongying Formation, and the Eocene Shahejie and Kongdian formations which are also composed of lacustrine sediments (Fig. 3.1b). The widely distributed Shahejie Formation (designated Es) is further subdivided into four members: the Sha1 (Es1), Sha2 (Es2), Sha3 (Es3) and Sha4 (Es4) members (Fig. 3.1b). Much evidence suggests that the Es1, the lower part of the Sha3 (Es3L) and the upper part of the Sha4 (Es4U) are the main oil-bearing intervals (Li et al., 2003; Zhang et al., 2009). The Es4 was deposited in a shallow, semi-enclosed brackish-saline lacustrine setting during the early stage of rift development, and the Es3 was deposited in a deeper and wider lake with fresh-brackish water salinity during the peak period of paralic lake development and regional subsidence (Bao and Li, 2001; Wang et al., 2013). The Es2 member is sandy and has been proven to be the main reservoir bed in the oilfield (Zhu et al., 2007). Although extensive volcanism and magma intrusion occurs in the Paleogene and Neogene sediments that are widespread in the Jiyang sub-basin, the Shahejie Formation contains high-quality hydrocarbon source rocks that are composed of lacustrine laminated calcareous mudstones and shales (Zhu et al., 2007) that are only rarely influenced by any magmatic activity. The laminated features in the sediments of the Dongying Depression probably indicate seasonal water stratification that may arise from seasonal palaeoclimate conditions (Zhang, 2008). The small-scale microbioturbation in the Es3 member suggests that oxygen was present in the bottom waters (Chen et al., 2016).

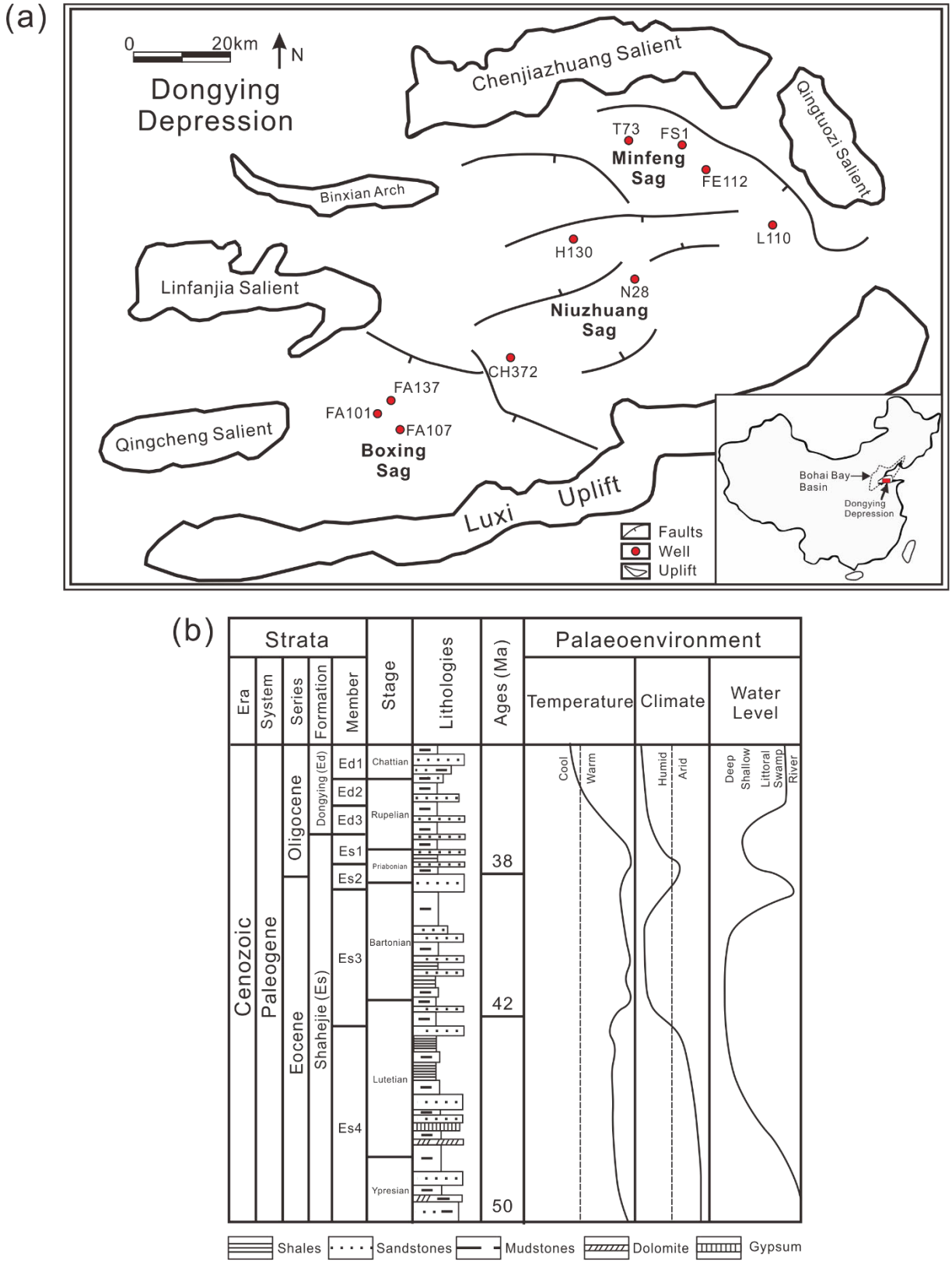


Fig. 3.1 Location map of the Dongying Depression, Bohai Bay Basin, showing the position of the subdivided sags, the wells and the structural elements (a), and a stratigraphic chart showing the Eocene to Oligocene strata of the Dongying Depression, Bohai Bay Basin (b).

## 3.3. Samples and analytical methods

### 3.3.1. Samples

For this study, a suite of thirty eight source rock samples was obtained from 10 different cores in the Dongying Depression, Bohai Bay Basin (Table 3.2). Twenty one samples are from three wells (FE112, FS1 and T73) in the north-eastern Minfeng sag, nine samples are from three wells (H130, N28 and L110) in the eastern Niuzhuang sag, and eight samples are from four wells (FA107, FA101, FA137 and CH372) in the southwestern Boxing sag (Fig. 3.1). The samples are from the middle part of the Sha3 (Es3M), the lower part of the Sha3 (Es3L) and the upper part of the Sha4 (Es4U) members (Table 3.2).

### 3.3.2. Extraction and Fractionation

The source rock samples were crushed into powder in a rotary mill. The homogenised powdered samples were extracted using a solvent mixture of dichloromethane/methanol (9:1 v/v) using an accelerated solvent extractor (ASE300). The extractable organic matter (EOM) was fractionated using two-step silica gel column liquid chromatography. Total hydrocarbons were collected from the first column by eluting with *n*-hexane/dichloromethane (4:1 v/v). The total hydrocarbons were fractionated on a second column into aliphatic hydrocarbons (elution with *n*-hexane), and aromatic hydrocarbons (elution with *n*-hexane/dichloromethane (4:1 v/v). UV light monitoring was used to ensure there were no mixed elution of aliphatic and aromatic hydrocarbons.

### 3.3.3. Gas chromatography-mass spectrometry

Gas chromatography-mass spectrometry (GC-MS) analyses of the aliphatic and aromatic hydrocarbon fractions were performed on an Agilent GC (6890N) coupled to an

Agilent Mass Selective Detector (5975B) equipped with a J&W DB-5MS fused silica column (length 60 m, inner diameter 0.25 mm, film thickness 0.25 μm). The inlet was held at 35°C for 3 min., then programmed to 310 ℃ (0.4 min. isothermal) at a rate of 700 ℃/min. Samples were injected in splitless mode. The temperature of the GC oven was initially held at 35 ℃ for 4 min. and was programmed to 310 ℃ at 4 ℃ /min, then was held for 40 min. Helium (99.999%) was used as the carrier gas. The carrier gas flow rate (constant flow) was 1.5 mL/min. The ion source of the mass spectrometer was operated in EI mode at 70 eV. The MS data were acquired in full scan and selected ion monitoring (SIM) modes. The relative abundance of compounds was determined from peak areas (using selected mass chromatograms for the integration of the compounds). External standards North Sea Standard Oil 1 (NSO-1), and synthetic benzo[a]pyrene, benzo[b]anthracene, fluoranthene, benzo[b]fluoranthene, chrysene, triphenylene, perylene, indeno[1,2,3-cd]pyrene and coronene were analysed for hydrocarbon identification based on retention times, and MS data and the NIST14 library (Alexander et al., 1986; Trolio et al., 1999; Schade and Andersson, 2006; Li et al., 2012a; Fang et al., 2015; Huang et al., 2015)..

## 3.4. Results

### 3.4.1. Bulk organic matter

The Es3M source rocks consist of massive grey mudstones and black shales, with total organic carbon content (TOC) of 4.7-14.9% (avg. 8.1%), total nitrogen content (TN) of 0.46-0.66% (avg. 0.55%) and extractable organic matter (EOM mg/g) of 5.9-19.9 (avg. 12.5) (Table 3.2). The Es3L samples are composed of black and grey mudstones, laminated mudstones and black shales, with TOC of 1.1-10.0%, (avg. 4.6%), TN of 0.5-0.8% (avg. 0.62%) and EOM of 2.5-29.2 (avg. 9.5). The Es4U samples consist mainly of calcareous laminated dark mudstones and black shales, with TOC of 0.3-13.5%, (avg. 5.5%), TN of 0.2-

0.8% (avg. 0.45%) and EOM of 0.6-15.0 (avg. 7.6).The C/N ratio ranges from 8.3-22.5 (avg. 14.3), 1.4-14.4 (avg. 7.5) and 5.4-23.0 (avg. 12.9) for the Es3M, Es3L and Es4U member samples, respectively (Table 3.2). TOC correlates well with C/N and EOM, and are likely controlled by microbial activity by heterotrophic bacteria, cyanobacteria and chemoautotrophic bacteria, as well as purple and green sulphur bacteria with strong denitrification (van Mooy et al., 2002), and anoxic conditions enhancing preservation of organic matter (Meyers et al., 2009).

### 3.4.2. Identification and distribution of the PAHs

As shown by representative total ion chromatograms (TIC), the most abundant compounds in the aromatic hydrocarbon fractions of the rock extracts are alkylnaphthalenes, phenanthrene and alkylphenanthrenes (Fig. 3.2). Moderately abundant compounds include parent and alkylated benzenes, chrysenes, dibenzothiophenes and biphenyls, and their parent equivalents, and triaromatic steroids. Also present in relatively lower abundances are unsubstituted and substituted polycyclic aromatic hydrocarbons with 3-7 rings (Figs. 3.2 and 3.3). Biphenyl and its $C_1$ and $C_2$ alkylated isomers were highlighted by the *m/z* 154, 168 and 182 mass chromatograms of the aromatic fractions (Fig. 3.4a). Dibenzothiophene (Fig. 3.5), methyldibenzothiophenes, and dimethyldibenzothiophenes were selectively identified by monitoring the *m/z* 184, 198 and 212 mass chromatograms. Phenylnaphthalenes (Fig. 3.4b), terphenyl, quaterphenyls, tetralin, and tetramethyltetralins were observed by monitoring the *m/z* 204, 230, 306, 159 and 173 mass chromatograms, respectively. In the *m/z* 218 and 232 mass chromatograms, alkylated 2-phenylnaphthalenes could be detected (Fig. 3.4b). Representative $C_1$ and $C_2$ alkylphenanthrene distributions are shown in the summed *m/z* 192 +206 mass chromatograms (Fig. 3.4d).

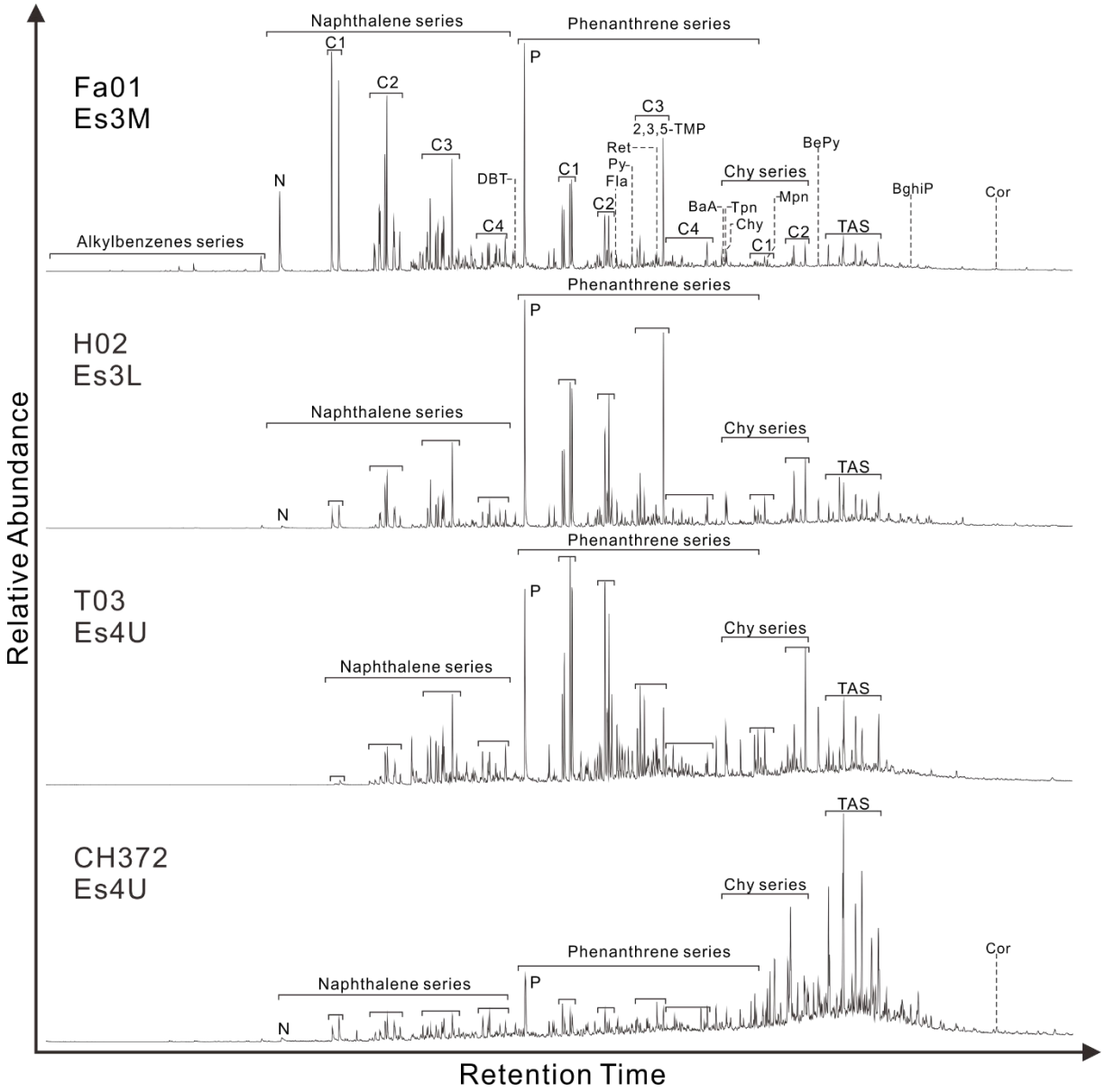


Fig. 3.2 Representative total ion chromatograms showing the distribution of polycyclic aromatic compounds in the Paleogene source rocks from the Shahejie Formation in the Dongying Depression, Bohai Bay Basin. Hydrocarbon abbreviations are defined in Table 3.1. Cx = Cx alkyl aromatic hydrocarbons. For explanation of sample codes see Table 3.2.

The relative distributions of some 2- and 3- ring unsubstituted PAHs (biphenyl, fluorene, diphenylmethane, dibenzofuran, dibenzothiophene and 2-phenylnaphthalene) with cadalene, 1-isohexyl-2-methylnaphthalene (iHMN) and retene are shown in the summed m/z (154+166+168+183+184+234) mass chromatograms (Fig. 3.5) and column charts (Fig. 3.3b) for representative samples from the Shahejie Formation. The average relative abundance of

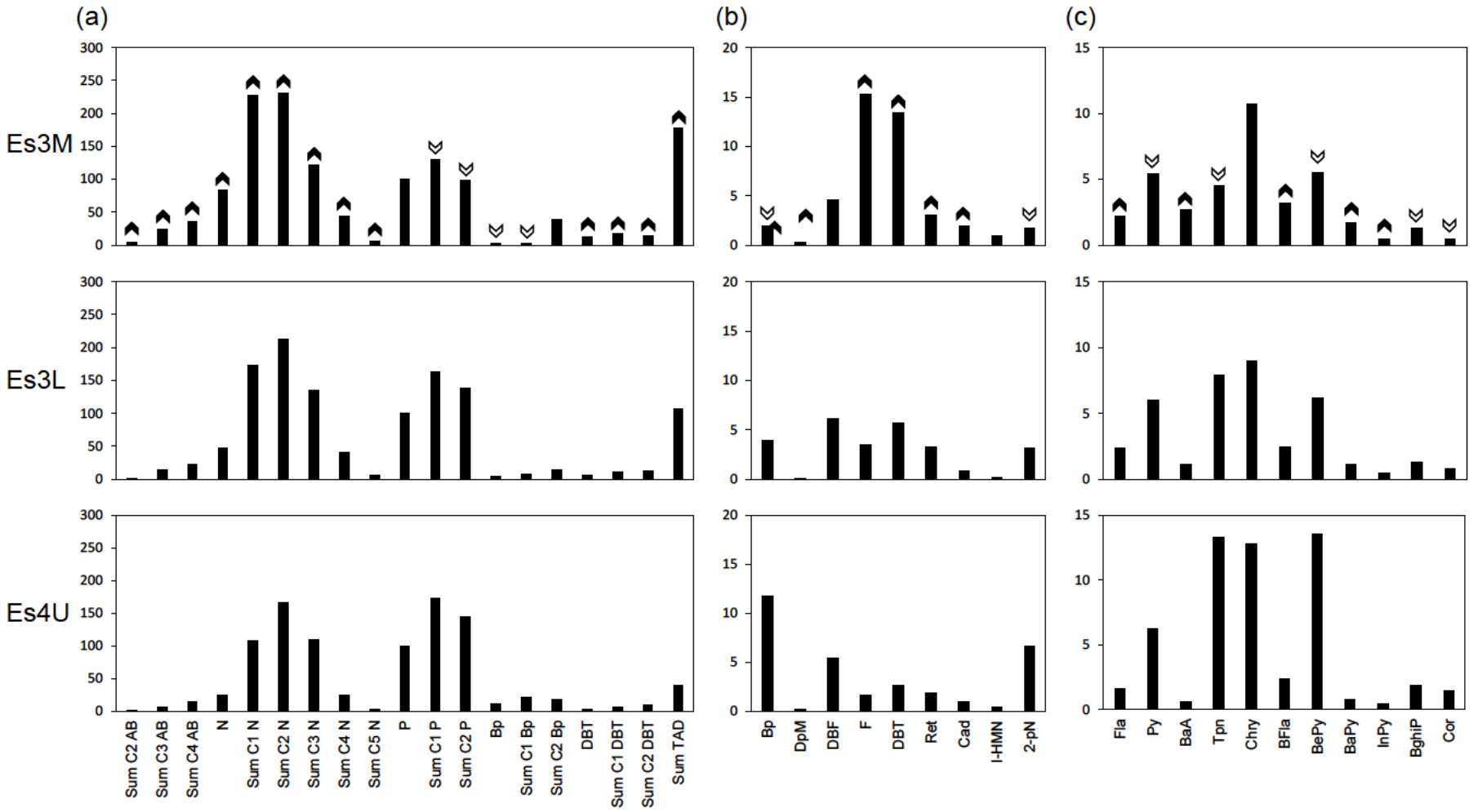


Fig. 3.3 Average relative abundances normalised to phenanthrene for three sections in the Shahejie Formation, showing (a) alkylbenzenes, naphthalene, alkylnaphthalenes, phenanthrene, alkylphenanthrenes, biphenyl, alkylbiphenyls, dibenzothiophene, alkyl dibenzothiophenes and triaromatic steroids, (b) selected aromatic compounds, and (c) PAHs. Hydrocarbon abbreviations are defined in Table 3.1. Solid up and hollow down arrows indicate an increase or decrease, respectively, of the relative abundance for each compound from the upper part of the 4$^{th}$ member (Es4U) to the middle part of the 3$^{rd}$ member (Es3M). Cx = degree of alkylation of aromatic hydrocarbons.

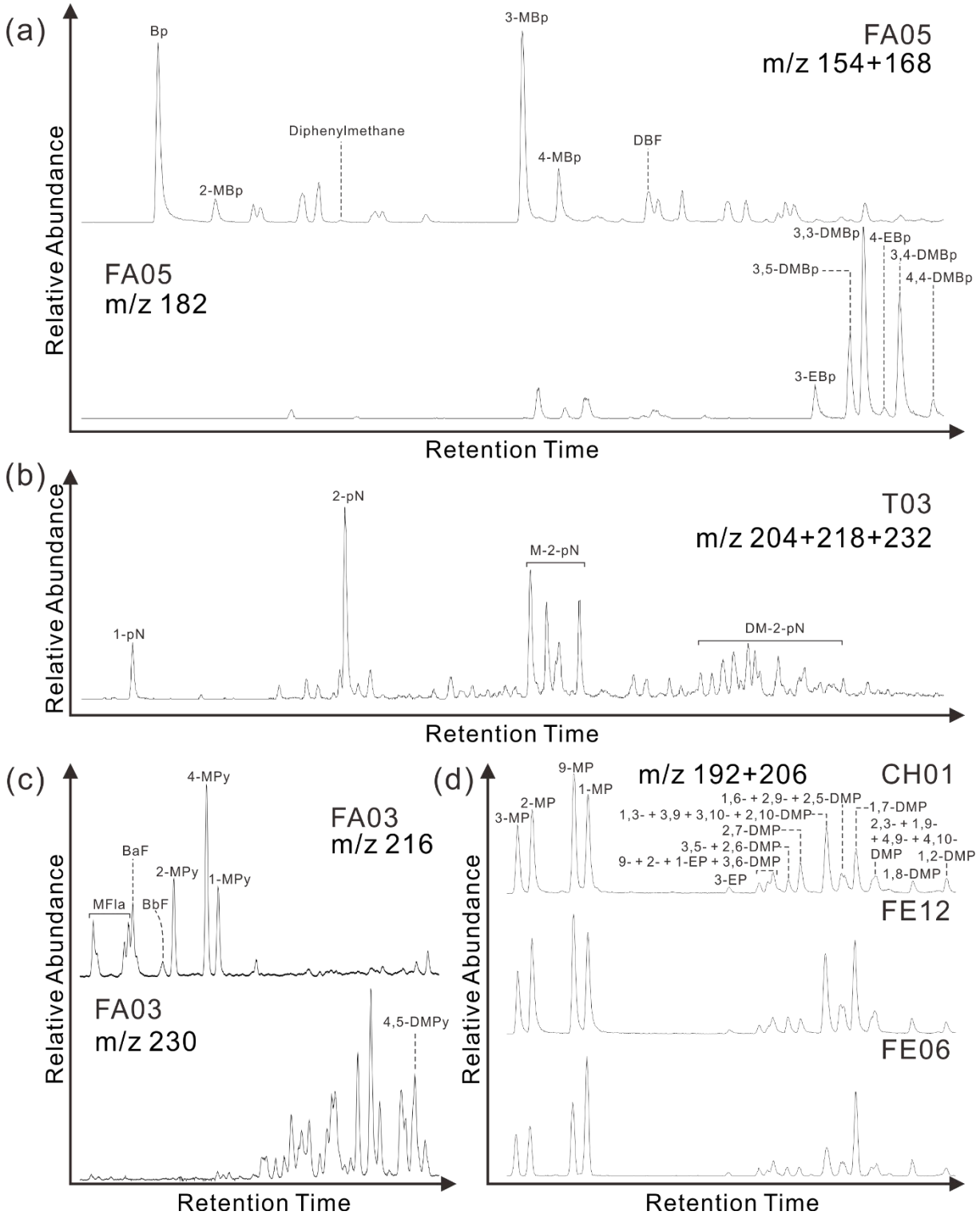


Fig. 3.4 Partial summed mass chromatograms for representative samples from the Shahejie Formation, Dongying Depression, showing the relative distribution of (a) biphenyl, $C_1$ alkylbiphenyls (m/z 154+168), and $C_2$ alkylbiphenyls (m/z 182); (b) phenylnaphthalenes, $C_1$ alkylphenylnaphthalenes and $C_2$ alkylphenylnaphthalenes (m/z 204+218+232); (c) $C_1$ alkylfluoranthenes, benzo[a]fluorene, benzo[b]fluorene and alkylpyrenes (m/z 216) and $C_2$ alkylfluoranthenes and alkylpyrenes (m/z 230); and (d) $C_1$ and $C_2$ alkylphenanthrenes (m/z 192+206). Hydrocarbon abbreviations are defined in Table 3.1. For explanation of sample codes see Table 3.2.

biphenyl and 2-phenylnaphthalene increases from the Es3M member to the Es4U member, whereas the relative abundance of dibenzothiophene, fluorene, and retene decreases (Fig. 3b). By monitoring the molecular ion *m/z* 202 (Fig. 3.6), fluoranthene and pyrene (Vassilaros et al., 1982) were identified in the aromatic fractions of the rock extracts. Fluoranthene is not present in large quantities in any of the samples from the Dongying Depression, and the abundance of pyrene is generally higher relative to fluoranthene (Fig. 3.6). Methylpyrenes (2-, 4-, and 1-MPy isomers) were identified in the *m/z* 216 mass chromatogram, which shows that 4-methylpyrene is always the dominant isomer (Fig. 3.4c). The peaks earlier eluting than the methylpyrenes in the *m/z* 216 mass chromatograms include benzo[a]fluorene, benzo[b]fluorene and methylfluoranthenes. In the *m/z* 230 mass chromatogram there are many unidentified peaks (Fig. 3.4c), but 4,5-dimethylpyrene was identified based on its retention time and isomer distribution reported in a previous publication (Fang et al., 2015).

Benzo[a]anthracene, triphenylene and chrysene are identified in the *m/z* 228 mass chromatogram of the aromatic fractions (Figs 3.6 and 3.7), with the former compound being the earlier eluting one. Generally, triphenylene is reported as coeluting with chrysene in the literature, but this study used a DB5MS capillary column and they are well separated (Fig. 3.7), as was proven by authentic standards. There is an increase in the relative abundance of triphenylene and a decrease in the relative abundance of benzo[a]anthracene from the Es3M member to the Es4U member, whereas chrysene shows no regular changes (Fig. 3.7). In addition, several groups of $C_1$-$C_3$ alkylated isomers of benzo[a]anthracene/chrysene/triphenylene were detected in the *m/z* 242, 256 and 270 mass chromatograms, respectively (Fig. 3.7). Li et al. (2012a) reported the elution order and assignment of 3-, 2-, 6-, and 1-methylchrysene by comparison of retention indices and the literature. We tentatively assign the first two peaks as methylbenzo[a]anthracenes (see (Kruge, 2000)) and the next three peaks as 3-, 2-, 1-methylchrysene in the *m/z* 242 mass

chromatogram. This was based on relative retention times and the mass spectra of these five isomers, which have diagnostic ions of *m/z* 120, 121, 239, 240, 241, 242 (base peak) and 243 (Li et al., 2012a).

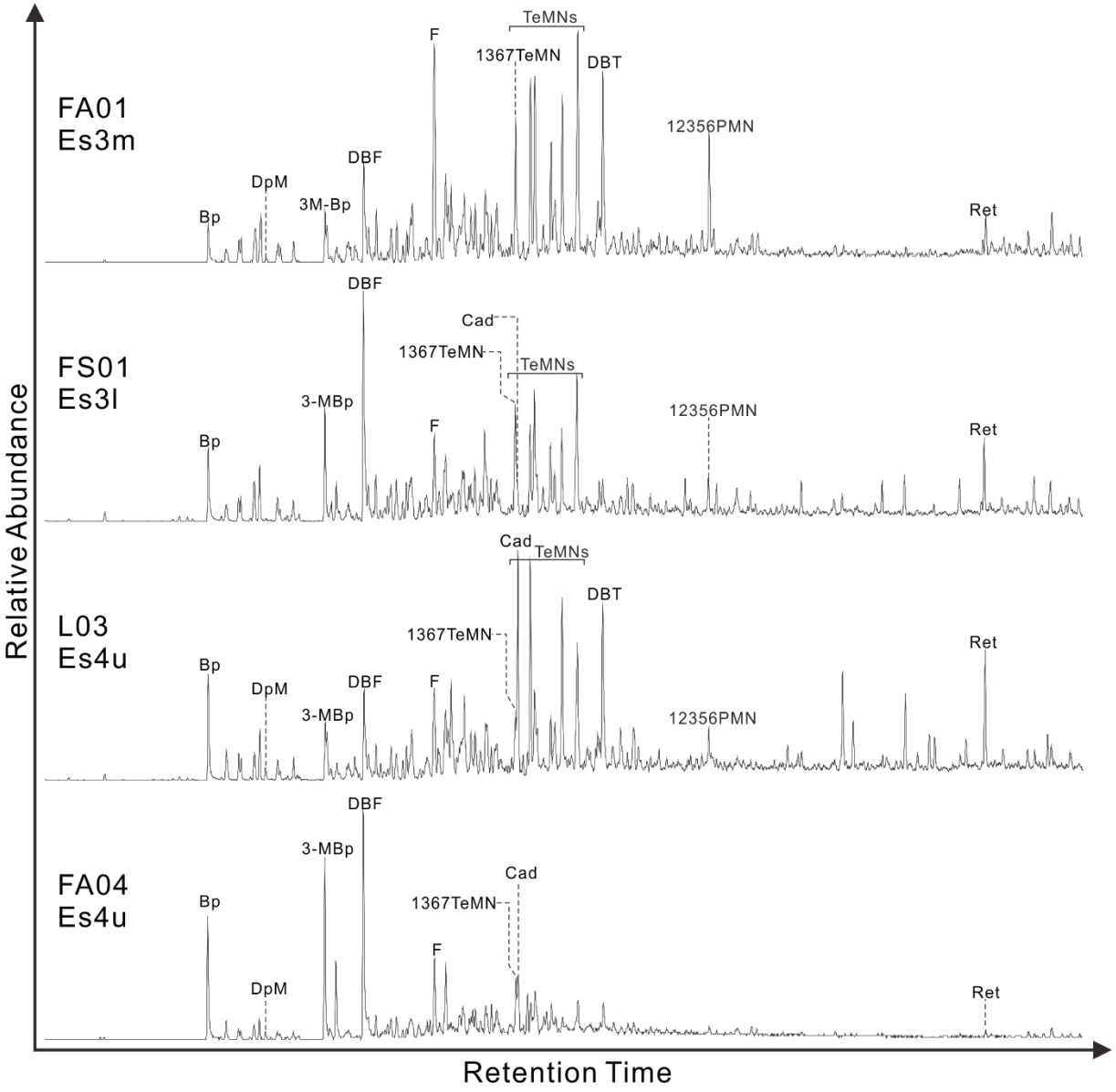


Fig. 3.5 Partial summed m/z (154+166+168+183+184+234) mass chromatograms for representative samples from the Shahejie Formation, showing the relative distributions of selected aromatic hydrocarbons (biphenyl, fluorene, dibenzofuran, cadalene, dibenzothiophene, and retene, respectively) and other alkylated aromatic hydrocarbons. Hydrocarbon abbreviations are defined in Table 3.1. For explanation of sample codes see Table 3.2.

Benzo[b,j,k]fluoranthene, benzo[e]pyrene and benzo[a]pyrene are present in most of the samples (Fig. 3.3c), but perylene could not be identified in the *m/z* 252 mass chromatogram

(Fig. 3.6). The relative amount of benzo[e]pyrene varies greatly in the various members of the Shahejie Formation, with samples from the Es4U member containing relatively higher abundances than samples from the Es3M and Es3L members (Figs 3.3c and 3.6). The three CH372 samples and three of the L110 samples have only minor amounts of benzopyrenes and benzofluoranthenes (Table 3.2). Benzo[g,h,i]perylene and coronene were identified in the *m/z* 276 and *m/z* 300 mass chromatograms, respectively. The presence of ≥5 rings PAHs may suggest the occurrence of combustion or other high temperature events (Jiang et al., 1998).

The possible controlling factors on the distributions of PAHs are various, and include the organic matter origins, diagenesis, catagenesis and other alteration processes (Marynowski and Simoneit, 2009). In general, alkylnaphthalenes and alkylphenanthrenes dominate the aromatic fraction of the rock extracts (Figs 3.2, 3.3a). The overall average-relative distributions of aromatic hydrocarbons (alkylbenzenes, alkylnaphthalenes, alkylphenanthrenes, alkyldibenzothiophenes, alkylchrysenes and triaromatic steroids) varies slightly from the top Es3M to the bottom Es4U (Fig. 3.3a). For example, the alkylbenzene series and the alkylnaphthalene series show a decreasing trend from the Es3M to the Es4U, and the phenanthrene series and triaromatic steroids show an increasing trend from the Es3M to the Es4U. This could be attributed to variation in thermal maturity or differences in source organic matter inputs. The 2- 3-ring PAHs such as biphenyl, diphenylmethane, fluorene, dibenzofuran, dibenzothiophene, retene, cadalene and 2-phenynaphthalene are present in varying concentrations (Fig. 3.3b). The Es3M member samples are dominated by dibenzothiophene, fluorene and to some extent dibenzofuran, while these compounds in the Es3L and Es4U member samples have lower relative abundance. Biphenyl and 2-phenynaphthalene are more abundant in the Es4U member samples than in the Es3M and Es3L members. The higher plant markers retene, cadalene and iHMN are more enriched in the Es3M member than in the Es4U member. Interestingly, dibenzothiophene is one of the most

prominent compounds in the Es4U member samples from the CH372 and L110 cores (e.g. L03 sample; Fig. 3.5). Retene and cadalene are much more abundant in these samples than in the other samples, and there is a predominance of cadalene over retene (Table 3.2).

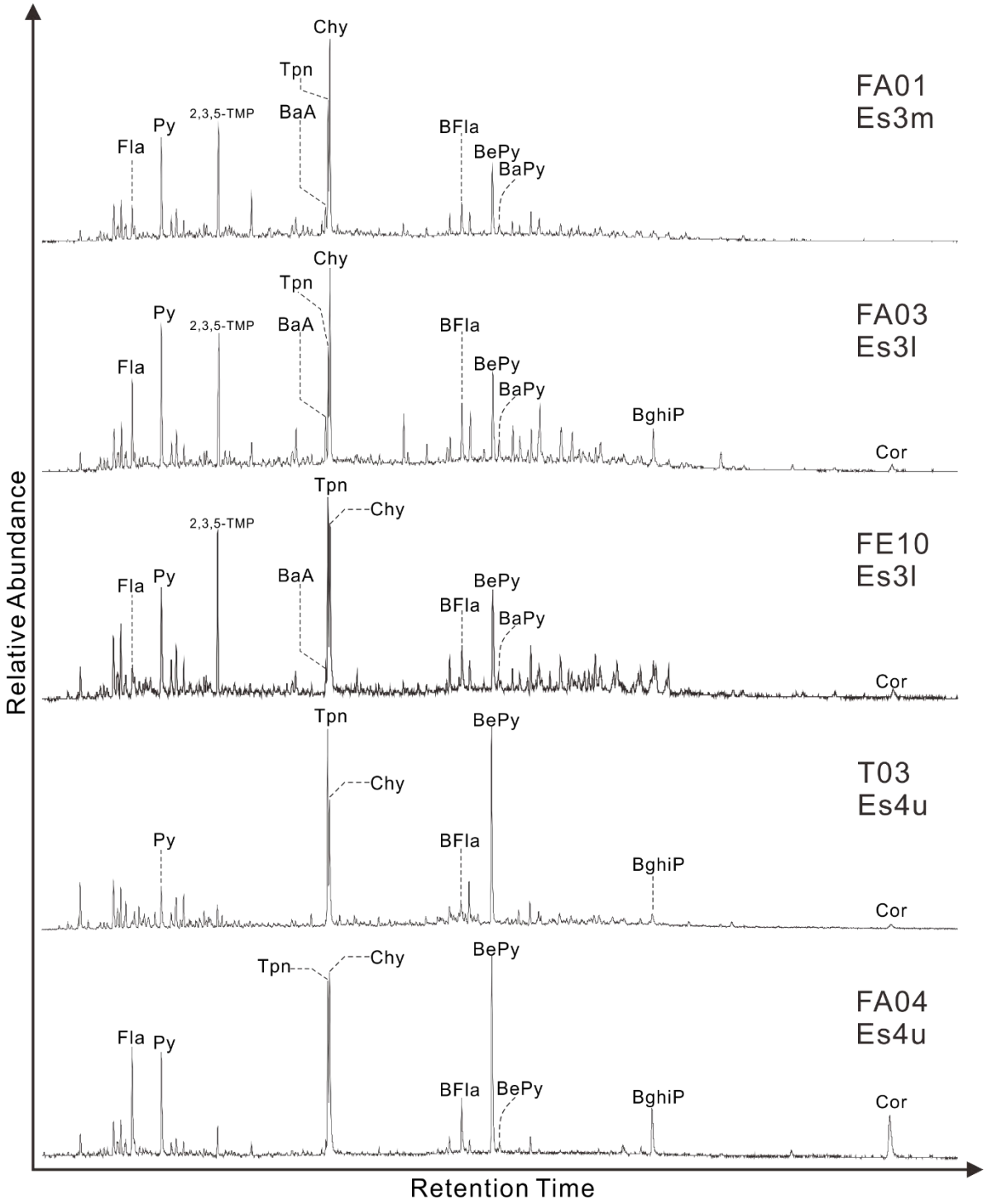


Fig. 3.6 Partial summed m/z (202+228+252+276+300) mass chromatograms for representative samples from the Shahejie Formation, showing the relative distributions of ≥4 ring unsubstituted PAHs (fluoranthene and pyrene; benzo[a]anthracene, triphenylene and chrysene; benzo[b,j,k]fluoranthene, benzo[e]pyrene, benzo[a]pyrene; benzo[ghi]perylene; and coronene, respectively). Hydrocarbon abbreviations are defined in Table 3.1. For explanation of sample codes see Table 3.2.

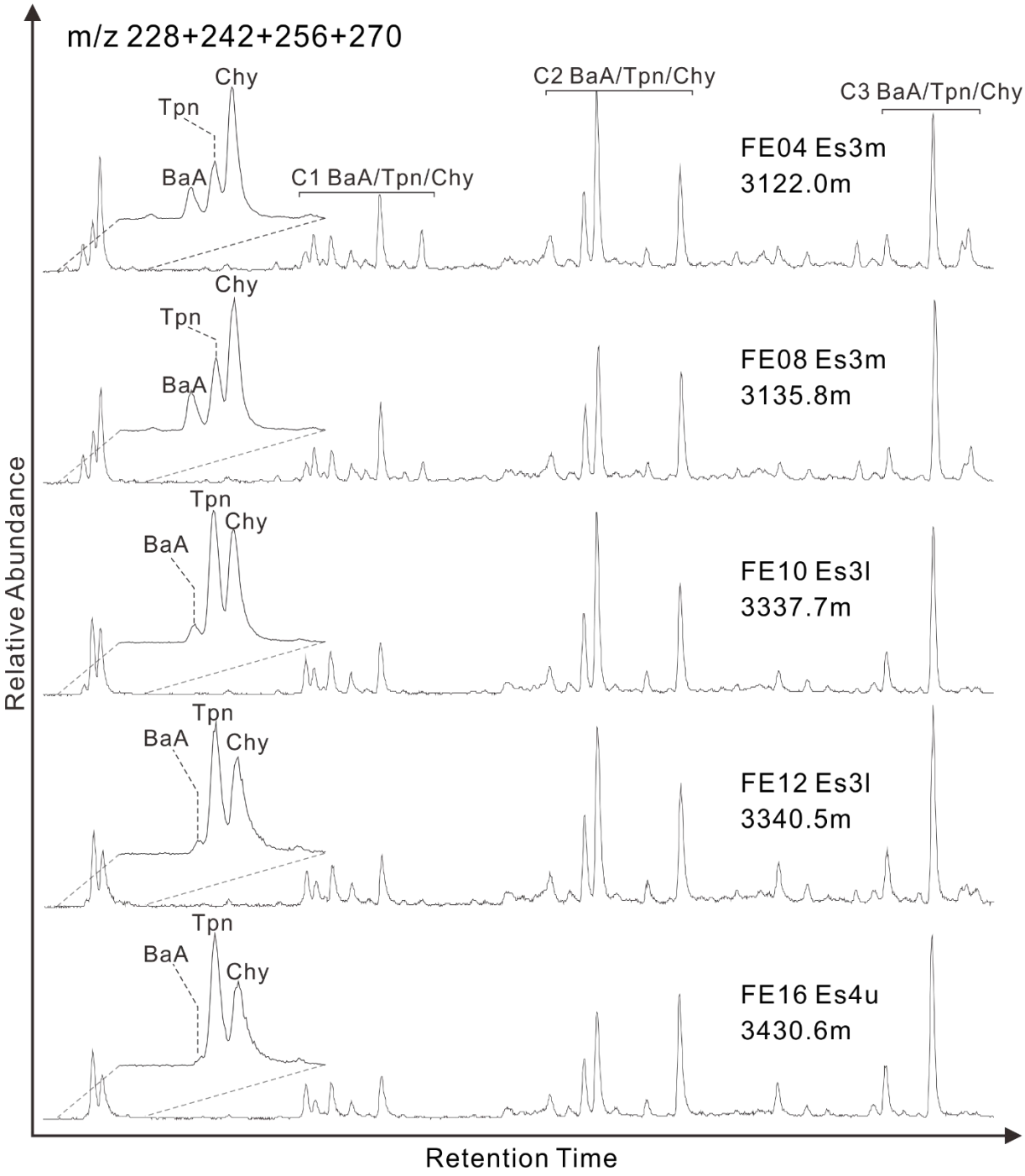


Fig. 3.7 Partial summed m/z (228+242+256+270) mass chromatograms for representative samples from the Shahejie Formation, showing the identification and distribution patterns of benzo[a]anthracene, triphenylene and chrysene and their $C_1$-$C_3$ alkylated homologues. The identification of $C_1$-$C_3$ alkylated homologues are tentative. Hydrocarbon abbreviations are defined in Table 3.1. The blow-ups show the relative abundance of benzo[a]anthracene, triphenylene and chrysene. For explanation of sample codes see Table 3.2.

The 4 rings PAHs fluoranthene, pyrene, benzo[a]anthracene, triphenylene and chrysene are widespread in the studied samples from the Dongying Depression (Figs 3.3c and

3.6 ). Pyrene, triphenylene and chrysene are generally more abundant than fluoranthene and benzo[a]anthracene. The average relative abundances of pyrene and triphenylene slightly increase from the Es3M to the Es4U members, and there is a decrease in the relative amount of fluoranthene and benzo[a]anthracene (Fig. 3c). The PAHs with 5 or more rings also exhibit varying relative abundance from the Es3M to the Es4U members. The Es4U member has a relatively higher abundance of benzo[e]pyrene, benzo[ghi]perylene and coronene, whereas the opposite is true for the benzo[b,j,k]fluoranthene, benzo[a]pyrene, indeno[1,2,3-cd]pyrene (Fig. 3.3c). This may be a result of the thermal behaviour due to their individual chemical stability, and could reflect varying organic matter inputs.

## 3.5. Discussion

### 3.5.1. Palaeoenvironment

Climate variation can trigger small scale fluctuations in ancient lake levels (Carroll and Bohacs, 2001; Renaut et al., 2013). Lakes can expand or contract in accordance with climate conditions, and these simultaneously can control the extent of terrigenous higher plant input resulted from the water runoff. Arid climates generally have scarce rainfall, high lake evaporation and low water input to the lake. Consequently, water salinity increases and bottom water stratification can develop. Conversely, under humid climates there is plentiful rainfall which may causes the expansion of a lake, the flourishing of terrigenous higher plants, and ample water flow to carry organic matter, sediments and nutrients into the lake. The number of aquatic organisms increases with the oxygen content of the water column. The Es4U member was deposited in a balanced-filled lake, a type that is often associated with a relatively closed hydrology (Carroll and Bohacs, 1999). Lake level fluctuations are strongly climatically driven (Zhang et al., 2009). However, the Es3M member was deposited in an over-filled lake that was bottom ventilated, instead of stratified as seen in the Es4U member.

In hydrologically-closed, balanced and overfilled lakes the palaeoclimate conditions largely control the water level fluctuations, which is explained by the frequent humid-arid cycle alteration (Carroll and Bohacs, 1999; Bohacs, 2000). The rhythmic resistivity logs for the Es4U member are consistent with laminated, excellent source rocks (Zhang et al., 2009) and alternating palaeoclimate conditions, as also indicated by periodic stratification and hypersalinity which preserves organic matter without bioturbation from benthic organisms (Liu et al., 2004). The abundant algal organic matter inputs to the Dongying Depression include dinoflagellates of the *Defladrea*, *Senegalinium*, *Palacostomocysts* species, and green algae (*Bohaiensis*, *Pediastrum* and *Botryococcus* genera) (Li et al., 2003). Some of these algae could be indicative of the salinity of the water body (Peters and Cassa, 1994). Coccoliths, which are an indication for high salinity, are only present in the Es4U member (Liu et al., 2000). From the Es4U member shales to the Es3M member mudstones there was an increase in sedimentation rate (Yao et al., 1994), and a decrease in water salinity, as the lake evolved from a shallow lake facies to a deep lake facies, and then to a semi-deep lake facies (Cai and Jiang, 1995). Changes from the strongly laminated Es4U member to the macro fabrics of the Es3 member likely reflect increasing oxygen level, with greater bioturbation when the Es3 member was deposited. Moreover, pyrite is more abundant in the Es4U member than the Es3L and Es3M members, which was ascribed to the higher salinity and sulphate content in the Es4U member (Zhang et al., 2009).

After intensive faulting, the palaeo-lake was severely evaporated, due to a prolonged period of arid climate when the Es4U member was being deposited, hence giving rise to saline water conditions (Li et al., 2003). This is corroborated by the fossils identified including *Discobis* sp., *Amrmmonia* and *Nonion* (Li et al., 2003). Gammacerane is a reduction product of tetrahymanol, which usually indicates enhanced water salinity and water body stratification accompanied with anoxic conditions (Ten Haven et al., 1988; Sinninghe Damsté et al., 1995).

In addition, the homohopane index (Table 3.2) is commonly considered to reflect reducing depositional environments in the water column. The gammacerane index correlates well with the pristane/phytane (Pr/Ph) ratio and the homohopane index (Table 3.2), which make them good indications for water salinity and redox conditions in the Dongying Depression. Our data (Table 3.2) show elevated concentrations of gammacerane in the Es4U member samples, and the gammacerane index is as high as 2.5. The Pr/Ph is generally less than 1.0, and is as low as 0.34, indicating anoxic conditions and saline or hypersaline stratification of the bottom waters. During deposition of the Es3 member, there was a higher subsidence rate than sedimentation rate, resulting in a deeper and wider lake (Zhang et al., 2004). The Pr/Ph ratio is higher, and the β-carotane and gammacerane content significantly reduced in the Es3 member (Table 3.2), suggesting decreased water salinity, increased oxygen, suboxic bottom waters and a less-stratified water body, consistent with humid and warm conditions during deposition (Chen et al., 2016; He et al., 2017).

Many PAHs preserved in sediments are useful for assessing the variability of the changing palaeo-conditions. The dibenzothiophene/phenanthrene (DBT/P) ratio reflects the source rock lithology (Hughes et al., 1995). The low values of the DBT/P (<1.0) and the Pr/Ph (<1.0) ratios indicate a saline anoxic lacustrine or marine setting for the deposition of the Shahejie Formation. Chakhmakhchev and Suzuki (1995) proposed that hypersaline depositional environments might contribute to the alkylation reactions of dibenzothiophene, leading to a very low concentration of unmethylated dibenzothiophene. The relative abundance of dibenzothiophene, methyldibenzothiophenes and dimethyldibenzothiophenes differs in each member investigated in this study (Table 3.2). For three hypersaline samples with a gammacerane index >1.4, the dimethyldibenzothiophene (%) is over 50% of all alkylated DBTs and the dibenzothiophene (%) is approximately 10% (Fig. 3.8a). These samples also

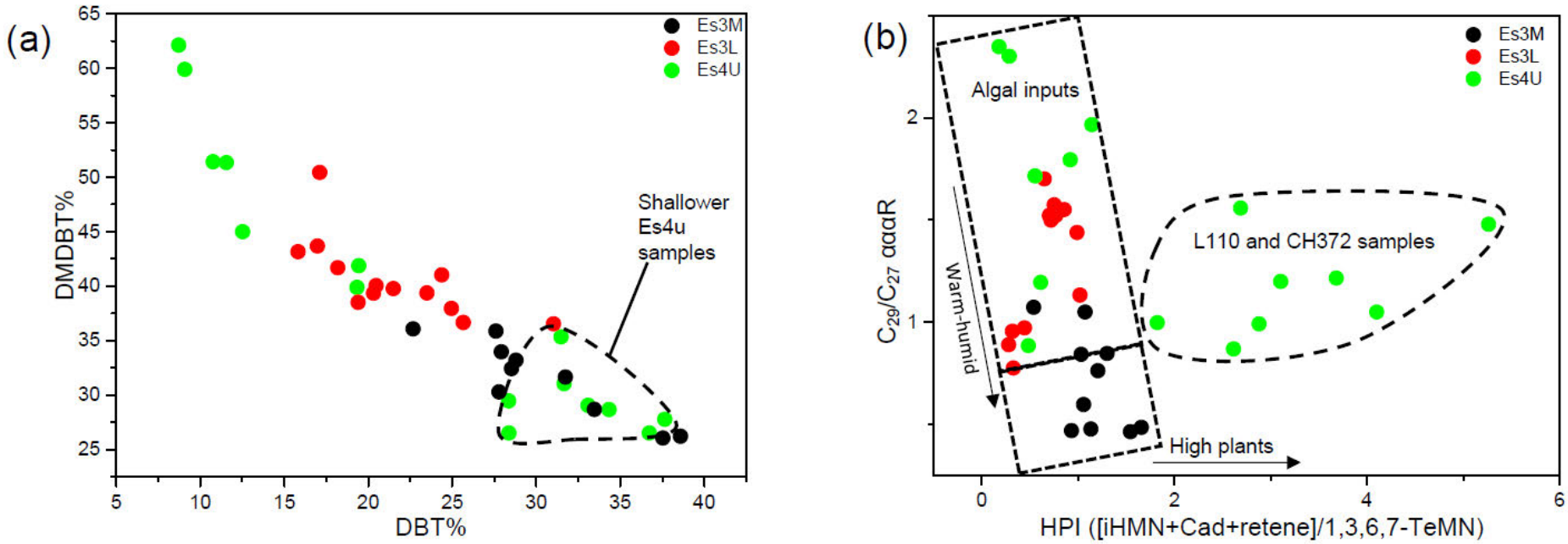


Fig. 3.8 Cross-plots of (a) the relative abundance of dibenzothiophene (% of total DBT + MDBT + DMDBT) against the relative abundance of dimethyldibenzothiophenes (% of total DBT + MDBT + DMDBT); (b) the $C_{29}/C_{27}$ ααα 20R sterane ratio against the higher plant index (HPI). The dashed circle indicates the samples from the L110 and CH372 core with shallower burial depth. Line charts showing (c) the ratios gammacerane/$C_{30}$ αβ hopanes, $C_{35}/(C_{35} + C_{34})$ homohopanes and DMDBT/(DBT + MDBT + DMDBT); and (d) the $C_{29}$ ααα 20S/(20S+20R) and $C_{29}$ αββ/(αββ+ααα) sterane ratios, and the DMDBT/(DBT + MDBT + DMDBT) ratio. The line charts showing variation in these ratios from the top Es3M member to the Es3L member, and then to the basal Es4U member of the Shahejie Formation. Hydrocarbon abbreviations are defined in Table 3.1. For explanation of sample codes see Table 3.2.

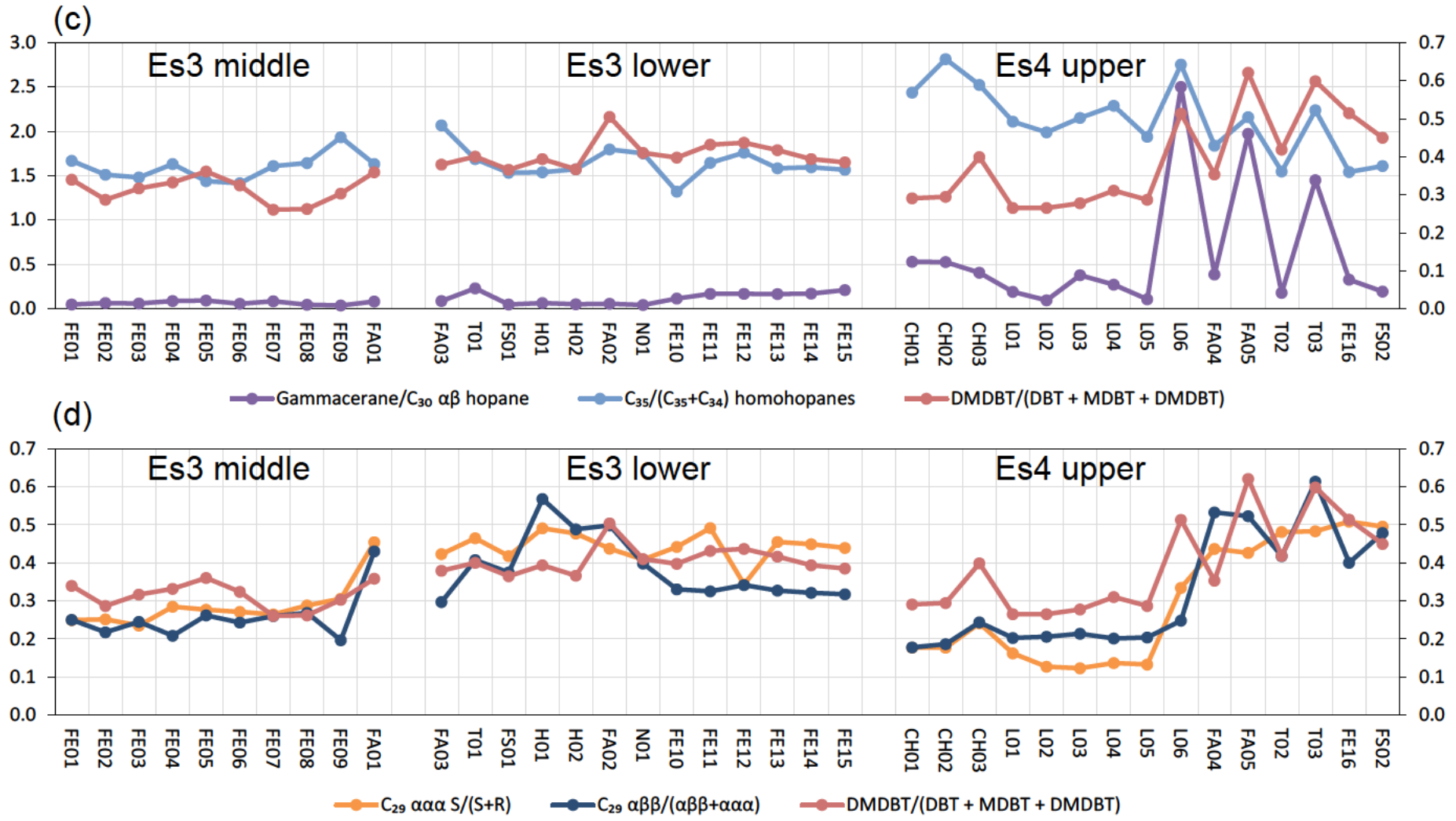


Fig. 3.8 (*continued*)

have high concentrations of $C_{35}$ homohopane (Table 3.2). In general, the Es4U member (except for the L110 and CH372 samples) has higher dimethyldibenzothiophene contents than the Es3L member, which in turn has higher dimethyldibenzothiophene contents than the Es3M member (Fig. 3.8a). Strong hypersalinity in three of the samples from the Es4U member, as shown by the elevated gammacerane and $C_{35}$ homohopane contents, correlate well with the relative abundance of dimethyldibenzothiophenes, thus creating a sawtooth-like pattern (Fig. 3.8c). However in this study, the low dimethyldibenzothiophene contents in the Es3M member may be mainly due to the lower thermal maturity in the shallower samples, rather than greater salinity. In order to assess the possible maturity effect on the distribution of alkyldibenzothiophenes, two sterane thermal maturity parameters were plotted against the relative abundance of dimethyldibenzothiophenes (Fig. 3.8d). Nine shallower Es4U member samples (L01-06 and CH01-03; 2571.5-2897.8m) with lower thermal maturity have relatively lower contents of dimethyldibenzothiophenes than the deeper samples, and are more similar to the Es3M samples (Fig. 3.8d). Therefore, thermal maturation is the primary control on the alkylation of the dibenzothiophenes in this study, with a slight enhancement of alkylation in the Es4U member samples deposited under hypersaline conditions.

In summary, saline/occasionally hypersaline water conditions are suggested for the Es4U member, and brackish/saline water conditions are suggested for the Es3L and Es3M member samples.

### 3.5.2. Algal-derived aromatic hydrocarbons

Retene, cadalene and simonellite widely occur in conifer resins (Grimalt et al., 1988; Otto et al., 2003; Grimalt et al., 2004), although Jiang et al. (1998) also suggested a potential microbial source for retene. These three compounds have commonly been used as higher plant indicators during oil-oil and oil-source rock correlation (van Aarssen et al., 1996). Retene is

mainly derived from higher plants that adapt well to a humid climate, whilst cadalene and simonellite are derived from higher plants that can survive and thrive in a relatively arid climate (Yakir et al., 1994; Lipp et al., 1996). Although the dominant organic matter inputs for the Shahejie Formation are conclusively algal and aquatic organisms (Liu and Wang, 2013), terrigenous higher plant input in the Es4U and Es3L member samples is not negligible. The ternary diagram of retene, cadalene and iHMN shows that the Es4U member samples contain relatively more cadalene, while the Es3L and Es3M member samples are more enriched in retene, especially so for the Es3L samples (Fig. 3.9a). This is consistent with the previously defined arid climate conditions for the Es4 member, and humid climate conditions for the Es3 member (Li et al., 2003; Wang et al., 2008). The proportion of $C_{27}$ sterane relative to $C_{28}$ and $C_{29}$ steranes varies through the members of the Shahejie Formation (Fig. 3.9b). The Es3M member contains larger proportions of $C_{27}$ steranes relative to $C_{29}$ steranes than the Es3L and Es4U members. The latter two sections contain $C_{29}$ steranes ≥ $C_{27}$ steranes. This is consistent with a greater contribution of organic matter from terrigenous land plants for the Es4U and Es3L members, and a greater algal/planktonic contribution for the Es3M member. The higher plant index (defined as HPI = ([iHMN + Cad + Ret]/1,3,6,7-TeMN); van Aarssen et al., 1996) plotted versus the $C_{29}/C_{27}$ ααα 20R sterane ratio can be used to differentiate the organic matter inputs from the bottom Es4U member to the top Es3M member (Fig. 3.8b). Oddly, there is no positive correlation, and indeed an inverse correlation through most of the data. Samples with higher $C_{29}/C_{27}$ ααα 20R sterane ratios have lower HPI values. Nevertheless, the saline lacustrine setting for the Dongying Depression, suggests another possible explanation for the anomalous sterane trend. It is known that specific algae can produce $C_{29}$ sterols as precursors for the $C_{29}$ steranes (Volkman et al., 1998). Moreover, an even-over-odd carbon number predominance for the *n*-alkanes has been recognised in samples from the Shahejie Formation (Wang et al., 2010). The even-over-odd

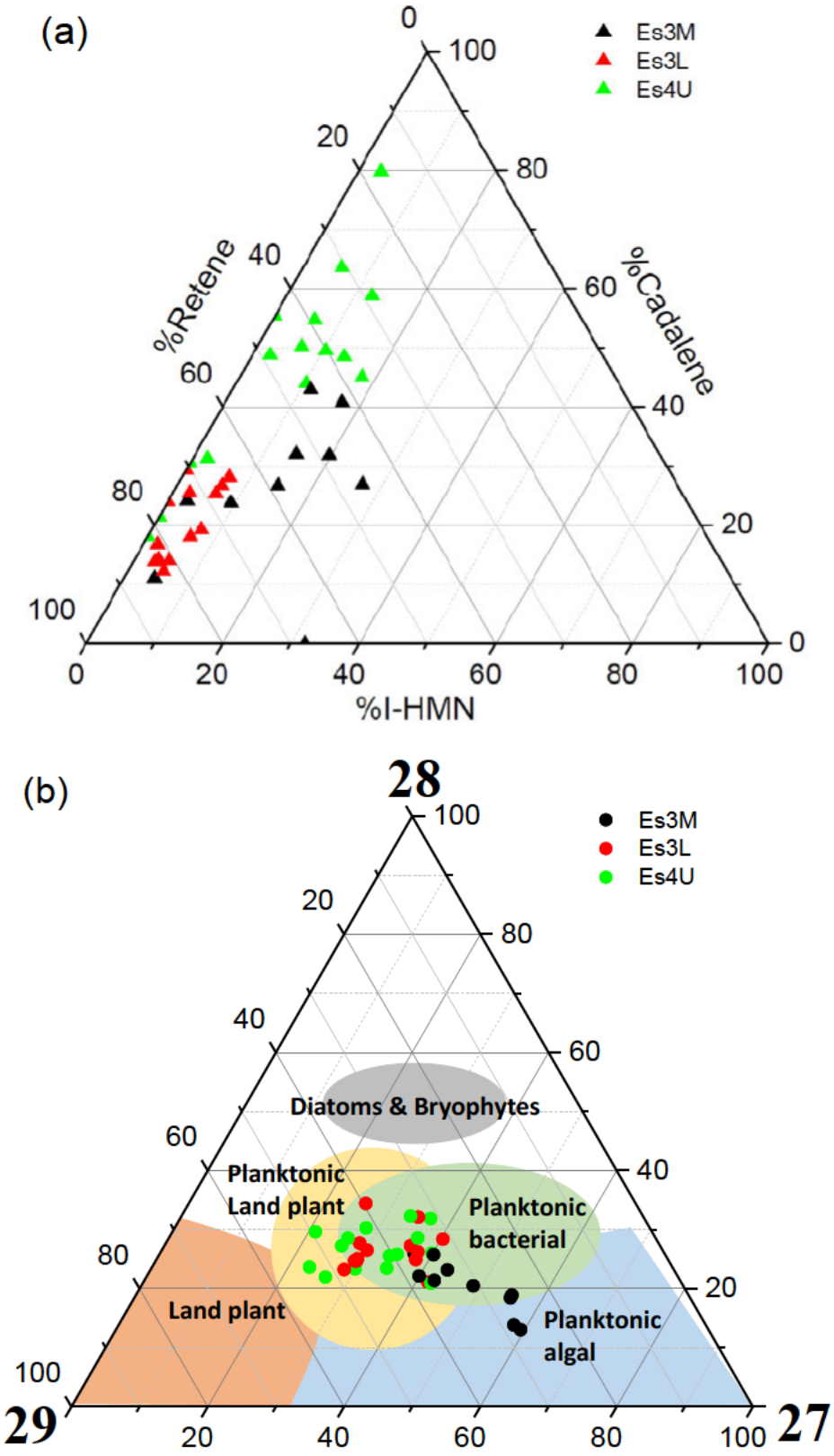


Fig. 3.9 Ternary diagrams showing the relative abundance of (a) retene, cadalene and 1-isohexyl-2-methylnaphthalene (iHMN) in the aromatic fractions, and (b) $C_{27}$, $C_{28}$ and $C_{29}$ ααα 20R steranes in the aliphatic fractions, of the source rocks from the Es3M, Es3L and Es4U members of the Shahejie Formation. Hydrocarbon abbreviations are defined in Table 3.1. 27 = $C_{27}$ ααα 20R %, 28 = $C_{28}$ ααα 20R %, and 29 = $C_{29}$ ααα 20R % (measured in m/z 217). Fields in the sterane diagram are from Huang and Meinschein (1979).

carbon number predominance for high molecular weight *n*-alkanes is likely associated with a low maturity, hypersaline environment with algal organism input (Metzger et al., 1991; Huang et al., 2003; Feng et al., 2007; Bechtel et al., 2012). This corroborates the significant algal input for $C_{29}$ steroids in the Shahejie Formation. The sterane/hopane ratio (Table 3.2) can help differentiate eukaryotic organic matter input (algae and higher plants) from prokaryotic organic matter (Grantham and Wakefield, 1988; Peters et al., 2005). Elevated concentrations of gammacerane and phytane indicate enhanced water column salinity and even water column stratification at times, conditions that are favourable for the algae contributing to steroidal biomarkers. There is a very good correlation ($R^2 = 0.92$) between the gammacerane index and the sterane/hopane ratio (Table 3.2), which suggests a close association between organism inputs and the palaeoredox conditions of the water column. Therefore, the predominance of $C_{29}$ steranes over $C_{27}$ and $C_{28}$ steranes as an indicator of higher plant input into the source rock is probably invalid for the Dongying Depression (Figs 3.8b and 3.9b). The Es4U member is interpreted to have been deposited in a stable stratified water column with organic matter inputs dominantly from algae that could produce $C_{29}$ sterols, which resulted in high $C_{29}/C_{27}$ ααα R sterane ratios (Fig. 3.8b). In the shallower Es3L member, the climate progressively became warmer and more humid, so that terrigenous higher plant input slightly increased, and algal input decreased (as indicated by the decrease of the sterane/hopane ratio; Table 3.2). The ample nutrient supply and higher dissolved oxygen content of the water column accelerated the growth of allochthonous aquatic organisms, as is corroborated by the larger proportions of $C_{27}$ steranes and the lowest sterane/hopane ratios for the Es3M member samples (Table 3.2).

The control on the relative distributions of the substituted and unsubstituted aromatic hydrocarbons includes organic matter inputs and thermal maturity. The aromatic hydrocarbons 1,2,5-trimethylnaphthalene (1,2,5-TMN), 1-methylphenanthrene (1-MP; Fig. 3.4d), 1,7-dimethylphenanthrene (1,7-DMP; Fig. 3.4d) and retene are commonly used to

characterise the relative contribution of coniferous terrigenous organic matter (Alexander et al., 1988; Volk et al., 2004). These parameters should be used with caution if there is the possibility of significant thermal maturity variation. Ratios using these compounds are used to differentiate organic matter inputs for the samples from the Es3M, Es3L and Es4U members (Fig. 3.10a and 10b). Exceptions which fall off the main correlation lines are the shallower and less mature Es4U samples from core L110 and CH372, which suggests a maturity effect on Log(Retene/9-MP) and Log(1,2,5-TMN/1,3,6-TMN). However, a satisfactory correlation ($R^2$ = 0.71) between Log(1-MP/9-MP) and Log(1,7-DMP/1,3- + 3,9- + 2,10- + 3,10-DMP) is observed for the whole sample set, regardless of the lower thermal maturity of the L110 and CH372 samples (Fig. 3.10c). The only explanation for this distinction between the members is that there are considerable differences in source inputs, as is supported by the poor relationships of Log(1-MP/9-MP) and Log(1,7-DMP/1,3- + 3,9- + 2,10- + 3,10-DMP) with maturity parameters (Table 3.2).

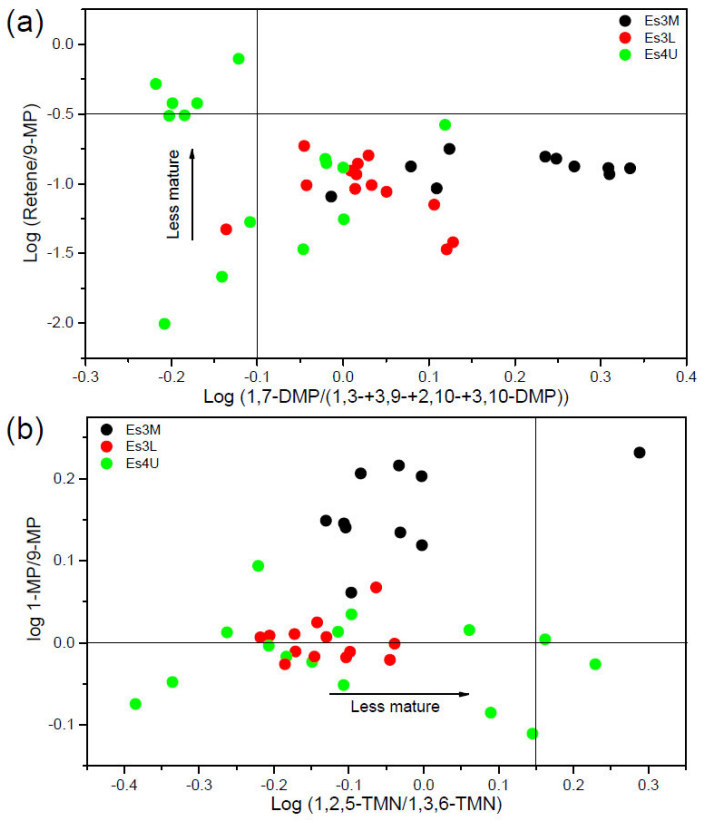

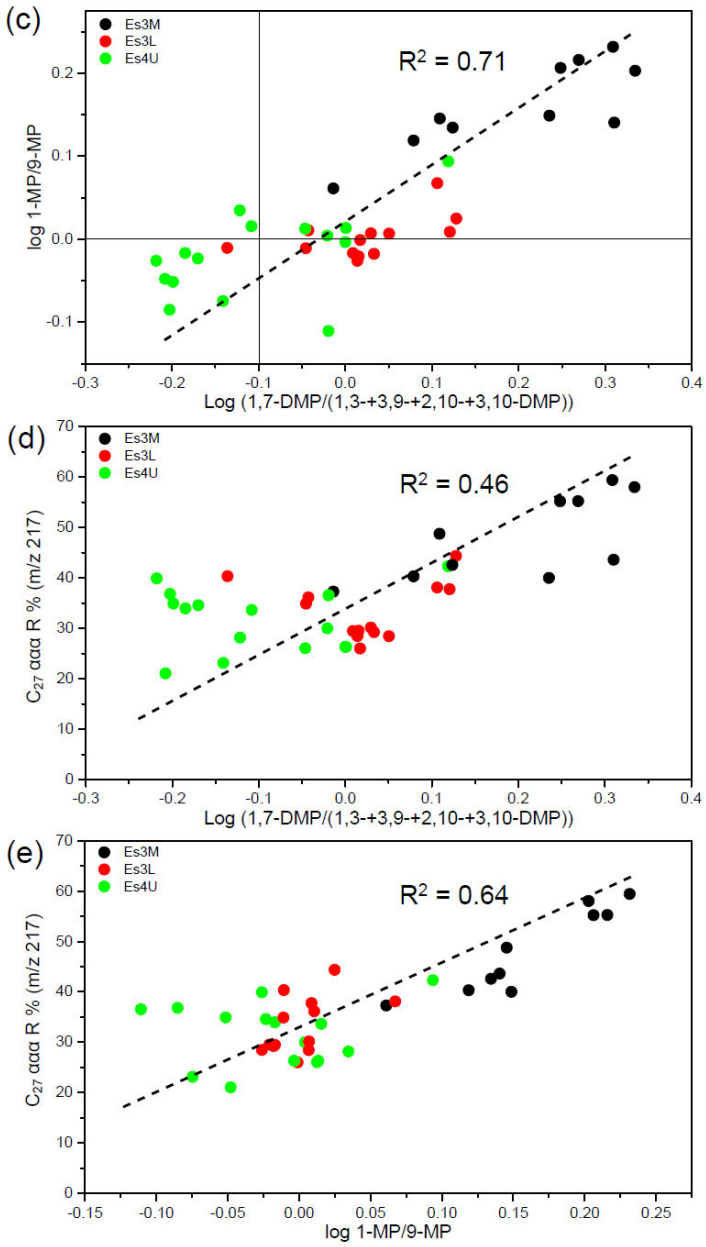


Fig. 3.10 Cross-plots of aromatic hydrocarbon source parameters for the Shahejie Formation samples. (a) Log(Retene/9-MP) versus Log(1,7-DMP/1,3- + 3,9- + 2,10- + 3,10-DMP); (b) Log(1-MP/9-MP) versus Log(1,2,5-TMN/1,3,6-TMN); (c) Log(1-MP/9-MP) versus Log(1,7-DMP/1,3- + 3,9- + 2,10- + 3,10-DMP). Cross-plots of the % $C_{27}$ ααα 20R steranes (of total $C_{27}$-$C_{29}$ ααα 20R steranes) with (d) Log(1,7-DMP/1,3- + 3,9- + 2,10- + 3,10-DMP) and (e) Log(1-MP/9-MP), showing consistent correlations. Hydrocarbon abbreviations are defined in Table 3.1.

There is strong support from the production of 1-MP and retene from rearranged phyllocladane precursors (Simoneit, 1997), and the similar carbon isotopic values ($\delta^{13}C$ = -23‰) of retene and phyllocladane in Gippsland Basin oils (Murray et al., 1998), suggested a mainly terrigenous land plant origins. However, intriguingly in the Dongying Depression

lacustrine setting, the relative abundance of $C_{27}$ ααα 20R steranes (%) is strongly correlated with Log(1-MP/9-MP) and Log(1,7-DMP/1,3- + 3,9- + 2,10- + 3,10-DMP) (Fig. 3.10d and 10e), regardless of thermal maturity level. This suggests an aquatic organism contribution to these phenanthrene-family compounds, in contrast to a combustion and/or higher plant source. The variation of these ratios may indicate the relative level of specific algal input, given that the $C_{27}$ steranes are known to be derived from phytoplankton/algae (Volkman et al., 1998; Peters et al., 2005; Volkman, 2005). The potential of phytoplankton (the green algae *Chlorella protothecoides*) and a cyanobacterium (*Synechocystis* sp.) as a possible source for retene was proposed by Zhou et al. (2000). Grice et al. (2007) suggested a common algal origin for 9-MP, chrysene and benzo[e]pyrene by noticing a similar carbon isotopic compositions of these aromatic hydrocarbons in the Perth Basin, Western Australia. There are good correlations of the relative abundance of alkylphenanthrenes (ΣMPs; 9-MP; 1-MP; 2,3- + 1,9- + 4,9- + 4,10-DMP; 1,6- + 2,9- + 2,5-DMP), 4-ring triphenylene (isochrysene) and 5-ring benzo[e]pyrene (Fig. 3.11a-f), suggesting a common source for these but with different levels of aromatisation (Fig. 3.11g), consistent with what Grice et al. (2007) suggested. Additionally, the relative abundance of phenanthrene-family compounds such as chrysene, triphenylene and 9-MP progressively increase as the sterane/hopane ratio and gammacerane index increase (Table 3.2), suggesting an increasing contribution from the eukaryotic algae that is bound up with water salinity.

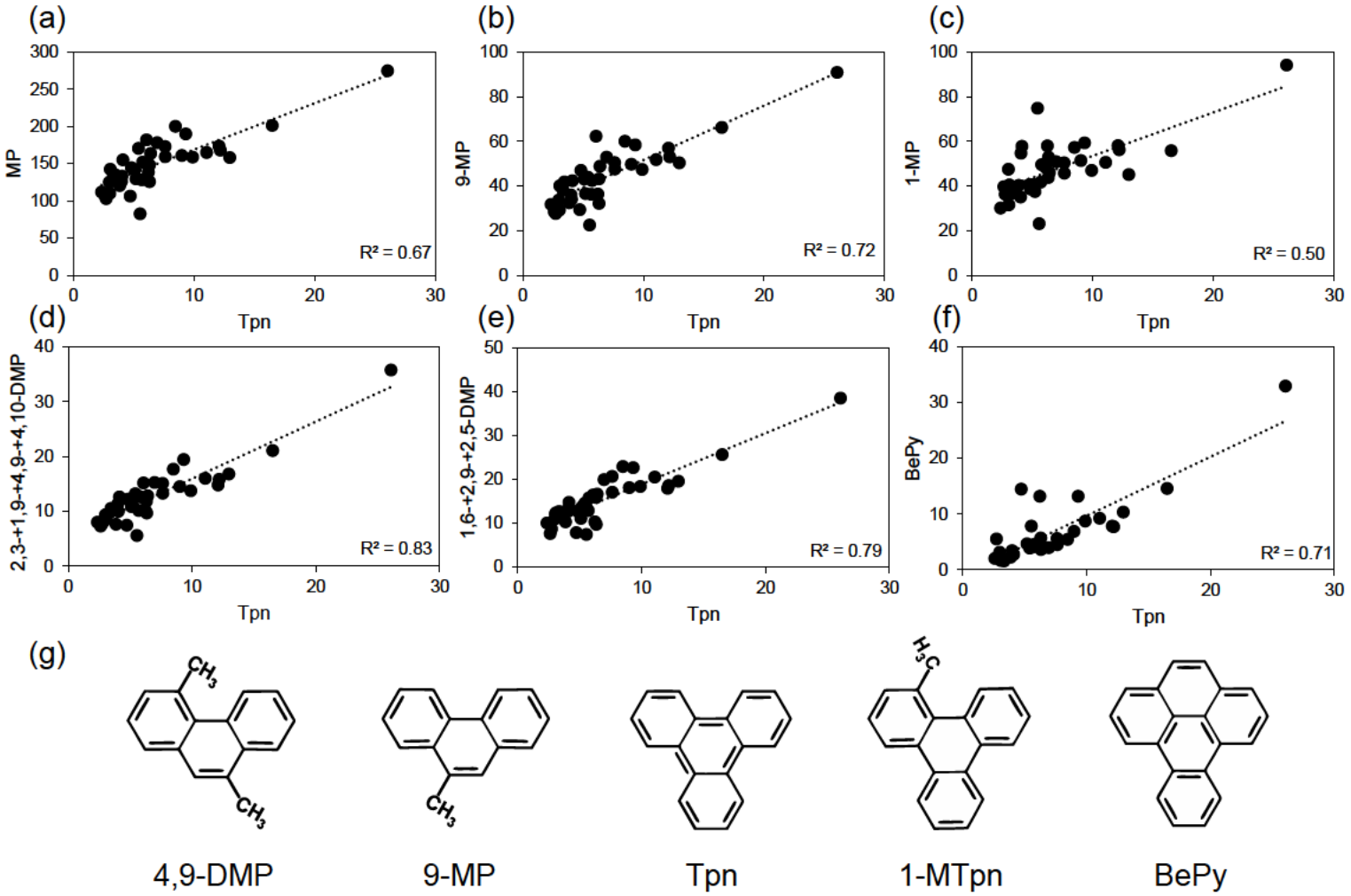


Fig. 3.11 Cross-plots for the Shahejie Formation samples of the relative abundance of triphenylene with (a) ΣMPs, (b) 9-MP, (c) 1-MP, (d) 2,3- + 1,9- + 4,9- + 4,10-DMP, (e) 1,6- + 2,9- + 2,5-MP and (f) benzo[e]pyrene. All relative abundances are normalised to phenanthrene. (g) The molecular structures of 4,9-DMP, 9-MP, triphenylene, 1-methyltriphenylene and benzo[e]pyrene, showing likely similar origins. Hydrocarbon abbreviations are defined in Table 3.1.

### 3.5.3. Diagenetic and petrogenic origins

The PAHs produced by incomplete combustion of organic matter can be preserved and transported long distances to lacustrine and marine depositional sites (Cope, 1981). The relative abundance of various PAHs in ancient sediments can reflect the frequency and extent of palaeo-vegetation fires, which is dependent on fuel loads and climatic conditions (Rundel, 1981; Scott, 2000). Warm and humid conditions favour the growth of land plants, and seasonally arid conditions can give rise to combustion events. The unsubstituted PAHs that are indicators of higher plant wildfires occur in relatively low abundance in the aromatic fractions from the rock extracts of the Dongying Depression, but exhibit significant trends in this study (Fig. 3.2). Since there is also no evidence for volcanic activity, the formation of PAHs was not caused by large scale vegetation wildfires due to volcanic activity, which is reasonable given the lacustrine setting. The unsubstituted (parent) PAHs detected in varying amounts have from 2 rings to 7 rings and include naphthalene, biphenyl, fluorene, dibenzothiophene, phenanthrene, fluoranthene, pyrene, benzo[a]anthracene, triphenylene, chrysene, 2-phenynaphthalene, benzo[b,j,k]fluoranthene, benzo[e]pyrene, benzo[a]pyrene, indeno[1,2,3-cd]pyrene, benzo[ghi]perylene and coronene, and the alkyl homologues of some of these. Abundant $C_2$-$C_4$ alkyl PAHs are normally considered to be non-combustion derived (Youngblood and Blumer, 1975). The level of resistance to biodegradation of PAHs and their alkyl homologous increases with increasing number of aromatic rings, and varies depending on the number and position of the alkyl groups (Huang et al., 2004; Greenwood et al., 2008; Chen et al., 2013). In addition, thermal maturity can also affect the distributions of PAHs and their alkyl isomers. The extent of alkyl-substitution of PAHs is determined by diagenetic/catagenetic reactions and sources (Yunker et al., 2002), including alkylation reactions (Alexander et al., 1995; Bastow et al., 2000).

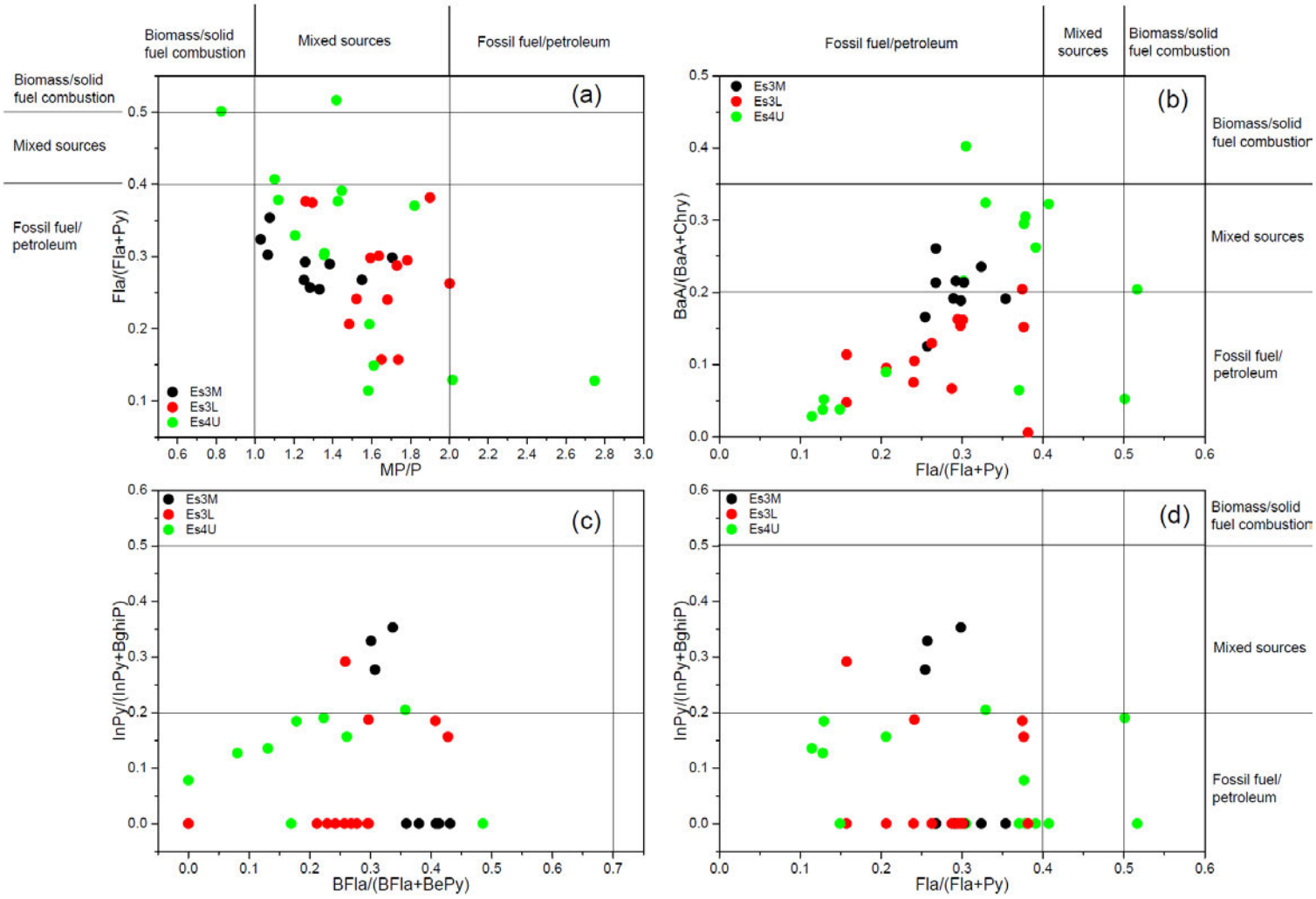


Fig. 3.12 PAH ratio cross-plots for the Shahejie Formation samples, characterising the origins of the PAHs. (a) MP/P versus Fla/(Fla + Py); (b) Fla/(Fla + Py) versus BaA/(BaA + Chy); (c) BFla/(BFla + BePy) versus InPy/(InPy + BghiP); and (d) Fla/(Fla + Py) versus InPy/(InPy + BghiP). Hydrocarbon abbreviations are defined in Table 3.1. Fields in the diagrams are from Budzinski et al. (1997), Zakir Hossain et al. (2013) and Yunker et al. (2015).

The methylphenanthrene/phenanthrene (MP/P) ratio was proposed to distinguish diagenetic/catagenetic and combustion/pyrogenic origins of PAHs in sediments (Prahl and Carpenter, 1983; Yunker et al., 2002). When the MP/P ratio is <1.0 it indicates mainly combustion or pyrogenic sources for the PAHs, due to the very abundant unsubstituted parent PAH that formed during a high temperature process. When the MP/P ratio is >2.0, diagenetic or catagenetic (i.e. fossil fuel/petroleum) sources for the PAHs are indicated (Prahl and Carpenter, 1983; Garrigues et al., 1995; Budzinski et al., 1997; Liu et al., 2005). The MP/P ratios of the samples from the Dongying Depression range from 0.83 to 2.8, with an average value of 1.5 (Fig. 3.12a), suggesting a mixed origin from both diagenesis/catagenesis and combustion/pyrogenic sources. Thermal maturity also has an influence on this ratio (Radke et al., 1982).

Heat is an essential prerequisite for the formation of PAHs (Oros et al., 2006; Denis et al., 2012). Of the PAHs with ⩾4 rings, fluoranthene, pyrene, benzo[a]anthracene, triphenylene, chrysene, benzo[b,j,k]fluoranthene, benzo[e]pyrene, benzo[a]pyrene, indeno[1,2,3-cd]pyrene, benzo[ghi]perylene and coronene are commonly recognised as combustion markers (Killops and Massoud, 1992; Bence et al., 1996; Jiang et al., 1998; Grimalt et al., 2004; Yunker et al., 2011). Characteristic combustion-related PAHs in some samples such as T03 and FA04 are triphenylene and chrysene, which are detected in the *m/z* 228 mass chromatogram (Figs 3.6 and 3.7). Benzo[a]anthracene is present in lower concentrations relative to the triphenylene and chrysene doublet peak, and the next most prominent peak is benzo[e]pyrene which is detected in the m/z 252 mass chromatogram (Fig. 3.6). The PAH ratios of Fla/(Fla + Py), BaA/(BaA + Chy), InPy/(InPy + BghiP) and BFla/(BFla + BePy) have also been proposed for assessing origins from fossil fuel/petroleum (petrogenic sources: thermal alteration of natural biolipids due to normal burial processes during diagenesis and catagenesis in sedimentary basins) or the combustion of biomass/solid

fuel (pyrogenic sources) (Grice et al., 2007; Quiroz et al., 2011; Zakir Hossain et al., 2013; Yunker et al., 2015). Relatively low values for these ratios (Fla/(Fla + Py) <0.4; InPy/(InPy + BghiP) <0.2; BaA(BaA + Chy) <0.2) collectively indicate petrogenic inputs, whereas high ratios (Fla/(Fla + Py) >0.5; InPy/(InPy + BghiP) >0.5; and BaA/(BaA + Chy) >0.35) indicate pyrogenic sources. The samples from the Dongying Depression have values of Fla/(Fla + Py) and BaA/(BaA + Chy) that are less than 0.52 and 0.40, respectively, and the values of InPy/(InPy + BghiP) and BFla/(BFla + BePy) are less than 0.35 and 0.49, respectively (Fig. 3.12b-12d). Almost all the samples analysed fall within the range of fossil fuel/petroleum (petrogenic) origin and liquid fuel combustion origin (Yunker et al., 2015), indicating that extensive wildfires did not occur in the Dongying Depression during the deposition of the Shahejie Formation (Fig. 3.12). These parameters suggest a dominant petrogenic source for the PAHs, and in some samples a mixed fossil fuel/petroleum (petrogenic) and combustion (pyrogenic) source. The latter is likely explained by low temperature (200-300 ℃) surface fires spread through surface fuels of grasses, bushes or woody debris (Scott, 2000), given that terrigenous input is limited in the Dongying Depression.

Li et al. (2012a) used the BaA/(BaA + Chy) ratio to distinguish the petroleum systems in the Tarim Basin of western China. This study suggested that when the BaA/(BaA + Chy) ratio is less than 0.35 it could imply a petrogenic input for the benzo[a]anthracene, which was attributed to differences in the depositional environment and/or organic matter input (Li et al., 2012a). In the Dongying Depression, the PAH ratios for samples from the Es3M and Es3L members are somewhat differentiated from each other, and the ratios for the Es4U member samples have a large range (Fig. 3.12). These variations are likely due to the thermal maturity behaviour of these PAHs associated with burial depth. It is noteworthy that the Es4U samples from the L110 and CH372 cores which have anomalous Fla/(Fla+Py), BaA/(BaA+Chy) and MP/P ratios relative to the Es3M and Es3L samples are from the shallower intervals

(approximately 2571.5-2897.8m). Furthermore, the Tpn/(Tpn+Chy), BaA/(BaA+Chy) and MP/P ratios have reasonable correlations with biomarker maturity parameters (Table 3.2) such as $C_{29}$ ααα 20S/(20S+20R), $C_{29}$ αββ/(αββ+ααα) and Ts/(Ts+Tm), which is also consistent with a maturity control on the occurrences of PAHs that were not sourced from abnormal heating. Since the detected PAHs were probably mainly formed during normal geological process, or may be sourced from low temperature (200-300 ℃) surface fires, it is more likely that the relatively low amounts of PAHs in the Dongying Depression are the products of 'slow' and 'microthermal' heating, rather than 'quick' and 'macrothermal' wildfires. Even with some terrigenous organic matter input in the Dongying Depression, there was no adequate seasonal climate variability leading to the occurrence of intense vegetation fires. In support of this conclusion is the relatively low abundance of the 6-ring indeno[1,2,3-cd]pyrene and benzo[ghi]perylene and the 7-ring coronene in the Dongying Depression, which if present in high abundance would indicate high intensity palaeo-vegetation fires (Finkelstein et al., 2005), including 800-900 ℃ crown fires (Pyne et al., 1996; Scott, 2000).

### 3.5.4. Distribution of benzo[a]anthracene, triphenylene and chrysene as indications of thermal maturity

Many conventional thermal maturity parameters based on aromatic hydrocarbons such as alkylnaphthalenes (e.g. TNR-1, TNR-2, TMNr, TeMNr; Table 3.2) and alkylphenanthrenes (e.g. MPI, MPDF, MPR, DPR; Table 3.2) are invalid (i.e., do not accurately reflect thermal maturity) in the Dongying Depression, probably due to the dominantly algal input to the source rocks. Some of these aromatic parameters show opposite trends with increasing burial depth in the Dongying Depression. A control group of three samples from the CH372 core and six samples from the L110 core, all from the Es4U member, were analysed to evaluate the maturity effects on the occurrence of the PAHs present in this study. These Es4U member

samples from the South Slope are important immature source rocks with burial depths of <2900 m (Li et al., 2003), because the South Slope is bounded by the Luxi Uplift in the south (Fig. 3.1a). These nine shallowest samples from this study should display a less mature signature that the other samples based on both aliphatic and aromatic thermal maturity parameters. The aliphatic maturity parameters such as the sterane ratios show that the six deeper Es4U samples have the highest maturity, followed by the Es3L member samples, then the Es3M member samples, and lastly the nine shallower samples from the Es4U member which have the lowest thermal maturity (Table 3.2, Fig. 3.8d, Fig 13d). In contrast, the abundance of triphenylene (and other PAHs such as methylphenanthrenes and benzo[e]pyrene) relative to phenanthrene increases with increasing burial depth (Fig. 3.13a), whereas the abundance of benzo[a]anthracene (and other PAHs such as fluoranthene and pyrene) decreases with increasing burial depth (Fig. 3.13b). These trends are likely due to thermal stress, although benzo[e]pyrene is the most stable and least susceptible PAH to post-depositional modifications (Marynowski et al., 2011; Quiroz et al., 2011; Yunker et al., 2011). However, the abundance of other PAH relative to phenanthrene, including chrysene (Fig. 3.13c), benzo[b,j,k]fluoranthene, biphenyl and fluorene show no regular trend with increasing depth. This suggests that the control on these PAHs is mainly due to source of the organic matter, or the depositional environment, and is not strongly influenced by thermal maturity.

Triphenylene, chrysene and benzo[e]pyrene are the most prominent and abundant unsubstituted PAHs (≥4 rings) in this study (Fig. 3.2). The $C_{18}$ benzo[a]anthracene elutes earlier than triphenylene/chrysene doublet on the m/z 228 mass chromatogram (Fig. 3.7). Many studies have reported that the retention time of triphenylene is very close to that of chrysene (Vassilaros et al., 1982; Grice et al., 2007; Drosos et al., 2010), but the thermodynamic behaviour of triphenylene in ancient sediments has not been reported in previous publications. However in this study, triphenylene is well separated on the DB5MS

column, and elutes between benzo[a]anthracene and chrysene (Fig. 3.7), so its geochemical behaviour can be investigated in detail for the first time. Chrysene and its alkylated homologues are carcinogenic and mutagenic (Wood et al., 1977), and are likely derived from the incomplete combustion of biomass/solid fuel, the degradation products of hopanes during diagenesis (Killops and Massoud, 1992; Borrego et al., 1997) or from algae (Grice et al., 2007). The maturity of the organic matter in the Dongying Depression rocks affects the relative abundance of the PAHs, depending on their chemical stability. The relative abundance of benzo[a]anthracene decreases and triphenylene increases with increasing burial depth (Fig. 3.13a and b). Triphenylene has a completely symmetrical chemical structure, whereas benzo[a]anthracene and chrysene are linear hydrocarbons (Appendix) which would be expected to exhibit weaker steric strain than triphenylene. Thus, triphenylene is expected to become more abundant with increasing thermal maturity than benzo[a]anthracene or chrysene. Therefore, we define the triphenylene-chrysene maturity ratio (TCR = Tpn/(Tpn + Chy)) which should increase as thermal maturity increases. In the shallower rocks in the Dongying Depression there is a relatively high abundance of benzo[a]anthracene and a low abundance of triphenylene (Figs 3.7, 3.13e). With increasing burial depth from the Es3M member to the deeper Es4U member samples, the relative abundance of benzo[a]anthracene decreases, and triphenylene becomes more abundant even than chrysene (Figs 3.7, 3.13e).

The consistent depth trends of the aliphatic biomarker maturity indicators $C_{29}$ ααα 20S/(20S+20R) steranes (Fig. 3.13d), $C_{29}$ αββ/(αββ+ααα) steranes, $C_{33}$ αβ S/(S+R) hopanes and Ts/(Ts+Tm) (Table 3.2) shows that thermal maturity does increase as expected with depth in the Dongying Depression. The TCR also increases with depth (Fig. 3.13e), and is well correlated with established biomarker ratios (e.g. $R^2 = 0.63$ with the $C_{29}$ ααα 20S/(20S+20R) sterane ratio). In contrast, the BaA/(BaA + Chy) ratio exhibits a general decrease with increasing depth (Fig. 3.13f), consistent with greatest instability of benzo[a]anthracene. The

values of the TCR and BaA/(BaA + Chy) range from 0.45-0.58 and 0.03-0.09 for the deeper Es4U member samples, 0.35-0.52 and 0.01-0.20 for the Es3L member samples, 0.24-0.38 and 0.13-0.26 for the Es3M member samples, and 0.19-0.34 and 0.06-0.40 for the shallower Es4U member samples, respectively (Fig. 3.14). The ratios for the shallow Es4U member samples are strongly separated from the deeper Es4U member samples. The increase of the TCR with increasing thermal maturity (Figs 3.13e and 3.14) is attributed mainly to a relative increase of the stable triphenylene, because of the larger fluctuations in the relative abundance of chrysene with burial depth (Fig. 3.13c). The parameter TCR increasing uniformly with burial depth, correlates well with biomarker thermal maturity parameters, and is proposed to be useful for the assessment of thermal maturity of the lacustrine oils and sediments in the Dongying Depression.

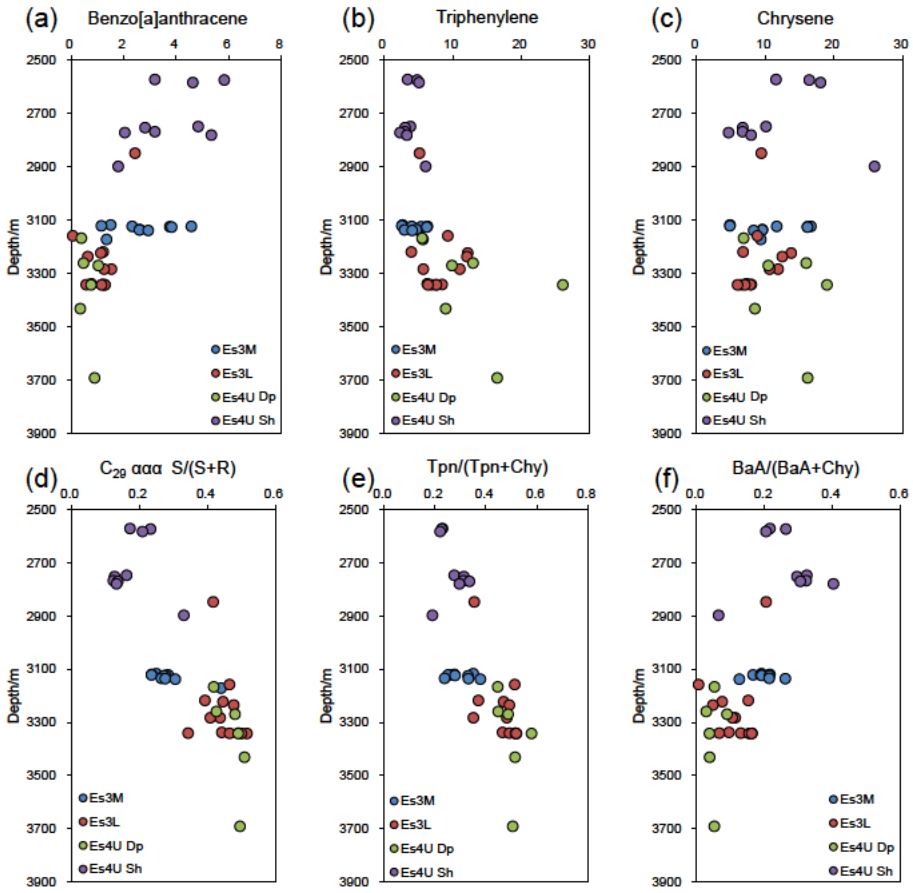


Fig. 3.13 The variation of hydrocarbon (%) ratios with burial depth for the samples from the Dongying Depression. (a) benzo[a]anthracene/phenanthrene; (b) triphenylene/phenanthrene; (c)

chrysene/phenanthrene; (d) $C_{29}$ ααα 20S/(20S+20R) steranes; (e) triphenylene-chrysene ratio (TCR) = Tpn/(Tpn + Chy); (f) BaA/(BaA + Chy). Hydrocarbon abbreviations are defined in Table 3.1. Dp = deepest, Sh = shallowest.

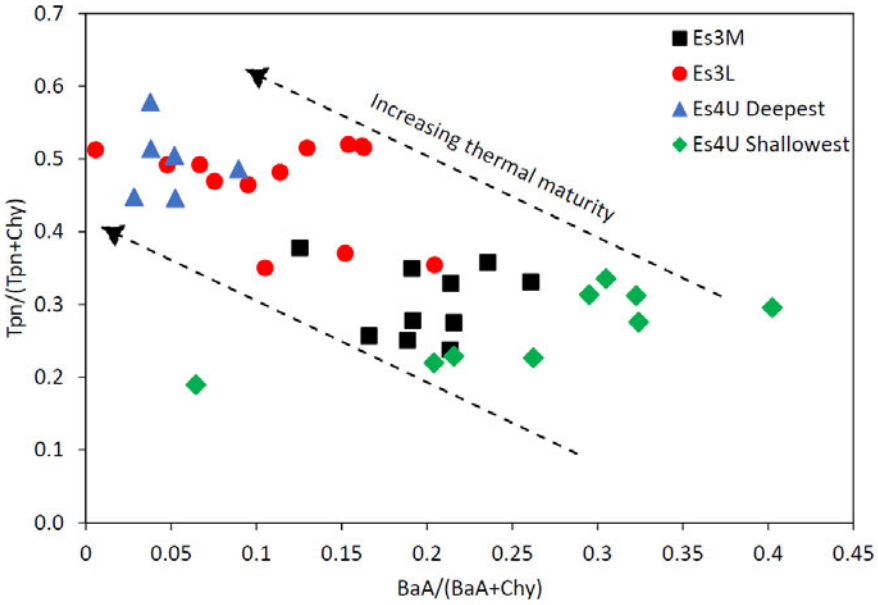


Fig. 3.14 Cross plot of the triphenylene-chrysene ratio (TCR) = Tpn/(Tpn + Chy) versus BaA/(BaA + Chy), showing four maturity groups for the source rock extracts from the Dongying Depression. Abbreviations are defined in Table 3.1.

## 3.6. Conclusions

The sources and origins of polycyclic aromatic hydrocarbons (PAHs) in thirty eight Paleogene organic-rich shales and mudstones from the paralic Dongying Depression, Bohai Bay Basin, China have been assessed. The PAHs included phenanthrene, retene, cadalene, fluoranthene, pyrene, benz[a]anthracene, triphenylene, chrysene, benzofluoranthenes, benzo[e]pyrene, benzo[a]pyrene, indeno[1,2,3-cd]pyrene, benzo[ghi]perylene and coronene. The PAHs in the sedimentary rocks are suggested to be mainly derived from diagenetic/catagenetic processes. The formation of the petrogenic PAHs resulted from 'slow' and 'microthermal' heating, rather than a 'quick' and 'macrothermal' palaeo-vegetation wildfires. The relative low abundance of the 6-ring indeno[1,2,3-cd]pyrene and benzo[ghi]perylene, and the 7-ring coronene, which are mainly derived from high intensity palaeo-vegetation fires, is either due to the inadequate seasonality of a humid-arid climate during deposition in the Dongying Depression, or to limited terrigenous organic matter input. The phenanthrene source parameters Log(1-MP/9-MP) and Log(1,7-DMP/1,3- + 3,9- + 2,10- + 3,10-DMP) are correlated with the relative abundance of $C_{27}$ regular steranes, suggesting an algal/planktonic source. The methylphenanthrenes, triphenylene, alkyltriphenylenes and benzo[e]pyrene may share a common source as their occurrences are closely correlated. Thermal maturation effects are the major control on the relative abundance and distribution of the non-combustion derived PAHs (e.g. biphenyl, fluorene, fluoranthene, pyrene, benz[a]anthracene, triphenylene) in lacustrine sediments. Triphenylene has been completely separated from chrysene and benzo[a]anthracene by gas chromatography. Benz[a]anthracene decreases in relative abundance while triphenylene increases in relative abundance with burial depth/thermal maturity. Correlation of the newly defined triphenylene-chrysene ratio (TCR; triphenylene/(triphenylene + chrysene) with burial depth and biomarker maturity parameters

was observed, showing that it is a useful maturity indicator for lacustrine oils and sediments in the Dongying Depression.

## Acknowledgements

This research was supported by the National Natural Science Foundation of China (Grant No. 41472108). The authors acknowledge the experimental assistance of Carl A. Peters, Sophia Aharonovich, Konstantinos Kotzakoulakis, Huaqing Xu, and Xiong Cheng. We thanks Se Gong in CSIRO for assistance with the MRM GC-MS analyses and molecular sieving. HX thanks the China University of Geosciences (Beijing) and Macquarie University for a co-tutelle PhD scholarship, and Macquarie University for analytical support funds.

# References

Aizenshtat, Z., 1973. Perylene and its geochemical significance. Geochimica et Cosmochimica Acta 37, 559-567.

Albrecht, P., Ourisson, G., 1971. Biogenic substances in sediments and fossils. Angewandte Chemie International Edition 10, 209-225.

Alexander, R., Kagi, R.I., Rowland, S.J., Sheppard, P.N., Chirila, T.V., 1985. The effects of thermal maturity on distributions of dimethylnaphthalenes and trimethylnaphthalenes in some ancient sediments and petroleums. Geochimica et Cosmochimica Acta 49, 385-395.

Alexander, R., Cumbers, K.M., Kagi, R.I., 1986. Alkylbiphenyls in ancient sediments and petroleums. Organic Geochemistry 10, 841-845.

Alexander, R., Larcher, A.V., Kagi, R.I., Price, P.L., 1988. The use of plant-derived biomarkers for correlation of oils with source rocks in the Cooper/Eromanga Basin system, Australia. The APPEA Journal 28, 310-324.

Alexander, R., Larcher, A., Kagi, R., Price, P., 1992a. An oil-source correlation study using age-specific plant-derived aromatic biomarkers. Biological markers in sediments and petroleum, 201-221.

Alexander, R., Larcher, A.V., Kagi, R.I., Price, P.L., 1992b. An oil-source correlation study using age-specific plant-derived aromatic biomarkers. Biological markers in sediments and petroleum, 201-221.

Alexander, R., Bastow, T.P., Fisher, S.J., Kagi, R.I., 1995. Geosynthesis of organic compounds: II. Methylation of phenanthrene and alkylphenanthrenes. Geochimica et Cosmochimica Acta 59, 4259-4266.

Bao, J., Li, M., 2001. Unprecedented occurrence of novel $C_{26}$-$C_{28}$ 21-norcholestanes and related triaromatic series in evaporitic lacustrine sediments. Organic Geochemistry 32, 1031–1036.

Bastow, T.P., Alexander, R., Fisher, S.J., Singh, R.K., Aarssen, B.G.K.V., Kagi, R.I., 2000. Geosynthesis of organic compounds. Part V— methylation of alkylnaphthalenes. Organic Geochemistry 31, 523-534.

Bechtel, A., Widera, M., Sachsenhofer, R.F., Gratzer, R., Lucke, A., Woszczyk, M., 2007. Biomarker and stable carbon isotope systematics of fossil wood from the second Lusatian lignite seam of the Lubstow deposit (Poland). Organic Geochemistry 38, 1850-1864.

Bechtel, A., Jia, J., Strobl, S.A.I., Sachsenhofer, R.F., Liu, Z., Gratzer, R., Püttmann, W., 2012. Palaeoenvironmental conditions during deposition of the Upper Cretaceous oil shale sequences in the Songliao Basin (NE China): Implications from geochemical analysis. Organic Geochemistry 46, 76–95.

Bence, A.E., Kvenvolden, K.A., Kennicutt, M.C., 1996. Organic geochemistry applied to environmental assessments of Prince William Sound, Alaska, after the Exxon Valdez oil spill—a review. Organic Geochemistry 24, 7-42.

Blumer, M., Youngblood, W.W., 1975. Polycyclic aromatic hydrocarbons in soils and recent sediments. Science 188, 53-55.

Bohacs, K.M., 2000. Keys to exploration: Lake-basin type, source potential, and hydrocarbon character within an integrated sequence-stratigraphic/geochemical framework.

Borrego, A.G., Blanco, C.G., Püttmann, W., 1997. Geochemical significance of the aromatic hydrocarbon distribution in the bitumens of the Puertollano oil shales, Spain. Organic Geochemistry 26, 219-228.

Budzinski, H., Jones, I., Bellocq, J., Pierard, C., Garrigues, P.H., 1997. Evaluation of sediment contamination by polycyclic aromatic hydrocarbons in the Gironde estuary. Marine Chemistry 58, 85-97.

Cai, J., Jiang, X., 1995. The Eocene sedimentary system and basin evolution of Dongying Basin. Acta Sedimentologia Sinica 13, 27-37.

Carroll, A.R., Bohacs, K.M., 1999. Stratigraphic classification of ancient lakes: Balancing tectonic and climatic controls. Geology 27, 99-102.

Carroll, A.R., Bohacs, K.M., 2001. Lake-type controls on petroleum source rock potential in nonmarine basins. AAPG Bulletin 85, 1033-1053.

Chakhmakhchev, A., Suzuki, N., 1995. Saturate biomarkers and aromatic sulfur compounds in oils and condensates from different source rock lithologies of Kazakhstan, Japan and Russia. Organic Geochemistry 23, 289-299.

Chen, J., Zhang, H., Huang, H., Li, X., Shi, S., Liu, F., Chen, L., 2013. Impact of anaerobic biodegradation on alkylphenanthrenes in crude oil. Organic Geochemistry 61, 6-14.

Chen, Z., Huang, W., Liu, Q., Zhang, L., Zhang, S., 2016. Geochemical characteristics of the Paleogene shales in the Dongying depression, eastern China. Marine and Petroleum Geology 73, 249–270.

Cope, M.J., 1981. Products of natural burning as a component of the dispersed organic matter of sedimentary rocks. Organic Maturation studies and fossil fuel exploration. Academic Press, London, 89-109.

Denis, E.H., Toney, J.L., Tarozo, R., Anderson, R.S., Roach, L.D., Huang, Y., 2012. Polycyclic aromatic hydrocarbons (PAHs) in lake sediments record historic fire events: validation using HPLC-fluorescence detection. Organic Geochemistry 45, 7-17.

Drosos, J.C., Viola-Rhenals, M., Vivas-Reyes, R., 2010. Quantitative structure–retention relationships of polycyclic aromatic hydrocarbons gas-chromatographic retention indices. Journal of Chromatography A 1217, 4411-4421.

Fan, C.W., Shiue, J., Wu, C.Y., Wu, C.Y., 2011. Perylene dominance in sediments from a subtropical high mountain lake. Organic Geochemistry 42, 116-119.

Fang, R., Li, M., Wang, T.G., Zhang, L., Shi, S., 2015. Identification and distribution of pyrene, methylpyrenes and their isomers in rock extracts and crude oils. Organic Geochemistry 83–84, 65-76.

Feng, Z., Fang, W., Zhang, J., Li, Z., Huang, C., Wang, X., Zhao, Q., Huo, Q., 2007. Distribution and significance of $C_{40+}$ alkanes in the extracts of Cretaceous source rocks from the Songliao Basin. Science in China Series D: Earth Sciences 50, 1510-1520.

Finkelstein, D.B., Pratt, L.M., Curtin, T.M., Brassell, S.C., 2005. Wildfires and seasonal aridity recorded in Late Cretaceous strata from south‐eastern Arizona, USA. Sedimentology 52, 587-599.

Fu, J., Sheng, G., 1989. Biological marker composition of typical source rocks and related crude oils of terrestrial origin in the People's Republic of China: a review. Applied Geochemistry 4, 13–22.

Garrigues, P., De Sury, R., Angelin, M.L., Bellocq, J., Oudin, J.L., Ewald, M., 1988. Relation of the methylated aromatic hydrocarbon distribution pattern to the maturity of organic matter in ancient sediments from the Mahakam delta. Geochimica et Cosmochimica Acta 52, 375-384.

Garrigues, P., Budzinski, H., Manitz, M.P., Wise, S.A., 1995. Pyrolytic and petrogenic inputs in recent sediments: a definitive signature through phenanthrene and chrysene compound distribution. Polycyclic Aromatic Compounds 7, 275-284.

Grantham, P.J., Wakefield, L.L., 1988. Variations in the sterane carbon number distributions of marine source rock derived crude oils through geological time. Organic Geochemistry 12, 61–73.

Greenwood, P.F., Wibrow, S., George, S.J., Tibbett, M., 2008. Sequential hydrocarbon biodegradation in a soil from arid coastal Australia, treated with oil under laboratory controlled conditions. Organic Geochemistry 39, 1336-1346.

Grice, K., Nabbefeld, B., Maslen, E., 2007. Source and significance of selected polycyclic aromatic hydrocarbons in sediments (Hovea-3 well, Perth Basin, Western Australia) spanning the Permian–Triassic boundary. Organic Geochemistry 38, 1795-1803.

Grice, K., Lu, H., Atahan, P., Asif, M., Hallmann, C., Greenwood, P., Maslen, E., Tulipani, S., Williford, K., Dodson, J., 2009. New insights into the origin of perylene in geological samples. Geochimica et Cosmochimica Acta 73, 6531-6543.

Grimalt, J.O., Simoneit, B.R.T., Hatcher, P.G., Nissenbaum, A., 1988. The molecular composition of ambers. Organic Geochemistry 13, 677-690.

Grimalt, J.O., van Drooge, B.L., Ribes, A., Fernandez, P., Appleby, P., 2004. Polycyclic aromatic hydrocarbon composition in soils and sediments of high altitude lakes. Environmental Pollution 131, 13-24.

Hasegawa, T., 2001. Predominance of terrigenous organic matter in Cretaceous marine fore-arc sediments, Japan and Far East Russia. International Journal of Coal Geology 47, 207-221.

He, J., Ding, W., Jiang, Z., Jiu, K., Li, A., Sun, Y., 2017. Mineralogical and chemical distribution of the Es3L oil shale in the Jiyang Depression, Bohai Bay Basin (East China): Implications for paleoenvironmental reconstruction and organic matter accumulation. Marine and Petroleum Geology 81, 196–219.

Hites, R.A., Laflamme, R.E., Windsor, J.G., Farrington, J.W., Deuser, W.G., 1980. Polycyclic aromatic hydrocarbons in an anoxic sediment core from the Pettaquamscutt River (Rhode Island, USA). Geochimica et Cosmochimica Acta 44, 873-878.

Hou, D., Wang, T., Zhang, Y., 1997. Dinosteranes in the tertiary terrestrial deposits, Eastern China—the marker of marine transgression facies. Geological Review 43, 524-528.

Huang, H., Zheng, Y., Zhang, Z., Li, J., 2003. Lacustrine biomass: An significant precursor of high wax oil. Chinese Science Bulletin 48, 1987–1994.

Huang, H., Bowler, B.F., Oldenburg, T.B., Larter, S.R., 2004. The effect of biodegradation on polycyclic aromatic hydrocarbons in reservoired oils from the Liaohe basin, NE China. Organic Geochemistry 35, 1619-1634.

Huang, H., Zhang, S., Su, J., 2015. Pyrolytically derived polycyclic aromatic hydrocarbons in marine oils from the Tarim Basin, NW China. Energy & Fuels 29, 5578-5586.

Huang, W., Meinschein, W.G., 1979. Sterols as ecological indicators. Geochimica et Cosmochimica Acta 43, 739-745.

Hughes, W.B., Holba, A.G., Dzou, L.I.P., 1995. The ratios of dibenzothiophene to phenanthrene and pristane to phytane as indicators of depositional environment and lithology of petroleum source rocks. Geochimica et Cosmochimica Acta 59, 3581-3598.

Ishiwatari, R., Ogura, K., Horie, S., 1980. Organic geochemistry of a lacustrine sediment (Lake Haruna, Japan). Chemical Geology 29, 261-280.

Jiang, C., 1998. Polycyclic Aromatic Hydrocarbons and Their Geochemical Significance, School of Applied Chemistry. Curtin University of Technology, Curtin p. 290.

Jiang, C., Alexander, R., Kagi, R.I., Murray, A.P., 1998. Polycyclic aromatic hydrocarbons in ancient sediments and their relationships to palaeoclimate. Organic Geochemistry 29, 1721-1735.

Jiang, C., Alexander, R., Kagi, R.I., Murray, A.P., 2000. Origin of perylene in ancient sediments and its geological significance. Organic Geochemistry 31, 1545-1559.

Jiang, N., Tong, Z., Ren, D., Song, F., Yang, D., Zhu, C., Gao, Y., 1995. The discovery of retene in Precambrian and Lower Paleozoic marine formations. Chinese Journal of Geochemistry 14, 41-51.

Jin, Z., Zhang, L., Yang, L., Hu, W., 2004. A preliminary study of mantle-derived fluids and their effects on oil/gas generation in sedimentary basins. Journal of Petroleum Science and Engineering 41, 45-55.

Kawamura, K., Ishiwatari, R., Ogura, K., 1987. Early diagenesis of organic matter in the water column and sediments: microbial degradation and resynthesis of lipids in Lake Haruna. Organic Geochemistry 11, 251-264.

Kawka, O.E., Simoneit, B.R., 1990. Polycyclic aromatic hydrocarbons in hydrothermal petroleums from the Guaymas Basin spreading center. Applied Geochemistry 5, 17-27.

Killops, S.D., Massoud, M.S., 1992. Polycyclic aromatic-hydrocarbons of pyrolytic origin in ancient sediments - evidence for Jurassic vegetation fires. Organic Geochemistry 18, 1-7.

Kruge, M.A., 2000. Determination of thermal maturity and organic matter type by principal components analysis of the distributions of polycyclic aromatic compounds. International Journal of Coal Geology 43, 27-51.

Kumar, A., Schimmelmann, A., Sauer, P.E., Brassell, S.C., 2017. Distribution and sources of polycyclic aromatic hydrocarbons (PAHs) in laminated Santa Barbara Basin sediments. Organic Geochemistry 113, 303-314.

Laflamme, R.E., Hites, R.A., 1978. The global distribution of polycyclic aromatic hydrocarbons in recent sediments. Geochimica et Cosmochimica Acta 42, 289-303.

Li, M.J., Shi, S.B., Wang, T.G., 2012a. Identification and distribution of chrysene, methylchrysenes and their isomers in crude oils and rock extracts. Organic Geochemistry 52, 55-66.

Li, M.J., Shi, S.B., Wang, T.G., Zhong, N.N., Wang, G.L., Cui, J.W., 2012b. The occurrence and distribution of phenylphenanthrenes, phenylanthracenes and binaphthyls in Palaeozoic to Cenozoic shales from China. Applied Geochemistry 27, 2560-2569.

Li, M.J., Simoneit, B.R.T., Zhong, N.N., Fang, R.H., 2013a. The distribution and origin of dimethyldibenzothiophenes in sediment extracts from the Liaohe Basin, East China. Organic Geochemistry 65, 63-73.

Li, M.J., Zhong, N.N., Shi, S.B., Zhu, L., Tang, Y.J., 2013b. The origin of trimethyldibenzothiophenes and their application as maturity indicators in sediments from the Liaohe Basin, East China. Fuel 103, 299-307.

Li, M.J., Wang, H., Shi, S.B., Fang, R.H., Tang, Q., Wang, D.W., 2016. The occurrence and distribution of phenylnaphthalenes, terphenyls and quaterphenyls in selected lacustrine shales and related oils in China. Organic Geochemistry 95, 55-70.

Li, S., Pang, X., Li, M., Jin, Z., 2003. Geochemistry of petroleum systems in the Niuzhuang South Slope of Bohai Bay Basin—part 1: source rock characterization. Organic Geochemistry 34, 389–412.

Lipp, J., Trimborn, P., Edwards, T., Waisel, Y., Yakir, D., 1996. Climatic effects on the $\delta^{18}O$ and $\delta^{13}$ C of cellulose in the desert tree Tamarix jordanis. Geochimica et Cosmochimica Acta 60, 3305-3309.

Liu, C., Wang, P., Xu, J., 2000. Algal blooms: the primary mechanism in the formation of lacustrine petroleum source rocks. Geological Review 47, 207-210.

Liu, C., Wang, P., 2013. The role of algal blooms in the formation of lacustrine petroleum source rocks - Evidence from Jiyang depression, Bohai Gulf Rift Basin, eastern China. Palaeogeography Palaeoclimatology Palaeoecology 388, 15–22.

Liu, G.Q., Zhang, G., Li, X.D., Li, J., Peng, X.Z., Qi, S.H., 2005. Sedimentary record of polycyclic aromatic hydrocarbons in a sediment core from the Pearl River Estuary, South China. Marine Pollution Bulletin 51, 912-921.

Liu, Q., Zhang, L., Shen, Z., Kong, X., Li, Z., 2004. Evolution of lake-basin types and occurrence of hydrocarbon source rocks in Dongying Depression. Acta Petrolei Sinica 25, 42-45 (in Chinese).

Louda, J.W., Baker, E.W., 1984. Perylene occurrence, alkylation and possible sources in deep-ocean sediments. Geochimica et Cosmochimica Acta 48, 1043-1058.

Lu, S., Kaplan, I.R., 1992. Diterpanes, triterpanes, steranes and aromatic hydrocarbons in natural bitumens and pyrolysates from different mimic coals. Geochimica et Cosmochimica Acta 56, 2761-2788.

Luo, X., Chen, S., Mai, B., Yang, Q., Sheng, G., Fu, J., 2006. Polycyclic aromatic hydrocarbons in suspended particulate matter and sediments from the Pearl River Estuary and adjacent coastal areas, China. Environmental Pollution 139, 9-20.

Luo, X., Gong, S., Sun, F.J., Wang, Z.H., Qi, J.S., 2017. Effect of volcanic activity on hydrocarbon generation: Examples in Songliao, Qinshui, and Bohai Bay Basins in China. Journal of Natural Gas Science and Engineering 38, 218-234.

Marynowski, L., Rospondek, M.J., zu Reckendorf, R.M., Simoneit, B.R.T., 2002. Phenyldibenzofurans and phenyldibenzothiophenes in marine sedimentary rocks and hydrothermal petroleum. Organic Geochemistry 33, 701-714.

Marynowski, L., Simoneit, B.R.T., 2009. Widespread Upper Triassic to Lower Jurassic wildfire records from Poland: evidence from charcoal and pyrolytic polycyclic aromatic hydrocarbons. Palaios 24, 785-798.

Marynowski, L., Kurkiewicz, S., Rakociński, M., Simoneit, B.R.T., 2011. Effects of weathering on organic matter: I. Changes in molecular composition of extractable organic compounds caused by paleoweathering of a Lower Carboniferous (Tournaisian) marine black shale. Chemical Geology 285, 144-156.

Marynowski, L., Smolarek, J., Bechtel, A., Philippe, M., Kurkiewicz, S., Simoneit, B.R.T., 2013. Perylene as an indicator of conifer fossil wood degradation by wood-degrading fungi. Organic Geochemistry 59, 143-151.

Messenger, S., Amari, S., Gao, X., Walker, R.M., Clemett, S.J., Chillier, X.D.F., Zare, R.N., Lewis, R.S., 1998. Indigenous polycyclic aromatic hydrocarbons in circumstellar graphite grains from primitive meteorites. The Astrophysical Journal 502, 284.

Metzger, P., Largeau, C., Casadevall, E., 1991. Lipids and macromolecular lipids of the hydrocarbon-rich microalga *Botryococcus braunii*. Chemical structure and biosynthesis. Geochemical and biotechnological importance, in: Herz, W., Kirby, G.W., Steglich, W., Tamm, C. (Eds.), Progress in the Chemistry of Organic Natural Products. Springer, Verlag, pp. 1–70.

Meyers, P.A., Yum, J.G., Wise, S.W., 2009. Origins and maturity of organic matter in mid-Cretaceous black shales from ODP Site 1138 on the Kerguelen Plateau. Marine and Petroleum Geology 26, 909–915.

Mimura, K., 1995. Synthesis of polycyclic aromatic hydrocarbons from benzene by impact shock: Its reaction mechanism and cosmochemical significance. Geochimica et Cosmochimica Acta 59, 579-591.

Moore, L.R., 1969. Geomicrobiology and geomicrobiological attack on sedimented organic matter, Organic Geochemistry. Springer, pp. 265-303.

Murchison, D.G., Raymond, A.C., 1989. Igneous activity and organic maturation in the Midland Valley of Scotland. International Journal of Coal Geology 14, 47-82.

Murray, A.P., Edwards, D., Hope, J.M., Boreham, C.J., Booth, W.E., Alexander, R.A., Summons, R.E., 1998. Carbon isotope biogeochemistry of plant resins and derived hydrocarbons. Organic Geochemistry 29, 1199-1214.

Oros, D.R., Simoneit, B.R.T., 2001. Identification and emission factors of molecular tracers in organic aerosols from biomass burning Part 1. Temperate climate conifers. Applied Geochemistry 16, 1513-1544.

Oros, D.R., Radzi bin Abas, M., Omar, N.Y.M.J., Rahman, N.A., Simoneit, B.R.T., 2006. Identification and emission factors of molecular tracers in organic aerosols from biomass burning: Part 3. Grasses. Applied Geochemistry 21, 919-940.

Otto, A., Simoneit, B.R.T., Rember, W.C., 2003. Resin compounds from the seed cones of three fossil conifer species from the Miocene Clarkia flora, Emerald Creek, Idaho, USA, and from related extant species. Review of Palaeobotany and Palynology 126, 225-241.

Peters, K.E., Cassa, M.R., 1994. Applied source rock geochemistry: Chapter 5: Part ii. Essential elements.

Peters, K.E., Walters, C.C., Moldowan, J.M., 2005. The Biomarker Guide. Cambridge University Press, Cambridge

Prahl, F.G., Carpenter, R., 1983. Polycyclic aromatic hydrocarbon (PAH)-phase associations in Washington coastal sediment. Geochimica et Cosmochimica Acta 47, 1013-1023.

Pyne, S.J., Andrews, P.L., Laven, R.D., 1996. Introduction to wildland fire. Wiley, New York.

Quiroz, R., Grimalt, J.O., Fernandez, P., Camarero, L., Catalan, J., Stuchlik, E., Thies, H., Nickus, U., 2011. Polycyclic aromatic hydrocarbons in soils from European high mountain areas. Water, Air, & Soil Pollution 215, 655-666.

Ramdahl, T., 1983. Retene—a molecular marker of wood combustion in ambient air. Nature 306, 580-582.

Renaut, R.W., Owen, R.B., Jones, B., Tiercelin, J.J., Tarits, C., Ego, J.K., Konhauser, K.O., 2013. Impact of lake-level changes on the formation of thermogene travertine in continental rifts: Evidence from Lake Bogoria, Kenya Rift Valley. Sedimentology 60, 428-468.

Rospondek, M.J., Marynowski, L., Góra, M., 2007. Novel arylated polyaromatic thiophenes: Phenylnaphtho[b]thiophenes and naphthylbenzo[b]thiophenes as markers of organic matter diagenesis buffered by oxidising solutions. Organic Geochemistry 38, 1729-1756.

Rospondek, M.J., Szczerba, M., Malek, K., Gora, M., Marynowski, L., 2008. Comparison of phenyldibenzothiophene distributions predicted from molecular modelling with relevant experimental and geological data. Organic Geochemistry 39, 1800-1815.

Rospondek, M.J., Marynowski, L., Chachaj, A., Gora, M., 2009. Novel aryl polycyclic aromatic hydrocarbons: Phenylphenanthrene and phenylanthracene identification, occurrence and distribution in sedimentary rocks. Organic Geochemistry 40, 986-1004.

Rullkötter, J., Peakman, T.M., Ten Haven, H.L., 1994. Early diagenesis of terrigenous triterpenoids and its implications for petroleum geochemistry. Organic Geochemistry 21, 215-233.

Rundel, P.W., 1981. Fire as an ecological factor, in: Lange, O.L., Nobel, P.S., Osmond, C.B., Ziegler, H. (Eds.), Physiological Plant Ecology I, Response to the Physical Environment. Springer, Berlin, pp. 501-538.

Schade, T., Andersson, J.T., 2006. Speciation of alkylated dibenzothiophenes through correlation of structure and gas chromatographic retention indexes. Journal of Chromatography A 1117, 206-213.

Scott, A.C., Jones, T.P., 1994. The nature and influence of fire in Carboniferous ecosystems. Palaeogeography, Palaeoclimatology, Palaeoecology 106, 91-112.

Scott, A.C., 2000. The Pre-Quaternary history of fire. Palaeogeography, Palaeoclimatology, Palaeoecology 164, 281-329.

Simoneit, B.R.T., 1977. Diterpenoid compounds and other lipids in deep-sea sediments and their geochemical significance. Geochimica et Cosmochimica Acta 41, 463-476.

Simoneit, B.R.T., Lonsdale, P.F., 1982. Hydrothermal petroleum in mineralized mounds at the seabed of Guaymas Basin.

Simoneit, B.R.T., Grimalt, J.O., Wang, T.G., Cox, R.E., Hatcher, P.G., Nissenbaum, A., 1986. Cyclic terpenoids of contemporary resinous plant detritus and of fossil woods, ambers and coals. Organic Geochemistry 10, 877-889.

Simoneit, B.R.T., Rogge, W.F., Mazurek, M.A., Standley, L.J., Hildemann, L.M., Cass, G., 1993. Lignin pyrolysis products, lignans, and resin acids as specific tracers of plant classes in emissions from biomass combustion. Environmental Science & Technology 27, 2533-2541.

Simoneit, B.R.T., Fetzer, J.C., 1996. High molecular weight polycyclic aromatic hydrocarbons in hydrothermal petroleums from the Gulf of California and Northeast Pacific Ocean. Organic Geochemistry 24, 1065-1077.

Simoneit, B.R.T., 1997. Compound-specific carbon isotope analyses of individual long-chain alkanes and alkanoic acids in Harmattan aerosols. Atmospheric Environment 31, 2225-2233.

Sinninghe Damsté, J.S., Kenig, F., Koopmans, M.P., Köster, J., Schouten, S., Hayes, J., de Leeuw, J.W., 1995. Evidence for gammacerane as an indicator of water column stratification. Geochimica et Cosmochimica Acta 59, 1895–1900.

Stubblefield, S.P., Taylor, T.N., Beck, C.B., 1985. Studies of paleozoic fungi. IV. Wood-decaying fungi in Callixylon newberryi from the upper Devonian. American Journal of Botany, 1765-1774.

Suzuki, N., Yessalina, S., Kikuchi, T., 2010. Probable fungal origin of perylene in Late Cretaceous to Paleogene terrestrial sedimentary rocks of northeastern Japan as indicated from stable carbon isotopes. Organic Geochemistry 41, 234-241.

Tan, Y., Heit, M., 1981. Biogenic and abiogenic polynuclear aromatic hydrocarbons in sediments from two remote Adirondack lakes. Geochimica et Cosmochimica Acta 45, 2267-2279.

Tan, Y., Kong, A., Monetti, M.A., 1996. Biogenic polycyclic aromatic hydrocarbons in an Alaskan arctic lake sediment. Polycyclic Aromatic Compounds 9, 185-192.

Ten Haven, H.L., De Leeuw, J.W., Sinninghe Damsté, J.S., Schenck, P.A., Palmer, S.E., Zumberge, J.E., 1988. Application of biological markers in the recognition of palaeohypersaline environments. Geological Society, London, Special Publications 40, 123-130.

Thomas, B.R., 1969. Kauri resins—modern and fossil, in: Eglinton, G., Murphy, M.T.J. (Eds.), Organic Geochemistry. Springer, pp. 599-618.

Trolio, R., Grice, K., Fisher, S.J., Alexander, R., Kagi, R.I., 1999. Alkylbiphenyls and alkyldiphenylmethanes as indicators of petroleum biodegradation. Organic Geochemistry 30, 1241-1253.

van Aarssen, B.G.K., Alexander, R., Kagi, R.I., 1996. The origin of Barrow Sub-basin crude oils: a geochemical correlation using land-plant biomarkers. The APPEA Journal 36, 465-476.

van Mooy, B.A.S., Keil, R.G., Devol, A.H., 2002. Impact of suboxia on sinking particulate organic carbon: Enhanced carbon flux and preferential degradation of amino acids via denitrification. Geochimica et Cosmochimica Acta 66, 457–465.

Varnosfaderany, M.N., Bakhtiari, A.R., Gu, Z., Chu, G., 2014. Perylene as an indicator of land-based plant biomarkers in the southwest Caspian Sea. Marine Pollution Bulletin 80, 124-131.

Vassilaros, D.L., Kong, R.C., Later, D.W., Lee, M.L., 1982. Linear retention index system for polycyclic aromatic compounds: critical evaluation and additional indices. Journal of Chromatography A 252, 1-20.

Venkatesan, M.I., 1988. Occurrence and possible sources of perylene in marine sediments-a review. Marine Chemistry 25, 1-27.

Venkatesan, M.I., Dahl, J., 1989. Organic geochemical evidence for global fires at the Cretaceous/Tertiary boundary. Nature 338, 57-60.

Volk, H., George, S.C., Boreham, C.J., Kempton, R.H., 2004. Geochemical and compound specific carbon isotopic characterisation of fluid inclusion oils from the offshore Perth Basin, Western Australia: Implications for recognising effective oil source rocks. The APPEA Journal 44, 223-240.

Volkman, J.K., Barrett, S.M., Blackburn, S.I., Mansour, M.P., Sikes, E.L., Gelin, F., 1998. Microalgal biomarkers: A review of recent research developments. Organic Geochemistry 29, 1163–1179.

Volkman, J.K., 2005. Sterols and other triterpenoids: source specificity and evolution of biosynthetic pathways. Organic Geochemistry 36, 139-159.

Wakeham, S.G., Schaffner, C., Giger, W., Boon, J.J., de Leeuw, J.W., 1979. Perylene in sediments from the Namibian Shelf. Geochimica et Cosmochimica Acta 43, 1141-1144.

Wakeham, S.G., Schaffner, C., Giger, W., 1980a. Polycyclic aromatic hydrocarbons in recent lake sediments—II. Compounds derived from biogenic precursors during early diagenesis. Geochimica et Cosmochimica Acta 44, 415-429.

Wakeham, S.G., Schaffner, C., Giger, W., 1980b. Polycyclic aromatic hydrocarbons in recent lake sediments—I. Compounds having anthropogenic origins. Geochimica et Cosmochimica Acta 44, 403-413.

Wang, G., Wang, T.G., Simoneit, B.R.T., Chen, Z., Zhang, L., Xu, J., 2008. The distribution of molecular fossils derived from dinoflagellates in Paleogene lacustrine sediments (Bohai Bay Basin, China). Organic Geochemistry 39, 1512–1521.

Wang, G., Li, S., Wang, T., Zhang, L., 2010. Applications of molecular fossils in lacustrine stratigraphy. Chinese Journal of Geochemistry 29, 15–20.

Wang, G., Wang, T.G., Simoneit, B.R.T., Zhang, L., 2013. Investigation of hydrocarbon biodegradation from a downhole profile in Bohai Bay Basin: Implications for the origin of 25-norhopanes. Organic Geochemistry 55, 72–84.

Wang, K., Lu, X., Chen, M., Ma, Y., Liu, K., Liu, L., Li, X., Hu, W., 2012. Numerical modelling of the hydrocarbon generation of Tertiary source rocks intruded by doleritic sills in the Zhanhua depression, Bohai Bay Basin, China. Basin Research 24, 234-247.

Wood, A.W., Levin, W., Ryan, D., Thomas, P.E., Yagi, H., Mah, H.D., Thakker, D.R., Jerina, D.M., Conney, A.H., 1977. High mutagenicity of metabolically activated chrysene 1, 2 dihydrodiol: Evidence for bay region activation of chrysene. Biochemical and Biophysical Research Communications 78, 847-854.

Yakir, D., Issar, A., Gat, J., Adar, E., Trimborn, P., Lipp, J., 1994. $^{13}C$ and $^{18}O$ of wood from the Roman siege rampart in Masada, Israel (AD 70–73): Evidence for a less arid climate for the region. Geochimica et Cosmochimica Acta 58, 3535-3539.

Yao, Y.M., Liang, H., Cai, Z., Guan, X., Zhao, Z., Chen, Z., Sun, Z., Yang, S., 1994. Tertiary in petroliferous regions of China (IV): The Bohai Gulf Basin. Petroleum Industry Press, Beijing.

Youngblood, W.W., Blumer, M., 1975. Polycyclic aromatic hydrocarbons in the environment: homologous series in soils and recent marine sediments. Geochimica et Cosmochimica Acta 39, 1303-1314.

Yunker, M.B., Macdonald, R.W., Vingarzan, R., Mitchell, R.H., Goyette, D., Sylvestre, S., 2002. PAHs in the Fraser River basin: a critical appraisal of PAH ratios as indicators of PAH source and composition. Organic Geochemistry 33, 489-515.

Yunker, M.B., Macdonald, R.W., 2003. Alkane and PAH depositional history, sources and fluxes in sediments from the Fraser River Basin and Strait of Georgia, Canada. Organic Geochemistry 34, 1429-1454.

Yunker, M.B., Macdonald, R.W., Snowdon, L.R., Fowler, B.R., 2011. Alkane and PAH biomarkers as tracers of terrigenous organic carbon in Arctic Ocean sediments. Organic Geochemistry 42, 1109-1146.

Yunker, M.B., Perreault, A., Lowe, C.J., 2012. Source apportionment of elevated PAH concentrations in sediments near deep marine outfalls in Esquimalt and Victoria, BC, Canada: is coal from an 1891 shipwreck the source? Organic Geochemistry 46, 12-37.

Yunker, M.B., Macdonald, R.W., Ross, P.S., Johannessen, S.C., Dangerfield, N., 2015. Alkane and PAH provenance and potential bioavailability in coastal marine sediments subject to a gradient of anthropogenic sources in British Columbia, Canada. Organic Geochemistry 89-90, 80-116.

Zakir Hossain, H.M., Sampei, Y., Roser, B.P., 2013. Polycyclic aromatic hydrocarbons (PAHs) in late Eocene to early Pleistocene mudstones of the Sylhet succession, NE Bengal Basin, Bangladesh: Implications for source and paleoclimate conditions during Himalayan uplift. Organic Geochemistry 56, 25-39.

Zhang, L., 2008. The progress on the study of lacustrine source rocks. Petroleum Geology & Experiment 30, 591–595.

Zhang, L., Liu, Q., Zhu, R., Li, Z., Lu, X., 2009. Source rocks in Mesozoic-Cenozoic continental rift basins, East China: A case from Dongying Depression, Bohai Bay Basin. Organic Geochemistry 40, 229–242.

Zhang, S., Wang, Y., Shi, D., Xu, H., Pang, X., Li, M., 2004. Fault-fracture mesh petroleum plays in the Jiyang Superdepression of the Bohai Bay Basin, eastern China. Marine and Petroleum Geology 21, 651-668.

Zhang, T., Zhang, M., Bai, B., Wang, X., Li, L., 2008. Origin and accumulation of carbon dioxide in the Huanghua depression, Bohai Bay Basin, China. AAPG Bulletin 92, 341–358.

Zhou, W., Wang, R., Radke, M., Wu, Q., Sheng, G., Liu, Z., 2000. Retene in pyrolysates of algal and bacterial organic matter. Organic Geochemistry 31, 757-762.

Zhu, D., Jin, Z., Hu, W., Song, Y., Gao, X., 2007. Effect of igneous activity on hydrocarbon source rocks in Jiyang Sub-basin, Eastern China. Journal of Petroleum Science and Engineering 59, 309–320.

# Tables

Table 3.1 Names and abbreviations of the aromatic compounds referred to in this study. Note: Benzo [b,j,k]fluoranthene (BFla) is reported as the integrated sum of benzo[b]fluoranthene, benzo[j]fluoranthene and benzo[k]fluoranthene.

| Abbreviation | Compound name | Diagnostic *m/z* ion |
|---|---|---|
| AB | Alkylbenzenes | 106, 120, 134 |
| N | Naphthalene | 128 |
| MN | Methylnaphthalenes | 142 |
| DMN | Dimethylnaphthalenes | 156 |
| TMN | Trimethylnaphthalenes | 170 |
| TeMN | Tetramethylnaphthalenes | 184 |
| PMN | Pentamethylnaphthalenes | 198 |
| Cad | Cadalene | 183 |
| iHMN | 1-Isohexyl-2-methylnaphthalene | 197 |
| 1-pN | 1-Phenynaphthalene | 204 |
| 2-pN | 2-Phenynaphthalene | 204 |
| M-2-pN | $C_1$ alkylphenylnaphthalenes | 218 |
| DM-2-pN | $C_2$ alkylphenylnaphthalenes | 232 |
| TrP | Terphenyl | 230 |
| QtP | Quaterphenyls | 306 |
| Te | Tetralin | 159 |
| TeMT | Tetramethyltetralins | 173 |
| Bp | Biphenyl | 154 |
| MBp | Methylbiphenyls | 168 |
| EBp | Ethylbiphenyls | 182 |
| DMBp | Dimethylbiphenyls | 182 |
| DBF | Dibenzofuran | 168 |
| DpM | Diphenylmethane | 168 |
| F | Fluorene | 166 |
| MF | Methylfluorenes | 180 |
| Phen | Phenanthrene | 178 |
| MP | Methylphenanthrenes | 192 |
| EP | Ethylphenanthrenes | 206 |
| DMP | Methylphenanthrenes | 206 |
| TMP | Dimethylphenanthrenes | 220 |
| TeMP | Trimethylphenenthrenes | 234 |
| Ret | Retene (l-methyl-7-isopropylphenanthrene) | 219 |
| Sim | Simonellite | 237 |
| DBT | Dibenzothiophene | 184 |
| Fla | Fluoranthene | 202 |
| Py | Pyrene | 202 |
| M-2-pN | Methyl-2-phenylnaphthalenes | 218 |
| DM-2-pN | Dimethyl-2-phenylnaphthalenes | 232 |
| MPy | Methylpyrenes | 216 |
| BaF | Benzo[a]fluorene | 216 |
| BbF | Benzo[b]fluorene | 216 |
| DMPy | Dimethylpyrenes | 230 |
| BaA | Benz[a]anthracene | 228 |
| BbA | Benz[b]anthracene | 228 |
| Tpn | Triphenylene | 228 |
| Chy | Chrysene | 228 |
| MChy | Methylchrysenes | 242 |
| MBaA | Methylbenz[a]anthracenes | 242 |
| BFla | Benzo[b,j,k]fluoranthene | 252 |
| BePy | Benzo[e]pyrene | 252 |
| BaPy | Benzo[a]pyrene | 252 |
| Pery | Perylene | 252 |
| InPy | Indeno[1,2,3-cd]pyrene | 276 |
| BghiP | Benzo[ghi]perylene | 276 |
| Cor | Coronene | 300 |
| TAS | Triaromatic steroids | 231 |

Table 3.2 Organic geochemical parameters of the Paleogene lacustrine core samples investigated from the Dongying Depression, Bohai Bay Basin. Hydrocarbon abbreviations are defined in Table 3.1.

| Sample Name | Wells | Formation | Depth | TOC (%) | TN (%) | C/N | EOM mg/g | Pr/Ph | β | Ts | 33S/(S+R) | 35/(35 + 34) | Ga/30H | St/H | $C_{27}$ αα α R % | $C_{28}$ α αα R % | $C_{29}$ α αα R % |
|---|---|---|---|---|---|---|---|---|---|---|---|---|---|---|---|---|---|
| FE01 | FE112 | Es3M | 3116.80 | 4.7 | 0.47 | 9.9 | | 0.89 | 4.9 | 0.29 | 0.52 | 0.39 | 0.05 | 0.67 | 40 | 26 | 34 |
| FE02 | FE112 | Es3M | 3120.00 | | | | | 0.94 | 2.3 | 0.30 | 0.53 | 0.35 | 0.06 | 0.47 | 49 | 20 | 31 |
| FE03 | FE112 | Es3M | 3122.00 | 14.3 | 0.66 | 21.7 | 17.2 | 1.04 | 5.1 | 0.36 | 0.57 | 0.35 | 0.06 | 0.28 | 55 | 18 | 26 |
| FE04 | FE112 | Es3M | 3122.00 | 14.9 | 0.66 | 22.4 | 19.9 | 1.03 | 2.4 | 0.26 | 0.55 | 0.38 | 0.09 | 0.39 | 55 | 19 | 26 |
| FE05 | FE112 | Es3M | 3123.40 | | | | | 1.24 | 4.6 | 0.42 | 0.58 | 0.34 | 0.09 | 0.41 | 59 | 13 | 28 |
| FE06 | FE112 | Es3M | 3124.90 | 5.7 | 0.52 | 10.9 | | 0.94 | 3.4 | 0.38 | 0.58 | 0.33 | 0.06 | 0.30 | 58 | 14 | 28 |
| FE07 | FE112 | Es3M | 3134.10 | 4.7 | 0.56 | 8.3 | | 1.01 | 4.0 | 0.35 | 0.57 | 0.38 | 0.08 | 0.49 | 44 | 23 | 33 |
| FE08 | FE112 | Es3M | 3135.80 | 5.2 | 0.46 | 11.3 | 7.0 | 1.20 | 4.1 | 0.32 | 0.57 | 0.38 | 0.05 | 0.37 | 40 | 22 | 38 |
| FE09 | FE112 | Es3M | 3137.90 | 10.2 | 0.51 | 19.8 | | 1.22 | 1.5 | 0.26 | 0.56 | 0.45 | 0.04 | 0.39 | 43 | 21 | 36 |
| FA01 | FA107 | Es3M | 3171.00 | 5.0 | 0.52 | 9.5 | 5.9 | 1.43 | 3.1 | 0.43 | 0.59 | 0.38 | 0.08 | 0.15 | 37 | 26 | 37 |
| FA03 | FA137 | Es3L | 2847.60 | 1.1 | 0.83 | 1.4 | 2.4 | 1.52 | nd | 0.37 | 0.59 | 0.48 | 0.09 | 0.45 | 36 | 27 | 37 |
| T01 | T73 | Es3L | 3158.00 | 3.7 | 0.55 | 6.8 | 12.1 | 0.64 | 5.4 | 0.37 | 0.59 | 0.39 | 0.23 | 0.98 | 30 | 27 | 43 |
| FS01 | FS1 | Es3L | 3217.93 | 2.5 | 0.64 | 3.9 | 4.2 | 1.00 | 1.8 | 0.40 | 0.57 | 0.36 | 0.05 | 0.24 | 35 | 32 | 33 |
| H01 | H130 | Es3L | 3222.00 | 3.6 | 0.51 | 7.1 | 7.6 | 0.99 | 1.3 | 0.55 | 0.58 | 0.36 | 0.06 | 0.24 | 44 | 23 | 33 |
| H02 | H130 | Es3L | 3235.25 | 5.9 | 0.67 | 8.8 | 11.3 | 1.05 | 2.5 | 0.48 | 0.58 | 0.37 | 0.05 | 0.23 | 38 | 26 | 36 |
| FA02 | FA101 | Es3L | 3282.44 | 5.5 | 0.50 | 10.9 | 5.9 | 1.02 | 2.8 | 0.49 | 0.57 | 0.42 | 0.06 | 0.36 | 40 | 28 | 31 |
| N01 | N28 | Es3L | 3282.43 | 1.9 | 0.48 | 4.0 | 4.0 | 1.24 | 0.9 | 0.49 | 0.57 | 0.41 | 0.04 | 0.15 | 38 | 25 | 37 |
| FE10 | FE112 | Es3L | 3337.70 | nd | nd | nd | 5.8 | 0.65 | 3.7 | 0.38 | 0.59 | 0.31 | 0.12 | 0.56 | 28 | 23 | 48 |
| FE11 | FE112 | Es3L | 3340.20 | nd | nd | nd | nd | 0.50 | 7.3 | 0.34 | 0.57 | 0.38 | 0.17 | 1.22 | 30 | 25 | 46 |
| FE12 | FE112 | Es3L | 3340.50 | 7.3 | 0.73 | 10.0 | 29.2 | 0.43 | 10.1 | 0.34 | 0.57 | 0.41 | 0.17 | 1.13 | 26 | 34 | 40 |
| FE13 | FE112 | Es3L | 3341.00 | nd | nd | nd | 12.2 | 0.42 | 6.8 | 0.33 | 0.57 | 0.37 | 0.16 | 1.41 | 29 | 25 | 46 |
| FE14 | FE112 | Es3L | 3341.40 | 10.0 | 0.70 | 14.4 | nd | 0.45 | 6.4 | 0.36 | 0.59 | 0.37 | 0.17 | 1.35 | 29 | 25 | 46 |
| FE15 | FE112 | Es3L | 3341.50 | nd | nd | nd | nd | 0.37 | 10.5 | 0.40 | 0.58 | 0.37 | 0.21 | 2.20 | 28 | 28 | 44 |
| CH01 | CH372 | Es4U | 2571.50 | 6.1 | 0.41 | 14.9 | 6.3 | 0.42 | 4.4 | 0.31 | 0.47 | 0.57 | 0.53 | 2.70 | 35 | 26 | 39 |
| CH02 | CH372 | Es4U | 2573.50 | nd | nd | nd | nd | 0.81 | 7.0 | 0.32 | 0.46 | 0.66 | 0.53 | 6.96 | 37 | 32 | 31 |
| CH03 | CH372 | Es4U | 2583.00 | 7.4 | 0.32 | 23.0 | 15.0 | 0.34 | 18.9 | 0.29 | 0.49 | 0.59 | 0.41 | 4.22 | 40 | 26 | 34 |
| L01 | L110 | Es4U | 2747.70 | 13.5 | 0.60 | 22.5 | 5.7 | 1.53 | 3.8 | 0.31 | 0.49 | 0.49 | 0.19 | 0.61 | 42 | 21 | 37 |
| L02 | L110 | Es4U | 2752.10 | nd | nd | nd | nd | 1.09 | 2.8 | 0.25 | 0.44 | 0.46 | 0.09 | 1.15 | 30 | 23 | 47 |
| L03 | L110 | Es4U | 2767.50 | 4.0 | 0.33 | 12.0 | 5.5 | 0.70 | 11.1 | 0.35 | 0.48 | 0.50 | 0.38 | 1.54 | 28 | 30 | 42 |
| L04 | L110 | Es4U | 2770.40 | nd | nd | nd | nd | 0.63 | 26.9 | 0.25 | 0.45 | 0.53 | 0.27 | 2.50 | 35 | 23 | 42 |
| L05 | L110 | Es4U | 2779.80 | 6.2 | 0.42 | 14.6 | 7.8 | 0.80 | 6.1 | 0.30 | 0.48 | 0.45 | 0.11 | 2.35 | 34 | 26 | 41 |
| L06 | L110 | Es4U | 2897.80 | nd | nd | nd | nd | 0.34 | 11.4 | 0.23 | 0.51 | 0.64 | 2.50 | 10.79 | 37 | 29 | 35 |
| FA04 | FA137 | Es4U | 3166.40 | 0.3 | 0.19 | 1.4 | 0.55 | 0.88 | 1.9 | 0.57 | 0.53 | 0.43 | 0.39 | 1.12 | 26 | 27 | 47 |
| FA05 | FA137 | Es4U | 3259.52 | 4.4 | 0.20 | 22.1 | 3.8 | 0.44 | 23.7 | 0.43 | 0.51 | 0.50 | 1.97 | 12.07 | 21 | 30 | 49 |
| T02 | T73 | Es4U | 3269.38 | 5.3 | 0.53 | 10.2 | 14.6 | 0.70 | 4.8 | 0.47 | 0.59 | 0.36 | 0.18 | 0.77 | 26 | 22 | 52 |
| T03 | T73 | Es4U | 3341.66 | 3.0 | 0.46 | 6.6 | 9.5 | 0.46 | 7.0 | 0.79 | 0.54 | 0.52 | 1.45 | 12.56 | 34 | 32 | 34 |
| FE16 | FE112 | Es4U | 3430.68 | 6.2 | 0.69 | 9.0 | 11.4 | 0.52 | 5.5 | 0.47 | 0.58 | 0.36 | 0.33 | 1.93 | 26 | 29 | 45 |
| FS02 | FS1 | Es4U | 3690.40 | 4.3 | 0.79 | 5.4 | 3.6 | 0.71 | 1.2 | 0.68 | 0.55 | 0.38 | 0.19 | 1.35 | 23 | 24 | 53 |

Table 3.2 (*continued*)

| 29/27 | $C_{27}$ 20S | $C_{29}$ 20S | 29S/R | $C_{29}$ αββ | TNR-1 | TNR-2 | 125 | 127 | TMNr | TeMNr | HPI | I-HMN % | Cadalene % | Retene% | MPI-1 |
|---|---|---|---|---|---|---|---|---|---|---|---|---|---|---|---|
| 0.84 | 0.34 | 0.25 | 0.33 | 0.25 | 0.80 | 0.65 | -0.002 | -0.05 | 0.35 | 0.34 | 0.56 | 32.0 | 0.00 | 67.99 | 0.52 |
| 0.63 | 0.32 | 0.25 | 0.34 | 0.22 | 0.82 | 0.68 | -0.11 | -0.19 | 0.42 | 0.37 | 0.92 | 17.1 | 40.80 | 42.06 | 0.51 |
| 0.48 | 0.35 | 0.24 | 0.31 | 0.25 | 0.79 | 0.65 | -0.03 | -0.02 | 0.37 | 0.33 | 1.13 | 14.8 | 26.72 | 58.52 | 0.46 |
| 0.47 | 0.33 | 0.28 | 0.40 | 0.21 | 0.81 | 0.65 | -0.08 | -0.05 | 0.39 | 0.37 | 0.94 | 9.4 | 23.76 | 66.86 | 0.49 |
| 0.46 | 0.36 | 0.28 | 0.38 | 0.26 | 1.08 | 0.79 | 0.29 | 0.14 | 0.21 | 0.27 | 1.54 | 4.5 | 11.07 | 84.42 | 0.47 |
| 0.49 | 0.34 | 0.27 | 0.37 | 0.24 | 0.69 | 0.58 | -0.003 | -0.05 | 0.33 | 0.34 | 1.66 | 19.7 | 31.80 | 48.48 | 0.47 |
| 0.76 | 0.36 | 0.26 | 0.36 | 0.26 | 0.72 | 0.63 | -0.10 | -0.20 | 0.42 | 0.37 | 1.21 | 11.4 | 42.97 | 45.61 | 0.47 |
| 0.95 | 0.34 | 0.29 | 0.41 | 0.27 | 0.72 | 0.64 | -0.13 | -0.17 | 0.44 | 0.42 | 1.07 | 14.8 | 32.01 | 53.20 | 0.51 |
| 0.85 | 0.38 | 0.31 | 0.44 | 0.20 | 0.73 | 0.64 | -0.03 | -0.13 | 0.38 | 0.40 | 1.30 | 27.0 | 26.91 | 46.04 | 0.56 |
| 0.98 | 0.53 | 0.45 | 0.83 | 0.43 | 0.97 | 0.72 | -0.10 | -0.11 | 0.41 | 0.38 | 0.54 | 2.8 | 24.10 | 73.14 | 0.60 |
| 1.01 | 0.46 | 0.42 | 0.73 | 0.30 | 0.99 | 0.73 | -0.17 | -0.13 | 0.45 | 0.43 | 0.70 | 7.0 | 28.08 | 64.90 | 0.68 |
| 1.44 | 0.48 | 0.46 | 0.87 | 0.41 | 0.73 | 0.61 | -0.13 | -0.20 | 0.41 | 0.44 | 0.99 | 3.2 | 13.83 | 82.97 | 0.66 |
| 0.95 | 0.44 | 0.42 | 0.72 | 0.37 | 0.97 | 0.75 | -0.10 | 0.01 | 0.42 | 0.43 | 1.02 | 6.3 | 18.03 | 75.71 | 0.69 |
| 0.75 | 0.49 | 0.49 | 0.97 | 0.57 | 0.88 | 0.61 | -0.14 | -0.20 | 0.37 | 0.44 | 0.28 | nd | 24.01 | 75.99 | 0.56 |
| 0.96 | 0.48 | 0.48 | 0.91 | 0.49 | 0.79 | 0.57 | -0.21 | -0.31 | 0.40 | 0.48 | 0.32 | nd | 29.29 | 70.71 | 0.54 |
| 0.78 | 0.48 | 0.44 | 0.78 | 0.50 | 0.90 | 0.66 | -0.17 | -0.26 | 0.42 | 0.43 | 0.33 | 2.5 | 25.44 | 72.11 | 0.63 |
| 0.97 | 0.47 | 0.41 | 0.69 | 0.40 | 0.90 | 0.67 | -0.06 | -0.15 | 0.37 | 0.36 | 0.44 | 6.6 | 26.74 | 66.69 | 0.65 |
| 1.70 | 0.45 | 0.44 | 0.79 | 0.33 | 0.79 | 0.61 | -0.22 | -0.24 | 0.44 | 0.50 | 0.65 | 5.1 | 14.02 | 80.84 | 0.69 |
| 1.55 | 0.50 | 0.49 | 0.97 | 0.33 | 0.78 | 0.58 | -0.05 | -0.10 | 0.32 | 0.42 | 0.86 | 5.3 | 12.25 | 82.49 | 0.75 |
| 1.52 | 0.47 | 0.34 | 0.52 | 0.34 | 0.89 | 0.65 | -0.04 | -0.06 | 0.33 | 0.44 | 0.92 | 2.1 | 16.75 | 81.17 | 0.73 |
| 1.55 | 0.48 | 0.46 | 0.84 | 0.33 | 0.73 | 0.60 | -0.15 | -0.19 | 0.41 | 0.46 | 0.75 | 7.3 | 19.26 | 73.45 | 0.74 |
| 1.58 | 0.48 | 0.45 | 0.82 | 0.32 | 0.89 | 0.64 | -0.10 | -0.13 | 0.37 | 0.44 | 0.78 | 3.5 | 14.21 | 82.30 | 0.70 |
| 1.54 | 0.47 | 0.44 | 0.78 | 0.32 | 0.76 | 0.60 | -0.19 | -0.20 | 0.42 | 0.49 | 0.72 | 6.3 | 25.30 | 68.36 | 0.72 |
| 1.13 | 0.29 | 0.18 | 0.22 | 0.18 | 0.82 | 0.84 | -0.11 | -0.09 | 0.53 | 0.36 | 3.10 | 6.2 | 54.70 | 39.12 | 0.67 |
| 0.85 | 0.29 | 0.18 | 0.21 | 0.19 | 0.80 | 0.89 | 0.09 | -0.03 | 0.45 | 0.31 | 4.08 | 10.4 | 49.48 | 40.16 | 0.67 |
| 0.85 | 0.35 | 0.24 | 0.32 | 0.24 | 0.68 | 0.78 | 0.23 | 0.01 | 0.36 | 0.36 | 2.75 | 2.6 | 48.72 | 48.69 | 0.66 |
| 0.87 | 0.27 | 0.16 | 0.19 | 0.20 | 0.76 | 0.64 | -0.22 | -0.01 | 0.47 | 0.39 | 2.62 | 5.7 | 63.53 | 30.73 | 0.60 |
| 1.56 | 0.25 | 0.13 | 0.15 | 0.21 | 1.00 | 0.80 | 0.16 | 0.25 | 0.28 | 0.29 | 2.65 | 6.5 | 50.12 | 43.38 | 0.73 |
| 1.48 | 0.26 | 0.12 | 0.14 | 0.21 | 0.71 | 0.63 | -0.10 | 0.09 | 0.41 | 0.33 | 5.26 | 13.6 | 48.45 | 37.92 | 0.68 |
| 1.22 | 0.26 | 0.14 | 0.16 | 0.20 | 0.70 | 0.63 | -0.15 | -0.03 | 0.44 | 0.36 | 3.68 | 12.6 | 58.74 | 28.69 | 0.69 |
| 1.19 | 0.26 | 0.13 | 0.15 | 0.20 | 0.80 | 0.72 | -0.18 | -0.17 | 0.50 | 0.47 | 0.60 | 10.2 | 44.01 | 45.77 | 0.75 |
| 0.95 | 0.36 | 0.33 | 0.50 | 0.25 | 0.73 | 0.77 | 0.15 | -0.05 | 0.37 | 0.38 | 1.82 | 17.9 | 45.07 | 37.05 | 0.68 |
| 1.79 | 0.44 | 0.44 | 0.78 | 0.53 | 0.96 | 0.79 | -0.26 | -0.44 | 0.54 | 0.59 | 0.92 | 3.3 | 79.79 | 16.89 | 0.59 |
| 2.35 | 0.40 | 0.43 | 0.74 | 0.52 | 0.82 | 0.69 | -0.34 | -0.48 | 0.56 | 0.58 | 0.18 | nd | 55.38 | 44.62 | 0.66 |
| 1.97 | 0.46 | 0.48 | 0.93 | 0.42 | 0.84 | 0.61 | -0.21 | -0.23 | 0.42 | 0.50 | 0.81 | nd | 18.07 | 81.93 | 0.68 |
| 1.01 | 0.37 | 0.48 | 0.94 | 0.61 | 0.76 | 0.71 | 0.06 | -0.18 | 0.36 | 0.42 | 0.48 | nd | 21.40 | 78.60 | 0.58 |
| 1.72 | 0.50 | 0.51 | 1.04 | 0.40 | 0.72 | 0.66 | -0.11 | -0.30 | 0.44 | 0.49 | 0.55 | 2.2 | 31.25 | 66.57 | 0.60 |
| 2.30 | 0.45 | 0.50 | 0.98 | 0.48 | 0.92 | 0.74 | -0.38 | -0.40 | 0.59 | 0.69 | 0.29 | nd | 30.47 | 69.53 | 0.70 |

Table 3.2 (*continued*)

| MPDF | 1/9-MP | MPR | DPR | 1,7-DMP | Retene | DBT/P | MDR | DBT% | MDBT% | DMDBT% | MP/P | BFla/(BFla+BePy) | Fla/(Fla+Py) | InPy/(InPy+BghiP) | BaA/(BaA+Chy) | Tpn/(Tpn+Chy) |
|---|---|---|---|---|---|---|---|---|---|---|---|---|---|---|---|---|
| 0 38 | 0 12 | 0 59 | 0 31 | 0 08 | -0 88 | 0 11 | 0 99 | 28 | 38 | 34 | 1 03 | 0 41 | 0 32 | nd | 0 24 | 0 36 |
| 0 37 | 0 15 | 0 55 | 0 29 | 0 11 | -0 99 | 0 07 | 1 22 | 33 | 38 | 29 | 1 08 | 0 43 | 0 35 | nd | 0 19 | 0 35 |
| 0 32 | 0 22 | 0 42 | 0 24 | 0 27 | -0 88 | 0 15 | 0 72 | 32 | 37 | 32 | 1 26 | 0 38 | 0 29 | nd | 0 22 | 0 28 |
| 0 33 | 0 21 | 0 45 | 0 24 | 0 25 | -0 76 | 0 15 | 0 73 | 29 | 38 | 33 | 1 33 | 0 31 | 0 25 | 0 28 | 0 17 | 0 26 |
| 0 30 | 0 23 | 0 38 | 0 22 | 0 31 | -0 89 | 0 07 | 0 68 | 23 | 41 | 36 | 1 71 | 0 34 | 0 30 | 0 35 | 0 19 | 0 25 |
| 0 32 | 0 20 | 0 42 | 0 28 | 0 33 | -0 89 | 0 11 | 0 84 | 29 | 39 | 32 | 1 38 | 0 36 | 0 29 | nd | 0 19 | 0 28 |
| 0 34 | 0 14 | 0 51 | 0 30 | 0 31 | -0 93 | 0 15 | 0 91 | 38 | 36 | 26 | 1 06 | 0 41 | 0 30 | nd | 0 21 | 0 33 |
| 0 35 | 0 15 | 0 52 | 0 28 | 0 24 | -0 81 | 0 17 | 1 19 | 39 | 35 | 26 | 1 25 | nd | 0 27 | nd | 0 21 | 0 24 |
| 0 35 | 0 13 | 0 53 | 0 27 | 0 12 | -0 75 | 0 28 | 0 91 | 28 | 42 | 30 | 1 55 | 0 41 | 0 27 | nd | 0 26 | 0 33 |
| 0 39 | 0 06 | 0 69 | 0 21 | -0 01 | -1 09 | 0 07 | 1 70 | 28 | 37 | 36 | 1 28 | 0 30 | 0 26 | 0 33 | 0 13 | 0 38 |
| 0 43 | 0 01 | 0 83 | 0 27 | -0 04 | -1 01 | 0 04 | 2 50 | 25 | 37 | 38 | 1 29 | 0 41 | 0 37 | 0 18 | 0 20 | 0 35 |
| 0 38 | 0 01 | 0 71 | 0 26 | 0 03 | -0 80 | 0 06 | 2 54 | 20 | 39 | 40 | 1 90 | 0 28 | 0 38 | nd | 0 01 | 0 51 |
| 0 44 | -0 01 | 0 87 | 0 31 | -0 05 | -0 73 | 0 02 | 3 35 | 31 | 32 | 37 | 1 26 | 0 43 | 0 38 | 0 16 | 0 15 | 0 37 |
| 0 35 | 0 02 | 0 60 | 0 20 | 0 13 | -1 42 | 0 09 | 1 76 | 23 | 37 | 39 | 1 68 | 0 24 | 0 24 | nd | 0 08 | 0 47 |
| 0 34 | 0 01 | 0 58 | 0 20 | 0 12 | -1 47 | 0 11 | 1 51 | 26 | 38 | 37 | 1 74 | 0 21 | 0 16 | nd | 0 05 | 0 49 |
| 0 38 | -0 01 | 0 69 | 0 20 | -0 14 | -1 33 | 0 07 | 2 04 | 17 | 32 | 50 | 1 65 | 0 26 | 0 16 | 0 29 | 0 11 | 0 48 |
| 0 40 | 0 07 | 0 71 | 0 23 | 0 11 | -1 15 | 0 05 | 1 49 | 24 | 35 | 41 | 1 52 | 0 30 | 0 24 | 0 19 | 0 10 | 0 35 |
| 0 41 | 0 01 | 0 88 | 0 26 | 0 05 | -1 06 | 0 04 | 2 15 | 21 | 39 | 40 | 1 48 | 0 30 | 0 21 | nd | 0 10 | 0 46 |
| 0 41 | -0 02 | 0 90 | 0 25 | 0 02 | -0 93 | 0 04 | 2 07 | 16 | 41 | 43 | 2 00 | 0 23 | 0 26 | nd | 0 13 | 0 52 |
| 0 42 | -0 001 | 0 90 | 0 25 | 0 02 | -0 86 | 0 06 | 2 09 | 17 | 39 | 44 | 1 73 | 0 26 | 0 29 | nd | 0 07 | 0 49 |
| 0 42 | -0 02 | 0 90 | 0 25 | 0 01 | -0 91 | 0 06 | 2 01 | 18 | 40 | 42 | 1 78 | nd | 0 29 | nd | 0 16 | 0 52 |
| 0 41 | -0 02 | 0 90 | 0 25 | 0 03 | -1 01 | 0 04 | 2 02 | 20 | 40 | 39 | 1 59 | 0 27 | 0 30 | nd | 0 15 | 0 52 |
| 0 42 | -0 03 | 0 93 | 0 26 | 0 01 | -1 04 | 0 04 | 2 26 | 19 | 42 | 39 | 1 64 | 0 30 | 0 30 | nd | 0 16 | 0 52 |
| 0 42 | -0 05 | 0 86 | 0 41 | -0 20 | -0 42 | 0 45 | 0 65 | 33 | 38 | 29 | 1 36 | nd | 0 30 | nd | 0 22 | 0 23 |
| 0 41 | -0 09 | 0 85 | 0 32 | -0 20 | -0 56 | 0 39 | 0 53 | 28 | 42 | 29 | 1 45 | nd | 0 39 | nd | 0 26 | 0 23 |
| 0 41 | -0 03 | 0 84 | 0 22 | -0 22 | -0 39 | 0 27 | 0 86 | 19 | 41 | 40 | 1 42 | nd | 0 52 | nd | 0 20 | 0 22 |
| 0 40 | 0 09 | 0 67 | 0 48 | 0 12 | -0 58 | 0 29 | 0 69 | 37 | 37 | 27 | 1 21 | 0 36 | 0 33 | 0 20 | 0 32 | 0 28 |
| 0 44 | 0 004 | 0 89 | 0 48 | -0 02 | -0 85 | 0 10 | 1 04 | 28 | 45 | 27 | 1 43 | nd | 0 38 | 0 08 | 0 30 | 0 31 |
| 0 45 | 0 03 | 0 86 | 0 53 | -0 12 | -0 10 | 0 23 | 0 89 | 38 | 35 | 28 | 1 10 | nd | 0 41 | nd | 0 32 | 0 31 |
| 0 45 | -0 02 | 0 91 | 0 51 | -0 17 | -0 42 | 0 14 | 1 14 | 32 | 37 | 31 | 1 12 | nd | 0 38 | nd | 0 30 | 0 34 |
| 0 45 | -0 02 | 0 88 | 0 62 | -0 18 | -0 56 | 0 31 | 0 91 | 34 | 37 | 29 | 1 36 | 0 49 | 0 30 | nd | 0 40 | 0 30 |
| 0 39 | -0 11 | 0 91 | 0 23 | -0 02 | -0 85 | 0 12 | 2 32 | 12 | 37 | 51 | 1 82 | nd | 0 37 | nd | 0 06 | 0 19 |
| 0 45 | 0 01 | 0 96 | 0 28 | -0 05 | -1 47 | 0 02 | 4 30 | 31 | 33 | 35 | 0 83 | 0 22 | 0 50 | 0 19 | 0 05 | 0 45 |
| 0 40 | -0 05 | 0 82 | 0 21 | -0 21 | -2 00 | 0 005 | 7 25 | 9 | 29 | 62 | 1 58 | 0 13 | 0 11 | 0 14 | 0 03 | 0 45 |
| 0 41 | -0 003 | 0 81 | 0 24 | 0 000 | -0 93 | 0 02 | 3 86 | 19 | 39 | 42 | 1 59 | 0 26 | 0 21 | 0 16 | 0 09 | 0 49 |
| 0 33 | 0 02 | 0 61 | 0 18 | -0 11 | -1 28 | 0 05 | 7 82 | 9 | 31 | 60 | 2 75 | 0 08 | 0 13 | 0 13 | 0 04 | 0 58 |
| 0 37 | 0 01 | 0 71 | 0 23 | 0 001 | -1 26 | 0 02 | 5 58 | 11 | 38 | 51 | 1 61 | 0 17 | 0 15 | nd | 0 04 | 0 51 |
| 0 39 | -0 07 | 0 81 | 0 19 | -0 14 | -1 67 | 0 01 | 9 63 | 13 | 42 | 45 | 2 02 | 0 18 | 0 13 | 0 18 | 0 05 | 0 50 |

TOC = total organic carbon; TN = total nitrogen; EOM = extractable organic matter; β = β-carotane/n-$C_{20}$ (%); %Rc = calculated vitrinite relectance from the depth (Depth = 2409.5 × ln(Ro) + 4081.03, $R^2$ = 0.94; Ping, private communication, 2017); 33S/(S+R) = $C_{33}$ αβ hopanes (22S/(22S + 22R)); 35/(35 + 34) = Homohopane Index ($C_{35}$ α β hopanes/($C_{35}$ αβ hopanes + $C_{34}$ αβ hopanes)); Ga/H30 = Gammacerane Index (Gammacerane/$C_{30}$ αβ hopane); St/H = $C_{29}$ ααα + αββ steranes/$C_{29}$ αβ hopane (based on areas in m/z 217 and 191, respectively); 29/27 = $C_{29}$/$C_{27}$ αα α 20R steranes; $C_{27}$ 20S = $C_{29}$ ααα 20S/(20S + 20R) steranes; $C_{29}$ 20S = $C_{29}$ ααα 20S/(20S + 20R) steranes; 29S/R = $C_{29}$ 20S/20R ααα steranes; $C_{29}$ αββ = $C_{29}$ αββ/(αββ+ααα) steranes; TNR-1 = trimethylnaphthalene ratio-1 (2,3,6-TMN/[1,4,6- + 1,3,5-TMN]); TNR-2 = trimethylnaphthalene ratio-2 ([2,3,6- + 1,3,7-TMN]/[1,4,6- + 1,3,5- + 1,3,6-TMN]); 125 = log(1,2,5-TMN/1,3,6-TMN); 127 = log(1,2,7-TMN/1,3,7-TMN); TMNr = trimethylnaphthalene ratio (1,3,7-TMN/[1,3,7- + 1,2,5-TMN]); TeMNr = tetramethylnaphthalene ratio (1,3,6,7-TeMN/[1,3,6,7- + 1,2,5,6-TeMN]); HPI = (iHMN+Cadalene+Retene)/1,3,6,7-tetramethylnaphthalene; MPI-1 = methylphenanthrene index-1 (1.5 × [3-MP + 2-MP]/[P + 9-MP + 1-MP]); MPDF = methylphenanthrene distribution fraction ((3-MP + 2-MP)/PMPs); 1/9-MP = log(1-MP/9-MP); MPR = methylphenanthrene ratio (2-MP/1-MP); DPR = dimethylphenanthrene ratio (3,5- + 2,6-DMP + 2,7-DMP)/(1,3- + 3,9- + 2,10- + 3,10-DMP + 1,6- + 2,9- + 2,5-DMP); 1,7-DMP = log(1,7-DMP/1,3- + 3,9- + 2,10- + 3,10-DMP); Retene = log(Retene/9-MP); DBT/P = dibenzothiophene/phenanthrene; MDR = methyldibenzothiophene ratio (4-MDBT/1-MDBT); DBT/P = dibenzothiophene/phenanthrene; DBT% = DBT/∑(DBT + MDBT + DMDBT) (%); MDBT% = MDBT/∑(DBT + MDBT + DMDBT) (%); DMDBT% = DMDBT/∑(DBT + MDBT + DMDBT) (%); Abbreviations for PAHs referred to Table 2. nd = not determined.

# Appendix

Molecular structures referred to in the text, figures and tables.

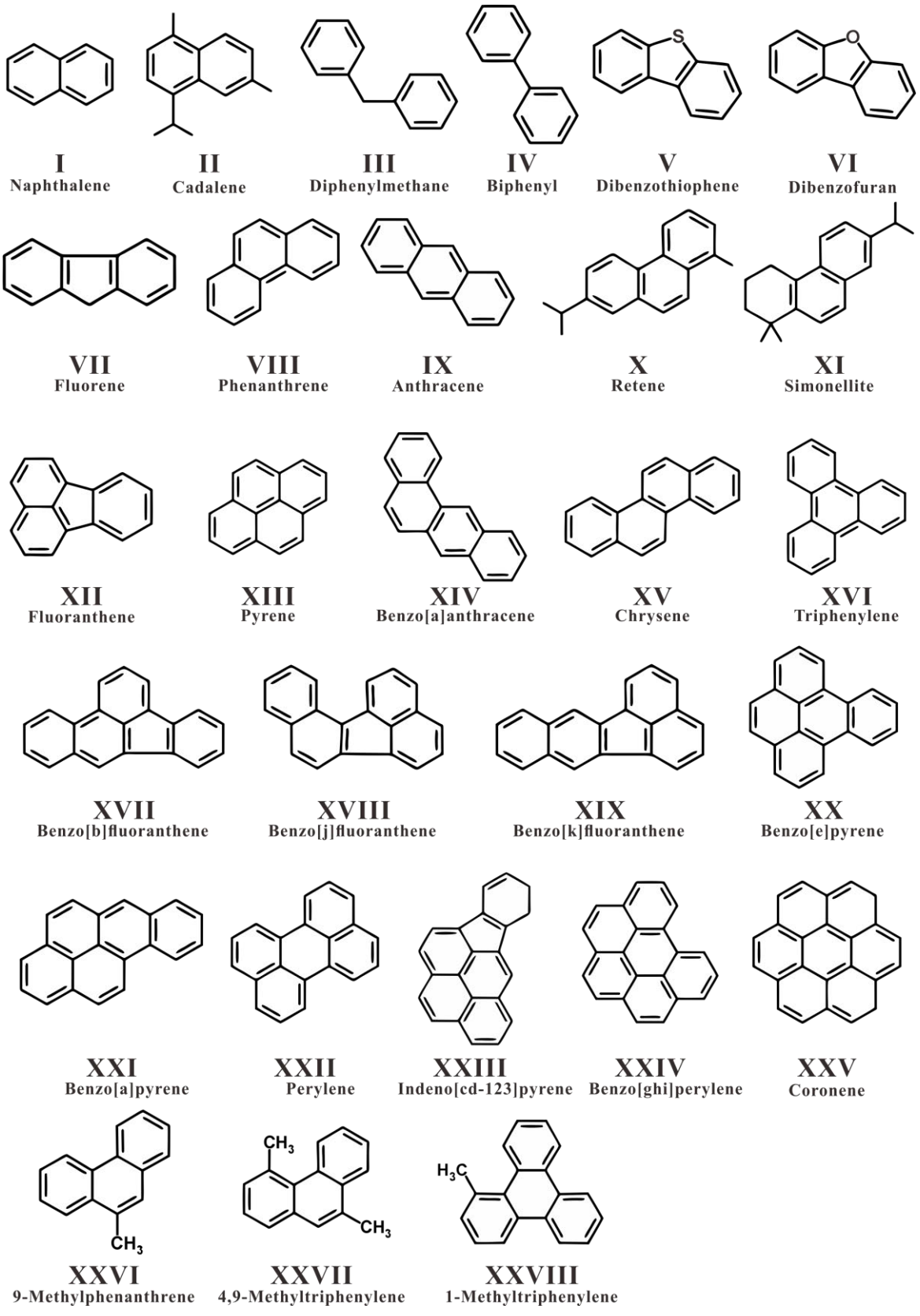

# Supplementary files

Supplementary Table 3.1 Weak $R^2$ values of correlations between PAHs and biomarker ratios. Ratios abbreviations are defined in Table 3.2.

| $R^2$ | 1,7-DMP | Retene | MP/P | BFla/(BFla+BePy) | Fla/(Fla+Py) | InPy/(InPy+BghiP) | BaA/(BaA+Chy) |
|---|---|---|---|---|---|---|---|
| Pr/Ph | 0.222 | 0.000 | 0.161 | 0.232 | 0.000 | 0.261 | 0.096 |
| β | 0.504 | 0.017 | 0.102 | 0.291 | 0.009 | 0.002 | 0.024 |
| 35/(35 + 34) | 0.397 | 0.122 | 0.001 | 0.341 | 0.136 | 0.015 | 0.066 |
| Ga/30H | 0.141 | 0.046 | 0.128 | 0.202 | 0.008 | 0.003 | 0.103 |
| St/H | 0.235 | 0.034 | 0.206 | 0.231 | 0.017 | 0.009 | 0.053 |
| 125 | 0.028 | 0.202 | 0.015 | 0.039 | 0.149 | 0.003 | 0.053 |
| HPI | 0.071 | 0.563 | 0.109 | 0.263 | 0.333 | 0.052 | 0.359 |
| DBT/P | 0.031 | 0.438 | 0.08 | 0.043 | 0.114 | 0.075 | 0.443 |

Chapter 4

# 4. Heterogeneity of hydrocarbons in a well-laminated shale from the Dongying Depression, Bohai Bay Basin: New insights on the mechanisms of organic matter preservation

Huiyuan Xu[a, b, c, *], Dujie Hou[a], , Stefan C. Löhr[b], Simon C. George[b, *]

[a] School of Energy Resources, China University of Geosciences (Beijing), Haidian District, Beijing 100083, China

[b] Department of Earth and Planetary Sciences and MQMarine Research Centre, Macquarie University, Sydney, NSW 2109, Australia

[c] State Key Laboratory of Shale Oil and Gas Enrichment Mechanisms and Effective Development, Beijing 100083, China

**Chapter 4** uses a newly improved experimental procedure to assess hydrocarbon heterogeneity at the microscale, and to tentatively unveil the precise mechanisms of organic matter accumulation and preservation. This chapter elucidates the formation of organic-rich shales in the Dongying Depression, and suggests an individual and dynamic process of organic matter enrichment.

**Statement of Author's Contribution:** 85% of the work was done by the first author Huiyuan Xu, including developing the project plan and timeframe, sampling,

designing and conducting laboratory experiments, processing and analysing the data, and writing the manuscript. Simon C. George helped with designing the laboratory experiments, directing the research, and improving the manuscript, which accounts for 8%. Dujie Hou helped with developing the project plan and timeframe, sampling, and improving the manuscript, which accounts for 4%. Stefan C. Löhr helped with designing and conducting the scanning electron microscopy (SEM) and Nanomin mineral mapping experiments, interpreting those data, and improving the manuscript, which accounts for 3%. This chapter is about to be submitted as an original research paper to *Geochimica et Cosmochimica Acta* (2019).

# Abstract

An organic-rich, low maturity and well-laminated shale from the Dongying Depression, Bohai Bay Basin was examined to assess the heterogeneity of hydrocarbons as proxies for depositional environment and source. This work provides the first organic-geochemical analysis of horizontal shale slices at the millimetre scale. The $^{13}C$ depleted (-31.6‰) *n*-$C_{25-31}$ alkanes support organic contributions from algae (e.g. *Botryococcus braunii* A race) rather than terrigenous plants. 24-*n*-Propylcholestane occurs in high relative abundance, indicating seawater influx. The presence of isorenieratane together with the varying aryl isoprenoid ratios suggest that the palaeo-lake experienced episodic water stratification and photic zone euxinia. The depositional environment varied repeatedly, instead of having permanent characteristics. Obligate anaerobes (e.g. sulphate-reducing bacteria) degraded and altered the organic matter, which was mainly derived by phytoplankton in the surface water layers. Sulphate-reducing bacteria were probably responsible for the formation of dolomite, based on their mediation of releasing $Mg^{2+}$ from sulphate. Autotrophic photosynthesisers (e.g. green-sulphur bacteria) episodically thrived and reduced the population of phytoplankton. The correlation of total organic carbon with parameters related to water body conditions provide a new dynamic organic matter preservation mechanism (at least at the millimetre scale), which is mainly controlled by the interactions of various micro-organisms and the sulphur cycle in the palaeowater column.

***Keywords***: aryl isoprenoids; 24-*n*-propylcholestane; photic zone euxinia; *n*-alkane isotopes; hydrocarbon heterogeneity; preservation; black shale; Bohai Bay Basin

## 4.1. Introduction

The deposition of organic-rich and fine grained shales and mudstones generally relies on high rates of primary productivity, continuous sediment delivery, low-energy conditions, balanced clastic sedimentation rate, persistent bottom water anoxia and non-bioavailability (Demaison and Moore, 1980; Pedersen and Calvert, 1990; Caplan and Bustin, 1999; Kennedy et al., 2002; Pacton et al., 2006; Mort et al., 2007a; Guo et al., 2010; Macquaker et al., 2010; Makeen et al., 2015). Lacustrine fine grained shales and mudstones are considered to be mainly associated with organic production (especially phytoplankton production) and preservation (Katz, 1990, 1995). Sedimentation in continental lake basins is relatively unstable due to highly variable climatic factors, affecting rainfall, evaporation and water level. Palaeolake water level expands and shrinks cyclically many times, resulting in sedimentary structures reflecting major cycles and superimposed micro-cycles at shorter time scales (Crossley et al., 1984; Weltje et al., 1998; Carroll and Bohacs, 2001; Ghinassi et al., 2012; Renaut et al., 2013). The embodiment of these cyclical changes are lamina in shales and mudstones, with possible bioturbation features. Depositional fluctuations in most lake basins can also result in significant heterogeneity in the distribution of organic matter and minerals (Chen et al., 2016). Apart from the observable laminae in hand specimens, lacustrine shales and mudstones can also be highly heterogeneous on the millimetre to micrometre scales, with commonly organised thin (< 10 mm) beds, reflecting complex depositional and diagenetic process (Macquaker et al., 2010; Trabucho-Alexandre et al., 2012). The fine grained rocks that are organised into individual thin beds were deposited as discrete events rather than during continuous settling of fine grained materials, under dynamic environments rather than permanent bottom water anoxia (Macquaker et al., 2007; 2010).

Liu and Wang (2013) and Zhang et al. (2009) noted multiple types of thin beds in the source rocks of the Shahejie Formation, Dongying Depression, eastern China. These consisted of algal laminae, organic matter laminae, carbonate laminae, clay-rich laminae, and reddish-grey rhythmites. The laminated structure and corrugated bedding of the fine grained rocks suggests intermittent stratification of the water column caused by palaeoclimatic changes (Chen et al., 2016). Ma et al. (2016) also suggested that climate controlled the deposition of well laminated shales and mudstones in the Zhanhua Depression, Jiyang Sub-basin. Higher rates of detrital input associated with increased river run-off increases oxygen content, the amount of terrigenous-derived nutrients and minerals, which together can break-up the oxygen-deficient and stratified water conditions, and dilute the organic matter (Tyson, 2001, 2005). The sedimentation rate of the Shahejie Formation generally increases from the upper part of the fourth member to the third member (Zhang et al., 2009), and the latter has a high sedimentation rate ranging from 200-500 mm/ka (Zhang et al., 2009; Gong et al., 2010; Guo et al., 2010). Thus, the environmental conditions leading to the alternating deposition of the thin beds in the Shahejie Formation may not be persistently anoxic and stagnant, but rather the settling of organic and inorganic materials through the water column fluctuated (Pearce et al., 2006; Hesselbo et al., 2007; McArthur et al., 2008). Additionally, the preservation of laminae requires a lack of bottom water current agitation and the absence of bioturbation. Zhu et al. (2005) suggested that the dark organic-rich laminae in the Dongying palaeolake were formed mainly in late autumn, winter and early spring, whilst the lighter calcite-rich laminae were formed in late spring, summer and early autumn, due to seasonal stratification and algal blooms. van Dongen et al. (2006) discussed the relationship between source inputs and preservation of organic carbon. However, uncertainty remains as to the depositional environments and the dominant organic inputs for different laminae at the millimetre scale. How do these vary between individual lamina? What chemical conditions at the sediment-

water interface trigger the changes from one another? What roles did aerobic and anaerobic bacteria play in the preservation of organic matter, apart from the dominant algal contribution?

Previous geochemical research on the source rocks in the Dongying Depression mostly utilised homogenised bulk powder as an averaging proxy for an individual sample at a specific depth to investigate the chemical conditions and origin (Li et al., 2003; Zhang et al., 2009; Hao et al., 2011; Chen et al., 2016; He et al., 2017; Chapter 2). Bulk powder neutralises and obscures the small scale variations in hydrocarbon composition preserved in the rocks. The variability of organic geochemistry has not often been assessed on well-laminated shales at the millimetre scale. To assess the micro-cyclicity of the depositional environment, the organic matter sources, and the influence of mineral nutrients, one black shale core sample from the Shahejie Formation, Dongying Depression was subjected to a horizontal slicing experiment at the millimetre scale. Solvent extracted fractions of the individual slices were analysed by gas chromatography-mass spectrometry, metastable reaction monitoring-gas chromatography-mass spectrometry, gas chromatography-isotope ratio mass spectrometry and scanning electron microscopy with energy dispersive spectrometry. In this study, the vertical variability of hydrocarbons in the core is illustrated by comparing multiple markers in each slice. The focus of this paper is on the geochemical heterogeneity of the laminated shales at the millimetre scale, so as to determine micro-changes in depositional environments and organic matter inputs. The goals were to determine if the Shehejie Formation shales or mudstones were deposited by the vertical aggradation of fine grained materials under permanent palaeowater conditions, and to define the proportions and variability of phytoplankton and bacteria as organic matter inputs.

## 4.2. Geological setting

The rise of the upper mantle behind the Western Pacific subduction margin caused the rifting of continental crust during the Late Mesozoic-Cenozoic (Fu and Sheng, 1989). The Bohai Bay Basin is an intracontinental extensional rift basin that formed since the Late Jurassic, and is located in the east of the North China Craton, adjacent to the Bohai Sea, and is bounded by the Tanlu Fault in the east (Fig. 4.1). There are six sub-basins within the Bohai Bay Basin. The Jiyang Sub-basin is the most petroliferous one, and formed in the rifting and subsiding phase. It is situated in the south of the Bohai Bay Basin, and covers most of the Yellow River Delta, with an area of 25,000 $km^2$, a width of 120 km and a length of 200 km, and is northeast-southwest trending. The Dongying Depression is developed in the southern part of the Jiyang Sub-basin, and covers an area of 5,500 $km^2$ (Fig. 4.1). The Dongying Depression is the second largest oil field in China, and contains five major Paleogene and Neogene formations. The Pliocene Minghuazhen Formation and the Miocene Guantao Formation are composed of alluvial and fluvial sediments, whereas the Oligocene Dongying Formation and the Eocene Shahejie and Kongdian formations are composed of lacustrine sediments. The widely distributed Eocene Shahejie Formation (designated Es in Fig. 4.2) is further subdivided into four members: the Sha1 (Es1), Sha2 (Es2), Sha3 (Es3) and Sha4 (Es4) members. Much evidence suggests that the Es1, the Sha3 (Es3) and the upper part of Sha4 (Es4U) are the main oil-bearing intervals (Li et al., 2003; Zhang et al., 2009). The Es4 member was deposited in a shallow, semi-enclosed brackish-saline lacustrine setting during the early stage of rift development, and the Es3 member was deposited in a deeper and wider lake with fresh-brackish water salinity during the peak period of paralic lake development and regional subsidence (Bao and Li, 2001; Wang et al., 2013). The sandy Es2 member has proven to be the main reservoir unit (Hao et al., 2011). The Es1 member was deposited in a brackish water depositional environment. The Es4U and the Es3 member sediments have

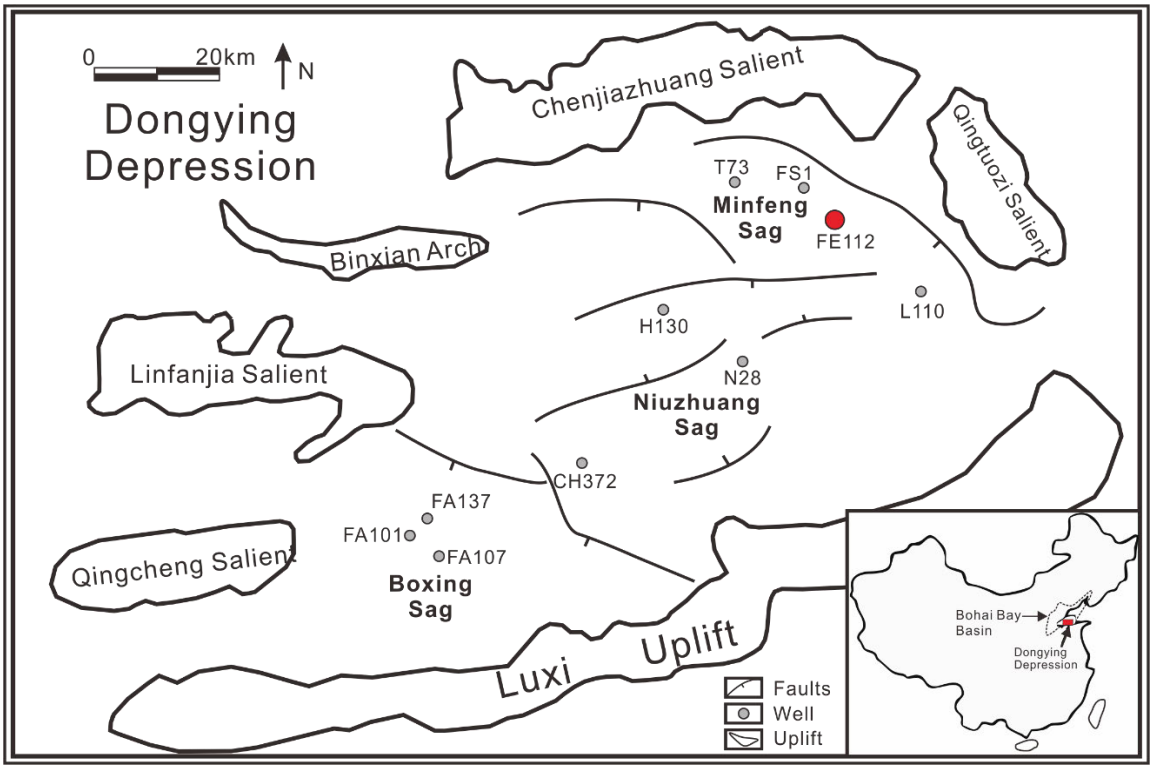


Fig. 4.1 Location map of the Dongying Depression in the Bohai Bay Basin, China, showing the position of the subdivided sags, the wells and the structural elements.

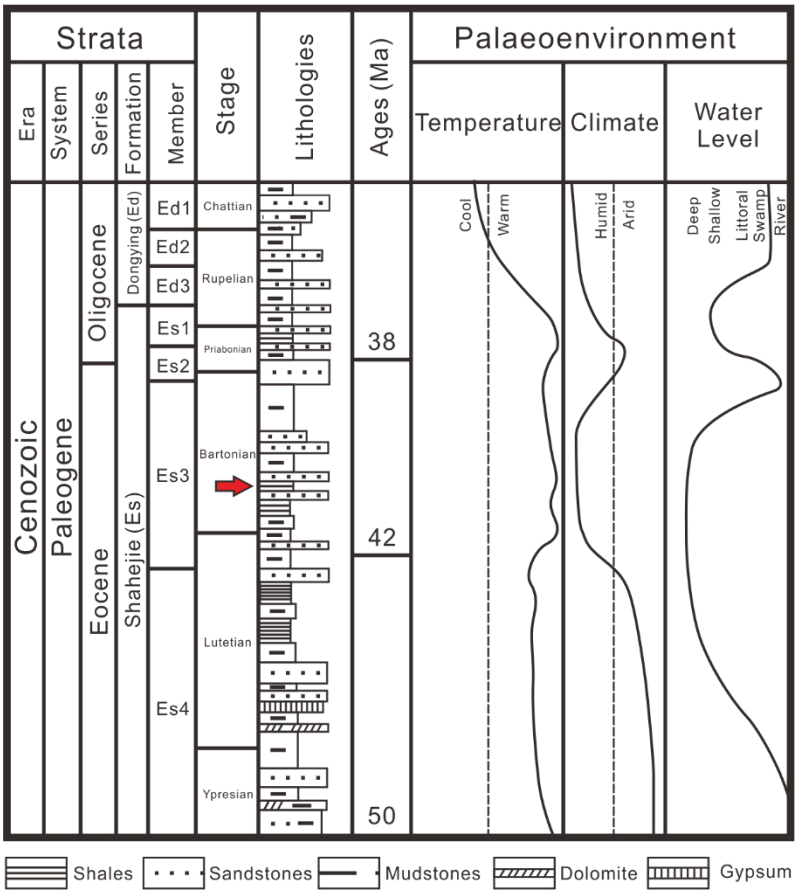


Fig. 4.2 Stratigraphic chart showing the Eocene to Oligocene strata of the Dongying Depression, Bohai Bay Basin.

strong climate-driven rhythmicity (Zhang et al., 2009). The lamination characteristics of these fine grained source rocks probably indicate seasonal water stratification that may have arisen from seasonal palaeoclimate conditions (Zhang, 2008). Source rocks in these two members mainly contain type I kerogen (Zhang et al., 2009).

## 4.3. Samples and experimental procedure

One black shale core sample from the FE112 well (3122.0 m; Es3 member of the Shahejie Formation; FE04; Chapter 2) was subjected to horizontal slice experiments at the millimetre scale. This well laminated bulk shale sample has the highest TOC (14.9%; higher than other samples from the Es3 to Es4 members in the FE112 well). Hand samples from the well are commonly fragile and fissile so were visually assessed, and an appropriate sample that was competent was sub-sampled for the slice experiment. No discernible grain size and textural variations could be visually observed, apart from dark and light layers. Before the slice analyses, part of the bulk sample was well ground and conventionally processed. The shale sample has abundant aliphatic and aromatic dinosteranes, 24-*n*-propylcholestanes (the relative signal intensity of these stereoisomers on the *m/z* 414→217 mass transition is 40.2% of the signal intensity on the *m/z* 414→231 mass transition), but diminished markers for a restricted depositional environment such as gammacerane, β-carotane, and homohopanes. The sample has a low thermal maturity (estimated VRE = 0.55; from $C_{29}$ S/R ααα (Sofer et al., 1993); Chapter 2), suggesting that biomarkers inside were fully preserved. Bacteria played a more important role in the high bioproductivity than eukaryotic organisms such as from algal blooms, based on the low $C_{29}$ sterane/$C_{29}$ αβ hopane ratio (0.39). Hypersaline water environments typically result in just a few simple microbial communities (Killops and Killops, 2005), which may give rise to a uniform organic matter distribution. However, the Es3 member was deposited in a hydrologically-open lake under varying palaeoclimate and

water chemistry (Zhang et al., 2009; Hao et al., 2011; Ma et al., 2016), so the discernible laminations probably record micro-fluctuations.

### 4.3.1. Scanning electron microscopy (SEM) and nanomin mineral mapping

The sample was polished using a Hitachi IM4000 Argon Ion Mill system and carbon-coated (5 nm carbon) before imaging and mineral mapping on a FEI Teneo field emission SEM equipped with dual EDS (energy dispersive X-ray spectroscopy) detectors (Bruker XFlash Series 6). High resolution back-scatter electron and mineral maps of the sample were collected to identify small-scale vertical variation in textural, mineralogical and organo-mineral associations in the sample (13 mm working distance, 15 kV accelerating voltage). Back-scatter electron image tilesets (150 nm pixel resolution) and EDS spectra (5 µm step size, 8 ms acquisition time) for mineral mapping were collected sequentially using the FEI Maps Mineralogy software, followed by classification of the individual EDS spectra using the FEI Nanomin software (Haberlah et al., 2015; Rahman et al., 2018). Mineral identification is achieved by comparing EDS spectra collected in the mapped area against reference spectra collected on known mineral standards. Unlike earlier SEM-based mineral mapping techniques (e.g. QEMSCAN), the Nanomin mineral classification system can de-convolve mixed X-ray spectra and assign up to three minerals per analysed spot (Löhr et al., 2018; Rahman et al., 2018). This is a critical advantage for the correct interpretation of the mixed phase X-ray spectra characteristic of heterogeneous fine grained sediments, which might otherwise lead to mineral misidentification. SEM photomicrographs and Nanomin maps provide direct visual evidence of the range and complex association of minerals and organic matter at the required mm to sub-mm scale.

### 4.3.2. Slicing

After cutting off the outside surfaces, the sample was horizontally sawn into ten slices with thickness ranging from 2 to 8 mm (slice sample codes: A-J) using a Buehler Isomet 4000 Linear Precision Saw with a 0.9 mm blade. Each slice and sample were treated with deionised water sonication and dichloromethane sonication to avoid laboratory and cross contamination, then was dried at room temperature. Even though these samples were sawn very carefully, a certain amount of sample was inevitably lost during the cutting process.

### 4.3.3. Crushing, solvent extraction, and fractionation

The slices and comparison samples were crushed into powder in a rotary mill. The homogenised powdered samples were extracted using an azeotropic solvent mixture of dichloromethane/methanol (9:1 v/v) using an accelerated solvent extractor (ASE300; Dionex). Then the extracts were fractionated using two phase silica gel column liquid chromatography. Total hydrocarbons were separated from polar compounds by eluting the extractable organic matter (EOM) with n-hexane/dichloromethane (4:1 v/v). Then the total hydrocarbons were separated into aliphatic hydrocarbons, which were collected by eluting with *n*-hexane, and aromatic hydrocarbons, which were collected by eluting with *n*-hexane/dichloromethane (4:1 v/v). UV light monitoring was used to ensure there were no mixed elution of aliphatic and aromatic hydrocarbons.

### 4.3.4. Gas chromatography-mass spectrometry (GC-MS)

Gas chromatography-mass spectrometry (GC-MS) analyses of the aliphatic and aromatic hydrocarbon fractions were performed on an Agilent GC (6890N) coupled to an Agilent Mass Selective Detector (5975B) equipped with a J&W DB-5MS fused silica column (length 60 m, inner diameter 0.25 mm, film thickness 0.25 μm). The inlet was held at 35 ℃

for 3 min then was programmed to 310 ℃ (0.4 min. isothermal) at a rate of 700 ℃/min. Samples were injected in splitless mode. The temperature of the GC oven was initially held at 35 ℃ for 4 min and was programmed to 310 ℃ at 4 ℃ /min, then was held for 40 min. Helium (99.999%) was used as the carrier gas. The carrier gas flow rate (constant flow) was 1.5 mL/min. The ion source of the mass spectrometer was operated in EI mode at 70 eV. The MS data were acquired in full scan and selected ion monitoring (SIM) modes. Compound identification were based on comparison of relative GC retention times and mass spectra with those previously reported (e.g., Li et al., 2012; Sousa Júnior et al., 2013). External standards including North Sea Oil 1 (NSO-1; Norwegian Petroleum Directorate) and an *n*-alkane mix were also analysed for comparison. The relative abundance of compounds was determined from peak areas (using selected ion mass chromatograms).

### 4.3.5. Gas chromatography-metastable reaction monitoring-mass spectrometry (GC-MRM-MS)

GC-MS analysis of the aliphatic hydrocarbon fraction was also performed on a Thermo Trace Ultra GC interfaced with a high resolution Thermo DFS MS system. Gas chromatography was carried out on a J&W DB-5MS fused silica column (60 x 0.25 mm i.d., 0.25 μm film thickness). Aliphatic hydrocarbons (1 μL) were injected using a splitless technique with a constant injector temperature of 260 ℃ and constant flow of 1.5 mL/min. The mass spectrometer was tuned to 1000 resolution (electron energy 70 eV; source temperature 280 ℃). The GC oven was programmed for an initial temperature of 40 ℃ for 2 min., followed by heating at 20 ℃ $min^{-1}$ to 200 ℃ and then a second heating ramp at 2 ℃ $min^{-1}$ to 310 ℃. The aliphatic fractions were analysed using a metastable reaction monitoring (MRM) programme with the following *m/z* transitions so as to examine the $C_{25-30}$ steranes:

344→217, 358→217, 372→217, 386→217, 400→217, 414→217, 414→231. An external standard (AGSO_NADD) was analysed for comparison of retention times.

### 4.3.6. Gas chromatography-isotope ratio-mass spectrometry (GC-ir-MS)

An aliquot of the aliphatic fraction from two slice samples was separated into purified n-alkanes by molecular sieving. An Agilent 6890 gas chromatograph (GC; BP-5 (SGE), 30m, 0.25mm O.D., 0.25mm film; constant flow 1.0mL/min) coupled to a Thermo MAT 253 through a GC-C-III combustion (with NiO/CuO/Pt at 950 ℃) interface was used to determine the $^{13}C$ of the selected compounds. The samples were injected at 290 ℃ using splitless mode (60 seconds). The GC oven temperature was initially held at 50 ℃ for 2 min and was programmed to increase to 120 ℃ at 25 ℃ /min then to 310 ℃ at 5 ℃ /min, where it was maintained isothermally for 8 min. Helium was used as the carrier gas. A standard mixture of *n*-alkanes with known $\delta^{13}C$ values was analysed to test the accuracy of the instrument. The isotopic compositions of all samples are reported relative to the international Vienna Peedee belemnite (VPDB) standard, and were determined at least twice. The standard deviations of the replicates were calculated to estimate reproducibility. The reproducibility was within 0.2‰.

### 4.3.7. Total organic carbon and nitrogen

500 mg of each ground slice sample was immersed in 10% HCl and heated in a water bath at 50 ℃ for 36 hours to remove the carbonates and dolomites (inorganic carbon). After HCl treatment, the samples were rinsed and centrifuged 3 times with deionised water to remove the acid, and then dried in an oven for 24 hours at 55 ℃. Dried samples (5-10 mg) were analysed using a Euro Vector EA3000 CHNS-O Elemental Analyser. The reaction gas products ($CO_2$ and $NO_x$) were carried by helium flow to a copper reactor where excess $O_2$ was

consumed to produce CuO, and NOx products were converted to $N_2$. The products were carried through a packed GC column that provided separation of the combustion gases which were detected by a thermal conductivity detector. Soil#6 (C = 3.429%; N = 0.228%) and acetanilide were used as standards every eight samples.

## 4.4. Results

The shale hand specimen have alternating horizontal light and dark bedding layers that are generally continuous and parallel (Fig. 4.3). Slices A-J have total organic carbon (TOC) contents of 10.6-17.5%, total nitrogen (TN) contents of 0.56-0.77%, carbon/nitrogen ratios of 18.5-23.6 and extractable organic matter (EOM) contents of 13.2-21.8 mg/g (Table 4.1).

### 4.4.1. SEM observations

SEM observations were used to determine the mineral compositions and sediment micro-fabric, which contribute to an understanding of the distribution/enrichment of the organic matter. The shale sample comprises five types of laminae (Table 4.2b and Fig. 4.3a and 3b): calcite laminae (white; on average, calcite: 83.2%, dolomite: 6.0%); dolomite (plus calcite) laminae (pale blue; on average, calcite: 35.2%, dolomite: 37.3%); clay mineral laminae (light green; on average, clay minerals: 21.7%); organic matter-rich laminae (dark green; on average, clay minerals: 17.9%); pyrite-rich laminae (yellow; on average, pyrite: 17.0%) (Fig. 4.4c and 4.4d). The thickness of all laminae range from 20 to 100 μm. The laminae are generally continuous and parallel, but occasionally, there are lenticular dolomite (plus calcite) fabrics and micro wavy-laminae fabrics. The clay minerals are predominantly composed of illite. In addition, the latter three clay-rich laminae contain more abundant feldspars than the carbonate laminae. The amount of apatite and fluorite varies slightly between the laminae (Fig. 4.4b). The clay mineral laminae are commonly mixed with the carbonate laminae (Fig. 4.3a). There are two repeated lamina sets (couplets) through the sample vertically, with cycles

of calcite laminae together with organic matter-rich laminae interspersed with alternating laminae of clay minerals and dolomite (Fig. 4.3a and 3b). The lamina couplets of thin carbonate and clay layers occur with thickness ranging from 50 to 150 μm. The organic matter stringers and disseminated organic matter are embedded in the clay mineral laminae (Fig. 4.3b). Framboid pyrite and pyrite clusters are present in almost every type of laminae (Fig. 4.3c). Calcareous microfossil was replaced by dolomite and calcite with 100% kaolinite infill (Fig. 4.3d). The clay mineral laminae contain relatively more pyrite than the carbonate laminae (Fig. 4.4c).

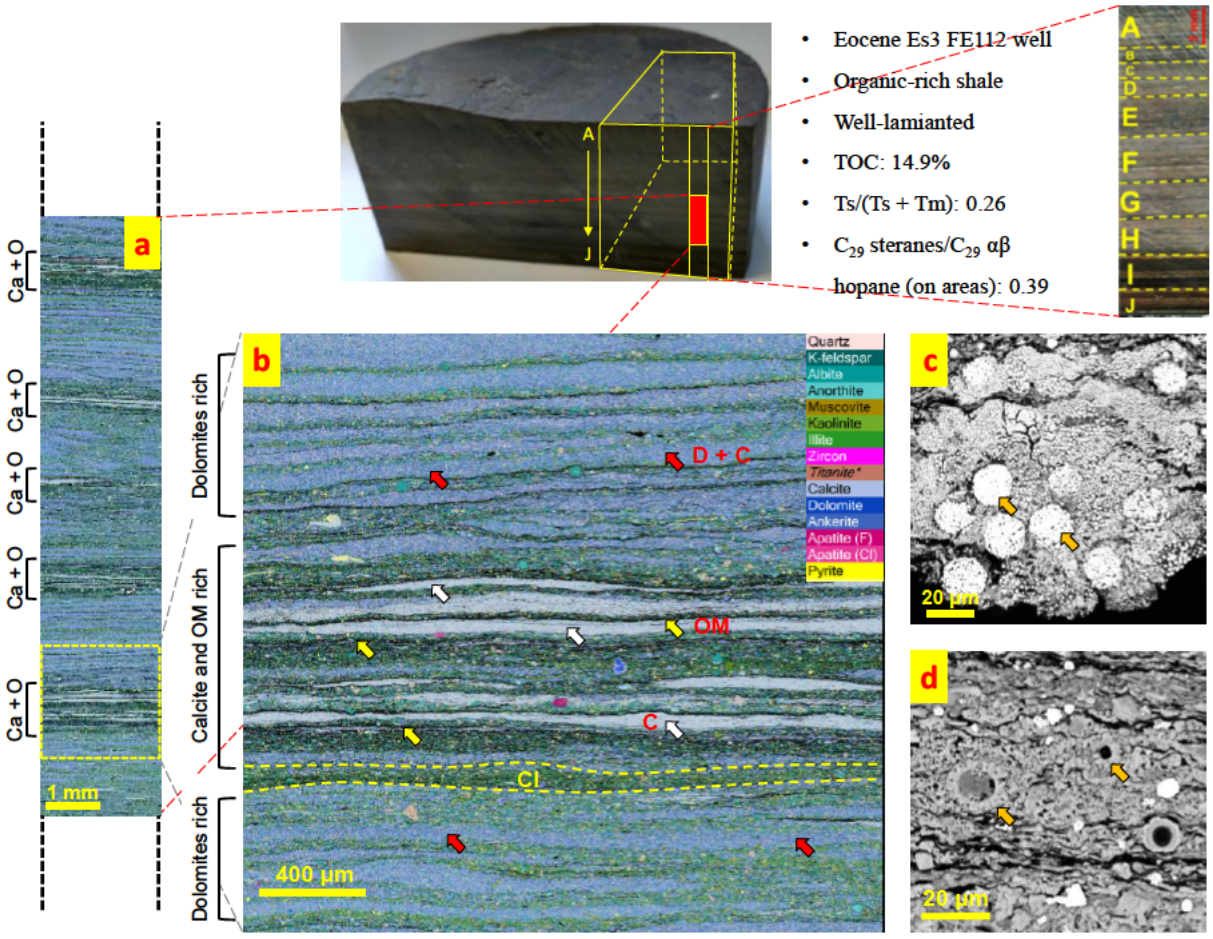


Fig. 4.3 Photomicrographs (a) showing the cyclical presence of clay and organic matter laminae sets from part of the sample (shown in red on the hand specimen photograph; summary of geochemistry parameters from bulk sample given); (b) showing the continuous and parallel alternating dolomite laminae (red arrows), calcite laminae (white arrows), organic matter stringers (yellow arrows) and clay mineral laminae (e.g. dashed line area); (c) showing framboid pyrite (orange arrows); (d) showing aggregates of calcareous microfossil composed of dolomite and calcite with 100% kaolinite infill (orange arrows). Ca + O = calcite and organic matter laminae sets; Cl = Clay minerals; D + C = dolomite and calcite laminae; OM = organic matter. Note the organic matter enrichment near the calcite laminae.

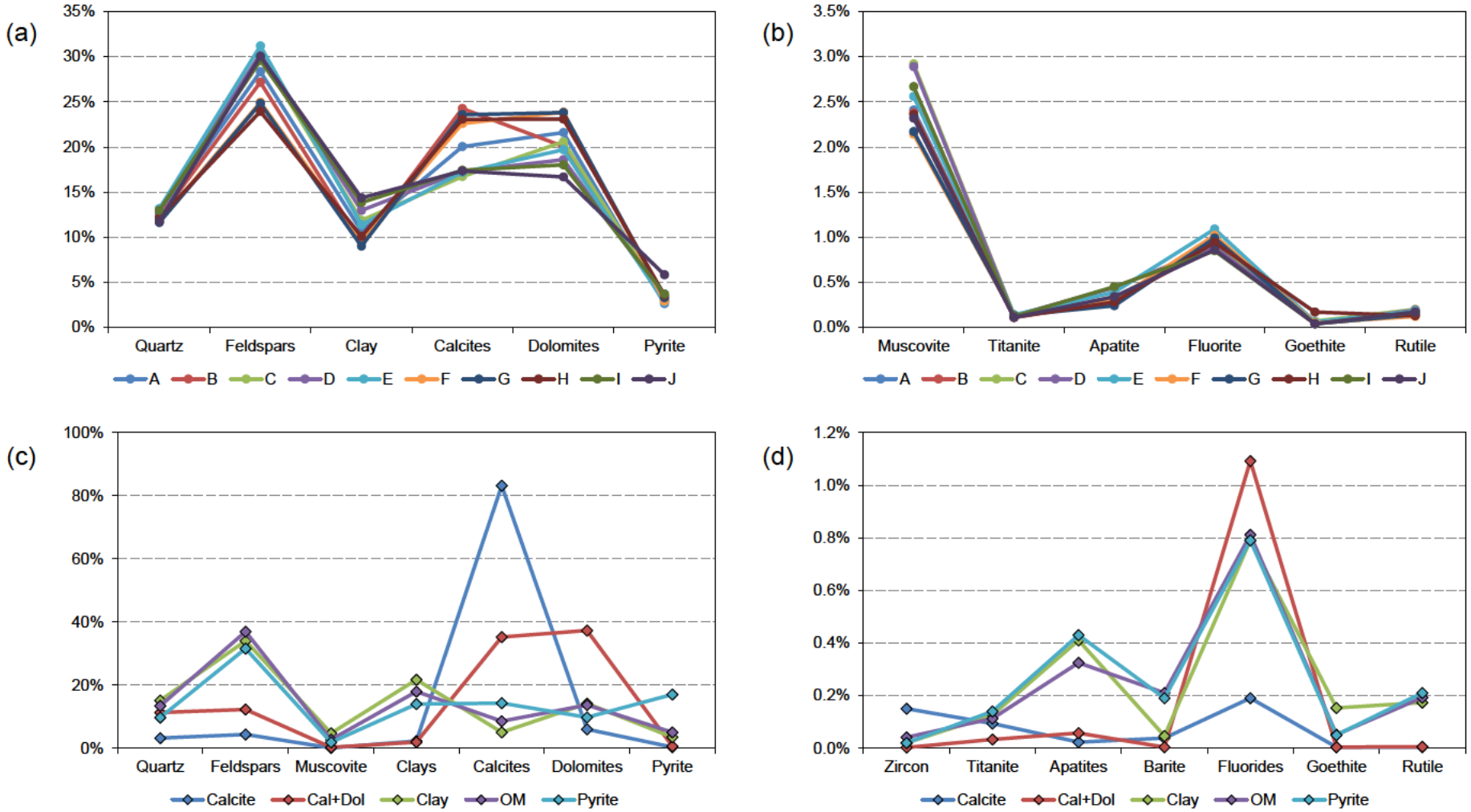


Fig. 4.4 Composite line charts (a) and (b) showing the mineral compositions of the sliced samples (A to J); (c) and (d) showing the mineral composition differences between the calcite laminae, calcite plus dolomite laminae, clay mineral laminae, organic matter-rich laminae and pyrite-rich laminae. Cal = calcite, Dol = dolomite, OM = organic matter.

### 4.4.2. Mineral compositions of the slices

In general, the ten slice samples are predominantly composed of feldspars (K-feldspar, albite, anorthite) (23.9-31.2%), dolomite and ankerite (16.7-23.8%), calcite (17.3-24.3%), quartz (11.6-13.2%) and clay minerals (9.0-14.4%). The subsidiary mineral components are pyrite (2.6-5.8%), muscovite (2.2-2.9%) and fluorite (0.85-1.1%). Apatite (0.24-0.81%), titanate (0.11-0.14%), rutile (0.12-0.20%) and goethite (0.04-0.07%) are present in trace amounts (Fig. 4.4a and 4.4b; Table 4.2a). The most varied mineral compositions between different slices include dolomite, calcite, clays, feldspars, apatite and fluorite. The sediment rate of the Es3 member in the Dongying depression is about 150-200 mm/ka (Zhang et al., 2009; Gong et al., 2010). The age span of the 10 sliced sample is about 225-300 years.

### 4.4.3. Molecular geochemistry

#### *4.4.3.1. Normal alkanes and isoprenoids*

The aliphatic fractions of the slice samples have abundant *n*-alkanes ranging from $C_{10}$-$C_{37}$, with a maximum at *n*-$C_{17}$ (Fig. 4.5). Slice C contains the highest relative abundance of middle to long chain *n*-alkanes (> $C_{20}$), whereas slice I has the lowest abundance. There is a prominent odd-over-even carbon number preference for the middle to long chain *n*-alkanes (Fig. 4.5). The relative abundance of summed *n*-$C_{27\text{-}31}$ alkanes to total *n*-alkanes ($\Sigma n$-$C_{27\text{–}31}$/$\Sigma n$-alkanes; %) is 21.2% for slice C, and is 9.6% for slice I. The pristane/phytane ratio (Pr/Ph) ranges from 0.84 to 0.92 (Table 4.1), which most likely reflects the redox conditions rather than other factors such as the micro-fractionation or micro-migration. There is no relationship ($R^2$ = 0.0083) between EOM (mg/g) and the $\sum$20-/$\sum$21+ *n*-alkane ratios, which corroborates the hypothesis that the differences in the relative abundance of the middle to long chain *n*-alkanes are not likely due to micro-fractionation. Moreover, low molecular weight *n*-

alkanes would more likely be influenced by micro-fractionation, but there is no evidence for this from the carbon isotope data such as similar $\delta^{13}C$ values of low and high molecular weight *n*-alkanes (Chapter 4.4.4).

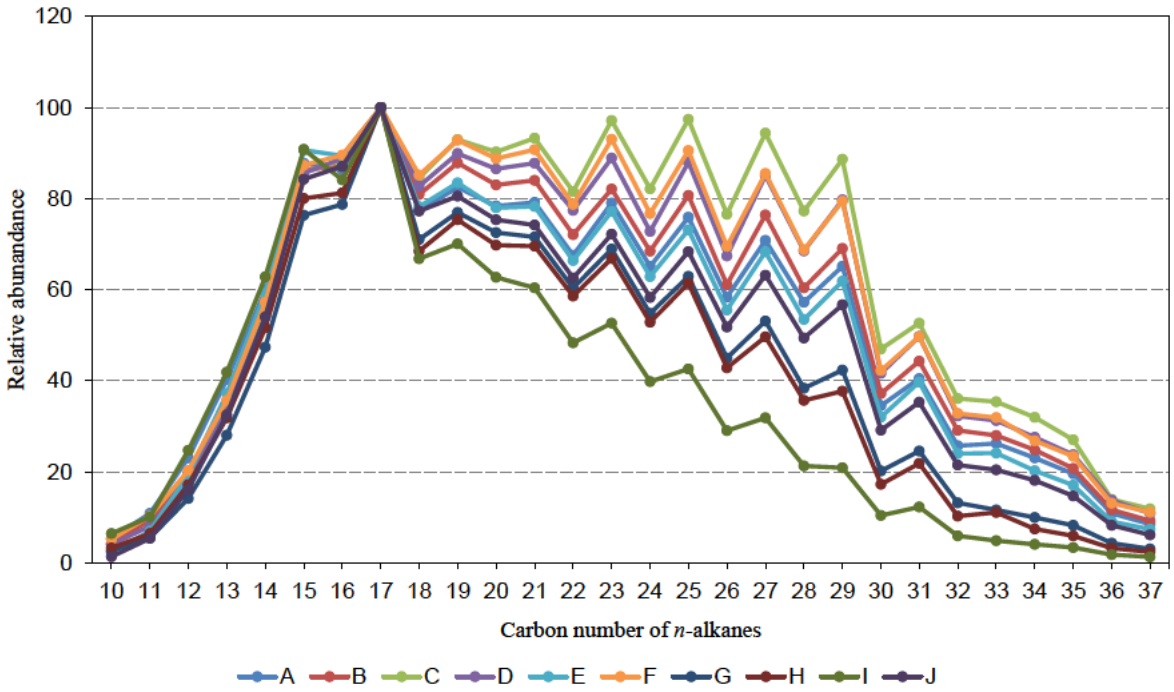


Fig. 4.5 *n*-Alkanes normalised to the *n*-alkane with highest concentration in each slice (always *n*-$C_{17}$), based on abundance in *m/z* 57 mass chromatograms.

### *4.4.3.2. Terpanes*

On the *m/z* 191 mass chromatograms (not shown), $C_{30}$ 17α,21β(H) hopane is predominant, followed in abundance by by $C_{29}$ norhopane. Most of the slice samples have $C_{29}/C_{30}$ hopane ratios less than 0.84 (Table 4.1). Other terpanes such as $C_{19\text{-}26}$ triterpanes, Ts (18α-22,29,30-trisnorneohopane), Tm (17α-22,29,30-trisnorhopane) and homohopanes ($C_{31}$-$C_{33}$) are present in varying concentrations. Gammacerane is near the limit of detection in all the slices, and there is no $C_{35}$ homohopane predominance over $C_{34}$ homohopane (Table 4.1). Tricyclic and tetracyclic diterpanes are absent. The $C_{21}$ tricyclic terpane has a comparable abundance to the $C_{23}$ tricyclic terpane, and $C_{19}$ and $C_{20}$ tricyclic terpanes are present in low relative abundances (Table 4.1). The Ts/(Ts + Tm) ratios are less than 0.28, and the

oleanane/$C_{30}$ hopane ratios are less than 0.04. On the *m/z* 205 mass chromatograms (not shown), 2α-methylhopanes are present in trace amounts.

*4.4.3.3. Steranes*

On the *m/z* 217 mass chromatograms (not shown), the regular steranes have a consistent $C_{27}$ predominance over $C_{28}$ and $C_{29}$ for all slices, and diasteranes were detected by MRM analyses in relatively low abundance (Fig. 4.6a; Table 4.1). $C_{30}$ dinosteranes (*m/z* 98; not shown) are present in significant abundance in all samples. Additionally, 24-*n*-propylcholestanes were detected in the bulk sample by monitoring the *m/z* 414→217 mass transitions (Fig. 4.6a; Chapter 2). The relative signal intensity on the *m/z* 414→217 mass transition is 40.2% of the signal intensity on the *m/z* 414→231 mass transition, ensuring no misidentification of dinosterane peaks from the *m/z* 414→217 mass transition. The $C_{29}$ regular steranes/$C_{29}$ αβ hopane ratios (St/H) ratios are less than 0.41 for all slices (Table 4.1).

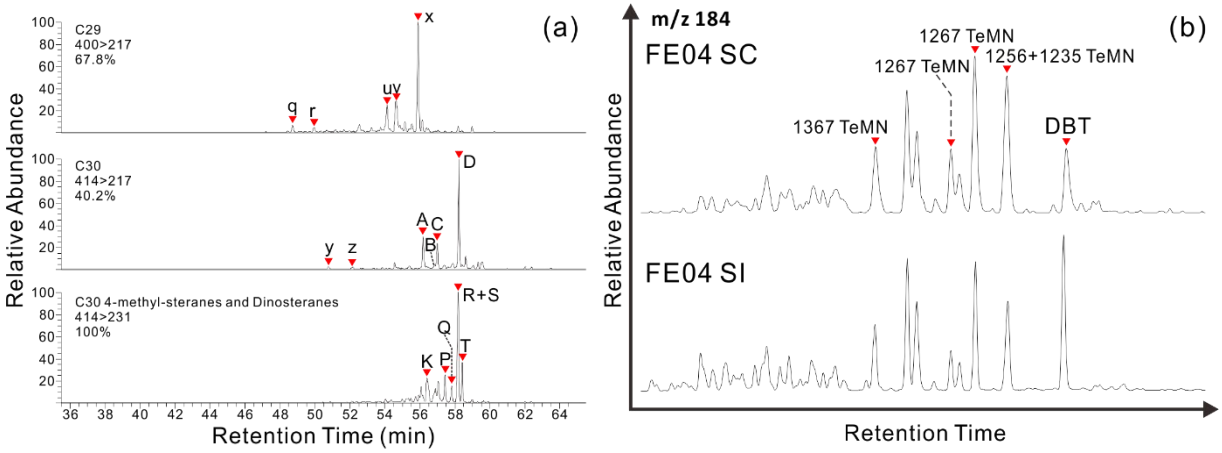


Fig. 4.6 (a) Partial MRM-GC-MS chromatograms (*m/z* 400→217, 414→217, 414→231 mass transitions) of the $C_{29}$–$C_{30}$ steranes (including 24-*n*-propylcholestanes in high amounts) for the bulk sample (Chapter 2). The xx% indicates the relative signal intensity for each MRM channel, compared to *m/z* 414→231 (100%). Marine organic matter contributions are shown by the abundant 24-*n*-propylcholestanes (peaks A, B, C and D). (b). Partial mass chromatograms (*m/z* 184) of the tetramethylnaphthalenes (TeMN) and dibenzothiophene (DBT) show the differences between slice C and slice I. Peak assignments: q = 24-ethyl-13β(H),17α(H)-diacholestane (20S); r = 24-ethyl-13β(H),17α(H)-diacholestane (20R); u = 24-ethyl-5α(H),14α(H),17α(H)-cholestane (20S); v = 24-ethyl-5α(H),14β(H),17β(H)-cholestane (20R); x = 24-ethyl-5α(H),14α(H),17α(H)-cholestane (20R); y = 24-*n*-propyl-13β(H),17α(H)-diacholestane (20S); z = 24-*n*-propyl-13β(H),17α(H)-diacholestane (20R); K = 4α-methyl-24-ethylcholestane 20S; P = 4α,23S,24S-trimethylcholestane (20R); Q = 4α,23S,24R-trimethylcholestane (20R); R = 4α-methyl-24-ethylcholestane (20R); S = 4α,23R,24R-trimethylcholestane (20R); T = 4α,23R,24S-trimethylcholestane (20R); 1367 TeMN means 1,3,6,7-tetramethylnaphthalene, etc.

*4.4.3.4. Aromatic compounds*

The most abundant compounds in the aromatic fractions of the rock slices are alkylnaphthalenes and alkylphenanthrenes, followed by alkylbenzenes, alkylchrysenes, alkyldibenzothiophenes (Fig. 4.6b), alkylbiphenyls, triaromatic steranes and triaromatic dinosteranes. Other relatively low abundance unsubstituted and substituted polycyclic aromatic hydrocarbons (PAH) with 3- to 7-rings that are present at varying but low concentrations include diphenylmethane, fluorene, dibenzofuran, retene and 2-phenylnaphthalene.

*4.4.3.4.1. Aryl isoprenoids, isorenieratane and derivatives*

In the aromatic fractions, the most prominent carotenoid skeleton compounds are aryl isoprenoids (with a 2,3,4/2,3,6/3,4,5-trimethyl substitution pattern) and isorenieratene derivatives, a series of which was detected on the *m/z* 133 mass chromatograms (Fig. 4.7a). The relative abundance of those homologues generally decreases as carbon number increases. These tail-to-tail-structure aromatic hydrocarbons include abundant monoaryl isoprenoids from $C_{10}$ to $C_{22}$ with maxima at $C_{13}$, diaryl isoprenoids from $C_{21}$ to $C_{24}$ and $C_{32}$ to $C_{33}$, $C_{40}$ triaryl isoprenoids, isorenieratane and four unknown compounds with a prominent *m/z* 133 molecular ion (Fig. 4.7a). The intensive aerobic degradation of aryl isoprenoids leads to more low molecular weight aryl isoprenoids (Schwark and Frimmel (2004). These authors proposed the aryl isoprenoid ratio (AIR) for comparing the abundance of low molecular weight to medium molecular weight aryl isoprenoids (defined as $\sum C_{13\text{-}17}/\sum C_{18\text{-}22}$ aryl isoprenoids), so as to assess the variability and persistence of photic zone euxinia (PZE). A low value of the AIR suggests persistent PZE, whereas a high AIR value (>3.0) suggests short-term episodic PZE conditions. The slice samples show significantly variation in the abundance of monoaryl isoprenoids (Fig. 4.7b), thus exhibiting variable AIR values (2.38-5.54; Table 4.1).

*4.4.3.4.2. Aromatic 8,14-secohopanoids*

On *m/z* 365 mass chromatograms (not shown), two regular D-ring monoaromatic $C_{29}$ and $C_{30}$ 8,14-secohopane were detected. There is a slight predominance of $C_{29}$ 8,14-secohopane over $C_{30}$ 8,14-secohopane. On *m/z* 363 mass chromatograms (not shown), the D,E-ring monoaromatic $C_{29}$ 8,14-secohopane dominates. On *m/z* 407 mass chromatograms (not shown), $C_{30}$ demethylated 8,14-secohopane are present.

*4.4.3.5. Thermal maturity*

The impact of any differential thermal maturation on the hydrocarbon distributions can be excluded for the slice samples, as they were so tightly sampled. A series of biomarker based parameters were calculated to estimate the thermal maturity of the FE112 3122.0 m sample (Table 4.1). The $CPI_{24\text{-}32}$ (carbon preference index) ranges from 1.28-1.34. The $C_{27}$ diasterane/ααα sterane ratio ranges from 0.05 to 0.09. The Ts/(Ts + Tm) ratios are less than 0.27, the $C_{29}$ 20S/(20S + 20R) sterane ratios are less than 0.29, and the $C_{29}$ αββ/(αββ + ααα) sterane ratios are less than 0.25, which all indicate that these rocks have similarly low maturity in the early oil window.

## 4.4.4. Carbon isotopic composition of individual n-alkanes

The $\delta^{13}C$ values of the individual *n*-alkanes of two slices (C and I) are shown in Table 4.3 and Fig. 4.8. The $\delta^{13}C$ values of the slice samples range from -31.6‰ to -23.6‰. The shapes of the *n*-alkane isotope profiles are very similar, and have slightly negative slopes, and an abrupt negative shift from the *n*-$C_{25}$ to *n*-$C_{31}$ alkanes. It is easy to identify the profiles of these slice samples from the Es3 member in the FE112 well and two comparison samples from the deeper Es3 and Es4U members of the Shahejie Formation in the same FE112 well (sample code FE10: $CPI_{24\text{-}32}$ = 1.17, St/H = 0.56, Ts/(Ts + Tm) = 0.38; sample code FE16: $CPI_{24\text{-}32}$ = 1.01, St/H = 1.93, Ts/(Ts + Tm) = 0.47; Chapter 2). The comparison samples have rather flat

isotope profiles, with $\delta^{13}C$ values ranging from -29.6‰ to -28.0‰ (average = -29.1‰) for sample FE10, and from -30.3‰ to -29.0‰ (average = -29.7‰) for sample FE16.

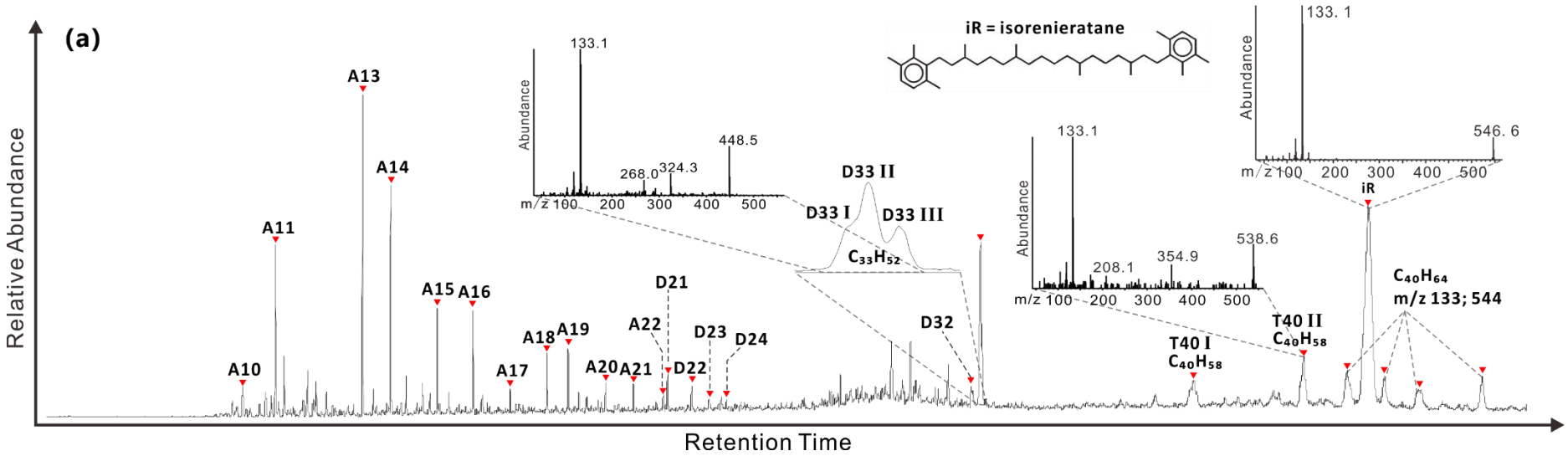


Fig. 4.7 Representative *m/z* 133 mass chromatograms for slice A in detail (a) and all the slices (b), showing the characteristic aryl isoprenoids in the aromatic hydrocarbon fractions. The detailed chromatogram (a) shows the monoaryl isoprenoids (Axx), the diaryl isoprenoids (Dxx) and the triaryl isoprenoids (Txx) with 2,3,4/2,3,6/3,4,5-trimethyl substitution pattern, and the $C_{40}$ biomarker isorenieratane (iR) and other structurally unidentified derivative $C_{33}$ and $C_{40}$ compounds which are typical biomarkers for green sulphur bacteria. The chemical structure of isorenieratane with 1-alkyl-2,3,6-trimethyl substitution is shown, and the insets are the mass spectra of isorenieratane and two of the corresponding derivatives. These hydrocarbons were identified by comparison of retention times and typical mass spectra with reference samples.

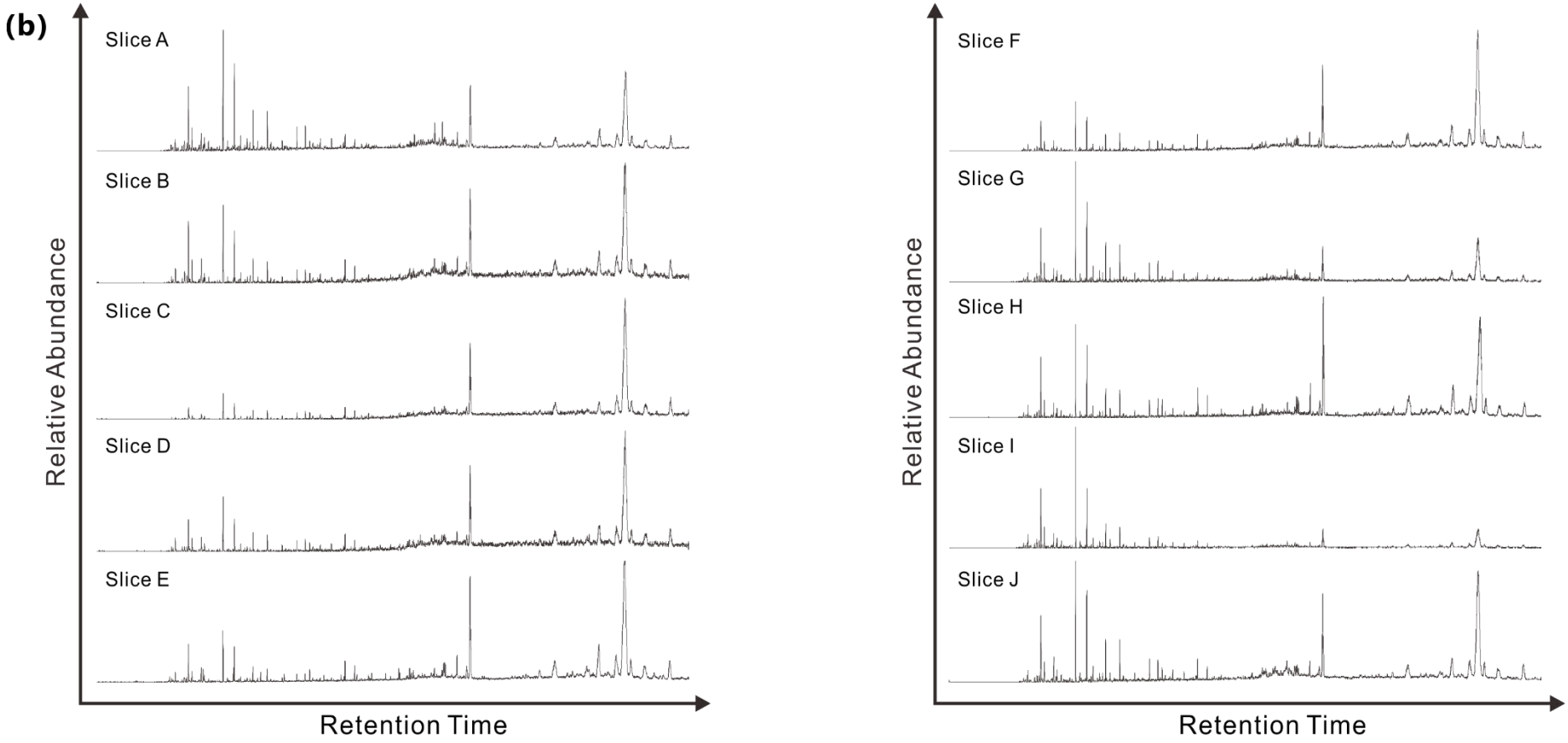


Fig. 4.7 (*continued*)

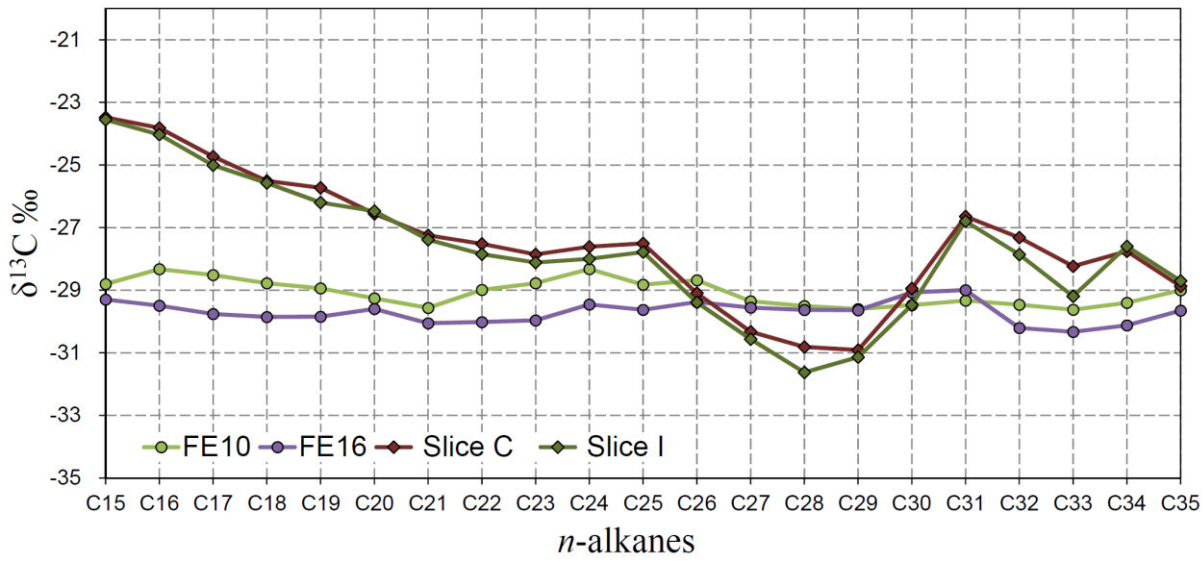


Fig. 4.8 $\delta^{13}C$ values of individual *n*-alkanes in slices C and I (diamonds) and comparison samples (codes FE10 and FE16; circles).

## 4.5. Discussion

Fine grained sediments such as mudstones and shales are widely distributed in the Es3 and Es4U members in the Dongying Depression (Zhang et al., 2009). However, the reasons for the organic matter enrichment of these organic-rich sediments remains unclear, and may be related to multiple aspects including source inputs, settling mechanisms, and quality of preservation conditions (Ingall et al., 1993; Tyson, 2005; Gallego-Torres et al., 2007; Bentum et al., 2009). It is reasonable to apply this framework at the large scale, but dynamic details at the micro-scale are usually not fully addressed. The approach in this paper is to assess a laminated organic-rich shale at the millimetre scale, and to document micro-changes of the hydrocarbons and recalcitrant biomarkers, so as to reveal more detailed geochemical information about the causes of organic matter enrichment.

### 4.5.1. Organic matter contributions

The direct use of dissolved $CO_2$ by phototrophs in the water column avoids the photosynthetic pathways (C3, C4 or CAM [crassulacean acid metabolism]) typical of

terrigenous higher plants, and results in almost no carbon isotopic fractionation (Farquhar et al., 1989). The long chain waxy *n*-alkanes have been proposed as products of specific algae (e.g. lacustrine *Botryococcus braunii* A race can biosynthesise precursors of exclusively odd carbon numbered $C_{25–31}$ *n*-alkanes) and aquatic micro-organisms (Derenne et al., 1988; Metzger et al., 1991; Huang et al., 2003; Feng et al., 2007; Riboulleau et al., 2007; Bechtel et al., 2012). Probable origins of middle and long chain *n*-alkanes from macrophytes and bacteria, respectively, have also been noted (Volkman et al., 1998; Zhang et al., 2004). Therefore, these features have cast doubt on the interpretation of terrigenous land derived sources for the long chain odd carbon numbered *n*-alkanes (Bechtel et al., 2012). The most likely organisms responsible for the isotopic depletion of the *n*-$C_{25-31}$ alkanes relative to the *n*-$C_{20-25}$ alkanes and the odd-over-even carbon number predominance include freshwater green algae (Metzger et al., 1991), various diatom communities (Henderson et al., 1972) and several other species of algae (Lichtfouse et al., 1994). Previous palynofacies analyses reported the presence of some non-marine algae in the Dongying Depression (e.g. *Botryococcus braunii, B. Granulata, Palacostomocysts and R. Bohaiensis*) (Li et al., 2003).

The *n*-alkane carbon isotopic compositions and the rather flat profiles of the comparison samples (Fig. 4.8) are consistent with a relatively closed saline lacustrine environment (Xiong et al., 2005). The isotopic profiles of the comparison samples reflect a uniform carbon source (algae, bacteria or combination of those) for the organisms prevalent in the palaeowater, which was possibly constrained by the water conditions. The deeper comparison sample (code 11) is relatively more mature than the other sample (code 10), but has lighter average $\delta^{13}C$ values. The isotopic compositions herein have been attributed only to source effects, and not to other controls such as thermal maturation.

In contrast, the slice samples have isotopic signatures typical of a relatively freshwater paralic lacustrine environment (Murray et al., 1994). This is supported by the negative carbon

isotope shifts of the *n*-$C_{25-31}$ alkanes (Fig. 4.8) as well as the prominent odd-over-even carbon number predominance of the n-alkanes ($CPI_{24-32}$ > 1.28; Fig. 4.5). The $\delta^{13}C$ values of the *n*-$C_{25-31}$ alkanes are very close to and even isotopically lighter than the values of phytoplanktonic and heterotrophic bacteria (*n*-$C_{20-29}$ alkanes, $\delta^{13}C$ = *c.*-30.0‰) in the Parachute Creek Member of the Green River Formation (Colorado) (Collister, 1994). Previous research on the *n*-alkane isotope compositions of these kind of fine-grained shales has revealed the derivation of *n*-alkanes from algae, and not from higher plants (Lichtfouse and Collister, 1992; Freeman et al., 1994; Lichtfouse et al., 1994; Spooner, 1994).

The $C_{27}$, $C_{28}$ and $C_{29}$ regular steranes and diasteranes are associated with red algae, chlorophyll-c algae (e.g. diatoms) and brown/green algae, respectively (Moldowan et al., 1985; Volkman et al., 1998). Additionally, terrigenous land plants are strongly related to the $C_{29}$ steranes (Moldowan et al., 1985; Volkman et al., 1998; Volkman, 2005). $C_{27}$ regular steranes are predominant (> 53%) over $C_{28}$ and $C_{29}$ regular steranes in all the slice samples (Table 4.1), suggesting a dominant algal organic input to the steranes. Based on the strong co-occurrence of $C_{29}$ regular steranes with gammacerane ($R^2$ = 0.92; data from thirty eight core samples in the Dongying Depression; Chapter 2), the $C_{29}/C_{27}$ ααα R sterane ratio may thus indicate the relative contribution of different algae rather than being a terrigenous-versus-aqueous organic input proxy. Moreover, the relative abundance of summed *n*-$C_{27-31}$ alkanes to total *n*-alkanes and the $C_{29}/C_{27}$ ααα R sterane ratio have a similar increasing trend from slice J to slice A, suggesting different algal contributions.

$C_{30}$ 24-*n*-proplycholestanes are present in the bulk sample FE04 (e.g. Fig. 4.6a; Chapter 2), and are indicative of a contribution from marine *Pelagophyte/Chrysophyte* algae, and hence a seawater influx. The relative abundance of dinosteranes to regular steranes generally increases from slices J to A, suggesting a slight rise in the proportion of dinoflagellates in the algal community over the time period represented by the sliced core.

Trace amounts of oleanane in all slices are suggestive of limited angiosperm contributions to the organic matter (Table 4.1). Similarly low abundances of $C_{19}$ and $C_{20}$ tricyclic terpanes are consistent with low input of terrigenous organic matter (Noble et al., 1986). Moreover, no tetracyclic or tricyclic diterpanes were detected, indicative of no vascular plant inputs (Simoneit et al., 1986). A number of specific aromatic hydrocarbons have been proposed as diagnostic markers for terrigenous land plants. 1,2,7-Trimethylnaphthlane can be derived from angiosperms (Strachan et al., 1988). When they have a high relative abundance, retene, 1-methylphenanthrene (1-MP), 1,7-dimethyphenanthrene and 1,2,5-trimethylnaphthalene may be associated with input from gymnosperms, including the conifer *Araucariaceae* (Alexander et al., 1988). There is no obvious correlation of Log(1-MP /9-MP) with the higher plant index (HPI), and these even have a slight negative correlation with the oleanane/$C_{30}$ αβ hopane ratio. The $C_{20}/C_{23}$ tricyclic terpane ratio irregularly varies between the slices, and has a weak correlation with terrigenous parameters such as Log(1,7-dimethylphenanthrene/1,3-+3,9-+2,10-+3,10-dimethylphenanthrene) and the oleanane/$C_{30}$ αβ hopane ratio. In summary, there is no evidence from these hydrocarbon distributions for any significant terrigenous organic matter input.

The terrigenous/aquatic ratio and the relative abundance of summed *n*-$C_{27\text{-}31}$ alkanes reflect similar trends. Odd-over-even carbon number predominance often over-estimates the input of terrigenous organic matter, because land-plant organic matter typically contains more *n*-alkanes than aquatic organic matter, resulting in disproportionate weight assigned to land-plant input (Peters et al., 2005). The best interpretation of these phenomena is organic matter inputs from freshwater green algae (e.g. lacustrine *Botryococcus braunii* biosynthesise precursors of exclusively odd carbon numbered *n*-$C_{25–31}$ alkanes) and aquatic micro-organisms (Derenne et al., 1988; Metzger et al., 1991; Huang et al., 2003; Feng et al., 2007; Riboulleau et al., 2007; Bechtel et al., 2012). Similarly, the $C_{29}$ regular steranes herein may represent a

specific algal input, instead of being derived from terrigenous land plants. This assumption is supported by the very good correlation between the $C_{29}$ regular steranes/$C_{29}$ αβ hopane ratio and the gammacerane/$C_{30}$ αβ hopane ratio ($R^2$ = 0.92), suggesting the co-occurrence of $C_{29}$ regular steranes and gammacerane in a common water body conditions.

One likely contributory cause for the low amount of land-derived organic matter in the sliced sample is that enhanced microbial organic carbon productivity diluted the input of terrigenous organic matter (French et al., 2014). Additionally, the relatively humid climate would have prompted dense vegetation acting as traps and baffles, then reduced terrigenous clastic input (Bohacs et al., 2003; Jiang et al., 2007; Smith et al., 2014), but allowing for the inflow of water and dissolved inorganic nutrients (Smith et al., 2008; Chetel et al., 2011). In summary, in the studied slices, micro-organisms were the main organic contributors, and the terrigenous land plant contribution to the organic matter enrichment is interpreted to have been minor.

### 4.5.2. Microbial community structure

The St/H ratio is commonly used to indicate the relative contributions of eukaryotic organisms (mainly algae and higher plants) versus prokaryotic organisms (bacteria in general) to the organic matter (Mackenzie, 1984; Tissot and Welte, 1984; Moldowan et al., 1985). In comparison with other samples in the Es3 and Es4U members which have St/H ratios > 1.0 (as high as 12.6; data not shown; Chapter 2), the sliced samples have evidence for significant bacterial input to the organic matter in the Es3 member. This evidence includes the relatively low St/H ratios (0.28 to 0.40; Table 4.1), and the presence of β-carotanes, gammacerane, hopanes, homohopanes, methylhopanes, sesquiterpanes, monomethyl alkanes, alkylbenzenes, pristane, phytane, isorenieratane and carotenoid diagenetic products. The low and rather variable St/H ratios can be interpreted as reflecting slight changes in the relative proportions

of organic matter sources (e.g. algae versus bacteria). Although the St/H ratios vary slightly, the microbial community structures were not significantly altered, and the palaeowater environment was still dominated by bacteria. 2α-Methylhopanes are not abundant in the slice samples. However, elevated 2α-methylhopanes are present in other samples (St/H = 0.28) with almost the same burial depths from the same well (Chapter 2), suggesting that the environmental conditions favourable for those microbial groups occurred randomly, or varies strongly at the mm resolution of the slices analysed.

Various hydrocarbon indicators of bacteria show reasonable correlations among the slices, which is consistent with different bacterial communities sharing the same environment (Fig. 4.9). However, it is not possible to determine the exact proportions of the sources of the bacteria. Isorenieratane, and other biomarkers derived from isorenieratene, are generally abundant, and are unambiguously derived from green sulphur bacteria (*Chlorobiaceae*) (Kuypers et al., 2002). These phototrophic bacteria are obligate anaerobes and require free hydrogen sulphide (i.e. euxinic conditions) in order to fix $CO_2$ in the photic zone. The relative abundance of isorenieratane can potentially indicate the relative organic matter contributions from green sulphur bacteria under PZE conditions. The isorenieratane/phenanthrene ratio is used to record the intensity of green sulphur bacteria activity (Table 4.1). Despite the low relative abundance of β-carotane (and gammacerane), there is a good correlation between these and isorenieratane and other derivatives ($R^2 > 0.85$; e.g. Fig. 4.10c). Likewise, the homohopane index has a good correlation ($R^2 = 0.80$) with the relative abundance of isorenieratane.

The methylphenanthrene/phenanthrene (MP/P) ratio has been proposed to distinguish diagenetic, combustion and pyrogenic sources for PAHs (Yunker et al., 2002; 2012; 2014). The MP/P ratios of the slices are > 1.0, suggesting that combustion/pyrogenic sources of land plants are not a major source (Budzinski et al., 1997; Liu et al., 2005). The correlation of

MP/P with the gammacerane/$C_{30}$ αβ hopane ratio ($R^2$ = 0.77), $C_{30}$ αβ hopane/*n*-$C_{17}$ ($R^2$ = 0.80), $C_{35}$/($C_{35}$ + $C_{34}$) homohopane ratio ($R^2$ = 0.82) and isorenieratane/phenanthrene ($R^2$ = 0.92; Fig. 4.10b), suggests that the methylphenanthrenes have bacterially-derived precursors. Additionally, Püttmann and Villar (1987) and Killops (1991) reported the close association between 8,14-secohopanoids and naphthalene and phenanthrene derivatives, probably reflecting a restricted range of conditions necessary for the bacterial production of the precursors, and their subsequent transformations.

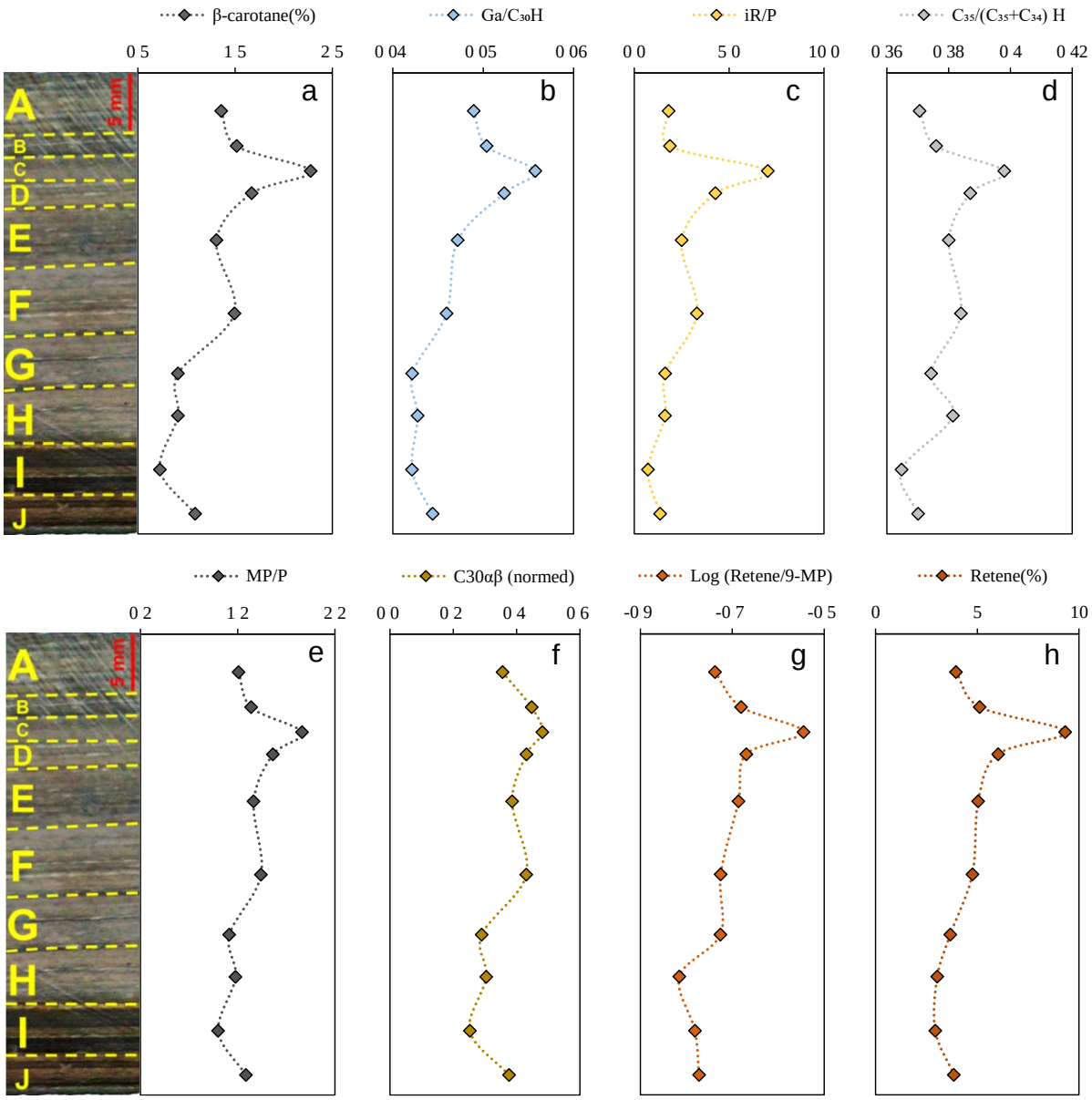


Fig. 4.9 Variation of multiple molecular parameters based on bacteria in the ten slices. (a) β-carotane/*n*-$C_{17}$ alkane ratio, as a %; (b) gammacerane/$C_{30}$ 17α,21β(H) hopane ratio; (c) isorenieratane/phenanthrene ratio;

(d) $C_{35}/(C_{35} + C_{34})$ homohopane ratio; (e) total methylphenanthrene/phenanthrene ratio; (f) $C_{30}$ 17α,21β(H) hopane normalised to *n*-$C_{17}$ alkane; (g) Log(retene/9-methylphenanthrene); (h) retene/phenanthrene ratio, as a %.

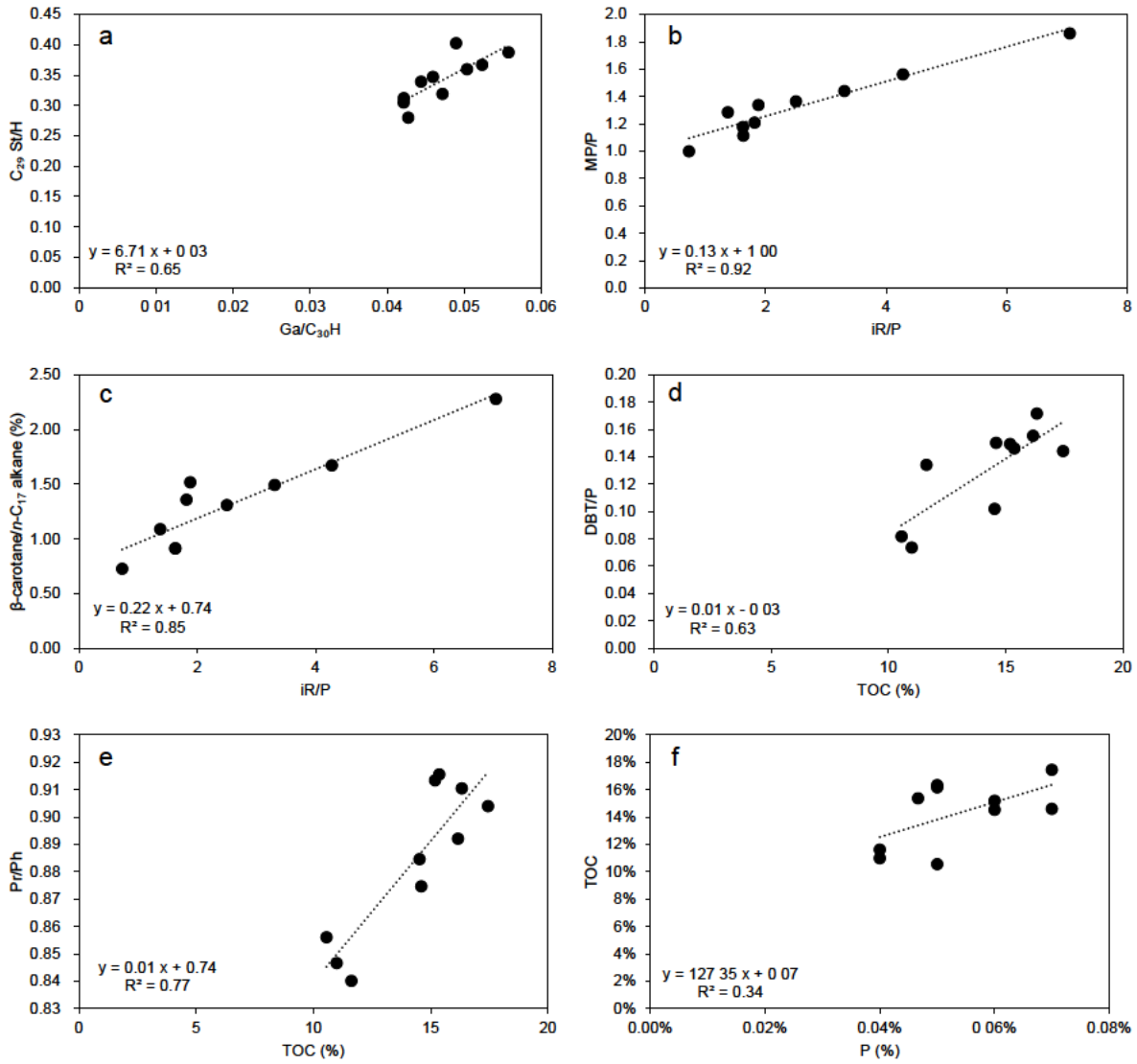


Fig. 4.10 Cross-plots of (a) $C_{29}$ regular steranes/$C_{29}$ αβ hopane ratio versus gammacerane/$C_{30}$ 17α,21β(H) hopane ratio; (b) total methylphenanthrene/phenanthrene ratio versus isorenieratane/phenanthrene ratio; (c) β-carotane/*n*-$C_{17}$ alkane ratio, as a % versus isorenieratane/phenanthrene ratio; (d) dibenzothiophene/phenanthrene ratio versus total organic carbon (%); (e) Pr/Ph ratio versus total organic carbon (%); (f) total organic carbon (%) versus phosphorous content (%).

Retene is a common biomarker for coniferous resins (Jiang et al., 1998; Grice et al., 2005), but in this study it is interpreted to be derived from algal and bacterial sources (Zhang et al., 1999). Retene can be produced by the pyrolysis of pure strains of green alga and cyanobacterium (Zhou et al., 2000). The low St/H ratio (< 0.40), the high TOC (as high as

17.5%), the predominance of $C_{27}$ over $C_{28}$ and $C_{29}$ regular steranes, the absence of prominent terrigenous land plant markers (Chapter 4.5.1), the $^{13}C$ depleted *n*-$C_{25-31}$ alkanes (Chapter 4.4.4), the correlation of the St/H ratio with the gammacerane//$C_{30}$ αβ hopane ratio, and the correlation of the relative abundance of retene with other bacterial marker ($R^2$ = 0.81 with gammacerane; $R^2$ = 0.92 with isorenieratane; Table 4.1), together argue for retene to have been derived from aqueous organisms.

In short, the microbial community structure was complex. Although microbial biomarkers show similarity in the relative distributions, there are also marked differences between the slices (Fig. 4.9). This suggests that the microbial community responded to variations in the depositional environment, and that they were the main participators in the contribution and modification of organic matter.

### 4.5.3. Organic matter alteration and preservation

Good preservation of organic matter generally requires a relatively stagnant water column where water column stratification, bottom/pore water anoxia (<0.5 ml oxygen/L water) or PZE (anoxic with abundant hydrogen sulphide) frequently occur and benthic metazoan life is eliminated (Peters et al., 2017). However, the controls on the net preservation of organic carbon are various and dynamic. These include a stable nutrient supply, generally low-energy conditions, enhanced organic substrate concentrations, a continuous settling rain of discrete particles (transport process), a low oxygen concentration, bioavailability of organic matter, adsorption of organics onto clays, natural vulcanisation, microbial degradation (e.g. anaerobic sulphate reduction, hence sulphide concentration rises), availability of electron acceptors, energy returning rates, bacterial productivity and local sedimentation rates (Tissot and Welte, 1984; Ingall et al., 1993; Boussafir and Lallier-Verg ès, 1997; Kennedy et al., 2002; Killops and Killops, 2005; Tyson, 2005; Pacton et al., 2006; van Dongen et al., 2006;

Gallego-Torres et al., 2007; Bentum et al., 2009; Sousa Júnior et al., 2013; Zhu et al., 2015). During deposition of the Es3 member, the climate fluctuated and the level of the Dongying palaeolake changed (Zhu et al., 2005; Zhang et al., 2009; Hao et al., 2011). Lamination and formation of organic-rich shales embodies the variation in biological and chemical environments in the palaeowater column (e.g. salinity, temperature, alkalinity/acidity, $O_2$, $CO_2$, organisms, etc.), which were mainly controlled by fluctuating climate (Zhang et al., 2009; Hao et al., 2011; Chen et al., 2016; Ma et al., 2016). Biomarkers sensitive to water chemistry derive from bacteria dwelling in different vertical positions in the water column (Killops and Killops, 2005; Peters et al., 2005; Grice and Brocks, 2011), and hence are perfect for tracking variations in depositional environment.

Pristane and phytane are largely derived from the chlorophyll phytyl side chain from photoautotrophs and bacteria (Didyk et al., 1978; Peters et al., 2005). Pr/Ph ratios < 1 indicate reducing environments (suboxic or anoxic), while values > 1 generally indicate oxic conditions (Didyk et al., 1978). For slices J to A the Pr/Ph ratios range from 0.84 to 0.92, suggesting an overall anoxic depositional environment, but with the redox conditions fluctuating slightly (Fig. 4.11a). Additional proxies for specific water column conditions include homohopanes, β-carotane, gammacerane, and the carotenoid products (Fig. 4.9a-d). For example, crude oils from the Sergipe-Alagoas Basin, Brazil have low Pr/Ph ratios, and abundant gammacerane, β-carotane, isorenieratane, aryl/diaryl isoprenoids, indicative of a reducing saline environment (Sousa Júnior et al., 2013). However in the organic-rich slice samples from the Es3 member, except for the low Pr/Ph ratios and the abundant aromatic carotenoids, only trace amounts of the high salinity indicators gammacerane and β-carotane are present. The slices do not have elevated $C_{35}$ homohopanes or a high γ-/δ-methylated-2-methyltrimethyltride-cylchromans ratio (γ-/δ-MTTC), thus not supporting a high water salinity. This is a bit unusual and not helpful for good organic matter preservation, because

anoxic water conditions are often accompanied by enhanced salinity which protects organic matter from significant degradation (hence the use of salt in food preservation). This also slightly contradicts the evidence for PZE, which is shown by the detection of abundant green-sulphur bacteria and maybe purple-sulphur bacteria carotenoids, and abundant pyrite.

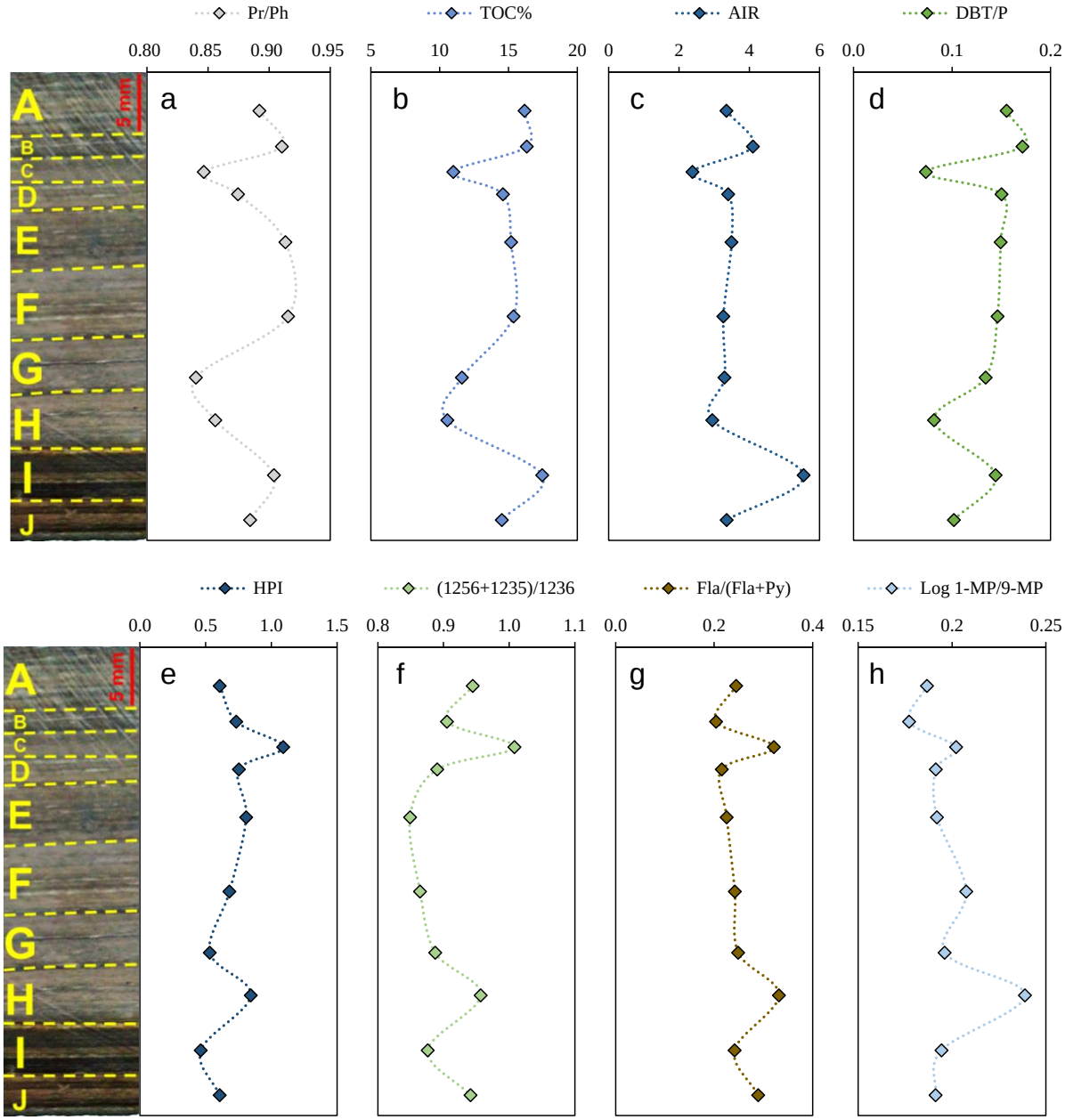


Fig. 4.11 Variation of multiple parameters in the ten slices. (a) Pr/Ph ratio; (b) total organic carbon (TOC; %); (c) aryl isoprenoid ratio (AIR; defined as $\sum C_{13\text{-}17}/\sum C_{18\text{-}22}$ aryl isoprenoids); (d) dibenzothiophene/phenanthrene ratio; (e) higher plant index (HPI); (f) (1256+1235)/1236 = (1,2,5,6- + 1,2,3,5-)/1,2,3,6-tetramethylnaphthalene ratio; (g) fluoranthene/(fluoranthene + pyrene) ratio; (h) Log 1-methylphenanthrene/9-methylphenanthrene. Note that in this study the HPI simplifies to (retene/1,3,6,7-tetramethylnaphthalene), due to the absence of cadalene and 1-isohexyl-2-methylnaphthalene (iHMN).

Elevated concentrations of gammacerane usually indicate a stratified water body due to its precursor tetrahymanol in ciliates thriving beneath the chemocline in anaerobic hypersaline conditions (Sinninghe Damsté et al., 1995). Additional sources include certain protozoa (Ourisson et al., 1987) and phototrophic bacteria (Kleemann et al., 1990). The gammacerane index slightly increases from slices J to A, which means an increasing possibility of development of water column stratification reflected up through the sample. However, the Pr/Ph ratio does not correlate with the gammacerane index for the slices (Table 4.1). Therefore, the generally low values (<0.06) of the gammacerane index provide little direct evidence of high salinity or low oxygen content. Highly reducing and hypersaline conditions do not always result in high gammacerane ratios (Moldowan et al., 1985), and additionally Wakeham et al. (2007) noted an association of tetrahymanol with suboxic waters. The similar changes in the bacterial populations with slice position in the sample (Fig. 4.9) reflects a shared response to external environmental dynamics of a closely associated consortia. One likely cause for the low gammacerane and β-carotane contents is grazing pressure or space competition. Bacteria and bacteria-eating ciliates may be supressed by more intense bacterial sulphate reduction (BSR), hence leading to gammacerane potentially being an invalid salinity indicator. Because sulphate reduction causes the degradation of carotenoids, and the survival of potential precursors of β-carotane requires the absence or limitation of sulphate reduction (Killops and Killops, 2005), which may account for the low concentration of β-carotane and gammacerane in the slices. The homohopanes ($C_{31}$-$C_{35}$) originate from bacteriohopanetetrol and other polyfunctional $C_{35}$ hopanoids common in prokaryotic micro-organisms (Ourisson et al., 1979; Rohmer et al., 1992). The $C_{35}/(C_{35}+C_{34})$ homohopane ratio reflects redox potentials (Eh) (Peters et al., 2005). In the slices, the $C_{35}/(C_{35}+C_{34})$ homohopane ratios have a relatively consistent trend with Ga/C30H ratios, suggesting that they were probably suppressed as well.

Aromatic carotenoids and their diagenetic/catagenetic derivatives have been used as proxies for anoxic or euxinic conditions in the photic zone during the deposition of organic-rich source rocks or sediments (Koopmans et al., 1996; Clifford et al., 1998). The 2,3,6-aryl isoprenoids, isorenieratane and other derivatives (Fig. 4.7) derived from green sulphur bacteria (*Chlorobiaceae*) or purple sulphur bacteria (*Chromatiaceae*) are markers of PZE (Bowden et al., 2006; Brocks and Schaeffer, 2008). Isorenieratane is uniquely biosynthesised by green sulphur bacteria (Sinninghe Damsté et al., 2001). Isorenieratane and other $C_{40}$ derivatives are rather abundant in the slice samples (Fig. 4.7), but the AIR values vary (Table 4.1), indicating fluctuating development of PZE conditions. Relatively low AIR values suggest more persistent PZE, whereas the high values suggest episodic PZE (Schwark and Frimmel, 2004). The AIR, DBT/P and Pr/Ph are positively correlated with TOC (e.g. Figs 4.10d and 4.10e, 4.11a-4.11d,), suggesting that the relatively low AIR, DBT/P and Pr/Ph are associated with a certain loss of organic carbon, and the relatively high values of these are associated with better preservation of organic carbon (Fig. 4.10a-10d). Thus, small fluctuations of water column environmental conditions seem to be modifiers to organic carbon preservation.

Previous studies mostly focused on algal productivity as a major control on the enrichment of organic matter in lacustrine petroleum source rocks in the Dongying Depression. Algal blooms can indeed provide high amounts of organic material (Liu and Wang, 2013). However, just as fungi degrade land plant material, aerobic and anaerobic bacteria are important decomposers of organic matter in aqueous environments (Killops and Killops, 2005). Organic material produced by phytoplankton can be partially consumed by herbivorous zooplankton within the photic zone, albeit with lesser efficiency during planktonic blooms (Killops and Killops, 2005). After being transported to the sediment surface, the phytoplankton remains (the detritus) and the bacterially-colonised particulate

material (that is being broken down) are assimilated and disseminated by detritivores (if there is sufficient oxygen), creating a high surface area to volume ratio, resulting in the organic matter being more readily available to the aerobic and anaerobic decomposers. Dissolved organic matter (DOM) and oxygen are diffused within pore waters (Killops and Killops, 2005). With abundant DOM and intense decomposition, the oxygen supply balance between pore waters and the overlying water column can be rapidly broken. Then, anoxicity occurs within the hypolimnion of the eutrophic lake. The obligate aerobes rapidly shrink in abundance as the activity of anaerobes broadens. Bacteria keep breaking down macromolecular components to smaller molecules (e.g. sugars, amino acids, fatty acids, alcohols, amines and volatile acids; together termed organic substrates) by hydrolysis and fermentation (Fenchel and Jørgensen, 1977). Then anaerobic heterotrophic bacteria such as denitrifiers, sulphate reducers and methanogens use the oxidising agents as terminal electron acceptors to consume these substrates, thus completing mineralisation. Under such oxygen-deficient conditions, sulphate reduction is the most important process, even if its energy-return is lower than during nitrate reduction, because the nitrate concentration in pore water is commonly very low (And and Saffarini, 1994; Rickard and Luther, 2007). The sulphate reducers (e.g. proteobacteria and eubacteria with wide tolerances of pH, pressure, temperature and salinity) are generally obligate anaerobes, and are merely controlled by the sulphate supply (Killops and Killops, 2005). Seawater influx, as shown by the presence of abundant 24-*n*-propylcholestanes, must have brought abundant sulphate to fuel the high levels of sulphate reduction in the Dongying palaeolake. Intense BSR would have consumed the organic substrates, and released its main by-product hydrogen sulphide ($H_2S$). $H_2S$ is extremely toxic to most organisms, thus other anaerobic competitions for the organic substrates would have been largely inhibited or eliminated (Jørgensen, 1982). Pyrite is formed during BSR. When $H_2S$ extended up into photic zone, the populations of phytoplanktonic

algae were probably reduced in the upper layer, and instead anaerobic photosynthesisers such as green sulphur bacteria and purple sulphur bacteria survived and prevailed. This would have led to the development of PZE, as shown by detection of varying amounts of isorenieratane and other $C_{40}$ derivatives.

This scenario accounts for why relatively low TOC values are accompanied with relatively low AIR values in the different slices, as these conditions are consistent with BSR and persistent PZE, and vice versa. Obligate anaerobic respiration and metabolism cause significant organic carbon loss (Fig. 4.12). Additionally, the build-up of $H_2S$ can increase the acidity of a water column (Killops and Killops, 2005), resulting in the decalcification of calcareous tests and shells, thus releasing $CO_2$. Those anaerobic photosynthetic bacteria which can use the products of anaerobic degradation processes (e.g. $H_2S$ and $CO_2$) amount to much less (approximately half) the productivity of phytoplankton (e.g. the Black Sea water column; (Repeta, 1989)). Thus, the whole process negatively influences total productivity.

By comparison with the dissimilatory process of BSR, the incorporation of sulphur into organic compounds requires assimilatory sulphate reduction to survive from poisoning of $H_2S$. In the slices, DBT/P co-varies with AIR (Fig. 4.11c and d). Thus, the incorporation of sulphur into organic compounds (the formation of S-containing compound: DBT) seems to have been restrained by PZE persistence. Any single group of organisms would be poisoned by a build-up of their own 'by-products', which are 'anoxicity' for aerobes, 'toxicity' for SRB, '$H_2S$ depletion' for green sulphur bacteria/purple sulphur bacteria, and '$CO_2$ depletion' for phytoplankton. The different and interdependent bacterial communities formed the whole decomposer system in the water column. The interactive bacterial system, together with the phytoplankton, are a cycle (Fig. 4.12), which is boosted or stalled by various direct/indirect factors such as climate, seasonality, terrigenous input, water acidity/salinity, temperature, electron acceptors supply, oxygen level, availability of organic substrates, etc (Kaeberlein et

al., 2002). Considering the episodic anoxia at the bottom-water interface and episodic euxinia in the photic zone, the aerobic and anaerobic reworking of organic matter might proceed simultaneously in different proportions.

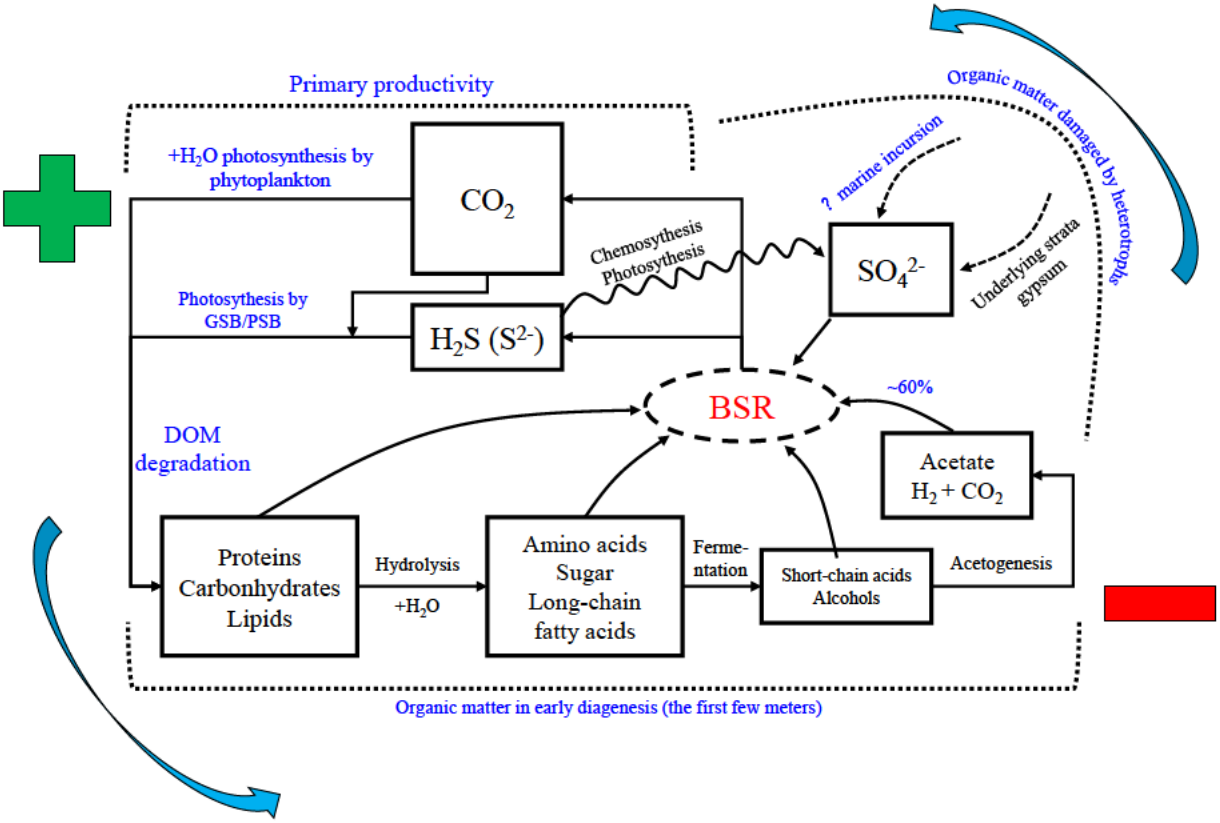


Fig. 4.12 Simplified scheme of the roles of phytoplankton and anaerobic bacteria in organic matter production and preservation in the Dongying Depression. DOM = dissolved organic matter, BSR = bacterial sulphate reduction.

Some aromatic parameters such as HPI, (1,2,5,6- + 1,2,3,5-)/1,2,3,6-tetramethylnaphthalene, fluoranthene/(fluoranthene + pyrene) and Log(1-MP/9-MP) negatively correlate with TOC in the slices (Fig. 4.11h), which is probably indicative of a negative effect on organic matter preservation. The HPI is commonly used as an indicator for terrigenous input (Volk et al., 2004). The most likely explanation for this negative correlation is that retene is derived in this sample from algal or bacterial sources (Zhang et al., 1999; Zhou et al., 2000). The alkyl derivatives of naphthalene and phenanthrene (e.g 1,2,5,6-

tetramethylnaphthalene) are probably derived from the degradation of aromatic 8,14-secohopanoids under restricted conditions by the pathway including cleavage, 1,2-methyl shift and aromatisation (Püttmann and Villar, 1987; Killops, 1991). That pathway involving hopanoidal species is apparently characteristic of bacterial inputs, which is consistent with the low St/H ratios of the slices (Fig. 4.10a; Table 4.1). The presence of a series of aromatic 8,14-secohopanoids in the slices supports this hypothesis. Additionally, anaerobic degradation of benzene, naphthalene, methylnaphthalene, phenanthrene, fluorene, and fluoranthene have been noticed under sulphate-reducing conditions (Thierrin et al., 1993; Coates et al., 1997; Kazumi et al., 1997; Reinhard et al., 1997; Zhang and Young, 1997). The fluoranthene/(fluoranthene + pyrene) ratio has been proposed to characterise combustion sources when it is > 0.4 (Yunker et al., 2012; Zakir Hossain et al., 2013). This ratio in the slices is <0.33, suggesting a minor or zero contribution from combustion (Yunker et al., 2015). Fluoranthene and pyrene can be used as carbon and energy sources by microbial communities (Juhasz et al., 1997), which makes the Fla/(Fla + Py) ratio likely bacterially controlled.

Algal blooms stimulate the precipitation of carbonate minerals by the high rate of assimilation of $CO_2$ (Kelts and Hsü, 1978; Zhu et al., 2005; Liu and Wang, 2013), which accounts for the cyclic presence of the calcite-rich laminae (Fig. 4.3A). On the basis of the occurrence of 24-*n*-propylcholestanes, the Dongying palaeolake must have experienced seawater incursions, which is consistent with the global high sea level during the Lutetian to Bartonian (Haq et al., 1987, 1988; Miller et al., 2005; 2008). The formation of dolomite laminae is closely associated with seawater influx, which supplies abundant magnesium and slightly enhances the salinity and alkalinity (Curtis and Coleman, 1986; Tian et al., 1998). The change from the calcite-rich laminae to the dolomite laminae (Fig. 4.3B) fits with the hypothesis of a slight change in depositional environments. The seawater influxes occurred

after a period with relatively fresh and nutrient-rich surface layer waters (hence leading to an algal bloom). The dolomite-rich laminae (D + C in Fig. 4.3B) and the calcite-rich laminae (C in Fig. 4.3B) are alternately expressed. SRB can remove a kinetic inhibitor and promote the formation of dolomite and high Mg-calcite under more oxygen-deficient and saline conditions (Warthmann et al., 2000; Deng et al., 2010). BSR removes sulphate and releases magnesium and calcium ions, and the dissociated and free $Mg^{2+}$ would tend to combine with bicarbonate ions, thus resulting in the formation of dolomite (Deng et al., 2010). It has been shown that BSR induces significant amounts of dolomite precipitation (Cole and Picard, 1978; Vasconcelos and Mckenzie, 1997; Warthmann et al., 2000; Wright and Wacey, 2005; Braissant et al., 2007; Deng et al., 2010). BSR accompanies the whole process of organic matter transport, accumulation and preservation. The sliced layers dominated by calcite and clay contain more organic matter than the layers of dolomite and clay (Fig. 4.3A and 3B), which is in agreement with the hypothesis of loss of organic matter during intense anaerobic degradation.

The adsorption of carbon compounds onto clay mineral surfaces much favours organic matter preservation (Kennedy et al., 2002; Rahman et al., 2018). The alternating thick and thin black organic matter laminae which are accompanied by clay minerals (Fig. 4.3B) may represent repeating conditions of organism growth or seasonal blooms (Schieber, 2010; Liu and Wang, 2013). However, there is no obvious relationship ($R^2 = 0.07$) between the clay content and the TOC content for the slices, suggesting that the adsorption of organic matter onto clays is not a primary control, at least at the millimetre scale. Dissolved phosphorous as limiting nutrient is not as effective in bioturbated shales as in laminated shales, because under anoxic conditions the ability of phosphorous to sustain further productivity is restrained (Ingall et al., 1993). The phosphorous content has a weak correlation with TOC content in the slices (Fig. 4.10f). The role of phosphorous (inorganic P) in controlling primary productivity

is thus not closely associated with the amount of finally-preserved organic matter (Ingall et al., 1993; Mort et al., 2007b).

The foregoing interpretations now make possible an integrated model of the water column in the Dongying palaeolake (Fig. 4.12). Abundant sulphate supported BSR and anoxicity at a relatively low position in the water column. Higher up in the water column, photosynthetic bacteria such as green sulphur bacteria and purple sulphur bacteria were active, and in the uppermost water layers planktonic organisms and heterotrophic oxidisers were present. Together they formed a syntrophic community (Fig. 4.12). This may account for the fluctuations of organic carbon content, recorded in high resolution by the various slices. Bacterially-mediated reduction of sulphate to sulphide would have been accompanied by the oxidation of organic matter to $CO_2$, so the different bacteria groups/communities directly or indirectly altered the net organic carbon content (Fig. 4.12). It is likely that the water column biological structure (i.e., composition of syntrophic bacterial consortia) and chemical conditions fluctuated as a result of fluctuating seawater and freshwater influxes. The varying sulphate content and periodic inputs of terrigenous nutrients played an important role in organic matter enrichment.

## 4.6. Summary

This study has shown the organic geochemical, isotopic and petrographic data of a high-TOC and well-laminated shale at the millimetre scale, which has led to new insights into the mechanism of organic matter preservation in the Dongying Depression, which are applicable more generally. Appropriate terrigenous-derived fresh water brought in nutrients and freshwater algae to the palaeolake. Planktonic blooms in the surface waters promoted high primary productivity and provided copious organic substrates. Periodic seawater influxes enhanced sulphate concentration. Bacteria such as SRB used dissolved sulphate (as electron acceptors) to oxidise organic matter and generate $H_2S$, then further lowering the oxygen content in the hypolimnion. Bottom water anoxia extended up into the photic zone where the increasing $H_2S$ supported more green sulphur bacteria/and possibly also purple sulphur bacteria to thrive. These had relatively low productivity, compared to phytoplankton, and reduced the phytoplankton populations, so overall productivity was consequently reduced. Episodic PZE conditions suggests cyclically BSR, which can cause the loss of organic matter and induce dolomite precipitation under more oxygen-deficient and saline conditions. Consequently, anaerobic respiration and metabolism significantly influences the water column biological and chemical conditions. Anaerobic micro-organisms (e.g. SRB) can thus play a vital role in organic matter preservation and carbonate (i.e. dolomite and high Mg-calcite) precipitation. However, the roles and interactions of different bacteria in the sedimentary environments are very complex and are not yet fully understood, so more research is needed.

## Acknowledgements

This research was supported by the National Natural Science Foundation of China (Grant No. 41472108). The authors acknowledge the experimental assistance of Carl A. Peters, Sophia Aharonovich, Konstantinos Kotzakoulakis, Huaqing Xu, and Xiong Cheng. We thank Se Gong at CSIRO for assistance with the MRM GC-MS analyses and molecular sieving. HX thanks the China University of Geosciences (Beijing) and Macquarie University for a co-tutelle PhD scholarship, and Macquarie University for analytical support funds.

# References

Alexander, R., Larcher, A.V., Kagi, R.I., Price, P.L., 1988. The use of plant-derived biomarkers for correlation of oils with source rocks in the Cooper/Eromanga Basin system, Australia. The APPEA Journal 28, 310-324.

And, K.H.N., Saffarini, D., 1994. Iron and manganese in anaerobic respiration: Environmental significance, physiology, and regulation. Annual Review of Microbiology 48, 311.

Bao, J., Li, M., 2001. Unprecedented occurrence of novel $C_{26}$-$C_{28}$ 21-norcholestanes and related triaromatic series in evaporitic lacustrine sediments. Organic Geochemistry 32, 1031–1036.

Bechtel, A., Jia, J., Strobl, S.A.I., Sachsenhofer, R.F., Liu, Z., Gratzer, R., Püttmann, W., 2012. Palaeoenvironmental conditions during deposition of the Upper Cretaceous oil shale sequences in the Songliao Basin (NE China): Implications from geochemical analysis. Organic Geochemistry 46, 76–95.

Bentum, E.C., van Hetzel, A., Brumsack, H.J., Forster, A., Reichart, G.J., Sinninghe Damste, J.S., 2009. Reconstruction of water column anoxia in the equatorial Atlantic during the Cenomanian-Turonian oceanic anoxic event using biomarker and trace metal proxies. Palaeogeography Palaeoclimatology Palaeoecology 280, 489-498.

Bohacs, K.M., Carroll, A.R., Neal, J.E., 2003. Lessons from large lake systems–Thresholds, nonlinearity, and strange attractions, in: Chan, M.A., Archer, A.W. (Eds.), Extreme depositional environments: Mega end members in geologic time. Geological Society of America Special Paper 370, Boulder, Colorado, pp. 75-90.

Boussafir, M., Lallier-Vergès, E., 1997. Accumulation of organic matter in the Kimmeridge Clay formation (KCF): an update fossilisation model for marine petroleum source-rocks. Marine and Petroleum Geology 14, 75-83.

Bowden, S.A., Farrimond, P., Snape, C.E., Love, G.D., 2006. Compositional differences in biomarker constituents of the hydrocarbon, resin, asphaltene and kerogen fractions: An example from the Jet Rock (Yorkshire, UK). Organic Geochemistry 37, 369-383.

Braissant, O., Decho, A.W., Dupraz, C., Glunk, C., Przekop, K.M., Visscher, P.T., 2007. Exopolymeric substances of sulfate-reducing bacteria: Interactions with calcium at alkaline pH and implication for formation of carbonate minerals. Geobiology 5, 401-411.

Brocks, J.J., Schaeffer, P., 2008. Okenane, a biomarker for purple sulfur bacteria (Chromatiaceae), and other new carotenoid derivatives from the 1640Ma Barney Creek Formation. Geochimica et Cosmochimica Acta 72, 1396-1414.

Budzinski, H., Jones, I., Bellocq, J., Pierard, C., Garrigues, P., 1997. Evaluation of sediment contamination by polycyclic aromatic hydrocarbons in the Gironde estuary. Marine Chemistry 58, 85-97.

Caplan, M.L., Bustin, R.M., 1999. Palaeoceanographic controls on geochemical characteristics of organic-rich Exshaw mudrocks: role of enhanced primary production. Organic Geochemistry 30, 161-188.

Carroll, A.R., Bohacs, K.M., 2001. Lake-type controls on petroleum source rock potential in nonmarine basins. AAPG Bulletin 85, 1033-1053.

Chen, Z., Huang, W., Liu, Q., Zhang, L., Zhang, S., 2016. Geochemical characteristics of the Paleogene shales in the Dongying depression, eastern China. Marine and Petroleum Geology 73, 249–270.

Chetel, L.M., Janecke, S.U., Carroll, A.R., Beard, B.L., Johnson, C.M., Singer, B.S., 2011. Paleogeographic reconstruction of the Eocene Idaho River, North American Cordillera. Geological Society of America Bulletin 123, 71-88.

Clifford, D.J., Clayton, J.L., Sinninghe Damste, J.S., 1998. 2,3,6-/3,4,5-Trimethyl substituted diaryl carotenoid derivatives (Chlorobiaceae) in petroleums of the Belarussian Pripyat River Basin. Organic Geochemistry 29, 1253-1267.

Coates, J.D., Woodward, J., Allen, J., Philp, P., Lovley, D.R., 1997. Anaerobic degradation of polycyclic aromatic hydrocarbons and alkanes in petroleum-contaminated marine harbor sediments. Applied Environmental Microbiology 63, 3589-3593.

Cole, R.D., Picard, M.D., 1978. Comparative mineralogy of nearshore and offshore lacustrine lithofacies, Parachute Creek Member of the Green River Formation, Piceance Creek Basin, Colorado, and eastern Uinta Basin, Utah. Geological Society of America Bulletin 89, 1441-1454.

Collister, J.W., 1994. Partial resolution of sources of *n*-alkanes in the saline portion of the Parachute Creek Member, Green River Formation (Piceance Creek Basin, Colorado). Organic Geochemistry 21, 645-659.

Crossley, R., Davison-Hirschmann, S., Owen, R.B., Shaw, P., 1984. Lake-level fluctuations during the last 2,000 Cal yrs in Malawi, in: Vogel, J.C. (Ed.), Late Cenozoic palaeoclimates of the southern hemisphere. Balkema, Rotterdam, pp. 305-316.

Curtis, C.D., Coleman, M.L., 1986. Controls on the precipitation of early diagenetic calcite, dolomite and siderite concretions in complex depositional sequences. Special Publications of SEPM 38, 23-33.

Demaison, G.J., Moore, G.T., 1980. Anoxic environments and oil source bed genesis. Organic Geochemistry 2, 9-31.

Deng, S., Dong, H., Lv, G., Jiang, H., Yu, B., Bishop, M.E., 2010. Microbial dolomite precipitation using sulfate reducing and halophilic bacteria: Results from Qinghai Lake, Tibetan Plateau, NW China. Chemical Geology 278, 151-159.

Derenne, S., Largeau, C., Casadevall, E., Connan, J., 1988. Comparison of torbanites of various origins and evolutionary stages. Bacterial contribution to their formation. Causes of the lack of botryococcane in bitumens. Organic Geochemistry 12, 43–59.

Didyk, B.M., Simoneit, B.R.T., Brassell, S.C., Eglinton, G., 1978. Organic geochemical indicators of palaeoenvironmental conditions of sedimentation. Nature 272, 216-222.

Farquhar, G.D., Ehleringer, J.R., Hubick, K.T., 1989. Carbon isotope discrimination and photosynthesis. Annual Review of Plant Biology 40, 503-537.

Fenchel, T.M., Jørgensen, B.B., 1977. Detritus food chains of aquatic ecosystems: the role of bacteria, in: Alexander, M. (Ed.), Advances in Microbial Ecology. Plenum Press, New York, pp. 1-58.

Feng, Z., Fang, W., Zhang, J., Li, Z., Huang, C., Wang, X., Zhao, Q., Huo, Q., 2007. Distribution and significance of $C_{40+}$ alkanes in the extracts of Cretaceous source rocks from the Songliao Basin. Science in China Series D: Earth Sciences 50, 1510-1520.

Freeman, K.H., Wakeham, S.G., Hayes, J.M., 1994. Predictive isotopic biogeochemistry: Hydrocarbons from anoxic marine basins. Organic Geochemistry 21, 629-644.

French, K.L., Sepúlveda, J., Trabucho-Alexandre, J., Gröcke, D.R., Summons, R.E., 2014. Organic geochemistry of the early Toarcian oceanic anoxic event in Hawsker Bottoms, Yorkshire, England. Earth and Planetary Science Letters 390, 116-127.

Fu, J., Sheng, G., 1989. Biological marker composition of typical source rocks and related crude oils of terrestrial origin in the People's Republic of China: a review. Applied Geochemistry 4, 13–22.

Gallego-Torres, D., Martínez-Ruiz, F., Paytan, A., Jiménez-Espejo, F.J., Ortega-Huertas, M., 2007. Pliocene–Holocene evolution of depositional conditions in the eastern Mediterranean: Role of anoxia vs. productivity at time of sapropel deposition. Palaeogeography Palaeoclimatology Palaeoecology 246, 424-439.

Ghinassi, M., D'Oriano, F., Benvenuti, M., Awramik, S., Bartolini, C., Fedi, M., Ferrari, G., Papini, M., Sagri, M., Talbot, M., 2012. Shoreline fluctuations of Lake Hayk (northern Ethiopia) during the last 3500 years: Geomorphological, sedimentary, and isotope records. Palaeogeography Palaeoclimatology Palaeoecology 365, 209-226.

Gong, Z., Zhu, W., Chen, P.P.-H., 2010. Revitalization of a mature oil-bearing basin by a paradigm shift in the exploration concept. A case history of Bohai Bay, Offshore China. Marine and Petroleum Geology 27, 1011-1027.

Grice, K., Backhouse, J., Alexander, R., Marshall, N., Logan, G.A., 2005. Correlating terrestrial signatures from biomarker distributions, $\delta^{13}C$, and palynology in fluvio-deltaic deposits from NW Australia (Triassic–Jurassic). Organic Geochemistry 36, 1347-1358.

Grice, K., Brocks, J.J., 2011. Biomarkers (organic, compound-specific isotopes), in: Reitner, J., Thiel, V. (Eds.), Encyclopedia of Geobiology. Springer, Netherlands, pp. 167-182.

Guo, X., He, S., Liu, K., Song, G., Wang, X., Shi, Z., 2010. Oil generation as the dominant overpressure mechanism in the Cenozoic Dongying depression, Bohai Bay Basin, China. AAPG Bulletin 94, 1859-1881.

Haberlah, D., Loehr, S., Kennedy, M., Debenham, N., Lattanzi, D., 2015. Innovative sub-micron SEM-EDS mineral mapping and analysis applied to Australian shale samples, AAPG International Exhibition and Conference. Society of Exploration Geophysicists and American Association of Petroleum Geologists, Melbourne, Australia, pp. 419-419.

Hao, F., Zhou, X., Zhu, Y., Yang, Y., 2011. Lacustrine source rock deposition in response to co-evolution of environments and organisms controlled by tectonic subsidence and climate, Bohai Bay Basin, China. Organic Geochemistry 42, 323–339.

Haq, B.U., Hardenbol, J., Vail, P.R., 1987. Chronology of fluctuating sea levels since the Triassic. Science 235, 1156–1167.

Haq, B.U., Hardenbol, J., Vail, P.R., 1988. Mesozoic and Cenozoic chronostratigraphy and cycles of sea-level change. Special Publications of SEPM 42, 71–108.

He, J., Ding, W., Jiang, Z., Jiu, K., Li, A., Sun, Y., 2017. Mineralogical and chemical distribution of the Es3L oil shale in the Jiyang Depression, Bohai Bay Basin (East China): Implications for paleoenvironmental reconstruction and organic matter accumulation. Marine and Petroleum Geology 81, 196–219.

Henderson, W., Reed, W.E., Steel, G., 1972. The origin and incorporation of organic molecules in sediments as elucidated by studies of the sedimentary sequence from a residual Pleistocene lake, 5th International Meeting on Advances in organic geochemistry 1971, Hanover, Germany, pp. 335-351.

Hesselbo, S.P., Jenkyns, H.C., Duarte, L.V., Oliveira, L.C.V., 2007. Carbon isotope record of the Early Jurassic (Toarcian) Oceanic Anoxic Event from fossil wood and marine carbonate (Lusitanian Basin, Portugal). Earth and Planetary Science Letters 253, 455–470.

Huang, H., Zheng, Y., Zhang, Z., Li, J., 2003. Lacustrine biomass: An significant precursor of high wax oil. Chinese Science Bulletin 48, 1987–1994.

Ingall, E.D., Bustin, R.M., van Cappellen, P., 1993. Influence of water column anoxia on the burial and preservation of carbon and phosphorus in marine shales. Geochimica et Cosmochimica Acta 57, 303-316.

Jørgensen, B.B., 1982. Mineralization of organic matter in the sea bed—the role of sulphate reduction. Nature 296, 643-645.

Jiang, C., Alexander, R., Kagi, R.I., Murray, A.P., 1998. Polycyclic aromatic hydrocarbons in ancient sediments and their relationships to palaeoclimate. Organic Geochemistry 29, 1721-1735.

Jiang, Z., Chen, D., Qiu, L., Liang, H., Jun, M.A., 2007. Source‐controlled carbonates in a small Eocene half‐graben lake basin (Shulu Sag) in central Hebei Province, North China. Sedimentology 54, 265–292.

Juhasz, A.L., Britz, M.L., Stanley, G.A., 1997. Degradation of fluoranthene, pyrene, benz[a]anthracene and dibenz[a,h]anthracene by Burkholderia cepacia. Journal of Applied Microbiology 83, 189-198.

Kaeberlein, T., Lewis, K., Epstein, S.S., 2002. Isolating "uncultivable" microorganisms in pure culture in a simulated natural environment. Science 296, 1127.

Katz, B.J., 1990. Controls on distribution of lacustrine source rocks through time and space, in: Katz, B.J. (Ed.), Lacustrine basin exploration: Case studies and modern analogs. AAPG Memoir 50, pp. 61-76.

Katz, B.J., 1995. Factors controlling the development of lacustrine petroleum source rocks - An update, in: Alain-Yves, H. (Ed.), Paleogeography, Paleoclimate, And Source Rocks. Studies in Geology 40, pp. 61-79.

Kazumi, J., Caldwell, M.E., Suflita, J.M., Lovley, D.R., Young, L.Y., 1997. Anaerobic degradation of benzene in diverse anoxic environments. Environmental Science & Technology 31, 813-818.

Kelts, K., Hsü, K.J., 1978. Freshwater carbonate sedimentation. Springer New York.

Kennedy, M.J., Pevear, D.R., Hill, R.J., 2002. Mineral surface control of organic carbon in black shale. Science 295, 657-660.

Killops, S.D., 1991. Novel aromatic hydrocarbons of probable bacterial origin in a Jurassic lacustrine sequence. Organic Geochemistry 17, 25-36.

Killops, S.D., Killops, V.J., 2005. Introduction to organic geochemistry, 2nd ed. Blackwell Publishing, Oxford.

Kleemann, G., Poralla, K., Englert, G., Kjosen, H., Liaaen-Jensen, S., Neunlist, S., Rohmer, M., 1990. Tetrahymanol from the phrototrophic bacterium *Rhodopseudomonas palustris*: First report of a gammacerane triterpene from a prokaryote. Journal of General Microbiology 136, 2551-2553.

Koopmans, M.P., Schouten, S., Kohnen, M.E.L., Sinninghe Damsté, J.S., 1996. Restricted utility of aryl isoprenoids as indicators for photic zone anoxia. Geochimica et Cosmochimica Acta 60, 4873-4876.

Kuypers, M.M.M., Pancost, R.D., Nijenhuis, I.A., Sinninghe Damste, J.S., 2002. Enhanced productivity led to increased organic carbon burial in the euxinic North Atlantic basin during the late Cenomanian oceanic anoxic event. Paleoceanography 17, 21-41.

Löhr, S., Kennedy, M., George, C.S., Williamson, R., Xu, H., 2018. Sediment microfabric records mass sedimentation of colonial cyanobacteria, rapid onset of seafloor anoxia and extensive metazoan reworking in Pliocene sapropels. The Depositional Record, in press.

Li, M.J., Shi, S.B., Wang, T.G., 2012. Identification and distribution of chrysene, methylchrysenes and their isomers in crude oils and rock extracts. Organic Geochemistry 52, 55-66.

Li, S., Pang, X., Li, M., Jin, Z., 2003. Geochemistry of petroleum systems in the Niuzhuang South Slope of Bohai Bay Basin—part 1: source rock characterization. Organic Geochemistry 34, 389–412.

Lichtfouse, E., Derenne, S., Mariotti, A., Largeau, C., 1994. Possible algal origin of long chain odd *n*-alkanes in immature sediments as revealed by distributions and carbon isotope ratios. Organic Geochemistry 22, 1023-1027.

Lichtfouse, E.A., Collister, J.W., 1992. Tracing biogenic links of natural organic substances at the molecular level with stable carbon isotopes: *n*-Alkanes and *n*-alkanoic acids from sediments. Tetrahedron Letters 33, 8093-8094.

Liu, C., Wang, P., 2013. The role of algal blooms in the formation of lacustrine petroleum source rocks - Evidence from Jiyang depression, Bohai Gulf Rift Basin, eastern China. Palaeogeography Palaeoclimatology Palaeoecology 388, 15–22.

Liu, G.Q., Zhang, G., Li, X.D., Li, J., Peng, X.Z., Qi, S.H., 2005. Sedimentary record of polycyclic aromatic hydrocarbons in a sediment core from the Pearl River Estuary, South China. Marine Pollution Bulletin 51, 912-921.

Ma, Y., Fan, M., Lu, Y., Liu, H., Hao, Y., Xie, Z., Liu, Z., Peng, L., Du, X., Hu, H., 2016. Climate-driven paleolimnological change controls lacustrine mudstone depositional process and organic matter accumulation: Constraints from lithofacies and geochemical studies in the Zhanhua Depression, eastern China. International Journal of Coal Geology 167, 103-118.

Mackenzie, A.S., 1984. Applications of biological markers in petroleum geochemistry, in: Brooks, J., Welte, D.H. (Eds.), Advances in petroleum geochemistry. Academic Press, London, pp. 115–214.

Macquaker, J.H.S., Taylor, K.G., Gawthorpe, R.L., 2007. High-resolution facies analyses of mudstones: Implications for paleoenvironmental and sequence stratigraphic interpretations of offshore ancient mud-dominated successions. Journal of Sedimentary Research 77, 324-339.

Macquaker, J.H.S., Keller, M.A., Davies, S.J., 2010. Algal Blooms and "Marine Snow": Mechanisms that enhance preservation of organic carbon in ancient fine-grained sediments. Journal of Sedimentary Research 80, 934-942.

Makeen, Y.M., Abdullah, W.H., Hakimi, M.H., 2015. Biological markers and organic petrology study of organic matter in the Lower Cretaceous Abu Gabra sediments (Muglad Basin, Sudan): origin, type and palaeoenvironmental conditions. Arabian Journal of Geosciences 8, 489-506.

McArthur, J.M., Algeo, T.J., van de Schootbrugge, B., Li, Q., Howarth, R.J., 2008. Basinal restriction, black shales, Re-Os dating, and the Early Toarcian (Jurassic) oceanic anoxic event. Paleoceanography 23, PA4127.

Metzger, P., Largeau, C., Casadevall, E., 1991. Lipids and macromolecular lipids of the hydrocarbon-rich microalga *Botryococcus braunii*. Chemical structure and biosynthesis. Geochemical and biotechnological importance, in: Herz, W., Kirby, G.W., Steglich, W., Tamm, C. (Eds.), Progress in the Chemistry of Organic Natural Products. Springer, Verlag, pp. 1–70.

Miller, K.G., Kominz, M.A., Browning, J.V., Wright, J.D., Mountain, G.S., Katz, M.E., Sugarman, P.J., Cramer, B.S., Christie-Blick, N., Pekar, S.F., 2005. The Phanerozoic record of global sea-level change. Science 310, 1293–1298.

Miller, K.G., Browning, J.V., Aubry, M.P., Wade, B.S., Katz, M.E., Kulpecz, A.A., Wright, J.D., 2008. Eocene-Oligocene global climate and sea-level changes: St. Stephens Quarry, Alabama. Geological Society of America Bulletin 120, 34–53.

Moldowan, J.M., Seifert, W.K., Gallegos, E.J., 1985. Relationship between petroleum composition and depositional environment of petroleum source rocks. AAPG Bulletin 69, 1255–1268.

Mort, H.P., Adatte, T., Föllmi, K.B., Keller, G., Steinmann, P., Matera, V., Berner, Z., Stüben, D., 2007a. Phosphorus and the roles of productivity and nutrient recycling during oceanic anoxic event 2. Geology 35, 483-486.

Mort, H.P., Adatte, T., Föllmi, K.B., Keller, G., Steinmann, P., Matera, V., Berner, Z., Stüben, D., 2007b. Phosphorus and the roles of productivity and nutrient recycling during oceanic anoxic event 2. Geology 35, 483–486.

Murray, A.P., Summons, R.E., Boreham, C.J., Dowling, L.M., 1994. Biomarker and *n*-alkane isotope profiles for Tertiary oils - relationship to source-rock depositional setting. Organic Geochemistry 22, 521-542.

Noble, R.A., Alexander, R., Kagi, R.I., Nox, J.K., 1986. Identification of some diterpenoid hydrocarbons in petroleum. Organic Geochemistry 10, 825-829.

Ourisson, G., Albrecht, P., Rohmer, M., 1979. The hopanoids: Palaeochemistry and biochemistry of a group of natural products. Pure & Applied Chemistry 51, 709-729.

Ourisson, G., Rohmer, M., Poralla, K., 1987. Prokaryotic hopanoids and other polyterpenoid sterol surrogates. Annual Review of Microbiology 41, 301-333.

Püttmann, W., Villar, H., 1987. Occurrence and geochemical significance of 1,2,5,6-tetramethylnaphthalene. Geochimica et Cosmochimica Acta 51, 3023-3029.

Pacton, M., Fiet, N., Gorin, G., 2006. Revisiting amorphous organic matter in Kimmeridgian laminites: what is the role of the vulcanization process in the amorphization of organic matter? Terra Nova 18, 380-387.

Pearce, C.R., Cohen, A.S., Coe, A.L., Burton, K.W., 2006. Changes in the extent of marine anoxia during the Early Jurassic: Evidence from molybdenum isotopes. Geochimica et Cosmochimica Acta 70, A476-A476.

Pedersen, T.F., Calvert, S.E., 1990. Anoxia vs. productivity: what controls the formation of organic-carbon-rich sediments and sedimentary Rocks?(1). AAPG Bulletin 74, 454-466.

Peters, K.E., Walters, C.C., Moldowan, J.M., 2005. The Biomarker Guide. Cambridge University Press, Cambridge

Peters, K.E., Walters, C.C., Moldowan, J.M., 2017. Biomarkers: Assessment of petroleum source-rock age and depositional environment, in: Sorkhabi, R. (Ed.), Encyclopedia of Petroleum Geoscience. Springer International Publishing, pp. 1-11.

Rahman, H.M., Kennedy, M., Löhr, S., Dewhurst, D.N., Sherwood, N., Yang, S., Horsfield, B., 2018. The influence of shale depositional fabric on the kinetics of hydrocarbon generation through control of mineral surface contact area on clay catalysis. Geochimica et Cosmochimica Acta 220, 429-448.

Reinhard, M., Shang, S., Kitanidis, P.K., Orwin, E., Hopkins, G.D., LeBron, C.A., 1997. In situ BTEX biotransformation under enhanced nitrate- and sulfate-reducing conditions. Environmental Science & Technology 31, 28-36.

Renaut, R.W., Owen, R.B., Jones, B., Tiercelin, J.J., Tarits, C., Ego, J.K., Konhauser, K.O., 2013. Impact of lake-level changes on the formation of thermogene travertine in continental rifts: Evidence from Lake Bogoria, Kenya Rift Valley. Sedimentology 60, 428-468.

Repeta, D.J., 1989. Carotenoid diagenesis in recent marine sediments: II. Degradation of fucoxanthin to loliolide. Geochimica et Cosmochimica Acta 53, 699-707.

Riboulleau, A., Schnyder, J., Riquier, L., Lefebvre, V., Baudin, F., Deconinck, J.-F., 2007. Environmental change during the Early Cretaceous in the Purbeck-type Durlston Bay section (Dorset, Southern England): A biomarker approach. Organic Geochemistry 38, 1804–1823.

Rickard, D., Luther, G.W., 2007. Chemistry of iron sulfides. Chemical Reviews 107, 514-562.

Rohmer, M., Bisseret, P., Neunlist, S., 1992. The hopanoids, prokaryotic triterpenoids and precursors of ubiquitous molecular fossils. Biological markers in sediments and petroleum 54, 1-17.

Schieber, J., 2010. The possible role of benthic microbial mats during the formation of carbonaceous shales in shallow Mid‐Proterozoic basins. Sedimentology 33, 521-536.

Schwark, L., Frimmel, A., 2004. Chemostratigraphy of the Posidonia black shale, SW-Germany: II. Assessment of extent and persistence of photic-zone anoxia using aryl isoprenoid distributions. Chemical Geology 206, 231–248.

Simoneit, B.R.T., Grimalt, J.O., Wang, T.G., Cox, R.E., Hatcher, P.G., Nissenbaum, A., 1986. Cyclic terpenoids of contemporary resinous plant detritus and of fossil woods, ambers and coals. Organic Geochemistry 10, 877-889.

Sinninghe Damsté, J.S., Kenig, F., Koopmans, M.P., Köster, J., Schouten, S., Hayes, J.M., Leeuw, J.W.D., 1995. Evidence for gammacerane as an indicator of water column stratification. Geochimica et Cosmochimica Acta 59, 1895.

Sinninghe Damsté, J.S., Schouten, S., Duin, A.C.T.V., 2001. Isorenieratene derivatives in sediments: possible controls on their distribution. Geochimica et Cosmochimica Acta 65, 1557-1571.

Smith, M.E., Carroll, A.R., Mueller, E.R., 2008. Elevated weathering rates in the Rocky Mountains during the Early Eocene Climatic Optimum. Nature Geoscience 1, 370-374.

Smith, M.E., Carroll, A.R., Scott, J.J., Singer, B.S., 2014. Early Eocene carbon isotope excursions and landscape destabilization at eccentricity minima: Green River Formation of Wyoming. Earth & Planetary Science Letters 403, 393-406.

Sofer, Z., Regan, D.R., Muller, D.S., 1993. Sterane isomerization ratios of oils as maturity indicators and their use as an exploration tool, Neuquen basin, Argentina, XII Congreso de Geológico Argentino y II Congreso de Exploración de Hidrocarburos Actas, pp. 407-411.

Sousa Júnior, G.R., Santos, A.L.S., de Lima, S.G., Lopes, J.A.D., Reis, F.A.M., Santos Neto, E.V., Chang, H.K., 2013. Evidence for euphotic zone anoxia during the deposition of Aptian source rocks based on aryl isoprenoids in petroleum, Sergipe–Alagoas Basin, northeastern Brazil. Organic Geochemistry 63, 94-104.

Spooner, N., 1994. Stable carbon isotopic correlation of individual biolipids in aquatic organisms and a lake bottom sediment. Organic Geochemistry 21, 823-827.

Strachan, M.G., Alexander, R., Kagi, R.I., 1988. Trimethylnaphthalenes in crude oils and sediments: Effects of source and maturity. Geochimica et Cosmochimica Acta 52, 1255-1264.

Thierrin, J., Davis, G., Barber, C., Patterson, B., Pribac, F., Power, T., Lambert, M., 1993. Natural degradation rates of BTEX compounds and naphthalene in a sulphate reducing groundwater environment. International Association of Scientific Hydrology Bulletin 38, 309-322.

Tian, J., Yin, G., Qin, J., Zeng, Y., Li, Y., 1998. The relationship between the transgression of eogene and the origin of lacustrine dolomite in Eastern China. China Offshore Oil and Gas. (Geology) 12, 250-254.

Tissot, B.P., Welte, D.H., 1984. From kerogen to petroleum, in: Tissot, B.P., Welte, D.H. (Eds.), Petroleum formation and occurrence, 2nd Edition. Springer, Berlin Heidelberg, pp. 160–198.

Trabucho-Alexandre, J., Dirkx, R., Veld, H., Klaver, G., de Boer, P.L., 2012. Toarcian black shales in the Dutch central graben: Record of energetic, variable depositional conditions during an oceanic anoxic event. Journal of Sedimentary Research 82, 104-120.

Tyson, R.V., 2001. Sedimentation rate, dilution, preservation and total organic carbon: some results of a modelling study. Organic Geochemistry 32, 333-339.

Tyson, R.V., 2005. The "productivity versus preservation" controversy: cause, flaws, and resolution, in: Harris, N.B. (Ed.), The Deposition of Organic-carbon-rich Sediments: Models, Mechanisms, and Consequences. SEPM Special Publication, pp. 17-33.

van Dongen, B.E., Schouten, S., Damsté, J.S.S., 2006. Preservation of carbohydrates through sulfurization in a Jurassic euxinic shelf sea: Examination of the Blackstone Band TOC cycle in the Kimmeridge Clay Formation, UK. Organic Geochemistry 37, 1052-1073.

Vasconcelos, C., Mckenzie, J.A., 1997. Microbial mediation of modern dolimite precipitation and diagenesis under anoxic conditions (Lagoa Vermelha, Rio De Janeiro, Brazil). Journal of Sedimentary Research 67, 378-390.

Volk, H., George, S.C., Boreham, C.J., Kempton, R.H., 2004. Geochemical and compound specific carbon isotopic characterisation of fluid inclusion oils from the offshore Perth Basin, Western Australia: Implications for recognising effective oil source rocks. The APPEA Journal 44, 223-240.

Volkman, J.K., Barrett, S.M., Blackburn, S.I., Mansour, M.P., Sikes, E.L., Gelin, F., 1998. Microalgal biomarkers: A review of recent research developments. Organic Geochemistry 29, 1163–1179.

Volkman, J.K., 2005. Sterols and other triterpenoids: source specificity and evolution of biosynthetic pathways. Organic Geochemistry 36, 139-159.

Wakeham, S.G., Amann, R., Freeman, K., H, Hopmans, E., C, Jørgensen, B., Barker, Putnam, I.F., Schouten, S., Sinninghe Damste, J.S., Talbot, H.M., Woebken, D., 2007. Microbial ecology of the stratified water column of the Black Sea as revealed by a comprehensive biomarker study. Organic Geochemistry 38, 2070-2097.

Wakeham, S.G., Turich, C., Schubotz, F., Podlaska, A., Li, X.N., Varela, R., Astor, Y., Sáenz, J.P., Rush, D., Sinninghe Damste, J.S., 2012. Biomarkers, chemistry and microbiology

show chemoautotrophy in a multilayer chemocline in the Cariaco Basin. Deep-Sea Research Part I 63, 133-156.

Wang, G., Wang, T.G., Simoneit, B.R.T., Zhang, L., 2013. Investigation of hydrocarbon biodegradation from a downhole profile in Bohai Bay Basin: Implications for the origin of 25-norhopanes. Organic Geochemistry 55, 72–84.

Warthmann, R., van Lith, Y., Vasconcelos, C., McKenzie, J.A., Karpoff, A.M., 2000. Bacterially induced dolomite precipitation in anoxic culture experiments. Geology 28, 1091-1094.

Weltje, G.J., Meijer, X.D., de Boer, P.L., 1998. Stratigraphic inversion of siliciclastic basin fills: A note on the distinction between supply signals resulting from tectonic and climatic forcing. Basin Research 10, 129-153.

Wright, D.T., Wacey, D., 2005. Precipitation of dolomite using sulphate-reducing bacteria from the Coorong Region, South Australia: significance and implications. Sedimentology 52, 987-1008.

Xiong, Y., Geng, A., Pan, C., Liu, D., Peng, P., 2005. Characterization of the hydrogen isotopic composition of individual *n*-alkanes in terrestrial source rocks. Applied Geochemistry 20, 455-464.

Yunker, M.B., Macdonald, R.W., Vingarzan, R., Mitchell, R.H., Goyette, D., Sylvestre, S., 2002. PAHs in the Fraser River basin: a critical appraisal of PAH ratios as indicators of PAH source and composition. Organic Geochemistry 33, 489-515.

Yunker, M.B., Perreault, A., Lowe, C.J., 2012. Source apportionment of elevated PAH concentrations in sediments near deep marine outfalls in Esquimalt and Victoria, BC, Canada: is coal from an 1891 shipwreck the source? Organic Geochemistry 46, 12-37.

Yunker, M.B., McLaughlin, F.A., Fowler, M.G., Fowler, B.R., 2014. Source apportionment of the hydrocarbon background in sediment cores from Hecate Strait, a pristine sea on the west coast of British Columbia, Canada. Organic Geochemistry 76, 235-258.

Yunker, M.B., Macdonald, R.W., Ross, P.S., Johannessen, S.C., Dangerfield, N., 2015. Alkane and PAH provenance and potential bioavailability in coastal marine sediments subject to a gradient of anthropogenic sources in British Columbia, Canada. Organic Geochemistry 89-90, 80-116.

Zakir Hossain, H.M., Sampei, Y., Roser, B.P., 2013. Polycyclic aromatic hydrocarbons (PAHs) in late Eocene to early Pleistocene mudstones of the Sylhet succession, NE Bengal Basin, Bangladesh: Implications for source and paleoclimate conditions during Himalayan uplift. Organic Geochemistry 56, 25-39.

Zhang, L., Huang, D., Liao, Z., 1999. High concentration retene and methylretene in Silurian carbonate of Michigan Basin. Chinese Science Bulletin 44, 2083-2086.

Zhang, L., 2008. The progress on the study of lacustrine source rocks. Petroleum Geology & Experiment 30, 591–595.

Zhang, L., Liu, Q., Zhu, R., Li, Z., Lu, X., 2009. Source rocks in Mesozoic-Cenozoic continental rift basins, East China: A case from Dongying Depression, Bohai Bay Basin. Organic Geochemistry 40, 229–242.

Zhang, X., Young, L.Y., 1997. Carboxylation as an initial reaction in the anaerobic metabolism of naphthalene and phenanthrene by sulfidogenic consortia. Applied Environmental Microbiology 63, 4759-4764.

Zhang, Z., Zhao, M., Yang, X., Wang, S., Jiang, X., Oldfield, F., Eglinton, G., 2004. A hydrocarbon biomarker record for the last 40 kyr of plant input to Lake Heqing, southwestern China. Organic Geochemistry 35, 595–613.

Zhou, W., Wang, R., Radke, M., Wu, Q., Sheng, G., Liu, Z., 2000. Retene in pyrolysates of algal and bacterial organic matter. Organic Geochemistry 31, 757-762.

Zhu, D., Wang, Y., Yin, Y., Yang, W., Zhu, D., Ning, F., SINOPEC, 2015. Study on the relationship between saline environmental deposition and shale oil-gas in faulted basin:A case study of areas of Dongying sag and Bonan subsag. Petroleum Geology & Recovery Efficiency 22, 7-13.

Zhu, G., Jin, Q., Zhang, S., Dai, J., Wang, G., Zhang, L., Li, J., 2005. Characteristics and origin of deep lake oil shale of the Shahejie Formation of Paleogene in Dongying Sag, Jiyang Depression. Journal of Palaeogeography 7, 59-69.

# Tables

Table 4.1 Organic geochemical parameters of the sliced shale sample from the Es3 member, FE112 well, Dongying Depression, Bohai Bay Basin.

| Slice codes | A | B | C | D | E | F | G | H | I | J |
|---|---|---|---|---|---|---|---|---|---|---|
| TOC (%) | 16 2 | 16 3 | 11 0 | 14 6 | 15 2 | 15 4 | 11 6 | 10 6 | 17 4 | 14 5 |
| N (%) | 0 73 | 0 69 | 0 56 | 0 70 | 0 72 | 0 66 | 0 57 | 0 57 | 0 77 | 0 62 |
| EOM (mg/g) | 16 4 | 16 1 | 13 2 | 18 3 | 16 1 | 21 8 | 17 0 | 14 8 | 16 7 | 21 3 |
| Pr/Ph | 0 892 | 0 911 | 0 847 | 0 875 | 0 913 | 0 916 | 0 840 | 0 856 | 0 904 | 0 885 |
| CPI 24-32 | 1 291 | 1 303 | 1 282 | 1 315 | 1 317 | 1 297 | 1 330 | 1 340 | 1 287 | 1 313 |
| β-carotane (%) | 1 36 | 1 52 | 2 28 | 1 67 | 1 31 | 1 49 | 0 91 | 0 91 | 0 73 | 1 09 |
| TAR | 0 65 | 0 69 | 0 86 | 0 78 | 0 62 | 0 75 | 0 47 | 0 43 | 0 25 | 0 59 |
| ∑20-/∑21+ | 0 81 | 0 75 | 0 62 | 0 69 | 0 84 | 0 70 | 0 97 | 1 06 | 1 59 | 0 86 |
| ∑n-$C_{15-19}$/∑n-A (%) | 29 7 | 29 3 | 26 3 | 28 0 | 31 2 | 28 1 | 34 6 | 35 5 | 40 7 | 32 4 |
| ∑n-$C_{21-25}$/∑n-A (%) | 25 1 | 25 7 | 26 6 | 26 0 | 25 3 | 26 1 | 27 3 | 27 1 | 24 1 | 25 3 |
| ∑n-$C_{27-31}$/∑n-A (%) | 18 4 | 19 1 | 21 2 | 20 3 | 18 0 | 19 8 | 15 3 | 14 2 | 9 6 | 17 6 |
| $C_{29}/C_{30}$ αβ hopane | 0 715 | 0 713 | 0 707 | 0 719 | 0 773 | 0 741 | 0 786 | 0 837 | 0 804 | 0 731 |
| Ts/(Ts+Tm) | 0 270 | 0 260 | 0 257 | 0 274 | 0 254 | 0 260 | 0 254 | 0 264 | 0 262 | 0 247 |
| 35/(35 + 34) | 0 371 | 0 376 | 0 398 | 0 387 | 0 380 | 0 384 | 0 374 | 0 381 | 0 365 | 0 370 |
| $C_{30}$αβ/*n*-$C_{17}$ | 0 355 | 0 447 | 0 481 | 0 431 | 0 386 | 0 430 | 0 289 | 0 304 | 0 252 | 0 376 |
| O/H | 0 038 | 0 039 | 0 028 | 0 033 | 0 025 | 0 028 | 0 030 | 0 027 | 0 032 | 0 024 |
| G/H | 0 049 | 0 050 | 0 056 | 0 052 | 0 047 | 0 046 | 0 042 | 0 043 | 0 042 | 0 044 |
| 19/23 | 0 165 | 0 146 | 0 155 | 0 171 | 0 205 | 0 184 | 0 136 | 0 149 | 0 159 | 0 154 |
| 20/23 | 0 568 | 0 492 | 0 585 | 0 694 | 0 532 | 0 581 | 0 467 | 0 709 | 0 533 | 0 581 |
| (19+20)/23 | 0 733 | 0 637 | 0 740 | 0 865 | 0 736 | 0 765 | 0 603 | 0 858 | 0 692 | 0 735 |
| St/H | 0 403 | 0 360 | 0 387 | 0 367 | 0 319 | 0 347 | 0 312 | 0 280 | 0 305 | 0 339 |
| $C_{29}$ 20S | 0 270 | 0 268 | 0 244 | 0 263 | 0 270 | 0 255 | 0 265 | 0 290 | 0 268 | 0 252 |
| $C_{29}$ αββ | 0 247 | 0 214 | 0 240 | 0 244 | 0 244 | 0 236 | 0 246 | 0 204 | 0 234 | 0 264 |
| Dino/$C_{27-29}$ (on area) | 0 088 | 0 085 | 0 094 | 0 083 | 0 084 | 0 087 | 0 082 | 0 081 | 0 081 | 0 081 |
| 29/27 | 0 457 | 0 459 | 0 483 | 0 453 | 0 431 | 0 456 | 0 427 | 0 439 | 0 439 | 0 425 |
| $C_{27}$ ααα R % (m/z 217) | 54 88 | 54 97 | 53 47 | 55 01 | 56 16 | 54 34 | 56 33 | 56 18 | 56 00 | 56 36 |
| $C_{28}$ ααα R % (m/z 217) | 20 02 | 19 82 | 20 71 | 20 08 | 19 63 | 20 89 | 19 61 | 19 18 | 19 41 | 19 68 |
| $C_{29}$ ααα R % (m/z 217) | 25 10 | 25 22 | 25 82 | 24 91 | 24 22 | 24 77 | 24 06 | 24 64 | 24 58 | 23 97 |
| (1256+1235)/1236 | 0 945 | 0 905 | 1 008 | 0 891 | 0 849 | 0 864 | 0 887 | 0 957 | 0 876 | 0 941 |
| HPI | 0 607 | 0 732 | 1 090 | 0 752 | 0 808 | 0 681 | 0 532 | 0 844 | 0 462 | 0 606 |
| Log(1-MP/9-MP) | 0 187 | 0 177 | 0 202 | 0 191 | 0 192 | 0 208 | 0 196 | 0 239 | 0 194 | 0 191 |
| Log(1,7-DMP/X) | 0 251 | 0 230 | 0 253 | 0 294 | 0 204 | 0 248 | 0 257 | 0 317 | 0 265 | 0 252 |
| MP/P | 1 208 | 1 338 | 1 861 | 1 561 | 1 364 | 1 440 | 1 113 | 1 177 | 0 999 | 1 284 |
| DBT/P | 0 155 | 0 171 | 0 074 | 0 150 | 0 149 | 0 146 | 0 134 | 0 082 | 0 144 | 0 102 |
| Log(Retene/9-MP) | -0 74 | -0 68 | -0 55 | -0 67 | -0 69 | -0 73 | -0 73 | -0 82 | -0 78 | -0 77 |
| Fla/(Fla+Py) | 0 24 | 0 20 | 0 32 | 0 22 | 0 23 | 0 24 | 0 25 | 0 33 | 0 24 | 0 29 |
| AIR | 3 35 | 4 10 | 2 38 | 3 40 | 3 49 | 3 26 | 3 29 | 2 95 | 5 54 | 3 36 |
| iR/P | 1 82 | 1 88 | 7 05 | 4 28 | 2 50 | 3 31 | 1 63 | 1 62 | 0 73 | 1 37 |
| Retene (%) | 3 95 | 5 12 | 9 33 | 6 03 | 5 05 | 4 76 | 3 68 | 3 04 | 2 94 | 3 85 |
| Phosphorus (Wt%) | 0 050 | 0 050 | 0 040 | 0 070 | 0 060 | 0 047 | 0 040 | 0 050 | 0 070 | 0 060 |

EOM = extractable organic matter; CPI 24-32 = Carbon Preference Index of *n*-$C_{24-32}$ alkanes ; β-carotane (%) = percentage of β-carotane relative to the highest concentration *n*-$C_{17}$ alkane; TAR = *n*-$C_{27+29+31}$/*n*-$C_{15+17+19}$ alkanes; ∑*n*-$C_{15-19}$ (%) = ∑*n*-$C_{15-19}$/∑n-alkanes (%); ∑*n*-$C_{21-25}$ (%) = ∑*n*-$C_{21-25}$/∑*n*-alkanes (%); ∑*n*-$C_{27-31}$ (%) = ∑*n*-$C_{27-31}$/∑n-alkanes (%); $C_{29}$ 20S = $C_{29}$ ααα 20S/(20S + 20R) steranes; $C_{29}$ αββ = $C_{29}$ αββ/(αββ + ααα) steranes; 35/(35 + 34) = $C_{35}$ αβ hopanes/($C_{35}$ ab hopanes + $C_{34}$ ab hopanes); $C_{30}$αβ/*n*-C17 = $C_{30}$ 17α,21β(H) hopane/*n*-$C_{17}$ alkane; O/H = Oleanane/$C_{30}$ αβ hopane; G/H = Gammacerane/$C_{30}$ αβ hopane; 19/23 = $C_{19}$ tricyclic terpane/$C_{23}$ tricyclic terpane; 20/23 = $C_{20}$ tricyclic terpane/$C_{23}$ tricyclic terpane; (19+20)/23 = ($C_{19}$ tricyclic terpane + $C_{20}$ tricyclic terpane)/$C_{23}$ tricyclic terpane; St/H = $C_{29}$ ααα + αββ steranes/$C_{29}$ αβ hopanes (on areas); 29/27 = $C_{29}/C_{27}$ aaa 20R steranes; Dino/$C_{27-29}$ (on area) = Sum of relative abundance of dinosteranes (4α,23S,24S-trimethylcholestane (20R) + 4α,23S,24R-trimethylcholestane (20R) + 4α,23R,24R-trimethylcholestane (20R) + 4 α,23R,24S-trimethylcholestane (20R)) to sum of relative abundance of $C_{27-29}$ regualar steranes; DBT/P = dibenzothiophene/phenanthrene; AIR = ∑$C_{13-17}$/∑$C_{18-22}$ monoaryl isoprenoids; (1256+1235)/1236 = 1,2,5,6- + 1,2,3,5-)/1,2,3,6-Tetramethylnaphthalene; HPI = ([iHMN+Cadalene+Retene]/1,3,6,7-Tetramethylnaphthalene), note the absence of iHMN and Cadalene; Log(1-MP/9-MP) = Log(1-methylphenanthrene/9-methylphenanthrene); Log(1,7-DMP/X) = Log(1,7-dimethylphenanthrene/1,3-+3,9-+2,10-+3,10-dimethylphenanthrene); Log(Retene/9-MP) = Log(Retene/9-methylphenanthrene); MP/P = total methylphenanthrene/phenanthrene; Fla/(Fla + Py) = fluoranthene/(fluoranthene + pyrene); iR/P = isorenieratane/phenanthrene; Retene (%) = percentage of retene relative to phenanthrene

Table 4.2 Mineral compositions (wt%) of the ten slices (a) and the five types of laminae (b). Note that a few additional minerals are not shown because of extremely low abundances.

(a)

| Slices | A | B | C | D | E | F | G | H | I | J |
|---|---|---|---|---|---|---|---|---|---|---|
| Quartz (%) | 12.57 | 12.17 | 12.87 | 12.80 | 13.16 | 11.78 | 11.62 | 12.14 | 12.97 | 11.73 |
| Feldspars (%) | 28.35 | 27.19 | 30.23 | 30.33 | 31.21 | 24.97 | 24.83 | 23.94 | 29.59 | 30.05 |
| Clay (%) | 10.68 | 9.38 | 11.85 | 12.97 | 11.40 | 9.53 | 9.01 | 10.09 | 13.85 | 14.36 |
| Zircon (%) | 0.02 | 0.03 | 0.02 | 0.03 | 0.02 | 0.03 | 0.03 | 0.02 | 0.03 | 0.03 |
| Calcite (%) | 20.05 | 24.27 | 16.73 | 17.29 | 17.19 | 22.60 | 23.59 | 23.07 | 17.43 | 17.33 |
| Dolomites (%) | 21.60 | 20.06 | 20.57 | 18.60 | 19.71 | 23.85 | 23.81 | 23.10 | 18.02 | 16.68 |
| Pyrite (%) | 2.63 | 2.96 | 3.11 | 3.32 | 2.81 | 2.90 | 3.30 | 3.56 | 3.70 | 5.83 |
| Muscovite (%) | 2.41 | 2.38 | 2.92 | 2.89 | 2.56 | 2.14 | 2.17 | 2.36 | 2.67 | 2.32 |
| Titanite (%) | 0.13 | 0.11 | 0.14 | 0.13 | 0.14 | 0.13 | 0.13 | 0.11 | 0.12 | 0.11 |
| Apatites (%) | 0.33 | 0.29 | 0.28 | 0.44 | 0.39 | 0.81 | 0.24 | 0.28 | 0.45 | 0.34 |
| Fluorite (%) | 0.91 | 0.90 | 0.95 | 0.89 | 1.09 | 1.02 | 0.99 | 0.94 | 0.85 | 0.86 |
| Goethite (%) | 0.06 | 0.04 | 0.07 | 0.05 | 0.06 | 0.05 | 0.04 | 0.17 | 0.04 | 0.04 |
| Rutile (%) | 0.18 | 0.14 | 0.20 | 0.19 | 0.18 | 0.12 | 0.14 | 0.13 | 0.17 | 0.17 |

(b)

| Laminae types | Calcite | Cal + Dol | Clay | OM | Pyrite |
|---|---|---|---|---|---|
| Quartz (%) | 3.21 | 11.28 | 15.10 | 13.45 | 9.70 |
| Feldspars (%) | 4.38 | 12.27 | 34.01 | 36.94 | 31.57 |
| Muscovite (%) | 0.08 | 0.27 | 4.72 | 2.71 | 1.85 |
| Clays (%) | 2.30 | 1.89 | 21.69 | 17.93 | 13.96 |
| Calcite (%) | 83.21 | 35.19 | 5.05 | 8.55 | 14.28 |
| Dolomites (%) | 5.99 | 37.28 | 14.16 | 13.64 | 9.78 |
| Pyrite (%) | 0.33 | 0.62 | 3.50 | 5.02 | 16.99 |
| Zircon (%) | 0.15 | 0.00 | 0.02 | 0.04 | 0.02 |
| Titanite (%) | 0.09 | 0.03 | 0.13 | 0.11 | 0.14 |
| Apatites (%) | 0.02 | 0.06 | 0.41 | 0.33 | 0.43 |
| Barite (%) | 0.04 | 0.00 | 0.05 | 0.21 | 0.19 |
| Fluorides (%) | 0.19 | 1.09 | 0.79 | 0.81 | 0.79 |
| Goethite (%) | 0.00 | 0.00 | 0.15 | 0.05 | 0.05 |
| Rutile (%) | 0.00 | 0.01 | 0.17 | 0.19 | 0.21 |

Cal + Dol = calcite plus dolomite laminae; OM = organic matter laminae

Table 4.3 Compound specific stable carbon isotope data for *n*-$C_{15-35}$ alkanes in slice C and slice I from the shale sample, and two comparison bulk samples (FE10, FE16) from the FE112 well in the Dongying Depression, Bohai Bay Basin.

| Sample codes | FE10 | FE16 | Slice C | Slice I |
|---|---|---|---|---|
| C15 | -28.8 | -29.3 | -23.5 | -23.6 |
| C16 | -28.3 | -29.5 | -23.8 | -24.0 |
| C17 | -28.5 | -29.8 | -24.7 | -25.0 |
| C18 | -28.8 | -29.9 | -25.5 | -25.6 |
| C19 | -28.9 | -29.8 | -25.7 | -26.2 |
| C20 | -29.3 | -29.6 | -26.6 | -26.5 |
| C21 | -29.6 | -30.1 | -27.3 | -27.4 |
| C22 | -29.0 | -30.0 | -27.5 | -27.8 |
| C23 | -28.8 | -30.0 | -27.9 | -28.1 |
| C24 | -28.3 | -29.5 | -27.6 | -28.0 |
| C25 | -28.8 | -29.6 | -27.5 | -27.8 |
| C26 | -28.7 | -29.4 | -29.1 | -29.4 |
| C27 | -29.4 | -29.6 | -30.3 | -30.6 |
| C28 | -29.5 | -29.6 | -30.8 | -31.6 |
| C29 | -29.6 | -29.6 | -30.9 | -31.1 |
| C30 | -29.5 | -29.1 | -28.9 | -29.5 |
| C31 | -29.3 | -29.0 | -26.6 | -26.8 |
| C32 | -29.5 | -30.2 | -27.3 | -27.9 |
| C33 | -29.6 | -30.3 | -28.2 | -29.2 |
| C34 | -29.4 | -30.1 | -27.8 | -27.6 |
| C35 | -29.0 | -29.7 | -28.9 | -28.7 |

Cxx = *n*-alkane

Chapter 5

# 5. Paradoxical photic zone euxinia in the Dongying Depression: A detailed organic geochemical assessment of the distribution of hydrocarbons on a very small scale

Huiyuan Xu[a, b, c, *], Simon C. George[b, *], Dujie Hou[a, *], Stefan C. Löhr[b]

[a] School of Energy Resources, China University of Geosciences (Beijing), Haidian District, Beijing 10083, China

[b] Department of Earth and Planetary Sciences and Macquarie University Marine Research Centre, Macquarie University, Sydney, NSW 2109, Australia

[c] State Key Laboratory of Shale Oil and Gas Enrichment Mechanisms and Effective Development, Beijing 100083, China

**Chapter 5** shows a comparison of hydrocarbons between two adjacent and contrasting parts of a core at the millimetre scale: a dark-coloured laminae, and a light-colour laminae in a well-laminated shale in the Dongying Depression. The selected sample in **Chapter 5** has a major difference in organic matter input from the sample chosen in **Chapter 4**. The former has a dominated eukaryotic organic input (the regular steranes/hopanes ratio > 3), whilst the latter has the regular steranes/hopanes < 0.41 indicating a dominated prokaryotic organic input. This

chapter postulates that the accumulation and preservation of organic matter should be considered to be the sum of many individual and temporally-varying processes, rather than long-period aggregation in a persistent depositional environment.

**Statement of Author's Contribution:** 85% of the work was done by the first author Huiyuan Xu, including developing the project plan and timeframe, sampling, conducting laboratory experiments, processing and analysing the data, and writing the manuscript. Simon C. George helped with designing the laboratory experiments, directing the research, and improving the manuscript, which accounts for 8%. Dujie Hou helped with developing the project plan and timeframe, sampling, and improving the manuscript, which accounts for 4%. Stefan C. Löhr helped with designing and conducting the scanning electron microscopy (SEM) and Nanomin mineral mapping experiments, interpreting those data, and improving the manuscript, which accounts for 3%. This chapter is about to be submitted as an original research paper to *Chemical Geology* (2019).

## Abstract

A well laminated shale from the upper part of the fourth member of the Shahejie Formation, Dongying Depression, Bohai Bay Basin was horizontally sliced in two and investigated using organic geochemical techniques to assess the heterogeneity of hydrocarbons within the rock layers. The distributions of aliphatic and aromatic hydrocarbons were compared between slices at the millimetre scale. Rapid fluctuations in environment are shown by variation in the aryl isoprenoid ratio, the relative amount of isorenieratane, and other molecular indicators including the relative amounts of dibenzothiophene, dibenzofuran, methyldibenzothiophene, and methyltrimethyltridecylchromans. The two slices have been interpreted as embodiments of different euxinic water conditions. No terrigenous land plant biomarkers were detected, but micro-scale changes in other source inputs were noted. For instance, the 4α-methylsteranes, dinosteranes and the triaromatic dinosteranes show varying distributions between the two slices, attributed to slight differences in dinoflagellate contributions. Additionally, we report the first stable carbon isotopic fractionation of long-chain *n*-alkanes on a millimetre-scale in a shale, for which bacterial sulphate reduction and photic zone euxinia are responsible. The micro-variations of source and environment in well-laminated shales have not been extensively documented. In this study, two different laminations in the fine-grained shale reflect variation in organic input (i.e. primary production) and preservation environment (during diagenetic processes). The accumulation and preservation of organic matter should probably be considered to be the sum of many individual processes, rather than long-period aggregation in a persistent depositional environment.

## 5.1. Introduction

Much previous research on the organic geochemical properties of hydrocarbons within sediment rocks has addressed issues about petroleum accumulation, palaeoenvironment, thermal maturity, organic inputs, etc. These have mostly been carried out on homogenised rock from a relatively large sample (cm size), where the hydrocarbons are treated as representative of specific beds, units, members or formations. Discrepancies have sometime been noted due to multiple effects on the relative content and distribution of hydrocarbons (e.g. Radke et al., 1998; Grice et al., 2007). Vertical textural or mineralogical physical heterogeneity at the micron-scale in fine-grained rocks (termed shales hereafter), has been shown using optical and scanning electron microscope (SEM) techniques (Macquaker and Adams, 2003; Röhl and Schmid-Röhl, 2005; Macquaker et al., 2010a; Macquaker et al., 2010b; Aplin and Macquaker, 2011; Trabucho-Alexandre et al., 2012; Löhr et al., 2018; Rahman et al., 2018). SEM techniques allow very detailed comparisons of rock properties such as mineralogy, micro-fossil, and micro-fabric. Although high resolution SEM and photomicrographs may provide sophisticated imaging of vertical variation at the micron scale, little chemical information is available. Small-scale variability of hydrocarbons in shales is not readily documented using existing organic geochemical techniques, especially when the rock samples are highly heterogeneous, so possible composition differences in hydrocarbons in laminated shales at such scales are commonly ignored. It is important to know how subtly different depositional environments (e.g. bottom water anoxia, photic zone euxinia (PZE), etc.) and organic matter input sources (e.g. bacteria, algae, land plants, etc.) interact to produce different hydrocarbons. The possible chemical processes generating those distinctions

are also of great importance, as well as the mechanism(s) of organic matter enrichment. An attempt to determine the controls on hydrocarbon variability at the millimetre-scale will enhance our understanding and utilisation of organic geochemistry.

Fundamental controls on hydrocarbons within rock frameworks include organic matter sources, depositional environment and thermal maturity (Peters et al., 2005, 2017). However, the relative contents and distributions of specific hydrocarbons are not usually fully constrained by one single control. For example, retene is generally produced during diagenesis by dehydrogenation of abietic acid, which is a major constituent of coniferous resins. But Zhou et al. (2000) identified retene in pure strains of the green alga *Chlorella protothecoides* and the *cyanobacterium Synechocystis* sp. A microbial origin for long-chain *n*-alkanes (Summons et al., 2013), which are often considered to be mainly derived from terrigenous or algal organic matter, and algal-derived polycyclic aromatic hydrocarbons (PAHs) (Grice et al., 2007) have been noted. In addition, the sensitivity of organic geochemical parameters to the environment may vary due to the different chemical properties of hydrocarbon biomarkers.

In this study, in order to assess the spatial variation of hydrocarbons in a laminated shale, a black well-laminated Eocene Dongying shale sample was selected that comprises two adjacent and contrasting parts at the millimetre scale: a dark-coloured laminae, and a light-colour laminae. The selected sample in **Chapter 5** has a major difference in organic matter input from the sample chosen in **Chapter 4**. The former has a dominated eukaryotic organic input (the regular steranes/hopanes ratio > 3), whilst the latter has the regular steranes/hopanes < 0.41 indicating a dominated prokaryotic organic input. Under high-resolution optical

imaging techniques, obvious physical property changes in texture and fabric are visible. This study set out to answer two questions. Firstly, how are these lithological changes related to possible organic geochemical changes? Secondly, are these changes a function of primary production, transport, secondary reworking or diagenetic process, or a combination thereof?

This study, in addition to showing the physicochemical rock framework properties, provides a new perspective in showing a distinction in the organic geochemical properties of generated and indigenous fluids (the aliphatic and aromatic hydrocarbons) adsorbed on a fine-grained shale at the millimetre scale. Controls on the distributions of the aliphatic and aromatic hydrocarbons are discussed, and are used in an attempt to unravel the exact trigger for the sudden change in organic matter sources, depositional environment and petrological properties.

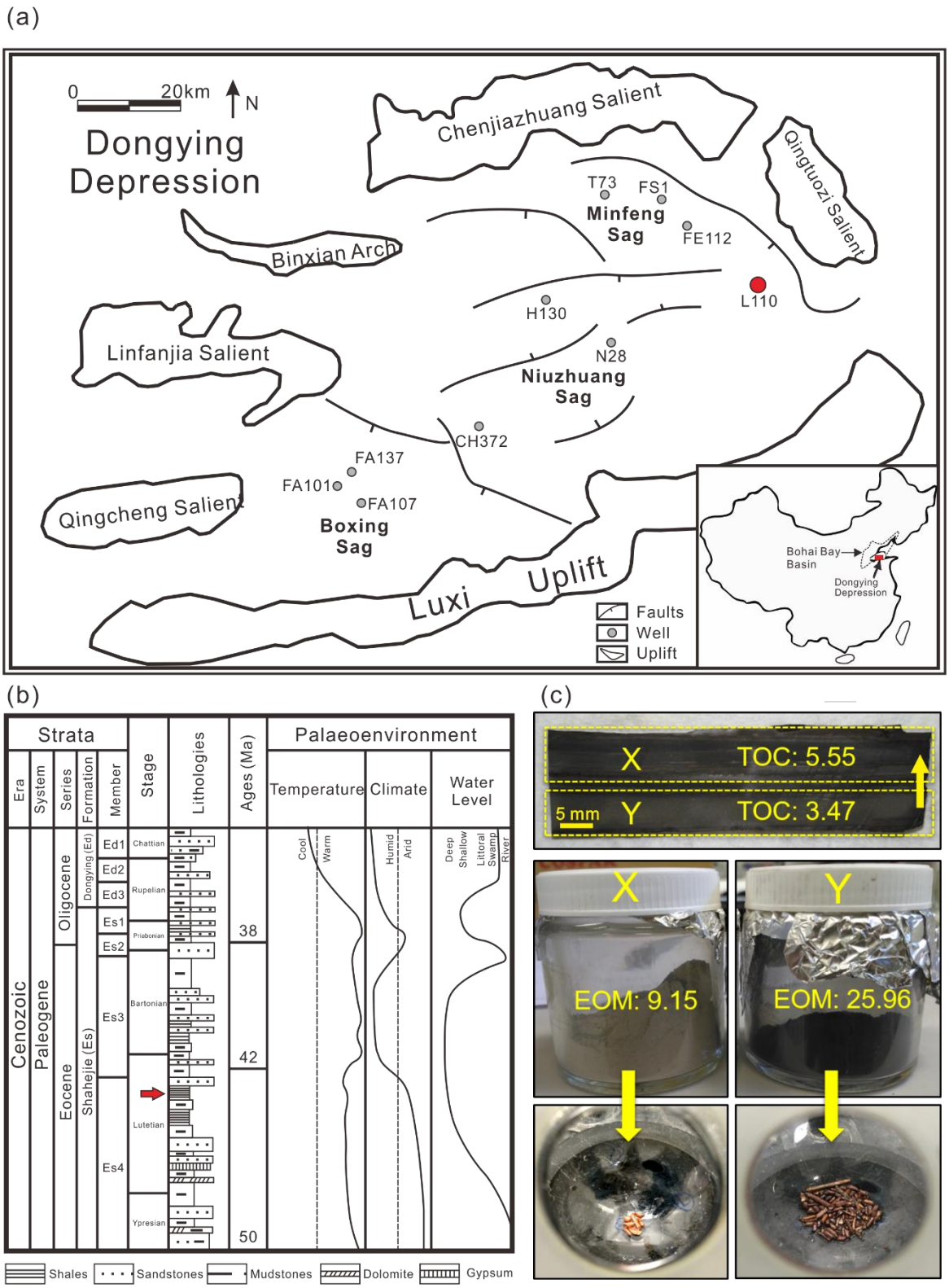


Fig. 5.1 a: Location map of the Dongying Depression, Bohai Bay Basin, showing the position of the subdivided sags, the L110 well, and the structural elements. b: Stratigraphic chart showing the Eocene to Oligocene strata in the Dongying Depression. c: The low-maturity shale sample (2770.4 m), showing how it was sawn into two consecutive slices (X and Y), based on differences in texture. TOC data (%), extractable organic matter yield (EOM; mg/g rock), and presence (Y) and absence (X) of elemental sulphur based on discolouration of copper metal are also shown.

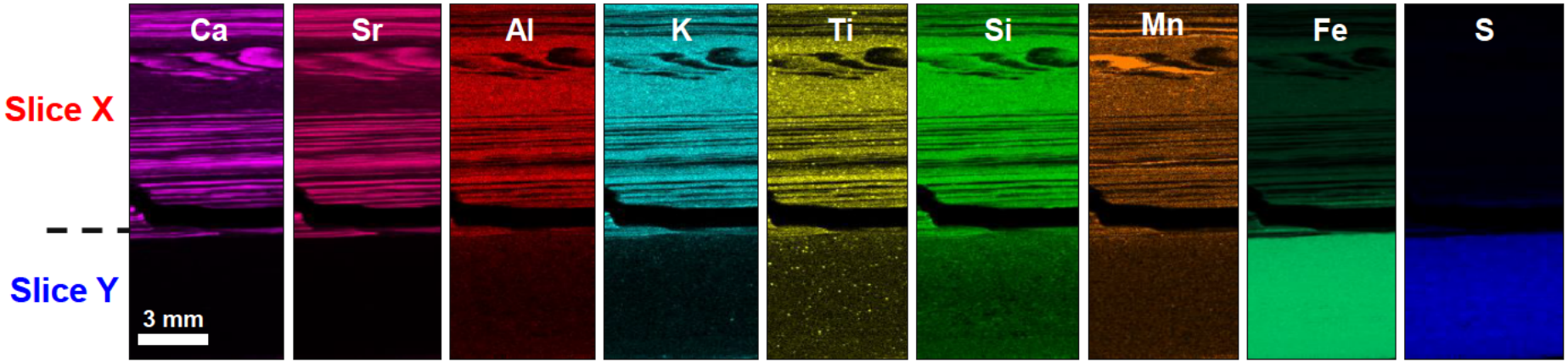


Fig. 5.2 Single element distribution images (partial) of a series of elements in the sample, displayed in individual frames. Each colour represents an individual element. The visible crack in the middle (black) was formed during sample preparation. The upper slice X is much more laminated than slice Y.

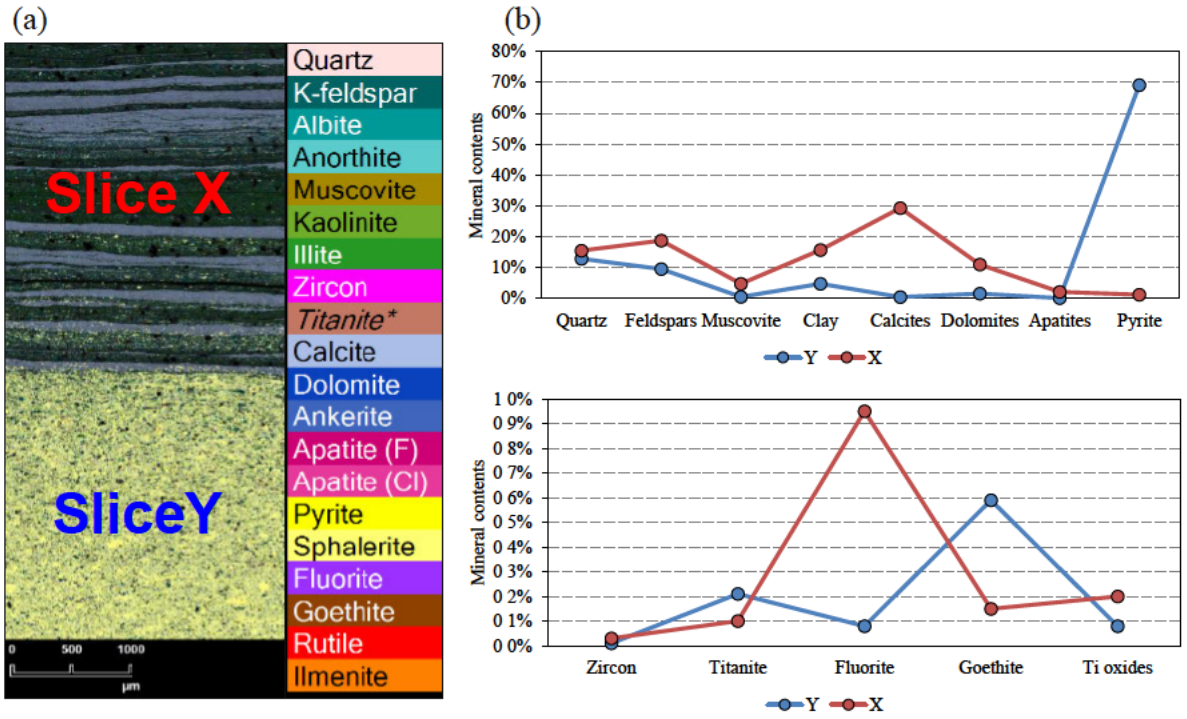


Fig. 5.3 a: Partial Nanomin mineral map of the sample showing interbedded clays (dark green) and carbonate laminae (light blue) in slice X, and minerals such as abundant pyrite (yellow) in slice Y. More minerals are identified in the colour legend. b: Composite line charts showing the mineral differences between slice X (red) and slice Y (blue).

## 5.2. Materials and methods

### 5.2.1. Sample

The low-maturity black shale sample (2770.4 m) was collected from the upper part of the fourth member of the Shahejie Formation (Es4U) of the L110 well, which is located in the northeast of the Dongying Depression. The Es4U was deposited in a shallow, closed, saline lake, under a relative arid climate (Hao et al., 2009).

## 5.2.2. Methods

### *5.2.2.1. Micro X-ray fluorescence (Micro-XRF)*

The laminated shale is inhomogeneous. Micro-XRF offers very good spatial resolution combined with high sensitivity for small element concentrations. The measurements were performed on a Bruker M4 TORNADO with a rhodium anode. The polished sample was scanned with an electron source at 50 kV, 600 µA to image the elemental distributions (Fig. 5.2). The spot size was 25 mm, the step size was 40 µm, the dwell time was 20 ms.

### *5.2.2.2. Scanning electron microscopy (SEM) and mineral mapping*

The sample was polished using a Hitachi IM4000 Argon Ion Mill system and carbon-coated (5 nm carbon) before imaging and mineral mapping on a FEI Teneo field emission SEM equipped with dual EDS (energy dispersive X-ray spectroscopy) detectors (Bruker XFlash Series 6). High resolution back-scatter electron and mineral maps of the sample were collected to identify small-scale vertical variation in textural, mineralogical and organo-mineral associations in the sample (13 mm working distance, 15 kV accelerating voltage). Back-scatter electron image tilesets (150 nm pixel resolution) and EDS spectra (5 µm step size, 8 ms acquisition time) for mineral mapping were collected sequentially using the FEI Maps Mineralogy software, followed by classification of the individual EDS spectra using the FEI Nanomin software (Haberlah et al., 2015; Rahman et al., 2018). Mineral identification is achieved by comparing EDS spectra collected in the mapped area against reference spectra collected on known mineral standards. Unlike earlier SEM-based mineral mapping techniques (e.g. QEMSCAN), the Nanomin mineral classification system can de-convolve mixed X-ray

spectra and assign up to three minerals per analysed spot. This is a critical advantage for the correct interpretation of the mixed phase X-ray spectra characteristic of heterogeneous fine-grained sediments, which might otherwise lead to mineral misidentification. SEM photomicrographs and Nanomin maps provide direct visual evidence of the range of complex association of minerals and organic matter at the required mm to sub-mm scale.

*5.2.2.3. Slicing and crushing*

After cutting off the outside surface of the shale core sample using a Buehler Isomet 4000 Linear Precision Saw with a 0.9 mm blade, the selected area was sawn into two horizontal slices (slices X and Y) (Fig. 5.1c). Each slice was treated with deionised water sonication and dichloromethane sonication to remove any possible laboratory contamination, and then was dried at room temperature. It is noticeable that the ground slice Y is darker than the ground slice X. Very thin (submillimeter scale) laminae are observable with the naked eye in slice X, but not in slice Y which has a fine uniform texture (Fig. 5.1c). The slices and comparison samples were crushed into powder in a rotary mill.

*5.2.2.4. Total organic carbon*

Five hundred milligrams of each well ground homogenised sample were immersed in 10% HCl and were heated in a water bath at 50 ℃ for 36 hours to remove any carbonate carbon. After HCl treatment, the samples were rinsed and centrifuged 3 times with deionised water to remove the acid, and then were dried in an oven for 24 hours at 55 ℃. Dried samples were mixed well, and then 5-10 mg were analysed using a Euro Vector EA3000 CHNS-O Elemental Analyser. The reaction gas products ($CO_2$ and $NO_X$) were carried by helium flow to

a copper reactor where excess $O_2$ was consumed to produce CuO, and NOx products were converted to $N_2$. The products were carried through a packed GC column that provided separation of the combustion gases which were detected by a thermal conductivity detector. Soil#6 (C = 3.429 %; N = 0.228 %) and acetanilide were used as standards that were analysed every eight samples. Total sulphur (TS) content then was measured using a LECO CS744 Elemental Analyser.

*5.2.2.5. Solvent extraction, sulphur removal and fractionation*

The homogenised powdered samples (25.3–27.2 g) were extracted using an azeotropic solvent mixture of dichloromethane/methanol (9:1 v/v) in an accelerated solvent extractor (ASE300; Dionex). Hydrochloric acid activated copper metal was used to remove any elemental sulphur present in the extractable organic matter (EOM). The EOM was refluxed for 15 minutes (in ~50 mL solvent) in a round bottom flask with activated copper (~2 g). More activated copper was added when necessary until a black CuO coating was no longer produced.

A known aliquot (1 ml from 10 ml) of the EOM was transferred to a pre-weighed vial. Solvent was blown off using a mild flow of dry and purified nitrogen at a heater-block temperature of 40 ℃. The vial containing the EOM aliquot was cooled at room temperature, then a stable weight for the aliquot was obtained and the extractability (mg EOM / g rock) was calculated. Then the EOM was fractionated using two phases of silica gel column chromatography. Firstly, EOM was separated into total hydrocarbons and polar compounds, the former collected by elution with n-hexane/dichloromethane (4:1 v/v). Secondly, total

hydrocarbons were fractioned into aliphatic hydrocarbons which were collected by elution with *n*-hexane, and aromatic hydrocarbons which were collected by elution with *n*-hexane/dichloromethane (4:1 v/v). Ultraviolet light monitoring was used to ensure there were no mixed elution of aliphatic and aromatic hydrocarbons.

*5.2.2.6. Gas chromatography-mass spectrometry (GC-MS)*

Gas chromatography-mass spectrometry (GC-MS) analyses of the aliphatic and aromatic fractions were performed on an Agilent GC (6890N) coupled to an Agilent Mass Selective Detector (5975B) equipped with a J&W DB-5MS fused silica column (length 60 m, inner diameter 0.25 mm, film thickness 0.25 μm). The inlet was held at 35 °C for 3 min., then was programmed to 310 ℃ (0.4 min. isothermal) at a rate of 700 ℃ $min^{-1}$. Samples were injected in splitless mode. The temperature of the GC oven was initially held at 35 ℃ for 4 min, then was programmed to 310 ℃ at 4 ℃ $min^{-1}$, and held for 40 min. Helium (99.999 %) was used as the carrier gas. The carrier gas flow rate was 1.5 mL $min^{-1}$ (constant flow). The ion source of the mass spectrometer was operated in EI mode at 70 eV. The MS data were acquired in full scan mode. Compound identification was based on comparison of relative GC retention times and mass spectra with those previously reported (e.g., Li et al., 2012; Sousa Júnior et al., 2013). An external laboratory standard (North Sea Oil 1, NSO-1) was also analysed for comparison. The relative abundance of compounds was determined from peak areas (using selected mass chromatograms for the integration of the compounds).

*5.2.2.7. Gas chromatography-metastable reaction monitoring-mass spectrometry (GC-MRM-MS)*

GC-MS analysis of the aliphatic hydrocarbon fractions was also performed on a Thermo Trace Ultra GC interfaced with a high resolution Thermo DFS GC-MS system. Gas chromatography was carried out on a J&W DB-5MS fused silica column (60 x 0.25 mm i.d., 0.25 μm film thickness). Aliphatic hydrocarbons (1 μL) were injected using a splitless technique with an injector temperature of 260 ℃ and helium carrier gas at a constant flow of 1.5 mL $min^{-1}$. The mass spectrometer was tuned to 1000 resolution (electron energy 70 eV; source temperature 280 ℃). The GC oven was programmed for an initial temperature of 40 ℃ for 2 min., followed by heating at 20 ℃ $min^{-1}$ to 200 ℃ and then a second heating ramp at 2 ℃ $min^{-1}$ to 310 ℃. The aliphatic fractions were analysed using a metastable reaction monitoring (MRM) programme with the following *m/z* transitions so as to examine the $C_{25\text{-}30}$ steranes: 344→217, 358→217, 372→217, 386→217, 400→217, 414→217, 414→231. An external standard (AGSO_NADD) was analysed for comparison of retention times.

*5.2.2.8. Gas chromatography-isotope ratio-mass spectrometry (GC-ir-MS)*

An aliquot of the aliphatic hydrocarbon from selected samples was separated into purified n-alkanes by molecular sieving. An Agilent 6890 gas chromatograph coupled to a Thermo MAT 253 through a GC-C-III combustion interface (with NiO/CuO/Pt at 950 ℃) was used to determine $\delta^{13}C$ of the selected compounds. Gas chromatography was carried out on an SGE BP5 fused silica column (30 x 0.25 mm i.d., 0.25 μm film thickness), with constant flow

of 1.0 mL $min^{-1}$. The samples were injected at 290 ℃ using splitless mode (60 seconds). The GC oven temperature was initially held at 50 ℃ for 2 min and was programmed to increase to 120 ℃ at 25 ℃ $min^{-1}$, then to 310 ℃ at 5 ℃ $min^{-1}$, where it was maintained isothermally for 8 min. Helium was used as the carrier gas. A standard mixture of *n*-alkanes with known $\delta^{13}C$ values was analysed to test the accuracy of the instrument. The isotopic compositions of samples are reported relative to the international Vienna Peedee belemnite (VPDB) standard, and were determined at least twice. The standard deviations of the replicates were calculated to estimate reproducibility, which was within 0.2 ‰.

## 5.3. Results

### 5.3.1. Inorganic compositions

By micro-XRF mapping (Fig. 5.2), slice X is rich in Ca, Sr, Al, K, Ti and Si, and slice Y is rich in Fe and S. Under SEM imaging, the main minerals in slice X include calcite, feldspar, quartz, clay, dolomite, muscovite, with minor apatite and pyrite (Fig. 5.3). Slice X has distinct laminae. In contrast, slice Y is morphologically or textually homogeneous, and is dominated by pyrite, with quartz, feldspar, clays, dolomite and calcite. Slice Y contain more dolomite than calcite, although both are in relatively low abundance. There are tests and skeletal products of algae (e.g. coccoliths) in the carbonate laminae, and there is abundant organic matter in amorphous form or in elongate lenticular stringers. There are apatite granules/concretions in slice X. Slice Y contains abundant biological materials, as observed under SEM, including calcareous microfossils (e.g. foraminifers and ostracods). Many shells and tests are pyritised; Fig. 5.4), attesting to the role of (PZE) in exceptional preservation of

the organic materials (Melendez et al., 2013).

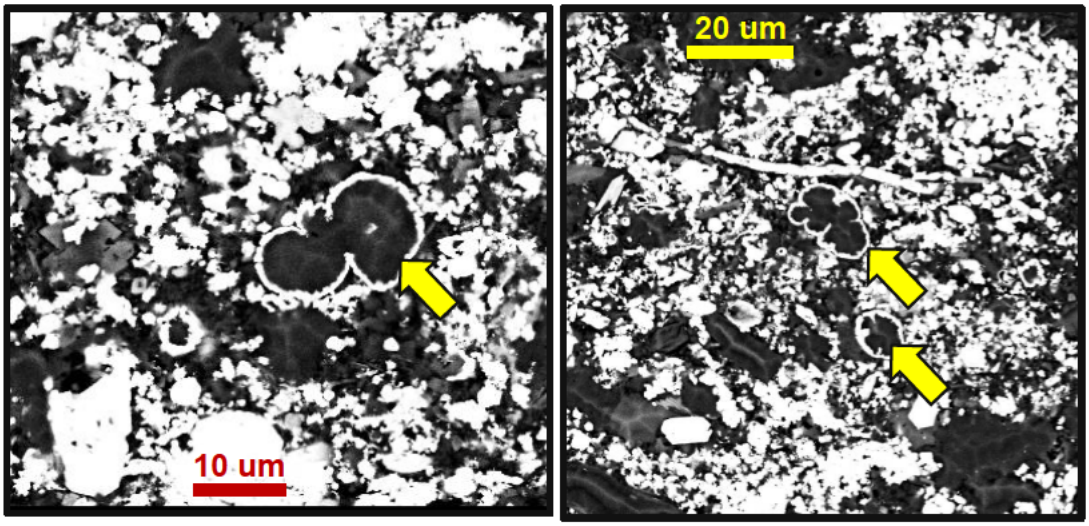


Fig. 5.4 Backscattered SEM photomicrographs of the slice Y part of the sample at different resolutions, showing very abundant pyrite (white). Yellow arrows indicate pyritised biological material such as algae.

### 5.3.2. Organic geochemistry

Slice X slice has a higher TOC (5.6 %) than slice Y (3.5 %), which contrasts their EOM yields (X = 9.2 mg/g; Y = 26.0 mg/g). The most likely cause for this phenomenon is that slice Y contains 69.1 % pyrite by weight (determined by mineral mapping). After removing the carbonates (abundant in X), the iron-rich (higher density) slice Y contains less organic carbon per unit weight (i.e. TOC). If this density difference is taken into account, and the TOC is calibrated as total organic carbon per unit volume ($TOC_v$), then $TOC_v$ is 142.3 mg/cm$^3$ for slice Y and 125.8 mg/cm$^3$ for slice X. A second reason for the discrepancy between TOC and EOM yield is that slice X contains > 40 % carbonates, but slice Y only contains 2.0 % carbonates, thus reducing the apparent EOM of slice X. Therefore, it is reasonable to conclude that slice Y contains more organic carbon than slice X.

It is noteworthy that only slice Y had a reaction with fresh copper metal during the sulphur removal procedure, and required a large amount of copper to react with all the elemental sulphur (Fig. 5.1c). This is in accordance with high total sulphur (TS) and pyrite content (42.4%) for slice Y, and the much lower TS (0.78%) of slice X, based on elemental analysis.

The terpanes (*m/z* 191) and regular steranes (*m/z* 217) of the two sliced samples (Fig. 5.5b and 5.5c) have near identical distributions, with characteristics including elevated gammacerane, predominance of $C_{29}$ over $C_{28}$ and $C_{27}$ regular steranes, and very low amounts of tricyclic terpanes. No diterpanes were detected. Dinosteranes and 4α-methylsteranes (*m/z* 231) are abundant in both slices (Fig. 5.5a). Slice X has a predominance of $C_{30}$ over $C_{29}$ and $C_{28}$ 4α-methylsteranes, but no such predominance is present in slice Y. The *n*-alkanes of the two slices have similar bimodal distributions, with a maximum at *n*-$C_{28}$.and a slight odd-over-even carbon number predominance (Table 5.1). However, the relative abundance of low molecular weight (LMW) and high molecular weight (HMW) *n*-alkanes are slightly different, with slice X relatively enriched in the LMW *n*-alkanes (∑20-/∑21+ *n*-alkane ratio, Table 5.1). The HMW *n*-alkanes are generally more depleted in $^{13}C$ than the LMW *n*-alkanes (Fig. 5.6). The HMW *n*-alkanes (>$C_{26}$) in slice Y are more depleted in $^{13}C$ than in slice X.

Differences between the two slices are more noticeable in the aromatic fractions than in the aliphatic fractions, as shown by summed mass chromatograms (Fig. 5.7). The aryl isoprenoids (AIs) and $C_{40}$ carotenoid derivatives (e.g. isorenieratane) are the most characteristic features of the *m/z* 133 mass chromatograms (Fig. 5.8). Slice X contains more abundant $C_{13\text{-}17}$ AIs (relative to the $C_{18\text{-}22}$ AIs) than slice Y, hence the aryl isoprenoid ratio

(AIR) of slice X is higher (2.5) than for slice Y (1.6; Table 5.2). The isorenieratane/phenanthrene (iR/P) and isorenieratane/$C_{18}$ AI (iR/$C_{18}$ AI) ratios of slice Y are higher. There are many differences in the alkylnaphthalenes between the two slices (Fig. 5.9), for example in the relative amounts of 2,6-dimethylnaphthalene (DMN), 1,4- + 2,3- DMN, 1,3- + 1,7- DMN, 1,6-DMN, 1,3,6-trimethylnaphthalene (TMN), 1,2,6-TMN, 1,3,6- + 1,4,6-TMN, 2,3,6-TMN, 1,2,5,7-tetramethylnaphthalene (TeMN) and 1,2,3,6-TeMN. The distribution of methyldibenzothiophenes (MDBT) is quite different in the two slices (Fig. 5.10). The 4-MDBT/1-MDBT ratio is 0.8 in slice Y, but 1.0 in slice X (Table 5.2). In addition, dibenzofuran (Fig. 5.10) were also detected in greater abundance in slice X than in slice Y. Relative to phenanthrene, slice Y contain more abundant methylphenanthrenes (MPs) (Fig. 5.11a). Slice Y also contains more of the commonly described terrigenous biomarkers such as retene, cadalene and iHMN (1-isohexyl-2-methylnaphthalene), so the higher plant index (HPI) is higher than in slice X (Table 5.2). The *m/z* 245 ion mass chromatograms show that the $C_{29}$ triaromatic dinosteranes (TAD) vary only slightly in isomeric composition between the slices (Fig. 5.12c), but slice Y contains more abundant TAD relative to other aromatic hydrocarbons (Fig. 5.7). On the *m/z* 231 ion mass chromatograms, $C_{28}$ 20R triaromatic steroids (TAS) are slightly more abundant in slice Y, and $C_{26}$ 20R + $C_{27}$ 20S is slightly more abundant in slice X (Fig 12b), but slice Y contains more abundant TAS relative to other aromatic hydrocarbons (Fig. 5.7). Monoaromatic steroids (MAS) vary slightly in isomeric composition between the two slices (Fig. 5.12a). Methyltrimethyltridecylchromans (MTTCs) are present in both slices, with the δ-MTTC isomer in relatively higher abundance in slice X than in slice Y (Fig. 5.11b).

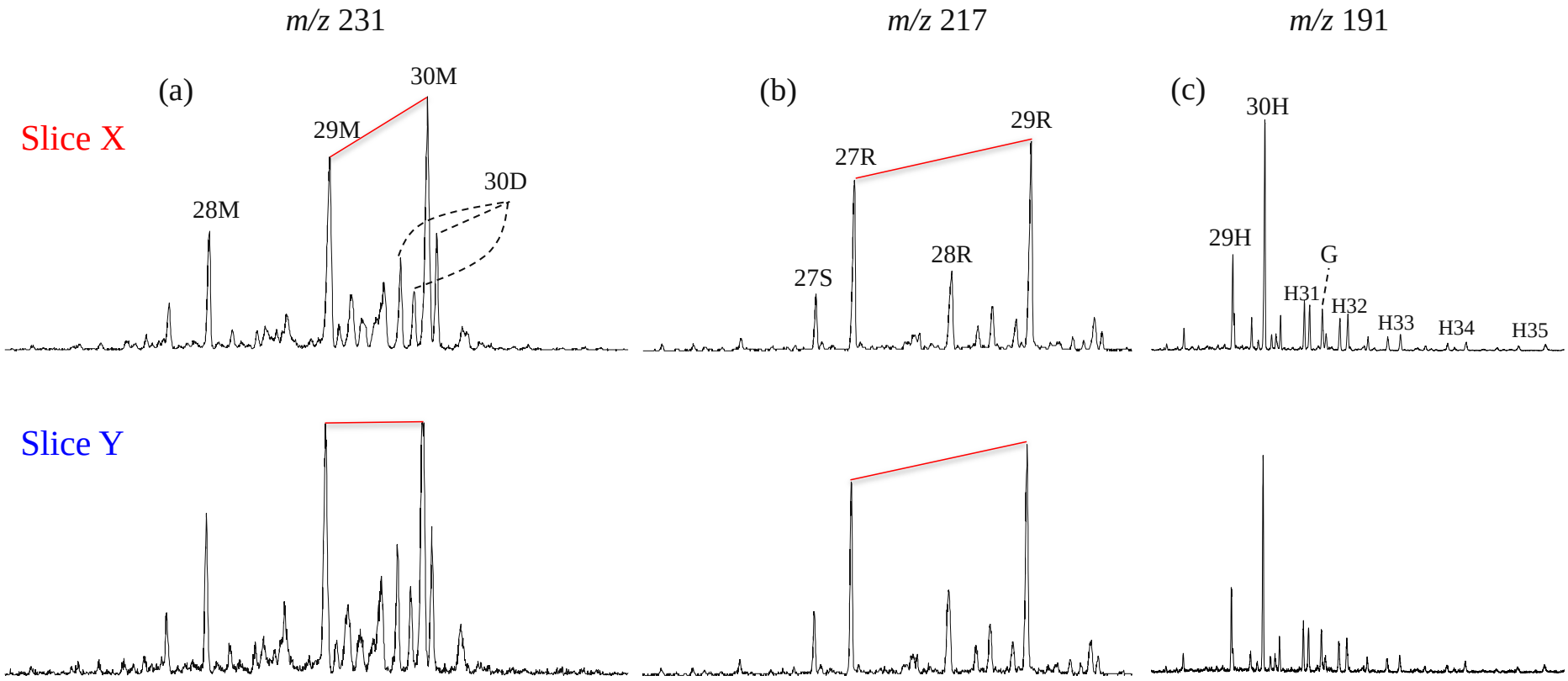


Fig. 5.5 Partial *m/z* 231 (a), *m/z* 217 (b) and *m/z* 191 (c) mass chromatograms, showing the distribution of 4α-methylsteranes, regular steranes and hopanes in the aliphatic fractions of slices X and Y. 28M to 30M = $C_{28}$–$C_{30}$ 4α-methylsteranes, 30D = $C_{30}$ dinosteranes, 27S = $C_{27}$ ααα 20S sterane, 27R to 29R = $C_{27}$–$C_{29}$ ααα 20R sterane, 30H = $C_{30}$ αβ hopane, 29H = $C_{29}$ αβ hopane, G = gammacerane, H31 to H35 = $C_{31}$–$C_{35}$ αβ homohopanes (S+R).

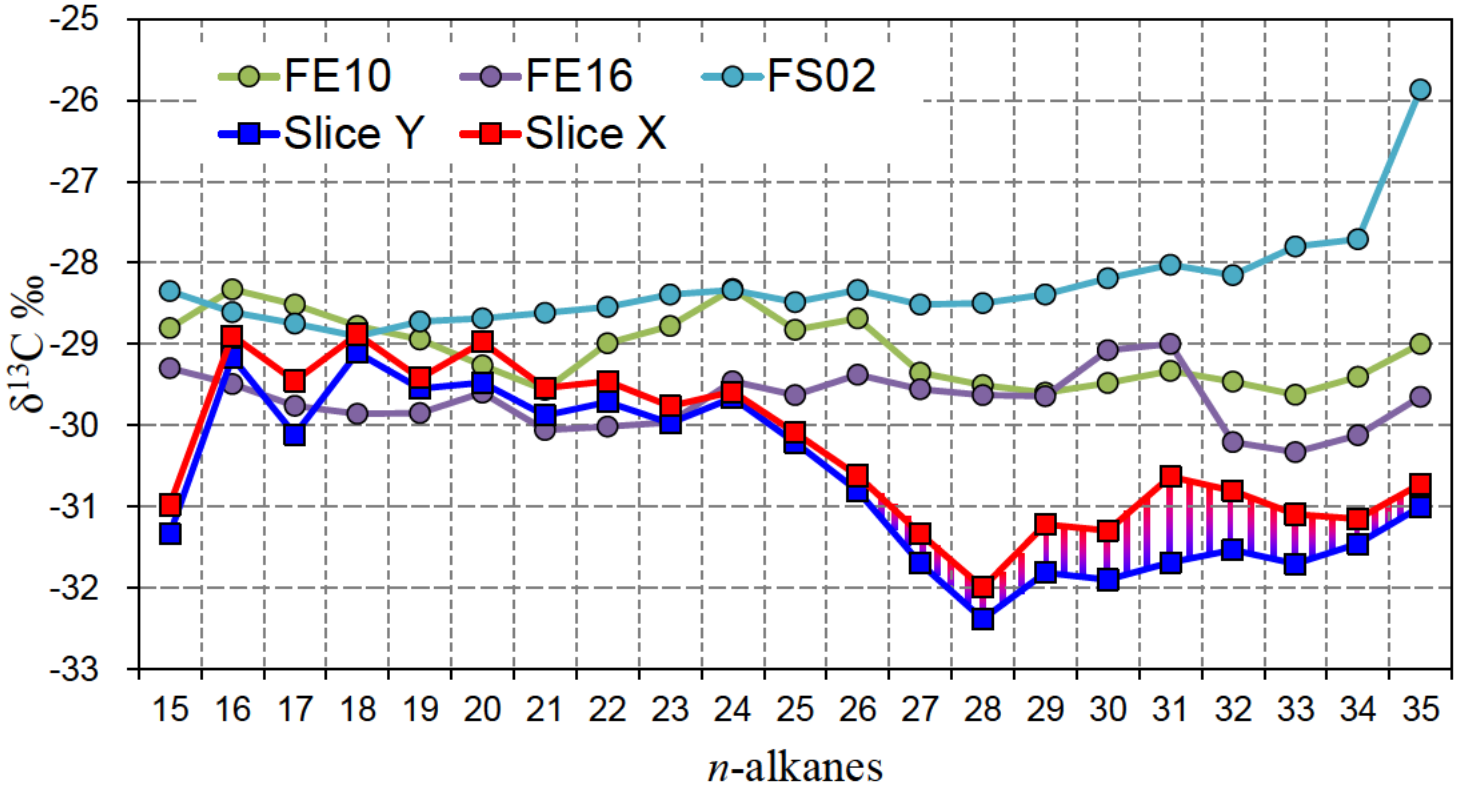


Fig. 5.6 $\delta^{13}C$ values of individual *n*-alkanes in slices X and Y (squares) in comparison to three homogenised bulk samples from the Dongying Depression (code: FE10, FE16 and FS02; circles).

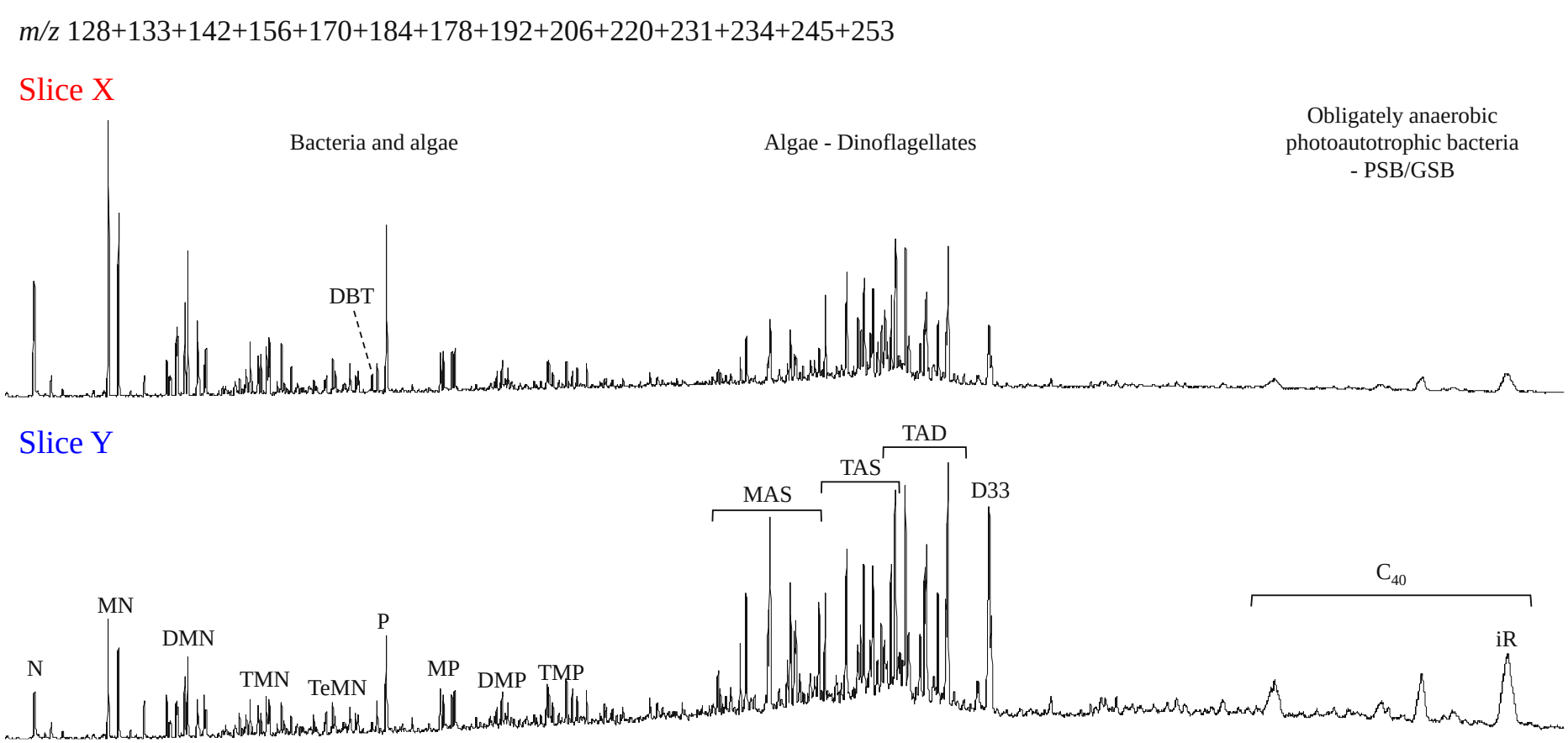


Fig. 5.7 Summed *m/z* 128+133+142+156+170+184+178+192+206+220+231+234+245+253 mass chromatograms, showing the distribution of aromatic hydrocarbons in slices X and Y. N = naphthalene, MN = methylnaphthalene, DMN = dimethylnaphthalene, TMN = trimethylnaphthalene, TeMN = tetramethylnaphthalene, P = phenanthrene, MP = methylphenanthrene, DMP = dimethylphenanthrene, TMP = trimethylphenanthrene, MAS = monoaromatic sterane, TAS = triaromatic sterane, TAD = triaromatic dinosteranes, DBT = dibenzothiophene, D33 = $C_{33}$ diaryl isoprenoid, iR = isorenieratane.

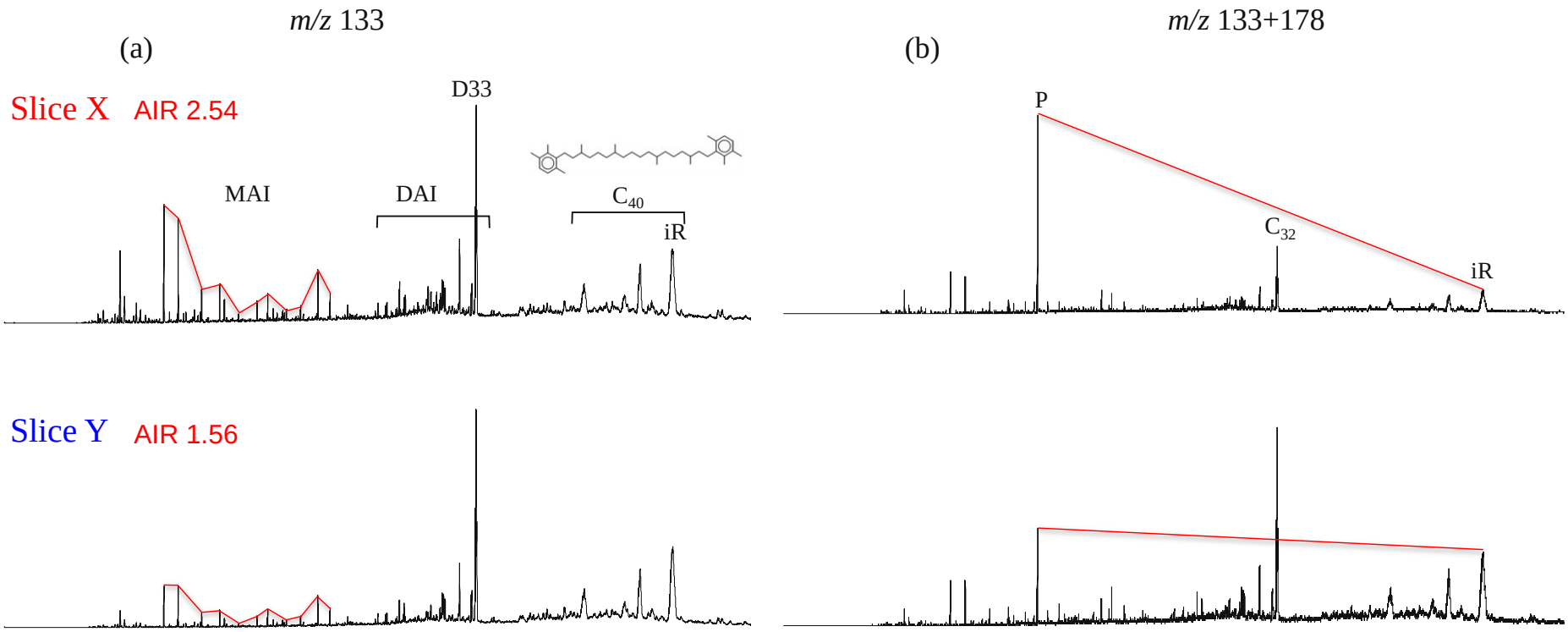


Fig. 5.8 The *m/z* 133 (a) and summed *m/z* 133+178 (b) mass chromatograms of the aromatic hydrocarbon fractions, showing the distributions of aryl isoprenoids and isorenieratane (iR) derivatives. The chemical structure of isorenieratane is shown. P = phenanthrene, MAI = monoaryl isoprenoids, DAI = diaryl isoprenoids, D33 = $C_{33}$ diaryl isoprenoid, iR = isorenieratane.

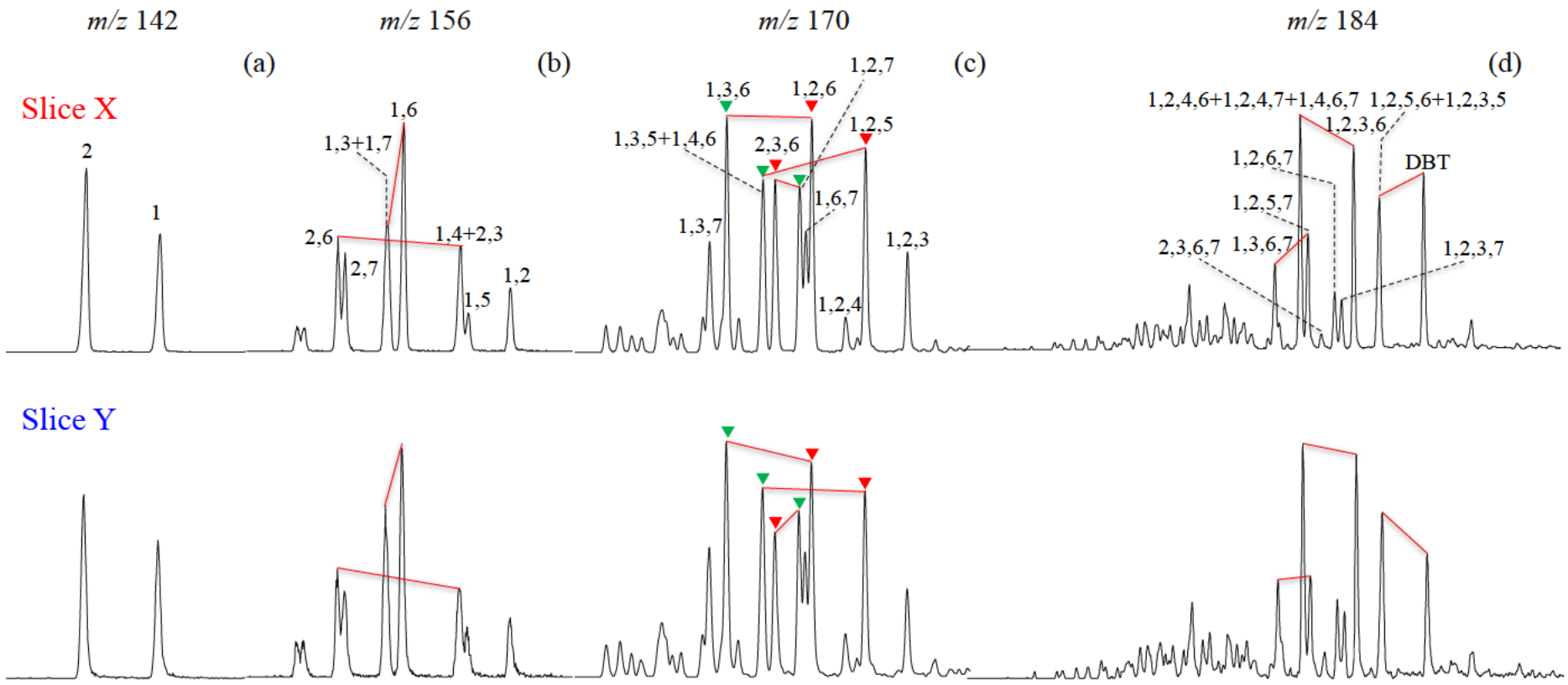


Fig. 5.9 Partial *m/z* 142 (a), *m/z* 156 (b), *m/z* 170 (c) and *m/z* 184 (d) mass chromatograms of the aromatic hydrocarbon fractions, showing the distributions of $C_1$-$C_4$ alkylnaphthalenes and dibenzothiophene (DBT). Numbers show the alkylation position of the methylnaphthalenes, dimethylnaphthalenes, trimethylnaphthalenes and tetramethylnaphthalenes. 1,2,5-TMN (red triangle) has a phytoplankton origin, 1,2,7-TMN (green triangle) can indicate an angiosperm input, and 1,3,6-TMN (green triangle) has been related to bacteria.

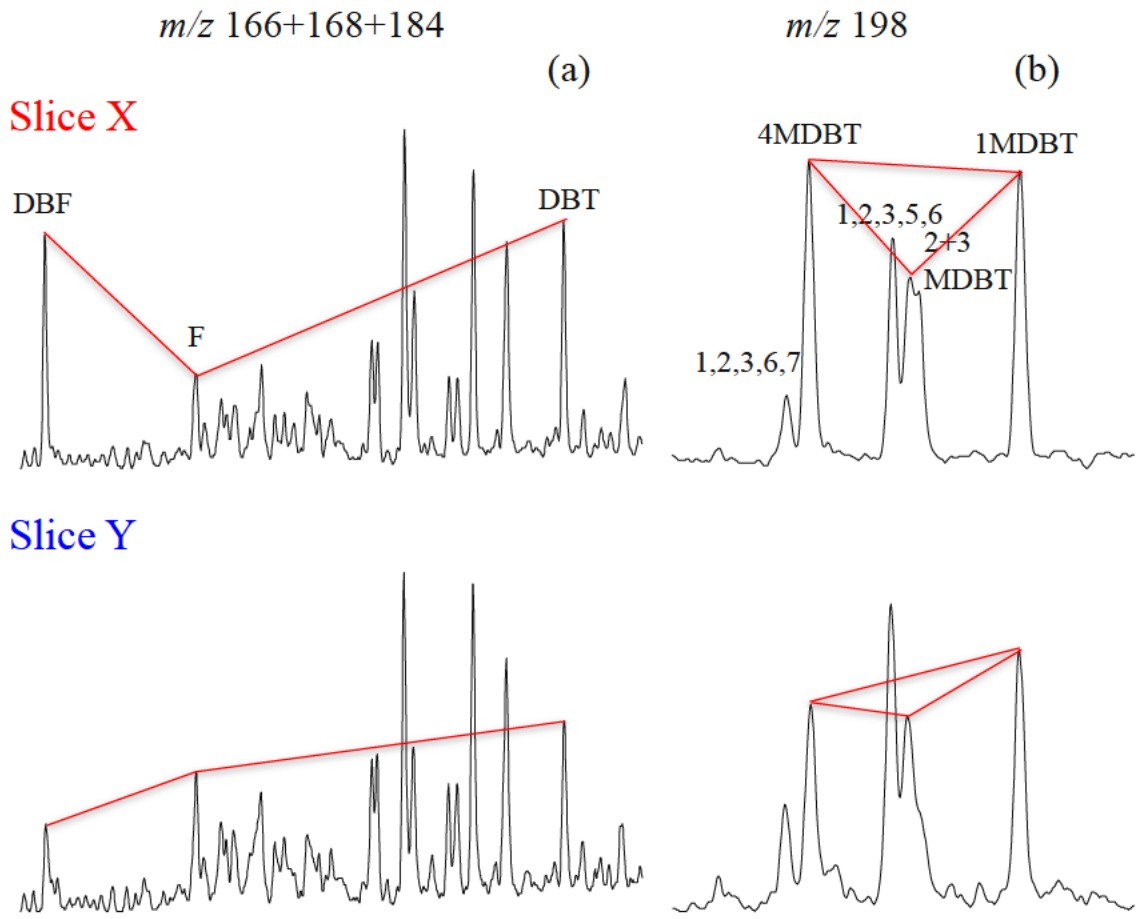


Fig. 5.10 Partial summed *m/z* 166+168+184 (a) and m/z 198 (b) mass chromatograms of the aromatic hydrocarbon fractions, showing the distributions of dibenzothiophene (DBT), dibenzofuran (DBF), fluorene (F), methyldibenzothiophenes (MDBT) and pentamethylnaphthalenes (1,2,3,6,7- and 1,2,3,5,6-PMN).

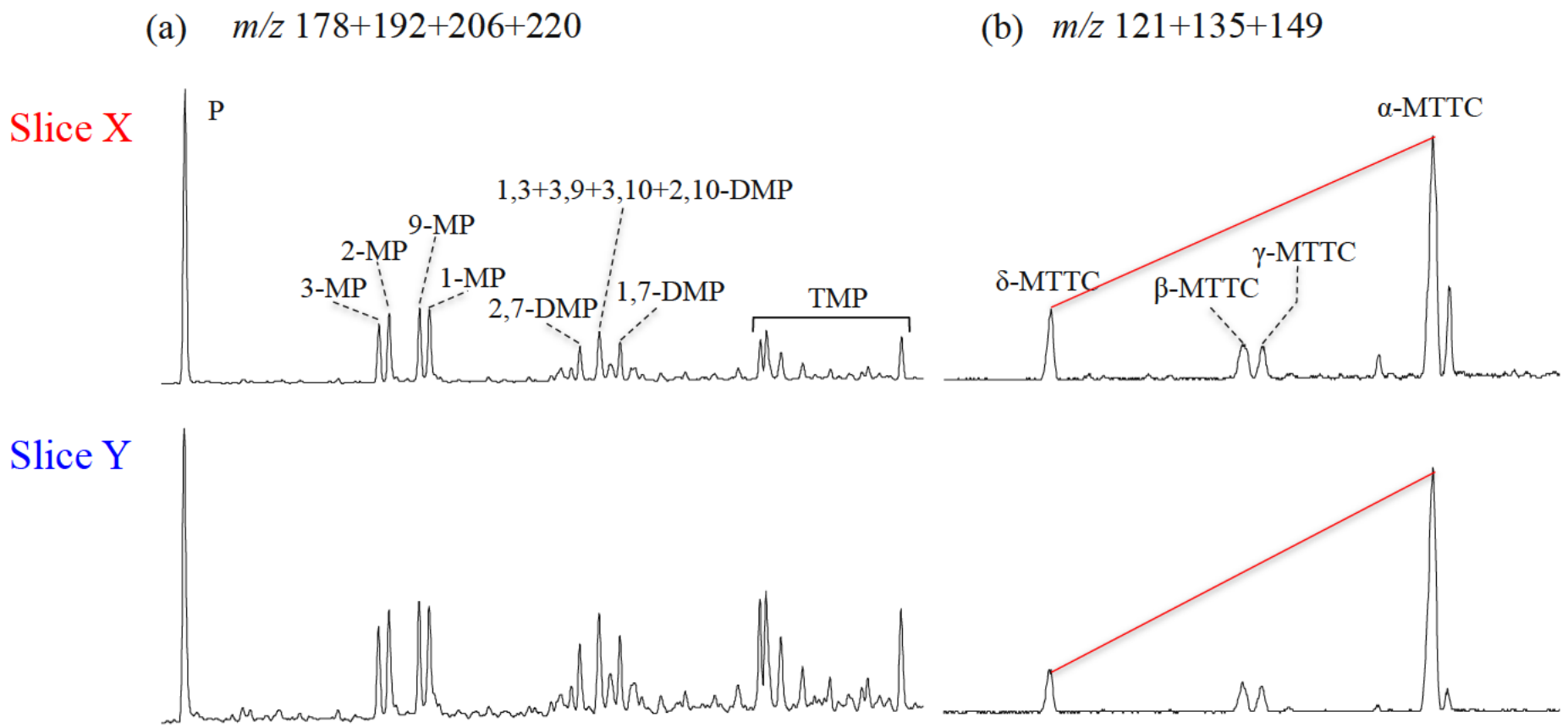


Fig. 5.11 Summed *m/z* 178+192+206+220 (a) and summed *m/z* 121+135+149 (b) mass chromatograms of the aromatic hydrocarbon fractions, show the distributions of phenanthrene, alkylphenanthrenes, and methyltrimethyltridecylchromans (MTTCs). MP = methylphenanthrene, DMP = dimethylphenanthrene, TMP = trimethylphenanthrene.

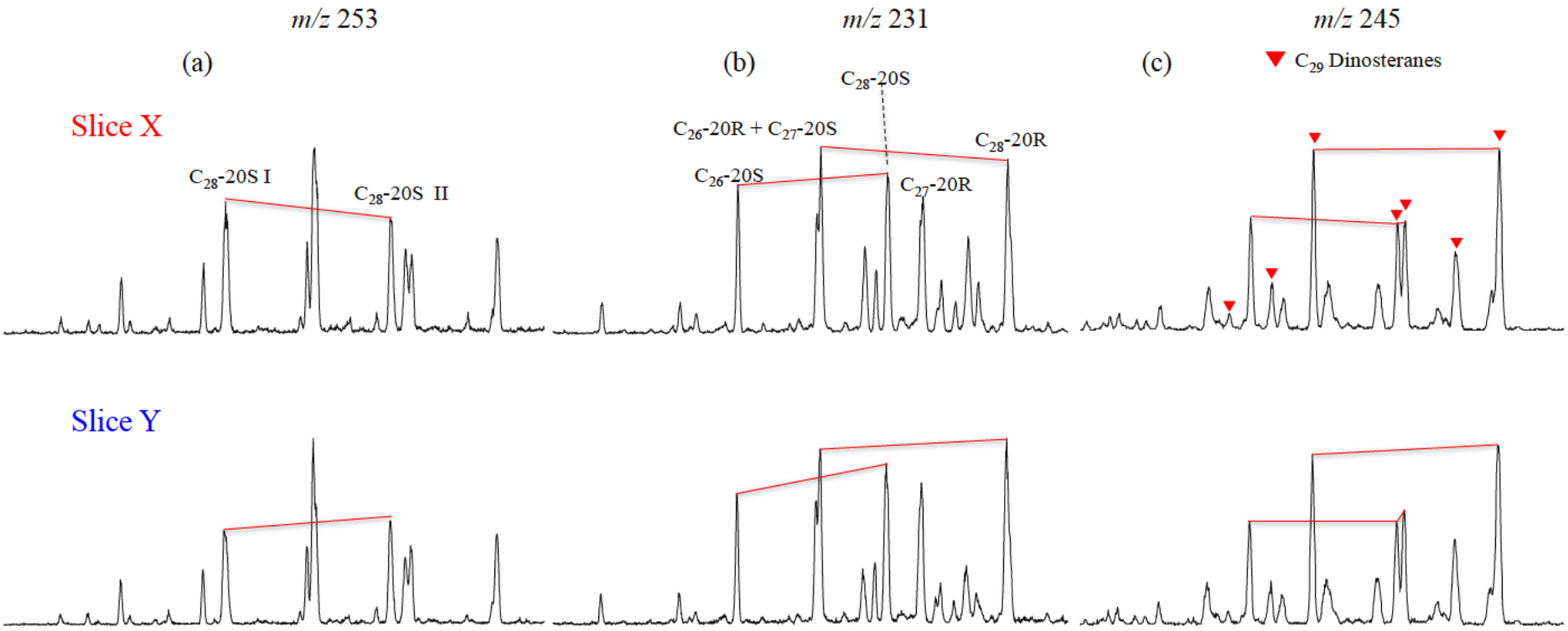


Fig. 5.12 Partial *m/z* 253 (a), *m/z* 231 (b) and *m/z* 245 (c) mass chromatograms of the aromatic hydrocarbon fractions, showing the distributions of monoaromatic steroids, triaromatic steroids and triaromatic dinosteroids, respectively. Red triangles show the identification of $C_{29}$ 4,23,24-trimethyldinosteroids (TAD).

## 5.4. Discussion

In this study any effect of thermal maturity can be excluded because the two sliced samples are only separated by a few mm burial depth. The most likely controls on the distribution of the aliphatic and aromatic hydrocarbons are organic source inputs and depositional environment. The pristane/phytane (Pr/Ph) ratios are very low for the two slices (X = 0.52; Y = 0.51), suggesting generally anoxic conditions. However, many more sensitive hydrocarbons indicators are different in the two slices, which reflects more detailed distinctions between those two periods of deposition in palaeowater chemical conditions and organic source inputs.

### 5.4.1. Small-scale anoxia event

In comparison to slice X, slice Y is interpreted to be the result of a small-scale anoxia event that affected both the deeper bottom waters and the upper photic zone. This conclusion is reached because of the greater amount of gammacerane and β-carotane in slice Y, the high (69 wt.%) pyrite content, and the higher iR/$C_{18}$ AI ratio, lower AIR and greater EOM content (per unit weight of rock) in slice Y compared to slice X (Tables 5.1 and 5.2). The pyrite enrichment in slice Y was significantly prompted by abundant $H_2S$, as deduced by the iR/P ratio in slice Y which is much higher than in slice X (Table 5.1). The $H_2S$ was copious enough to form a high amount of pyrite, and to drive greater amounts of anaerobic photosynthesisers (e.g. green sulphur bacteria (GSB)). The lower AIR (Table 5.2) is consistent with more persistent PZE in slice Y than in slice X (Schwark and Frimmel, 2004). Consequently, there was more intense bacterial sulphate reduction (BSR) which generated the oxidant $H_2S$ for the

GSB/PSB that are interpreted to have thrived during deposition of slice Y (Grice et al., 1996; Melendez et al., 2013). Given that the sulphate-reducing bacteria (SRB) are obligate anaerobes, the terminal electron acceptor (sulphate) supply is important in this anaerobic environment. Canfield (2001) proposed four possible external inputs of sulphate for lake waters: dissolved gypsum and pyrite from old strata, atmospheric precipitation, emissions from a volcano or hydrothermal system, and marine sulphate from seawater incursions. No discernible 24-*n*/*iso*-propylcholestanes were identified in the slices, due to a detection issue related to crosstalk fragments from the *m/z* 414→231 mass transition to the *m/z* 414→217 mass transition (Peters et al., 2005), therefore a marine sulphate source is not ascertained by biomarkers. Nonetheless, a marine source cannot be fully ruled out because the sulphur isotopes ($\delta^{34}S$ = 15–24‰) (Yuan et al., 2008), have a similar isotope range to marine sulphur isotopes during deposition. There is a suite of gypsum and halite interbeds in the Es4 member in the north-eastern Dongying Depression, close to where the L110 well (Li et al., 2003). Given the arid palaeoclimate (Hao et al., 2009), one other possible origin of the sulphate for the BSR is dissolution of gypsum or pyrite (reduced $S^{2-}$) in the Es4 member during the intensive faulting.

Based on the higher sulphate content, slice Y was probably deposited in a more saline water column than slice X, which is also consistent with the higher gammacerane index (G/H; Table 5.1) and the higher β-carotane relative abundance in slice Y (Table 5.1). Interestingly, the MTTC index (MTTCI = α-MTTC/total MTTCs) (Schwark et al., 1998) and the α/δ-MTTC ratio (Grice et al., 1998) (Fig. 5.11b) suggest a lower water salinity in slice Y (cf. slice X) than the aliphatic indicators in slice Y suggest (Schwark et al., 1998; Wang et al., 2011), thus

complicating the interpretation. Nevertheless, other reliable molecular biomarkers show significant differences in the biogeochemical-environment between the slices. The biomarkers show that slice Y must have experienced a small-scale anoxia event both in the deeper bottom waters and the upper photic zone, and the water column was more saturated with $H_2S$. The formation of abundant pyrite in slice Y is interpreted to be related to intense BSR. Thus, PZE conditions during deposition of slice Y were more persistent than in slice X.

### 5.4.2. Differences in algal species and genera

There is rarity of land plant biomarkers in the two slices. The slight *n*-alkane odd-over-even carbon number preference and the abundant HMW *n*-alkanes (Table 5.1) may not be indicative of terrigenous land plant input, but of aqueous organisms (e.g. lacustrine *Botryococcus braunii*, and SRB) (Derenne et al., 1988; Metzger et al., 1991; Huang et al., 2003; Feng et al., 2007; Riboulleau et al., 2007; Bechtel et al., 2012; Summons et al., 2013). Similarly, the weak predominance of $C_{29}$ over $C_{27}$ and $C_{28}$ regular steranes might not reflect a dominant terrigenous organic input in this case (Volkman et al., 1998). The $C_{27}$ versus $C_{29}$ regular steranes and the LMW versus HMW *n*-alkanes are probably suggestive of two different algal/bacterial contributions, as suggested by the *n*-alkane isotope profiles (Fig. 5.6). Also, the sterane/hopane ratios (St/H > 3) suggest that eukaryotic organisms (herein mainly algae) made greater organic contributions than the prokaryotic ones (e.g. heterotrophic/photosynthetic bacteria) (Grantham and Wakefield, 1988; Peters et al., 2005).

There are two groups of $\delta^{13}C$ values for the LMW and HMW *n*-alkanes, respectively (Fig. 5.6). The $\delta^{13}C$ values of the LMW *n*-alkanes are close to -30 ‰, suggesting a

heterotrophic bacterial source, consistent with photoautotrophic GSB/PSB in the photic zone (Collister, 1994). The $\delta^{13}C$ values of the HMW *n*-alkanes in the two slices are more negative than the values of HMW *n*-alkanes in the saline portion of the Parachute Creek Member, Green River Formation, Piceance Creek Basin, Colorado, and in an oil shale from Pula, Hungary, which has been attributed to a phytoplanktonic source (Collister, 1994; Lichtfouse, 1994). These reference samples have rather flat isotope profiles, but in the slice samples the *n*-alkane $\delta^{13}C$ values vary strongly with molecular weight (Fig. 5.6), suggesting there were at least two different organic inputs. The $^{13}C$ depleted HMW *n*-alkanes corroborates the non-terrigenous origins of these hydrocarbons, because higher plants are usually enriched in $^{13}C$ due to the carbon fixation pathways that leads to significant carbon isotopic fractionation (Farquhar et al., 1989; Schouten et al., 1998; van der Meer et al., 1998; Chikaraishi et al., 2004).

The palaeowater column conditions, especially the salinity, have a large impact on the composition of primary producer communities, and their diversity changes as salinity changes (Killops and Killops, 2005). Fresh, oxygenated open water has a greater diversity of organisms, whereas in closed hypersaline waters very few species survive and diversity is low (Fu et al., 1990). Dinoflagellates and coccoliths are two of the most important primary producers in the Shahejie Formation (Wang et al., 2008; Liu and Wang, 2013). Abundant dinoflagellates-related biomarkers were detected in the slice samples of this study, including 4α-methylsteranes, dinosteranes and triaromatic dinosteranes (Figs. 5.5 and 5.12). However these could have been supported by a few different environments, as Fu et al. (1990) concluded that dinoflagellate blooms occur mainly in freshwater settings, while others have

shown that dinoflagellate blooms occur mainly in saline or marine settings (Moldowan et al., 1996; Moldowan and Talyzina, 1998).

Both slices X and Y have a $C_{29}$ 4α-methylsterane predominance over the $C_{28}$ homologue, but only slice X has a $C_{30}$ 4α-methylsterane predominance over the $C_{29}$ homologue (Fig. 5.6a). Varying distributions of $C_{28\text{-}30}$ 4α-methylsteranes suggests slightly different species and genera of dinoflagellates living in differing environments (Fu et al., 1990). Moreover, slice Y contains slightly more dinosteranes and triaromatic dinosteranes than slice X (Tables 5.1 and 5.2), which is consistent with the higher St/H ratio (3.6) for slice Y. The distribution of the triaromatic dinosteranes relative to other aromatic hydrocarbons also corroborates that there was a slight difference in dinoflagellate contributions (Fig. 5.7). This variation is likely the result of changes in water column conditions, and cannot be due to thermal maturity which is invariant.

### 5.4.3. Micro-changes in environment and source inputs

Thermal maturation exerts an impact on the distribution of many aromatic hydrocarbons (e.g. Alexander et al., 1985; Chakhmakhchev and Suzuki, 1995; Li et al., 2013b). However, variations in the distribution of aromatic hydrocarbons are also used to differentiate organic sources (e.g. Alexander et al., 1988; George et al., 2007) and depositional environments (e.g. salinity, carbonate vs shale) (e.g. Riolo et al., 1985; Moldowan et al., 1986; Fan et al., 1990; Fan et al., 1991; Murillo et al., 2016). In order to record the micro-change between slices, several more aromatic compounds were compared.

The influence of microorganisms (e.g. bacterial activity) on the distribution of aromatic

hydrocarbons is significant. For example, alkylnaphthalenes in rock samples may derive from the degradation of the known bacterial biomarkers aromatic 8,14-secohopanoids (Killops, 1991). Additionally, bacterial enzymes may be catalysts for the removal of sulphur (desulphurisation) through specific pathways, and some are even capable of metabolising DBT and its alkylated derivatives (Kirimura et al., 2001; Rashidi and Ghasemali, 2006). In this study, microorganism communities are interpreted to have played a more vital role than thermal maturation in controlling the distribution of aromatic hydrocarbons, resulting in some of the observed small-scale variation between the slices, in addition to rapid differences in source inputs and environmental conditions.

*5.4.3.1. Sulphur-containing compounds*

The two slices have completely different TeMN, DBT and MDBT isomer distributions, as highlighted by the *m/z* 184 and *m/z* 198 chromatograms (Fig. 5.10a, 5.10c). The DBT content is slightly lower in slice Y than slice X (Table 5.2), with both having low DBT/P values (< 0.15), consistent with a lacustrine setting (Hughes et al., 1995). However, the DBT content relative to tetramethylnaphthalenes (DBT/1,3,6,7-TeMN and DBT/1,2,5,6 + 1,2,3,5-TeMN) differs between the slices, with relatively more DBT in slice X, consistent with micro-changes in environment. These results are somewhat surprising, given the large difference in total sulphur content between the samples (Table 5.1). This may be because incorporation of sulphur into organic compounds (the assimilatory formation of S-containing compounds such as DBT) is restrained by PZE. In comparison with the dissimilatory process of BSR, the assimilatory process requires assimilatory sulphate reduction to continue despite possible

poisoning by $H_2S$. Additionally, the formation of pyrite during early diagenesis may take-up all available $H_2S$ prior to other processes, which is in agreement with the 69.1 % pyrite content of slice Y.

Theoretically, 1-MDBT is less thermally stable than 4-MDBT due to a weak valency electron, hence the 4-MDBT/1-MDBT ratio can be used to estimate the level of thermal maturity of rocks and oils (Radke et al., 1986; George et al., 2007). However, thermal maturity is invariant for the two slices, so the higher 4-MDBT/1-MDBT ratio in slice X (Table 5.2; Fig. 5.10c) must be due to depositional environment or source input. Wang and Fingas (1995) characterised different groups of oils using isomeric ratios of MDBTs, showing a source control. Another interesting observation is that the relative amounts of dibenzofuran (DBF), fluorene and DBT vary markedly (Fig. 5.10b). The DBF content is similar to that of DBT in slice X, whereas DBF is less abundant than both DBT and fluorene in slice Y. The dominance of DBT over DBF and fluorene in slice Y may be consistent with the higher water salinity during deposition of slice Y (Fan et al., 1991; Hughes et al., 1995; Li et al., 2013a).

*5.4.3.2. Aromatic steroids*

The TAD are the most characteristic compounds in the aromatic fraction of the rock extracts (Fig. 5.12c). Based on the summed aromatic chromatograms, slice Y contains more abundant TAD than slice X (Fig. 5.7). Algae such as dinoflagellates are responsible for the TADs (Wang et al., 2008), thus slice Y may contain a greater dinoflagellate contribution than slice X. The TAS originate from the aromatisation of monoaromatic steroids (Wang et al., 2010). A similar situation is observed for the monoaromatic/triaromatic steroids (MAS/TAS;

Fig. 5.7). However in detail, the MAS, TAS and TAD distribution patterns are different for the two slices (Fig. 5.12). The main distinction is that the $C_{28}$ 20R TAS dominates in slice Y, but the $C_{27}$ 20S TAS dominates in slice X (Fig. 5.12b). This may suggest that the depositional environments are different between the two slices, or that the contributors (from algae and bacteria) to these compounds varies on a small time scale. The TAD (Fig. 5.12c) and MAS (Fig. 5.12a) distributions also subtly differ between the slices, mirroring differences in the TAS and the aliphatic 4-methylsteranes (*m/z* 231).

These characteristics could indicate either differences in depositional environment or organic source inputs, or both. Some studies have reported a dominance of $C_{28}$ TAS in fresh water environments, and more abundant $C_{26}$ TAS in more brackish and saline water environments. Saline water generally yield more total aromatic steroids (Fan et al., 1991; Meng et al., 2011). This conflicts with the salinity indicators (e.g. the gammacerane index) in the aliphatic fractions, which suggest a higher salinity for slice Y, but are consistent with the MTTCs indicators in the aromatic fractions. Nevertheless, those variations in biomarker compositions show that slice Y was deposited under slightly different water conditions to slice X.

*5.4.3.3. Alkylphenanthrenes and alkylnaphthalenes*

The total alkylphenanthrene content is higher in slice Y than in slice X relative to phenanthrene (Fig. 5.11a), but there are no obvious differences in their isomer distributions. Although some alkylphenanthrenes (i.e. 1,7-DMP and 1-MP) have been used to characterise the relative contribution of higher plants (Alexander et al., 1988; Volk et al., 2004), the OM of

these slices do not include a higher plant origin. A co-occurrence of alkylphenanthrenes and retene (Radke et al., 1998) with similar carbon isotopic compositions (Grice et al., 2001), showed they can both be derived from phyllocladane and pimarane-type (diterpanes) natural and aromatised products. However, no abietane-type diterpenoids and only trace amounts of oleanane were detected in the slices (Fig. 5.6c), suggesting they were not the source of the alkylphenanthrenes. Alkylphenanthrenes from marine shales are typically depleted in $^{13}C$ compared to terrigenous coaly samples (Radke et al., 1998). Grice et al. (2007) also suggested an algal origin for 9-methylphenanthrene. The different abundances of alkylphenanthrenes relative to phenanthrene in slice X and Y are thus attributed to different algal source inputs, rather than thermal maturity differences.

The alkylnaphthalenes ($C_2$-$C_4$) have incredibly different patterns in slices X and Y (Fig. 5.9). These differences could have resulted from variation in organic source inputs, with reworking by microorganisms during early diagenesis, rather than thermal maturity. In comparison to slice X, 1,3- + 1,7-DMN in slice Y are more abundant relative to 1,6-DMN, and 2,6-DMN is more abundant relative to 1,4- + 2,3-DMN (Fig. 5.9b). The 1,2,5-TMN, 1,2,6-TMN and 2,3,6-TMN contents also vary between the two slices. These compounds (reversed red triangles in Fig. 5.9c) have lower relative abundance compared to 1,3,5 + 1,4,6-TMN, 1,3,6-TMN and 1,2,7-TMN, respectively, (reversed green triangles in Fig. 5.9c) in slice Y than in slice X. In slice Y, 1,3,6,7-TeMN and 1,2,3,6-TeMN have a higher relative abundance than 1,2,5,7-TeMN and 1,2,4,6- + 1,2,4,7- + 1,4,6,7-TeMN, respectively (Fig. 5.9d).

The effect of thermal maturity effect on the alkylnaphthalenes has been well addressed

(Alexander et al., 1985; Strachan et al., 1988; van Aarssen et al., 1999). However, given the same level of thermal maturity experienced by the two slices, the isomeric differences must be controlled by source inputs and depositional environment differences. For example, 1,6-DMN and 1,2,5-TMN are associated mostly with *Araucariaceae* conifers (Alexander et al., 1992), and could be derived from pentacyclic triterpanes or diterpanes. Abundant 1,2,7-TMN can indicate angiosperm input in immature sediments (Strachan et al., 1988). Other isomers such as 1,3,6-TMN and 1,3,6,7-TeMN have been related to bacteria (van Aarssen et al., 2000; Peters et al., 2005). Grice et al. (2001) noted that 1,2,5-TMN has a similar $\delta^{13}C$ composition as drimanes, hopanes, regular isoprenoids, pristane and phytane, which suggests a common phytoplankton origin (cyanobacteria and algae). In addition, other alkylnaphthalenes also have similar $\delta^{13}C$ compositions with 1,2,5-TMN, suggesting a common euphotic zone source. Thus, the different alkylnaphthalene isomer distributions of the slices is further evidence for differences in organic matter input.

Coccolithophore and dinoflagellate blooms in the ancient Dongying lakes characterise the coccolith laminae and dinoflagellate laminae of shales in the Dongying Depression (Liu and Wang, 2013). The high sterane/hopane ratios of slices X and Y (>3; Table 5.1) are consistent with these being the main primary producers. Zhou et al. (2001) reported that the EOM of dried coccolithophore cells contained alkylnaphthalenes, alkylphenanthrenes, alkylbenzenes and alkylthiophenes. Coccolithophores may therefore be one of the major sources of aromatic hydrocarbons in these sources rock slices.

The absence of diterpanes, the trace amounts of oleanane, the slight odd-over-even carbon number predominance and the $^{13}C$ depleted long-chain *n*-alkanes, along with the

interpreted highly euxinic deposition conditions, collectively indicate that higher plants were not responsible for the alkyl aromatics that are abundant in both slices. It can therefore be concluded that algae and bacteria can be important sources of the aromatic hydrocarbons, as previously suggested by Killops (1991) and Radke et al. (1994). As for the variations between the slices, the most likely controls are depositional environment and algal source inputs.

### 5.4.4. BSR influence on the $\delta^{13}C$ of long-chain n-alkanes

There is a small but consistent $^{13}C$ depletion shift in the $C_{25}$ to $C_{35}$ *n*-alkanes for slice Y relative to slice X (Fig. 5.6). Given the very similar $\delta^{13}C$ values for < *n*-$C_{25}$ alkanes in both slices, this slight shift is interpreted to be mostly due to source inputs or depositional environment. To assess possible primary controls on this $C_{25}$ to $C_{35}$ *n*-alkane $^{13}C$ depletion in slice Y, prominent and distinctive biomarkers in the slices such as AIR (as shown in Fig. 5.8) were compared to the composition of three homogenised bulk samples (FS02, FE10 and FE16) from the Dongying Depression, with similar and flat isotope profiles that suggest a uniform and common microbial organic input. These three additional samples, and the two slices, are in the immature to early oil window thermal maturity range (Ro < *c.* 0.75; before or at the onset of hydrocarbon generation). They all have similar $\delta^{13}C$ values for the LMW *n*-alkanes. The three additional samples contain no diterpanes, which suggests that other effects on the HMW *n*-alkanes carbon isotopes (e.g. terrigenous land plant inputs, or thermal maturity) can be excluded in this case (Bjorøy et al., 1992; Clayton and Bjoroy, 1994).

The AIR and isorenieratane concentration seem to be very sensitive to small degrees of PZE and BSR (French et al., 2014; Liu et al., 2014; Aderoju and Bend, 2018). The FS02

sample contains no isorenieratane, has an AIR of 8.5 and the average $\delta^{13}C$ values for the $C_{25}$ to $C_{35}$ *n*-alkanes is -28.3 ‰. The FE10 and FE16 samples have similar average $\delta^{13}C$ values for the HMW *n*-alkanes (approx. -29.5‰) but lower AIR (approx. 2.4). Their iR/$C_{18}$ AI ratios are 3.7 and 5.8. These two samples thus show a relatively greater PZE and BSR signature. The average $\delta^{13}C$ values of the HMW *n*-alkanes for slices X and Y are -31.3 ‰ and -31.9 ‰, respectively (Fig. 5.6). The higher AIR in slice X (2.5) than in slice Y, and the higher iR/$C_{18}$ AI ratio in slice Y (75.4) than in slice X (Table 5.1) indicates greater PZE and BSR characteristics for slice Y relative to slice X. The $\delta^{13}C$ values of the HMW *n*-alkanes for slice Y are consistently more negative (< 1‰ difference) (Fig. 5.6). The average $\delta^{13}C$ values of the HMW *n*-alkanes of the five samples show a reasonable correlation with each of iR/$C_{18}$ AI, AIR and Pr/Ph (Fig. 5.13a-5.13c). It therefore appears that the greater $^{13}C$ depletion of the HMW *n*-alkanes in the slices is related to PZE and BSR in these samples. Little has been previously reported about the effects of BSR on the carbon isotopic compositions of *n*-alkanes. From this study, it appears that increasing PZE and BSR conditions (sourer water) leads to lower $\delta^{13}C$ values of the HMW *n*-alkanes, as described in the next paragraph.

For the two slices, the main aqueous producers contributing to the HMW *n*-alkanes were eukaryotic, based on sterane/hopane ratios >3. Their $\delta^{13}C$ values were controlled by the $\delta^{13}C$ value of the $CO_2$ that the primary producers used. The depletion in $^{13}C$ must be ascribed to a source of isotopically lighter $CO_2$. Heterotrophs have $\delta^{13}C$ values *c*. 1.0 ‰ greater than their food source (Deniro and Epstein, 1981; Hayes, 1993). Their main output is respired $CO_2$, which is isotopically lighter as a consequence of the citric acid cycle (involving decarboxylation of organic acids). Additionally, bacterial heterotrophs (such as SRB) yield

more significant isotopic fractionations (Coffin et al., 1990; Pancost and Sinninghe Damsté 2003). This $CO_2$ can be fixed by phototrophic primary producers in the upper water column, which will result in an isotopically lighter signature preserved in the rocks. Thus, it is postulated that significant PZE and BSR may lead to carbon isotopic fractionation of HMW *n*-alkanes. Furthermore, more intense BSR (and PZE) conditions may give rise to greater $^{13}C$ depletion of the HMW *n*-alkanes. This depletion may be the result of variable degrees of BSR, because SRB are heterotrophs that can oxidise organic substrates by reducing sulphate as an electron acceptor. The output $CO_2$ will then be recycled. Thus, the $\delta^{13}C$ values of the HMW *n*-alkanes vary as a function of BSR.

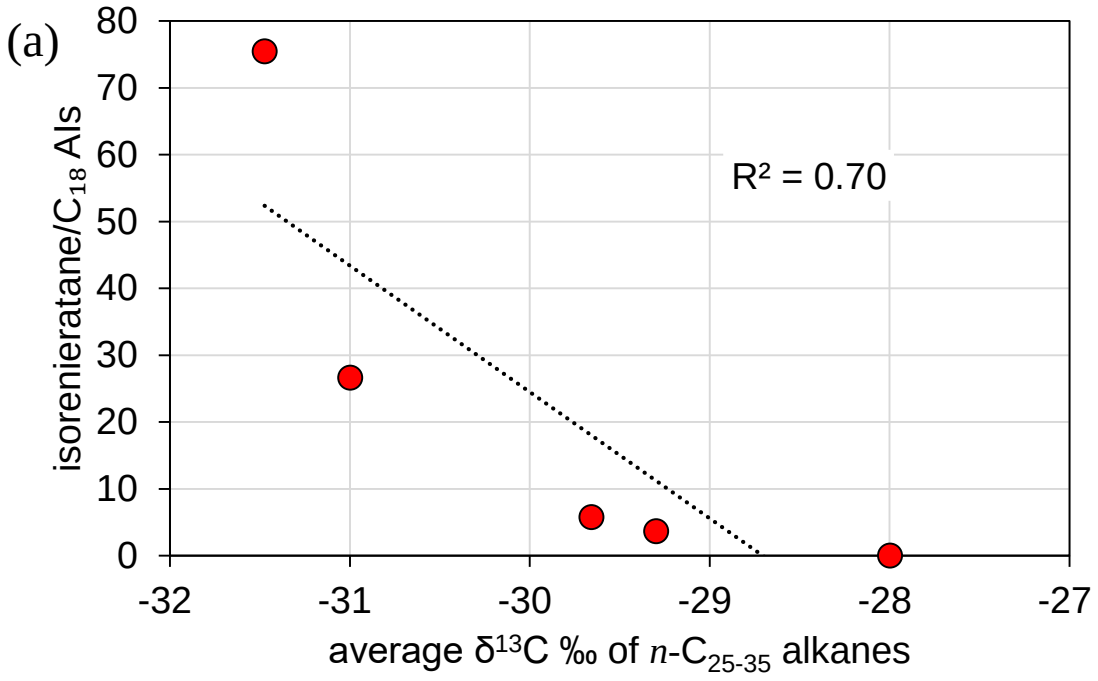


Fig. 5.13 Cross-plots of the average $\delta^{13}C$ (‰) of the $C_{25\text{-}35}$ *n*-alkanes versus (a) isorenieratane/$C_{18}$ AI ratio, (b) aryl isoprenoid ratio (AIR), and (c) pristane/phytane (Pr/Ph), showing reasonably good correlations between the HMW *n*-alkane isotopic compositions and the environment indicators.

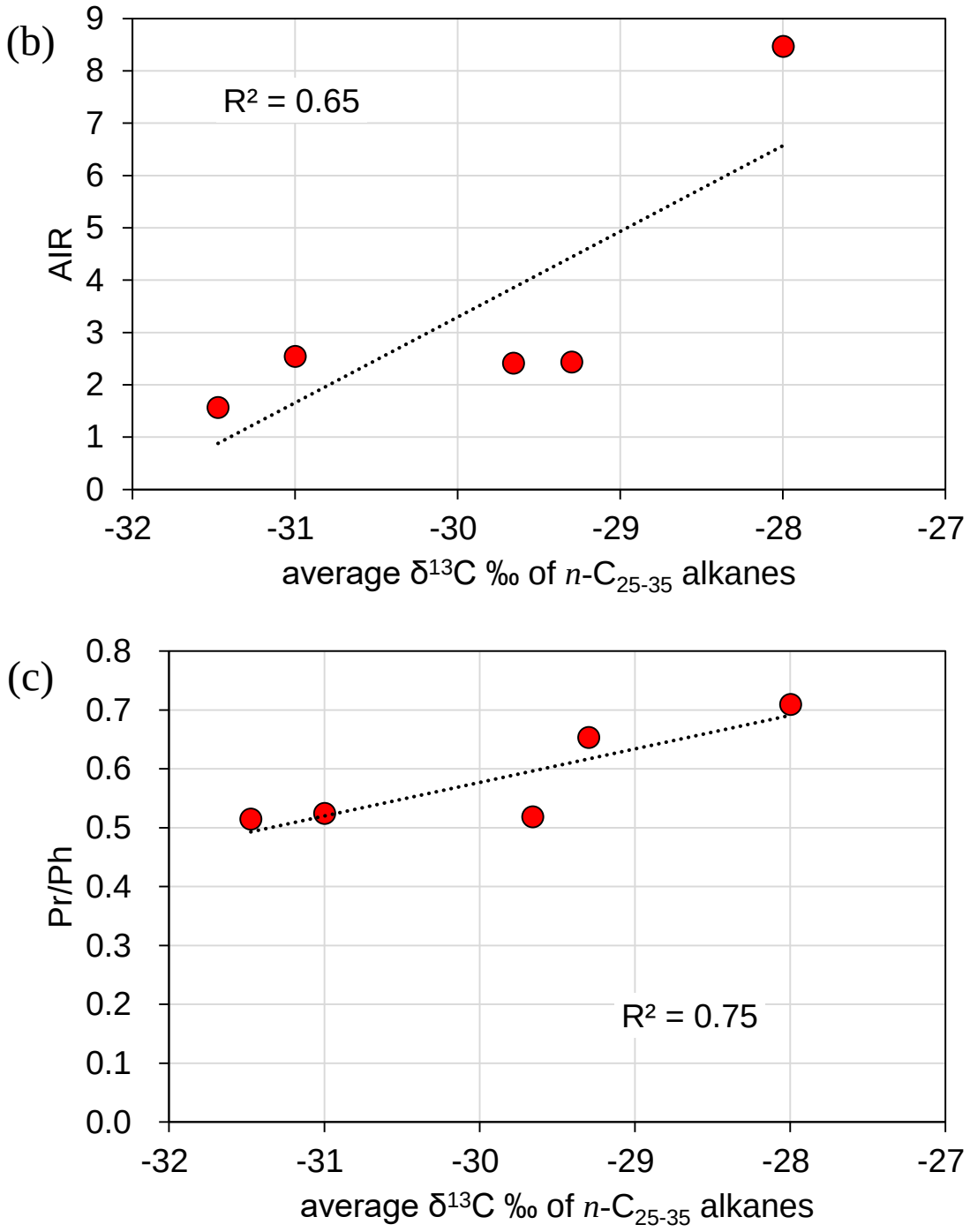


Fig. 5.13 (*continued*)

## 5.5. Summary

A well-laminated and organic-rich shale from the upper part of the fourth member of the Shahejie Formation, Dongying Depression, Bohai Bay Basin was horizontally sliced in two and investigated using mainly organic geochemical technique to unravel significant hydrocarbon variations on the millimetre scale. Heterogeneity of hydrocarbons in the organic-rich shales was recorded. In this low-maturity and organic-rich shale sample, the variation in the aliphatic and aromatic hydrocarbons shows there was rapid change in the source inputs and depositional environments.

The two slices are interpreted as having been deposited during different euxinic conditions. There are also slight differences in organic source inputs between the two slices, as shown by variations in biomarkers and aromatic hydrocarbon distributions. Water column anoxia or euxinia were not persistent as a whole during the production, transport and burial of the organic matter. Micro-scale variations of source and depositional environment in well laminated shales have not been extensively documented yet. The accumulation and preservation of organic matter is probably composed of many individual processes, rather than representing a long-period of steady-state aggregation in a depositional environment. A reasonable correlation between the HMW *n*-alkane carbon isotope ratios and the AIR, Pr/Ph and iR/$C_{18}$ AI ratios suggest that the negative $\delta^{13}C$ shift evident in the two slices (cf. the other Dongying Depression samples) is mainly controlled by the depositional environment, especially the variation of euxinic conditions on the millimetre scale.

This study records organic geochemical variability at a small scale, and helps to evaluate

the shale oil quality of the Dongying Depression, which is essential for the predictive model of future unconventional petroleum exploration and production.

## Acknowledgements

This research was supported by the National Natural Science Foundation of China (Grant No. 41472108). The authors acknowledge the experimental assistance of Carl A. Peters, Sophia Aharonovich, Konstantinos Kotzakoulakis, Huaqing Xu, and Xiong Cheng. We thanks Se Gong at CSIRO Energy for assistance with the MRM GC-MS analyses and molecular sieving. HX thanks the China University of Geosciences (Beijing) and Macquarie University for a co-tutelle PhD scholarship, and Macquarie University for analytical support funds.

# References

Aderoju, T., Bend, S., 2018. Reconstructing the palaeoecosystem and palaeodepositional environment within the Upper Devonian–Lower Mississippian Bakken Formation: A biomarker approach. Organic Geochemistry 119, 91-100.

Alexander, R., Kagi, R.I., Rowland, S.J., Sheppard, P.N., Chirila, T.V., 1985. The effects of thermal maturity on distributions of dimethylnaphthalenes and trimethylnaphthalenes in some ancient sediments and petroleums. Geochimica et Cosmochimica Acta 49, 385-395.

Alexander, R., Larcher, A.V., Kagi, R.I., Price, P.L., 1988. The use of plant-derived biomarkers for correlation of oils with source rocks in the Cooper/Eromanga Basin system, Australia. The APPEA Journal 28, 310-324.

Alexander, R., Kralert, P.G., Kagi, R.I., 1992. Kinetics and mechanism of the thermal decomposition of esters in sediments. Organic Geochemistry 19, 133–140.

Aplin, A.C., Macquaker, J.H.S., 2011. Mudstone diversity: Origin and implications for source, seal, and reservoir properties in petroleum systems. AAPG Bulletin 95, 2031-2059.

Bechtel, A., Jia, J., Strobl, S.A.I., Sachsenhofer, R.F., Liu, Z., Gratzer, R., Püttmann, W., 2012. Palaeoenvironmental conditions during deposition of the Upper Cretaceous oil shale sequences in the Songliao Basin (NE China): Implications from geochemical analysis. Organic Geochemistry 46, 76–95.

Bjorøy, M., Hall, P.B., Hustad, E., Williams, J.A., 1992. Variation in stable carbon isotope ratios of individual hydrocarbons as a function of artificial maturity. Organic Geochemistry 19, 89-105.

Canfield, D.E., 2001. Biogeochemistry of sulfur isotopes. Reviews in Mineralogy and Geochemistry 43, 607–636.

Chakhmakhchev, A., Suzuki, N., 1995. Aromatic sulfur compounds as maturity indicators for petroleums from the Buzuluk depression, Russia. Organic Geochemistry 23, 617-625.

Chikaraishi, Y., Naraoka, H., Poulson, S.R., 2004. Hydrogen and carbon isotopic fractionations of lipid biosynthesis among terrestrial (C3, C4 and CAM) and aquatic plants. Phytochemistry 65, 1369-1381.

Clayton, C.J., Bjoroy, M., 1994. Effect of maturity on $^{13}C/^{12}C$ ratios of individual compounds in North Sea oils. Organic Geochemistry 21, 737-750.

Coffin, R.B., Velinsky, D.J., Devereux, R., Price, W.A., Cifuentes, L.A., 1990. Stable carbon isotope analysis of nucleic acids to trace sources of dissolved substrates used by estuarine bacteria. Applied and Environmental Microbiology 56, 2012.

Collister, J.W., 1994. Partial resolution of sources of *n*-alkanes in the saline portion of the Parachute Creek Member, Green River Formation (Piceance Creek Basin, Colorado). Organic Geochemistry 21, 645-659.

Deniro, M.J., Epstein, S., 1981. Influence of diet on the distribution of carbon isotopes in animals. Geochimica et Cosmochimica Acta 42, 495-506.

Derenne, S., Largeau, C., Casadevall, E., Connan, J., 1988. Comparison of torbanites of various origins and evolutionary stages. Bacterial contribution to their formation. Causes of the lack of botryococcane in bitumens. Organic Geochemistry 12, 43–59.

Fan, P., Philp, R.P., Li, Z., Ying, G., 1990. Geochemical characteristics of aromatic hydrocarbons of crude oils and source rocks from different sedimentary environments.

Organic Geochemistry 16, 427-435.

Fan, P., Philp, R.P., Li, Z., Yu, X., Ying, G., 1991. Biomarker distributions in crude oils and source rocks from different sedimentary environments. Chemical Geology 93, 61-78.

Farquhar, G.D., Ehleringer, J.R., Hubick, K.T., 1989. Carbon isotope discrimination and photosynthesis. Annual Review of Plant Biology 40, 503-537.

Feng, Z., Fang, W., Zhang, J., Li, Z., Huang, C., Wang, X., Zhao, Q., Huo, Q., 2007. Distribution and significance of $C_{40+}$ alkanes in the extracts of Cretaceous source rocks from the Songliao Basin. Science in China Series D: Earth Sciences 50, 1510-1520.

French, K.L., Sepúlveda, J., Trabucho-Alexandre, J., Gröcke, D.R., Summons, R.E., 2014. Organic geochemistry of the early Toarcian oceanic anoxic event in Hawsker Bottoms, Yorkshire, England. Earth and Planetary Science Letters 390, 116-127.

Fu, J., Sheng, G., Xu, J., Eglinton, G., Gowar, A.P., Jia, R., Fan, S., Peng, P., 1990. Application of biological markers in the assessment of paleoenvironments of Chinese non-marine sediments. Organic Geochemistry 16, 769-779.

George, S.C., Volk, H., Ahmed, M., Pickel, W., Allan, T., 2007. Biomarker evidence for two sources for solid bitumens in the Subu wells: Implications for the petroleum prospectivity of the East Papuan Basin. Organic Geochemistry 38, 609–642.

Grantham, P.J., Wakefield, L.L., 1988. Variations in the sterane carbon number distributions of marine source rock derived crude oils through geological time. Organic Geochemistry 12, 61–73.

Grice, K., Schaeffer, P., Schwark, L., Maxwell, J.R., 1996. Molecular indicators of palaeoenvironmental conditions in an immature Permian shale (Kupferschiefer, Lower

Rhine Basin, north-west Germany) from free and S-bound lipids. Organic Geochemistry 25, 131–147.

Grice, K., Schouten, S., Peters, K.E., Sinninghe Damsté, J.S., 1998. Molecular isotopic characterisation of hydrocarbon biomarkers in Palaeocene-Eocene evaporitic, lacustrine source rocks from the Jianghan Basin, China. Organic Geochemistry 29, 1745-1764.

Grice, K., Audino, M., Boreham, C.J., Alexander, R., Kagi, R.I., 2001. Distributions and stable carbon isotopic compositions of biomarkers in torbanites from different palaeogeographical locations. Organic Geochemistry 32, 1195-1210.

Grice, K., Nabbefeld, B., Maslen, E., 2007. Source and significance of selected polycyclic aromatic hydrocarbons in sediments (Hovea-3 well, Perth Basin, Western Australia) spanning the Permian–Triassic boundary. Organic Geochemistry 38, 1795-1803.

Haberlah, D., Loehr, S., Kennedy, M., Debenham, N., Lattanzi, D., 2015. Innovative sub-micron SEM-EDS mineral mapping and analysis applied to Australian shale samples, AAPG International Exhibition and Conference. Society of Exploration Geophysicists and American Association of Petroleum Geologists, Melbourne, Australia, pp. 419-419.

Hao, F., Zhou, X., Zhu, Y., Zou, H., Bao, X., Kong, Q., 2009. Mechanisms of petroleum accumulation in the Bozhong sub-basin, Bohai Bay Basin, China. Part 1: Origin and occurrence of crude oils. Marine and Petroleum Geology 26, 1528-1542.

Hayes, J.M., 1993. Factors controlling $^{13}C$ contents of sedimentary organic compounds: Principles and evidence. Marine Geology 113, 111-125.

Huang, H., Zheng, Y., Zhang, Z., Li, J., 2003. Lacustrine biomass: An significant precursor of high wax oil. Chinese Science Bulletin 48, 1987–1994.

Hughes, W.B., Holba, A.G., Dzou, L.I.P., 1995. The ratios of dibenzothiophene to phenanthrene and pristane to phytane as indicators of depositional environment and lithology of petroleum source rocks. Geochimica et Cosmochimica Acta 59, 3581-3598.

Killops, S.D., 1991. Novel aromatic hydrocarbons of probable bacterial origin in a Jurassic lacustrine sequence. Organic Geochemistry 17, 25-36.

Killops, S.D., Killops, V.J., 2005. Introduction to organic geochemistry, 2nd ed. Blackwell Publishing, Oxford.

Kirimura, K., Furuya, T., Nishii, Y., Ishii, Y., Kino, K., Usami, S., 2001. Biodesulfurization of dibenzothiophene and its derivatives through the selective cleavage of carbon-sulfur bonds by a moderately thermophilic bacterim Bacillus subtilis WU-S2B. Journal of Bioscience and Bioengineering 91, 262-266.

Löhr, S., Kennedy, M., George, C.S., Williamson, R., Xu, H., 2018. Sediment microfabric records mass sedimentation of colonial cyanobacteria, rapid onset of seafloor anoxia and extensive metazoan reworking in Pliocene sapropels. The Depositional Record, in press.

Li, M.J., Shi, S.B., Wang, T.G., 2012. Identification and distribution of chrysene, methylchrysenes and their isomers in crude oils and rock extracts. Organic Geochemistry 52, 55-66.

Li, M.J., Wang, T.G., Zhong, N.N., Zhang, W.B., Sadik, A., Li, H.B., 2013a. Ternary diagram

of fluorenes, dibenzothiophenes and dibenzofurans: Indicating depositional environment of crude oil source rocks. Energy Exploration & Exploitation 31, 569-588.

Li, M.J., Zhong, N.N., Shi, S.B., Zhu, L., Tang, Y.J., 2013b. The origin of trimethyldibenzothiophenes and their application as maturity indicators in sediments from the Liaohe Basin, East China. Fuel 103, 299-307.

Li, S., Pang, X., Li, M., Jin, Z., 2003. Geochemistry of petroleum systems in the Niuzhuang South Slope of Bohai Bay Basin—part 1: source rock characterization. Organic Geochemistry 34, 389–412.

Lichtfouse, E., Derenne, S., Mariotti, A., & Largeau, C., 1994. Possible algal origin of long chain odd *n*-alkanes in immature sediments as revealed by distributions and carbon isotope ratios. Organic Geochemistry 22, 1023-1027.

Liu, C., Wang, P., 2013. The role of algal blooms in the formation of lacustrine petroleum source rocks - Evidence from Jiyang depression, Bohai Gulf Rift Basin, eastern China. Palaeogeography Palaeoclimatology Palaeoecology 388, 15–22.

Liu, Z., Liu, J., Gardner, W.S., Shank, G.C., Ostrom, N.E., 2014. The impact of Deepwater Horizon oil spill on petroleum hydrocarbons in surface waters of the northern Gulf of Mexico. Deep Sea Research Part II: Topical Studies in Oceanography 125, 383-391.

Macquaker, J.H.S., Adams, A.E., 2003. Maximizing information from fine-grained sedimentary rocks: An inclusive nomenclature for mudstones. Journal of Sedimentary Research 73, 735-744.

Macquaker, J.H.S., Bentley, S.J., Bohacs, K.M., 2010a. Wave-enhanced sediment-gravity

flows and mud dispersal across continental shelves: Reappraising sediment transport processes operating in ancient mudstone successions. Geology 38, 947-950.

Macquaker, J.H.S., Keller, M.A., Davies, S.J., 2010b. Algal Blooms and "Marine Snow": Mechanisms that enhance preservation of organic carbon in ancient fine-grained sediments. Journal of Sedimentary Research 80, 934-942.

Melendez, I., Grice, K., Trinajstic, K., Ladjavardi, M., Greenwood, P., Thompson, K., 2013. Biomarkers reveal the role of photic zone euxinia in exceptional fossil preservation: An organic geochemical perspective. Geology 41, 123–126.

Meng, J., Liu, L., Zhang, M., Wang, Y., 2011. Indicative function of aromatic hydrocarbon in crude oil on depositional environment. Journal of China University of Mining & Technology 40, 901-907.

Metzger, P., Largeau, C., Casadevall, E., 1991. Lipids and macromolecular lipids of the hydrocarbon-rich microalga *Botryococcus braunii*. Chemical structure and biosynthesis. Geochemical and biotechnological importance, in: Herz, W., Kirby, G.W., Steglich, W., Tamm, C. (Eds.), Progress in the Chemistry of Organic Natural Products. Springer, Verlag, pp. 1–70.

Moldowan, J.M., Sundararaman, P., Schoell, M., 1986. Sensitivity of biomarker properties to depositional environment and/or source input in the Lower Toarcian of SW-Germany. Organic Geochemistry 10, 915-926.

Moldowan, J.M., Dahl, J., Jacobson, S.R., Huizinga, B.J., Fago, F.J., Shetty, R., Watt, D.S., Peters, K.E., 1996. Chemostratigraphic reconstruction of biofacies: molecular evidence linking cyst-forming dinoflagellates with pre-Triassic ancestors. Geology 24,

159–162.

Moldowan, J.M., Talyzina, N.M., 1998. Biogeochemical evidence for dinoflagellate ancestors in the Early Cambrian. Science 281, 1168–1170.

Murillo, W.A., Vieth-Hillebrand, A., Horsfield, B., Wilkes, H., 2016. Petroleum source, maturity, alteration and mixing in the southwestern Barents Sea: New insights from geochemical and isotope data. Marine and Petroleum Geology 70, 119-143.

Pancost, R.D., Sinninghe Damsté, J.S., 2003. Carbon isotopic compositions of prokaryotic lipids as tracers of carbon cycling in diverse settings. Chemical Geology 195, 29-58.

Peters, K.E., Walters, C.C., Moldowan, J.M., 2005. The Biomarker Guide. Cambridge University Press, Cambridge

Peters, K.E., Walters, C.C., Moldowan, J.M., 2017. Biomarkers: Assessment of petroleum source-rock age and depositional environment, in: Sorkhabi, R. (Ed.), Encyclopedia of Petroleum Geoscience. Springer International Publishing, pp. 1-11.

Röhl, H.J., Schmid-Röhl, A., 2005. Lower Toarcian (Upper Liassic) black shales of the Central European Epicontinental Basin: A sequence stratigraphic case study from the SW German Posidonia Shale. Bangladesh Journal of Scientific & Industrial Research 82, 165-189.

Radke, M., Welte, D.H., Willsch, H., 1986. Maturity parameters based on aromatic hydrocarbons: Influence of the organic matter type. Organic Geochemistry 10, 51-63.

Radke, M., Rullkötter, J., Vriend, S.P., 1994. Distribution of naphthalenes in crude oils from the Java Sea: Source and maturation effects. Geochimica et Cosmochimica Acta 58, 3675-3689.

Radke, M., Hilkert, A., Rullkötter, J., 1998. Molecular stable carbon isotope compositions of alkylphenanthrenes in coals and marine shales related to source and maturity. Organic Geochemistry 28, 785-795.

Rahman, H.M., Kennedy, M., Löhr, S., Dewhurst, D.N., Sherwood, N., Yang, S., Horsfield, B., 2018. The influence of shale depositional fabric on the kinetics of hydrocarbon generation through control of mineral surface contact area on clay catalysis. Geochimica et Cosmochimica Acta 220, 429-448.

Rashidi, L., Ghasemali, M., 2006. Biodesulfurization of dibenzothiophene and its alkylated derivatives through the sulfur-specific pathway by the bacterium RIPI-S81. African Journal of Biotechnology 5, 351-356.

Riboulleau, A., Schnyder, J., Riquier, L., Lefebvre, V., Baudin, F., Deconinck, J.-F., 2007. Environmental change during the Early Cretaceous in the Purbeck-type Durlston Bay section (Dorset, Southern England): A biomarker approach. Organic Geochemistry 38, 1804–1823.

Riolo, J., Hussler, G., Albecht, P., Connan, J., 1985. Distribution of aromatic steroids in geological samples: Their evaluation as geochemical parameters. Organic Geochemistry 10, 981-990.

Schouten, S., Breteler, W.C.M.K., Blokker, P., Schogt, N., Rijpstra, W.I.C., Grice, K., Baas, M., Sinninghe Damsté, J.S., 1998. Biosynthetic effects on the stable carbon isotopic compositions of algal lipids: Implications for deciphering the carbon isotopic biomarker record. Geochimica et Cosmochimica Acta 62, 1397-1406.

Schwark, L., Vliex, M., Schaeffer, P., 1998. Geochemical characterization of Malm Zeta

laminated carbonates from the Franconian Alb, SW-Germany (II). Organic Geochemistry 29, 1921-1952.

Schwark, L., Frimmel, A., 2004. Chemostratigraphy of the Posidonia black shale, SW-Germany: II. Assessment of extent and persistence of photic-zone anoxia using aryl isoprenoid distributions. Chemical Geology 206, 231–248.

Sousa Júnior, G.R., Santos, A.L.S., de Lima, S.G., Lopes, J.A.D., Reis, F.A.M., Santos Neto, E.V., Chang, H.K., 2013. Evidence for euphotic zone anoxia during the deposition of Aptian source rocks based on aryl isoprenoids in petroleum, Sergipe–Alagoas Basin, northeastern Brazil. Organic Geochemistry 63, 94-104.

Strachan, M.G., Alexander, R., Kagi, R.I., 1988. Trimethylnaphthalenes in crude oils and sediments - effects of source and maturity. Geochimica et Cosmochimica Acta 52, 1255-1264.

Summons, R.E., Bird, L.R., Gillespie, A.L., Pruss, S.B., Roberts, M., Sessions, A.L., 2013. Lipid biomarkers in ooids from different locations and ages: evidence for a common bacterial flora. Geobiology 11, 420-436.

Trabucho-Alexandre, J., Dirkx, R., Veld, H., Klaver, G., de Boer, P.L., 2012. Toarcian black shales in the Dutch central graben: Record of energetic, variable depositional conditions during an oceanic anoxic event. Journal of Sedimentary Research 82, 104-120.

van Aarssen, B.G., Bastow, T.P., Alexander, R., Kagi, R.I., 1999. Distributions of methylated naphthalenes in crude oils: indicators of maturity, biodegradation and mixing. Organic Geochemistry 30, 1213-1227.

van Aarssen, B.G.K., Alexander, R., Kagi, R.I., 2000. Higher plant biomarkers reflect palaeovegetation changes during Jurassic times. Geochimica et Cosmochimica Acta 64, 1417-1424.

van der Meer, M.T.J., Schouten, S., Sinninghe Damsté, J.S., 1998. The effect of the reversed tricarboxylic acid cycle on the $^{13}C$ contents of bacterial lipids. Organic Geochemistry 28, 527-533.

Volk, H., George, S.C., Boreham, C.J., Kempton, R.H., 2004. Geochemical and compound specific carbon isotopic characterisation of fluid inclusion oils from the offshore Perth Basin, Western Australia: Implications for recognising effective oil source rocks. The APPEA Journal 44, 223-240.

Volkman, J.K., Barrett, S.M., Blackburn, S.I., Mansour, M.P., Sikes, E.L., Gelin, F., 1998. Microalgal biomarkers: A review of recent research developments. Organic Geochemistry 29, 1163–1179.

Wang, G., Wang, T.G., Simoneit, B.R.T., Chen, Z., Zhang, L., Xu, J., 2008. The distribution of molecular fossils derived from dinoflagellates in Paleogene lacustrine sediments (Bohai Bay Basin, China). Organic Geochemistry 39, 1512–1521.

Wang, G., Wang, T.G., Simoneit, B.R.T., Zhang, L., Zhang, X., 2010. Sulfur rich petroleum derived from lacustrine carbonate source rocks in Bohai Bay Basin, East China. Organic Geochemistry 41, 340-354.

Wang, L., Song, Z., Yin, Q., George, S.C., 2011. Paleosalinity significance of occurrence and distribution of methyltrimethyltridecyl chromans in the Upper Cretaceous Nenjiang Formation, Songliao Basin, China. Organic Geochemistry 42, 1411-1419.

Wang, Z., Fingas, M., 1995. Use of methyldibenzothiophenes as markers for differentiation and source identification of crude and weathered oils. Environmental Science & Technology 29, 2842-2849.

Yuan, B., Chen, S., Yuan, W., Zhu, J., 2008. Characteristics of strontium and sulfur isotopes in Shahejie Formation of Jiyang Depression. Journal of Jilin University (Earth Science Edition) 38, 613–617. (in Chinese).

Zhou, W., Wang, R., Radke, M., Wu, Q., Sheng, G., Liu, Z., 2000. Retene in pyrolysates of algal and bacterial organic matter. Organic Geochemistry 31, 757-762.

Zhou, W., Wu, Q., Wang, R., Song, Y., Zhang, L., Liu, Z., 2001. Distribution of aromatic biomarkers in pyrolysates of coccolithophore. Chinese Science Bulletin 46, 246-252.

# Tables

Table 5.1 Aliphatic hydrocarbon parameters of the two slice samples from the Es4U member of the L110 well, Dongying Depression, Bohai Bay Basin.

| Bulk and aliphatic hydrocarbon parameters | X | Y |
|---|---|---|
| TOC (%) | 5.6 | 3.5 |
| TS (%) | 0.8 | 42.4 |
| EOM (mg/g) | 9.2 | 26.0 |
| Pr/Ph | 0.52 | 0.51 |
| Pr/n-$C_{17}$ | 1.9 | 2.2 |
| Ph/n-$C_{18}$ | 5.2 | 5.1 |
| $CPI_{24-32}$ | 1.1 | 1.1 |
| n-$C_{31}$/n-$C_{19}$ | 1.8 | 2.8 |
| β-carotane/n-$C_{28}$ alkane (on areas; %) | 9.1 | 9.7 |
| β/$C_{30}$ H (on areas; %) | 21.1 | 35.4 |
| TAR | 1.8 | 3.5 |
| Σ21-/Σ22+ | 0.47 | 0.25 |
| 17/31 | 0.83 | 0.41 |
| Σ20-/Σ21+ | 0.40 | 0.20 |
| ∑n-$C_{15-19}$ (%) | 19 | 11 |
| ∑n-$C_{21-25}$ (%) | 21 | 20 |
| ∑n-$C_{27-31}$ (%) | 36 | 43 |
| Ts/(Ts+Tm) | 0.25 | 0.25 |
| $C_{30}$ αβ/(αβ+βα) hopanes | 0.88 | 0.85 |
| $C_{31}$ αβ S/(S+R) hopanes | 0.50 | 0.50 |
| 35/(35+34) | 0.49 | 0.49 |
| Homohopanes/$C_{30}$ αβ hopane | 1.16 | 1.56 |
| O/H | 0.05 | 0.07 |
| G/H | 0.22 | 0.27 |
| G/31H | 1.01 | 1.00 |
| 23/21 | 1.9 | 1.8 |
| 24/26 | 0.54 | 0.49 |
| 20/23 | 0.45 | 0.43 |
| (19+20)/23 | 0.45 | 0.43 |
| St/H | 3.1 | 3.6 |
| $C_{27}$ 20S | 0.23 | 0.24 |
| $C_{29}$ 20S | 0.11 | 0.13 |
| $C_{29}$ S/R ααα steranes | 0.12 | 0.15 |
| VRE from $C_{29}$ S/R ααα steranes (Sofer et al., 1993) | 0.41 | 0.42 |
| $C_{29}$ αββ | 0.18 | 0.21 |
| Dinosteranes/$C_{27-29}$ (on areas) | 0.30 | 0.31 |
| Dinosteranes/$C_{29}$ (on areas) | 0.65 | 0.70 |
| 29/27 | 1.3 | 1.4 |
| 28/29 | 0.46 | 0.50 |
| D/S | 0.05 | 0.06 |
| $C_{27}$ ααα 20R % | 34 | 33 |
| $C_{28}$ ααα 20R % | 21 | 22 |
| $C_{29}$ ααα 20R % | 45 | 45 |

Table 5.1 (*continued*)

TOC = total organic carbon; TS = total sulphur; EOM = extractable organic matter; β/$C_{30}$ H (%) = β-carotane/C30 αβ hopanes (%); TAR = terrigenous/aquatic ratio, ($C_{27}$ + $C_{29}$ + $C_{31}$)/($C_{15}$ + $C_{17}$ + $C_{19}$) n-alkanes; Σ21-/Σ22+ = Σn-$C_{21-}$/Σn-$C_{22+}$; 17/31 = n-$C_{17}$/n-$C_{31}$ n-alkane; Σ20-/Σ21+ = Σn-$C_{21-}$/Σn-$C_{22+}$; Σn-$C_{15-19}$ (%) = Σn-$C_{15-19}$/Σn-alkanes (%); Σn-$C_{21-25}$ (%) = Σn-$C_{21-25}$/Σn-alkanes (%); Σn-$C_{27-31}$ (%) = Σn-$C_{27-31}$/Σn-alkanes (%); $C_{27}$ 20S = $C_{27}$ ααα 20S/(20S + 20R) steranes; $C_{29}$ 20S = $C_{29}$ ααα 20S/(20S + 20R) steranes; $C_{29}$ αββ = $C_{29}$ αββ/(αββ + ααα) steranes; D/S = $C_{27}$ βα diasteranes/$C_{27}$ ααα steranes; 35/(35 + 34) = $C_{35}$ αβ hopanes/($C_{35}$ αβ hopanes + $C_{34}$ αβ hopanes); O/H = Oleanane/$C_{30}$ αβ hopane; G/H = Gammacerane/$C_{30}$ αβ hopane; G/31H = Gammacerane/C31 αβ hopane; (19 + 20)/23 = ($C_{19}$ tricyclic terpane + $C_{20}$ tricyclic terpane)/$C_{23}$ tricyclic terpane; 23/21 = $C_{23}$ tricyclic terpane/$C_{21}$ tricyclic terpane; 24/26 = $C_{24}$ tertracyclic terpane/$C_{26}$ tricyclic terpane; 20/23 = $C_{20}$ tricyclic terpane/$C_{23}$ tricyclic terpane; St/H = $C_{29}$ (ααα + αββ) steranes/$C_{29}$ αβ hopanes (on areas in m/z 191 and m/z 217); 29/27 = $C_{29}$/$C_{27}$ ααα 20R steranes; 28/29 = $C_{28}$/$C_{29}$ ααα 20R steranes.

Table 5.2 Aromatic hydrocarbon parameters of the two slice samples from the Es4U member of the L110 well, Dongying Depression, Bohai Bay Basin.

| Aromatic hydrocarbon parameters | X | Y |
|---|---|---|
| 2-MN/1-MN (MNR) | 1.5 | 1.3 |
| 2,3,6,7-/1,2,3,6-TeMN | 0.10 | 0.14 |
| 1,2,5,6-+1,2,3,5-TeMN/1,2,3,6-TeMN | 0.93 | 0.94 |
| TMNr | 0.33 | 0.33 |
| HPI | 3.5 | 4.4 |
| MPI | 0.66 | 0.78 |
| Rc (0.6xMPI)+0.4 | 0.79 | 0.87 |
| MPDF | 0.46 | 0.46 |
| 1-MP/9-MP | 1.0 | 1.1 |
| Log 1-MP/9-MP | 0.00 | 0.03 |
| 2-MP/1-MP (MPR) | 0.94 | 0.93 |
| %Rc from MPR =(0.99*Log MPR)+0.94 | 0.91 | 0.91 |
| DBT/1,3,6,7-TeMN | 2.0 | 1.4 |
| DBT/(1,2,5,6-+1,2,3,5-TeMN) | 1.0 | 0.7 |
| TeMNs/MPs | 0.61 | 0.64 |
| MPs/P | 0.92 | 1.34 |
| DBT/P | 0.11 | 0.12 |
| DBF/DBT | 1.06 | 0.65 |
| DBF/F | 3.64 | 1.07 |
| Log (1,7-DMP/X) | -0.16 | -0.12 |
| Log (Retene/9-MP) | -0.32 | -0.11 |
| Fla/(Fla+Py) | 0.38 | 0.39 |
| 4-MDBT/1-MDBT | 1.0 | 0.8 |
| α/δ-MTTC | 4.3 | 6.4 |
| MTTCI | 0.65 | 0.72 |
| TAD/(TAD+P) | 0.80 | 0.92 |
| AIR | 2.5 | 1.6 |
| iR/$C_{18}$ AI | 26.6 | 75.4 |
| iR/P | 1.4 | 8.9 |
| Log(1,7-DMP/2,3-+1,9-+4,9-+4,10-DMP) | 0.23 | 0.22 |
| Retene/P (on areas; %) | 8.1 | 17.8 |

MNR = methylnaphthalene ratio; TMNr = trimethylnaphthalene ratio (1,3,7-TMN/[1,3,7- + 1,2,5-TMN]); HPI = highe rplant index ([iHMN + Cadalene + Retene]/1,3,6,7-tetramethylnaphthalene); MPI = methylphenanthrene index (1.5 × [3-MP + 2-MP]/[P + 9-MP + 1-MP]); MPDF = methylphenanthrene distribution fraction ((3-MP + 2-MP)/ΣMPs); 1-MP/9-MP = 1-methylphenanthrene/9-methylpheanthrene; MPR = 2-methylphenanthrene/1-methylpheanthrene; DBT/1,3,6,7-TeMN = dibenzothiophene/1,3,6,7tetramethylnaphthalene; TeMNs/MPs = Σ tetramethylnaphthalenes/Σmethylphenanthrenes; MPs/P = Σ methylphenanthrenes/phenanthrene; DBT/P = dibenzothiophene/phenanthrene; DBF/DBT = dibenzofluorene/dibenzothiophene; DBF/F = dibenzofluorene/fluorene; Log(1,7-DMP/X) = Log(1,7-dimethylphenanthrene/1,3+3,9+3,10+2,10-dimethylphenanthrene; Fla/(Fla+Py) = fluoranthene/(fluoranthene+pyrene); 4-MDBT/1-MDBT = 4-methyldibenzothiophene/1-methyldibenzothiophene; MTTCI = methyltrimethyltridecylchromans index (α-MTTC/total MTTCs); TAD/(TAD+P) = triaromatic dinosterans/(triaromatic dinosterans+phenanthrene); AIR = $C_{13-17}/C_{18-22}$ monoaryl isoprenoids; iR/$C_{18}$ = isorenieratane/$C_{18}$ aryl isoprenoid; iR/P = isorenieratane/phenanthrene; Retene/P = retene/phenantherene.

Chapter 6

# 6. Petroleum sources in the Xihu Depression, East China Sea: Evidence from stable carbon isotopic compositions of individual *n*-alkanes and isoprenoids

Huiyuan Xu[a, b, c, d, *], Simon C. George[c], Dujie Hou[a, b, *], Bing Cao[d], Xiaodong Chen[d]

[a] School of Energy Resources, China University of Geosciences (Beijing), Haidian District, Beijing 100083, China

[b] Key Laboratory of Reservoir Evolution and Hydrocarbon Accumulation, Ministry of Education, Beijing 100083, China

[c] Department of Earth and Planetary Sciences and MQMarine Research Centre, Macquarie University, Sydney, NSW 2109, Australia

[d] Shanghai Branch of China National Offshore Oil Corporation, Shanghai 200030, China

---

**Chapter 6** is an oil-source correlation in the Xihu Depression, East China Sea Basin that was made for discriminating the relative contributions of mudstones and coals to petroleum.

**Statement of Author's Contribution:** This chapter is an original research paper that has been submitted to the *Journal of Petroleum Science and Engineering* (2019). 90% of this chapter was done by the first author Huiyuan Xu, including developing the project plan and timeframe, sampling, conducting laboratory experiments, processing and analysing the data, and writing the manuscript. Simon C. George helped with analysing the data and improving the manuscript, which accounts for 3%. Dujie Hou helped with designing the research, sampling, arranging the experiments, and improving the manuscript, which accounts for 3%. Bing Cao (2% contribution) and Xiaodong Chen (2% contribution) helped with developing the project plan and timeframe and sampling.

# Abstract

The molecular composition and individual *n*-alkane and isoprenoid carbon isotope compositions were determined for oils and extracts of Paleogene mudstones (TOC: 0.45-2.3%), carbonaceous mudstones (12.7-19.6%), and coals (48-60%) in the Xihu Depression, East China Sea, so as to discriminate the hydrocarbon sources of coals and associated mudstones to the petroleum generated in the basin. Abundant diterpanes (e.g., isopimarane, phyllocladane) are present in all the samples, indicative of common terrigenous inputs. Variations in the diterpenoid distributions indicate differences in the relative contribution of main plant types (e.g., gymnosperm and angiosperm plants). Coal composition reflects very high plant input (e.g., high $C_{29}$ steranes) and mudstones relatively more aqueous input (higher $C_{27}$ steranes). Other molecular differences in the relative proportions of low versus high MW *n*-alkanes (algal versus plant sources) and the isoprenoid distributions (Pr>>Ph; higher plant signature of the mudstones) were noted between samples. The differences in the $\delta^{13}C$ values of pristane and phytane indicate separate origins for these isoprenoids. A general negative sloping profile with increasing *n*-alkane carbon chain length was observed in coals, mudstones and oils from the Huangyan oilfield of the Xihu Depression, with individual *n*-alkane $\delta^{13}C$ values between -25.6‰ and -34.4‰. These values are characteristic of the isotopic compositions of C3 plants, and are also typical of fluvial/lacustrine depositional settings. Fluctuations in the isotope compositions of individual *n*-alkanes in the extracts of the coals and mudstones correlate with the relative concentration of terrigenous higher plant-derived diterpenoids, which suggests that the relative contribution of OM from plant phyla/classes (for example gymnosperm-derived diterpanes versus angiosperm-derived diterpanes) controls the carbon isotope profiles of *n*-alkanes. For samples dominated by terrigenous organic matter, long chain *n*-alkanes with a large proportion of gymnosperm input are approximately 2-3‰ enriched in $^{13}C$ relative to those with angiosperm input, regardless of lithology. This provides

a way of differentiating specific source contributions to petroleum. Oils generated from the coals have heavier $\delta^{13}C$ values with increasing chain length within a narrow range (approx. 2-3‰) and have more heterotrophic origins, whereas oils from the mudstones are more depleted in $^{13}C$ with increasing carbon number (*n*-$C_{20-31}$) and have a greater derivation from land plants. The 825B oils in the Huangyan oilfield have a greater angiosperm-sourced hydrocarbon contribution than those of the 825AD oils, which have a greater gymnosperm-sourced hydrocarbon contribution. The tricyclic and tetracyclic diterpanes and the isotopic compositions of individual *n*-alkanes and isoprenoids are effective in differentiating contributions of coals and associated mudstones to petroleum.

*Keywords*: carbon isotopes; *n*-alkanes; isoprenoids; coals; mudstones; Xihu Depression

## 6.1. Introduction

In order to correlate or mathematically group oils and source rocks in coaly basins that contain dominantly terrigenous organic matter, input from specific plant phyla can be determined using biomarkers (Weston et al., 1989; Sykes et al., 2014). Thermal maturation, depositional environment, and mixing of organic matter from multiple source rocks can obscure the discrimination of various source contributions for petroleum. In addition, the measurement of bulk isotope compositions and molecular compositions may blur or integrate the distinctions of organic matter from specific sources (e.g. chlorophyll, cuticular waxes and bacteria).

The *n*-alkanes in source rocks and oils are derived mainly from algae, photosynthetic bacteria, and leaf waxes of land plants (Eglinton and Hamilton, 1967a; Gelpi et al., 1970). They are useful for identifying source inputs, and their carbon isotopic ($\delta^{13}C$) compositions provide more accurate biogeochemical information than their molecular (i.e., relative abundance) information alone. The $\delta^{13}C$ of individual hydrocarbons has commonly been used to make oil-source and oil-oil correlations (Sofer, 1984; Murray et al., 1994; Dawson et al., 2007; Li et al., 2016). However, isotopic variations among different *n*-alkanes can complicate the interpretations. Sun et al. (2000) reported a depletion in $^{13}C$ for high molecular weight *n*-alkanes of mudstones associated with coals in the Turpan Basin, and attributed this to a large amount of algal input due to aqueous biota, resulting in $^{13}C$ depletion of specific molecules. However, Xiong et al. (2005) and Liu et al. (2006) studied the *n*-alkane carbon isotopes of source rocks in the Turpan and Huanghua basins, and did not observe significant differences in $\delta^{13}C$ values between coals and interbedded mudstones. This discrepancy may be explained by (1) the carbon source which led to significantly isotopically heavier *n*-alkanes contributed equally to both lithologies, or (2) that solely using the carbon isotopic composition of

individual hydrocarbons to make correlations may neglect the possibility of different organic matter sources contributing to identical lithologies.

However, there are several major controls on the stable carbon isotopic characteristics of *n*-alkanes in crude oils and corresponding source rocks, including organic matter sources (Rieley et al., 1991; Boreham et al., 1994; Collister et al., 1994; Murray et al., 1994), thermal maturity (due to carbon bond cracking energy) (Clayton, 1991; Schwab et al., 2005; Sackett et al., 2015), transport fractionation (Leythaeuser et al., 1984; Brother et al., 1991), and mixing of multi-charge oils (Mackenzie et al., 1988; Rooney et al., 1998; Cheng et al., 2015). Local factors such as temperature, humidity of the environment, growth rate of plants and partial pressure of $CO_2$ are also likely to influence the isotopic compositions (Schwarzbauer et al., 2013). It is generally accepted that enrichment in $^{13}C$ (heavier $\delta^{13}C$ values) of odd carbon number *n*-alkanes (>*n*-$C_{21}$) is a source indicator for the input of higher plants (Collister et al., 1992). However, Zhou et al. (2010) studied the sawtooth patterns of the $\delta^{13}C$ of these *n*-alkanes and showed that both odd and even carbon number *n*-alkanes could have originated from terrigenous higher plants, but via different biochemical pathways. Diverse vegetation controlled by palaeoenvironmental and palaeoclimatic conditions will impact the carbon isotopic compositions of plants assimilating $CO_2$. Thus, molecular compounds from specific plants detected in sediments should ultimately inherit the corresponding isotopic compositions of their source plants (Grice et al., 2005a). Consequently, fluids generated from the varying source rocks should exhibit unique organic geochemical characteristics.

The Xihu Depression is an elongate NNE trending feature that is located in the northeast of the Cenozoic East China Sea Basin on the continental shelf, offshore from Shanghai (Fig. 6.1a). It covers a region of about 46,000 $km^2$, and is the depression with the best potential source rocks in the basin (Li and Li, 2003; Ye et al., 2007). The Xihu Depression is separated into five tectonic belts which are designated, from west to east, the West Slope Belt, the West

Sub-depression, the Central Inversion Tectonic Belt, the East Sub-depression and the East Fault Belt. The traps discovered in the Xihu Depression are mostly distributed in two oilfields, the Pinghu oilfield in the Pinghu Slope Belt (part of the West Slope Belt), and the Huangyan oilfield in the Huangyan Tectonic Belt (part of the Central Inversion Tectonic Belt). Four key oil- and gas-bearing intervals have been recognised (Gu et al., 2005; Ye et al., 2007), including the Pinghu, Huagang, Longjing and Yuquan formations. The Oligocene Huagang and Eocene Pinghu formations are the major source intervals (Fig. 6.1b). The Pinghu Formation contains the main reservoir rocks. The Huagang and Pinghu formations are mainly comprised of siltstones, mudstones, carbonaceous mudstones and coals (the latter with an aggregate thickness of 22-42 m and a maximum total organic carbon (TOC) of 60.3%), which were deposited in fluvial, deltaic and lacustrine environments (Chen, 1998; Zhu et al., 2012). The crude oils have a low density (0.75-0.82 g/cm$^3$), low wax content (<1%), low sulphur, and low V/Ni ratios (Ye et al., 2007; Zhu et al., 2012; Su et al., 2013). Dominant higher plant inputs are suggested by abundant diterpenoids, a predominance of $C_{29}$ over $C_{27}$ and $C_{28}$ steranes, and low methyldibenzothiophene/methyldibenzofuran ratios and high pristane/phytane (Pr/Ph) ratios (> 3.0) indicate oxic depositional conditions (Philp et al., 1983; Mackenzie, 1984; Noble et al., 1985; Hughes et al., 1995). Tricyclic- and tetracyclic diterpenoids are abundant; they are the most characteristic biomarkers of the sediments in the Xihu Depression coal-bearing petroleum system (Zhu et al., 2012).

Diterpenoids are also common in other terrigenous-organic matter-dominated basins, including the Gippsland and Cooper-Eromanga basins in Australia (Noble et al., 1985; Alexander et al., 1988, 1992), the Beaufort-MacKenzie Basin in Canada (Snowdon, 1980), and the Taranaki Basin in New Zealand (Murray et al., 1998; Killops et al., 2003). Due to different carbon fixation pathways the respective contribution from higher plant and resin-derived organic matter can affect the composition and carbon isotopic values of hydrocarbons

in sedimentary organic matter. Organic matter differences can also arise from input from different parts of land plants (e.g. leaf wax, cuticle wax, heartwood resin) (Leavitt and Long, 1982; Tegelaar et al., 1989; Collister et al., 1994; Lloyd and Farquhar, 1994; Lockheart et al., 1997; Murray et al., 1998), as well as different plant phylum (Tuo et al., 2003). For example, typical $\delta^{13}C$ values for gymnosperm conifer woods are -23‰, and for angiosperm woods are -26‰ (Murray et al., 1998; Lucke et al., 1999; Cernusak et al., 2008). More generally, there have been long, ongoing and to some extent unresolved discussions of the relative contribution of coals and terrigenous mudstones to oil in these type of basins (Murchison, 1987; Pepper and Corvi, 1995; Wilkins and George, 2002; Abbassi et al., 2016).

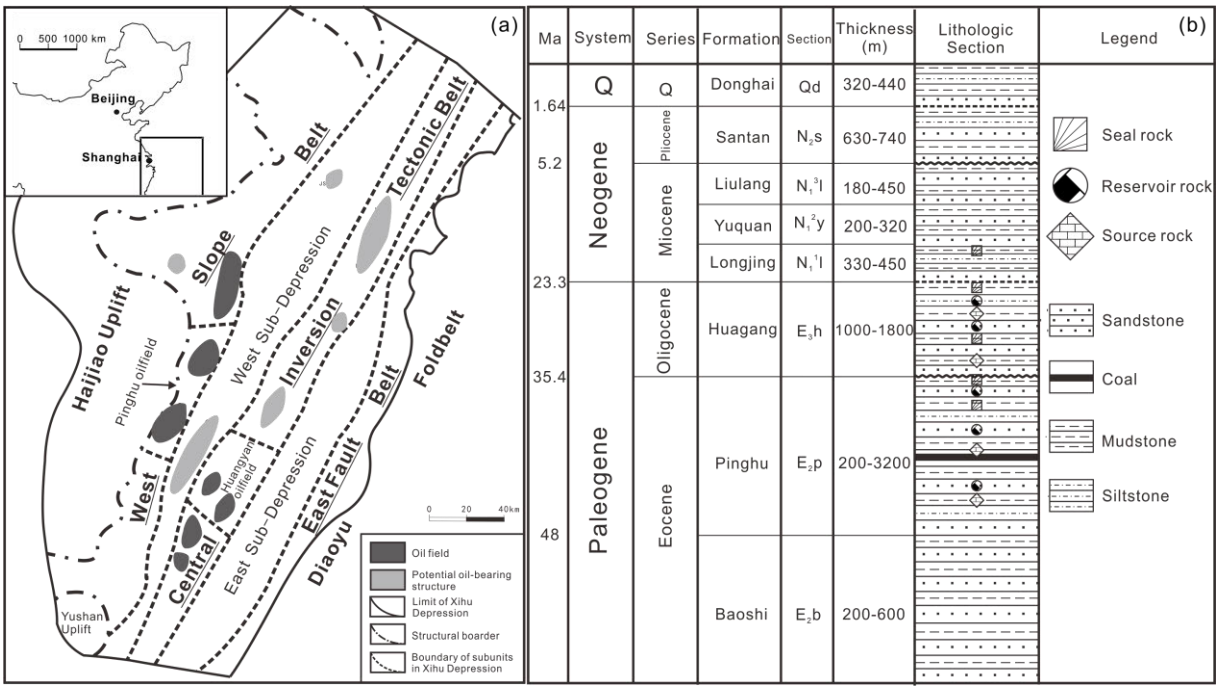


Fig. 6.1 Geological map showing the location, structural divisions and stratigraphy of the Xihu Depression, East China Sea Basin.

### 6.1.1. Study Objective

It is important for the efficiency of oil exploration to better define oil-source correlations in the Xihu Depression. In order to assess the relative contributions of coal or terrigenous mudstones to the generated oil and gas, this study relates carbon isotopic variations of *n*-alkanes and isoprenoids to the varied input of different organic matter sources. These data reveal connections between the oils, coals, and mudstones, and allow determination of the patterns and variations in hydrocarbon contributions of different sources. We observed many distinctive isotopic phenomena, such as large $\delta^{13}C$ excursions (> 4‰) in the long chain *n*-alkanes (> *n*-$C_{23}$), and variations in $\delta^{13}C$ values of *n*-$C_{17}$, pristane and phytane with depth. The likely causes of these seems to be (1) the complex interbedded coals and mudstones, (2) variations of higher plant biomarker (diterpenoid) from different classes/species, e.g. phyllocladane derived from resins of *Podocarpaceae*, *Araucariaceae*, *Taxodiaceae* and *Cupressaceae* (Noble et al., 1985; Schulze and Michaelis, 1990; Rieley et al., 1991; Otto et al., 1997), and/or (3) biogeochemical reworking (Murray et al., 1994). A detailed $\delta^{13}C$ CSIA study has been undertaken here to identify reliable correlations as well as to distinguish differences. Our results, combined with the biomarker compositions, provide unique evidence for the different terrigenous organic matter inputs to the petroleum generated in the Xihu Depression.

## 6.2. Samples and analytical methods

### 6.2.1. Samples

A suite of 10 coals, 2 carbonaceous mudstones, 7 mudstones and 5 oils from the Huangyan Oilfield (Table 6.1) of the Xihu Depression, East China Sea Basin were selected for this study. All the rock samples are from cores, and are from two Paleogene formations, the

Oligocene Huagang ($E_3h$) Formation and the Eocene Pinghu ($E_2p$) Formation (Fig. 6.1b). The coals and mudstone samples analysed are thought to be potential source rocks for the Huangyan Oilfield, based on their thermal maturity, TOC content, thickness, and widespread distribution (Ye et al., 2007). TOC values range from 0.45-2.3% for the non-carbonaceous mudstones (n=7), 12.7-19.6% for the carbonaceous mudstones (n=2), and 48-60% for the coals (n=10; Table 6.1). Organic matter is mainly comprised of vitrinite (Liu, 2004). Three Huangyan Oilfield oils and six Huangyan Oilfield mudstones and coals (Table 6.2) were analysed by gas chromatography-isotope ratio mass spectrometry (GC-IRMS).

### 6.2.2. Solvent extraction and fractionation

Homogenised rock powders of source rock samples were solvent extracted using a mixture of methanol and dichloromethane (1:9, v/v) in a Soxhlet apparatus for 72 hours. Asphaltenes were precipitated from the extractable organic matter of the rocks, and from the oils, by adding an excess volume of *n*-hexane equal to 50 times the sample volume, followed by filtration to recover the maltene fractions. The maltenes were fractionated using silica gel/ aluminium oxide (alumina) columns into saturated fractions (*n*-hexane), aromatic fractions (*n*-hexane:dichloromethane, 1:2, v:v), and polar fractions (chloroform:ethanol, 2:1, v:v).

### 6.2.3. Gas chromatography-mass spectrometry (GC-MS)

GC-MS analyses of the saturated and aromatic fractions were performed on an Agilent 6890-GC/5973-MS instrument equipped with an HP-5MS capillary column (30 m × 0.25 mm i.d. × 0.25 μm film thickness). The GC oven temperature was initially held at 50 ℃ for 1 min and was programmed to increase to 120 ℃ at 20 ℃ /min and then to 310 ℃ at 3 ℃ /min. The temperature was then held at 310 ℃ for 25 min. Helium (99.999%) was used as the carrier gas. The carrier gas flow rate (constant flow) was 1 mL/min. The inlet was held at 300 ℃, and

the samples were injected in split mode (20:1). The ion source of the mass spectrometer was operated in EI mode at 70 eV in full scan and selected ion monitoring (SIM) modes. The relative abundance of compounds was determined from peak areas using total ion current chromatograms for the integration of *n*-alkanes and isoprenoids, and selected mass chromatograms for other compounds.

### 6.2.4. Gas chromatography-isotope ratio mass spectrometry (GC-IRMS)

An aliquot of the saturated fraction from selected samples was separated into purified *n*-alkanes and branched/cyclic alkanes by urea adduction. Carbon isotopic analyses of the purified *n*-alkanes and isoprenoids were separately performed on a Thermo Scientific Delta V Advantage stable isotope ratio mass spectrometer system (IRMS) interfaced to a Trace Ultra GC (Thermo Scientific; J&W DB-5 fused silica column: 30 m × 0.25 mm i.d. and 0.25 μm film thickness). The temperature of the splitless injector was held at 300 ℃, and samples were injected in splitless mode. The GC oven temperature was initially held at 80 ℃ for 2 min and was programmed to increase to 320 ℃ at 3 ℃ /min, where it was maintained isothermally for 30 min. Helium was used as the carrier gas. The temperature of the IRMS oxidation oven was 980 ℃ and that of the reduction oven was 640 ℃. A standard mixture of *n*-alkanes and isoprenoids with known $\delta^{13}C$ values was analysed daily to test the accuracy of the instrument. The isotopic compositions of all samples are relative to VPDB, and were determined at least twice, and the standard deviation of the replicates were calculated to estimate reproducibility. The reproducibility was within 0.4‰.

## 6.3. Results and discussion

### 6.3.1. Molecular compositions

#### *6.3.1.1. n-Alkanes and isoprenoids*

The *n*-alkane distributions of the coal and mudstone source rocks differ from one another (Figs 6.2 and 6.3, respectively). Most of the mudstone samples are dominated by long chain *n*-alkanes with a unimodal distribution, maximising at *n*-$C_{27}$ and *n*-$C_{29}$, with a strong odd-over-even carbon number predominance for the high molecular weight *n*-alkanes (>*n*-$C_{23}$). The carbon preference index ($CPI_{24-34}$) of the mudstones varies from 1.16 to 1.78 (Table 6.1). This likely indicates that long chain *n*-alkanes in the mudstone samples are derived from epicuticular waxes from terrigenous vascular plants (Eglinton and Hamilton, 1967b), although several species of algae have also been reported to contribute to long chain *n*-alkanes with odd-over-even carbon number predominance (Metzger et al., 1991; Lichtfouse et al., 1994; Grice et al., 1998b). Some of the mudstone samples have slight to significant bimodal *n*-alkane distributions (e.g. well 825AD-1, 2956.0 m; Fig. 6.2), indicating mixed algal and terrigenous inputs. One sample from well 825G-1 (3044.6 m) is dominated by low molecular weight *n*-alkanes, which could suggest an algal or bacterial input. However, this sample may be overprinted by a well bore contaminant, as its thermal maturity is relatively higher than that of a nearby sample (3044.0 m) based on a lesser odd-carbon number n-alkane predominance and the lower isoprenoid/*n*-alkane ratio (Fig. 6.2). Overall, mudstones in the Huangyan Oilfield are dominated by terrigenous input, with a possible contribution from algal organic matter. In contrast the coal samples contain *n*-alkanes dominated by short- and mid-chain *n*-alkanes ranging from *n*-$C_{13}$ to *n*-$C_{34}$ and have a unimodal trace maximising in the *n*-$C_{18}$ to *n*-$C_{20}$ range (Fig. 6.3). $CPI_{24-34}$ of the mudstones is mostly lower than for the coals, varying from 1.03 to 1.2 (Table 6.1). Low molecular weight *n*-alkanes are traditionally

thought to mostly originate from bacterial and algal derivatives (Gelpi et al., 1970). A high abundance of low molecular weight *n*-alkanes has previously been considered to be related to the thriving of some specific species of algae (van Kaam-Peters et al., 1997). Given the oxic depositional conditions in the Xihu Depression (Zhu et al., 2012), the shift towards low molecular weight *n*-alkane distributions in the coals is not likely due to algal sources.

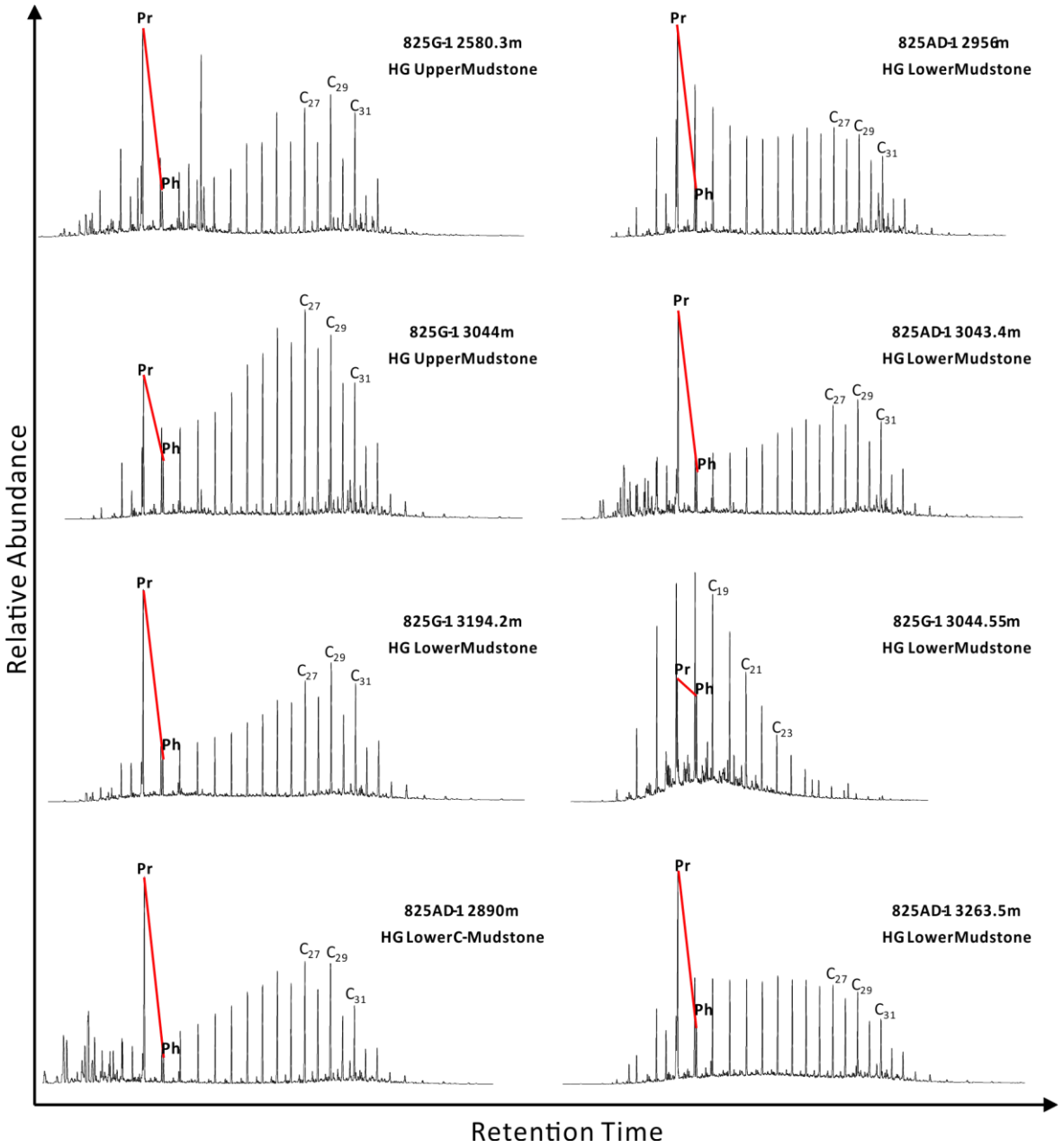


Fig. 6.2 Total ion current chromatograms showing the distribution of *n*-alkanes of selected mudstones from the Huangyan Oilfield. Numbers show the carbon number of *n*-alkanes. Pr = pristane, Ph = phytane.

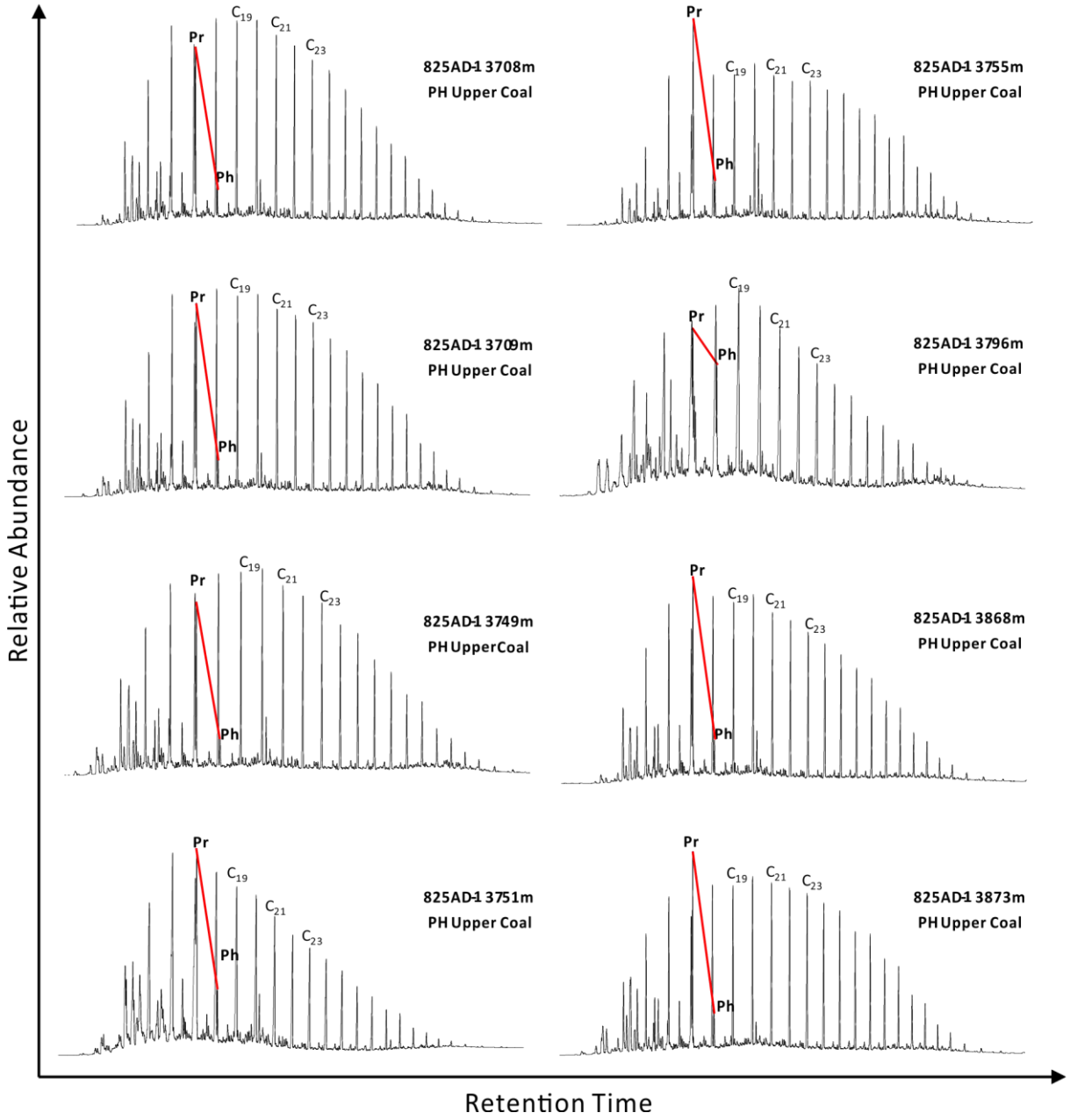


Fig. 6.3 Total ion current chromatograms showing the distribution of *n*-alkanes of selected coals from the Huangyan Oilfield. Numbers show the carbon number of *n*-alkanes. Pr = pristane, Ph = phytane.

The *n*-alkane distributions of the coals in the Xihu Depression (Fig. 6.3), which are dominated by short- and mid-chain *n*-alkanes, with an abrupt decrease towards higher molecular weight *n*-alkanes, are similar to those observed in Niger coals (Disnar and Harouna, 1994), Malgasy coals (Ramanampisoa et al., 1990) and Indian coals (Mukhopadhyay et al., 1979). There is also no significant odd-over-even carbon number preference in the Xihu

Depression coal samples (Fig. 6.3). These characteristics differ from the typical dominance of odd carbon number *n*-alkanes from $C_{27}$ to $C_{33}$ that is inherited in most coals from terrigenous angiosperm plant waxes (Eglinton and Hamilton, 1963; Tissot et al., 1977). *n*-Alkane distributions without a well-marked odd over even carbon number predominance have frequently been attributed to bacterial lipids (Tissot et al., 1977). The high abundance of the relatively thermally unstable $C_{20}$ tetracyclic diterpanes (Fig. 6.4) indicate the maturity is below the levels for thermal cracking (Powell and Snowdon, 1983; Dzou and Hughes, 1993), and indicates that maturity is not the cause of the low MW *n*-alkane dominance, or other variations in biomarker distributions. Therefore, the *n*-alkane distributions of Xihu Depression coal samples are attributed to the lipids inherited from biological precursors.

Pr/Ph ratios are known to be affected by both thermal maturation (Tissot and Welte, 1984) and variations in the precursors of these acyclic isoprenoids (Blumer and Snyder, 1965; Goossens et al., 1984; Rowland, 1990a). The high abundance of pristane (average Pr/Ph >4.0) for almost all the sample extracts in the Xihu Depression is consistent with predominantly higher plant derived organic matter deposited in a suboxic to oxic environment (Simoneit and Didyk, 1978). Inspection of the *m/z* 125 mass chromatograms indicates that β-carotane was not present in any samples above detection limit.

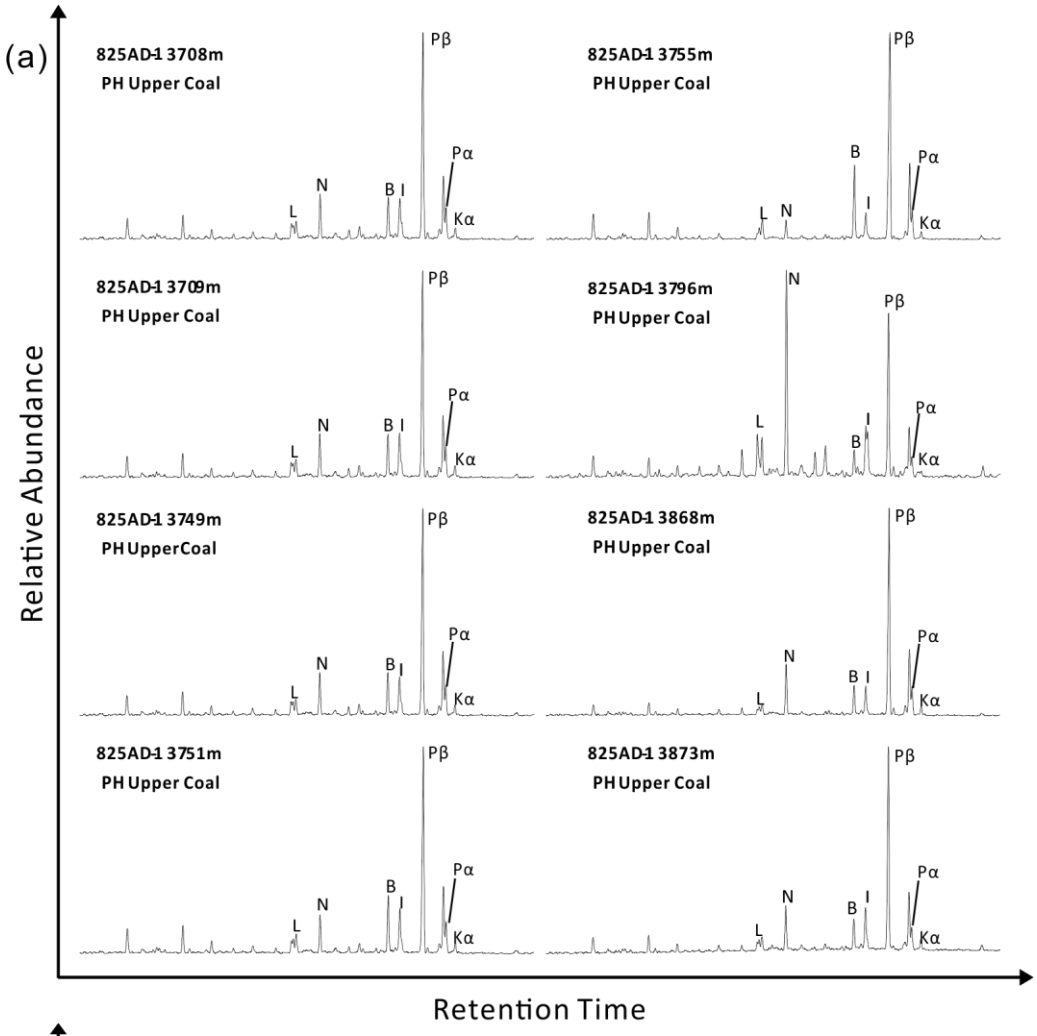
(a)
825AD-1 3708m
PH Upper Coal
825AD-1 3755m
PH Upper Coal
825AD-1 3709m
PH Upper Coal
825AD-1 3796m
PH Upper Coal
825AD-1 3749m
PH UpperCoal
825AD-1 3868m
PH Upper Coal
825AD-1 3751m
PH Upper Coal
825AD-1 3873m
PH Upper Coal
Pβ
Pα
Kα
L
N
B
I
Relative Abundance
Retention Time

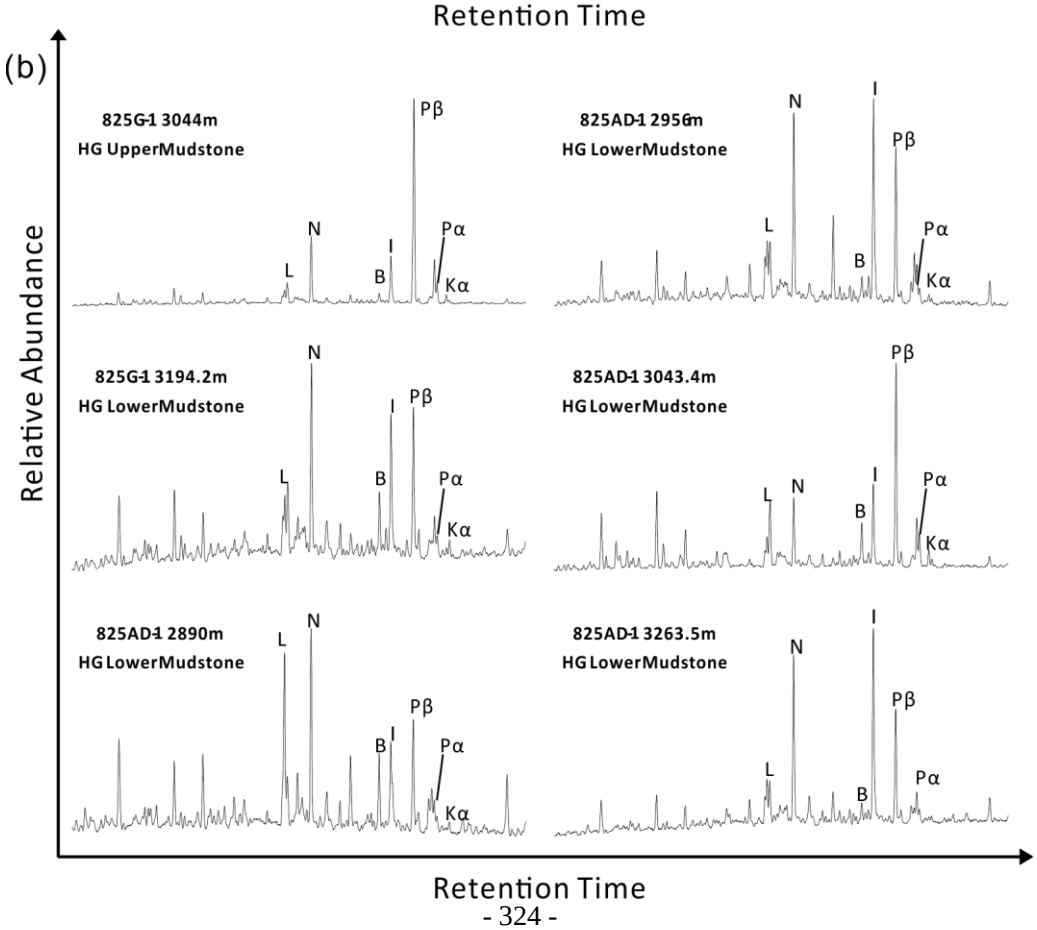
(b)
825G-1 3044m
HG UpperMudstone
825AD-1 2956m
HG LowerMudstone
825G-1 3194.2m
HG LowerMudstone
825AD-1 3043.4m
HG LowerMudstone
825AD-1 2890m
HG LowerMudstone
825AD-1 3263.5m
HG LowerMudstone
Pβ
Pα
Kα
L
N
B
I
Relative Abundance
Retention Time

Fig. 6.4 Partial mass *m/z* 123 chromatograms showing the distribution of diterpenoids in representative (a) coal extracts and (b) mudstone extracts from the Huangyan Oilfield. Peak annotations: L = 8β(H)-labdane; N = 4β(H)-19-norisopimarane; B = beyerane; I = isopimarane; Pβ = 16β(H)-phyllocladane; Pα = 16α(H)-phyllocladane; Kα = 16α(H)-kaurane.

### *6.3.1.2. Tricyclic and tetracyclic diterpenoids*

In the Xihu Depression, one of the most characteristic features of the molecular composition of oils and rocks is the abundant diterpane content (base peak *m/z* 123) eluting at retention times near that of *n*-$C_{19}$ and *n*-$C_{20}$. Diterpanes are considered to be derived primarily from vascular plants (Simoneit et al., 1986), and are widely used to evaluate terrigenous input. The Xihu coals and mudstones contain varying abundances of diterpanes in the *m/z* 123 chromatograms (Fig. 6.4), including a bicyclic diterpane (8β(H)-labdane), tricyclic diterpanes (4β(H)-norisopimarane and isopimarane) with a molecular weight of 276 amu, and tetracyclic diterpanes (*ent*-beyerane, 16β(H)-phyllocladane, 16α(H)-phyllocladane, 16α(H)-kaurane) with a molecular weight of 274 amu.

Unlike the tricyclic diterpanes, which have a broad range of precursors, the tetracyclic diterpanes are derived from a more restricted range of gymnosperm conifer resins (Alexander et al., 1987). 4β(H)-Norisopimarane (N) and isopimarane (Pβ) are relatively more abundant in the mudstones than the coals, with the exception of a coal sample from the 825AD-1 well (3796.0m; Fig. 6.4). This is consistent with different land plant contributions to the organic matter in the interbedded mudstones compared to the coals, as shown by spider diagrams of the diterpane distributions (Fig. 6.5a and b). The ratios isopimarane/16β(H)-phyllocladane and 4β(H)-norisopimarane/(4β(H)-norisopimarane + 16β(H)-phyllocladane) are 0.07-1.41 (average 0.29) and 0.06-0.55 (average 0.18) for the coal extracts, and 0.04-1.74 (average 0.78) and 0.11-0.64 (average 0.40) for the mudstone extracts, respectively, showing a significant difference from one another (Fig. 6.5c). These ratios, along with the relative amounts of

tricyclic and tetracyclic diterpanes (Fig. 6.5d), can preliminarily differentiate coals and mudstones, as these are source-related biomarkers that are suggestive of their distinct origins.

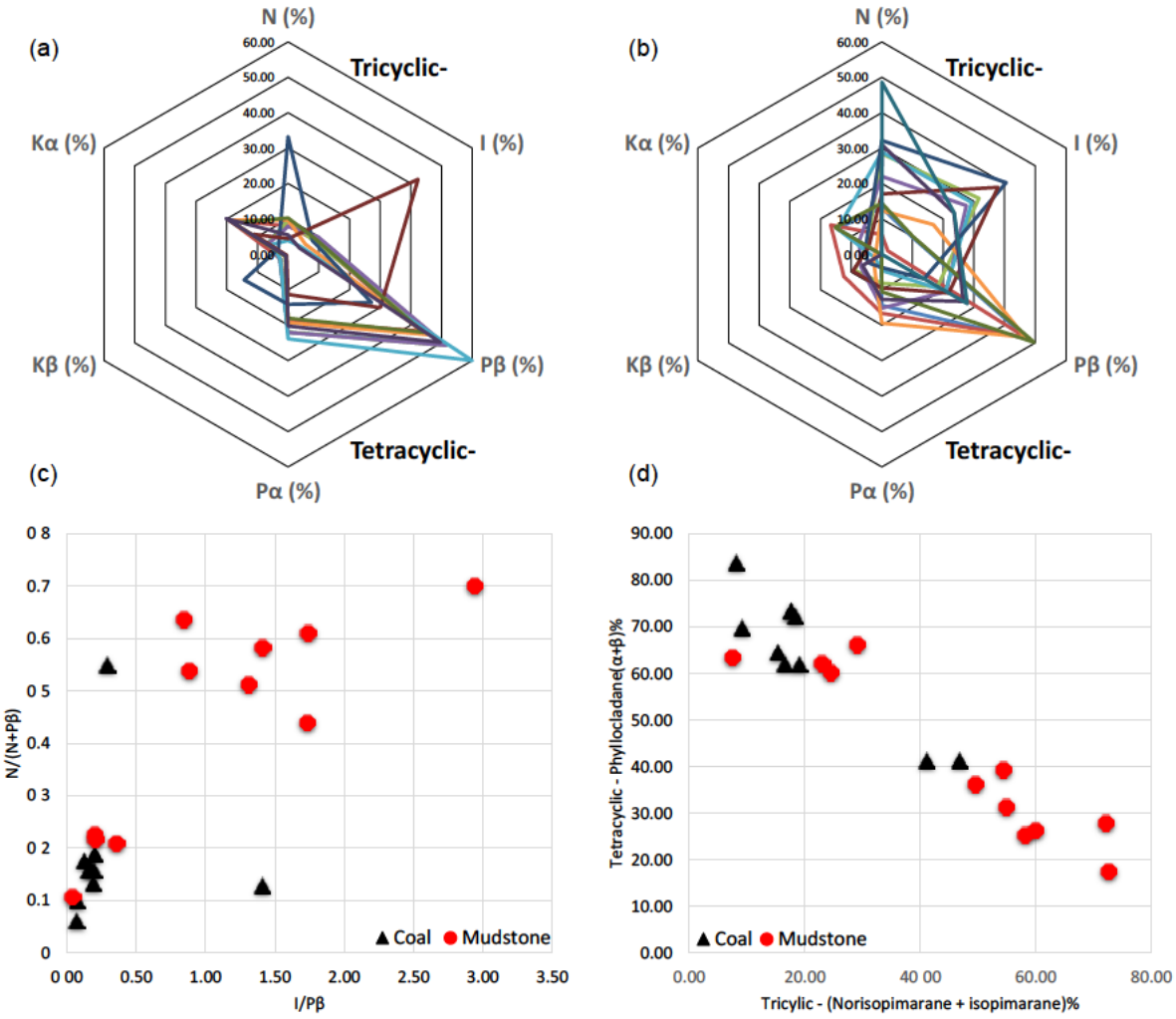


Fig. 6.5 Diterpane distributions for source rocks from the Xihu depression, East China Sea Basin. Spider diagrams show the variation in higher plant related diterpenoids for (a) coal extracts and (b) mudstone extracts. Cross-plots are shown for (c) % tetracyclic diterpanes (16β(H)-phyllocladane + 16α(H)-phyllocladane versus % tricyclic diterpanes (4β(H)-19-norisopimarane + isopimarane), and (d) 4β(H)-norisopimarane/(4β(H)-norisopimarane + 16β(H)-phyllocladane) versus isopimarane/16β(H)-phyllocladane. For peak abbreviations see the caption to Fig. 6.4.

There are no unambiguous reports that the relative distributions of diterpanes are influenced by thermal maturity. On the contrary, in New Zealand there was variation in the diterpane distributions in samples from both outcrop (vitrinite reflectances < 0.7% Ro) and mature sediments (petroleum exploration wells from the *Trichotomosulcites subgranulatus* zone), but no straightforward correlation between these biomarker groups and thermal

maturity was observed (Killops et al., 2003). In this study, the coal sample 825AD-1 3796m has a dominant peak of 4β(H)-19-norisopimarane over the other diterpanes, whereas the other coal samples (from 3708m to 3873m) are characterised by dominant 16β(H)-phyllocladane (Fig. 6.4a). This distribution is inconsistent with any maturity effects on the abundance of the diterpanes, but instead most likely reflects variations in the source of organic matter or the depositional environment.

*6.3.1.3. Steranes*

$C_{29}$-steroids are typically derived from land plants in the age ranges being considered in the Xihu trough (Volkman, 1986), Phytoplankton are the dominant source of $C_{27}$ steroids; apart from several well known exceptions (Volkman et al., 1998; Volkman, 2005). The investigated coal samples had a high relative abundance of $C_{29}$ steranes (60%-70%; Table 6.1; Fig. 6.6), consistent with a dominance of terrigenous higher plant organic matter input (Huang and Meinschein, 1979; Volkman, 2003).

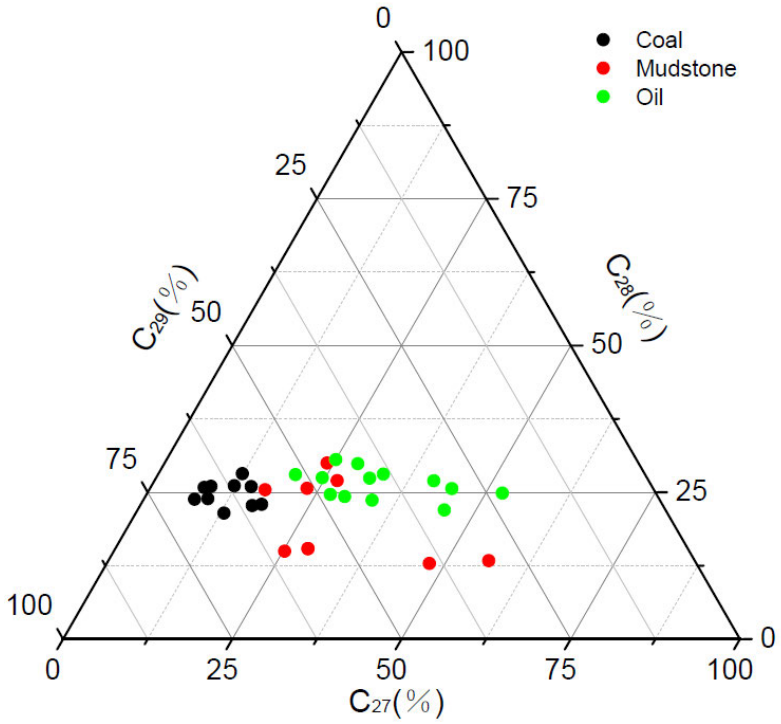


Fig. 6.6 Ternary diagram showing the relative abundance of $C_{27}$, $C_{28}$ and $C_{29}$ regular steranes (20S-ααα + 20R-αββ + 20S-αββ + 20R-ααα) in the aliphatic fractions of coals, mudstones and oils in the Huangyan Oilfield.

In comparison, the interbedded mudstone samples contain relatively less $C_{29}$ steranes along with a wider range (30%-60%; Table 6.1), and relatively more $C_{27}$ sterane content; nevertheless, they still have a considerable contribution of $C_{29}$ steranes. The oils plot, in part, over the range of the mudstones on a sterane ternary diagram (Fig. 6.6), suggesting that they may have been sourced from the mudstones. The obvious distinction in the sterane distribution between the coals and the mudstones can be explained by additional aqueous organic matter inputs into the mudstones.

The $C_{29}$ sterane 20S/(20S + 20R) and ββ/(ββ + αα) ratio ranges of the Huangyan Oilfield coals are 0.41-0.56 (average 0.45) and 0.27-0.58 (average 0.52), respectively (Table 6.1). In contrast, the mudstones have ratio ranges of 0.36-0.42 (average 0.44) and 0.33-0.51 (average 0.45), respectively (Table 6.1). The sterane ratios have approached their pseudo-equilibrium values (0.52-0.55 for 20S/(20S + 20R), 0.67-0.70 for ββ/(ββ + αα); (Seifert and Moldowan, 1986; Peters et al., 2005), which suggests that the coals and the mudstones are within the oil window (Table 6.1). The thermal maturity of the coals is slightly higher than that of the mudstones, based on the average $C_{29}$ αββ/(αββ + ααα) ratios (Table 6.1). However, the slight differences in thermal maturity are unlikely to be responsible for the variation in the distributions of the diterpanes and the carbon isotopic compositions of the *n*-alkanes.

### 6.3.2. Individual hydrocarbon carbon isotopes

The carbon isotope compositions of modern plants and palaeosediments have been studied extensively (Collister et al., 1994; Huang et al., 1995; Lockheart et al., 1997; Murray et al., 1998), and this section will discuss the main controls on these compositions. Palaeoenvironment and palaeoclimate are major factors controlling isotope shifts (Korner et al., 1988; Hasegawa et al., 2003). Other important factors related to the growth of plants include pressure of $CO_2$ ($pCO_2$), cell geometry features (Popp et al., 1998), and phytoplankton

growth rate (Bidigare et al., 1997). For higher plants, the photosynthetic pathway (C3, C4 or CAM [crassulacean acid metabolism]) is the original determinant of their carbon isotopic fractionation profile (Farquhar et al., 1989), and there can be up to 20‰ differences in $\delta^{13}C$ within the carbon of an individual organism (Schouten et al., 1998; van der Meer et al., 1998). Gymnosperms are relatively enriched in $^{13}C$ compared to angiosperms, by up to ca. 4-5‰ (Chikaraishi et al., 2004), the most likely cause being that their different stomatal structures influence their carbon sequestration (Grice and Brocks, 2011). The diverse organic matter precursors might also be apparent in the shapes of the *n*-alkane isotopic profiles (Murray et al., 1994). As a generalisation, the $\delta^{13}C$ values of short-chain, mid-chain and long chain *n*-alkanes are likely to reflect the carbon isotopic compositions of organic matter derived from bacteria, aquatic organisms and land plants, respectively (Song et al., 2013). Sun et al. (2000) examined the carbon isotopic compositions of coals and interbedded shales in the Turpan Basin, China, and suggested that land plant organic matter inputs in the coals caused enrichment in $^{13}C$ of *n*-alkanes relative to mudstones, which had more dominant algal organic matter inputs. Moreover, Kotarba and Clayton (2003) have concluded that the isotopic shift for coals on the Sofer (1984) diagram is caused by different mechanisms of isotopic fractionation during coalification of organic matter in comparison to that of carbonaceous mudstones. A mineral catalysis effect could also contribute different isotopic fractionations of coals and carbonaceous mudstones (McCollom and Seewald, 2006). Thermal maturity or burial depth can also affect the $\delta^{13}C$ compositions of individual *n*-alkanes, but in a very limited carbon number range (Bjorøy et al., 1991; Tuo et al., 2003; Song et al., 2013; Cheng et al., 2015). Evaporative fractionation can slightly alter the carbon isotopic composition of fluvial-deltaic oils or condensates by less than 0.5‰ (Dzou and Hughes, 1993). For fluvial-deltaic oils, negatively sloping *n*-alkane isotope curves are considered to indicate abundant land plant inputs (Murray et al., 1994). In summary, for predominantly terrigenous

sedimentary systems, source inputs are largely thought to be the primary factor determining isotopic compositions of *n*-alkanes and isoprenoids across a carbon number range from $C_{13}$ to $C_{35}$.

*6.3.2.1. Carbon isotopes of n-alkanes*

In this study GC-IRMS analyses were carried out to help resolve differences. The carbon isotopic data of *n*-alkanes, pristane and phytane in the source rocks extracts and oils from the Huangyan Oilfield are listed in Table 6.2. Figure 6.7 shows a general negatively sloping trend with carbon chain length, with $\delta^{13}C$ values between -25.6‰ and -34.4‰. These values are characteristic of the isotopic compositions of C3 plants (-23‰ to -34‰, with an average value of about -27‰) (Smith and Epstein, 1971). Thus, these data are consistent with typical fluvial/lacustrine depositional settings (Murray et al., 1994), and are also in agreement with other higher plant-derived coals as reported by Schoell et al. (1994), Simoneit et al. (1995), Sun et al. (2000) and Tuo et al. (2003). The increased$^{13}C$ depletion of the long chain *n*-alkanes are typical of C3 land plants, and the enriched $^{13}C$ values for short-chain alkanes are suggestive of significant contributions from bacterial or aquatic organisms. Thus the *n*-alkanes analysed here could have mixed sources, including phytoplankton as well as terrigenous and aquatic plants (Collister et al., 1994; Tulipani et al., 2014).

In the Huangyan Oilfield samples, a distinct difference is observed between the mudstones and the coals. The coals have relatively flat *n*-alkane isotopic distribution profiles from *n*-$C_{15}$ to *n*-$C_{29,}$ whereas the one non-carbonaceous mudstone (M1) displays a slightly negatively sloping profile (Fig. 6.7). However, the carbonaceous mudstone (M2) has a relatively flat and uniform *n*-alkane isotopic pattern from *n*-$C_{19}$ to *n*-$C_{29}$, with a relatively depleted $\delta^{13}C$ range (-29.9‰ to -30.5‰) compared to coals (-26 to -28‰). This may be a result of differences in the plant community composition due to large inter-species variation in

the isotope composition of higher plant waxes (Rieley et al., 1991), which could contribute to the 19.6% TOC of this sample and typical coaly sources or homogeneous precursors, placing it between coals and mudstones (Eglinton, 1994; Murray et al., 1994; Sun et al., 2000; Ahmed et al., 2009). The three oils have large isotopic differences. One oil sample (O1) is relatively isotopically heavy up to the n-$C_{27}$ alkane, and the higher molecular weight *n*-alkanes are isotopically lighter by a few ‰. The other two oil samples (O2 and O3) display the most negatively sloping isotopic profile from *n*-$C_{15}$ to *n*-$C_{30}$.

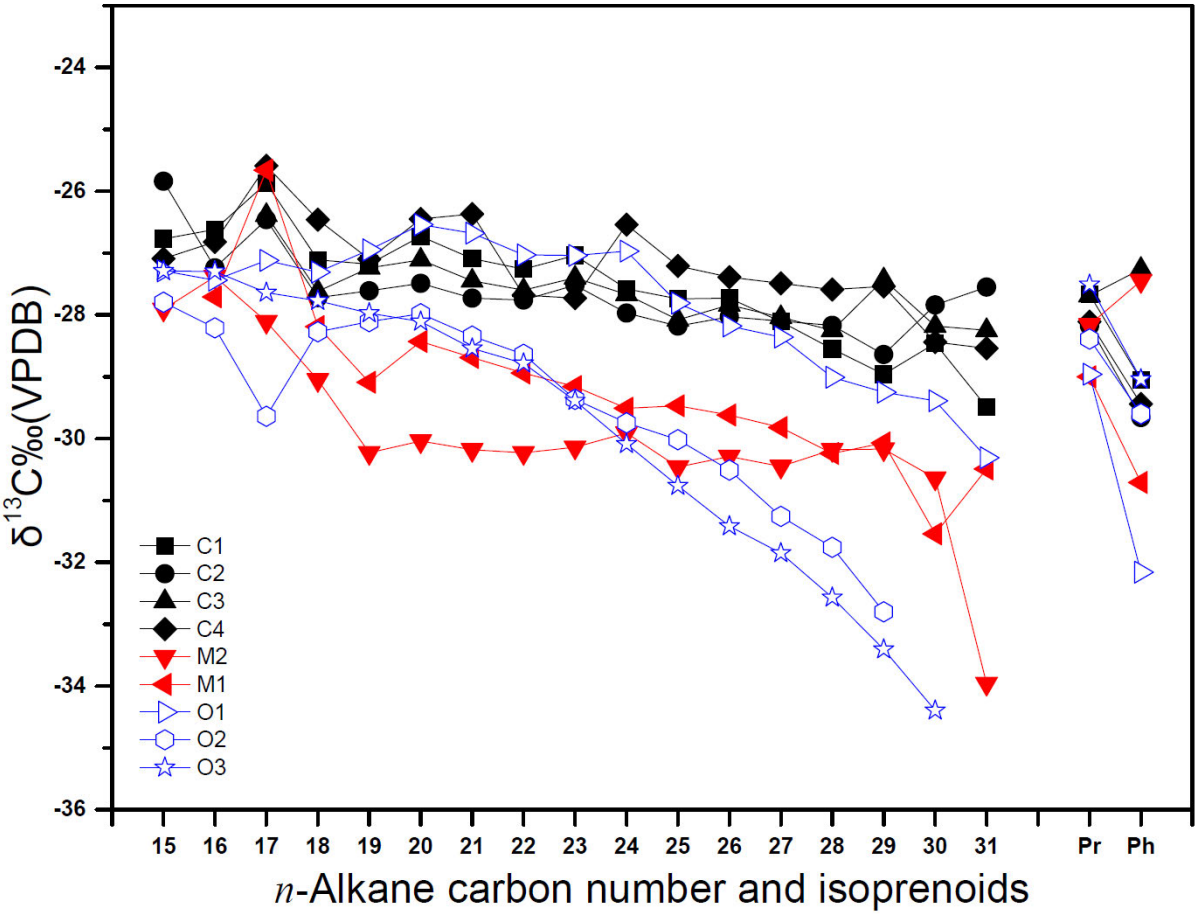


Fig. 6.7 $\delta^{13}C$ values of individual *n*-alkanes and isoprenoids in coals, mudstones and oils from the Huangyan Oilfield. For letter-number designations see Table 6.2.

The isotope profiles of the $C_{15}$ to $C_{20}$ *n*-alkanes for all samples seem to be relatively heavy and rather similar to each other, except for the M2 sample. However, the >$C_{21}$ *n*-alkanes of two of the oils (O2, O3) and the M1 mudstone become isotopically lighter with

increasing carbon chain length. These prominent variations are ascribed to different source inputs rather than other factors. Two of the oil samples (O2, O3) have isotopically lighter mid-chain and long chain long chain *n*-alkanes (*n*-$C_{21}$ to *n*-$C_{29}$) relative to the other samples, especially for >$C_{27}$ (Fig. 6.7). One of the oil samples (O1) and the coal extracts (C1, C2, C3, C4) have similar *n*-alkane compound specific isotope compositions (Fig. 6.7), suggesting an oil-source correlation. The M1 sample has a nearly identical *n*-alkane carbon isotope composition profile as the coal extracts, but is a few permil more negative, indicating some similarity in organic matter sources with the coals.

The relatively enriched $^{13}C$ of the *n*-alkanes in the coals compared to the mudstones could be consistent with higher thermal maturities for the coals. However, this possibility is discounted for three reasons. Firstly, there is no correlation between the $\delta^{13}C$ values of the *n*-alkanes and the sterane thermal maturity parameters, or with depth (Tables 1 and 2). Secondly, the possible $\delta^{13}C$ fractionation of approximately 2–4‰ (Table 6.2 and Fig. 6.7) between the coals and mudstones is greater than can be attributed to thermal maturity alone (Clayton, 1991; Summons et al., 1994). Thirdly, during increasing thermal maturity, the low molecular weight fractions (< *n*-$C_{20}$) become more $^{13}C$ enriched than the high molecular weight fractions (Clayton, 1991). This means that the isotopic differences for the low molecular weight n-alkanes between the mudstones and coals would be greater than those of high molecular weight n-alkanes if thermal maturity was a significant influence, whereas the reverse is apparent for the Huangyan Oilfield samples (Fig. 6.7).

It is generally accepted that short-chain *n*-alkanes (<*n*-$C_{20}$) are primarily attributed to algal and photosynthetic bacteria source inputs in samples at low to moderate thermal maturities (Gelpi et al., 1970). Here the short-chain *n*-alkanes are interpreted as mainly representing the primary input. The $\delta^{13}C$ values for the *n*-$C_{15}$ to *n*-$C_{19}$ alkanes vary between -25.6‰ and -27.7‰ for the coals and between -25.7‰ and -30.7‰ for the mudstones, and

have a minor decrease with increasing carbon chain length (Fig. 6.7). An isotopic anomaly for the $C_{17}$ *n*-alkane is apparent, which exhibits up to 2.3‰ enrichment in $^{13}C$ relative to the average values of the rest of *n*-alkanes from $C_{15}$ to $C_{18}$. There was baseline resolution between *n*-$C_{17}$ and Pr on the GC-IRMS, so this does not seem to be due to an instrumentation artefact. Unusual $^{13}C$ enrichment of *n*-$C_{17}$ has been interpreted to be due to the use of bicarbonate rather than $CO_2$ by photoautotrophic precursors (Huang et al., 1996) or a restriction of dissolved $CO_2$ in the upper water column (Hollander et al., 1993) for photoautotrophic microorganisms (Schwab and Spangenberg, 2007). Murray et al. (1994) also noted this phenomenon, and pointed out a possible correlation between algal-related steranes and *n*-$C_{17}$ isotope enrichment, which likely resulted from the abundant *n*-$C_{17}$ in marine phytoplankton (Saliot, 1981). However, microbial reworking of higher plant biomass cannot be excluded, especially in interpreting the isotopic characteristics of lacustrine and fluvial-deltaic samples. Interestingly, one of the oils (O2) displays the opposite pattern, with *n*-$C_{17}$ depleted in $^{13}C$ by ca. 1.6‰. The M2 mudstone does not exhibit any obvious isotopic deviation for *n*-$C_{17}$ (Fig. 6.7). Xiong and Geng (2000) showed $C_{15}$ *n*-alkane isotopic depletion in $^{13}C$, but did not further discuss it.

Our coals and mudstones exhibit marked distinctions in the abundance of tricyclic and tetracyclic diterpanes (Fig. 6.5), with some exceptions as discussed below. A thermal maturation effect can be excluded because there is no correlation between diterpenoid parameters and maturity parameters. The magnitude of the *n*-$C_{17}$ isotope enrichment and the summed relative abundances of 16α(H)-phyllocladane and 16β(H)-phyllocladane (tetracyclic diterpanes) and 4β(H)-norisopimarane and isopimarane (tricyclic diterpanes) are plotted in Fig. 6.8a and 6.8b, respectively. Reasonably good correlations ($R^2$ = 0.86; 0.71) can be readily identified. The coals and M1 mudstone have a higher abundance of tetracyclic diterpanes and a lower abundance of tricyclic diterpanes. In contrast, the M2 mudstone has a relatively lower

abundance of tetracyclic diterpanes and a higher abundance of tricyclic diterpanes. All samples have positive or near zero $\delta^{13}C$ values for the term (*n*-$C_{17}$ - av. $C_{15+16+18}$), except for one of the oils (O2) which has a negative value, due to the *n*-$C_{17}$ being depleted in $^{13}C$. The samples with more positive $\delta^{13}C$ values of (*n*-$C_{17}$ - av. $C_{15+16+18}$) may be associated with the tetracyclic diterpanes derived from gymnosperms, which would explain why the coals exhibit slightly heavier isotopic compositions. This anomaly at *n*-$C_{17}$ correlates well with tetracyclic diterpane resin-biomarkers, including 16α(H)-phyllocladane and 16β(H)-phyllocladane, which are abundant in fluvial-deltaic depositional systems (Dzou and Hughes, 1993; Philp, 1994). The negative value for the O2 oil could be the result of relatively abundant angiosperm organic matter input.

Resinites derived from gymnosperm resins, especially those associated with conifers, are isotopically heavier than those from angiosperm resins (Murray et al., 1998). Biomarkers related to different resins may show distinct isotopic profiles (Anderson and Crelling, 1995; Nissenbaum and Yakir, 1995; Peters et al., 2005). Murray et al. (1998) noted that the most abundant diterpane in the Tuna-2 oil from the Australian Gippsland Basin is 16β(H)-phyllocladane (a tetracyclic diterpane), which has a $\delta^{13}C$ value of -23‰, very close to the average $\delta^{13}C$ value of -22.8‰ for fossil conifer resins. Isopimarane (a tricyclic diterpane) is the most abundant diterpane in the Maui oil from New Zealand and has a $\delta^{13}C$ value of -25.9‰, slightly heavier than that of fossil angiosperm resins (-26.4‰) (Lloyd and Farquhar, 1994). These isotopic variations are due to angiosperms having a broader and spreading leaf morphology with high stomatal leaf conductance, whereas gymnosperm conifers generally have a narrow and compact leaf morphology with lower stomatal conductance, and thus are relatively water conservative and less efficient in $CO_2$ assimilation (Farquhar et al., 1989; Lloyd and Farquhar, 1994; Saurer et al., 1995). As a result, angiosperms fractionate carbon isotopes more than gymnosperms (Stuiver and Braziunas, 1987; Marshall and Zhang, 1993),

and the carbon isotope values of angiosperm-derived compounds are more negative. The phyllocladanes have fewer precursors compared to the tricyclic diterpanes, and the broader precursor input to the tricyclic diterpanes may result in a relatively wider variation of their carbon isotope compositions (Otto and Wilde, 2001). In contrast to other diterpenoids derived from angiosperms, phyllocladane is commonly considered a strictly gymnosperm-related biomarker (Alexander et al., 1987), and thus the $\delta^{13}C$ of the coal samples from the Upper Pinghu Formation in the Huangyan Oilfield can be seen as representative of a specific carbon source, with the exception of the C2 coal which has relatively abundant tricyclic diterpanes. This is consistent with two distinct groups of Tertiary brown coals in China, which have heavier carbon isotopic compositions for gymnosperm-related compounds, and lighter values for angiosperm-related compounds (Schoell et al., 1994).

These diterpane variations may be reflected by the isotopic compositions of the *n*-alkanes. However, the diterpenoids are ca. 4-6‰ enriched in $^{13}C$ compared to the *n*-alkanes, due to the relative isotope fractionation of the different biosynthetic pathways (Tuo et al., 2003). The mudstones are generally $^{13}C$ depleted with increasing carbon number for the $C_{25}$ to $C_{31}$ *n*-alkanes (Fig. 6.7). The average carbon isotopic compositions of the odd carbon numbered long chain *n*-alkanes (*n*-$C_{27}$, *n*-$C_{29}$ and *n*-$C_{31}$) are likely to be representative of carbon inputs from higher plant photosynthetic pathways (Eglinton and Hamilton, 1967b). There is a correlation between the average $\delta^{13}C$ of the $C_{27+29+31}$ *n*-alkanes and the relative content of tricyclic and tetracyclic diterpanes (Fig. 6.8c and 6.8d, respectively). The three coal extracts (C1, C3, and C4) that are rich in gymnosperm-related tetracyclic diterpanes contain $C_{27+29+31}$ *n*-alkanes enriched in $^{13}C$ by 2.7-3.7‰ relative to the mudstone M2, which has more abundant tricyclic diterpanes. This trend is interpreted to be due to the coals contain isotopically heavier carbon from gymnosperm resinite, whereas a higher proportion of angiosperm resinite contributed to the M2 mudstone. The M1 mudstone sample has a

completely different biomarker distribution compared to the M2 mudstone, with substantially lower tricyclic diterpanes, and $C_{27+29+31}$ *n*-alkanes that are enriched in $^{13}C$ (Fig. 6.8c and 6.8d), presumably because of less angiosperm-derived resinite. Unlike the other coal samples, C2 contains diterpanes dominated by 4β (H)-norisopimarane (Fig. 6.4a), but has $C_{27+29+31}$ *n*-alkanes with similar isotopic compositions as those of the other coals (Fig. 6.8c and 6.8d). This could either be because 4β(H)-19-norisopimarane had a different source compared to the *n*-alkanes, or because of a limited angiosperm origin for the 4β(H)-19-norisopimarane.

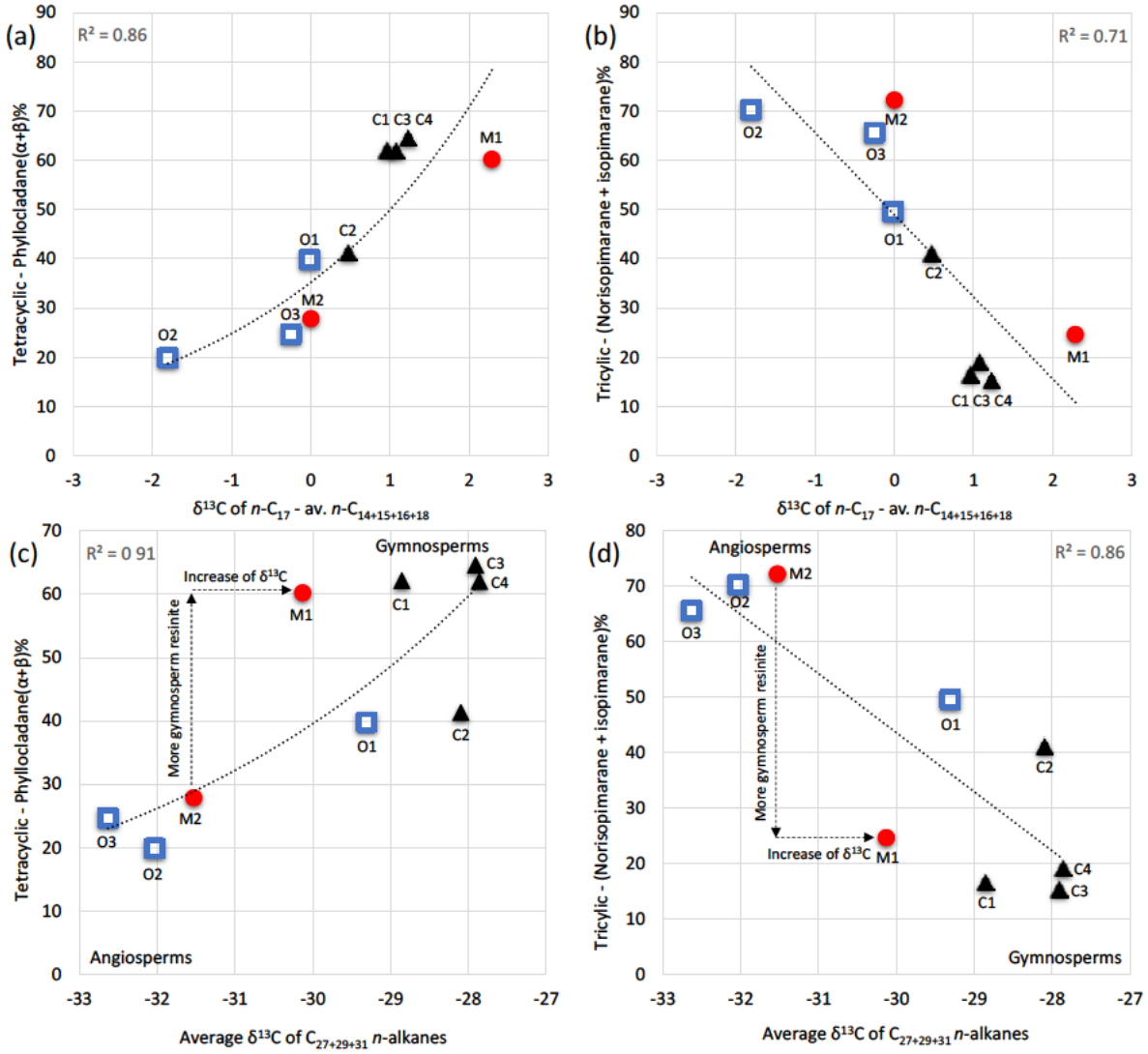


Fig. 6.8 Correlations of $\delta^{13}C$ values of *n*-$C_{17}$ minus the average of *n*-$C_{14+16+18}$ versus the relative abundance of tetracyclic diterpanes (a) and tricyclic diterpanes (b). Correlations of average $\delta^{13}C$ values of *n*-$C_{27+29+31}$ alkanes versus the relative abundance of (c) tetracyclic diterpanes and (d) tricyclic diterpanes. % tetracyclic diterpanes = 16β(H)-phyllocladane + 16α(H)-phyllocladane; % tricyclic diterpanes = 4β(H)-19-norisopimarane + isopimarane. For letter-number designations see Table 6.2. Coals: black triangles; mudstones: red circles; oils: blue squares.

Oil sample O1 has similar *n*-alkane isotopic profiles as the coal samples (Fig. 6.7), and contains high relative amounts of gymnosperm-related tetracyclic diterpanes, suggesting it was derived from a source rock containing gymnosperm resinite. In contrast the other two oils (O2 and O3) contain less gymnosperm-related tetracyclic diterpanes and thus are interpreted to have been derived from source rocks with a greater proportion of angiosperm-derived resinite (Fig. 6.8c and 8d). Consequently, the $C_{27+29+31}$ *n*-alkanes in the O1 oil sample are 2.7-3.3‰ enriched in $^{13}C$ compared with those in the O2 and O3 oil samples.

*6.3.2.2. Carbon isotopes of acyclic isoprenoids*

Variations in the $\delta^{13}C$ of the multisource-derived acyclic isoprenoids pristane, phytane and short-chain *n*-alkanes (*n*-$C_{17}$ and *n*-$C_{18}$) were observed in the studied samples and provide a way of distinguishing various source contributions for petroleum generated from the Xihu Depression. Pristane and phytane are isotopically heavier than *n*-$C_{17}$ and *n*-$C_{18}$ if derived from primary producers through the mevalonate pathway, whereas they are isotopically lighter if derived from heterotrophs utilising primary photosynthates or bacterial biomass (Freeman et al., 1990; Hartgers et al., 2000; Grice et al., 2005b; Schouten et al., 2008; Nabbefeld et al., 2010). Pristane and phytane in the Xihu Depression samples are mostly $^{13}C$ depleted relative to *n*-$C_{17}$ and *n*-$C_{18}$ (Table 6.2; Fig. 6.7), which indicates that the acyclic isoprenoids were derived from lipids of various bacteria.

For most Huangyan Oilfield samples, pristane is enriched in $^{13}C$ by an average of 1.6‰ relative to that of phytane, except for two samples in which pristane is slightly depleted in $^{13}C$ (by 0.4‰ and 0.7‰). The $\delta^{13}C$ of pristane does not vary consistently with depth (Table 6.2; Fig. 6.9a). This may suggest separate origins for the two isoprenoids (Volkman et al., 2015). Freeman et al. (1990) suggested that $^{13}C$-depletion of phytane relative to pristane in the Messel shale was due to an additional contribution from methanogenic bacteria (Brassell et

al., 1981). Grice et al. (1997) attributed a similar isotopic shift in the Permian Kupferschiefer to different biological sources for pristane and phytane. Schwarzbauer et al. (2013) interpreted isotopically lighter phytane to be due to distinct diagenetic pathways, as both isoprenoids show similar trends resulting from the dominant terrigenous inputs. Nabbefeld et al. (2010) explained depletion in $^{13}C$ of pristane as due to large intramolecular isotopic fractionation during the biosynthesis of phytol.

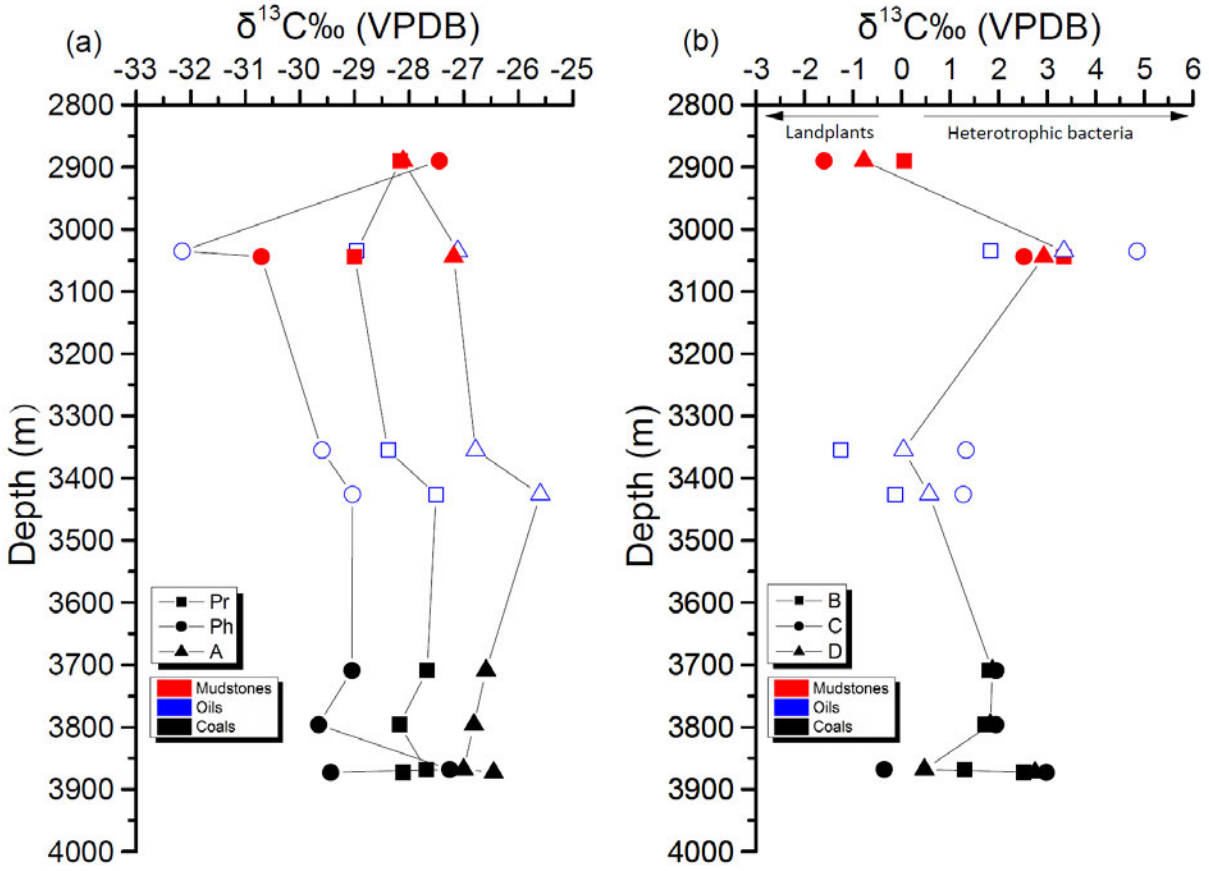


Fig. 6.9 The variation of (a) $\delta^{13}C$ of pristane, phytane, average *n*-$C_{14-18}$ (A) and (b) three isotopic difference values (B, C, D) with depth for mudstone and coal samples from the Huangyan Oilfield. B = $\delta^{13}C$ of *n*-$C_{17}$ - Pr, C = $\delta^{13}C$ of *n*-$C_{18}$ - Ph, D = $\Delta\delta$ = [average $\delta^{13}C$ of *n*-$C_{17}$ + *n*-$C_{18}$] - [average $\delta^{13}C$ of Pr + Ph].

The phytanyl core of $^{13}C$ enriched archaeal lipids are one source for phytane that will give rise to relatively positive values of $\delta^{13}C$ (Rowland, 1990b; Rowland, 1990a; Grice et al., 1998a). Indeed, considering the dominant terrigenous sources for our Xihu Depression samples, a possible contribution of higher plant-derived tocopherol for pristane (Goossens et

al., 1984), as well as a contribution of archaea to phytane (Rowland, 1990a; Grice et al., 1998a) cannot be excluded.

Comparison of the $\delta^{13}C$ of Pr and Ph with the $\delta^{13}C$ of the *n*-$C_{17}$ and *n*-$C_{18}$ alkanes provides an additional approach to interpret source contributions. The $\delta^{13}C$ values of the isoprenoids in the M2 mudstone, which contains a high tricyclic diterpane content, are slightly $^{13}C$ enriched relative to the short-chain *n*-alkanes (Table 6.2; Fig. 6.9b). This likely reflects an origin from primary producers via the mevalonate pathway (Hayes, 1993), as is also indicated by the flat shape of the n-alkane isotopic profile (Fig. 6.7). The anomalous M1 mudstone sample which contains a relatively high tetracyclic diterpane content has acyclic isoprenoids that are more $^{13}C$ depleted, indicating a heterotrophic bacterial origin for these compounds. The Huangyan Oilfield coal samples have a consistent depletion in $^{13}C$, or similar $\delta^{13}C$ values for isoprenoids relative to short-chain *n*-alkanes, consistent with heterotrophic bacterial origins (Grice et al., 2005b). There are differences between the 825AD oil (O1) and the two 825B oils (O2 and O3), even though they are both indicated as having heterotrophic origins by having positive $\Delta\delta$ values (where $\Delta\delta$ = [average $\delta^{13}C$ of *n*-$C_{17}$ + *n*-$C_{18}$] - [average $\delta^{13}C$ of Pr + Ph] (Grice et al., 2005b)). The $\Delta\delta$ value of oil O1 is 3.4, whereas the $\Delta\delta$ values of O2 and O3 are 0.04 and 0.57 (Fig. 6.9b), probably suggesting organic matter source differences for these oils, although it is possible that mixing of the oils may have masked or neutralised real isotopic distinctions. The origins of the acyclic isoprenoids in the O2 and O3 oils are likely genetically closer to land plants, whereas the origin of the O1 oil appears closer to a heterotrophic bacterial source (Hayes, 1993; Schouten et al., 1998; Grice et al., 2005b; Nabbefeld et al., 2010).

## 6.4. Summary

The source contributions of Paleogene coals and associated mudstones to generated oils from Xihu Depression, East China Sea, were differentiated using land plant-derived diterpenoid biomarkers and compound-specific isotope analyses. The coal samples analysed have a relatively higher content of tetracyclic diterpanes (e.g., 16β(H)-phyllocladane, 16α(H)-phyllocladane, 16α(H)-kaurane) than the mudstone samples, which have a relatively higher content of tricyclic diterpanes (e.g., 4β(H)-norisopimarane and isopimarane). These diterpane differences correlate with the $\delta^{13}C$ variation of *n*-alkanes for coals, mudstones and oils, which indicates that the plant phyla/classes (e.g. gymnosperms vs. angiosperms) could be a major factor affecting the carbon isotopic compositions of individual *n*-alkanes, and also provides evidence for differentiating specific hydrocarbon contributions to Xihu Depression petroleum. For terrigenously-dominated organic matter, long chain *n*-alkanes with a large proportion of gymnosperm organic inputs are approximately 2-3‰ enriched in $^{13}C$ than those with a large proportion of angiosperm organic inputs, regardless of variation in lithologies.

A general trend was observed towards isotopically lighter values for *n*-alkanes with increasing carbon numbers, which is consistent with typical fluvial/deltaic depositional settings and with previous studies. The differences between the $\delta^{13}C$ values of pristane and phytane are suggestive of separate origins for the isoprenoids. The differences in the $\delta^{13}C$ values of the *n*-$C_{17}$ and *n*-$C_{18}$ alkanes relative to pristane and phytane are indicative of different origins for these hydrocarbons, from land plants as well as possibly from heterotrophic bacteria. Oils generated from the coals have a small increase (<3‰) in the *n*-alkane $\delta^{13}C$ values with increasing chain length and have pristane and phytane more depleted in $^{13}C$ relative to *n*-$C_{17}$ and *n*-$C_{18}$, suggesting a more heterotrophic origin. In contrast, oils generated from organic matter in the mudstones have increased $^{13}C$ depletion with increasing

carbon number over the *n*-$C_{20}$ to *n*-$C_{30}$ range, and have pristane and phytane less depleted in $^{13}C$ relative to *n*-$C_{17}$ and *n*-$C_{18}$, suggesting greater derivation from land plants. Recognition of these isotopic trends in several oils of the Huangyan Oilfield showed that some had a major mudstone-source (e.g., 825B), whereas coals contributed more significantly to other oils (e.g., 825AD).

## Acknowledgements

This research was supported by the Major Special Project for National Science and Technology (Project No. 2016ZX05027-001-003) and the National Natural Science Foundation of China (Grant No. 41472108). The authors acknowledge the assistance of Hui Diao. However, any opinions, findings, conclusions, or recommendations expressed herein are those of the authors and do not necessarily reflect the views of the project. HX thanks China University of Geosciences (Beijing) and Macquarie University for a PhD scholarship. We thank Dr Joe Curiale for a review that substantially improved an earlier version of this manuscript.

# References

Abbassi, S., Edwards, D.S., George, S.C., Volk, H., Mahlstedt, N., di Primio, R., Horsfield, B., 2016. Petroleum potential and kinetic models for hydrocarbon generation from the Upper Cretaceous to Paleogene Latrobe Group coals and shales in the Gippsland Basin, Australia. Organic Geochemistry 91, 54-67.

Ahmed, M., Volk, H., George, S.C., Faiz, M., Stalker, L., 2009. Generation and expulsion of oils from Permian coals of the Sydney Basin, Australia. Organic Geochemistry 40, 810-831.

Alexander, R., Noble, R.A., Kagi, R.I., 1987. Fossil resin biomarkers and their application in oil to source-rock correlation, Gippsland Basin, Australia. The APPEA Journal 27, 63-72.

Alexander, R., Larcher, A.V., Kagi, R.I., Price, P.L., 1988. The use of plant derived biomarkers for correlation of oils with source rocks in the Cooper/Eromanga Basin System, Australia. The APPEA Journal 28, 310-324.

Alexander, R., Larcher, A.V., Kagi, R.I., Price, P.L., 1992. An oil-source correlation study using age-specific plant-derived aromatic biomarkers, in: Moldowan, J.M., Albrecht, P., Philp, R.P. (Eds.), Biological markers in sediments and petroleum. Prentice Hall, Englewood Cliffs, pp. 201-221.

Anderson, K.B., Crelling, J.C., 1995. Amber, Resinite, and Fossil Resins. American Chemical Society, Washington, D.C.

Bidigare, R.R., Fluegge, A., Freeman, K.H., Hanson, K.L., Hayes, J.M., Hollander, D., Jasper, J.P., King, L.L., Laws, E.A., Milder, J., 1997. Consistent fractionation of $^{13}C$ in nature and in the laboratory: Growth‐rate effects in some haptophyte algae. Global Biogeochemical Cycles 11, 279-292.

Bjorøy, M., Hall, K., Gillyon, P., Jumeau, J., 1991. Carbon isotope variations in *n*-alkanes and isoprenoids of whole oils. Chemical Geology 93, 13-20.

Blumer, M., Snyder, W.D., 1965. Isoprenoid hydrocarbons in recent sediments: presence of pristane and probable absence of phytane. Science 150, 1588-1589.

Boreham, C.J., Summons, R.E., Roksandic, Z., Dowling, L.M., Hutton, A.C., 1994. Chemical, molecular and isotopic differentiation of organic facies in the Tertiary lacustrine duaringa oil-shale deposit, Queensland, Australia. Organic Geochemistry 21, 685-712.

Brassell, S.C., Wardroper, A.M.K., Thomson, I.D., Maxwell, J.R., Eglinton, G., 1981. Specific acyclic isoprenoids as biological markers of methanogenic bacteria in marine-sediments. Nature 290, 693-696.

Brother, L., Engel, M.H., Krooss, B.M., 1991. The effects of fluid flow through porous media on the distribution of organic compounds in a synthetic crude oil. Organic Geochemistry 17, 11-24.

Cernusak, L.A., Winter, K., Aranda, J., Turner, B.L., 2008. Conifers, angiosperm trees, and lianas: Growth, whole-plant water and nitrogen use efficiency, and stable isotope composition (delta C-13 and delta O-18) of seedlings grown in a tropical environment. Plant Physiology 148, 642-659.

Chen, L., 1998. Depositional environment evolution of Pinghu formation in Xihu Depression, the East China Sea. Marine Geology & Quaternary Geology 18, 69-78.

Cheng, P., Xiao, X.M., Gai, H.F., Li, T.F., Zhang, Y.Z., Huang, B.J., Wilkins, R.W.T., 2015. Characteristics and origin of carbon isotopes of *n*-alkanes in crude oils from the western Pearl River Mouth Basin, South China sea. Marine and Petroleum Geology 67, 217-229.

Chikaraishi, Y., Naraoka, H., Poulson, S.R., 2004. Hydrogen and carbon isotopic fractionations of lipid biosynthesis among terrestrial (C3, C4 and CAM) and aquatic plants. Phytochemistry 65, 1369-1381.

Clayton, C.J., 1991. Effect of maturity on carbon isotope ratios of oils and condensates. Organic Geochemistry 17, 887-899.

Collister, J.W., Summons, R.E., Lichtfouse, E., Hayes, J.M., 1992. An isotopic biogeochemical study of the Green River oil shale. Organic Geochemistry 19, 265-276.

Collister, J.W., Rieley, G., Stern, B., Eglinton, G., Fry, B., 1994. Compound-specific $\delta^{13}C$ analyses of leaf lipids from plants with differing carbon dioxide metabolisms. Organic Geochemistry 21, 619-627.

Dawson, D., Grice, K., Alexander, R., Edwards, D., 2007. The effect of source and maturity on the stable isotopic compositions of individual hydrocarbons in sediments and crude oils from the Vulcan Sub-basin, Timor Sea, Northern Australia. Organic Geochemistry 38, 1015-1038.

de Leeuw, J.W., Largeau, C., 1993. A review of macromolecular organic compounds that comprise living organisms and their role in kerogen, coal, and petroleum formation, in: Engel, M.H., Macko, S.A. (Eds.), Organic Geochemistry. Plenum Press, New York, pp. 23-72.

Disnar, J.R., Harouna, M., 1994. Biological origin of tetracyclic diterpanes, *n*-alkanes and other biomarkers found in Lower Carboniferous Gondwana coals (Niger). Organic Geochemistry 21, 143-152.

Dzou, L.I.P., Hughes, W.B., 1993. Geochemistry of oils and condensates, K-field, offshore Taiwan - a case-study in migration fractionation. Organic Geochemistry 20, 437-462.

Eglinton, G., Hamilton, R.J., 1963. The distribution of alkanes. Chemical Plant Taxonomy, 187-217.

Eglinton, G., Hamilton, R.J., 1967a. Leaf epicuticular waxes. Science 156, 1322–1335.

Eglinton, G., Hamilton, R.J., 1967b. Leaf epicuticular waxes. Science 156, 1322-1335.

Eglinton, T.I., 1994. Carbon isotopic evidence for the origin of macromolecular aliphatic structures in kerogen. Organic Geochemistry 21, 721-735.

Farquhar, G.D., Ehleringer, J.R., Hubick, K.T., 1989. Carbon isotope discrimination and photosynthesis. Annual Review of Plant Biology 40, 503-537.

Freeman, K.H., Hayes, J.M., Trendel, J.M., Albrecht, P., 1990. Evidence from carbon isotope measurements for diverse origins of sedimentary hydrocarbons. Nature 343, 254-256.

Gelpi, E., Schneider, H., Mann, J., Oro, J., 1970. Hydrocarbons of geochemical significance in microscopic algae. Phytochemistry 9, 603-612.

Goossens, H., de Leeuw, J.W., Schenck, P.A., Brassell, S.C., 1984. Tocopherols as likely precursors of pristane in ancient sediments and crude oils. Nature 312, 440-442.

Grice, K., Schaeffer, P., Schwark, L., Maxwell, J.R., 1997. Changes in palaeoenvironmental conditions during deposition of the Permian Kupferschiefer (Lower Rhine Basin, northwest Germany) inferred from molecular and isotopic compositions of biomarker components. Organic Geochemistry 26, 677-690.

Grice, K., Schouten, S., Nissenbaum, A., Charrach, J., Sinninghe Damste, J.S., 1998a. Isotopically heavy carbon in the $C_{21}$ to $C_{25}$ regular isoprenoids in halite-rich deposits from the Sdom Formation, Dead Sea Basin, Israel. Organic Geochemistry 28, 349-359.

Grice, K., Schouten, S., Peters, K.E., Sinninghe Damsté, J.S., 1998b. Molecular isotopic characterisation of hydrocarbon biomarkers in Palaeocene-Eocene evaporitic,

lacustrine source rocks from the Jianghan Basin, China. Organic Geochemistry 29, 1745-1764.

Grice, K., Backhouse, J., Alexander, R., Marshall, N., Logan, G.A., 2005a. Correlating terrestrial signatures from biomarker distributions, $\delta^{13}C$, and palynology in fluvio-deltaic deposits from NW Australia (Triassic–Jurassic). Organic Geochemistry 36, 1347-1358.

Grice, K., Cao, C., Love, G.D., Bottcher, M.E., Twitchett, R.J., Grosjean, E., Summons, R.E., Turgeon, S.C., Dunning, W., Jin, Y., 2005b. Photic zone euxinia during the Permian-Triassic superanoxic event. Science 307, 707-709.

Grice, K., Brocks, J.J., 2011. Biomarkers (organic, compound-specific isotopes), in: Reitner, J., Thiel, V. (Eds.), Encyclopedia of Geobiology. Springer, Netherlands, pp. 167-182.

Gu, H., Ye, J., Hao, F., 2005. Distribution pattern of oil and gas in Pinghu structural zone in Xihu depression, East China Sea. Oil & Gas Geology 26, 104-108.

Hartgers, W.A., Schouten, S., Lopez, J.F., Sinninghe Damsté, J.S., Grimalt, J.O., 2000. $^{13}C$-contents of sedimentary bacterial lipids in a shallow sulfidic monomictic lake (Lake Ciso, Spain). Organic Geochemistry 31, 777-786.

Hasegawa, T., Pratt, L.M., Maeda, H., Shigeta, Y., Okamoto, T., Kase, T., Uemura, K., 2003. Upper Cretaceous stable carbon isotope stratigraphy of terrestrial organic matter from Sakhalin, Russian Far East: a proxy for the isotopic composition of paleoatmospheric $CO_2$. Palaeogeography Palaeoclimatology Palaeoecology 189, 97-115.

Hayes, J.M., 1993. Factors controlling $^{13}C$ contents of sedimentary organic compounds: Principles and evidence. Marine Geology 113, 111-125.

Hollander, D.J., Mckenzie, J.A., Hsü, K.J., 1993. Carbon-isotope evidence for unusual plankton blooms and fluctuations of surface-water $CO_2$ in "Strangelove Ocean" after

terminal Cretaceous event. Palaeogeography Palaeoclimatology Palaeoecology 104, 229-237.

Huang, W., Meinschein, W.G., 1979. Sterols as ecological indicators. Geochimica et Cosmochimica Acta 43, 739-745.

Huang, Y., Lockheart, M.J., Collister, J.W., Eglinton, G., 1995. Molecular and isotopic biogeochemistry of the Miocene Clarkia Formation: Hydrocarbons and alcohols. Organic Geochemistry 23, 785-801.

Huang, Y., Lockheart, M.J., Logan, G.A., Eglinton, G., 1996. Isotope and molecular evidence for the diverse origins of carboxylic acids in leaf fossils and sediments from the Miocene Lake Clarkia deposit, Idaho, USA. Organic Geochemistry 24, 289-299.

Hughes, W.B., Holba, A.G., Dzou, L.I.P., 1995. The ratios of dibenzothiophene to phenanthrene and pristane to phytane as indicators of depositional environment and lithology of petroleum source rocks. Geochimica et Cosmochimica Acta 59, 3581-3598.

Killops, S., Cook, R., Raine, I., Weston, R., Woolhouse, T., 2003. A tentative New Zealand chemostratigraphy for the Jurassic - Cretaceous based on terrestrial plant biomarkers. New Zealand Journal of Geology and Geophysics 46, 63-77.

Korner, C., Farquhar, G.D., Roksandic, Z., 1988. A global survey of carbon isotope discrimination in plants from high altitude. Oecologia 74, 623-632.

Kotarba, M.J., Clayton, J.L., 2003. A stable carbon isotope and biological marker study of Polish bituminous coals and carbonaceous shales. International Journal of Coal Geology 55, 73-94.

Leavitt, S.W., Long, A., 1982. Evidence for $^{13}C/^{12}C$ fractionation between tree leaves and wood. Nature 298, 742-744.

Leythaeuser, D., Mackenzie, A., Schaefer, R.G., Bjoroy, M., 1984. A novel approach for recognition and quantification of hydrocarbon migration effects in shale-sandstone sequences. AAPG Bulletin 68, 196-219.

Li, S., Li, C., 2003. Analysis on the petroleum resource distribution and exploration potential of the Xihu depression, the East China Sea. Petroleum Geology and Experiment 25, 728-733.

Li, Y., Song, Z., Cao, X., George, S.C., 2016. Sedimentary organic matter record of Early Cretaceous environmental changes in western Liaoning Province, NE China. Organic Geochemistry 98, 54-65.

Lichtfouse, E., Derenne, S., Mariotti, A., Largeau, C., 1994. Possible algal origin of long chain odd n-alkanes in immature sediments as revealed by distributions and carbon isotope ratios. Organic Geochemistry 22, 1023-1027.

Liu, D.Y., 2004. Characteristics of source rocks and their hydrocarbons in East China Sea continental shelf basin, in: Jiang, L. (Ed.), Proceedings of Petroleum Resources Exploration in East China Sea Shelf Basin. The Press of the Petroleum Industry, Beijing,, pp. 181-187 (in Chinese).

Liu, J., Geng, A., Xiong, Y., 2006. The application of stable carbon and hydrogen isotopic compositions of individual *n*-alkanes to Paleozoic oil/source rock correlation enigmas in the Huanghua depression, China. Journal of Petroleum Science and Engineering 54, 70-78.

Lloyd, J., Farquhar, G.D., 1994. $^{13}C$ discrimination during $CO_2$ assimilation by the terrestrial biosphere. Oecologia 99, 201-215.

Lockheart, M.J., Van Bergen, P.F., Evershed, R.P., 1997. Variations in the stable carbon isotope compositions of individual lipids from the leaves of modern angiosperms:

implications for the study of higher land plant-derived sedimentary organic matter. Organic Geochemistry 26, 137-153.

Lucke, A., Helle, G., Schleser, G.H., Figueiral, I., Mosbrugger, V., Jones, T.P., Rowe, N.P., 1999. Environmental history of the German Lower Rhine Embayment during the Middle Miocene as reflected by carbon isotopes in brown coal. Palaeogeography Palaeoclimatology Palaeoecology 154, 339-352.

Mackenzie, A.S., 1984. Applications of biological markers in petroleum geochemistry, in: Brooks, J., Welte, D.H. (Eds.), Advances in petroleum geochemistry. Academic Press, London, pp. 115–214.

Mackenzie, A.S., Leythaeuser, D., Muller, P., Quigley, T.M., Radke, M., 1988. The movement of hydrocarbons in shales. Nature 331, 63-65.

Marshall, J.D., Zhang, J., 1993. Altitudinal variation in carbon isotope discrimination by conifers, in: Ehleringer, J.R., Hall, A.E., Farquhar, G.D. (Eds.), Stable isotopes and plant carbon-water relations. Academic Press, London, pp. 187-200.

McCollom, T.M., Seewald, J.S., 2006. Carbon isotope composition of organic compounds produced by abiotic synthesis under hydrothermal conditions. Earth and Planetary Science Letters 243, 74-84.

Metzger, P., Largeau, C., Casadevall, E., 1991. Lipids and macromolecular lipids of the hydrocarbon-rich microalga *Botryococcus braunii*. Chemical structure and biosynthesis. Geochemical and biotechnological importance, in: Herz, W., Kirby, G.W., Steglich, W., Tamm, C. (Eds.), Progress in the Chemistry of Organic Natural Products. Springer, Verlag, pp. 1–70.

Mukhopadhyay, P.K., Hagemann, H.W., Hollerbach, A., Welte, D.H., 1979. The relation between organic geochemical and petrological parameters of coal in Indian Coal Basins. Energy Sources 4, 313-328.

Murchison, D.G., 1987. Recent advances in organic petrology and organic geochemistry: an overview with some reference to 'oil from coal'. Geological Society, London, Special Publications 32, 257-302.

Murray, A.P., Summons, R.E., Boreham, C.J., Dowling, L.M., 1994. Biomarker and *n*-alkane isotope profiles for Tertiary oils - relationship to source-rock depositional setting. Organic Geochemistry 22, 521-542.

Murray, A.P., Edwards, D., Hope, J.M., Boreham, C.J., Booth, W.E., Alexander, R.A., Summons, R.E., 1998. Carbon isotope biogeochemistry of plant resins and derived hydrocarbons. Organic Geochemistry 29, 1199-1214.

Nabbefeld, B., Grice, K., Twitchett, R.J., Summons, R.E., Hays, L., Bottcher, M.E., Asif, M., 2010. An integrated biomarker, isotopic and palaeoenvironmental study through the Late Permian event at Lusitaniadalen, Spitsbergen. Earth and Planetary Science Letters 291, 84-96.

Nissenbaum, A., Yakir, D., 1995. Stable isotope composition of amber, in: Anderson, K.B., Crelling, J.C. (Eds.), Amber, Resinite, and Fossil Resins. American Chemical Society, Washington, pp. 32-42.

Noble, R.A., Alexander, R., Kagi, R.I., Knox, J., 1985. Tetracyclic diterpenoid hydrocarbons in some Australian coals, sediments and crude oils. Geochimica et Cosmochimica Acta 49, 2141-2147.

Otto, A., Walther, H., Püttmann, W., 1997. Sesqui-and diterpenoid biomarkers preserved in Taxodium-rich Oligocene oxbow lake clays, Weisselster Basin, Germany. Organic Geochemistry 26, 105-115.

Otto, A., Wilde, V., 2001. Sesqui-, di-, and triterpenoids as chemosystematic markers in extant conifers - A review. Botanical Review 67, 141-238.

Pepper, A.S., Corvi, P.J., 1995. Simple kinetic models of petroleum formation. Part III: Modelling an open system. Marine and Petroleum Geology 12, 417-452.

Peters, K.E., Walters, C.C., Moldowan, J.M., 2005. The Biomarker Guide. Cambridge University Press, Cambridge

Philp, R.P., Simoneit, B.R.T., Gilbert, T.D., 1983. Diterpenoids in crude oils and coals of South Eastern Australia, in: Bjorøy, M. (Ed.), Advances in Organic Geochemistry 1981. Wiley, Chichester, pp. 698-704.

Philp, R.P., 1994. Geochemical characteristics of oils derived predominantly from terrigenous source materials. Geological Society, London, Special Publications 77, 71-91.

Popp, B.N., Laws, E.A., Bidigare, R.R., Dore, J.E., Hanson, K.L., Wakeham, S.G., 1998. Effect of phytoplankton cell geometry on carbon isotopic fractionation. Geochimica et Cosmochimica Acta 62, 69-77.

Powell, T.G., Snowdon, L.R., 1983. Composite hydrocarbon generation model. Erdol Kohle Erdgas Petrochem 36, 163-170.

Ramanampisoa, L., Radke, M., Schaeffer, R.G., Littke, R., Rullkötter, J., Horsfield, B., 1990. Organic geochemical characterisation of sediments from the Sakoa coalfield, Madagascar. Organic Geochemistry 16, 235-246.

Rieley, G., Collier, R.J., Jones, D.M., Eglinton, G., Eakin, P.A., Fallick, A.E., 1991. Sources of sedimentary lipids deduced from stable carbon isotope analyses of individual compounds. Nature 352, 425-427.

Rooney, M.A., Vuletich, A.K., Griffith, C.E., 1998. Compound-specific isotope analysis as a tool for characterizing mixed oils: An example from the west of Shetlands area. Organic Geochemistry 29, 241-254.

Rowland, S.J., 1990a. Production of acyclic isoprenoid hydrocarbons by laboratory maturation of methanogenic bacteria. Organic Geochemistry 15, 9-16.

Rowland, S.J., 1990b. The widespread occurrence of highly branched acyclic $C_{20}$, $C_{25}$ and $C_{30}$ hydrocarbons in recent sediments and biota - A review. Marine Environmental Research 30, 191-216.

Sackett, W.M., Nakaparksin, S., Dalrymple, D., 2015. Carbon isotope effects in methane production by thermal cracking, Advances in Organic Geochemistry: Proceedings of the Third International Congress 1966, pp. 37-53.

Saliot, A., 1981. Natural hydrocarbons in sea water. Elsevier Oceanography Series 31, 327-374.

Saurer, M., Siegenthaler, U., Schweingruber, F., 1995. The climate-carbon isotope relationship in tree-rings and the significance of site conditions. Tellus B 47, 320-330.

Schoell, M., Simoneit, B.R.T., Wang, T.G., 1994. Organic geochemistry and coal petrology of Tertiary brown-coal in the Zhoujing Mine, Baise Basin, South China—4. Biomarker sources inferred from stable carbon-isotope compositions of individual compounds. Organic Geochemistry 21, 713-719.

Schouten, S., Breteler, W.C.M.K., Blokker, P., Schogt, N., Rijpstra, W.I.C., Grice, K., Baas, M., Sinninghe Damsté, J.S., 1998. Biosynthetic effects on the stable carbon isotopic compositions of algal lipids: Implications for deciphering the carbon isotopic biomarker record. Geochimica et Cosmochimica Acta 62, 1397-1406.

Schouten, S., Ozdirekcan, S., van der Meer, M.T.J., Blokker, P., Baas, M., Hayes, J.M., Sinninghe Damsté, J.S., 2008. Evidence for substantial intramolecular heterogeneity in the stable carbon isotopic composition of phytol in photoautotrophic organisms. Organic Geochemistry 39, 135-146.

Schulze, T., Michaelis, W., 1990. Structure and origin of terpenoid hydrocarbons in some German coals. Organic Geochemistry 16, 1051-1058.

Schwab, V., Spangenberg, J.E., Grimalt, J.O., 2005. Chemical and carbon isotopic evolution of hydrocarbons during prograde metamorphism from 100 degrees to 550 degrees: Case study in the Liassic black shale formation of Central Swiss Alps. Geochimica et Cosmochimica Acta 69, 1825-1840.

Schwab, V.F., Spangenberg, J.E., 2007. Molecular and isotopic characterization of biomarkers in the Frick Swiss Jura sediments: A palaeoenvironmental reconstruction on the northern Tethys margin. Organic Geochemistry 38, 419-439.

Schwarzbauer, J., Littke, R., Meier, R., Strauss, H., 2013. Stable carbon isotope ratios of aliphatic biomarkers in Late Palaeozoic coals. International Journal of Coal Geology 107, 127-140.

Seifert, W.K., Moldowan, J.M., 1986. Use of biological markers in petroleum exploration. Methods in Geochemistry and Geophysics 24, 261-290.

Simoneit, B.R.T., Didyk, B.M., 1978. Organic geochemistry of a Chilean paraffin dirt. Chemical Geology 23, 21-40.

Simoneit, B.R.T., Grimalt, J.O., Wang, T.G., Cox, R.E., Hatcher, P.G., Nissenbaum, A., 1986. Cyclic terpenoids of contemporary resinous plant detritus and of fossil woods, ambers and coals. Organic Geochemistry 10, 877-889.

Simoneit, B.R.T., Schoell, M., Stefanova, M., Stojanova, G., Nosyrev, I.E., Goranova, M., 1995. Composition of the extract from a Carboniferous bituminous coal. 2. Compound-specific isotope analyses. Fuel 74, 1194-1199.

Smith, B.N., Epstein, S., 1971. Two categories of $^{13}C/^{12}C$ ratios for higher plants. Plant Physiology 47, 380-384.

Snowdon, L.R., 1980. Resinite—A potential petroleum source in the upper Cretaceous/Tertiary of the Beaufort-Mackenzie Basin, in: Miall, A.D. (Ed.), Facts and

Principles of World Oil Occurrence. Canadian Society of Petroleum Geologists Memoir 6, pp. 509-521.

Sofer, Z., 1984. Stable carbon isotope compositions of crude oils - application to source depositional-environments and petroleum alteration. AAPG Bulletin 68, 31-49.

Song, Z., Qin, Y., George, S.C., Wang, L., Guo, J., Feng, Z., 2013. A biomarker study of depositional paleoenvironments and source inputs for the massive formation of Upper Cretaceous lacustrine source rocks in the Songliao Basin, China. Palaeogeography Palaeoclimatology Palaeoecology 385, 137-151.

Stuiver, M., Braziunas, T.F., 1987. Tree cellulose $^{13}C/^{12}C$ isotope ratios and climatic change. Nature 328, 58-60.

Su, A., Chen, H., Wang, C., Li, P., Zhang, H., Xiong, W., Lei, M., 2013. Genesis and maturity identification of oil and gas in the Xihu Sag, East China Sea Basin. Petroleum Exploration and Development 40, 558-565.

Summons, R.E., Jahnke, L.L., Roksandic, Z., 1994. Carbon isotopic fractionation in lipids from methanotrophic bacteria: Relevance for interpretation of the geochemical record of biomarkers. Geochimica et Cosmochimica Acta 58, 2853-2863.

Sun, Y., Sheng, G., Peng, P.a., Fu, J., 2000. Compound-specific stable carbon isotope analysis as a tool for correlating coal-sourced oils and interbedded shale-sourced oils in coal measures: an example from Turpan basin, north-western China. Organic Geochemistry 31, 1349-1362.

Sykes, R., Volk, H., George, S.C., Ahmed, M., Higgs, K.E., Johansen, P.E., Snowdon, L.R., 2014. Marine influence helps preserve the oil potential of coaly source rocks: Eocene Mangahewa Formation, Taranaki Basin, New Zealand. Organic Geochemistry 66, 140-163.

Tegelaar, E.W., Matthezing, R.M., Jansen, J.B.H., Horsfield, B., de Leeuw, J.W., 1989. Possible origin of *n*-alkanes in high-wax crude oils. Nature 342, 529-531.

Tissot, B., Pelet, R., Roucach, J., Combaz, A., 1977. Utilisation des alcanes comme fossiles géochimiques indicateurs des environnements géologiques. Advance in Organic Geochemistry 1975, 117-154.

Tissot, B.P., Welte, D.H., 1984. From kerogen to petroleum, in: Tissot, B.P., Welte, D.H. (Eds.), Petroleum formation and occurrence, 2nd Edition. Springer, Berlin Heidelberg, pp. 160–198.

Tulipani, S., Grice, K., Krull, E., Greenwood, P., Revill, A.T., 2014. Salinity variations in the northern Coorong Lagoon, South Australia: Significant changes in the ecosystem following human alteration to the natural water regime. Organic Geochemistry 75, 74-86.

Tuo, J., Wang, X., Chen, J., Simoneit, B.R.T., 2003. Aliphatic and diterpenoid hydrocarbons and their individual carbon isotope compositions in coals from the Liaohe Basin, China. Organic Geochemistry 34, 1615-1625.

van der Meer, M.T.J., Schouten, S., Sinninghe Damsté, J.S., 1998. The effect of the reversed tricarboxylic acid cycle on the $^{13}C$ contents of bacterial lipids. Organic Geochemistry 28, 527-533.

van Kaam-Peters, H.M.E., Schouten, S., de Leeuw, J.W., Sinninghe Damsté, J.S., 1997. A molecular and carbon isotope biogeochemical study of biomarkers and kerogen pyrolysates of the Kimmeridge Clay Facies: palaeoenvironmental implications. Organic Geochemistry 27, 399-422.

Volkman, J.K., 1986. A review of sterol markers for marine and terrigenous organic matter. Organic Geochemistry 9, 83-99.

Volkman, J.K., Barrett, S.M., Blackburn, S.I., Mansour, M.P., Sikes, E.L., Gelin, F., 1998. Microalgal biomarkers: A review of recent research developments. Organic Geochemistry 29, 1163–1179.

Volkman, J.K., 2003. Sterols in microorganisms. Applied Microbiology and Biotechnology 60, 495-506.

Volkman, J.K., 2005. Sterols and other triterpenoids: source specificity and evolution of biosynthetic pathways. Organic Geochemistry 36, 139-159.

Volkman, J.K., Zhang, Z., Xie, X., Qin, J., Borjigin, T., 2015. Biomarker evidence for *Botryococcus* and a methane cycle in the Eocene Huadian oil shale, NE China. Organic Geochemistry 78, 121-134.

Weston, R.J., Philp, R.P., Sheppard, C.M., Woolhouse, A.D., 1989. Sesquiterpanes, diterpanes and other higher terpanes in oils from the Taranaki basin of New-Zealand. Organic Geochemistry 14, 405-421.

Wilkins, R.W.T., George, S.C., 2002. Coal as a source rock for oil: a review. International Journal of Coal Geology 50, 317-361.

Xiong, Y., Geng, A., 2000. Carbon isotopic composition of individual *n*-alkanes in asphaltene pyrolysates of biodegraded crude oils from the Liaohe Basin, China. Organic Geochemistry 31, 1441-1449.

Xiong, Y., Geng, A., Pan, C., Liu, D., Peng, P., 2005. Characterization of the hydrogen isotopic composition of individual *n*-alkanes in terrestrial source rocks. Applied Geochemistry 20, 455-464.

Ye, J., Qing, H., Bend, S.L., Gu, H., 2007. Petroleum systems in the offshore Xihu Basin on the continental shelf of the East China Sea. AAPG Bulletin 91, 1167-1188.

Zhou, Y., Grice, K., Stuart-Williams, H., Farquhar, G.D., Hocart, C.H., Lu, H., Liu, W., 2010. Biosynthetic origin of the saw-toothed profile in $\delta^{13}C$ and $\delta^{2}H$ of *n*-alkanes and

systematic isotopic differences between *n*-, *iso*- and *anteiso*-alkanes in leaf waxes of land plants. Phytochemistry 71, 388-403.

Zhu, Y., Li, Y., Zhou, J., Gu, S., 2012. Geochemical characteristics of Tertiary coal-bearing source rocks in Xihu depression, East China Sea basin. Marine and Petroleum Geology 35, 154-165.

# Tables

Table 6.1 General organic geochemical characteristics of the rock samples investigated from the Huangyan Oilfield in the Xihu Depression, East China Sea Basin. PH = Pinghu Formation, HG = Huagang Formation.

| Well | Depth/m | Fm | Lithology | TOC (%) | N (%) | I (%) | Pβ (%) | Pα (%) | Kβ (%) | Kα (%) | I/Pβ | N/(N+Pβ) | $C_{27}$ (%) | $C_{28}$ (%) | $C_{29}$ (%) | $CPI_{24-34}$ | Pr/Ph | $C_{29}$ 20S | $C_{29}$ αββ |
|---|---|---|---|---|---|---|---|---|---|---|---|---|---|---|---|---|---|---|---|
| 825G-1 | 2580 3 | HG Upper | C-Mudstone | 12 7 | 5 6 | 2 0 | 46 8 | 16 7 | 12 4 | 16 7 | 0 04 | 0 11 | 24 | 30 | 46 | 1 78 | 4 5 | 0 46 | 0 51 |
| 825G-1 | 3044 0 | HG Lower | Mudstone | 1 6 | 14 5 | 10 1 | 49 6 | 10 6 | 0 1 | 15 2 | 0 20 | 0 23 | 28 | 15 | 56 | 1 31 | 1 5 | 0 47 | 0 51 |
| 825G-1 | 3044 6 | HG Lower | Mudstone | 1 5 | 13 1 | 9 9 | 47 7 | 14 4 | 0 3 | 14 6 | 0 21 | 0 22 | 28 | 15 | 56 | nd | 1 2 | 0 47 | 0 51 |
| 825G-1 | 3194 2 | HG Lower | Mudstone | 2 3 | 31 0 | 23 5 | 26 5 | 12 7 | 6 3 | 0 1 | 0 88 | 0 54 | 56 | 13 | 30 | 1 45 | 4 3 | 0 47 | 0 44 |
| 825AD-1 | 2890 0 | HG Lower | C-Mudstone | 19 6 | 48 7 | 23 5 | 27 8 | 0 0 | 0 0 | 0 0 | 0 85 | 0 64 | 25 | 15 | 60 | 1 41 | 7 2 | 0 44 | 0 46 |
| 825AD-1 | 2956 0 | HG Lower | Mudstone | 1 2 | 22 0 | 27 6 | 21 0 | 15 2 | 6 8 | 7 4 | 1 31 | 0 51 | 27 | 27 | 46 | 1 20 | 6 1 | 0 36 | 0 33 |
| 825AD-1 | 3043 4 | HG Lower | Mudstone | 1 5 | 12 3 | 16 8 | 46 8 | 19 4 | 2 8 | 1 9 | 0 36 | 0 21 | 48 | 13 | 39 | 1 38 | 4 7 | 0 41 | 0 38 |
| 825AD-1 | 3263 5 | HG Lower | Mudstone | 0 96 | 28 4 | 31 6 | 18 2 | 8 1 | 9 0 | 4 8 | 1 74 | 0 61 | 17 | 25 | 57 | 1 16 | 4 8 | 0 42 | 0 47 |
| 825AD-1 | 3263 5 | HG Lower | Mudstone | 0 45 | 28 9 | 29 3 | 20 7 | 4 5 | 2 2 | 14 4 | 1 41 | 0 58 | 23 | 26 | 51 | 1 16 | 4 1 | 0 42 | 0 47 |
| 825AD-1 | 3708 0 | PH Upper | Coal | 55 6 | 9 7 | 8 7 | 50 3 | 22 0 | 2 8 | 6 6 | 0 17 | 0 16 | 8 | 24 | 69 | 1 10 | 5 6 | 0 46 | 0 57 |
| 825AD-1 | 3709 0 | PH Upper | Coal | 58 5 | 8 1 | 8 5 | 43 3 | 18 9 | 2 4 | 18 9 | 0 20 | 0 16 | 9 | 24 | 67 | 1 11 | 6 3 | 0 46 | 0 53 |
| 825AD-1 | 3749 0 | PH Upper | Coal | 49 3 | 9 6 | 8 0 | 51 4 | 21 9 | 2 6 | 6 4 | 0 16 | 0 16 | 9 | 26 | 65 | 1 09 | 5 6 | 0 44 | 0 55 |
| 825AD-1 | 3751 0 | PH Upper | Coal | 55 7 | 7 9 | 9 8 | 51 5 | 22 0 | 2 6 | 6 2 | 0 19 | 0 13 | 13 | 21 | 66 | 1 03 | 5 1 | 0 42 | 0 54 |
| 825AD-1 | 3755 0 | PH Upper | Coal | 59 8 | 3 9 | 4 2 | 60 0 | 23 9 | 2 5 | 5 5 | 0 07 | 0 06 | 17 | 23 | 61 | 1 15 | 5 5 | 0 41 | 0 48 |
| 825AD-1 | 3796 0 | PH Upper | Coal | 56 5 | 33 2 | 7 9 | 27 2 | 14 1 | 14 4 | 3 2 | 0 29 | 0 55 | 8 | 26 | 66 | 1 13 | 1 2 | 0 44 | 0 55 |
| 825AD-1 | 3867 0 | PH Upper | Coal | 48 0 | 5 5 | 3 7 | 49 6 | 20 2 | 0 7 | 20 2 | 0 07 | 0 10 | 15 | 26 | 59 | 1 20 | 7 0 | 0 46 | 0 53 |
| 825AD-1 | 3868 0 | PH Upper | Coal | 60 1 | 9 7 | 5 7 | 45 3 | 19 2 | 0 8 | 19 3 | 0 12 | 0 18 | 12 | 26 | 62 | 1 11 | 6 0 | 0 56 | 0 27 |
| 825AD-1 | 3869 0 | PH Upper | Coal | 54 9 | 4 4 | 42 4 | 30 0 | 11 3 | 0 5 | 11 3 | 1 41 | 0 13 | 12 | 28 | 59 | 1 13 | 6 6 | 0 41 | 0 58 |
| 825AD-1 | 3873 0 | PH Upper | Coal | 60 3 | 10 3 | 8 8 | 44 0 | 18 0 | 1 0 | 17 9 | 0 20 | 0 19 | 18 | 23 | 59 | 1 13 | 6 3 | 0 41 | 0 57 |
| 825A-1 | 3540 5 | | Oil | | 31 6 | 53 8 | 10 0 | 0 6 | 1 8 | 2 2 | 5 36 | 0 75 | 52 | 25 | 23 | nd | 4 1 | 0 66 | 0 45 |
| 825AD-1 | 2516 0 | | Oil | | 26 8 | 28 1 | 32 2 | 2 8 | 8 7 | 1 4 | 0 87 | 0 43 | 25 | 27 | 48 | 1 05 | 8 1 | 0 42 | 0 51 |
| 825AD-1 | 3035 3 | | Oil | | 22 8 | 26 7 | 36 4 | 3 3 | 8 9 | 1 9 | 0 73 | 0 36 | 45 | 22 | 33 | 1 13 | 3 1 | 0 46 | 0 52 |
| 825B-2 | 3355 5 | | Oil | | 24 3 | 45 9 | 17 7 | 2 1 | 4 5 | 5 5 | 2 60 | 0 55 | 41 | 27 | 32 | nd | 5 1 | 0 78 | 0 41 |
| 825B-3 | 3426 8 | | Oil | | 24 6 | 40 9 | 23 0 | 1 6 | 5 0 | 4 8 | 1 78 | 0 50 | 34 | 24 | 43 | nd | 5 3 | 0 62 | 0 49 |

Note: C-Mudstone = carbonaceous mudstone; N = 4β(H)-19-norisopimarane; I = isopimarane; Pβ = 16β(H)-phylloclodane; Pα = 16α(H)-phylloclodane; Kβ = 16β(H)-kaurane; Kα = 16α(H)-kaurane % are of these 6 diterpanes $C_{27}$, $C_{28}$ and $C_{29}$ are the % of total 4 regular (20S-ααα + 20R-αββ + 20S-αββ + 20R-ααα) steranes $CPI_{24-34}$ = carbon preference index (defined as $1/2 \times [\sum(C_{25}\sim C_{33})/\sum(C_{24}\sim C_{32}) + \sum(C_{25}\sim C_{33})/\sum(C_{26}\sim C_{34})]$, Bray and Evans, 1961) $C_{29}$ 20S = $C_{29}$ ααα 20S/(20S + 20R) steranes; $C_{29}$ αββ = $C_{29}$ αββ/(αββ + ααα) steranes nd = not determined

Table 6.2 Compound specific stable carbon isotope data for *n*-alkanes and isoprenoids in the source rocks extracts and oils from the Huangyan Oilfield in the Xihu Depression, East China Sea Basin.

| Well | 825AD-1 | 825AD-1 | 825AD-1 | 825AD-1 | 825AD-1 | 825G-1 | 825AD-1 | 825B-2 | 825B-3 |
|---|---|---|---|---|---|---|---|---|---|
| Depth (m) | 3709 | 3796 | 3868 | 3873 | 2890 | 3044 | 3035 | 3355 | 3426 |
| Type of sample | Coal | Coal | Coal | Coal | Mudstone | Mudstone | Oil | Oil | Oil |
| Formation | PH Upper | PH Upper | PH Upper | PH Upper | HG Lower | HG Lower | | | |
| Tag | C1 | C2 | C3 | C4 | M2 | M1 | O1 | O2 | O3 |
| C15 | -26.8 | -25.8 | | -27.1 | -27.9 | | -27.3 | -27.8 | -27.3 |
| C16 | -26.6 | -27.2 | | -26.8 | -27.4 | -27.7 | -27.4 | -28.2 | -27.3 |
| C17 | -25.9 | -26.5 | -26.4 | -25.6 | -28.1 | -25.7 | -27.1 | -29.6 | -27.6 |
| Pr | -27.7 | -28.2 | -27.7 | -28.1 | -28.2 | -29.0 | -29.0 | -28.4 | -27.5 |
| C18 | -27.1 | -27.7 | -27.6 | -26.5 | -29.1 | -28.2 | -27.3 | -28.3 | -27.8 |
| Ph | -29.1 | -29.7 | -27.3 | -29.4 | -27.5 | -30.7 | -32.2 | -29.6 | -29.0 |
| C19 | -27.2 | -27.6 | -27.2 | -27.1 | -30.2 | -29.1 | -27.0 | -28.1 | -28.0 |
| C20 | -26.7 | -27.5 | -27.1 | -26.5 | -30.0 | -28.4 | -26.5 | -28.0 | -28.1 |
| C21 | -27.1 | -27.7 | -27.5 | -26.4 | -30.2 | -28.7 | -26.7 | -28.3 | -28.5 |
| C22 | -27.3 | -27.8 | -27.6 | -27.7 | -30.2 | -28.9 | -27.0 | -28.6 | -28.8 |
| C23 | -27.0 | -27.5 | -27.4 | -27.7 | -30.1 | -29.2 | -27.0 | -29.4 | -29.4 |
| C24 | -27.6 | -28.0 | -27.7 | -26.5 | -29.9 | -29.5 | -27.0 | -29.7 | -30.1 |
| C25 | -27.7 | -28.2 | -28.1 | -27.2 | -30.5 | -29.5 | -27.8 | -30.0 | -30.8 |
| C26 | -27.7 | -28.0 | -27.8 | -27.4 | -30.3 | -29.6 | -28.2 | -30.5 | -31.4 |
| C27 | -28.1 | -28.1 | -28.0 | -27.5 | -30.5 | -29.8 | -28.4 | -31.3 | -31.9 |
| C28 | -28.6 | -28.2 | -28.3 | -27.6 | -30.2 | -30.2 | -29.0 | -31.8 | -32.6 |
| C29 | -29.0 | -28.6 | -27.4 | -27.5 | -30.2 | -30.1 | -29.3 | -32.8 | -33.4 |
| C30 | -28.5 | -27.8 | -28.2 | -28.4 | -30.6 | -31.5 | -29.4 | | -34.4 |
| C31 | -29.5 | -27.6 | -28.3 | -28.5 | -34.0 | -30.5 | -30.3 | | |

Chapter 7

# 7. Summary and conclusions

This thesis has documented a detailed investigation of the organic matter inputs and depositional environments of Eocene organic-rich shales and mudstones in the Dongying Depression, Bohai Bay Basin. The enrichment and preservation mechanisms of organic matter at the microscale were also constrained by assessing the heterogeneity of hydrocarbons within those shales and mudstones. An oil-source correlation in the Xihu Depression, East China Sea Basin was made for discriminating the relative contribution of mudstones and coals to petroleum.

## 7.1. Diversity in organic matter input in the Dongying Depression

The relative distribution and abundance of aliphatic and aromatic hydrocarbons in rock samples from the Dongying Depression suggest a great diversity in organic matter input.

In **Chapter 2**, various biomarkers were used to demonstrate that the organic matter input mainly included indigenous lacustrine algae, some additional marine algae, and minor terrigenous land plants. A prokaryotic bacterial contribution is also prominent, particularly in the third member of the Shahejie Formation, as the regular sterane/hopane ratios are

consistently less than 1. The presence of 2α-methylhopanes, β-carotane, aryl isoprenoids, isorenieratene derivatives and hopanes is consistent with intense bacterial activity. Gammacerane co-occurs with $C_{29}$ regular steranes, which shows that the $C_{29}$ regular steranes are related to aqueous organisms rather than higher plants (Volkman et al., 1998). Thus the large variation in the relative abundance of $C_{27\text{-}29}$ regular steranes through the third and fourth members of the Shahejie Formation represents a large diversity in algal and bacterial communities. The possibility of a marine transgressive event in the Dongying Depression has been debated for a long time. In this thesis, the occurrence of 24-*n*-propylcholestanes strengthens the link between marine organic matter and the Dongying palaeo-lake (Moldowan et al., 1990) (Section 7.2). Importantly, the identification of 24-*n*-propylcholestanes should consider the possibility of cross-talk of 4-methylsteranes and dinosteranes into the *m/z* 414→217 mass transition, particularly in samples with low concentrations of 24-*n*-propylcholestanes. Only samples from the west of the depression received significant terrigenous land plant organic matter input, based on biomarker evidence including oleanane, abundant $C_{19\text{-}21}$ tricyclic terpanes and low abundances of retene and cadalene. Other hydrocarbon biomarkers that might usually suggest terrigenous inputs have here been attributed to other sources in this case. For example, in **Chapter 3** 1-methylphenanthrene and 1,7-dimethylphenanthrene were suggested to be related to aqueous organisms, due to their correlations with $C_{27}$ regular steranes (Grice et al., 2007). The long-chain *n*-alkanes are also suggestive of specific algae (e.g. the lacustrine *Botryococcus braunii*) (Feng et al., 2007; Bechtel et al., 2012).

In the Dongying Depression, the high generative potential of the organic-rich source

rocks is not only a consequence of high algal productivity and the anoxic preservation conditions, but also of significant bacterial activity and organic matter input during deposition of the Shahejie Formation.

## 7.2. The varying depositional environment and palaeowater composition

After intense faulting, the Dongying palaeo-lake was severely evaporated, due to a prolonged period of arid climate when the Es4U member was being deposited (Li et al., 2003). The data in **Chapter 2** show elevated concentrations of gammacerane and low Pr/Ph ratios in the Es4U member samples, indicating anoxic conditions and saline or hypersaline stratification of the palaeowater column. During deposition of the overlying Es3 member, there was a higher subsidence rate than sedimentation rate, causing a deeper and wider lake (Zhang et al., 2004). The Pr/Ph ratio increased, and the β-carotane and gammacerane content significantly reduced, suggesting decreased water salinity, an increase in the oxygen concentration, suboxic bottom water conditions and a less-stratified water body, consistent with humid and warm climate conditions for deposition of the Es3 member (Chen et al., 2016; He et al., 2017). The decline of gammacerane is interpreted as reflecting palaeo-depositional dynamics, including a decrease in water salinity and water stratification from the basal Es4U member, through the Es3L member to the top Es3M member.

The pervasive presence of aryl isoprenoids and isorenieratene derivatives was inferred to indicate a stratified water column and episodic PZE conditions during deposition of the Shahejie Formation. This was probably due to enhanced water salinity, which played a pivotal

role in the preservation of organic matter. Algal blooms may have given rise to the oxygen-deficient conditions. Two periods of episodic seawater incursions into the Dongying palaeo-lake occurred during deposition of the Es3M and the Es4U members, as shown by the unambiguous detection of 24-*n*-propylcholestanes. There was decreasing PZE persistence from the NE to the SW of the palaeo-lake, as shown by an increasing aryl isoprenoid ratio. Seawater incursions may have contributed to development of stratification and photic zone euxinia. This is somewhat consistent with the direction of seawater incursions, based on palaeogeographic plate reconstructions (Scotese, 2001), and the absence of oleanane in the northeastern Dongying Depression. The Dongying palaeo-lake contained a high abundance of $H_2S$ that was necessary for anoxygenic photosynthesis by green sulphur bacteria. Sulphate-reducing bacteria supplied $H_2S$ by reducing the aqueous sulphate ($SO_4^{2-}$) that was carried into the palaeo-lake by episodic seawater flooding.

## 7.3. The enrichment of organic matter in the lacustrine shales

The evolution of the depositional environments and the primary mechanism of accumulation of organic matter in the lacustrine setting have been widely discussed in the literature and in this thesis. The formation of excellent petroleum source rocks usually depends on high productivity and restricted preservation conditions, with a low clastic sedimentation rate to avoid dilution. However, it is uncertain to what extent water column stratification, bottom water anoxia, photic zone euxinia and bacterial activity occurred, and their association with organic matter preservation at the microscale is also unknown. **Chapter 4** focuses on hydrocarbon heterogeneity at the microscale, and tries to unveil the precise

mechanisms of organic matter accumulation and preservation.

After organic substrates settled to the 'sediment-water' interface, abundant sulphate furthered bacterial sulphate reduction and anoxicity at a relatively low position in the water column. Bacterially-mediated reduction of sulphate to sulphide is accompanied by oxidation of organic matter to carbon dioxide ($CO_2$). At a higher position in the water column, photosynthetic bacteria such as green sulphur bacteria and purple sulphur bacteria can be active, and in the uppermost water layers planktonic organisms and heterotrophic oxidisers are present. Together they formed a syntrophic community, with a complete carbon cycle. Different bacterial groups/communities can directly or indirectly alter the net organic carbon content. This accounts for fluctuation of the organic carbon content at the millimetre scale as described in **Chapter 4**, with a change in persistence or intensity of photic zone euxinia consistent with the change in total organic carbon. Based on this finding, it has been postulated that in the Dongying Depression, these fine-grained rocks were deposited under a dynamic environment rather than permanent bottom water anoxia, and that net preservation of organic carbon occurred during dynamic carbon cycling. Various groups of micro-organisms together with their specific living features are the main controls.

## 7.4. Influences of photic zone euxinia and bacterial sulphate reduction on hydrocarbon biomarkers at the microscale

In **Chapter 5**, aromatic hydrocarbon distributions at the millimetre scale have significant variation. Almost every series of aromatic compounds has marked differences between two sliced samples, consistent with the effects of different sources or depositional environment.

These two sliced samples have been interpreted to record different levels of euxinic water conditions. Due to the different depositional environments, specific micro-organism assemblages adapted and thrived.

At the millimetre scale, biomarker parameters based on the relative distribution of the aliphatic and most of the aromatic hydrocarbons are not always loyal to indications based on a bulk sample. This is because the variability of different hydrocarbons may have different sensitivities and validities to the environment. For example, of the pristane/phytane ratio and the aryl isoprenoid ratio, the former barely shows any difference at the millimetre scale, while the latter shows significant change. This suggests that the isorenieratane derivatives are more sensitive and responsive to redox conditions in the photic zone. Biomarker evidence for the change in micro-organisms includes 4α-methylsteranes, triaromatic dinosteranes, isorenieratane, alkylnaphthalenes and alkylphenanthrenes. Micro-changes in environment and organisms at the 'water-sediment' interface and the photic zone can be recorded by such biomarkers.

Differences in stable carbon isotopic fractionation of long-chain *n*-alkanes was noted at the millimetre scale of sampling. Variations in magnitude of bacterial sulphate reduction (BSR) and photic zone euxinia (PZE) are responsible for these differences. The more intense BSR (and PZE conditions) are interpreted as giving rise to increased $^{13}C$ depletion of long-chain *n*-alkanes. SRB can oxidise organic substrates by reducing sulphate as an electron acceptor. The produced $CO_2$, which is isotopically lighter as a consequence of the citric acid cycle (involving decarboxylation of organic acids) can then be recycled. Additionally, bacterial heterotrophs (such as SRB) yield greater isotopic fractionations (Coffin et al., 1990;

Pancost and Sinninghe Damsté, 2003). This $CO_2$ can be fixed by those phototrophic producers in the upper water layers, which will result in an isotopically lighter signature of the lipids and subsequently the n-alkanes detected in the sedimentary organic matter record.

In summary, depositional environments in the Dongying Depression varied significantly at the millimetre scale. Organic matter enrichment is a very individual and location/time specific process, rather than being a persistent process. However, unusual differences in the distributions of hydrocarbons are due to unknown and complex effects, so more research is needed.

## 7.5. The relative contribution of mudstones and coals to petroleum in the Xihu Depression

Unlike source rocks from the Dongying Depression, the source rocks from the Xihu Depression contain biomarkers that are mainly derived from terrigenous organic matter. The Xihu Depression source rocks were deposited mainly in fluvial, deltaic and lacustrine environments, with oxic depositional conditions (Chen, 1998; Zhu et al., 2012). Tricyclic- and tetracyclic diterpenoids are abundant, and are the most characteristic biomarkers of the sediments in this coal-bearing petroleum system (Zhu et al., 2012). **Chapter 6** differentiates the hydrocarbon contribution of mudstones and associated coals to the reservoired petroleum. The carbon fixation pathways of higher plant and resin-sources is reflected in the molecular and carbon isotopic compositions of the preserved hydrocarbons. This influence extends to the components derived from different parts of land plants (e.g. leaf wax, cuticle wax, heartwood resin), as well as to the generated oil and gas. For terrigenously-dominated organic matter,

long chain *n*-alkanes with a large proportion of gymnosperm organic inputs are approximately 2-3‰ enriched in $^{13}C$ than those with a large proportion of angiosperm organic inputs, regardless of variation in lithologies. The carbon isotopic compositions of *n*-alkanes and isoprenoids, combined with the biomarker compositions, provide unique evidence for the different terrigenous organic matter inputs to the petroleum generated in the Xihu Depression.

## 7.6. Future work

Further possibilities for research in this area include improved experimental processes and spatially constrained techniques. One is to do slice experiments at even smaller scale to document more detailed fluctuations in organic matter input and depositional environment at a shorter time scale. This would be of great significance when these time slices are age constrained by using high-precision rhenium-osmium (Re-Os) isotopic dating techniques. Links between the open sea and the Dongying palaeo-lake could be highly strengthened if variation in marine-specific biomarkers were able to be documented at even smaller scale. Another avenue for further research is to establish an experiment procedure that works for bulk samples in three dimensions. The three dimensional variation in organic geochemistry could be assessed to understand the spatial heterogeneity of organic inputs and depositional environments at the microscale. Additionally, sediment mapping technique such as Nanomin, combined with spatially constrained techniques such as micro-drilling and sampling, and laser micropyrolysis GC-MS, would be helpful for understanding organic matter inputs and mineral interactions.

# References

Bechtel, A., Jia, J., Strobl, S.A.I., Sachsenhofer, R.F., Liu, Z., Gratzer, R., Püttmann, W., 2012. Palaeoenvironmental conditions during deposition of the Upper Cretaceous oil shale sequences in the Songliao Basin (NE China): Implications from geochemical analysis. Organic Geochemistry 46, 76–95.

Chen, L., 1998. Depositional environment evolution of Pinghu formation in Xihu Depression, the East China Sea. Marine Geology & Quaternary Geology 18, 69-78.

Chen, Z., Huang, W., Liu, Q., Zhang, L., Zhang, S., 2016. Geochemical characteristics of the Paleogene shales in the Dongying depression, eastern China. Marine and Petroleum Geology 73, 249–270.

Coffin, R.B., Velinsky, D.J., Devereux, R., Price, W.A., Cifuentes, L.A., 1990. Stable carbon isotope analysis of nucleic acids to trace sources of dissolved substrates used by estuarine bacteria. Applied and Environmental Microbiology 56, 2012.

Feng, Z., Fang, W., Zhang, J., Li, Z., Huang, C., Wang, X., Zhao, Q., Huo, Q., 2007. Distribution and significance of $C_{40+}$ alkanes in the extracts of Cretaceous source rocks from the Songliao Basin. Science in China Series D: Earth Sciences 50, 1510-1520.

Grice, K., Nabbefeld, B., Maslen, E., 2007. Source and significance of selected polycyclic aromatic hydrocarbons in sediments (Hovea-3 well, Perth Basin, Western Australia) spanning the Permian–Triassic boundary. Organic Geochemistry 38, 1795-1803.

He, J., Ding, W., Jiang, Z., Jiu, K., Li, A., Sun, Y., 2017. Mineralogical and chemical distribution of the Es3L oil shale in the Jiyang Depression, Bohai Bay Basin (East China): Implications for paleoenvironmental reconstruction and organic matter

accumulation. Marine and Petroleum Geology 81, 196–219.

Li, S., Pang, X., Li, M., Jin, Z., 2003. Geochemistry of petroleum systems in the Niuzhuang South Slope of Bohai Bay Basin—part 1: source rock characterization. Organic Geochemistry 34, 389–412.

Moldowan, J.M., Fago, F.J., Lee, C.Y., Jacobson, S.R., Watt, D.S., Slougui, N.E., Jeganathan, A., Young, D.C., 1990. Sedimentary 24-*n*-propylcholestanes, molecular fossils diagnostic of marine-algae. Science 247, 309–312.

Pancost, R.D., Sinninghe Damsté, J.S., 2003. Carbon isotopic compositions of prokaryotic lipids as tracers of carbon cycling in diverse settings. Chemical Geology 195, 29-58.

Scotese, C.R., 2001. The plate tectonic reconstructions. PALEOMAP Project. http://www.scotese.com/newpage9.htm

Volkman, J.K., Barrett, S.M., Blackburn, S.I., Mansour, M.P., Sikes, E.L., Gelin, F., 1998. Microalgal biomarkers: A review of recent research developments. Organic Geochemistry 29, 1163–1179.

Zhang, S., Wang, Y., Shi, D., Xu, H., Pang, X., Li, M., 2004. Fault-fracture mesh petroleum plays in the Jiyang Superdepression of the Bohai Bay Basin, eastern China. Marine and Petroleum Geology 21, 651-668.

Zhu, Y., Li, Y., Zhou, J., Gu, S., 2012. Geochemical characteristics of Tertiary coal-bearing source rocks in Xihu depression, East China Sea basin. Marine and Petroleum Geology 35, 154-165.

# Appendix

## A.1. Conferences

Xu, H., George, S.C., Hou, D. (2016) The stable carbon isotopic compositions of individual *n*-alkanes and isoprenoids provide evidence of source contributions for petroleum generated from the Xihu Depression, East China Sea. 19th Australian Organic Geochemistry Conference, Perth, Australia.

George, S.C., Xu, H., Löhr, S.C., and Kennedy, M.J. (2017) Organic geochemistry of Pliocene sapropels from ODP Sites 964 and 967, eastern Mediterranean Basin. In: Book of abstracts, 28th International Meeting on Organic Geochemistry, Florence, Italy.

## A.2. The IODP work (Copy of published paper)

Löhr, S.C., Kennedy, M.J., George, S.C., Williamson, R.J., Xu, H., 2018. Sediment microfabric records mass sedimentation of colonial cyanobacteria and extensive

syndepositional metazoan reworking in Pliocene sapropels. The Depositional Record 4, 293-317.

## A.3. A copy of published paper (Chapter 2)

Xu, H., George, S.C., Hou, D., 2019. The occurrence of isorenieratane and 24-n-propylcholestanes in Paleogene lacustrine source rocks from the Dongying Depression, Bohai Bay Basin: Implications for bacterial sulfate reduction, photic zone euxinia and seawater incursions. Organic Geochemistry 127, 59-80.

## A.4. A copy of published paper (Chapter 3)

Xu, H., George, S.C., Hou, D., 2019. Algal-derived polycyclic aromatic hydrocarbons in Paleogene lacustrine sediments from the Dongying Depression, Bohai Bay Basin, China. Marine and Petroleum Geology 102, 402-425.

**Appendix 2, 3 and 4 of this thesis have been removed as they contain published material. Please refer to the following citations for details of the article contained in this appendix.**

Löhr, S. C., Kennedy, M. J., George, S. C., Williamson, R. J., & Xu, H. (2018). Sediment microfabric records mass sedimentation of colonial cyanobacteria and extensive syndepositional metazoan reworking in Pliocene sapropels. *The Depositional Record*, *4*(2), 293-317. https://doi.org/10.1002/dep2.49.

Xu, H., George, S. C., & Hou, D. (2019). The occurrence of isorenieratane and 24-n-propylcholestanes in Paleogene lacustrine source rocks from the Dongying Depression, Bohai Bay Basin: Implications for bacterial sulfate reduction, photic zone euxinia and seawater incursions. *Organic Geochemistry*, *127*, 59-80. https://doi.org/10.1016/j.orggeochem.2018.11.008

Xu, H., George, S. C., & Hou, D. (2019). Algal-derived polycyclic aromatic hydrocarbons in Paleogene lacustrine sediments from the Dongying Depression, Bohai Bay Basin, China. *Marine and Petroleum Geology*, *102*, 402-425. https://doi.org/10.1016/j.marpetgeo.2019.01.004Get